Palladium-Catalyzed Decarbonylative Halogenation of Carboxylic Acid Derivatives

(パラジウム触媒によるカルボン酸誘導体の
脱カルボニル化を伴うハロゲン化反応)

2025.3

Tian TIAN

Graduate School of Natural Science and Technology
(Doctor's Course)
OKAYAMA UNIVERSITY

Contents

Abstract

Organic halides, especially aryl halides, are versatile synthetic building blocks and are essential components of organic synthesis. The synthesis and construction of aryl halides provide a strong foundation for the advancement of organic chemistry and related scientific fields. This significance arises not only from the widespread use of the carbon-halogen (C–X) bond in various applications — such as the total synthesis of natural products, organic functional materials, the pharmaceutical industry, agriculture, pesticide development, and molecular recognition — but also from the highly polarized nature of the C–X bond. This polarization allows for facile oxidative addition under transition metal catalysis. Additionally, aryl halides can undergo single electron transfer (SET) to generate aryl radicals or organometallic reagents, or they can form high-valent halogen reagents that enhance late-stage transformations and modifications. Consequently, developing practical, convenient, efficient, and cost-effective methods for constructing aryl halides has become a decisive step in the progress of science and technology.

The current methodologies for synthesizing aryl halides are still quite limited. Most approaches focus on the electrophilic halogenation of aromatic compounds, which often involves highly toxic, strongly oxidizing, difficult-to-handle, and costly electrophilic halogenating agents. As a result, many applications concentrate on the synthesis of aryl fluorides and chlorides, as these can be produced using high reactivity of highly electrophilic reagents. However, the use of relatively less reactive electrophilic bromine and iodine reagents presents significant challenges, leading to a limited variety and high cost of commercially available aryl bromides and iodides. Notably, aryl iodides make up only 2% of all commercially available aryl halides. Given these issues, exploring nucleophilic halogenation appears to be an ideal alternative, as nucleophilic halogenation reagents are non-toxic and more readily available at a lower cost. The nucleophilic halogenation process, particularly when catalyzed by transition metals, can greatly enhance efficiency. However, there are two main challenges that have hindered the design of these transformations: 1) the weak nucleophilicity of the nucleophilic halogen reagents, and 2) the thermodynamically unfavorable nature of the reductive elimination process involving C–X bonds. Fortunately, some studies have demonstrated that

palladium can mediate the reductive elimination of C–X bonds using relatively bulky ligands. However, this approach has limited applicability for constructing C–Br and C–Cl bonds, and it is inadequate for the formation of C–I bonds due to the extremely small equilibrium constant. This limitation may also stem from the highly exothermic oxidative addition involving aryl iodides, which poses significant thermodynamic and kinetic challenges. To address these intrinsic limitations and achieve the desired outcomes, the Author proposes exploring the concept of decarbonylation as a potential breakthrough. The Author proposes that the CO generated after decarbonylation will make the transition metal center more electron-deficient. This enhancement can theoretically accelerate the reductive elimination of C–X bonds, particularly the C–I bond. Therefore, this PhD Thesis focuses on the palladium-catalyzed decarbonylative nucleophilic halogenation process via the reductive elimination of C–X bonds, emphasizing nucleophilic iodination. This research successfully constructs a variety of aryl iodides, bromides, and chlorides through the reductive elimination of C–I, C–Br, and C–Cl bonds, achieving high atom utilization and excellent efficiency.

Chapter 2. Palladium-Catalyzed Decarbonylative Nucleophilic Halogenation of Acyl Fluorides and Acyl Chlorides

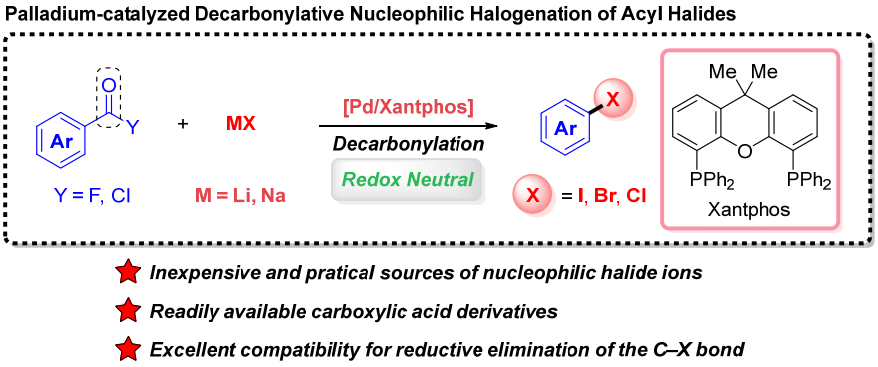

Carboxylic acid derivatives are inexpensive, readily available, air-stable, and easy-to-handle raw materials for organic synthesis. Over the past two decades, they have emerged as new electrophilic reagents for transition-metal-catalyzed carbonyl-retentive or decarbonylative coupling, with a particular focus on the decarbonylative process. In Chapter 2, the Author successfully developed a practical and versatile palladium-catalyzed decarbonylative nucleophilic halogenation method using acyl fluorides and chlorides.

The ligand Xantphos plays a dual role: it facilitates the challenging reductive elimination of Ar–I, Ar–Br, and Ar–Cl bonds due to its large bite angle, and it acts as a non-innocent additive that promotes unique outer-sphere nucleophilic substitutions by forming phosphonium halides. Importantly, this protocol utilizes low-cost lithium and sodium halides as sources of halogen, making it both cost-effective and aligned with the principles of green and sustainable development, since these are inorganic salts with low toxicity.

The Author conducted in-depth mechanistic studies and proposed that the coordination of released CO to the palladium center kinetically accelerates the reductive elimination of the C–X bond. Additionally, the coordination of excess Xantphos to the Pd(0) center may hinder the over-oxidative addition of the aryl iodide, promoting the progression of the catalytic cycle in the desired direction. The Author was pleased to discover highly reactive acyl iodides as unique reaction intermediates. This discovery enabled the in-situ generation of acyl iodides using stable acyl fluorides as mediators, facilitating indirect unimolecular fragmentation coupling (UFC) through decarbonylation under mild and practical conditions. Kinetic studies indicated that the rate of acyl iodide formation is crucial for the success of the transformation, with a slow and gradual formation helping to effectively prevent catalyst poisoning. Therefore, the Author demonstrated that the concept of "gradual generation" — where highly reactive intermediates are generated and consumed simultaneously — serves as an effective transformation model in this system.

Chapter 3. Palladium-Catalyzed Decarbonylative Nucleophilic Halogenation of Acid Anhydrides

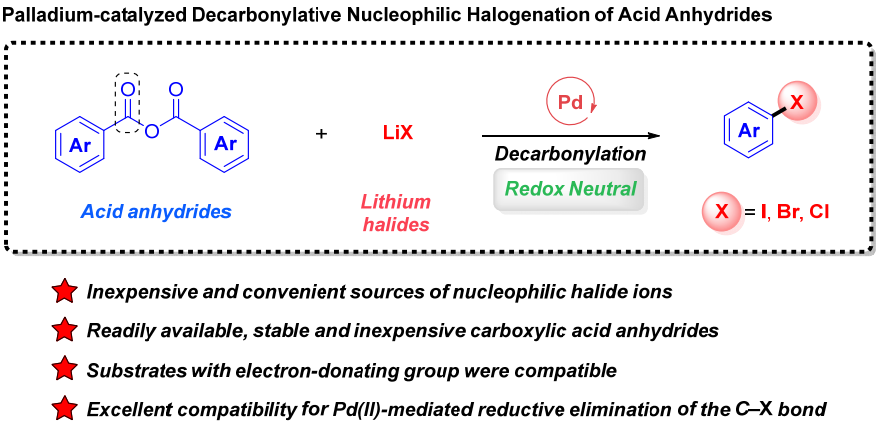

Acid anhydrides, often considered "activated carboxylic acid", have been developed by chemists as effective agents for acylation as well as arylation/alkylation, particularly in the decarbonylation process under transition metal catalysis. This area of research currently encompasses four main dimensions: elimination, insertion and cyclization, C–H bond functionalization, and cross-coupling. In the previous Chapter, the Author introduced an efficient palladium-catalyzed decarbonylative nucleophilic halogenation method for acyl fluorides and chlorides. However, the high instability of acyl chlorides and the considerable cost of acyl fluorides raised concerns for the Author. More importantly, substrates containing electron-donating substituents can be challenging to work with due to issues such as catalyst poisoning and the scrambling of phenyl groups that may occur after the oxidative addition of the C–P bond to the phosphorus–phenyl bond of Xantphos during outer-sphere nucleophilic substitution. In Chapter 3, the Authors explored the use of stable, active, and cost-effective acid anhydrides as substrates for catalytic decarbonylative halogenation. Importantly, the Authors managed to facilitate the spillover of a potential catalyst poison, molecular iodine (I_2), in an open system. This approach significantly reduced catalyst poisoning and enhanced catalytic efficiency, particularly when acid anhydrides with electron-donating substituents were employed as substrates. As a result, the Author successfully synthesized a series of aryl iodides, bromides, and chlorides through the reductive elimination of C–I, C–Br, and C–Cl bonds, achieving high atom utilization in this process. Mechanistic studies have revealed a Pd-catalyzed decarbonylative indirect unimolecular fragment coupling (IUFC) pathway. A key aspect of this process is the formation rate of acyl iodides, which is crucial for success. Using acid anhydrides as the substrates generates an antagonistic carboxylate (specifically, lithium carboxylate) alongside the formation of acyl iodides. This byproduct can slow down the generation rate of acyl iodides, ultimately ensuring high catalytic efficiency.

CHAPTER 1

General Introduction

1-1 Introduction

The synthesis and application of aryl halides is one of the foundational research projects within the scientific research community, as it plays a critical role in various fields, including the total synthesis of natural products,[1] pharmaceutical engineering,[2] organic functional materials,[3] and the agriculture and pesticide industry,[4] as well as molecular recognition.[5] This significance arises from the highly polarized C–X bond in aryl halides, which facilitates oxidative addition in the presence of low-valent transition metals,[6] and allows for single electron transfer (SET) in reducing environments. This process generates aryl radicals or constructs organometallic reagents.[7] Additionally, aryl halides can be oxidized to form high-valent halogen reagents, thereby providing numerous opportunities for subsequent late-stage modifications and transformations.[8] The C–X bond lengths of the simplest aryl halides, such as fluorobenzene, chlorobenzene, bromobenzene, and iodobenzene, are measured at 1.37, 174, 1.90, and 2.14 Å, respectively.[9] As the atomic radius increases, both bond length and bond energy change accordingly, leading to a gradual increase in reactivity. This characteristic makes aryl iodides particularly attractive to chemists due to their unique reactivity. However, the current method for synthesizing aryl halides, especially aryl iodides, are somewhat limited. In classical electrophilic halogenation, reagents such as F_2 and XeF_2 for fluorine, Cl_2 for chlorine, and Br_2 for bromine possess strong electrophilicity and oxidizing properties. As a result, they are highly reactive and often produce a variety of halogenated products during reactions.[10] Even with strict dosage control, it is challenging to avoid unwanted byproducts, complicating subsequent purification processes. Given these challenges, employing transition metal catalysis for the construction of carbon–halogen bonds presents an ideal approach.

Despite the advancements in the field, challenges remain in the actual operation process. One significant issue is the thermodynamically and kinetically unfavorable reductive elimination of the C–X bond.[11] Generally, for reductive elimination to occur, the two components bonded to the transition metal must have sufficient electron density overlap with the metal center. However, highly polarized metal–halogen bonds exhibit more ionic character, which stabilizes the bond and inhibits subsequent reductive elimination. Nevertheless, due to the extensive use of aromatic halides in organic chemistry, chemists

continue to actively seek strategies to overcome these challenges.[12] Over the past two decades, significant advancements have been made in catalytic halogenation through reductive elimination using highly oxidized transition metal complexes as intermediates. This process involves creating more electron-deficient transition metal central atoms. Since Ettorre first discovered the C–I bond reductive elimination promoted by Pt^{IV} in 1969,[13] various transition metals, including Pt^{IV},[14] Pd^{IV},[15] Pd^{III},[16] Ni^{III},[17] and Ni^{IV},[18] have effectively facilitated the smooth reductive elimination of carbon–halogen bonds to synthesize a range of aromatic halides. However, despite these breakthroughs in halogen chemistry, some critical issues remain unaddressed. For instance, there is often a need for customized catalysts or expensive ligands, as well as highly reactive halogenating agents or oxidants. These requirements limit the practicality of the processes and their compatibility with various functional groups. In light of these challenges, the Author is highly motivated and seeks to overcome these limitations by developing a more inclusive, mild, and redox-neutral methodology for nucleophilic halogenation.

1-2 Reversibility of Palladium-Mediated Oxidative Addition of Aryl Halides

The process of breaking old chemical bonds and forming new ones is effectively managed by transition metals through two essential reactions: oxidative addition and reductive elimination. These reactions are fundamental to the field of catalysis. In particular, oxidative addition—the initial step in reaction design—plays a crucial role in establishing new protocols. Aryl (pseudo)halides are often key players in this process because their properties facilitate thermodynamically and kinetically favorable oxidative addition. As a result, these transition-metal-catalyzed cross-coupling reactions have been developed over time by chemists and were recognized with the Nobel Prize in Chemistry in 2010.[19] A series of innovative cross-coupling reactions have been continuously demonstrated in synthetic organic chemistry and related fields. These reactions include, but are not limited to: Suzuki-Miyaura coupling reaction using boron reagents,[20] Negishi coupling reaction using zinc or aluminum reagents,[21] Kumada-Tamao-Corriu coupling reaction using Grignard reagents,[22] Murahashi coupling reaction using lithium reagents,[23] Migita-Kosugi-Stille coupling reaction using tin reagents,[24] Hiyama coupling reaction using

silicon reagents,[25] Sonogashira-Hagihara coupling reaction using terminal alkynes,[26] Mizoroki-Heck coupling reaction using alkenes,[27] Buchwald-Hartwig amination reaction using amines,[28] and new orthogonal cross-coupling reactions using germanium reagents.[29] These advancements have significantly accelerated progress and breakthroughs in chemistry and other interdisciplinary fields.

Currently, the mechanisms of nearly all coupling reactions have been fundamentally understood. These mechanisms include: 1) oxidative addition of low-valent transition metals facilitated by aryl (pseudo)halides; 2) transmetalation mediated by nucleophiles; and 3) reductive elimination, which releases the desired products and regenerates transition metal catalysts, particularly in the case of palladium-mediated oxidative addition of aryl halides.

1-2-1 Palladium-Mediated Oxidative Addition of Aryl Halides

This step involves the reaction of palladium(0) with an aryl halide (Ar–X, X is usually Cl, Br, or I) to form a palladium(II) intermediate (Ar–Pd–X). During this process, the oxidation state of the palladium center increases from 0 to +2. The palladium(0) species accept electrons from the aryl halide through its empty orbital, forming a coordination with the halogen in the C–X bond. As this occurs, the C–X bond stretches and eventually breaks, resulting in the formation of an aryl radical or ion. The palladium then establishes a new Pd–C σ-bond with the aryl group and a Pd–X σ-bond with the halogen.[30] Once this step is completed, a stable aryl palladium(II) intermediate (Ar–Pd–X) is formed (**Scheme 1-1**). In general, factors such as electron-rich ligands, polar solvents, and elevated temperatures can significantly accelerate oxidative addition. These factors enhance the reducibility of the transition metal palladium, stabilize the oxidative adduct, and facilitate the cleavage of the C–X bond, respectively.[31] The likelihood of oxidative addition varies with the nature of different aryl halides. Iodinated aromatics most readily undergo oxidative addition due to the relatively weak C–I bond and strong leaving ability. This is followed by aryl bromides, while aryl chlorides are comparatively more challenging to react. Fluorinated aromatics rarely participate in oxidative addition because of the extremely strong C–F bond. Due to the highly exothermic nature of the bonding process with metals,

when active aryl halides, such as aryl bromides and aryl iodides, participate in the reaction, the process is both thermodynamically and kinetically favorable. Over the past few decades, aryl halide-mediated oxidative addition has been generally regarded as an irreversible process. However, this seemingly accurate concept has been challenged and reevaluated over time.

Scheme 1-1. Palladium-mediated Oxidative Addition of Aryl Halides.

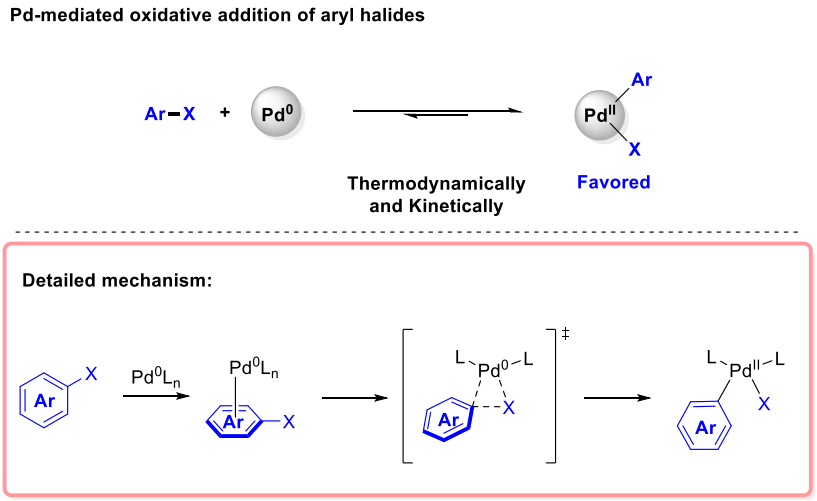

1-2-2 Discovery of Palladium-mediated Reductive Elimination of C–Cl Bonds

In 1987, Echavarren and Stille made an unexpected discovery while further investigating the well-known Migita-Kosugi-Stille cross-coupling reaction.[32] Their initial goal was to broaden the applicability of coupling reactions involving tin reagents with aryl halides or triflates. The protocol was successfully extended to incorporate various types of tin reagents, including alkyl, alkenyl, aryl, and alkynyl tin reagents as nucleophiles. This allowed for the efficient formation of a range of bonds, including C(sp^2)–C(sp^3), C(sp^2)–C(sp^2), C(sp^2)–C(sp) bonds. However, when the team employed $(TMSCH_2)_4Sn$ as the tin reagent and 4-nitrophenyl triflate as the electrophile, the desired cross-coupled product was not produced under the previously established Pd catalytic system. Instead, they obtained 4-nitrochlorobenzene as the final product, albeit in 25% yield (**Scheme 1-2**). The research

team was puzzled because there was no doubt that the chlorine atom originated from the transmetalation activating reagent LiCl. The formation of C–Cl bonds under these circumstances was quite remarkable at the time. To clarify, the process began with 4-nitrophenyl triflate, which triggered the palladium catalyst-mediated oxidative addition. This was followed by LiCl-mediated transmetalation, resulting in the formation of a 4-nitrophenyl–Pd–Cl intermediate. Remarkably, instead of undergoing further transmetalation with the tin reagent, this intermediate directly proceeded to a reductive elimination. This step released 4-nitrochlorobenzene as the final product while simultaneously regenerating the Pd catalyst. This finding caused quite a stir within the scientific community, which had generally believed that the Pd-mediated oxidative addition process of aryl (pseudo)halides was irreversible. This discovery challenged this long-standing assumption, prompting chemists to reconsider the reversibility of the process and initiate further studies.

Scheme 1-2. Unexpected Discovery on Palladium-mediated Reductive Elimination of C–Cl Bond.

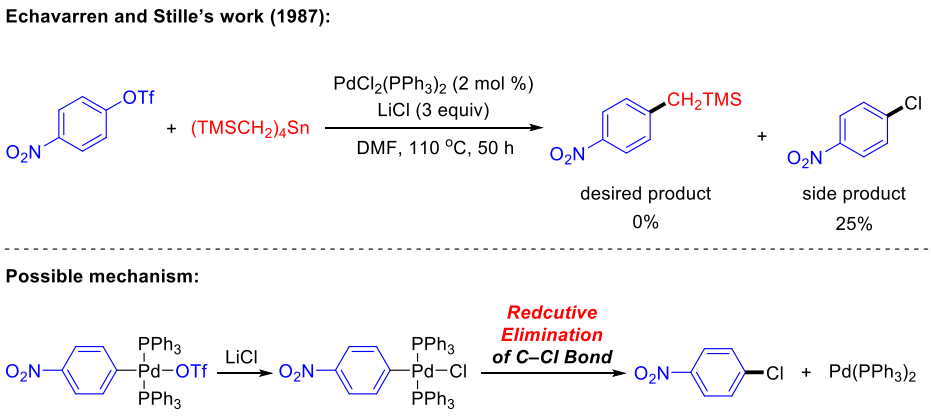

1-2-3 Palladium-Mediated Reductive Elimination of C–X bonds

Based on previous speculation, chemists sought to determine the feasibility of the reverse reaction of palladium-mediated oxidative addition of aryl halides, specifically the reductive elimination of carbon–halogen (C–X) bonds. In 2001, Hartwig and his co-workers conducted an in-depth investigation into the reductive elimination mechanism of aryl–Pd–halide dimers. They proposed a distinct reaction pathway facilitated by the coordination

of tri-*tert*-butylphosphine (P(*t*-Bu)$_3$). Traditionally, it has been thought that the reductive elimination of aryl halides is thermodynamically unfavorable. However, this study confirms for the first time that this trend can be effectively reversed by introducing the strong electron-donating ligand P(*t*-Bu)$_3$, thereby making reductive elimination a thermodynamic preference process (**Scheme 1-3**).[33]

The research demonstrated that the ligand P(*t*-Bu)$_3$ not only influences the electronic structure of the palladium (Pd) center through its strong electron-donating properties but also significantly alters the kinetic characteristics of the reaction due to its considerable steric hindrance. In the experiments, the author systematically investigated the reaction behavior of different halides, including chloride, bromide, and iodide, under various ligand conditions. Techniques such as nuclear magnetic resonance (NMR) were employed to monitor the rate constants and equilibrium constants of the reactions. The findings indicate that both the electronic and steric effects of ligands are crucial factors affecting the efficiency of reduction elimination. Furthermore, the experiments revealed that, during the dimer cleavage process, the addition of P(*t*-Bu)$_3$ enhances the generation of monomers through ligand exchange, thereby facilitating reductive elimination. Additionally, based on the calculations of the equilibrium constants, the author concluded that the tendency for reductive elimination of C–X bonds weakens progressively from chloride to iodide. Notably, the reductive elimination involving C–I was found to be the most challenging, with an equilibrium constant of only $3.7 * 10^{-5}$ (**Scheme 1-3**). Through kinetic and mechanistic studies, the authors ruled out other possible pathways and ultimately confirmed that the reaction follows an unusual ligand dissociative mechanism. This mechanism suggests that after P(*t*-Bu)$_3$ coordinates too the Pd center, the significant steric crowding and electronic effects render the dissociation of the ligand an irreversible step. This process leads to the formation of an active monomer that rapidly undergoes reduction and elimination.

Scheme 1-3. Dimeric Pd(II) Complex-mediated Reductive Elimination of C–X (X = I, Br, Cl) Bonds.

Pd(II)-mediated reductive elimination of C–X Bonds (Hartwig's work (2001)):

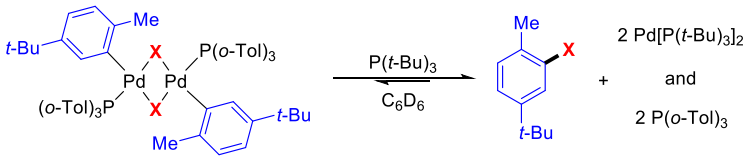

Equilibrium Constants and Yields:

X	Cl	Br	I
K_{eq}	9.0×10^{-2}	2.3×10^{-3}	3.7×10^{-5}
Yield	70%	70%	39%

Two years later, Hartwig's group directly observed the reductive elimination of aryl halides from three-coordinated aryl–Pd–halide complexes for the first time. They explored the key factors influencing the thermodynamics and kinetics of this reaction.[34] Their studies indicated that the thermodynamic favorability of reduction elimination is related to the strength of the carbon–halogen bond, whereas the reaction rate is more influenced by the energy of the transition state and the electronic properties of the halogen. Through experimental work, the equilibrium constants for oxidative addition and reductive elimination were determined again. They found that the thermodynamics of reductive elimination involving chlorine is more favorable, although the reaction rate is slower. In contrast, reactions involving bromine and iodide exhibit higher kinetic activity. Notably, while the equilibrium constant for the reductive elimination of the C–I bond has improved significantly over previous findings, it still shows the lowest value among the halogens, with an equilibrium constant of $1.79 * 10^{-1}$ (**Scheme 1-4**). Additionally, this research uncovered the distinct mechanism of the dissociation of the palladium central ligand, providing new theoretical insights and data that support the advancement of palladium-catalyzed cross-coupling and halogen exchange reactions.

Scheme 1-4. Monomeric Pd(II) Complex-mediated Reductive Elimination of C–X Bonds.

Hartwig's work (2003):

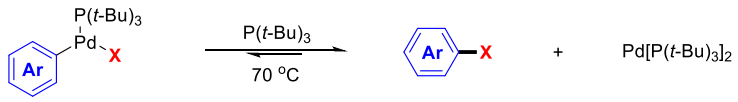

Equilibrium Constants:

X	Cl	Br	I
K_{eq}	1090	3.27	0.179

Based on the findings from two in-depth studies, there is strong evidence supporting the role of the ligand in facilitating the Pd-mediated reductive elimination of the C–X bond due to steric effects. Consequently, in 2004, the research group investigated how bulky ligands influence the reductive elimination of the C–X bond.[35] They screened various ligands with significant steric hindrance, including monodentate and bidentate phosphine ligands, and *N*-heterocyclic carbene ligands. The study revealed that the extremely bulky monodentate phosphine ligand, **L5** (QPhos), had a pronounced effect on this process. This ligand enabled the formation of products constructed from C–Br and C–Cl bonds, achieving yields of 87% and 69%, respectively (**Scheme 1-5**). As a result, this research provides innovative insights into regulating the thermodynamics and kinetics of transition-metal-catalyzed reactions through the use of strong electron donors and bulky ligands. It also broadens the potential applications of reductive elimination in Pd-catalyzed coupling reactions. This mechanism may serve as a basis for designing new catalyst systems and developing more efficient methods for converting aryl halides in the future.

Scheme 1-5. The Influence of Bulky Ligands on Pd-mediated Reductive Elimination of C–X Bonds.

Hartwig's work (2004):

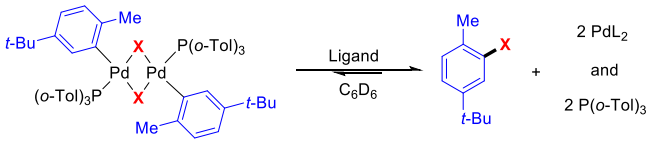

Ligand	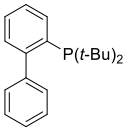	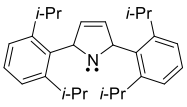	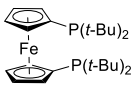	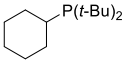	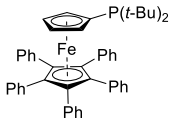	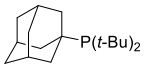
	L1	**L2**	**L3**	**L4**	**L5 (QPhos)**	**L6**
Yield (X = Br)	0%	0%	0%	15%	87%	42%
Yield (X = Cl)	0%	0%	0%	10%	69%	52%

1-3 Palladium-Catalyzed Nucleophilic Halogenation Method

The groundbreaking research on stoichiometry offers limitless possibilities for future halogenation modes. With the reversibility of the Pd-mediated oxidative addition of the C–X bond now confirmed, a key focus is on utilizing the reduction elimination of the C–X bond to develop new halogenation techniques, particularly nucleophilic halogenation. This represents a breakthrough in the field. Consequently, chemists have begun to explore and study catalysis derived from stoichiometric processes.

1-3-1 Palladium-Catalyzed Nucleophilic Bromination and Chlorination

Designing innovative ligands with palladium catalyst precursors to effectively facilitate the construction of C–X bonds and synthesize a variety of aryl halides via reductive elimination of C–X bonds is a highly sought-after research topic. The significance of developing nucleophilic halogenation processes could be unprecedented. However, chemists must select an electrophilic reagent to initiate the reaction, which is typically an aryl (pseudo)halide. If successfully designed, the product will still be an aryl halide. One of the key challenges in this protocol design is selecting a catalytic system that can simultaneously execute the oxidative addition of aryl (pseudo)halides and manipulate a similar or even identical reductive elimination of aryl halides after transmetalation. This task appears daunting. Remarkably, this research challenge was successfully tackled by

the Buchwald group, which feels akin to opening Pandora's box. In 2010, the research group successfully designed BrettPhos-type ligands, which proved to be highly effective in the construction of C–X bonds (**Scheme 1-6**).[36] Consequently, they developed a palladium-catalyzed method for the direct conversion of aryl triflates to the corresponding aryl halides (bromides and chlorides) using relatively inexpensive halide salts as halogen sources, resulting in high yields. Additionally, by optimizing catalysts, additives, and reaction conditions, the researchers were able to overcome the challenges associated with traditional methods, such as the need for high temperatures, high pressures, or multi-step operations.

Scheme 1-6. Pd-catalyzed Nucleophilic Halogenation of Aryl Triflates.

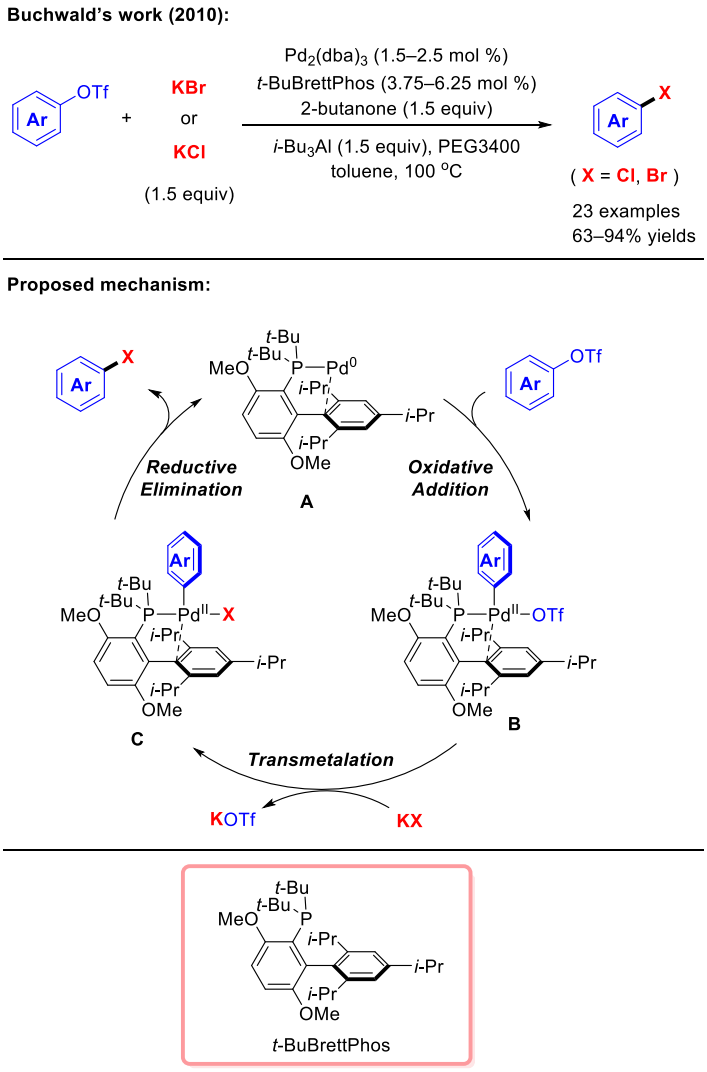

This methodology demonstrates strong adaptability to a variety of electron-poor and electron-rich aryl triflates, as well as to functionalized substrates such as heterocycles, esters, aromatic amines, and vinyl compounds. This flexibility makes it an excellent option for the synthesis of complex and multifunctional molecules. Based on the experimental results, the authors proposed a possible reaction mechanism (**Scheme 1-6**). It involves the active Pd(*t*-BuBrettPhos) species **A**, which facilitates the oxidative addition of aryl triflates, leading to the formation of oxidative adduct **B**. This is followed by a transmetalation process mediated by halide salts, resulting in the formation of a Pd intermediate **C**. Finally, reductive elimination occurs, catalyzed by the ligand *t*-BuBrettPhos, while builds the C–Br and C–Cl bonds while regenerating the Pd catalyst.

Scheme 1-7. Improved Pd-catalyzed Nucleophilic Halogenation of Aryl Triflates.

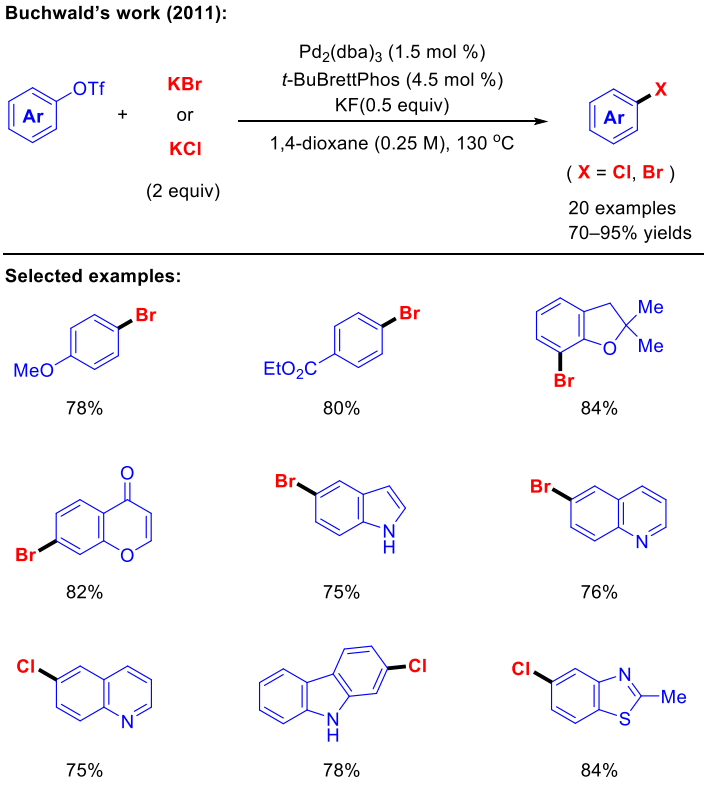

The limitations of the reaction conditions in this protocol necessitate the use of various additives. These include phase transfer catalysts, such as PEG3400, which enhance the solubility of the halide salts, and Lewis acid additives like *i*-Bu_3Al, which chelate KOTf and inhibit the reaction. These factors can limit the compatibility of the substrate. Consequently, the authors are eager to refine the reaction conditions to develop a more practical and easy-to-operate redox-neutral nucleophilic halogenation protocol. In 2011, the authors successfully improved the reaction conditions of their previously developed Pd/*t*-BuBrettPhos catalytic system by using a sole potassium fluoride (KF) as a sole additive. This significantly enhanced the reaction efficiency and simplified the reaction steps (**Scheme 1-7**).[37] The method demonstrated good applicability in reactions involving aryl triflate substrates, including those with various functional groups, both electron-donating and electron-withdrawing aromatic groups, and heterocyclic rings. This highlights the versatility and practicality of the approach.

1-3-2 Palladium-Catalyzed Nucleophilic Fluorination

In the previous section, the authors discussed the nucleophilic bromination and chlorination of aryl triflates under palladium catalysis. Remarkably, this catalytic system is also effective for the challenging task of nucleophilic fluorination.[38] In 2009, Buchwald and his team pioneered the use of the Pd/*t*-BuBrettPhos catalytic system, enabling the nucleophilic fluorination of aryl triflates and bromides (**Scheme 1-8**).[39] This methodology allowed for the conversion of aryl triflates into aryl fluorides under mild conditions, using CsF as the fluorine source. This approach overcomes the limitations of traditional methods, which often require harsh reaction conditions — such as strongly acidic or highly oxidizing environments — or rely on highly reactive electrophilic fluorinating agents that are poorly compatible with various functional groups. A key innovation of this protocol is the introduction of the biaryl monophosphine ligand *t*-BuBrettPhos, which is notably bulky (with a cone angle $\theta = 244°$).[40] This ligand was crucial in demonstrating, for the first time, that palladium(II) complexes can efficiently carry out the reductive elimination of C–F bonds. Previous studies indicated that there is a significant energy barrier associated with the reductive elimination of Ar–F bonds. The success of this study overcame this challenge and provided theoretical support and technical routes for the catalytic synthesis

of aryl fluorides. Nevertheless, in the end, a plausible reaction mechanism was proposed: it mainly includes three steps: oxidative addition of aryl triflates, CsF-mediated transmetalation, and reductive elimination.

Scheme 1-8. Pd-catalyzed Nucleophilic Fluorination of Aryl Triflates.

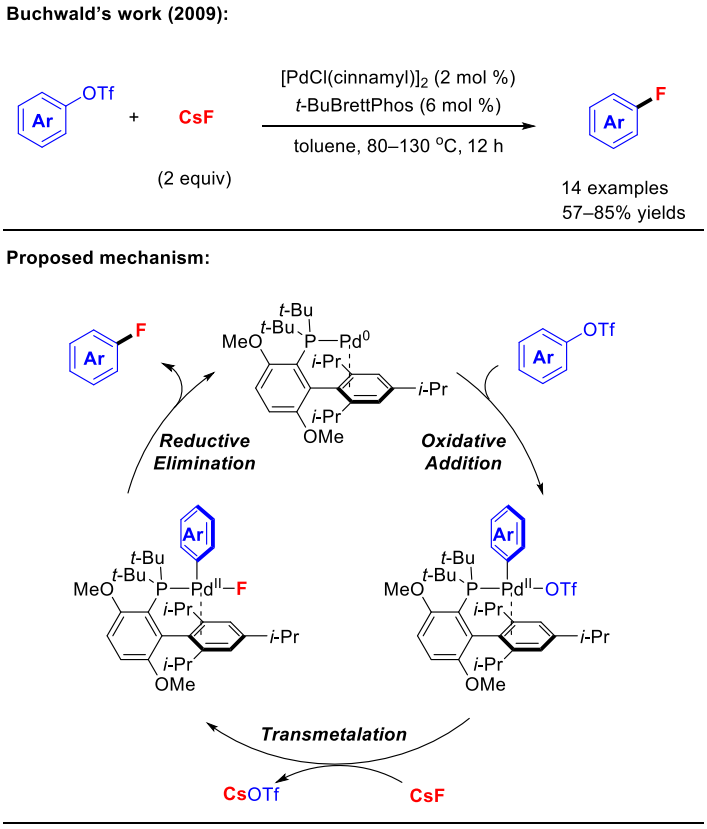

Nevertheless, Buchwald's group found that when aryl triflates were linked to electron-donating substituents, they always gave unsatisfactory regioselectivity, resulting in a mixture that was difficult to separate. But they did not know the reason for the generation of this isomer. In order to uncover the mystery, they began to further study the reaction mechanism of the proposal.[41] Firstly, they used 4-butyl bromobenzene as a reaction substrate combined with $Pd(CH_2TMS)_2(cod)$/RockPhos for stoichiometric experiments and successfully obtained the oxidative adduct **A** in 76% yield. Then the halogen exchange reaction was carried out. When AgF was used as the fluorine source, the aryl–Pd–F complex **B** was obtained in 86% yield. Finally, when they used it as a starting material to

verify whether it could undergo reductive elimination to release the desired aryl fluoride, however, unexpectedly, whether the corresponding ligand, aryl triflate or aryl bromide was added, the reductive elimination could not occur (**Scheme 1-9**).

Scheme 1-9. Mechanistic Study on Pd-catalyzed Nucleophilic Fluorination (first part).

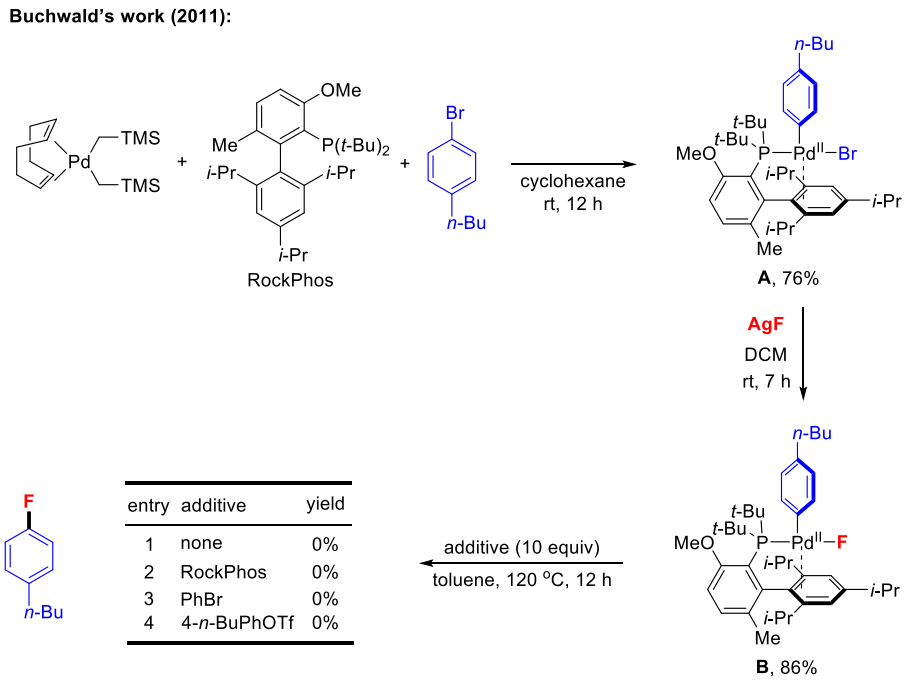

This result further proves that complex **B** may not be able to directly undergo reductive elimination to generate aryl fluoride. Simultaneously, the group found that complex **C**, which is very similar to complex **A**, is unstable. It will partially transform into Pd three-membered ring complex **D** in deuterated dichloromethane (CD_2Cl_2) and is accompanied by the aromatic migration process from the Pd center to the benzene ring in the ligand, and there is a balance between the two complexes (**Scheme 1-10(a)**). The discovery of this three-membered ring complex also further explains the reason for the generation of regioselective isomers in the catalytic nucleophilic fluorination protocol. If 4-butylbromobenzene is added to the system and DBU is used as a base, complex **C** will continuously form the three-membered ring Pd complex **D** and achieve complete C–H bond activation of the benzene ring in the ligand, and finally completely transform into a new

oxidized adduct **F** through intermediate **E**. This complex was proved to have sufficient thermal stability by the Buchwald research group (**Scheme 1-10(b)**).

Scheme 1-10. Mechanistic Study on Pd-catalyzed Nucleophilic Fluorination (second part).

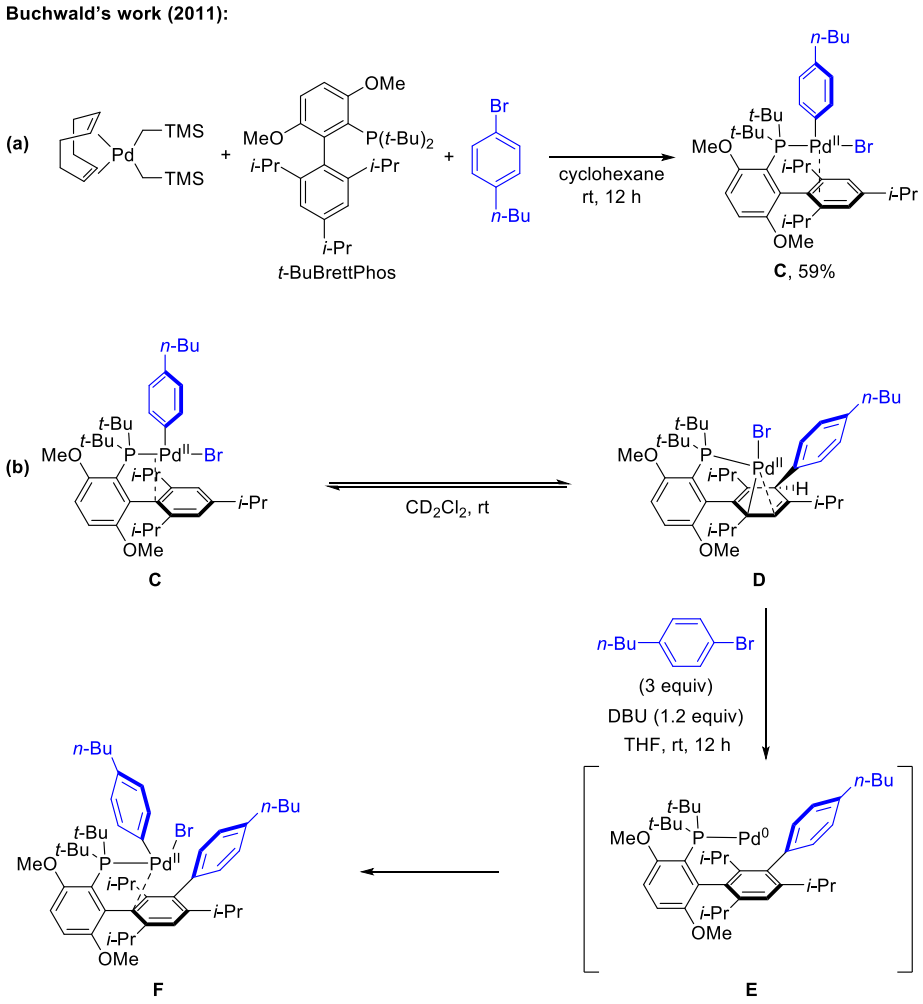

Finally, after halogen exchange of complex **F**, a new aryl–Pd–F complex **G** was generated, which was proved to be able to undergo C–F bond reductive elimination of C–F bond to release the expected product 4-butylfluorobenzene in 15% yield (**Scheme 1-11**). Therefore, the results show that reductive elimination of the C–F bond is through the activation of C–H bonds and arylation of ligands to form new ligands to activate the seemingly impossible reductive elimination step.

Scheme 1-11. Mechanistic Study on Pd-catalyzed Nucleophilic Fluorination (third part).

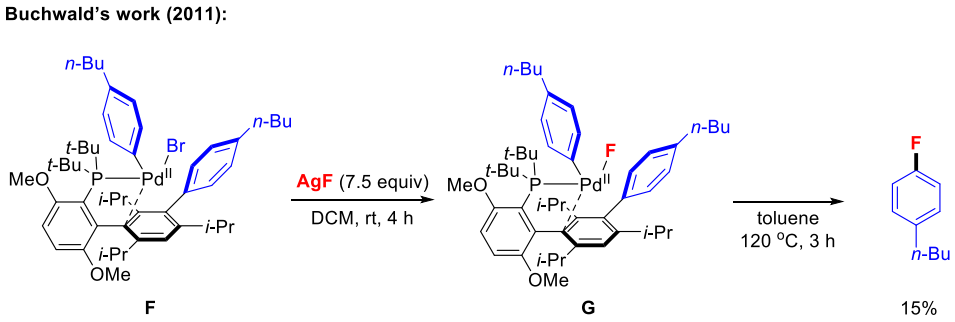

Based on that, the mechanism of this prestigious protocol was basically revealed, so Buchwald hoped to break through the previous limitations, so they improved the catalytic system and replaced the original *t*-BuBrettPhos with a bulkier AdBrettPhos ligand. A new Pd complex [Pd(AdBrettPhos)]$_2$(cod) was synthesized as a catalyst to achieve nucleophilic fluorination of aryl triflates in 2013.[42] The catalytic system significantly improves reaction performance and reduces the generation of by-products. Especially for aryl triflates and heteroaryl triflates with electron-donating substituents, the production of regioisomeric aryl fluorides can be effectively prevented (**Scheme 1-12**).

Scheme 1-12. Improved Pd-catalyzed Nucleophilic Fluorination of Aryl Triflates.

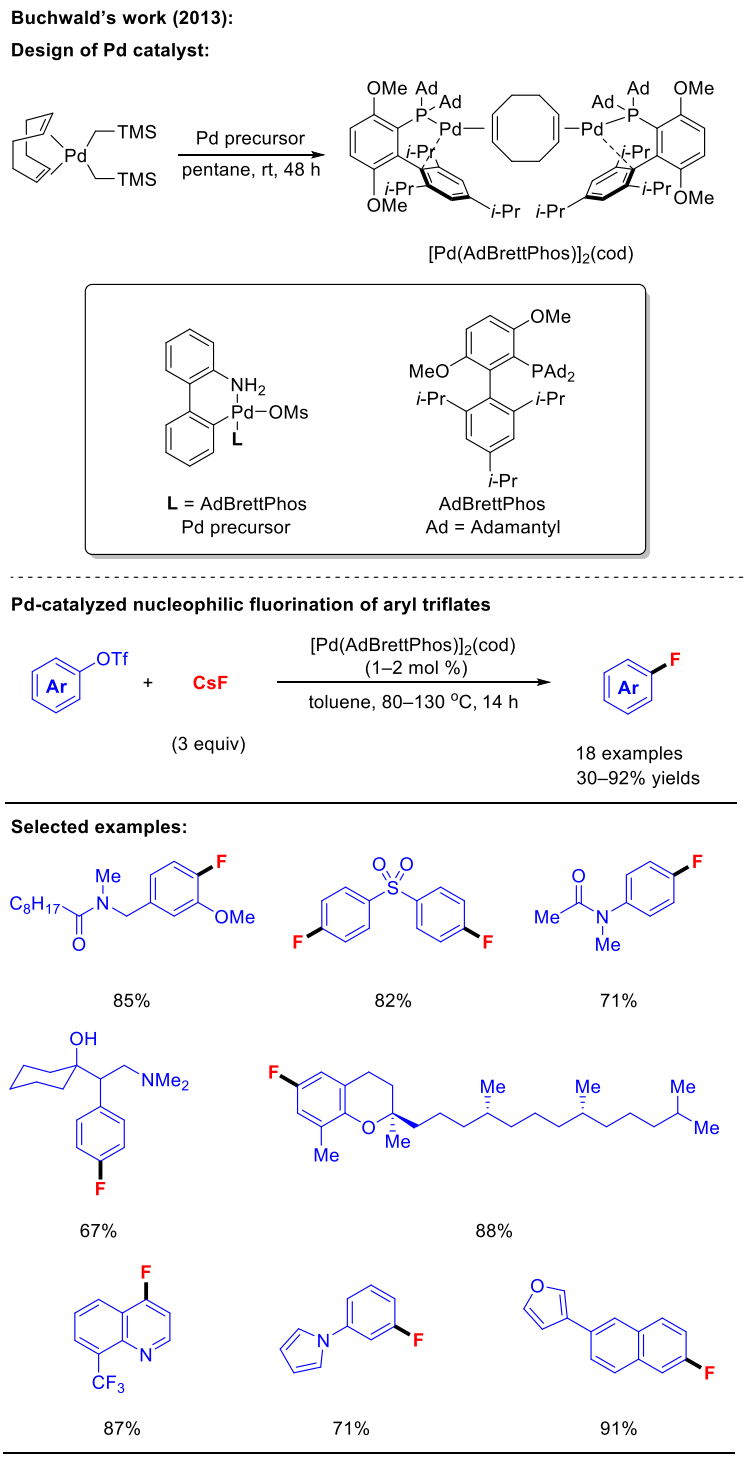

On the other hand, for the nucleophilic fluorination mode of aryl bromides, the group used AdBrettPhos, which had been arylated, as a ligand. In other words, it was the first to

introduce 4-butylphenyl substituent into the benzene ring in the ligand of AdBrettPhos as a new monodentate phosphine ligand HGPhos, thereby synthesizing a new Pd catalyst [Pd(HGPhos)]$_2$(cod) in 2014.[43] At the same time, using AgF as the fluorine source and KF as the base can significantly improve the compatibility of electron-rich aryl bromides or heteroaryl bromides and effectively suppress the formation of regioselective isomers (**Scheme 1-13**).

Scheme 1-13. Improved Pd-catalyzed Nucleophilic Fluorination of Aryl Bromides.

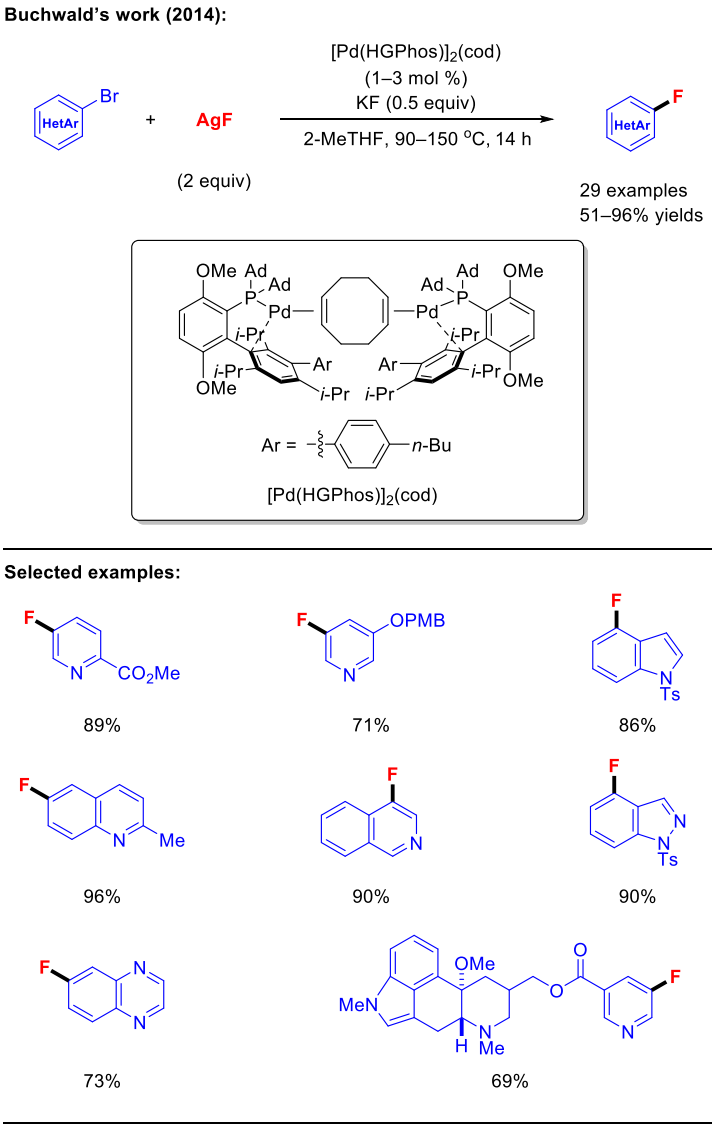

What is impressive is that the fluorine source required in previous catalytic systems, especially CsF, is highly sensitive to moisture, and the reductive elimination of C–F bonds is also highly sensitive to water, because this will make the generation of hydrogen bonding with F atom, it continues to raise the already unattainable energy barrier, dramatically inhibiting the reductive elimination of C–F bonds. Therefore, the CsF used for this conversion needs to be dried in a vacuum under high temperature for a long time before use, and the reaction needs to be operated in a glove box, which will undoubtedly affect the practicality and operability of this catalytic mode. Interestingly, the author developed a capsule strategy, which is to quantitatively store the catalyst and fluoride salt matched with aryl triflate and aryl bromide respectively in capsules, thus effectively avoiding the reaction of each group in 2015 (**Scheme 1-14**).[44] The parts are in contact with air, which can greatly improve the operability of this protocol, and all operations can be performed on the experimental bench. Because as the capsule material dissolves in the organic solvent, the corresponding reaction components are released in the reaction system, triggering nucleophilic fluorination, and constructing a series of aryl fluorides with high yield and good substrate compatibility.

Scheme 1-14. Capsule Strategy for Pd-catalyzed Nucleophilic Fluorination.

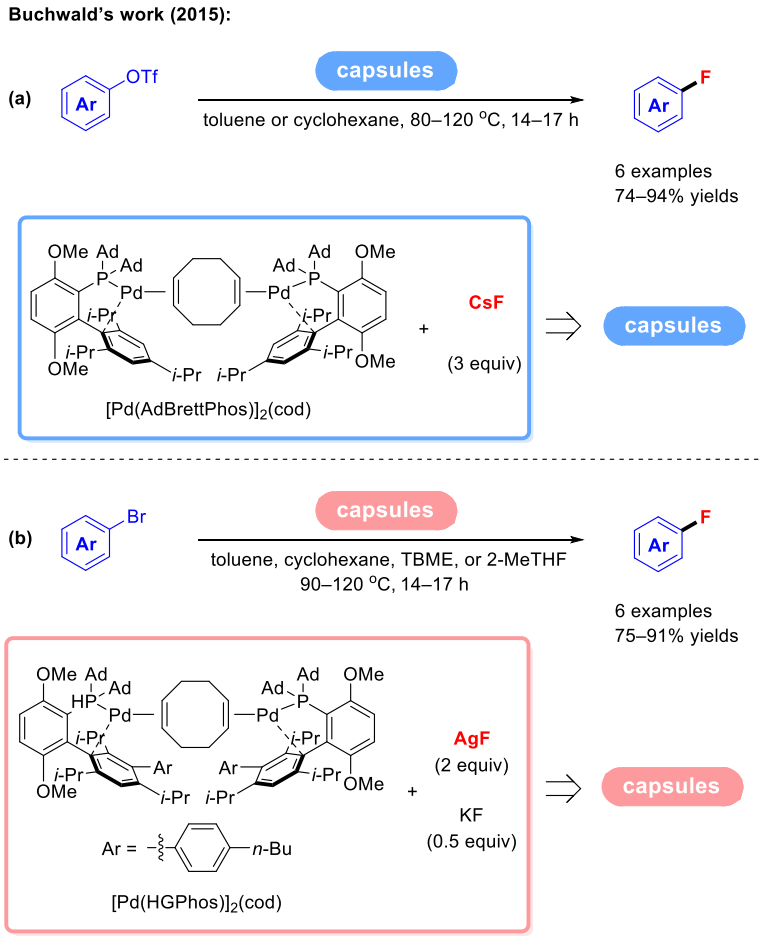

In the same year, Buchwald's group made further breakthroughs in this research field. It achieved the nucleophilic fluorination of aryl triflates under palladium catalysis at room temperature by further improving the HGPhos ligand. This time, the improvement mainly focused on the modification of the newly introduced aromatic group, that is, the previous 4-butylphenyl was changed to 2,3,5,6-tetrafluoro-4-butylphenyl, and the ligand was named AIPhos.[45] The new palladium catalyst [Pd(AIPhos)]$_2$(cod) was synthesized with this ligand and applied to the nucleophilic fluorination of aryl triflates (**Scheme 1-15**). Although this protocol is only more effective for substrates with electron-withdrawing substituents and requires a longer reaction time to complete the conversion, it is enough to show that reductive elimination of C–F bond can be full of unlimited potential in future synthetic chemistry and other related fields.

Scheme 1-15. Pd-catalyzed Nucleophilic Fluorination of Aryl Triflates at Room Temperature.

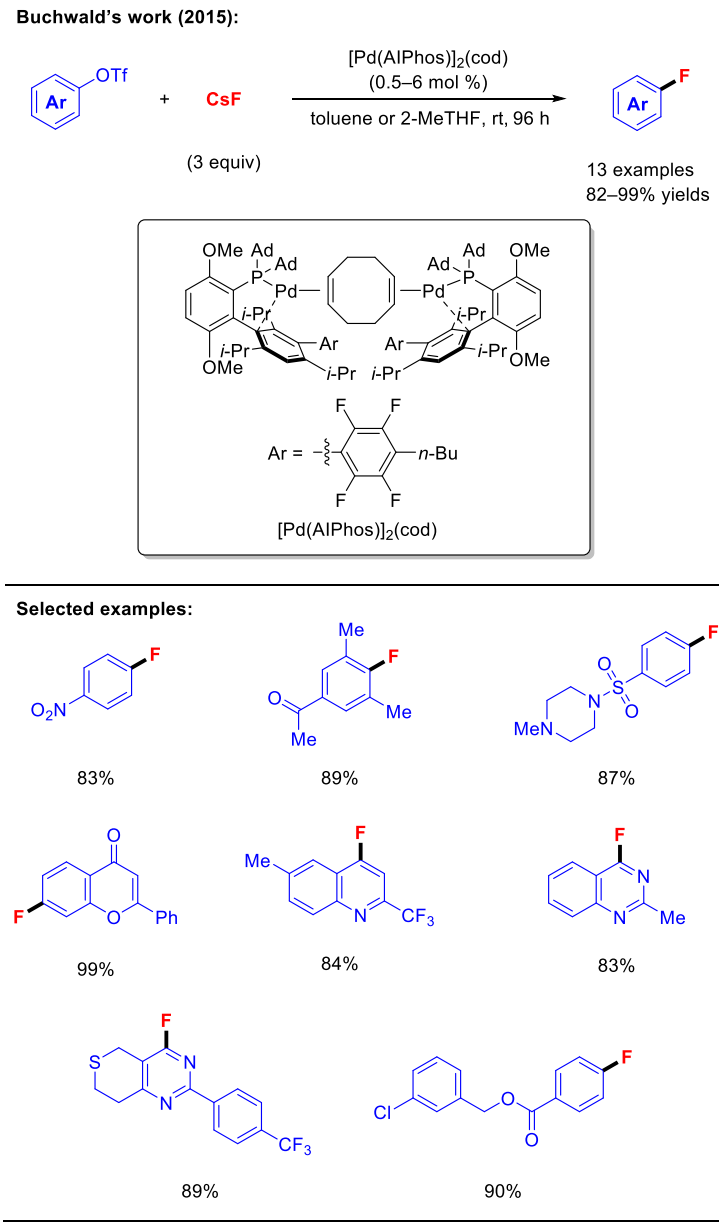

Finally, Buchwald and co-workers shifted their attention from the nucleophilic fluorination of aryl triflates to the nucleophilic fluorination of alkenyl triflates in an attempt to achieve palladium-mediated reductive elimination of C(alkenyl)–F bond.[46] However, based on previous research experience, it was found that they were not compatible with

alkenyl systems. In other words, they could only achieve the construction of alkenyl fluorides with poor regioselectivity, albeit after screening several rather bulky ligands **L1**–**L4**.[47] Fortunately, when the authors use $TESCF_3$ as an additive, the regioselectivity of the product can be significantly improved. The results show that when using **L1** as the ligand, the addition of 30 mol % $TESCF_3$ can increase the regioselectivity ratio from 1.8:1 to >99:1, and obtain the desired product alkenyl fluoride in 74% yield (**Scheme 1-16**). This "$TESCF_3$ effect" was revealed as a possible mechanism after the authors performed in-depth density functional theory (DFT) calculations (**Scheme 1-16**): Initially, $TESCF_3$ releases CF_3^-, a portion of which decomposes into CHF_3 or CF_2CF_2 without contributing to the reaction, while a smaller fraction interacts with the **L1**Pd^{II} species **D** to yield the dearomatized intermediates **E**. The fluoride ion then engages with species **E**, producing intermediate **F**, which subsequently releases CF_3^- to form the *cis*-**L1**Pd(alkenyl)F complex **G**. Subsequently, complex **G** undergoes reductive elimination, yielding the desired alkenyl fluoride **A** with good regioselectivity. Throughout the fluorination process, intermediates **F** reversibly release and capture CF_3^- in the presence of F^-, maintaining a relatively elevated CF_3^- concentration. This promotes the preferential formation of **E** over **G**.

Scheme 1-16. $TESCF_3$-promoted Pd-Catalyzed Regioselectively Nucleophilic Fluorination of Vinyl Triflates.

Buchwald's work (2023):

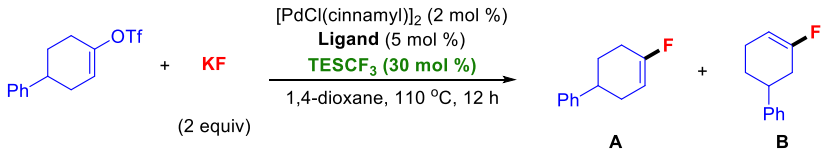

entry	ligand	A:B w/o $TESCF_3$ (yield%)	A:B w/ $TESCF_3$ (yield%)
1[a]	**L1**	1.8:1 (11)	>99:1 (74)
2	**L1**	2.0:1 (64)	36:1 (73)
3	**L2**	1.7:1 (59)	14:1 (60)
4	**L3**	2.7:1 (55)	63:1 (64)
5	**L4**	1.6:1 (51)	15:1 (64)

[a] 2-MeTHF was used as the solvent.

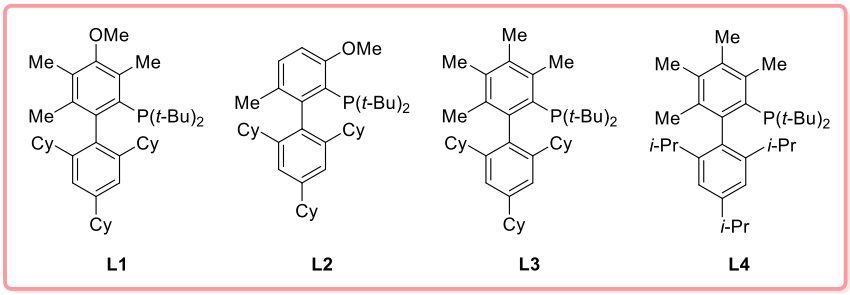

Possible mechanism:

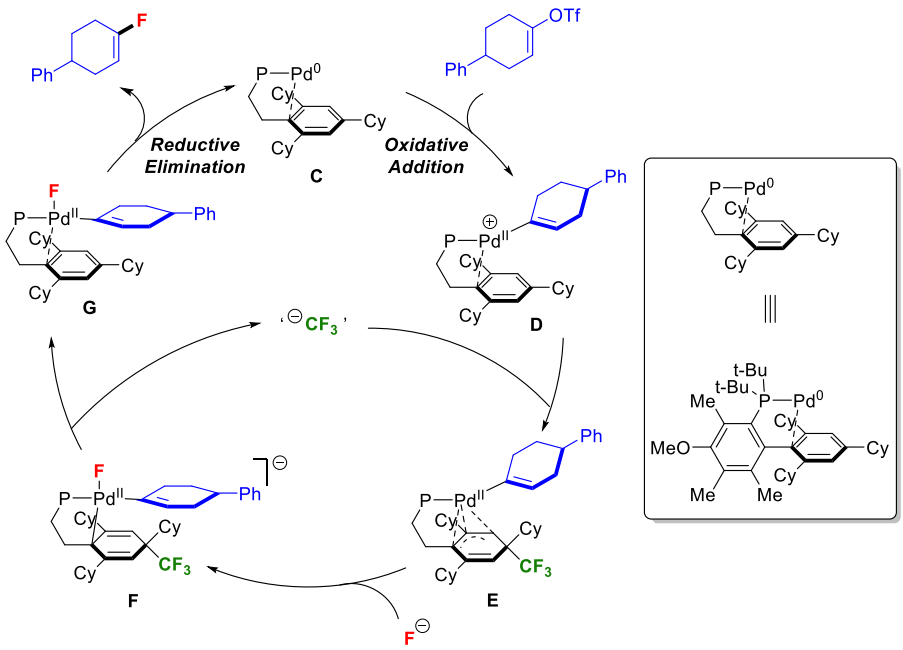

1-4 Transition-Metal-Catalyzed Carbohalogenation of Unsaturated Bonds

In the development of a model for the delicate nucleophilic halogenation of aryl (pseudo)halides using bulky ligands under palladium catalysis, chemists have successfully constructed a series of aryl bromides, aryl chlorides, and even aryl fluorides using a series of modified BrettPhos ligands. However, the construction of aryl iodides remains a huge challenge, which is probably due to the inherent instability of aryl iodides, because the reductive elimination of C–I bonds is not only thermodynamically unfavorable but also kinetically difficult to stay in this state. However, considering the important uses of organic iodides, chemists have also been exploring the construction of C–I bonds through the reductive elimination of C–I bonds. So far, a lot of research has focused on the construction of corresponding alkyl iodides or alkenyl iodides through the intramolecular or intermolecular carboiodination mode of unsaturated bonds. Next, the author will focus on the carboiodination of unsaturated bonds by the reductive elimination of C–I bonds under transition metal catalysis from two aspects.

1-4-1 Intramolecular Carbohalogenation

In 2011, Lautens and co-workers disclosed a palladium-catalyzed reaction that forms carbon-carbon bonds between aryl iodides and alkenes via reductive elimination of the C–I bond.[48] Unlike conventional cross-coupling methods, this process creates two new bonds while retaining all atoms from the starting materials in the final product. The incorporation of a palladium catalyst paired with bulky phosphine ligands, QPhos, is essential for achieving effective reactivity and constructed a series of iodinated dihydro-benzofurans, indolines, and indolin-2-ones (**Scheme 1-17(a)**).

Scheme 1-17. Pd-catalyzed Intramolecular Carboiodination of Alkenes.

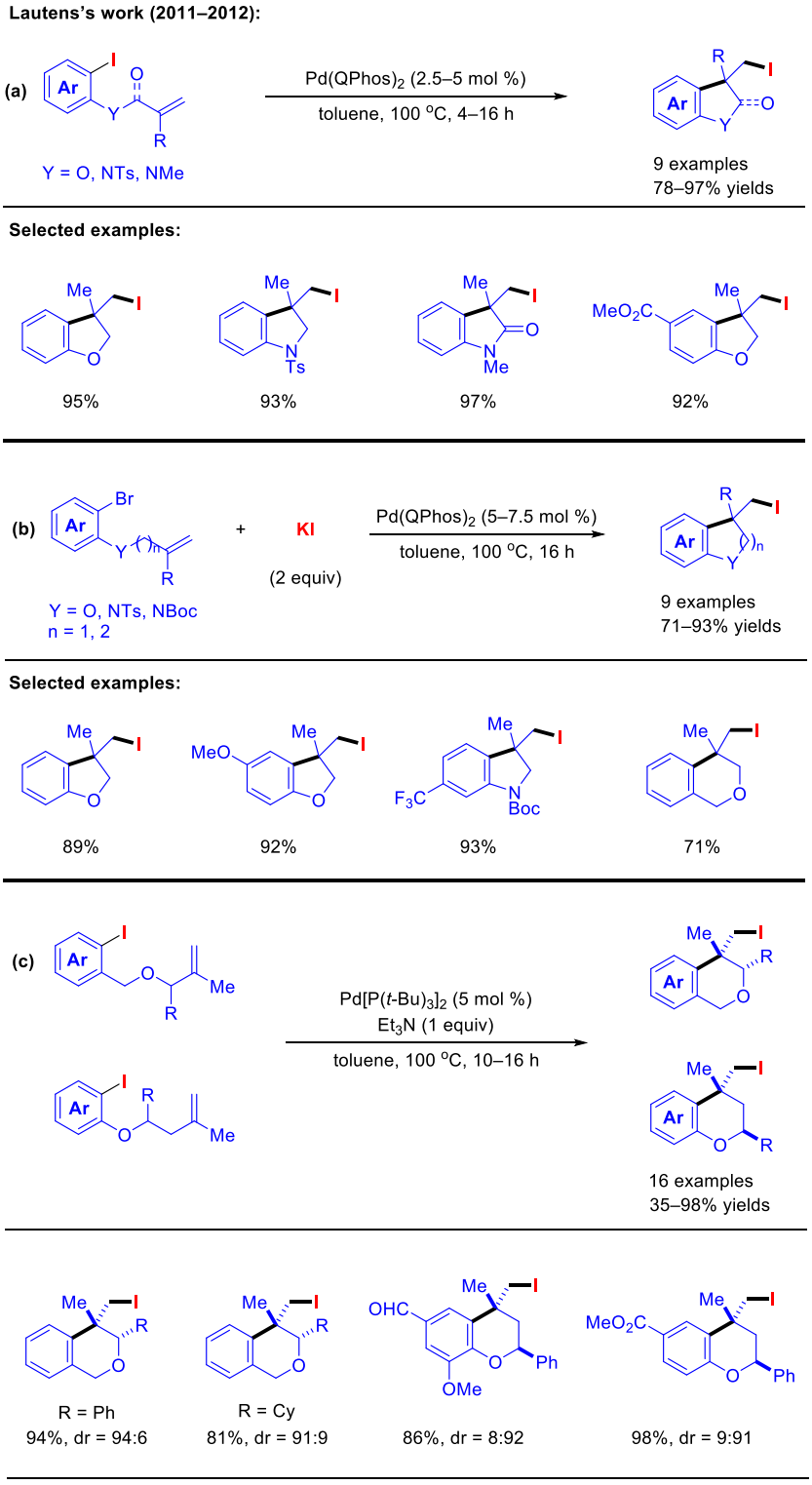

In the same year, they also introduced a similar reaction mode, that is, using lower-priced aromatic bromides and KI as iodine sources to achieve Pd/QPhos-catalyzed intramolecular carbon iodination mode, thereby synthesizing a series of iodinated nitrogen-containing and oxygen-containing five-membered heterocyclic compounds (**Scheme 1-17(b)**).[49] It is worth mentioning that this catalytic system can still be applied to the construction of six-membered rings. In order to further expand the construction of iodinated six-membered rings, in 2012, Lautens' group established a versatile method for the diastereoselective synthesis of isochroman and chroman scaffolds through a Pd-catalyzed carboiodination reaction (**Scheme 1-17(c)**).[50] These processes generally deliver good to excellent yields with high diastereoselectivity and exhibit wide compatibility with various functional groups. The stereochemical outcome of these cyclizations is believed to result from minimizing $A^{1,2}$ strain and axial–axial interactions, and a stereochemical model has been proposed.

Scheme 1-18. A Plausible Mechanism.

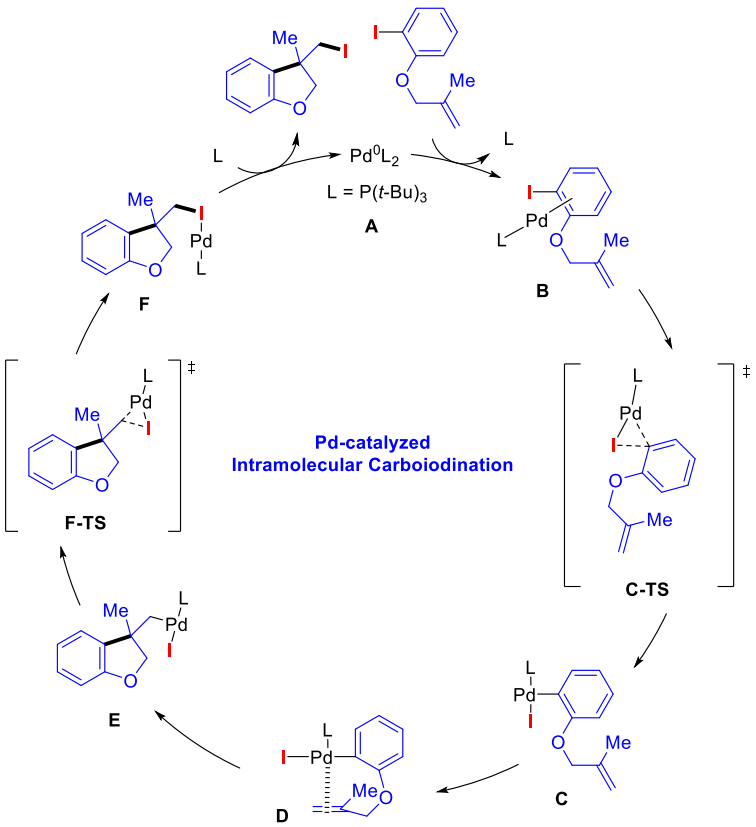

Based on a large number of research results and experience, they used DFT calculations to conduct an in-depth study of the possible mechanism of this transformation.[51] The group used the most classic aryl iodide tethered to an unsaturated bond moiety as a substrate for a detailed mechanism introduction (**Scheme 1-18**). Initially, the aryl iodide with a remote C=C double bond binds to the activated palladium catalyst **A** to form intermediate **B**, and then the aryl iodine moiety triggers the oxidative addition of the palladium catalyst through the three-membered ring transition state **C-TS** to form an oxidative adduct intermediate **C**, which undergoes intramolecular isomerization and coordinates with the Pd catalyst to form a Pd species **D**. Subsequently, migration insertion occurs to achieve cyclization and generate an alkyl–Pd–I intermediate **E**, which can be reductively eliminated under the acceleration of a relatively bulky ligand through the three-membered ring transition state **F-TS** to release the desired product and coordinate with the regenerated palladium catalyst **A** to form intermediate **F**. Finally, the following ligand exchange produces the final product and the activated Pd catalyst **A**.

Indeed, after a series of mechanistic studies, Lautens' team became more convinced that the oxidative addition initiated by aryl iodide in the developed carboiodination mode is reversible because their catalytic system can simultaneously manipulate oxidative addition and reductive elimination of C–I bonds. Forasmuch, in the next phase, the research team tried to get a firm answer to their hypothesis. So, they introduced two iodine atoms into the substrate, if one of the iodine atoms could undergo carboiodination whether the remaining iodine atom can be retained intact, it will undoubtedly be the best explanation for their postulation. In 2013, they revealed a Pd-catalyzed protocol for the intramolecular carboiodination of diiodo-aryl compounds (**Scheme 1-19(a)**).[52] Crucially, they found that the addition of 1,2,2,6,6-pentamethylpiperidine (PMP) as a weak base can significantly improve the catalytic efficiency, thereby promoting intramolecular carboiodination and allowing the other iodine atom to be completely retained. This further supports the inference that the oxidative addition initiated by aryl iodides is reversible. Interestingly, after mixing another molecule of terminal alkene into the system, two iodine atoms can perform intramolecular carboiodination and intermolecular Mizoroki-Heck cross-coupling respectively under the established Pd/QPhos/PMP system (**Scheme 1-19(b)**).

Scheme 1-19. PMP-promoted Simultaneous Intramolecular Carboiodination and Intermolecular Mizoroki-Heck Reaction of diiodo-alkenes, and PMP-promoted Intramolecular Carboiodination of Alkenes with High Diastereoselectivity.

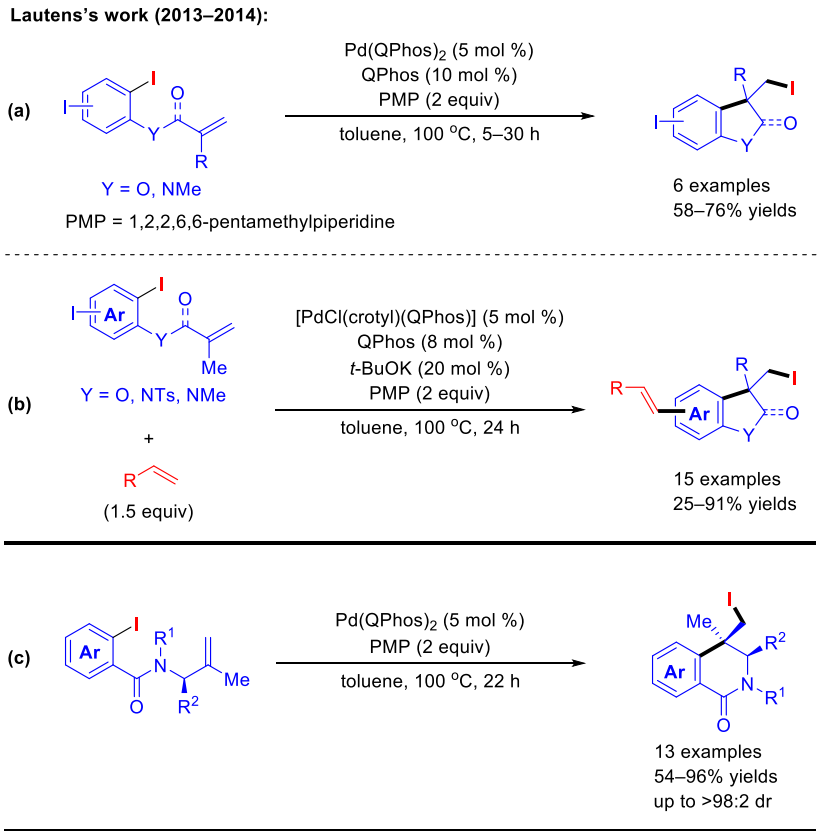

On the other hand, the team in this study also found that tertiary amine PMP can dramatically improve the diastereomeric selectivity ratio of carboiodination conversion. Although Pd-catalyzed carboiodination reaction uses bulkier ligands to accelerate the reductive elimination of carbon–halogens mediated by Pd(II), which has become an effective strategy to build C–I bonds when the substrate has low stereoselectivity, however, catalyst optimization becomes challenging because the number of ligands that can effectively promote reductive elimination is very limited. In 2014, they found that tertiary amines, as a weak coordination ligand, can significantly improve the diastereoselectivity of chiral *N*-allyl amides in Pd/QPhos-catalyzed carboiodination (**Scheme 1-19(c)**).[53] This methodology is a promising protocol and provides a highly efficient route for the synthesis of enantiomerically enriched and highly functionalized dihydroisoquinolinones.

Several important research topics described above focus on the intramolecular carboiodination of alkenes via Pd(II)-mediated C(sp^3)–I bond reductive elimination. To further demonstrate the value of this catalytic system and synthetic strategy, Lautens and co-colleagues sought to further expand the application of this field, namely, whether the previous carbon–carbon double bond moiety can be replaced by a carbon–carbon triple bond moiety to achieve intramolecular carboiodination of alkynes to construct vinyl iodides through a more challenging reductive elimination process of C(sp^2)–I bond. In 2015, they developed a method for intramolecular carbohalogenation of hindered alkynes, which again used the previously constructed Pd/QPhos catalyst system (**Scheme 1-20**).[54] The steric effect of the ligand and the substrate combined to improve the reaction efficiency. By introducing a larger alkynyl substituent, the tendency of C(sp^2)–X reductive elimination was enhanced, and the possibility of undesirable side reactions of the final vinyl halide product was effectively reduced. Taken together, the synergistic spatial effect of the catalyst and the substrate plays a key role in achieving this transformation, and it is difficult to achieve the same effect by relying on any one of the strategies alone.

Scheme 1-20. Pd-catalyzed Intramolecular Carboiodination of Alkynes.

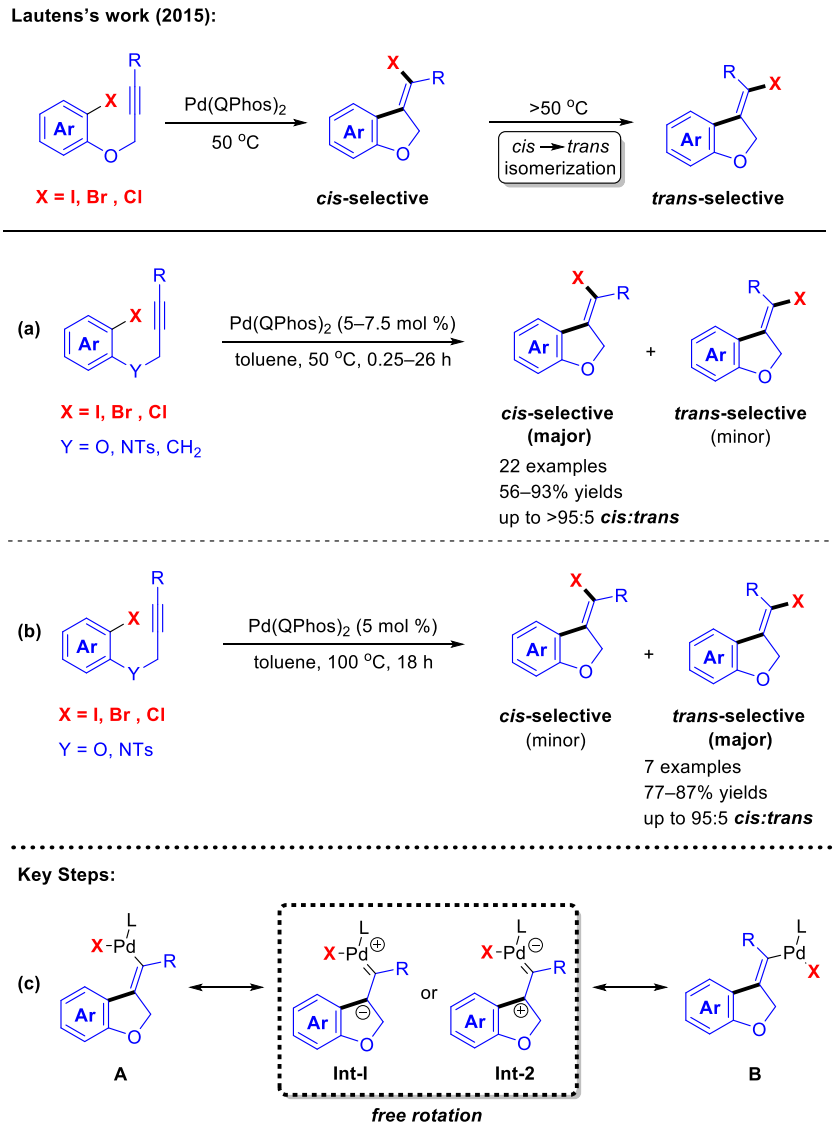

Crucially, they also found that temperature can promote the *cis-trans* interconversion of the alkenyl halide products. In other words, when the reaction temperature is 50 degrees, the *cis*-product is the main product (**Scheme 1-20(a)**), but when the temperature is higher than 50 degrees, the *trans*-product becomes the main product (**Scheme 1-20(b)**). Based on this phenomenon, the group proposed a corresponding mechanistic explanation (**Scheme 1-20(c)**).[55] There is no doubt that after the aryl halides undergo oxidative addition and migration insertion, Pd intermediate **A** is formed. This Pd species directly affects the

isomerization process because the intermediate may appear as a zwitterionic Pd carbene species **Int-1** or **Int-2**. Related studies have shown that similar Pd carbene intermediates have been applied to the stereoisomerization process of vinyl Pd(II) complexes by research teams such as Lipshutz,[56] Cook,[57] Amatore, and Jutand.[58] Either **Int-1** or **Int-2** may generate vinyl Pd species **A** or **B** through bond rotation, and finally release *cis* or *trans* products through reductive elimination, but higher temperature may accelerate the free rotation of intermediate **Int-1** to **Int-2**.

Along with the extensive experience in dealing with the intramolecular carbohalogenation of alkenes or alkynes under palladium catalysis, it is worth mentioning that the research group has also discovered a conceptually novel domino hydrohalogenation of intramolecular enynes to synthesize a series of halogenated pyridines with good yields and efficiency in 2017.[59] Importantly, the facile catalytic conditions can also achieve reductive elimination of $C(sp^3)$–I, $C(sp^3)$–Br, and $C(sp^3)$–Cl bonds via Pd(II) complexes. The reaction uses crystalline ammonium halide ($Et_3N \cdot HX$) as the source of hydro halide, replacing the traditional toxic and corrosive reagents, and can also use 1-iodobutane as an alternative source of non-ionic HI (**Scheme 1-21**). By introducing strategically placed O*t*-Bu nitrogen-protecting groups, the target products can be generated with high selectivity, which contain $C(sp^3)$–halogen groups and all-carbon quaternary centers located at the γ position of the carbonyl group. In-depth mechanistic studies revealed that the reaction involves a key *E*-to-*Z* vinyl-Pd(II) isomerization that proceeds via a formal *trans*-alkyne hydrogenation step.

Scheme 1-21. Pd-catalyzed Cyclohydrohalogenation of Enynes.

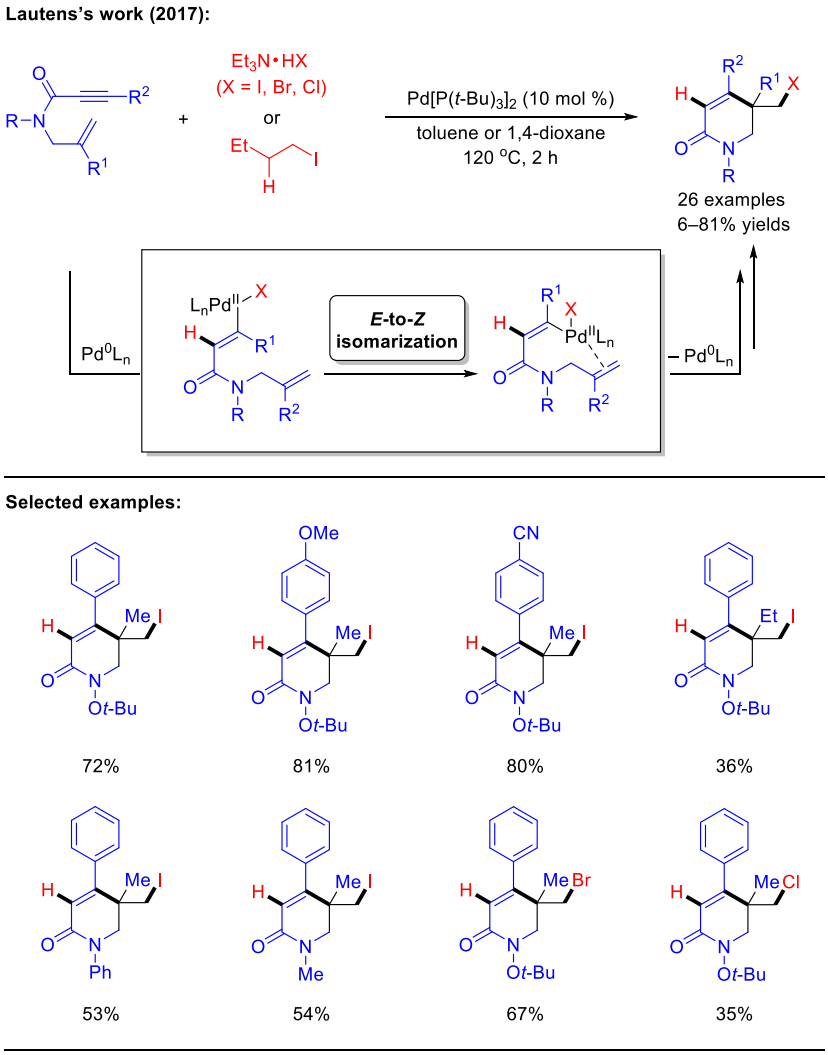

From another perspective, to further enhance the application potential of this transformation, Lautens hopes to design a more inexpensive nickel catalyst to replace the expensive palladium catalyst to achieve Ni(II)-mediated reductive elimination of C–X bonds. However, due to the high reducibility of Ni catalysts, it is inherently not conducive to reductive elimination, which may require more cumbersome or more harsh conditions to construct C–X bonds. Nevertheless, to their surprise, in 2018, they designed a simple, practical, and easy-to-operate $NiI_2(PPh_3)_2$ catalytic system to efficiently achieve the intramolecular carboiodination mode of aryl iodide tethered alkene moiety or aryl bromide tethered alkene moiety/KI, and successfully constructed a series of iodinated heterocyclic

compounds with good yields (**Scheme 1-22**).[60] Surprisingly, the enantioselectivity of the benzylic position can be effectively controlled by introducing chiral BINAP-type ligands.

Scheme 1-22. Ni-catalyzed Intramolecular Carboiodination of Alkenes.

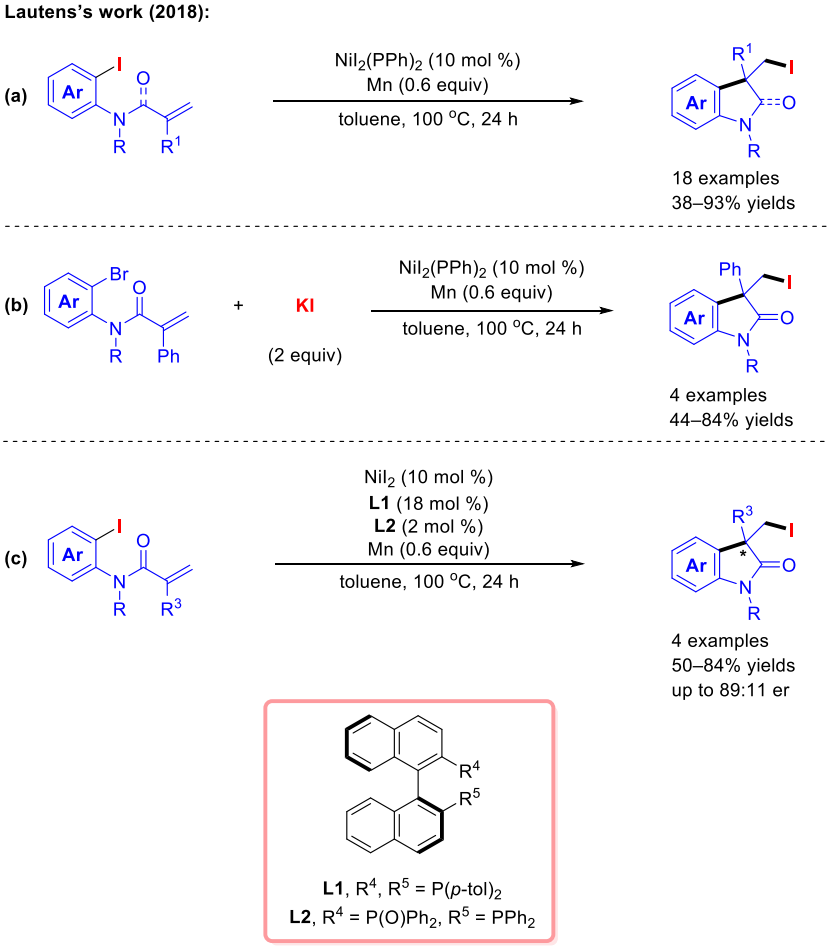

In addition, the research team also found that the Ni catalytic system can also show enough charm in the dearomative carboiodination. They also revealed a diastereoselective intramolecular carboiodination reaction achieved by a Ni/$P(OEt)_3$ catalytic system. Through substrate design, they replaced the previous vinyl units with an indole unit. Surprisingly, the carboiodination can be successfully carried out on the indole moiety and realize dearomative 1,2-difunctionalization, and the synthesis of secondary benzyl iodides is completed with moderate to good yields and excellent diastereoselectivity (**Scheme 1-**

23(a)).[61] Meanwhile, the carboiodination transformation controlled by a similar Ni/P(O*i*-Pr)$_3$ catalytic system can also be applied to the synthesis of 6-membered heterocyclic dihydroisoquinolones and tetrahydroquinolines derivatives (**Scheme 1-23(b)**).[62] Crucially, the six-membered heterocyclic compounds constructed by this method have *trans*-stereoselective six-membered heterocyclic compounds, which can serve as a powerful supplement to the palladium catalytic strategy introduced in the previous article.[53] This protocol can also efficiently obtain diastereomers of each iodinated dihydroisoquinolones product. Moreover, these new iodinated tetrahydroquinolines skeletons have important application value due to their similarity with many key pharmaceutical-related compounds and the potential provided by the alkyl iodide sites for subsequent functionalization. However, they did not give a specific explanation for why the palladium-catalyzed and nickel-catalyzed systems gave opposite diastereomers, because they are still further exploring through DFT theoretical calculations. The author believes that this mystery will be revealed shortly.

Scheme 1-23. Ni-catalyzed Intramolecular Dearomative Carboiodination of Indoles, and Ni-catalyzed Diastereoselectively Intramolecular Carboiodination of Alkenes.

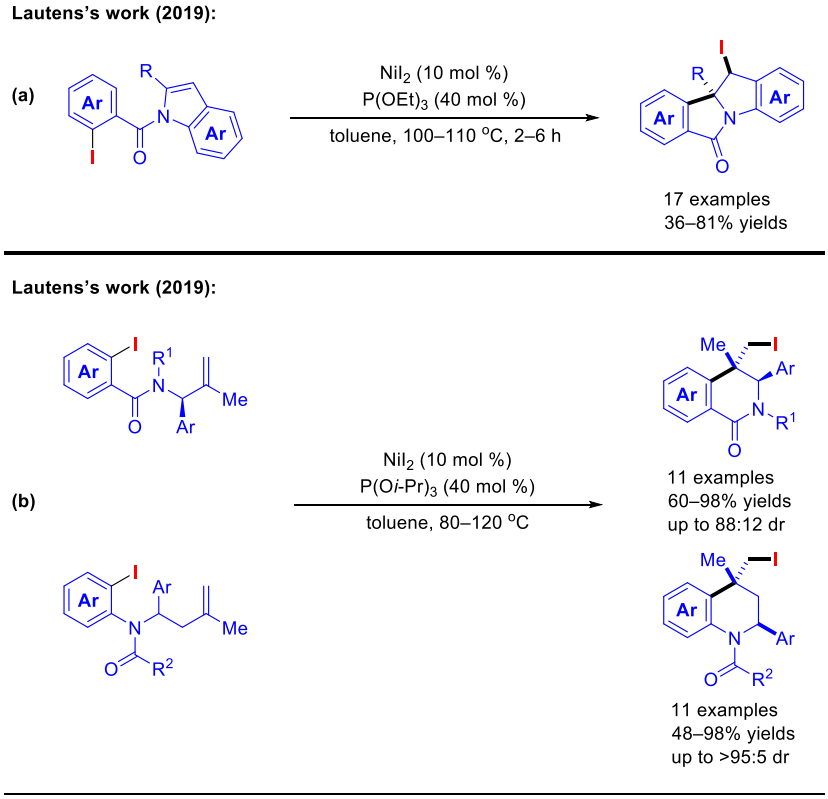

Recently, with the resurgence of free radical chemistry, photoredox or photoinduced catalytic systems have been increasingly applied to the fields of synthesis and catalysis, and have also demonstrated their increasing value. Lautens and co-workers recently found that combining the photoinduced system with the previous Pd-catalyzed system[63] or Ni-catalyzed system[64] can achieve intramolecular carbohalogenation of alkenes under milder conditions (**Scheme 1-24(a)** and **(b)**). Especially, for palladium-catalyzed systems, previous successes mainly relied on extremely bulky and expensive ligands, such as QPhos. If combined with the photoinduced system, the inexpensive DPEphos can be used as a ligand and the desired carboiodination can be achieved at even room temperature, while a series of dihydrobenzofurans, indolines, indolin-2-ones, and indene skeletons are constructed with good yields and broad functional group compatibility. Through in-depth mechanistic studies, especially isotope labeling experiments, they proposed the crucial concept: reversible single-electron reductive elimination of the C–I bond.

Scheme 1-24. Photo-induced Pd/Ni-catalyzed Intramolecular Carboiodination of Alkenes.

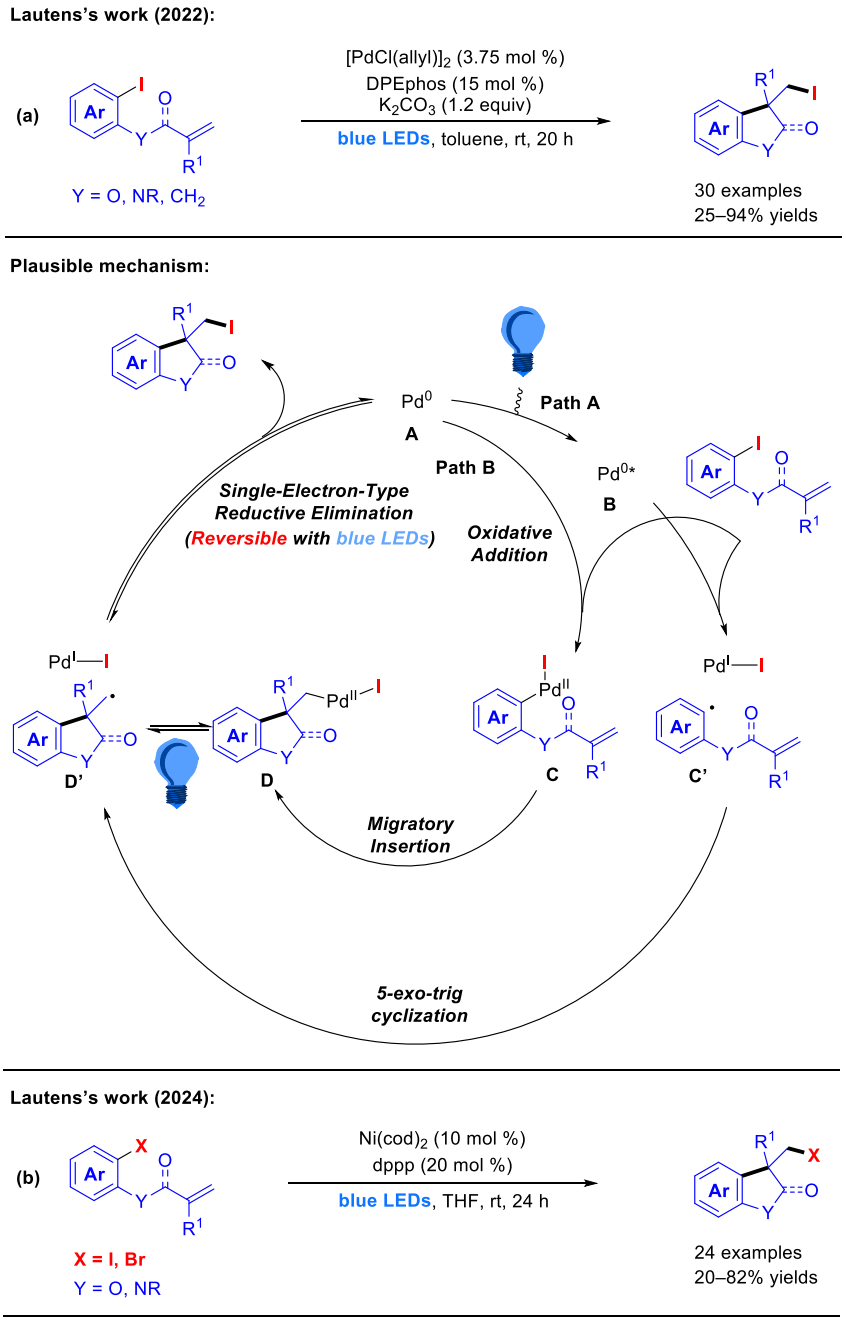

Here, the author uses the palladium catalytic system as an example to introduce the relevant mechanism (**Scheme 1-24**): **Path A**: Initially, the activated Pd catalyst **A** forms an excited state of Pd catalyst **B** under photo-irradiation, which can mediate the single electron

transfer (SET) of the substrate aryl iodide to generate an aryl radical intermediate **C'** and a Pd(I)–I complex, followed by intramolecular radical cyclization to form an alkyl radical intermediate **D'**. **Path B**: Simultaneously, the activated Pd catalyst **A** can also trigger the oxidative addition of aryl iodide to form an oxidative adduct intermediate **C**, followed by intramolecular migration insertion to form a Pd(II) species **D**. Crucially, under photoexcitation conditions, the C–Pd bond will be homolytically cleaved, resulting in the mutual conversion of intermediates **D** and **D'**. Finally, the alkyl radical intermediate **D'** will undergo a reversible single electron reductive elimination of the C–I bond with the Pd(I)–I complex to release the desired product and regenerate the activated Pd catalyst **A**.

Moreover, intramolecular carboiodination patterns of alkenes can also use alkenyl iodides as initiating moiety. In 2011, Tong's group built a Pd/dppf catalytic system to manipulate (*Z*)-1-iodo-1,6-diene to achieve a cycloisomerization reaction accompanied by the transfer of iodine atoms (**Scheme 1-25(a)**).[65] This method provides a simple and efficient route to the synthesis of 1,2,3,6-tetrahydropyridine with a quaternary carbon center. In addition, they also proved through mechanistic experiments that the construction of the C–I bond is stereoselective, thus indirectly proving that the construction of the C–I bond comes from Pd-mediated reductive elimination rather than the radical pathway. Ten years later, their research team improved the catalytic conversion. They proposed a hydrogen bond promotion strategy, that is, adding $[Et_3NH]^+$ salt to the catalytic system as a hydrogen bond donor (**Scheme 1-25(b)**).[66] According to DFT theoretical calculations, it was shown that the assumed hydrogen bond interaction in the **intermediate** significantly enhanced the heterolytic dissociation of Pd(II)–halogen, which plays a crucial role in reducing the reaction barrier of reductive elimination of $C(sp^3)$–I. At the same time, this strategy can also be applied to the construction of C–Br bonds. Importantly, they used modified chiral Ferrophos ligands to easily achieve asymmetric carboiodination and carbobromination with high reaction efficiency and enantioselectivity.

Scheme 1-25. Pd-catalyzed Intramolecular Carboiodination of Dienes.

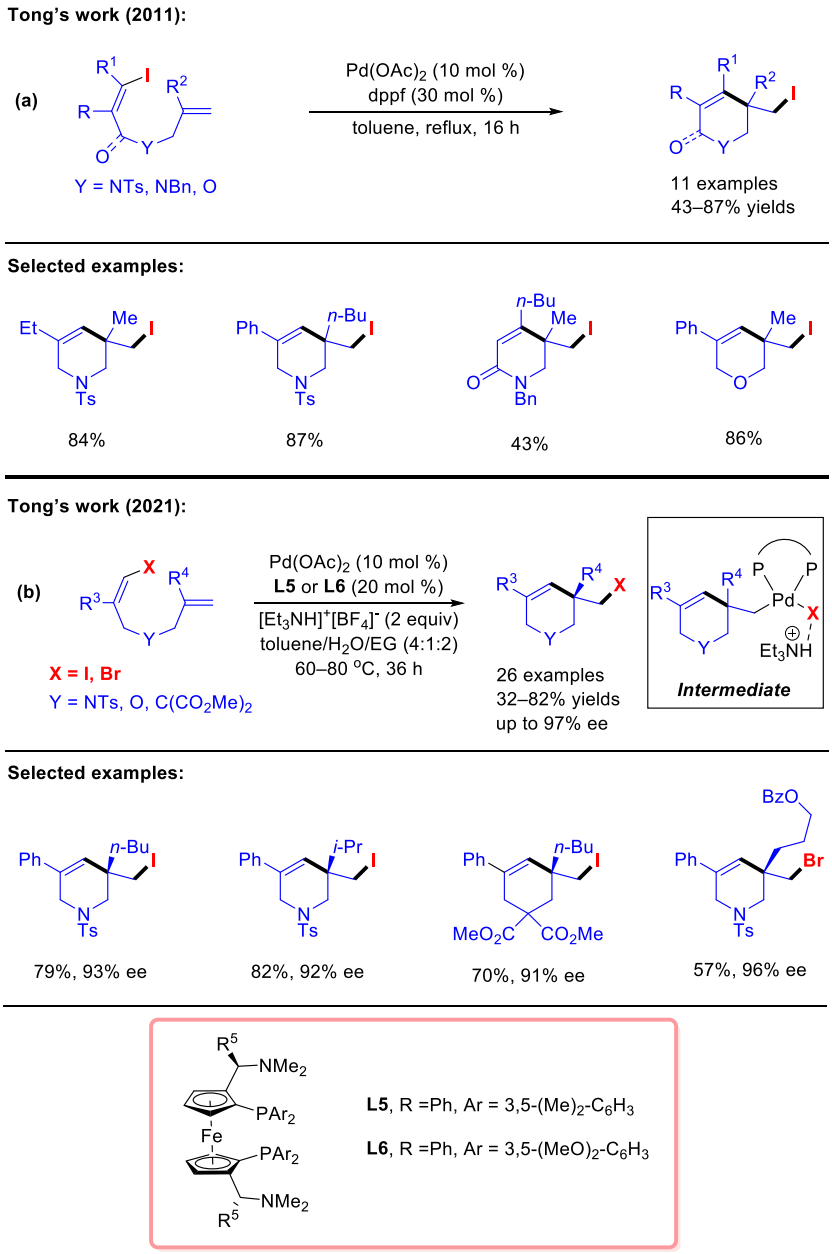

Finally, it is worth mentioning that in addition to the widely developed intramolecular carbohalogenation mode, Tong and co-workers also developed a palladium-catalyzed intramolecular iminohalogenation of oxime ester tethered to carbon–carbon double bonds by using an exogenous halide salt as a halogen source (**Scheme 1-26**).[67] They co-founded that the electron-deficient phosphine ligand used in this catalytic system is crucial for the

reductive elimination of the C–X bond, thereby ensuring that a series of dihydropyrroles were constructed with good efficiency.

Scheme 1-26. Pd-catalyzed Intramolecular Iminohalogenation of Oxime Ester.

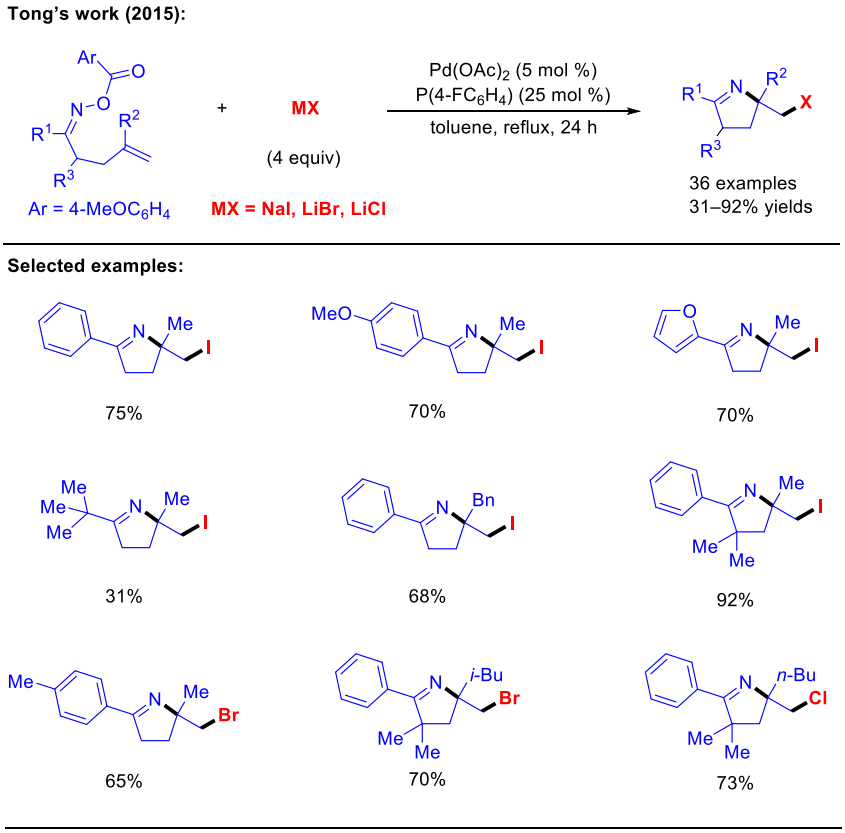

1-4-2 Intermolecular Carboiodination

The second key halogenation mode is the intermolecular carboiodination mode. It was first reported by the Lautens' group as early as 2011. They used the same catalytic system as the intramolecular strategy and were also eager to use aryl iodide as a bifunctional reagent with unsaturated compounds to achieve intermolecular carboiodination.[48] In other words, aryl iodide can be used as both a carbon source and an iodine source. However, only the special norbornene can perfectly interpret this perfect design (**Scheme 1-27(a)**). To further expand the potential application and value of this protocol, Morandi and colleagues created

a Pd/dAr^{F}pe catalytic system in 2019 to manipulate the intermolecular carboiodination of aryl iodides and alkynes, thereby synthesizing a series of valuable cis-alkenyl iodides via reductive elimination of C–I bonds (**Scheme 1-27(b)**).[68] Subsequently, the group also developed a unique intermolecular hydrogen iodination mode for alkynes, which uses a rhodium catalytic system to manipulate aromatic and aliphatic terminal alkynes to achieve *anti*-Markovnikov rule hydrogenation iodination. Crucially, they used commercially available aliphatic iodides as HI substitutes to construct a series of olefin iodides with high chemoselectivity and fully retained stereoselectivity, further demonstrating the charm of C–I bond reductive elimination.[69]

Scheme 1-27. Pd-catalyzed Intermolecular Carboiodination of Alkenes or Alkynes.

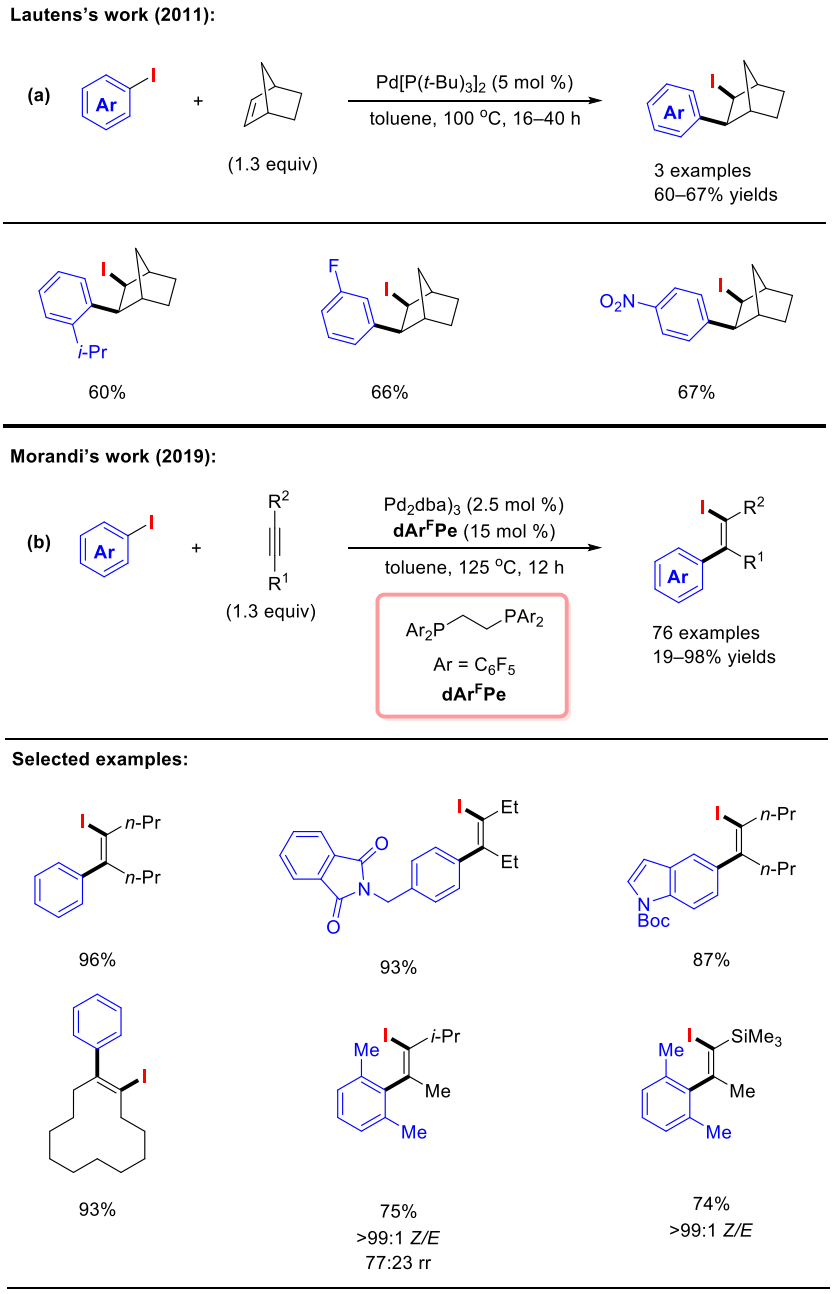

In addition, the intermolecular domino carboiodination of aryl iodides with alkynes was reported by Lautens and co-workers in 2012.[70] They used the classic Pd/QPhos catalytic system to effectively suture iodoaryl alkenes and internal alkynes, and synthesize a series of iodine-substituted indene derivatives (**Scheme 1-28**). Based on the experimental results,

they speculated a plausible mechanism: initially, the iodoaryl alkene coordinated with the activated Pd catalyst **A** to form intermediate **B**, and finally the aryl iodide moiety triggered the oxidative addition of the Pd center to generate the oxidative adduct Pd species **C**, which would undergo two migration insertions, including the intermolecular migration insertion with the alkyne to form intermediate **D**, and the intramolecular migration insertion with the alkene moiety, and finally form the alkyl–Pd(II)–I intermediate **E**, followed by the reductive elimination of C–I bond to release the final indene derivatives and regenerate the active palladium catalyst **A**.

Scheme 1-28. Pd-catalyzed Intermolecular Domino Carboiodination of Alkenes and Alkynes.

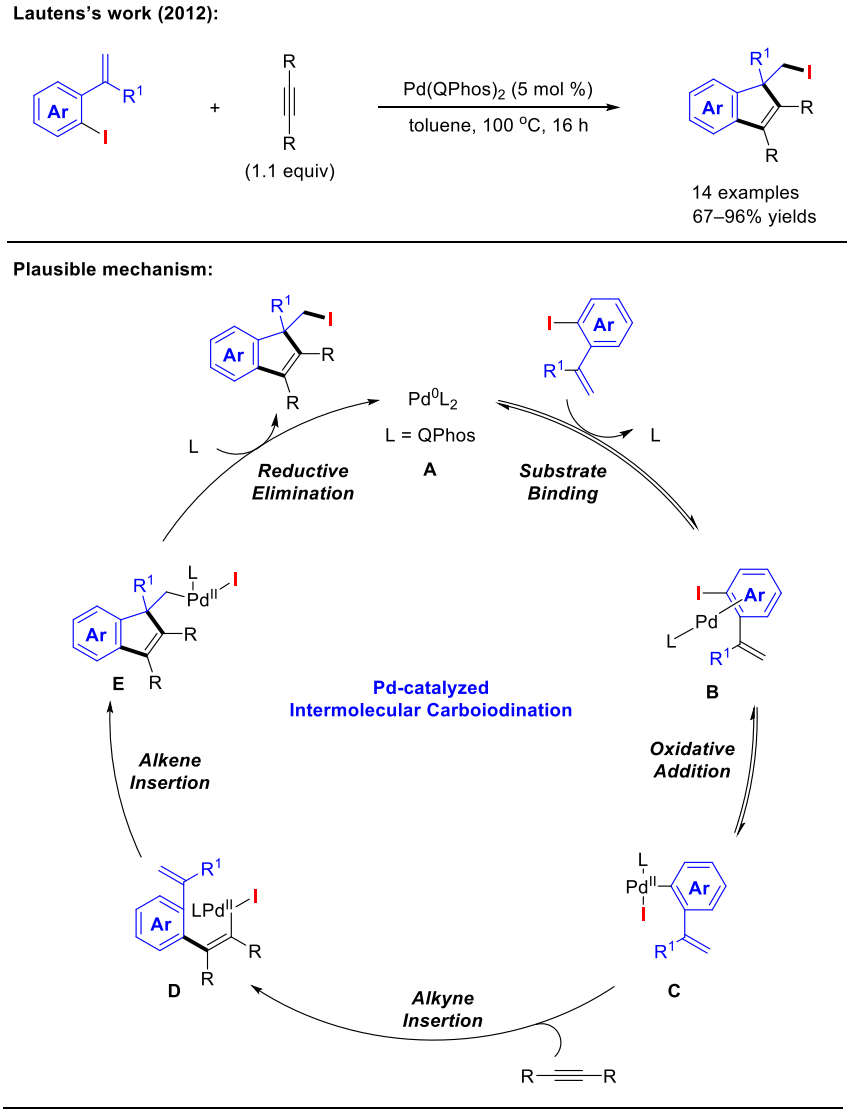

Finally, it is worth mentioning that the intermolecular iodination mode of iodoaniline derivatives with alkynes was reported by Xi's group in 2014.[71] Although this is not a typical intermolecular carboiodination mode, it is the first design of generating alkyl halides by reductive elimination in alkyl palladium(II) halides containing syn-β-hydrogen atoms (**Scheme 1-29**). Through in-depth mechanistic studies, the research team found that the reductive elimination reaction of this type of alkyl palladium halide **F** can take precedence over β-hydride abstraction, and even become the only reaction path in some cases. In addition, the reductive elimination of the C(sp^3)–I bond unexpectedly becomes a favorable step only when triphenylphosphine (PPh_3) is used as a ligand, which provides a fairly broad idea for subsequent research.

Scheme 1-29. Pd-Catalyzed Intermolecular Cycloiodination of Anilines and Alkynes.

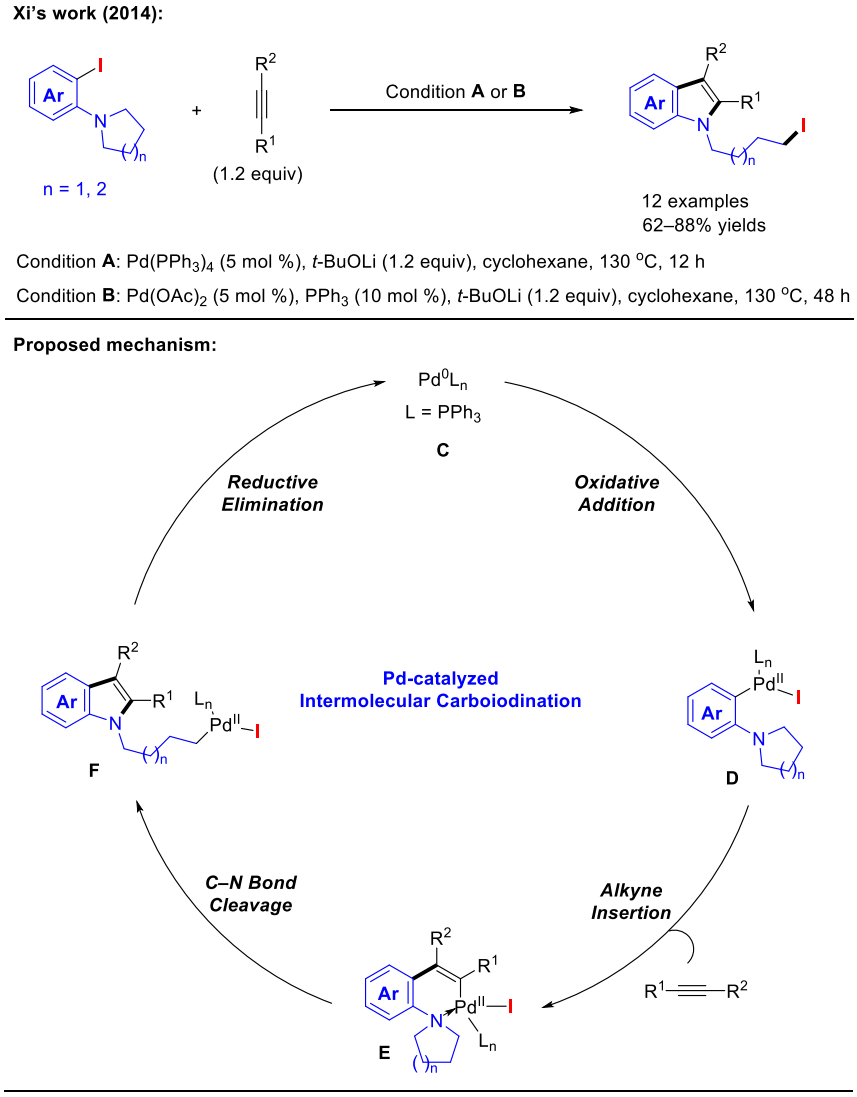

1-5 Summary

In summary, this chapter mainly focuses on the key points of using transition-metal-mediated reductive elimination steps of the C–X bond to achieve efficient organic synthesis transformations. Since the discovery of this step and its confirmation by stoichiometric experiments, chemists have built a series of Pd or Ni catalytic systems and synthesized a series of organic halides by screening and designing catalytic systems, especially ligands with both electronic and steric hindrance effects. However, as Hartwig revealed in his pioneering research, the reductive elimination trends of different C(Ar)–X bonds can be

derived from the equilibrium constant. Among them, the reductive elimination of C(Ar)–I bonds is the weakest, and this conclusion has also been confirmed in a large number of subsequent studies. Because the nucleophilic halogenation mode of aromatics perfectly integrates the formation of C–Br bonds, C–Cl bonds, and even C–F bonds, but only the construction of C(Ar)–I bonds remains a blank. Simultaneously, intramolecular and intermolecular carboiodination strategies undoubtedly provide a wealth of experience in the reductive elimination of C–I bonds, but all breakthroughs focus only on the reductive elimination of C(alkyl)–I and C(alkenyl)–I, therefore, the reductive elimination of C(Ar)-I bonds, which is a thermodynamically and kinetically unfavorable process, is still in high demand for further exploration and development. Therefore, the author's doctoral thesis focuses on how to achieve the nucleophilic iodination mode of aromatics through the design of catalytic systems, thereby breaking through the milestone of reductive elimination of C(Ar)–I bonds to build a series of aromatic iodides with good efficiency.

1-6 References

1. (a) Harper, D. B.; O'Hagan, D. *Nat. Prod. Rep.* **1994**, *11*, 123. (b) Murai, A. *Stud. Nat. Prod. Chem.* **1996**, *19*, 411. (c) Gribble, G. W. *Acc. Chem. Res.* **1998**, *31*, 141. (d) Gribble, G. W. Structure and Biosynthesis of Halogenated Alkaloids. In *Modern Alkaloids: Structure, Isolation, Synthesis, and Biology*; Fattorusso, E., Tagilialatela-Scafati, O., Eds.; Wiley-VCH: Weinheim, 2008. (e) Blunt, J. W.; Copp, B. R.; Keyzers, R. A.; Munro, M. H. G.; Prinsep, M. R. *Nat. Prod. Rep.* **2012**, *29*, 144.
2. (a) Böhm, H.-J.; Banner, D.; Bendels, S.; Kansy, M.; Kuhn, B.; Muller, K.; Obst-Sander, U.; Stahl, M. *ChemBioChem* **2004**, *5*, 637. (b) Bégué, J.-P.; Bonnet-Delpon, D. *J. Fluorine Chem.* **2006**, *127*, 992. (c) Müller, K.; Faeh, C.; Diederich, F. *Science* **2007**, *317*, 1881. (d) Purser, S.; Moore, P. R.; Swallow, S.; Gouverneur, V. *Chem. Soc. Rev.* **2008**, *37*, 320. (e) Hernandes, M. Z.; Cavalcanti, S. M. T.; Moreira, D. R. M.; de Azevedo, W. F. Jr.; Leite, A. C. L. *Curr. Drug Targets* **2010**, *11*, 303. (f) Kosjek, T.; Heath, E. Halogenated Heterocycles as Pharmaceuticals. In *Halogenated Heterocycles: Synthesis, Application and Environment*; Iskra, J., Ed.; Springer: New York, 2012. (g) Wilcken, R.; Zimmermann, M. O.; Lange, A.; Joerger, A. C.; Boeckler, F. M. *J. Med. Chem.* **2013**, *56*, 1363. (h) Wang, J.; Sánchez-Roselló, M.; Aceña, J.-L.; del Pozo, C.; Sorochinsky, A. E.; Fustero, S.; Soloshonok, V. A.; Liu, H. *Chem. Rev.* **2014**, *114*, 2432.
3. (a) Tang, M. L.; Bao, Z. *Chem. Mater.* **2011**, *23*, 446. (b) Amanchukwu, C. V.; Harding, J. R.; Shao-Horn, Y.; Hammond. P. T. *Chem. Mater.* **2015**, *27*, 550.
4. (a) Jeschke, P. *ChemBioChem* **2004**, *5*, 570. (b) Jeschke, P. *Pest Manage. Sci.* **2010**, *66*, 10. (c) Jeschke, P. The Unique Role of Halogen Substituents in the Design of Modern Crop Protection Compounds. In *Modern Methods in Crop Protection Research*; Jeschke, P., Krämer, W., Schirmer, U., Witschel, M., Eds.; Wiley-VCH: Weinheim, 2013.
5. (a) Beale, T. M.; Chudzinski, M. G.; Sarwar, M. G.; Taylor, M. S. *Chem. Soc. Rev.* **2013**, *42*, 1667. (b) Jentzsch, A. V. *Pure Appl. Chem.* **2015**, *87*, 15.
6. (a) Stille, J. K.; Lau, K. S. Y. *Acc. Chem. Res.* **1977**, *10*, 434. (b) Labinger, J. A. *Organometallics* **2015**, *34*, 4784. (c) Phapale, V. B.; Cardenas, D. J. *Chem. Soc. Rev.* **2009**, *38*, 1598. (d) Hartwig, J. F. *Synlett* **2006**, *9*, 1283. (e) Terao, J.; Kambe, N. *Acc. Chem. Res.* **2008**, *41*, 1545. (f) Weix, D. J. *Acc. Chem. Res.* **2015**, *48*, 1767. (g) Rio, J.; Liang, H.; Perrin, M.-E. L.; Perego, L. A.; Grimaud, L.; Payard, P.-A. *ACS Catal.* **2023**, *13*, 11399. (h) Zeni, G.; Larock, R. C. *Chem. Rev.* **2006**, *106*, 4644. (i) Jutand, A.; Pytkowicz, J.; Roland, S.; Mangeney, P. *Pure Appl. Chem.* **2010**, *82*, 1393. (j)

Xue, L.; Lin, Z. *Chem. Soc. Rev.* **2010**, *39*, 1692.

7. (a) Kvasovs, N.; Gevorgyan V. *Chem. Soc. Rev.* **2021**, *50*, 2244. (b) Ghosh, I.; Marzo, L.; Das A.; Shaikh, R.; König, B. *Acc. Chem. Res.* **2016**, *49*, 1566. (c) Pagire, S. K.; Föll, T.; Reiser O. *Acc. Chem. Res.* **2020**, *53*, 782. (d) Pan, Q.; Ping, Y.; Kong, W. *Acc. Chem. Res.* **2023**, *56*, 515.
8. (a) Zhdankin, V. V.; Stang, P. J. *Tetrahedron* **1998**, *54*, 10927. (b) Li, Y.; Hari, D. P.; Vita, M. V.; Waser, J. *Angew. Chem., Int. Ed.* **2016**, *55*, 4436; *Angew. Chem.* **2016**, *128*, 4512. (c) Brand, J. P.; Waser, J. *Chem. Soc. Rev.* **2012**, *41*, 4165. (d) Charpentier, J.; Früh, N.; Togni, A. *Chem. Rev.* **2015**, *115*, 650. (e) Wang, X.; Studer, A. *Acc. Chem. Res.* **2017**, *50*, 1712. (f) Hari, D. P.; Caramenti, P.; Waser, J. *Acc. Chem. Res.* **2018**, *51*, 3212. (g) Declas, N.; Pisella, G.; Waser, J. *Helv. Chim. Acta* **2020**, *103*, e2000191. (h) Allouche, E. M. D.; Grinhagena, E.; Waser, J. *Angew. Chem., Int. Ed.* **2022**, *61*, e202112287; *Angew. Chem.* **2022**, *134*, e202112287. (i) Vaillant, F. L.; Waser, J. *Chem. Sci.* **2019**, *10*, 8909. (j) Zhdankin, V. V. *J. Org. Chem.* **2011**, *76*, 1185.
9. (a) Becke, A. D.; Edgecombe, K. E. *J. Chem. Phys.* **1990**, *92*, 5397. (b) Cioslowski, J.; Mixon, S. T. *J. Am. Chem. Soc.* **1991**, *113*, 414. (c) Schleyer, P. V. R.; Jiao, H. *J. Am. Chem. Soc.* **1996**, *118*, 6317.
10. (a) Olah, G. A. *Acc. Chem. Res.* **1971**, *4*, 240. (b) Schlosser, M. *Pure Appl. Chem.* **1977**, *49*, 355.
11. (a) Jones, D. J.; Lautens, M.; McGlacken, G. P. *Nat. Catal.* **2019**, *2*, 843. (b) Hartwig, J. F. *Organotransition Metal Chemistry: From Bonding to Catalysis;* University Science Books: Sausalito, CA, 2010. (c) Sasson, Y. Formation of Carbon-Halogen Bonds (Cl, Br, I). In *Halides, Pseudo-Halides and Azides;* Patai, P., Rappoport, Z., Eds.; John Wiley and Sons: New York, 1995.
12. (a) Petrone, D. A.; Ye, J.; Lautens, M. *Chem. Rev.* **2016**, *116*, 8003. (b) Chen, C.; Tong, X. *Org. Chem. Front.* **2014**, *1*, 439.
13. Ettorre, R. *Inorg. Nucl. Chem. Lett.* **1969**, *5*, 45.
14. (a) Yahav-Levi, A.; Goldberg, I.; Vigalok, A. *J. Am. Chem. Soc.* **2006**, *128*, 8710. (b) Yahav-Levi, A.; Goldberg, I.; Vigalok, A.; Vedernikov, A. N. *Chem. Commun.* **2010**, *46*, 3324.
15. (a) Whitfield, S. R.; Sanford, M. S. *J. Am. Chem. Soc.* **2007**, *129*, 15142. (b) Furuya, T.; Ritter, T. *J. Am. Chem. Soc.* **2008**, *130*, 10060. (c) Ball, N. D.; Sanford, M. S. *J. Am. Chem. Soc.* **2009**, *131*, 3796. (d) Arnold, P. L.; Sanford, M. S.; Pearson, S. M. *J. Am. Chem. Soc.* **2009**, *131*, 13912. (e) Wang, X.; Mei, T.-S.; Yu, J.-Q. *J. Am. Chem. Soc.* **2009**, *131*, 7520. (f) Haines, B. E.; Xu, H.; Verma, P.; Wang, X.-C.; Yu, J.-Q.; Musaev, D. G. *J. Am. Chem. Soc.* **2015**, *137*, 9022. (g) Chu, L.; Xiao, K.-J.; Yu, J.-Q. *Science* **2014**, *346*, 451.
16. (a) Power, D. C.; Ritter, T. *Nat. Chem.* **2009**, *1*, 302. (b) Powers, D. C.; Benitez, D.; Tkatchouk,

E.; Goddard, W. A.; Ritter, T. *J. Am. Chem. Soc.* **2010**, *132*, 14092. (c) Nielsen, M. C.; Lyngvi, E.; Schoenebeck, F. *J. Am. Chem. Soc.* **2013**, *135*, 1978. (d) Bonney, K. J.; Proutiere, F.; Schoenebeck, F. *Chem. Sci.* **2013**, *4*, 4434.

17. (a) Higgs, A. T.; Zinn, P. J.; Simmons, S. J.; Sanford, M. S. *Organometallics* **2009**, *28*, 6142. (b). Zheng, B.; Tang, F.; Luo, J.; Schultz, J. W.; Rath, N. P.; Mirica, L. M. *J. Am. Chem. Soc.* **2014**, *136*, 6499. (c) Lee, H.; Börgel, J.; Ritter, T. *Angew. Chem., Int. Ed.* **2017**, *56*, 6966; *Angew. Chem.* **2017**, *129*, 7070.
18. Meucci, E. A.; Ariafard, A.; Canty, A. J.; Kampf, J. W.; Sanford, M. S. *J. Am. Chem. Soc.* **2019**, *141*, 13261.
19. (a) Suzuki, A. *Angew. Chem., Int. Ed.* **2011**, *50*, 6722; *Angew. Chem.* **2011**, *123*, 6855. (b) Negishi, E.-I. *Angew. Chem., Int. Ed.* **2011**, *50*, 6738; *Angew. Chem.* **2011**, *123*, 6870. (c) Wu, X.-F.; Anbarasan, P.; Neumann, H.; Beller, M. *Angew. Chem., Int. Ed.* **2010**, *49*, 9047; *Angew. Chem.* **2010**, *122*, 9231. (d) *Metal-Catalyzed Cross-Coupling Reactions*, 2nd ed., Vols. 1 and 2 (Eds: de Meijere, A.; Diederich, F.), Wiley-VCH: Weinheim, Germany, 2004. (e) Seechurn, C. C. C. J.; Kitching, M. O.; Colacot, T. J.; Snieckus, V. *Angew. Chem., Int. Ed.* **2012**, *51*, 5062; *Angew. Chem.* **2012**, *124*, 5150.
20. (a) Miyaura, N.; Suzuki, A. *Chem. Rev.* **1995**, *95*, 2457. (b) Miyaura, N.; Yanagi, T.; Suzuki, A. *Synth. Commun.* **1981**, *11*, 513.
21. (a) Negishi, E.-I. *Acc. Chem. Res.* **1982**, *15*, 340. (b) King, A. O.; Okukado, N.; Negishi, E.-I. *J. Chem. Soc. Chem. Commun.* **1977**, 683.
22. (a) Tamao, K.; Sumitani, K.; Kiso, Y.; Zembayashi, M.; Fujioka, A.; Kodama, S.; Nakajima, I.; Minato, A.; Kumada, M. *Bull. Chem. Soc. Jpn.* **1976**, *49*, 1958. (b) Tamao, K.; Sumitani, K.; Kumada, M. *J. Am. Chem. Soc.* **1972**, *94*, 4374. (c) R. J. P. Corriu, J. P. Massse, *J. Chem. Soc. Chem. Commun.* **1972**, 144.
23. (a) Yamamura, M.; Moritani, I.; Murahashi, S. *J. Organomet. Chem.* **1975**, *91*, C39. (b) Murahashi, S.; Yamamura, M.; Yanagisawa, K.; Mita, N.; Kondo, K. *J. Org. Chem.* **1979**, *44*, 2408.
24. (a) Stille, J. K. *Angew. Chem., Int. Ed.* **1986**, *25*, 508; *Angew. Chem.* **1986**, *98*, 504. (b) Kosugi, M.; Sasazawa, K.; Shimizu, Y.; Migita, T. *Chem. Lett.* **1977**, 301. (c) Milstein, D.; Stille, J. K. *J. Am. Chem. Soc.* **1978**, *100*, 3636.
25. (a) Hatanaka, Y.; Hiyama, T. *J. Org. Chem.* **1988**, *53*, 918. (b) Hiyama, T.; Hatanaka, Y. *Pure. Appl. Chem.* **1994**, *66*, 1471.

26. (a) Sonogashira, K.; Tohda, Y.; Hagihara, N. *Tetrahedron Lett.* **1975**, *16*, 4467. (b) Chinchilla, R.; Najera, C. *Chem. Rev.* **2007**, *107*, 874. (c) Chinchilla, R.; Najera, C. *Chem. Soc. Rev.* **2011**, *40*, 5084.
27. (a) Mizoroki, T.; Mori, K.; Ozaki, A. *Bull. Chem. Soc. Jpn.* **1971**, *44*, 581. (b) Heck, R. F.; Nolley, J. P. *J. Org. Chem*. **1972**, *37*, 2320.
28. (a) Paul, F.; Patt, J.; Hartwig, J. F. *J. Am. Chem. Soc.* **1994**, *116*, 5969. (b) Guram, A. S.; Buchwald, S. L. *J. Am. Chem. Soc.* **1994**, *116*, 7901. (c) Guram, A.; Rennels, R.; Buchwald, S. L. *Angew. Chem., Int. Ed.* **1995**, *34*, 1348. (d) Louie, J.; Hartwig, J. F. *Tetrahedron Lett.* **1995**, *36*, 3609.
29. Rogova, T.; Ahrweiler, E.; Schoetz, M. D.; Schoenebeck, F. *Angew. Chem., Int. Ed.* **2024**, *63*, e202314709; *Angew. Chem.* **2024**, *136*, e202314709.
30. Amatore, C.; Jutand, A. *Chem. Rev.* **1999**, *99*, 2011.
31. García-Melchor, M.; López, N. *J. Am. Chem. Soc.* **2015**, *137*, 4901.
32. Echavarren, A. M.; Stille, J. K. *J. Am. Chem. Soc.* **1987**, *109*, 5478.
33. Roy, A. H.; Hartwig, J. F. *J. Am. Chem. Soc.* **2001**, *123*, 1232.
34. Roy, A. H.; Hartwig, J. F. *J. Am. Chem. Soc.* **2003**, *125*, 13944.
35. Roy, A. H.; Hartwig, J. F. *Organometallics* **2004**, *23*, 1533.
36. Shen, X.; Hyde, A. M.; Buchwald, S. L. *J. Am. Chem. Soc.* **2010**, *132*, 14076.
37. Pan, J.; Wang, X.; Zhang, Y.; Buchwald, S. L. *Org. Lett.* **2011**, *13*, 4974.
38. (a) Sather, A. C.; Buchwald, S. L. *Acc. Chem. Res.* **2016**, *49*, 2146. (b) Brown, J. M.; Gouverneur, V. *Angew. Chem., Int. Ed.* **2009**, *48*, 8610; *Angew. Chem.* **2009**, *121*, 8762.
39. Watson, D. A.; Su, M.; Teverovskiy, G.; Zhang, Y.; GarcíaFortanet, J.; Kinzel, T.; Buchwald, S. L. *Science* **2009**, *325*, 1661.
40. For Kraken Library, see: Gensch, T.; Gomes, G. P.; Friederich, P.; Peters, E.; Gaudin, T.; Pollice, R.; Jorner, K.; Nigam, A.; LindnerD'Addario, M.; Sigman, M. S.; Aspuru-Guzik, A. *J. Am. Chem. Soc.* **2022**, *144*, 1205−1217. https://kraken.cs.toronto.edu.
41. Maimone, T. J.; Milner, P. J.; Kinzel, T.; Zhang, Y.; Takase, M. K.; Buchwald, S. L. *J. Am. Chem. Soc.* **2011**, *133*, 18106.
42. Lee, H. G.; Milner, P. J.; Buchwald, S. L. *Org. Lett.* **2013**, *15*, 5602.
43. Lee, H. G.; Milner, P. J.; Buchwald, S. L. *J. Am. Chem. Soc.* **2014**, *136*, 3792.
44. Sather, A. C.; Lee, H. G.; Colombe, J. R.; Zhang, A.; Buchwald, S. L. *Nature* **2015**, *524*, 208.
45. Sather, A. C.; Lee, H. G.; Rosa, V. Y. D. L.; Yang, Y.; Müller, P.; Buchwald, S. L. *J. Am. Chem.*

Soc. **2015**, *137*, 13433.

46. Ye, Y.; Takada, T.; Buchwald, S. L. *Angew. Chem., Int. Ed.* **2016**, *55*, 15559; *Angew. Chem.* **2016**, *128*, 15788.
47. Ye, Y.; Kim, S.-T.; King, R. P.; Baik, M.-H.; Buchwald, S. L. *Angew. Chem., Int. Ed.* **2023**, *62*, e202300109; *Angew. Chem.* **2023**, *135*, e202300109.
48. Newman, S. G.; Lautens, M. *J. Am. Chem. Soc.* **2011**, *133*, 1778.
49. Newman, S. G.; Howell, J. K.; Nicolaus, N.; Lautens, M. *J. Am. Chem. Soc.* **2011**, *133*, 14916.
50. Petrone, D. A.; Malik, H. A.; Clemenceau, A.; Lautens, M. *Org. Lett.* **2012**, *14*, 4806.
51. Lan, Y.; Liu, P.; Newman, S. G.; Lautens, M.; Houk, K. N. *Chem. Sci.* **2012**, *3*, 1987.
52. Petrone, D. A.; Lischka, M.; Lautens, M. *Angew. Chem., Int. Ed.* **2013**, *52*, 10635; *Angew. Chem.* **2013**, *125*, 10829.
53. Petrone, D. A.; Yoon, H.; Weinstabl, H.; Lautens, M. *Angew. Chem., Int. Ed.* **2014**, *53*, 7908; *Angew. Chem.* **2014**, *126*, 8042.
54. Le, C. M.; Menzies, P. J. C.; Petrone, D. A.; Lautens, M. *Angew. Chem., Int. Ed.* **2015**, *54*, 254; *Angew. Chem.* **2015**, *127*, 256.
55. Sperger, T.; Le, C. M.; Lautens, M.; Schoenebeck, F. *Chem. Sci.* **2017**, *8*, 2914.
56. (a) Krasovskiy, A.; Lipshutz, B. H. *Org. Lett.* **2011**, *13*, 3818. (b) Lu, G.-P.; Voigtritter, K. R.; Cai, C.; Lipshutz, B. H. *Chem. Commun.* **2012**, *48*, 8661. (c) Lu, G.-P.; Voigtritter, K. R.; Cai, C.; Lipshutz, B. H. *J. Org. Chem.* **2012**, *77*, 3700.
57. Fruchey, E. R.; Monks, B. M.; Patterson, A. M.; Cook, S. P. *Org. Lett.* **2013**, *15*, 4362.
58. Amatore, C.; Bensalem, S.; Ghalem, S.; Jutand, A. *J. Organomet. Chem.* **2004**, *689*, 4642.
59. Petrone, D. A.; Franzoni, I.; Ye, J.; Rodríguez, J. F.; Poblador-Bahamonde, A. I.; Lautens, M. *J. Am. Chem. Soc.* **2017**, *139*, 3546.
60. Yoon, H.; Marchese, A. D.; Lautens, M. *J. Am. Chem. Soc.* **2018**, *140*, 10950.
61. Marchese, A. D.; Lind, F.; Mahon, A. E.; Yoon, H.; Lautens, M. *Angew. Chem., Int. Ed.* **2019**, *58*, 5095; *Angew. Chem.* **2019**, *131*, 5149.
62. Marchese, A. D.; Kersting, L.; Lautens, M. *Org. Lett.* **2019**, *21*, 7163.
63. Marchese, A. D.; Durant, A. G.; Reid, C. M.; Jans, C.; Arora, R.; Lautens, M. *J. Am. Chem. Soc.* **2022**, *144*, 20554.
64. Arora, R.; Lautens, M. *ACS Catal.* **2024**, *14*, 1970.
65. Liu, H.; Li, C.; Qiu, D.; Tong, X. *J. Am. Chem. Soc.* **2011**, *133*, 6187.
66. Chen, X.; Zhao, J.; Dong, M.; Yang, N.; Wang, J.; Zhang, Y.; Liu, K.; Tong, X. *J. Am. Chem. Soc.*

2021, *143*, 1924.

67. Chen, C.; Hou, L.; Cheng, M.; Su, J.; Tong, X. *Angew. Chem., Int. Ed.* **2015**, *54*, 3092; *Angew. Chem.* **2015**, *127*, 3135.
68. Lee, Y. H.; Morandi, B. *Angew. Chem., Int. Ed.* **2019**, *58*, 6444; *Angew. Chem.* **2019**, *131*, 6510.
69. Boehm, P.; Kehl, N.; Morandi, B. *Angew. Chem., Int. Ed.* **2023**, *62*, e202214071. *Angew. Chem.* **2023**, *135*, e202214071.
70. Jia, X.; Petrone, D. A.; Lautens, M. *Angew. Chem., Int. Ed.* **2012**, *51*, 9870; *Angew. Chem.* **2012**, *124*, 10008.
71. Hao, W.; Wei, J.; Geng, W.; Zhang, W.-X.; Xi, Z. *Angew. Chem., Int. Ed.* **2014**, *53*, 14533; *Angew. Chem.* **2014**, *126*, 14761.

CHAPTER 2

Palladium-Catalyzed Decarbonylative Halogenation of Acyl Fluorides and Chlorides

2-1 Introduction

Indeed, after the introduction in the previous chapter, it goes without saying that the use of nucleophilic iodination to construct aryl iodides will be an urgent research topic. Therefore, due to many limitations, aryl iodide compounds are not only very limited in commercial types but also extremely expensive. Looking at all the commercially available aryl halides, aryl iodide accounts for only 2%, closely related aryl bromide accounts for 21%, aryl chloride accounts for 38%, and aryl fluoride accounts for 39% (**Scheme 2-1**).[1] However, in the previous large number of studies on nucleophilic halogenation of organic halides using reductive elimination of C–X bond, either aryl triflate and aryl bromide-mediated nucleophilic halogenation were developed,[2] or aryl iodide-mediated intramolecular or intermolecular carbohalogenation was revealed.[3] There is no doubt that these precious studies provide quite meaningful research experience and ideas for the subsequent reductive elimination of C(Ar)–I , but it must be mentioned that these extremely expensive starting materials and the rather bulky ligands and catalysts that require verbose routes to be designed and synthesized more or less limit future further applications.

Scheme 2-1. The Proportion of Aryl Iodides in all Commercially Available Aryl Halides.

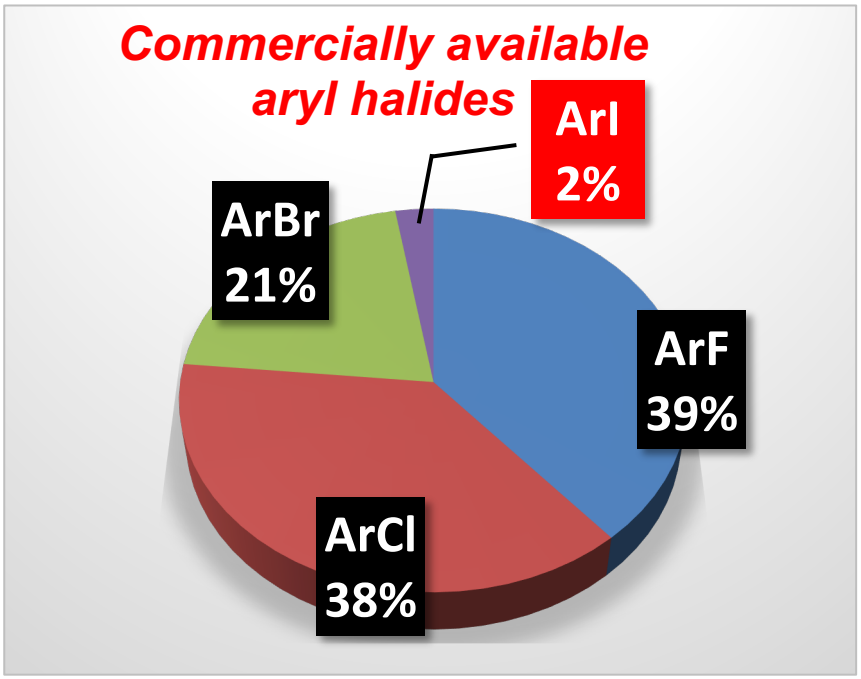

Based on them, the Authors concluded that in addition to the research idea of using the electronic effect and steric hindrance effect of the ligand to accelerate the reductive elimination of the C–X bond, whether other modes can be used to change the electron density of the transition metal center because if the electron density of the catalytic central atom is further reduced, it will undoubtedly accelerate the subsequent reductive elimination. Therefore, the Author wants to know whether a well-known decarbonylation strategy can be applied to this research proposal, because the Author postulates that in the transition-metal-catalyzed decarbonylation protocol, the carbon monoxide (CO) stripped from the reaction system will coordinate with the transition metal to some extent, making it more electron-deficient, which may achieve the seemingly impossible reductive elimination of C(Ar)–I bond (**Scheme 2-2**).[4]

Scheme 2-2. Reaction Design of Decarbonylative Iodination of Carboxylic Acid Derivatives.

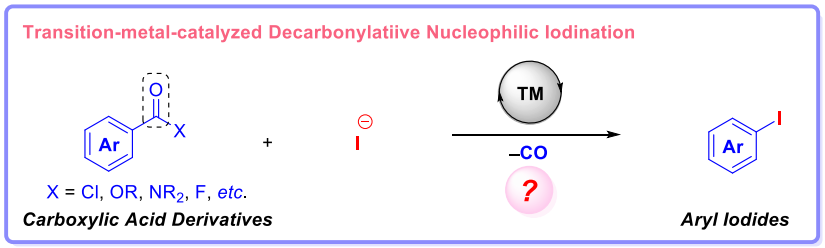

Focusing on the precursors for producing aryl iodides, carboxylic acid derivatives stand out as a cost-efficient and abundantly accessible group of chemical substances. These compounds can be conveniently transformed into numerous molecular structures through the application of transition metal-catalyzed processes.[5] Among the various approaches for converting carboxylic acid derivatives into high-value products, two key mechanisms—decarboxylation [6] and decarbonylation [7] —are commonly employed. Decarbonylation, in particular, has been identified as a crucial technique in contemporary research, and it has recently emerged as a simple yet effective alternative. The binding of the carbon monoxide generated in situ to the metallic center produces an electron-poor,

sterically hindered intermediate that enhances the reductive elimination of the carbon–halogen bond. Consequently, combining palladium-catalyzed halogenation with decarbonylation holds promise for the development of a more economical and efficient route to synthesize aryl halides.

Within this framework, the Author concentrates on acyl fluorides, a subset of carboxylic acid derivatives. Recently, acyl fluorides have attracted the attention of chemists and attracted a lot of research interests due to their unique metastable advantages, which balance activity and stability.[8] A considerable portion of these compounds is readily available on the market. For those not commercially accessible, they can be obtained in a single synthetic step from corresponding carboxylic acids and used directly in subsequent steps with minimal processing or simple filtration. Building on the groundbreaking discoveries of Schoenebeck and Keaveney in 2018,[9] who demonstrated palladium-catalyzed trifluoromethylation of acyl fluorides, further studies by multiple research groups,[10,11] including the Author's group,[12] have showcased the diverse transformations achievable through decarbonylation of acyl fluorides, underscoring their unique chemical behavior (**Scheme 2-3**).

Scheme 2-3. Transition metal-catalyzed Decarbonylative Transformations of Acyl Fluorides.

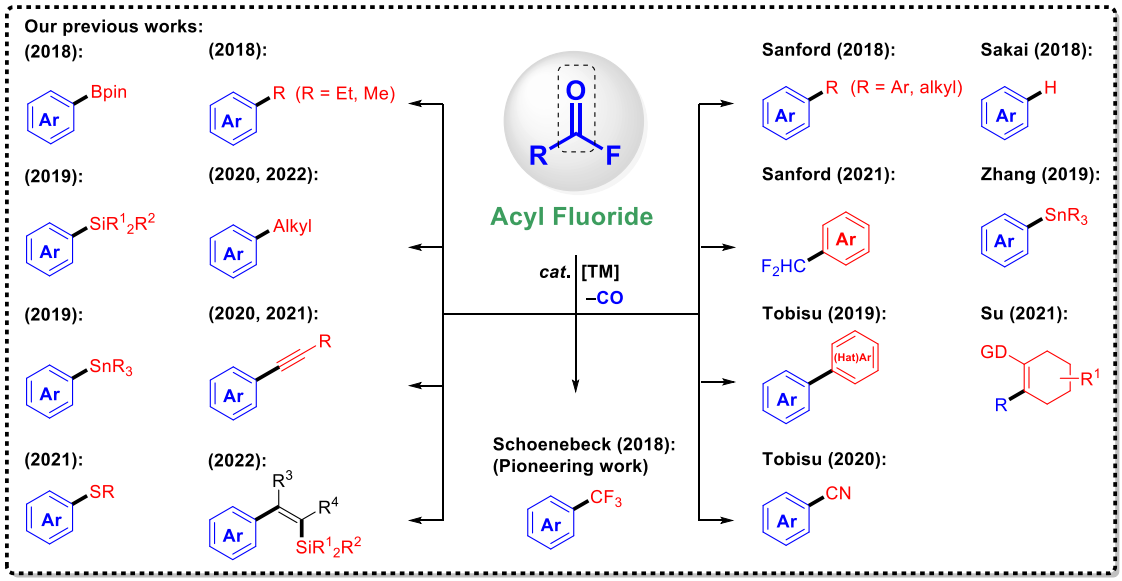

In the quest for efficient methods to generate organic iodides from carboxylic acid derivatives, Morandi [13, 14] and Arndtsen's [15] palladium-catalyzed decarbonylative iodination of acyl chlorides is particularly noteworthy (**Scheme 2-4**). Their innovation was celebrated for its significant advancement in forming aryl–iodine bonds via reductive elimination from Pd(II) intermediates. The Xantphos ligand, characterized by a large bite angle (β_n = 111°) and substantial steric bulk, was instrumental in accelerating the carbon–iodine bond formation.[16] Furthermore, this ligand proved effective in facilitating distinctive outer-sphere nucleophilic transhalogenation processes mediated by phosphonium salts (**Scheme 2-4**). To avoid dependence on organic iodides as iodine sources, the Author turns their attention to the use of more affordable inorganic halides.

Scheme 2-4. Pd-catalyzed Decarbonylative Iodination of Acyl Chlorides.

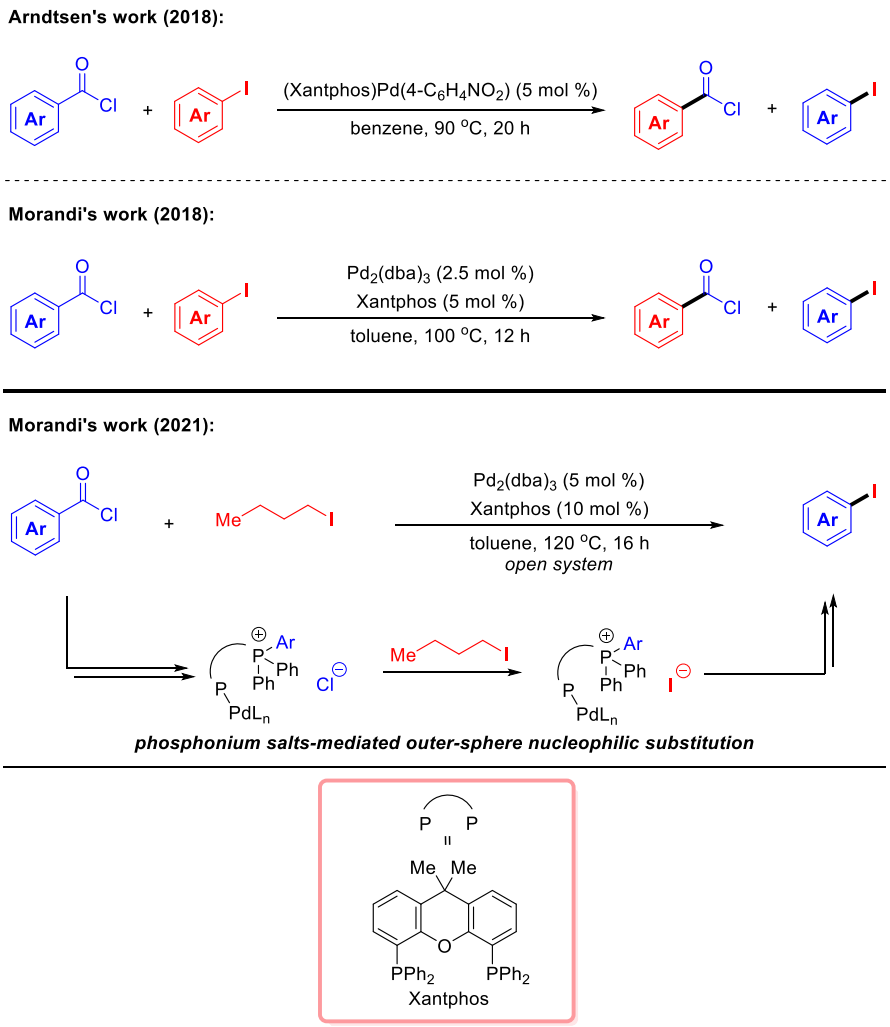

The Author postulates that employing LiI as the iodine source enables the in situ formation of acyl iodides from substrate-derived acyl fluorides. These acyl iodides can then transform aryl iodides through a mechanism termed unimolecular fragment coupling (UFC), which includes palladium-catalyzed oxidative addition, decarbonylation, and reductive elimination steps. Drawing inspiration from Sanford et al.'s prior study on the UFC of acyl chlorides,[17] this strategy was effectively adapted for the bromination and chlorination of acyl fluorides, as well as their iodination, by utilizing corresponding alkali metal halides (**Scheme 2-5**). This approach has demonstrated itself to be straightforward, efficient, versatile, and highly practical for synthesizing aryl chlorides, bromides, and iodides.

Scheme 2-5. Pd-catalyzed Decarbonylative Nucleophilic Halogenation of Acyl Halides (This Work).

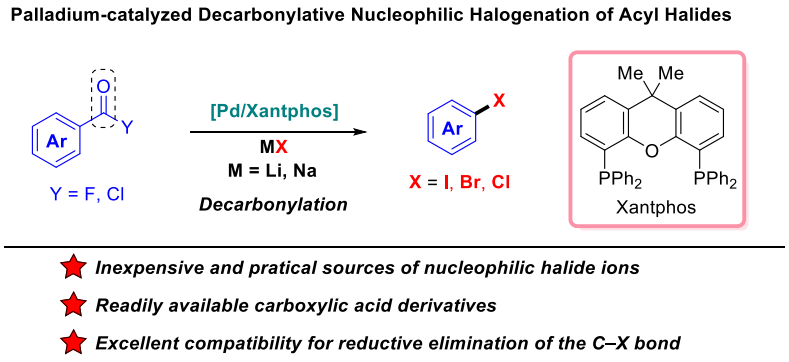

2-2 Results and Discussion

2-2-1 Design of Reaction Protocol

With strong confidence and passion for this research idea, the Author began to design the research proposal. Firstly, based on previous research experience, the Author designed the [PdCl(cinnamyl)]$_2$/Xantphos catalytic system and selected 1-naphthoyl fluoride (**1a**) as the reaction substrate, and used 3 equivalents of lithium iodide (LiI) with strong nucleophilicity as the iodine source and toluene as the solvent to start the exploration of reaction temperature.

2-2-2 Optimization of Reaction Condition for Acyl Fluorides

To the Author's delight, the reaction at 60 °C obtained the expected decarbonylation nucleophilic iodination product 1-iodonaphthalene (**2a**) with a yield of 16% (Table 2-1, entry 1). As the reaction temperature increased, the yield of the desired product continued to increase, until at 100 °C, the expected product 1-iodonaphthalene (**2a**) could be obtained with a yield of 95% (Table 2-1, entry 3). This also proves that the decarbonylation process, a thermodynamic endothermic process, is significantly affected by the reaction temperature. In addition, even if the temperature continues to rise to 120 °C and 140 °C, it still does not significantly affect the over-reaction or decomposition of highly activated 1-iodonaphthalene (**2a**) (Table 2-1, entries 4 and 5). Therefore, the appropriate temperature for the reaction was determined to be 100 °C. Crucially, the decarbonylative reduction product naphthalene (**3a**) was almost undetectable, which also highlights the high chemoselectivity of the catalytic system.

Table 2-1. Effect of Temperature in Catalytic Decarbonylative Iodination of **1a**.

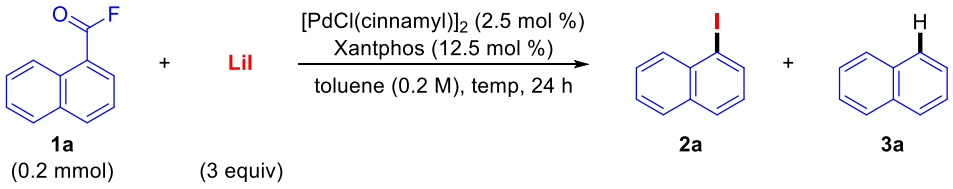

1a (0.2 mmol) (3 equiv) **2a** **3a**

entry	**temp (°C)**	**1a** (%)[a]	yield (%)[a]	
			2a	**3a**
1	60	0	16	<1
2	80	0	51	<1
3	**100**	**0**	**95**	**<1**
4	120	0	93	<1
5	140	0	79	<1

Reaction condition: **1a** (0.2 mmol, 1 equiv), $[PdCl(cinnamyl)]_2$ (2.5 mol %), Xantphos (12.5 mol %), LiI (3 equiv), toluene (0.2 M), 24 h, under N_2. [a] NMR yields were determined by ^1H NMR using dibromomethane as the internal standard.

Subsequently, to further improve the efficiency, the Author tried to screen the appropriate amount of LiI to match it. Unexpectedly, LiI showed super high efficiency in this conversion mode. As the amount of LiI continued to decrease, even when only 1 equivalent of LiI was present, the desired product 1-iodonaphthalene (**2a**) could be released with a yield of 92% with 3% of the starting material **1a** remaining (Table 2-2, entry 5). To better ensure a high conversion rate, the Author used a slight excess of LiI (1.1 equiv) as an iodine source to completely consume the raw material and obtain 1-iodonaphthalene (**2a**) with a yield of 96% (Table 2-2, entry 6).

Table 2-2. Effect of Amounts of LiI in Catalytic Decarbonylative Iodination of **1a**.

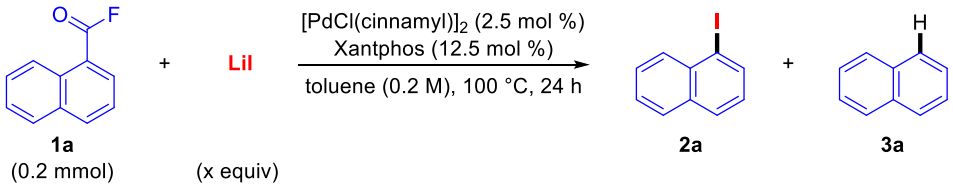

1a (0.2 mmol) (x equiv) **2a** **3a**

entry	**LiI (x equiv)**	**1a** (%)[a]	yield (%)[a]	
			2a	**3a**
1	3.0	0	95	<1
2	2.5	0	97	<1
3	2.0	0	97	<1
4	1.5	0	96	<1
5	1.0	3	92	<1
6	**1.1**	**0**	**96**	**<1**

Reaction condition: **1a** (0.2 mmol, 1 equiv), $[PdCl(cinnamyl)]_2$ (2.5 mol %), Xantphos (12.5 mol %), toluene (0.2 M), 100 °C, 24 h, under N_2. [a] NMR yields were determined by ^1H NMR using dibromomethane as the internal standard.

Based on them, the optimized LiI dosage was determined. Subsequently, the Author investigated the effects of different nucleophilic iodine sources on the catalytic conversion. After a series of iodine sources were screened, including NaI, KI, tetrabutylammonium iodide (TBAI), and 1-iodobutane (Table 2-3, entries 2–5) in addition to LiI, the Author found that these iodine sources were completely unable to initiate the reaction, resulting in

the complete residue of 1-naphthoyl fluoride (**1a**). This is probably due to the weak nucleophilicity of other iodine sources. Therefore, LiI was confirmed as the only matching iodine source for subsequent optimization condition exploration.

Table 2-3. Effect of Iodine Sources in Catalytic Decarbonylative Iodination of **1a**.

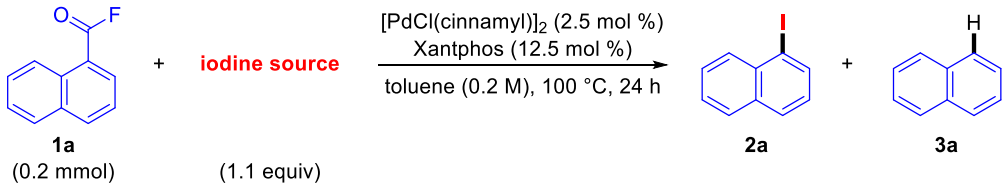

1a (0.2 mmol) (1.1 equiv) **2a** **3a**

entry	iodine source	**1a** (%)[a]	yield (%)[a]	
			2a	**3a**
1	**LiI**	**0**	**96**	**<1**
2	NaI	98	<1	0
3	KI	95	<1	0
4	tetrabutylammonium iodide (TBAI)	92	<1	0
5	1-iodobutane	99	<1	<1

Reaction condition: **1a** (0.2 mmol, 1 equiv), $[PdCl(cinnamyl)]_2$ (2.5 mol %), Xantphos (12.5 mol %), toluene (0.2 M), 100 °C, 24 h, under N_2. [a] NMR yields were determined by ^1H NMR using dibromomethane as the internal standard.

In the next stage, the Author began to investigate the factors affecting the catalytic system. The first is the effect of the ligand on the catalytic system (Table 2-4), and the specific structure of the ligands is shown in **Scheme 2-6**. The Author first screened a series of bidentate phosphine ligands and found that except for bulky DPEphos and Ferrophos-type (including dppf and dtbpf) ligands with large bite angles, which can build decarbonylative iodination products **2a** with low yields (Table 2-4, entries 4, 7 and 8), the remaining bidentate phosphine ligands have no obvious effect on the catalytic system. On the other hand, after screening monodentate phosphine ligands, the Author found that the extremely bulky BrettPhos and *t*-BuBrerrPhos can slightly give a small amount of the desired product 1-iodonaphthalene (**2a**), but they only show poor chemoselectivity, in other words, the decarbonylative reduction product **3a** will also be generated with it,

simultaneously (Table 2-4, entries 12 and 13). Other monodentate phosphine ligands are not suitable for this catalytic system. In particular, tricyclohexylphosphine (PCy_3) as a ligand can even give opposite chemoselectivity, that is, only 52% yield of decarbonylative reduction product naphthalene (**3a**) (Table 2-4, entry 10). Based on the above results, Xantphos was determined to be the only suitable ligand for the expected catalytic transformation.

Table 2-4. Effect of Ligands in Catalytic Decarbonylative Iodination of **1a**.

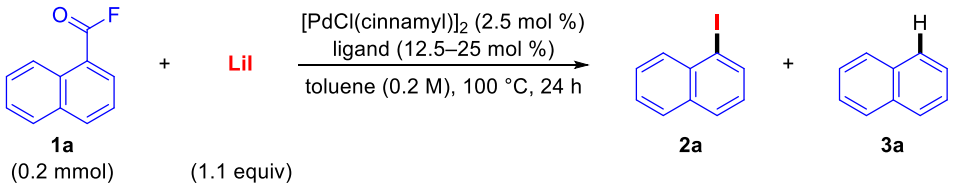

1a (0.2 mmol) (1.1 equiv) **2a** **3a**

entry	ligand	**1a** (%)[a]	yield (%)[a]	
			2a	**3a**
1	**Xantphos (12.5 mol %)**	**0**	**96**	**<1**
2	CyXantphos (12.5 mol %)	0	1	<1
3	*t*-BuXantphos (12.5 mol %)	0	3	<1
4	DPEphos (12.5 mol %)	0	18	3
5	dpppent (12.5 mol %)	19	0	3
6	dcype (12.5 mol %)	0	<1	<1
7	dppf (12.5 mol %)	<1	21	<1
8	dtbpf (12.5 mol %)	0	31	<1
9	PPh_3 (25 mol %)	0	0	<1
10	PCy_3 (25 mol %)	0	0	52
11	$P(t\text{-}Bu)_3$ (25 mol %)	0	3	<1
12	BrettPhos (25 mol %)	0	20	32
13	*t*-BuBrettPhos (25 mol %)	0	17	13
14	SPhos (25 mol %)	0	11	12
15	RuPhos (25 mol %)	0	7	21
16	*t*-BuXPhos (25 mol %)	0	3	<1
17	XPhos (25 mol %)	0	3	9

Reaction condition: **1a** (0.2 mmol, 1 equiv), $[PdCl(cinnamyl)]_2$ (2.5 mol %), LiI (0.22 mmol), toluene (0.2 M), 100 °C, 24 h, under N_2. [a] NMR yields were determined by ^1H NMR using dibromomethane as the internal standard.

Scheme 2-6. Structure of Ligands.

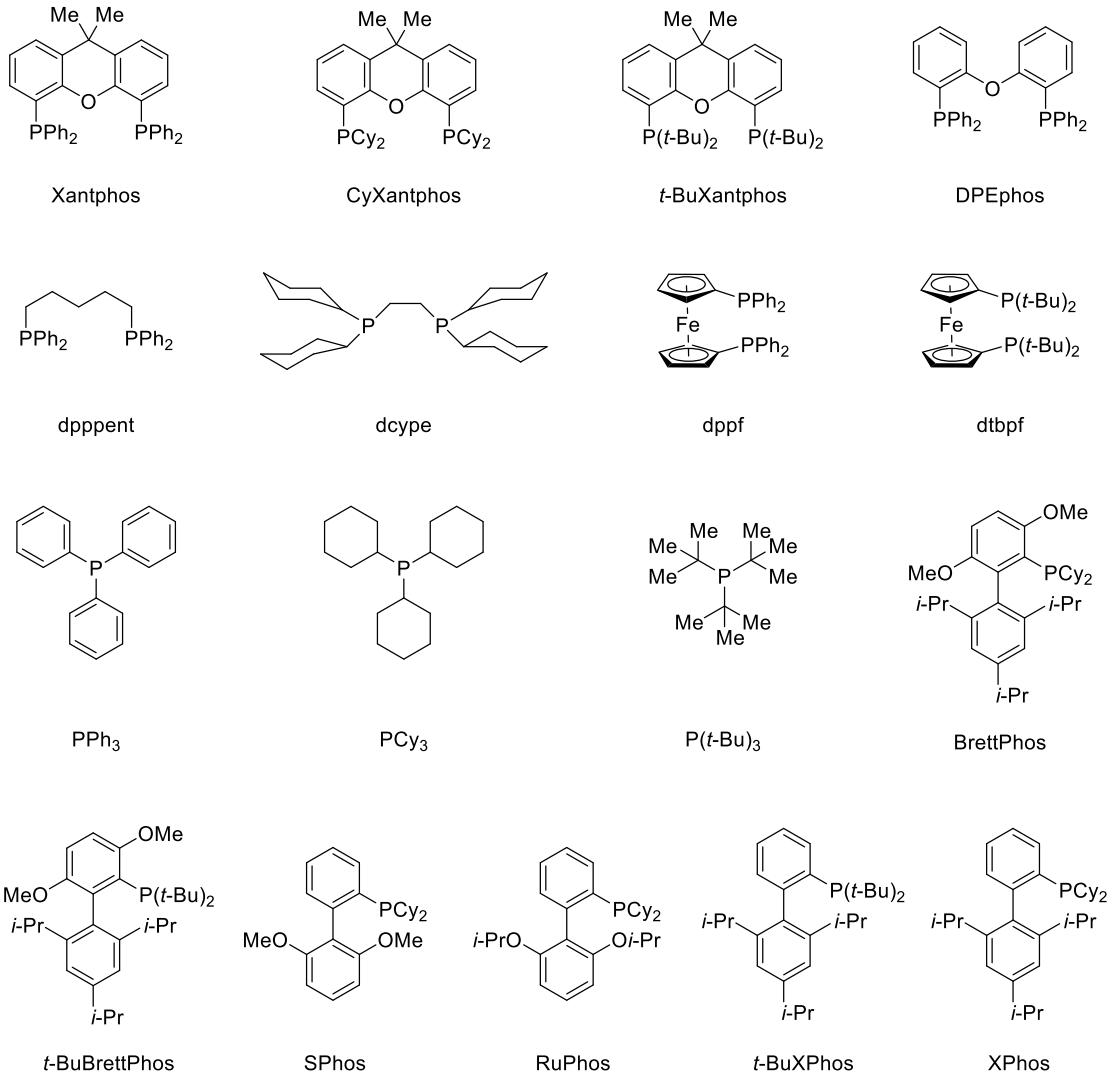

Meanwhile, when the Authors screened the catalyst precursors, they suggest that, except for $[PdCl(cinnamyl)]_2$, Pd(0) species, $Pd(dba)_2$ and $Pd_2(dba)_3$ can also perfectly fit the decarbonylative nucleophilic iodination mode and give excellent yields (Table 2-5, entries 4 and 5). However, other Pd(II) species, such as $PdCl_2$ and $Pd(OAc)_2$, are completely incompatible (Table 2-5, entries 2 and 3). In addition, the Authors tried to use a more inexpensive Ni catalyst instead of a Pd catalyst, but the transformation was not achieved (Table 2-5, entry 6). Finally, considering factors such as practicality, cost-effectiveness,

and experimental reproducibility, the Authors comprehensively considered $[PdCl(cinnamyl)]_2$ as the optimized catalyst precursor.

Table 2-5. Effect of Transition Metal Precursors in Catalytic Decarbonylative Iodination of **1a**.

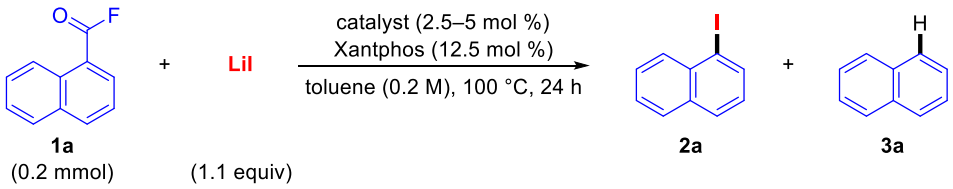

1a (0.2 mmol) (1.1 equiv) **2a** **3a**

entry	**catalyst**	**1a** (%)[a]	yield (%)[a]	
			2a	**3a**
1[b]	**$[PdCl(cinnamyl)]_2$**	**0**	**96**	**<1**
2[c]	$PdCl_2$	0	3	<1
3[c]	$Pd(OAc)_2$	0	2	<1
4[c]	$Pd(dba)_2$	0	94	<1
5[b]	$Pd_2(dba)_3$	0	95	<1
6[c]	$Ni(cod)_2$	0	2	<1

Reaction condition: **1a** (0.2 mmol, 1 equiv), catalyst (2.5–5 mol %), Xantphos (12.5 mol %), LiI (0.22 mmol), toluene (0.2 M), 100 °C, 24 h, under N_2. [a] NMR yields were determined by ^1H NMR using dibromomethane as the internal standard. [b] Catalyst (2.5 mol %). [c] Catalyst (5 mol %).

Finally, the Authors explored the effect of solvent on the decarbonylative transformation (Table 2-6). Based on this, common solvents used for reductive elimination of carbon–halogen bond and nucleophilic halogenation solvents were considered, including hexane, 1,2-dichloroethane (DCE), 1,4-dioxane, tetrahydrofuran (THF), and *N*,*N*-dimethylformamide (DMF), and they were respectively applied to the decarbonylative iodination of 1-naphthoyl fluoride (**1a**). The results indicated that ether solvents THF and 1,4-dioxane are more suitable for the designed catalytic system and can obtain the desired product in moderate yield (Table 2-6, entries 4 and 5), but they are accompanied by solvent ring-opening reaction as a side reaction, which may be one of the

reasons for the unsatisfactory yield. On the contrary, other solvents are not suitable for this transformation system.

Table 2-6. Solvent Effect in Catalytic Decarbonylative Iodination of **1a**.

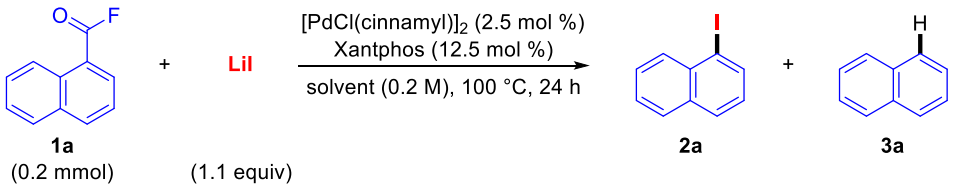

1a (0.2 mmol) (1.1 equiv) **2a** **3a**

entry	**solvent**	**1a** (%)[a]	yield (%)[a]	
			2a	**3a**
1	**toluene**	**0**	**96**	**<1**
2	hexane	0	9	<1
3	DCE	54	6	<1
4	THF	3	41	<1
5	1,4-dioxane	9	39	<1
6	DMF	49	<1	<1

Reaction condition: **1a** (0.2 mmol, 1 equiv), $[PdCl(cinnamyl)]_2$ (2.5 mol %), Xantphos (12.5 mol %), LiI (0.22 mmol), 100 °C, 24 h, under N_2. [a] NMR yields were determined by ^1H NMR using dibromomethane as the internal standard.

In summary, the optimized reaction conditions can be basically determined: $[PdCl(cinnamyl)]_2$ (2.5 mol %)/Xantphos (12.5 mol %) is used as a satisfactory catalytic system, 1-naphthoyl fluoride (**1a**) is used as a substrate, LiI (1.1 equiv) is used as an iodine source, and toluene is used as a solvent. The reaction is carried out at 100 °C for 24 h to obtain the expected decarbonylative nucleophilic iodination product 1-iodonaphthalene (**2a**) with nearly quantitative yield and good chemical selectivity.

2-2-3 Optimization of Reaction Condition for Acyl Chlorides

Based on the suitable reaction conditions explored in this way, the Authors explored the matching of other carboxylic acid derivatives. Through the screening of acyl chlorides,

acyl fluorides, esters, and amides (**Scheme 2-7**), the Authors were surprised to find that only acyl fluorides could be good substrate candidates. Acyl chlorides with better reactivity could only afford 1-iodonaphthalene (**2a**) with a yield of 22%. In addition, even the use of activated twisted amides[18] only gave a yield of 9%. Indeed, it is reasonable that stable and inert esters and amides cannot complete the expected catalytic design under this system. However, what puzzles the Authors is why acyl chlorides are not compatible with this catalytic system. After all, if inexpensive acyl chlorides can be used as candidates for substrates, it will undoubtedly greatly enhance the prospects and industrial applications of this protocol.

Scheme 2-7. Decarbonylative Iodination of Several Classical Carboxylic Acid Derivatives.

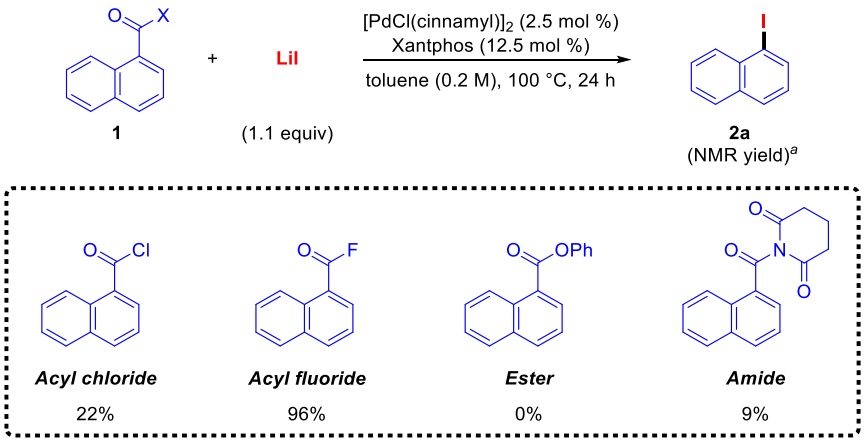

Although, the study of Morandi *et al.*,[14] also proved that LiI is not a good partner with acyl chlorides, meanwhile, the Author also checked the details of this transformation and showed that this transformation stopped only 15 min after the reaction started. To further explore the decarbonylative nucleophilic iodination conditions suitable for 1-naphthoyl chloride (**1a'**), the Author conducted a brief investigation of the reaction condition for this transformation of acyl chlorides (Table 2-7). Interestingly, when the Author used NaI instead of LiI as the iodine source, the catalytic iodination was efficiently achieved, and the desired 1-iodonaphthalene (**2a**) was obtained in 94% yield (Table 2-7, entry 2). Moreover, even if the Author shortened the reaction time to 12 h, there was no effect on the conversion efficiency (Table 2-7, entry 5). Therefore, through the investigation and

exploration of the above series of reaction conditions, the Authors suggested that the combination of different substrates, acyl fluorides or chlorides, and the countercation of alkali metal iodides is crucial for the implementation of the expected catalytic decarbonylative iodination.

Table 2-7. Effect of Iodine Salts in Decarbonylative Iodination of **1a'**.

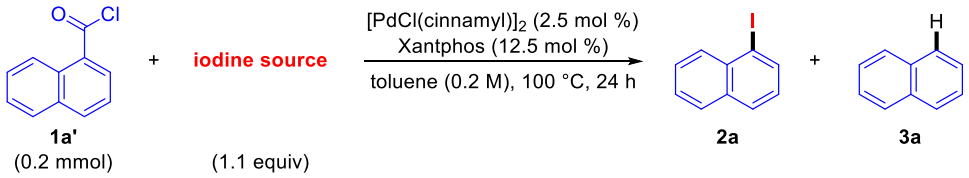

entry	iodine source	yield (%)[a]	
		2a	**3a**
1	LiI	22	<1
2	NaI	94	<1
3	KI	79	<1
4	tetrabutylammonium iodide (TBAI)	24	0
5[b]	**NaI**	**95**	**<1**

Reaction condition: **1a'** (0.2 mmol, 1 equiv), $[PdCl(cinnamyl)]_2$ (2.5 mol %), Xantphos (12.5 mol %), toluene (0.2 M), 100 °C, 24 h, under N_2. [a] NMR yields were determined by ^1H NMR using dibromomethane as the internal standard. [b] 12 h.

2-2-4 Substrate Scope of Decarbonylative Iodination

The reactivity of various acyl fluorides and chlorides was thoroughly evaluated under the established optimal conditions, as detailed in **Scheme 2-8**. Electron-neutral substrates, such as benzoyl fluoride (**1b**) and 2-naphthoyl fluoride (**1c**), displayed outstanding performance, producing the anticipated products **2b** and **2c** in high yields. Next, a variety of benzoyl fluorides containing electron-donating groups—including 4-*t*-Bu, 4-cyclohexyl, 3-OMe, 3-OPh, 4-SMe, 4-Ph, and 3-Ph—were tested. Due to the lower propensity of these electron-rich substrates for oxidative addition, elevated reaction temperatures were necessary, resulting in enhanced yields of the target compounds **2d**−**2j**.

Interestingly, the preparation of sterically hindered 2-iodobiphenyl (**2k**) was achieved in an open reaction setup, which promoted decarbonylation and mitigated the undesired formation of fluorenone via intramolecular C−H activation. Investigation of substrates with halogen substituents at the 4-position of the phenyl ring revealed compatibility with all halogens, producing dihaloarenes **2l**−**2o** with moderate to good efficiency. Although **2n** showed a minor side product, 1,4-diiodobenzene (**2o**), these polyhalogenated arenes are particularly valuable as precursors for selective synthesis of complex structures utilizing the diverse reactivity of multiple halogens.

Scheme 2-8. Substrate Scope for Decarbonylative Nucleophilic Iodination of Acyl Fluorides **1** and Acyl Chlorides **1'**.

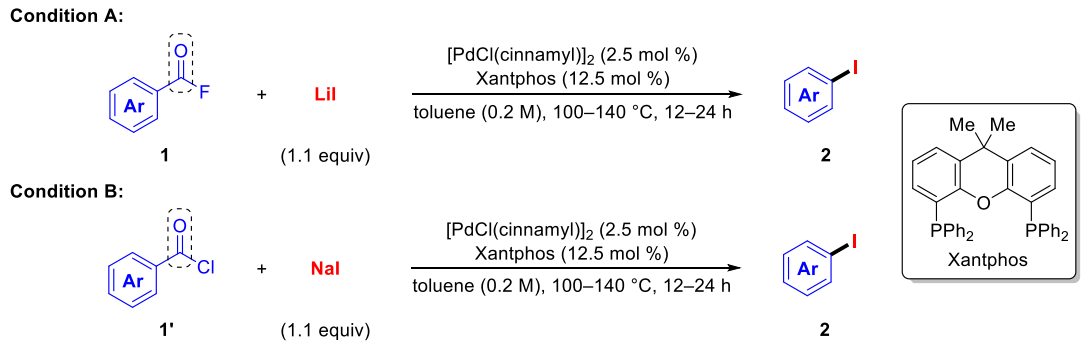

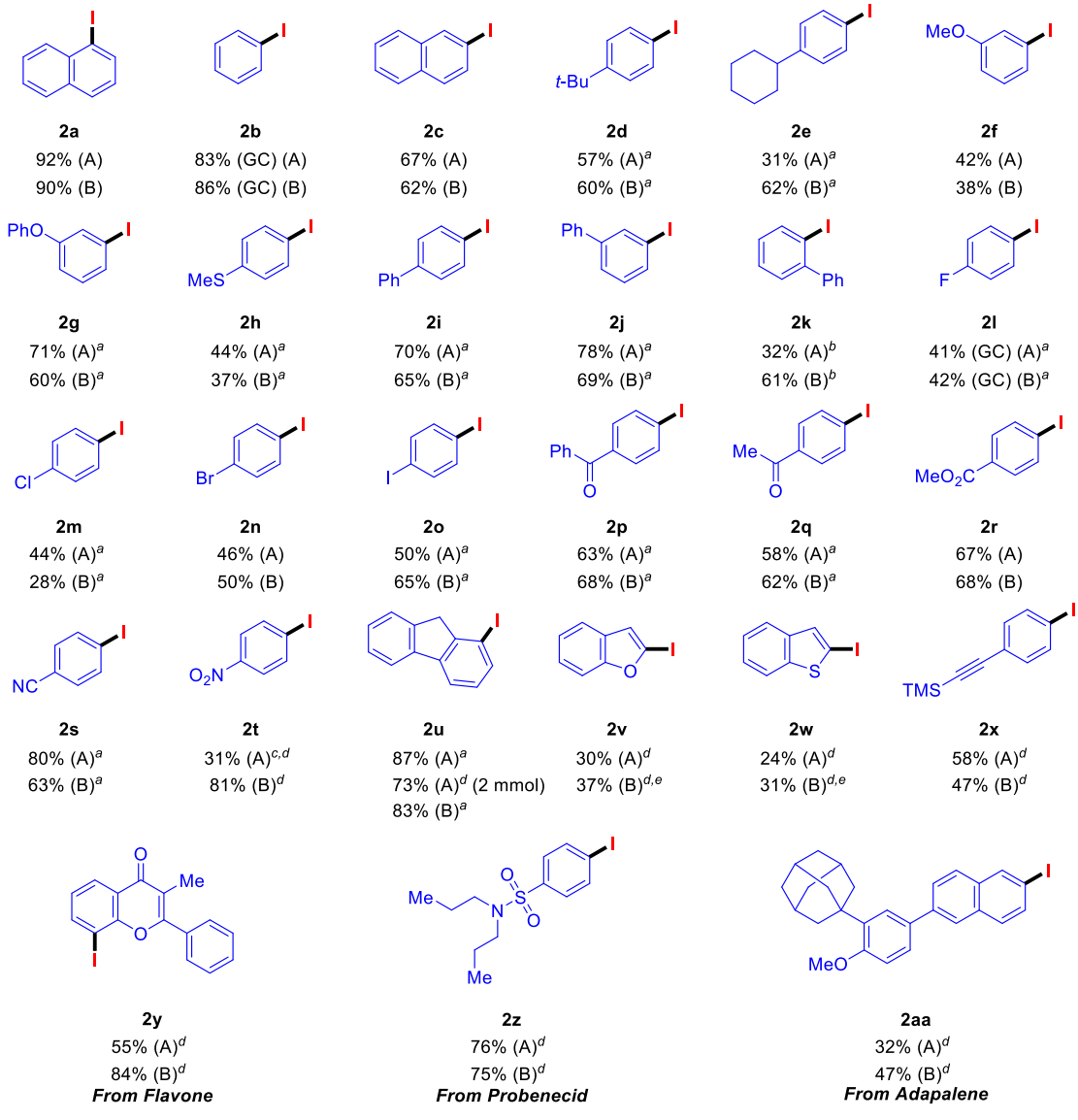

Condition A: acyl fluorides **1** (0.2 mmol, 1 equiv), $[PdCl(cinnamyl)]_2$ (2.5 mol %), Xantphos (12.5 mol %), LiI (1.1 equiv), toluene (0.2 M), 100 °C, 24 h. **Condition B**: acyl chlorides **1'** (0.2 mmol, 1 equiv), $[PdCl(cinnamyl)]_2$ (2.5 mol %), Xantphos (12.5 mol %), NaI (1.1 equiv), toluene (0.2 M), 100 °C, 12 h. Isolated yields were shown unless otherwise indicated. GC yields were determined by using *n*-dodecane as an internal standard. [a] 140 °C, 12 h. [b] Open system, toluene (0.1 M), 120 °C, 12 h. [c] Yields were determined by ^{1}H NMR, using dibromomethane as an internal standard. [d] 140 °C, 24 h. [e] Corresponding acyl chloride (0.4 mmol, 1 equiv).

Substrates containing electron-withdrawing groups, such as carbonyl, cyano, or nitro functionalities, proceeded smoothly to give products **2p**−**2t** in satisfactory yields. Additionally, 1-iodo-9*H*-fluorene (**2u**) was synthesized in an excellent yield. However, certain heterocyclic substrates, including benzofuran and benzo[*b*]thiophene, proved unsuitable in this system. The high electron density of these heterocycles significantly hindered iodination efficiency, leading to decarbonylative hydrogenation at the reactive 2-position as the predominant side reaction.

Remarkably, despite the presence of fluoride ions in the reaction, the silylethynyl group remained unaffected, enabling the isolation of product **2x** with moderate yield. To further expand the scope of this method, acyl fluorides derived from natural products and pharmaceutical compounds were tested. This effort successfully yielded iodo-flavonoid **2y**, a probenecid derivative **2z**, and an adapalene derivative **2aa**, all with moderate to good efficiency.

Importantly, both the acyl fluoride/LiI and acyl chloride/NaI systems delivered comparable outcomes (**Scheme 2-x**), offering flexibility to select between the more chemically stable acyl fluorides or the more accessible acyl chlorides based on specific experimental needs.

2-2-5 Substrate Scope of Decarbonylative Bromination

To further expand the potential of the constructed catalytic system, the Authors also wondered whether the decarbonylation strategy could be applied to decarbonylative nucleophilic bromination. Therefore, after a brief investigation of optimizing the reaction conditions by using 1-naphthoyl fluoride (**1a**) as the substrate and the corresponding LiBr (1.1 equiv) as the bromine source, the Authors were delighted that decarbonylative nucleophilic bromination could be efficiently achieved simply by

increasing the reaction temperature (Table 2-8). After screening the reaction temperature, the results suggested that when the temperature was above 160 °C, the highest efficiency could be afforded and the expected product 1-bromonaphthalene (**4a**) was obtained in 87% yield (Table 2-8, entry 4). Crucially, when 1-naphthoyl chloride (**1a'**) was used as the substrate, the desired decarbonylative bromination product could still be obtained in 79% yield.

Table 2-8. Effect of Temperature for Decarbonylative Bromination.

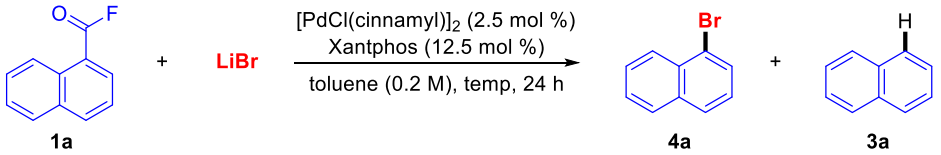

1a (0.2 mmol) (1.1 equiv) **4a** **3a**

entry	**temp (°C)**	**1a** (%)[a]	yield (%)[a]	
			4a	**3a**
1	100	82	<1	<1
2	120	30	7	<1
3	140	9	42	<1
4	**160**	**0**	**87**	**<1**
5	170	0	88	<1

Reaction condition: **1a** (0.2 mmol, 1 equiv), $[PdCl(cinnamyl)]_2$ (2.5 mol %), Xantphos (12.5 mol %), LiBr (0.22 mmol), 24 h, under N_2. [a] NMR yields were determined by ^1H NMR using dibromomethane as the internal standard.

Subsequently, considering the broad range of substrates anticipated to be compatible, a selection of compounds was investigated to verify their applicability to this bromination method. As anticipated, all tested substrates, regardless of the presence or absence of substituents, produced the desired products **4a**–**4k** with yields ranging from moderate to good (**Scheme 2-9**). Notably, the efficiency of bromination followed a pattern similar to that observed for iodination, where both the type and position of substituents were influential in determining the reaction outcome. However, in the case of acyl chlorides,

the current bromination method was predominantly effective only for substrates containing electron-donating groups. For instance, acyl chlorides with substituents like 3-OMe, 3-OPh, and 4-Ph exhibited moderate to high yields in the bromination reaction (**4c**−**4e**). In contrast, other acyl chlorides often resulted in a mixture of brominated and chlorinated products.

Scheme 2-9. Substrate Scope for Decarbonylative Nucleophilic Bromination of Acyl Fluorides **1** and Acyl Chlorides **1'**.

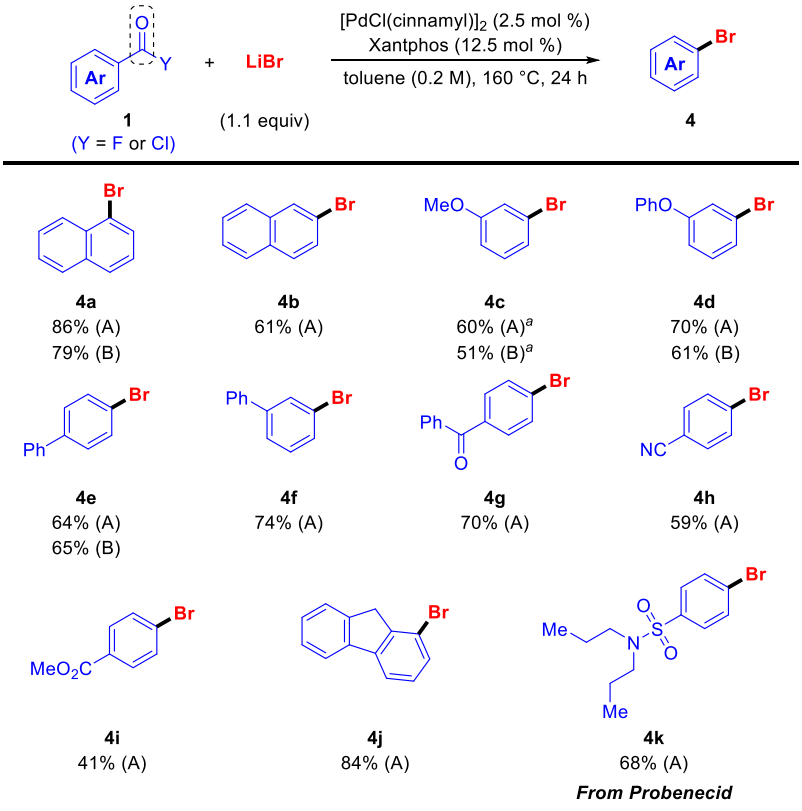

Condition A: acyl fluorides **1** (0.2 mmol, 1 equiv) were used as the substrates. **Condition B**: acyl chlorides **1'** (0.2 mmol, 1 equiv) were used as the substrates. $[PdCl(cinnamyl)]_2$ (2.5 mol %), Xantphos (12.5 mol %), LiBr (1.1 equiv), toluene (0.2 M), 160 °C, 24 h. Isolated yields were shown. [a] Yields were determined by ^1H NMR, using dibromomethane as an internal standard.

In conclusion, acyl fluorides were determined to be the more suitable substrates for achieving efficient and selective bromination under these conditions.

2-2-6 Substrate Scope of Decarbonylative Chlorination

Finally, after a brief investigation of the optimization of the reaction conditions by using 1-naphthoyl fluoride (**1a**) as substrate and corresponding LiCl as chlorine source, surprisingly, the developed Pd-catalyzed system can still be applied to decarbonylative nucleophilic chlorination (Table 2-9). Although the UFC of acyl chloride **1'** has been documented before,[17] the Author's research focuses on the use of acyl fluoride **1**. However, considering the low solubility and weak nucleophilicity of LiCl, the protocol requires not only an increase in temperature but also an increase in the amount of LiCl, which can afford the highest efficiency and obtain the desired product 1-chloronaphthalene (**5a**) in 79% yield (Table 2-9, entry 5).

Table 2-9. Effect of Temperature and Equivalents of LiCl for Decarbonylative Chlorination.

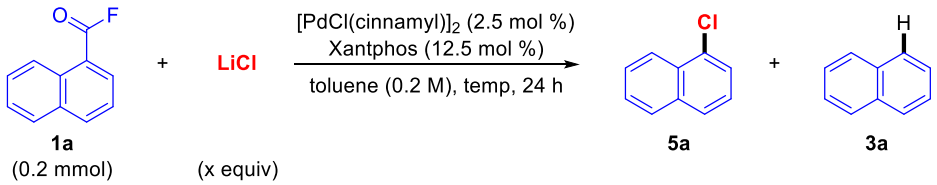

1a (0.2 mmol) (x equiv) **5a** **3a**

entry	temp (°C)	LiCl (x equiv)	1a (%)[a]	yield (%)[a]	
				5a	**3a**
1	150	1.1	37	42	<1
2	160	1.1	24	56	<1
3	170	1.1	26	57	<1
4	160	2	2	73	<1
5	**160**	**3**	**6**	**79**	**<1**

Reaction condition: **1a** (0.2 mmol, 1 equiv), $[PdCl(cinnamyl)]_2$ (2.5 mol %), Xantphos (12.5 mol %), 24 h, under N_2. [a] NMR yields were determined by ^1H NMR using dibromomethane as the internal standard.

Subsequent substrate screening revealed that a diverse array of compounds, both electronically and structurally, were compatible, delivering the corresponding chloroarenes **5** with moderate to good yields (**Scheme 2-10**). Although decarbonylative fluorination

remains a significant hurdle, the robust catalytic methodology established here enables the systematic synthesis of halogenated products from the same starting materials. This process utilizes cost-effective and user-friendly lithium and sodium salts while maintaining consistent reaction conditions, underscoring its practical and versatile application.

Scheme 2-10. Substrate Scope for Decarbonylative Nucleophilic Chlorination of Acyl Fluorides **1**.

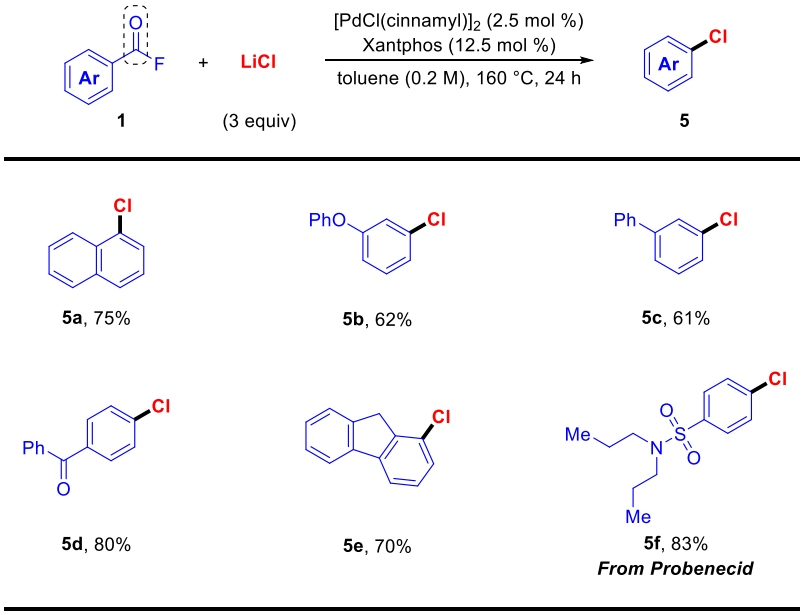

Reaction conditions: **1** (0.2 mmol, 1 equiv), $[PdCl(cinnamyl)]_2$ (2.5 mol %), Xantphos (12.5 mol %), LiCl (3 equiv), toluene (0.2 M), 160 °C, 24 h. Isolated yields were shown.

2-2-7 Mechanistic Study

To gain deeper insights into the mechanism of Pd-catalyzed decarbonylative nucleophilic halogenation of acyl fluorides (**1**) and chlorides (**1'**), the Author conducted mechanistic investigations using iodination as a representative reaction. Initially, the decarbonylative iodination of benzoyl fluoride (**1b**) was monitored at room temperature, 50 °C, and 100 °C via $^{31}P\{^{1}H\}$ NMR spectroscopy (**Scheme 2-11**).

Scheme 2-11. Monitoring the Catalytic Iodination of **1b** at Room Temperature, 50, and 100 °C by $^{31}P\{^{1}H\}$ NMR.

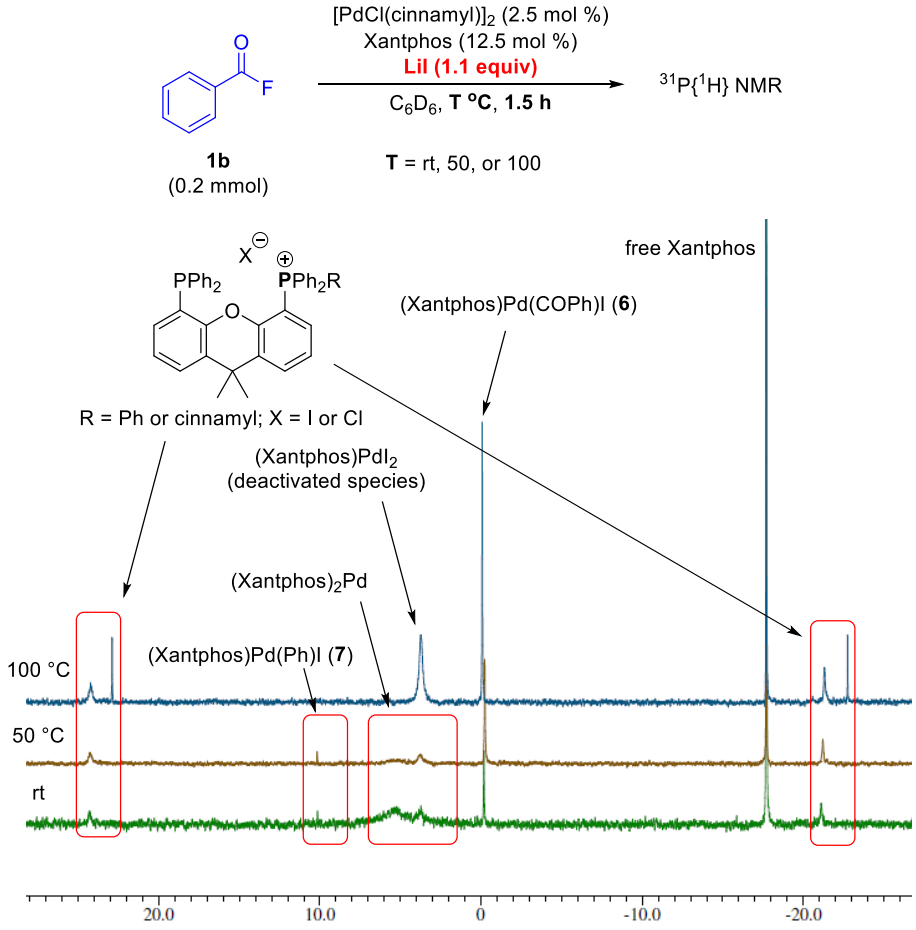

Three palladium intermediates were identified: (Xantphos)Pd(II)(COPh)I (**6**) at −0.3 ppm, $(Xantphos)_2Pd(0)$ at 3.5 and 5.2 ppm (two broad multiplets), and (Xantphos)Pd(II)(Ph)I (**7**) at 10.0 ppm. In parallel, the Authors also performed stoichiometric time-course studies to monitor possible intermediates during the experiment (**Scheme 2-12**). The results also suggested the same results as in the catalytic time-course studies. The signals for these intermediates were assigned by either preparing authentic samples or by comparison with previously reported data.[13,14,19]

Scheme 2-12. Monitoring the Stoichiometric Iodination of **1b** at Room Temperature, 50, and 75 °C by $^{31}P\{^{1}H\}$ NMR.

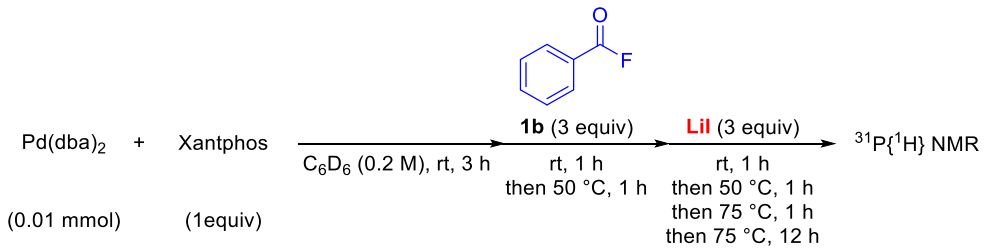

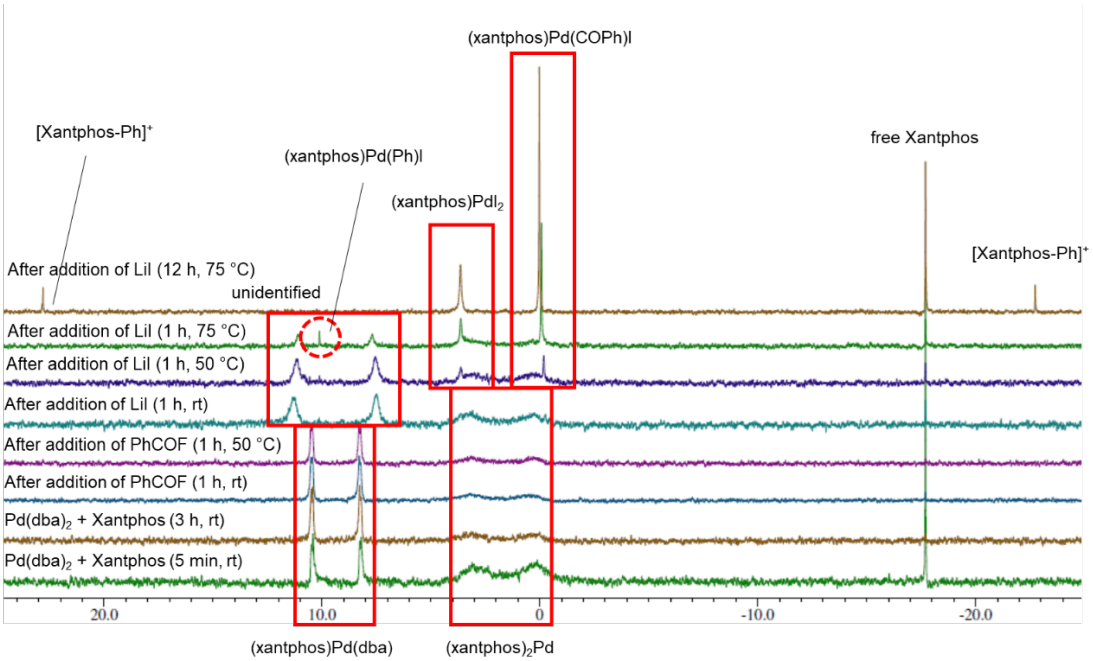

Complex **6** appeared to be a plausible resting state, while the other intermediates were predominantly observed during the initial stages of the reaction. To confirm the involvement of complexes **6** and **7** in the catalytic cycle, both were synthesized according to established methods and tested as catalysts for the iodination of acyl fluoride **1b** (Table 2-10). The expected product **2b** was obtained in all cases, regardless of the presence of an additional Xantphos ligand, confirming the intermediacy of complexes **6** and **7** in the reaction.

Table 2-10. Catalytic Reaction with Pd Complexes **6** and **7**.

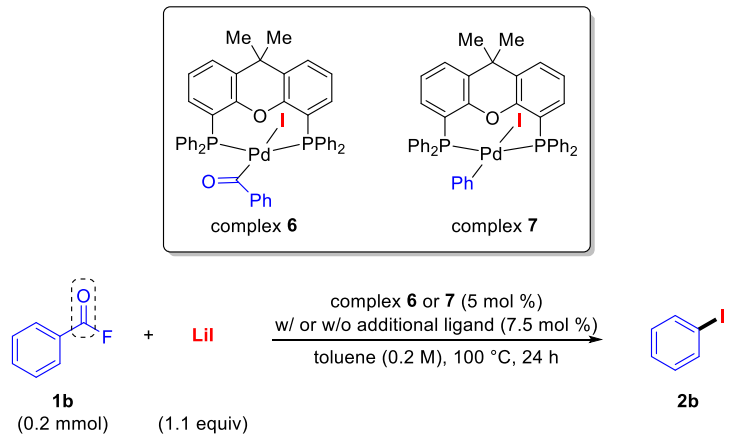

entry	Pd complex	additional ligand	yield of **2b** (%)[a]
1	**6**	Xantphos (7.5 mol %)	92
2	**6**	none	77[b]
3	**7**	Xantphos (7.5 mol %)	92
4	**7**	none	41[b]

Reaction conditions: **1b** (0.2 mmol, 1 equiv), Pd complex (5 mol %), LiI (1.1 equiv), toluene (0.2 M), 100 °C, 24 h. [a] Yields were determined by GC, using n-dodecane as an internal standard. [b] Average values of two experiments.

However, a lower yield of **2b** was observed in the absence of an external Xantphos ligand, suggesting that the ligand enhances catalytic turnover (Table 2-10, entry 2). Furthermore, while the yield of **2b** was similar with or without added Xantphos in the case of complex **7** (Table 2-10, entry 3), the yield was lower for complex **7** than for complex **6** without external Xantphos. This indicates that, in the absence of added Xantphos, CO eliminated from complex **6** coordinates with the palladium center, stabilizing the catalyst. It is proposed that both added Xantphos and the carbonyl ligands stabilize Pd(0) species formed after reductive elimination of Ar–I, enhancing the catalytic cycle's efficiency.[4,13,14,15,20]

Scheme 2-13. Catalytic Reaction with Pd Complex (Xantphos)PdI_2.

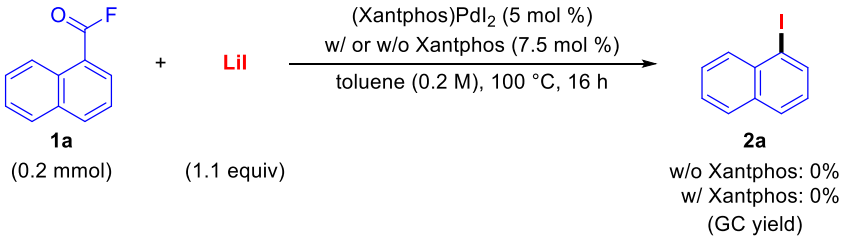

Additionally, the (Xantphos)Pd(II)I_2 complex, observed at 3.8 ppm, was found to be completely inactive with or without additional Xantphos as the ligand (**Scheme 2-13**).

Scheme 2-14. Reaction details of 4-Methoxybenzoyl Fluoride as the Substrate.

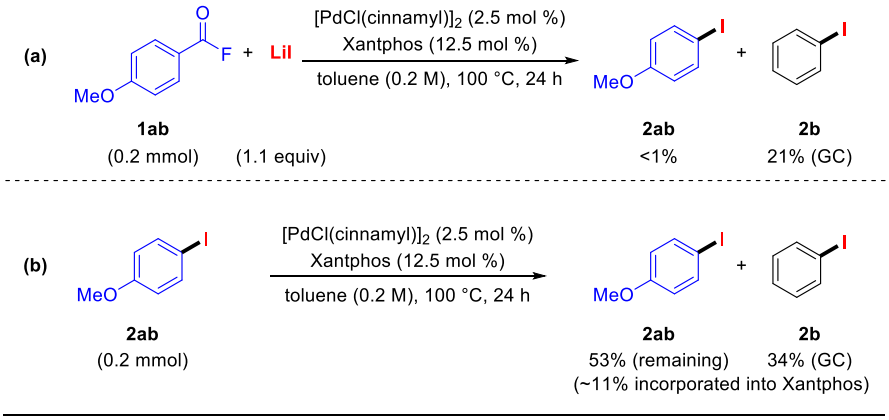

Suspiciously, when 4-methoxybenzoyl fluoride (**1ab**) was used as the substrate, the desired product, 4-methoxyiodobenzene (**2ab**), was scarcely formed, with iodobenzene (**2b**) being obtained in a 21% yield (**Scheme 2-14(a)**). Moreover, under standard reaction conditions, **2ab** itself was consumed, resulting in the formation of **2b** in a 34% yield (**Scheme 2-14(b)**). These findings, consistent with previous observations, suggest a phosphonium-mediated reversible mechanism involving reductive elimination and oxidative addition of the C(aryl)−P bond.[14]

Scheme 2-15. Possible Mechanism on Xantphos-mediated Scrambling Aryl and Phenyl Group.

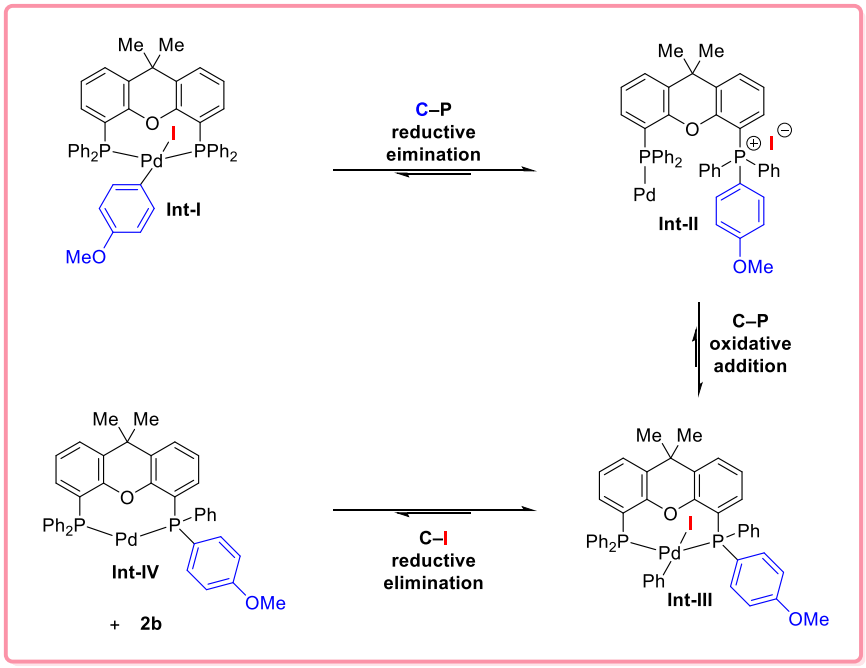

As depicted in **Scheme 2-15**, oxidative addition of **2ab** to (Xantphos)Pd(0) generates intermediate **Int-I**. Reductive elimination, driven by the electron-rich *p*-anisyl group and the formation of a carbon–phosphorus bond, then produces phosphonium salt-ligated Pd complex **Int-II**. Subsequent oxidative addition of the less electron-rich Ph group forms intermediate **Int-III**. This intermediate undergoes reductive elimination, creating a carbon−iodine bond and yielding **2b**. This proposed mechanism explains the lower yields of target products when using electron-rich substrates.

The presence of phosphonium salts is further supported by $^{31}P\{^{1}H\}$ NMR spectra shown in **Scheme 2-11**, where a signal at −22 ppm corresponds to phosphine and a signal around 24 ppm is attributed to phosphonium, observed in approximately a 1:1 ratio. It is plausible that the scrambling of aryl groups proceeds through an outer-sphere nucleophilic substitution pathway, consistent with the mechanism proposed by Morandi.[13,14]

Scheme 2-16. Control Experiment on the Formation of Acyl Iodide without Catalyst and Ligand.

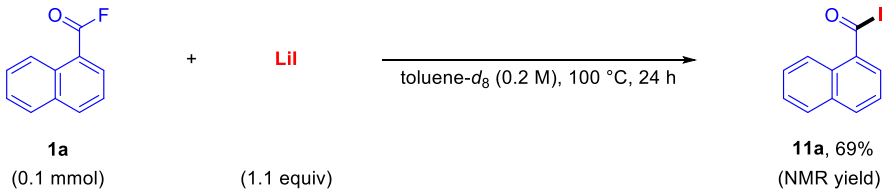

From another perspective, intermediate complex **6** is noteworthy, as it forms not only via the rapid oxidative addition of benzoyl fluoride followed by halogen exchange between fluorine and iodine but also through the oxidative addition of acyl iodides generated in situ, as evidenced by subsequent experiments. The reaction pathway proposed involves acyl iodides as transient intermediates, which then undergo decarbonylative UFC to establish aryl iodides. Control experiments conducted without [PdCl(cinnamyl)]$_2$ and Xantphos revealed that 1-naphthoyl fluoride (**1a**) reacts with LiI, yielding 1-naphthoyl iodide (**11a**) at 69% NMR efficiency (**Scheme 2-16**).

Scheme 2-17. Pd-catalyzed Decarbonylative Unimolecular Fragment Coupling (UFC) of Acyl Iodides.

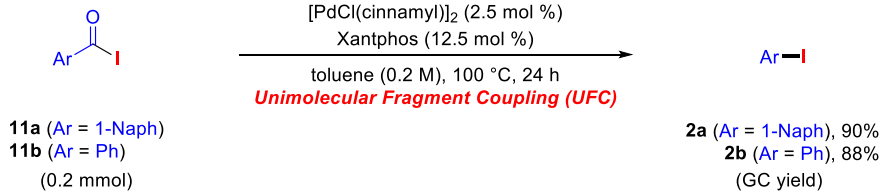

Similarly, when 1-naphthoyl iodide (**11a**) and benzoyl iodide (**11b**) were utilized as starting materials under standard conditions but without additional LiI, the products 1-iodonaphthalene (**2a**) and iodobenzene (**2b**) were obtained in 90% and 88% GC yields, respectively (**Scheme 2-17**). These findings strongly support the hypothesis that aryl iodides are generated through Pd-catalyzed UFC of the acyl iodides formed during the reaction, with acyl fluorides acting as facilitators. In contrast to conventional methods requiring elevated temperatures and catalysis by Wilkinson's catalyst,[21] this new approach

offers milder conditions and more stable starting materials, marking a significant improvement in aryl iodide synthesis.

Table 2-11. Stepwise Experiments on Acyl Fluorides or Chlorides with Different Iodine Salts.

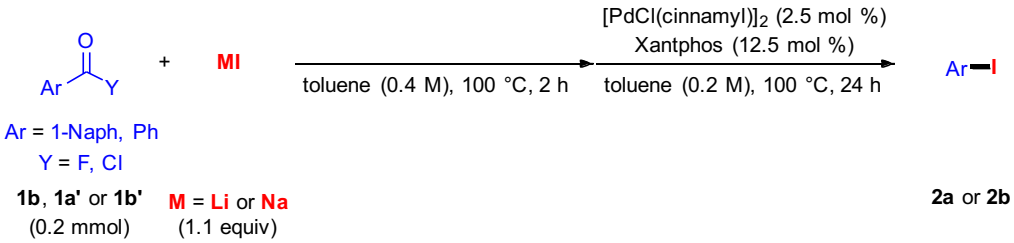

entry	**acyl halide**	**MI**	yield of **2** (%)[a]	*cf.*) yield of **2** under standard conditions (%)	*cf.*) yield of **2** under UFC conditions (%)
1	benzoyl fluoride (**1b**)	LiI	82	83	88
2	1-naphthoyl chloride (**1a'**)	NaI	96	90	84
3	benzoyl chloride (**1b'**)	NaI	77	86	88
4	1-naphthoyl chloride (**1a'**)	LiI	2	22	84
5	benzoyl chloride (**1b'**)	LiI	3	45	88

Reaction conditions: **1** (0.2 mmol, 1 equiv), **MI** (0.22 mmol), $[PdCl(cinnamyl)]_2$ (5 mol %), Xantphos (12.5 mol %), toluene (0.2 M), 100 °C, 24 h. [a] Yields were determined by GC, using *n*-dodecane as an internal standard.

Interestingly, **11a** was also generated from 1-naphthoyl chloride (**1a'**) in the presence of both LiI and NaI. However, under standard reaction conditions, the combination of **1a'** and LiI produced significantly lower yields of **2a** compared to **1a'**/NaI (Table 2-7, entries 1 and 2). To clarify this discrepancy, sequential experiments were carried out where acyl halides **1** and alkali metal iodides were heated at 100 °C for 2 h before catalyst introduction (Table 2-11). The expected outcomes were observed: acyl fluoride/LiI and

acyl chloride/NaI combinations yielded high amounts of the desired product **2** (Table 2-11, entries 1−3), while the acyl chloride/LiI system produced only negligible quantities (Table 2-11, entries 4 and 5).

Scheme 2-18. Monitoring Experiments on the Effect of Different Iodine Salts on the Decarbonylative Iodination of Benzoyl Chloride (**1b'**).

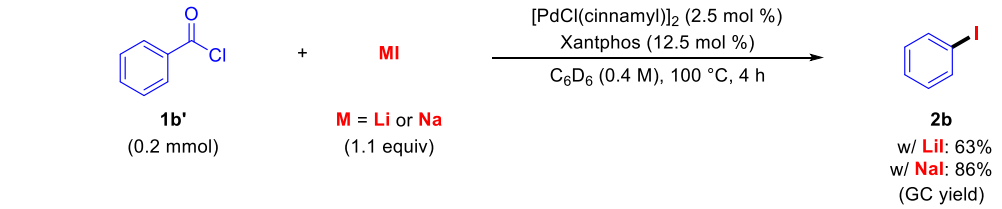

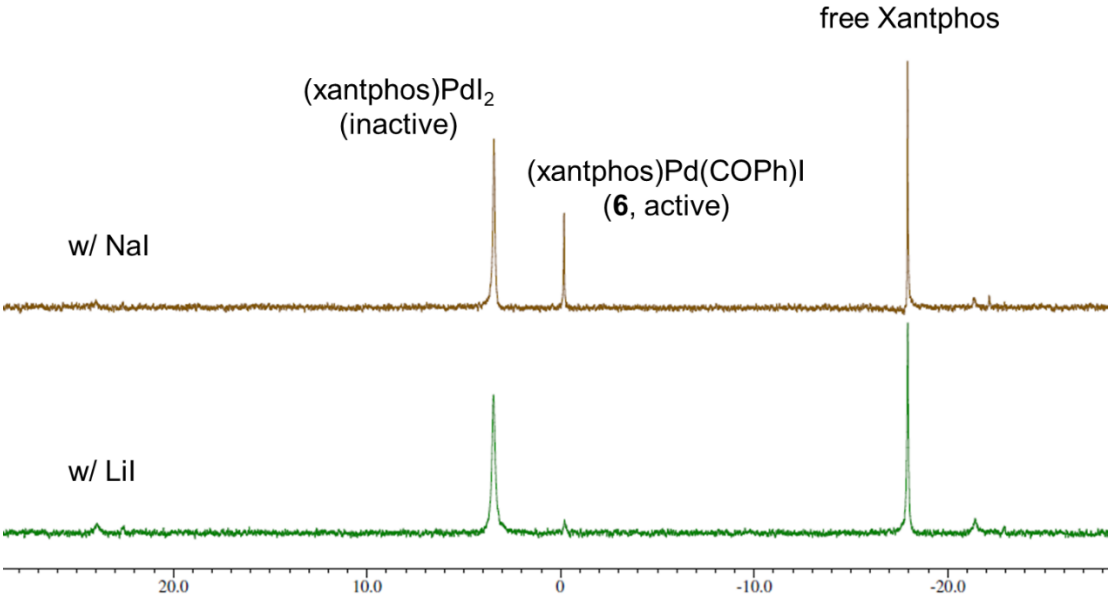

Notably, yields from the stepwise approach were even lower than those obtained using standard conditions (22% and 45% for **2a** and **2b**, respectively) (see Table 2-11, entries 4 and 5, for details). This suggests the formation of a catalyst poison during the reaction of acyl chlorides with LiI. Supporting this, the reaction of **1b'** with LiI under standard conditions significantly reduced the active (Xantphos)Pd(II)(COPh)I (**6**), whereas **6** remained unaffected in the **1b'**/NaI system (**Scheme 2-18**).

Scheme 2-19. Stepwise Experiments with Vacuum Procedures.

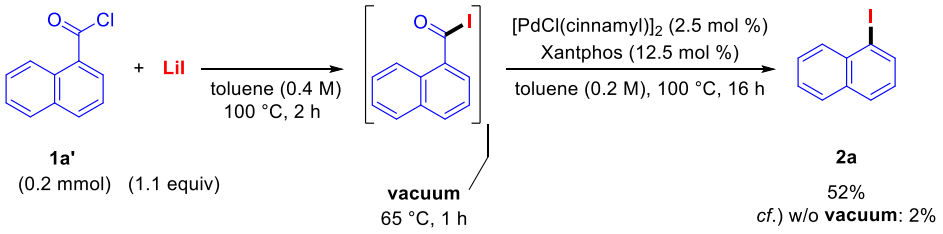

As shown in the scheme above (**Scheme 2-18**), the only inactive species identified in the acyl chloride **1'**/LiI reaction system is (Xantphos)PdI_2, therefore, this means a reasonable speculation: molecular iodine (I_2) may be a catalyst poison. On this basis, the Authors performed a stepwise reaction of 1-naphthoyl chloride (**1a'**) with LiI using a vacuum process (**Scheme 2-19**). Surprisingly, the yield of desired product **2a** was significantly improved compared to that without vacuum operation, which further confirmed this hypothesis.

Scheme 2-20. Controlled Experiments on Iodine (I_2) as a Possible Catalyst Poison.

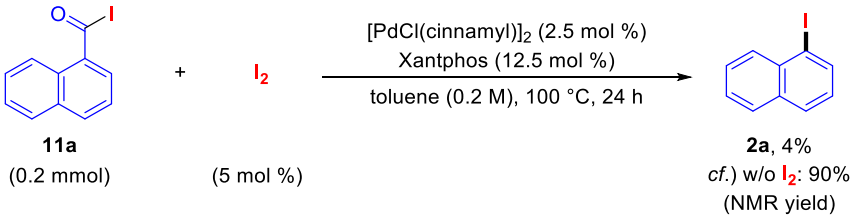

Additionally, small amounts of added iodine almost completely inhibited the UFC of 1-naphthoyl iodide (**11a**) (**Scheme 2-20**). $^{31}P\{^{1}H\}$ NMR analysis with benzoyl iodide (**11b**) as the substrate showed that iodine completely deactivated the Pd catalyst, leaving no trace of active species **6** (**Scheme 2-21**).

Scheme 2-21. Monitoring Experiments on the Effect of Iodine (I_2) as a Possible Catalyst Poison on Pd-catalyzed UFC of Benzoyl Iodide (**11b**).

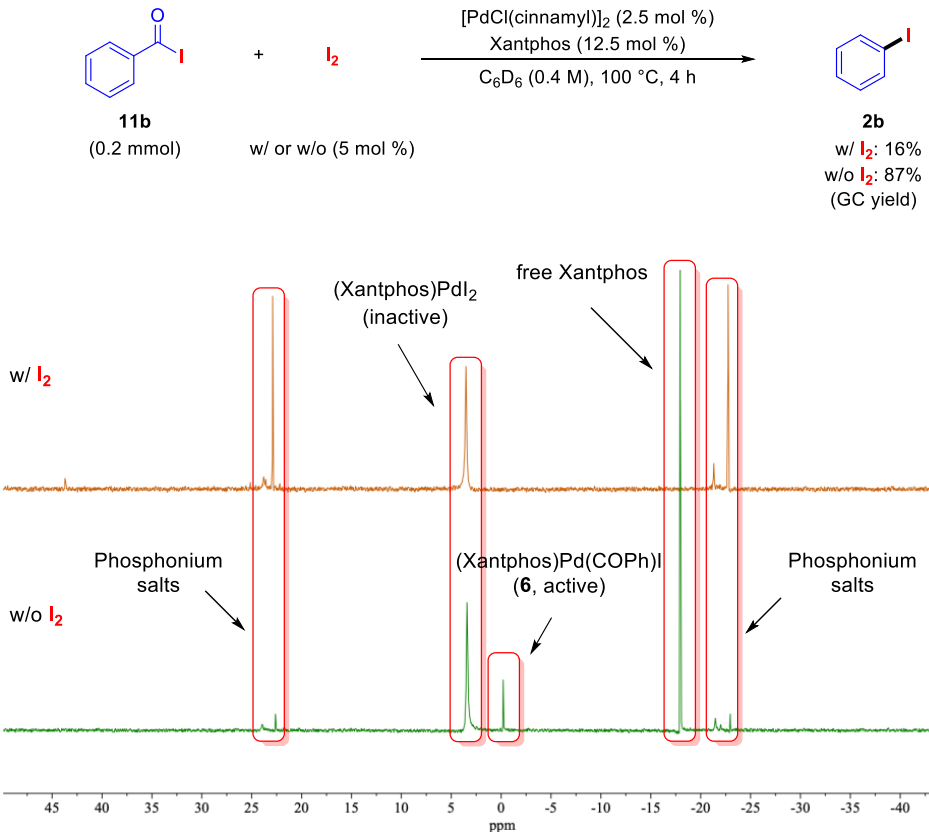

Furthermore, the possibility of (Xantphos)PdI_2 forming via disproportionation of the potential intermediate (Xantphos)Pd(Ph)I (**7**) is unlikely, as no biaryl formation was detected.

Table 2-12. Time-course Study of 1-Naphthoyl Fluoride (**1a**)/LiI Combination.

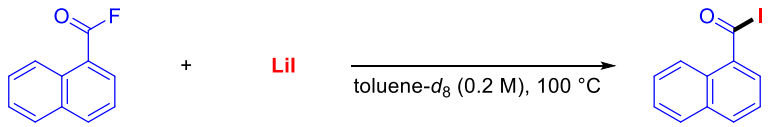

1a (0.1 mmol) (1.1 equiv) **11a**

entry	time (h)	yield of **1a** (%)[a]	yield of **11a** (%)[a]
1	0	>99	<1
2	0.5	87	13
3	1	71	29
4	2	46	44
5	3	31	47
6	6	4	65
7	12	0	68
8	24	0	69

Reaction conditions: **1a** (0.1 mmol, 1 equiv), LiI (0.11 mmol), toluene-d_8 (0.2 M), 100 °C. [a] Yields were determined by ^{1}H NMR, using dibromomethane as an internal standard.

Table 2-13. Time-course Study of 1-Naphthoyl Chloride (**1a'**)/NaI Combination.

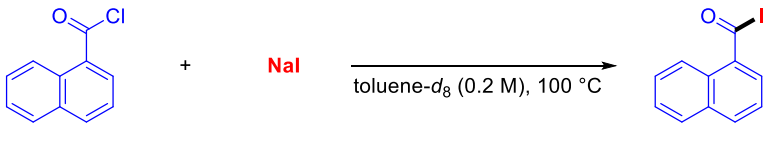

1a' (0.1 mmol) (1.1 equiv) **11a**

entry	time (h)	yield of **1a'** (%)[a]	yield of **11a** (%)[a]
1	0	>99	<1
2	0.5	87	13
3	1	75	27
4	2	60	44
5	3	48	52
6	6	37	67
7	18	27	81

Reaction conditions: **1a'** (0.1 mmol, 1 equiv), NaI (0.11 mmol), toluene-d_8 (0.2 M), 100 °C. [a] Yields were determined by ^{1}H NMR, using dibromomethane as an internal standard.

Table 2-14. Time-course Study of 1-Naphthoyl Chloride (**1a'**)/LiI Combination.

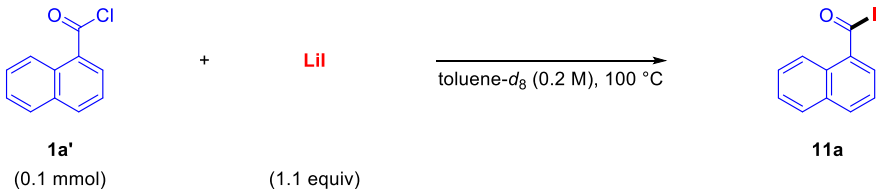

1a' (0.1 mmol) (1.1 equiv) **11a**

entry	time (h)	yield of **1a'** (%)[a]	yield of **11a** (%)[a]
1	0	>99	<1
2	0.5	67	33
3	1	42	54
4	2	17	74
5	3	12	78
6	6	11	76
7	18	12	78

Reaction conditions: **1a'** (0.1 mmol, 1 equiv), LiI (0.11 mmol), toluene-d_8 (0.2 M), 100 °C. [a] Yields were determined by ^{1}H NMR, using dibromomethane as an internal standard.

To explore the mechanism behind the formation of the catalytic inhibitor iodine, several time-dependent studies were performed to assess the rate of acyl iodide production using different combinations of acyl halides and iodide salts. The data revealed that the formation rates of acyl iodide were similar (approximately 28% after 1 hour) in the systems of 1-naphthoyl fluoride (**1a**) with LiI and 1-naphthoyl chloride (**1a'**) with NaI. However, the combination of 1-naphthoyl chloride (**1a'**) and LiI led to a much faster production of **11a**, reaching about 54% within 1 hour (Tables 2-12, 13 and 14, and **Scheme 2-22**).

Scheme 2-22. Comparison of the Formation Rates of 1-Naphthoyl Iodide (**11a**).

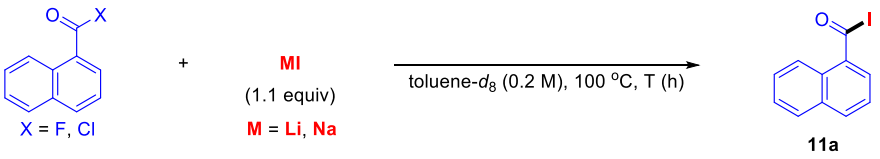

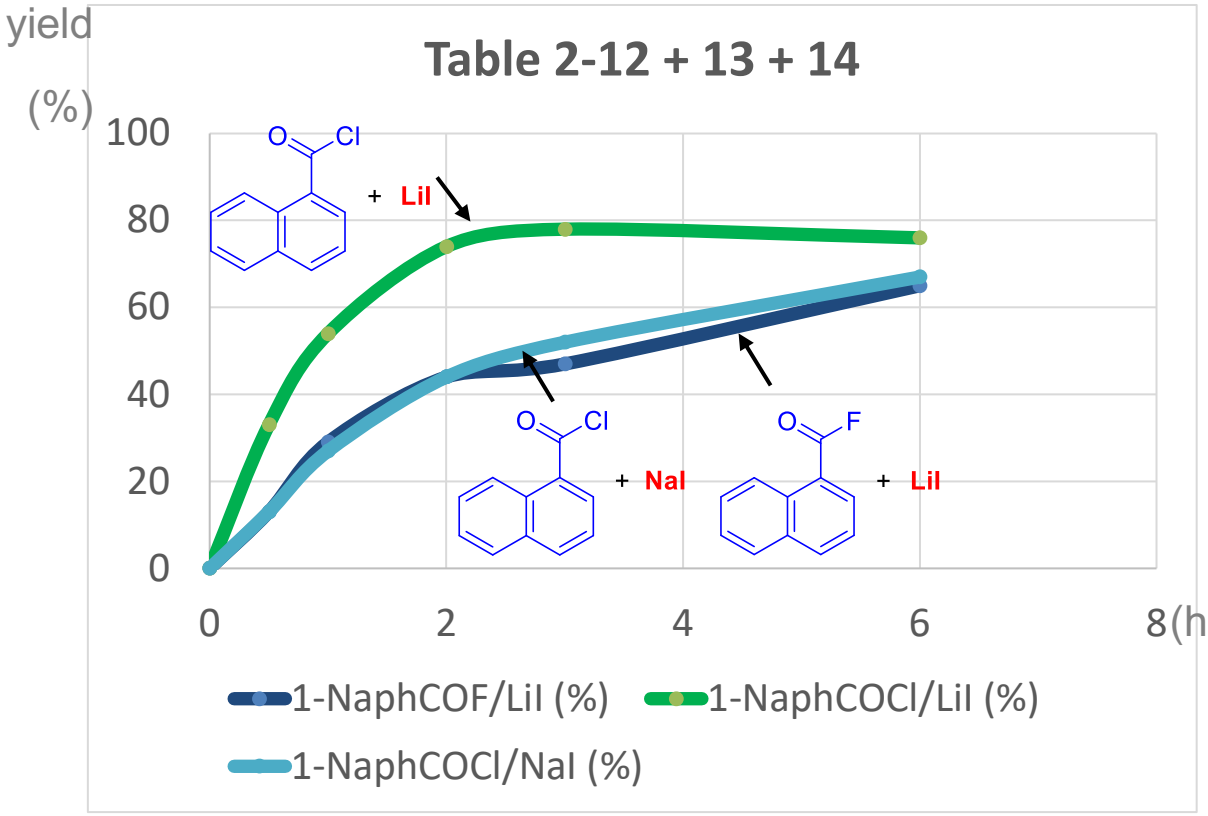

These observations suggest that a gradual formation of acyl iodides is crucial for effective catalysis. Conversely, a rapid accumulation of acyl iodides results in the creation and build-up of a catalytic inhibitor. Since the catalytic reaction was not halted by acyl iodide alone (**Scheme 2-17**), it was hypothesized that the catalyst poison could form from a combination of halide salts and acyl iodide.

Table 2-15. Effect of Li Salts on Pd-catalyzed Decarbonylative UFC of Acyl Iodides.

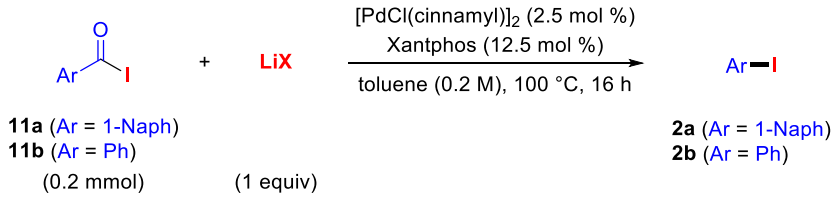

11a (Ar = 1-Naph)
11b (Ar = Ph)
(0.2 mmol)

(1 equiv)

2a (Ar = 1-Naph)
2b (Ar = Ph)

entry	LiX	yield of **2a** (%)[a]	yield of **2b** (%)[a]	*cf.)* yield of **2a** under standard conditions (%)	*cf.)* yield of **2b** under standard conditions (%)
1	none	73	87		
2	LiF	82	82		
3	LiCl	85	86	22	45
4	LiI	52	95	(1-naphthoyl	(benzoyl
5	LiF (0.5 equiv) + LiI (0.5 equiv)	38	97	chloride/LiI system)	chloride/LiI system)
6	LiCl (0.5 equiv) + LiI (0.5 equiv)	41	96		

Reaction conditions: **11** (0.2 mmol, 1 equiv), LiX (0.2 mmol), $[PdCl(cinnamyl)]_2$ (5 mol %), Xantphos (12.5 mol %), toluene (0.2 M), 100 °C, 16 h. [a] Yields were determined by GC, using *n*-dodecane as an internal standard.

To test this, the impact of additional lithium halide on the UFC of acyl iodides was evaluated (Table 2-15). When the Authors screened different lithium salts as exogenous additives, it was suggested that when 1-naphthoyl iodide (**11a**) was used as the reaction substrate, the addition of exogenous lithium iodide would significantly weaken the efficiency of decarbonylative iodination (Table 2-15, entries 4–6). This is consistent with previous reaction results. Because if the formation rate of acyl iodide is too fast, it will accumulate, so that it can fully coexist with the remaining LiI, thus forming a large number of catalytic poisons and deactivating the catalytic system. The findings indicate that LiI plays a significant role in reducing yield.

Table 2-16. Effect of Catalyst Poisoning Process on Preheating Experiments of Pd-catalyzed UFC.

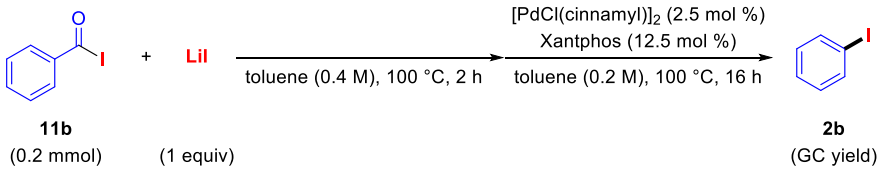

entry	preheating	yield of **2b** (%)[a]
1	benzoyl iodide (**11b**)	89
2	LiI	91
3	benzoyl iodide (**11b**) and LiI	15
4	none	87

Reaction conditions: **11b** (0.2 mmol, 1 equiv), LiI (0.2 mmol), $[PdCl(cinnamyl)]_2$ (5 mol %), Xantphos (12.5 mol %), toluene (0.2 M), 100 °C, 16 h. [a] Yields were determined by GC, using *n*-dodecane as an internal standard.

This deactivation effect was especially evident when acyl iodide and LiI were heated together prior to initiating the catalytic reaction, causing a marked decrease in efficiency (Table 2-16, entry 3). However, preheating either benzoyl iodide (**11b**) or LiI alone did not negatively affect the desired transformation (Table 2-16, entries 1, 2 and 4).

These results imply that heating a mixture of acyl iodide and LiI leads to the formation of a catalytic inhibitor, likely I_2, via a complex pathway, which in turn deactivates the catalytic system. In conclusion, the experiments suggest that in the non-catalytic reaction between acyl chloride and LiI, rapid accumulation of acyl iodide and LiI results in the production of a substantial amount of the catalytic inhibitor I_2. On the other hand, reactions involving acyl fluoride with LiI or acyl chloride with NaI proceed more slowly, allowing the acyl iodide to be efficiently consumed by the Pd catalyst as it forms.

2-2-8 Proposed Mechanism

Based on the experimental results discussed above, the Author logically proposes two possible mechanisms for decarbonylative nucleophilic halogenation (**Scheme 2-x**). In

pathway A, Pd(0) species **A** initiates oxidative addition with acyl fluoride **1** or chloride **1'**, forming the acyl−Pd(II)−Y complex **B** (where Y represents F or Cl). This complex undergoes reductive elimination of the C−P bond, similar to the mechanism shown in **Scheme 2-23**, producing the phosphonium halide intermediate **C**.[22] Next, **C** undergoes halogen exchange through an outer-sphere nucleophilic substitution reaction with lithium or sodium halide, yielding the corresponding phosphonium halide **D**. This leads to the formation of acyl−Pd−X complex **E** via oxidative addition of the C−P bond. The Xantphos ligand, acting as a hemilabile monodentate ligand in the square planar Pd(II) species **F**, facilitates partial CO deinsertion, promoting the reductive elimination of the C−X bond. This step produces the desired halogenated products **2**, **4**, and **5**, while simultaneously regenerating the Pd(0) catalyst **A**. The steric bulk of the Xantphos bidentate ligands hinders the Pd center, delaying reverse oxidative addition of the products **2**, **4**, and **5**. Additionally, the acyl−Pd−X complex **E** is thermodynamically more stable than the aryl−Pd−X complex **F** according to the DFT calculation, indicating that **E** may serve as a resting state within the catalytic cycle.

Scheme 2-23. Two Plausible Reaction Mechanisms.

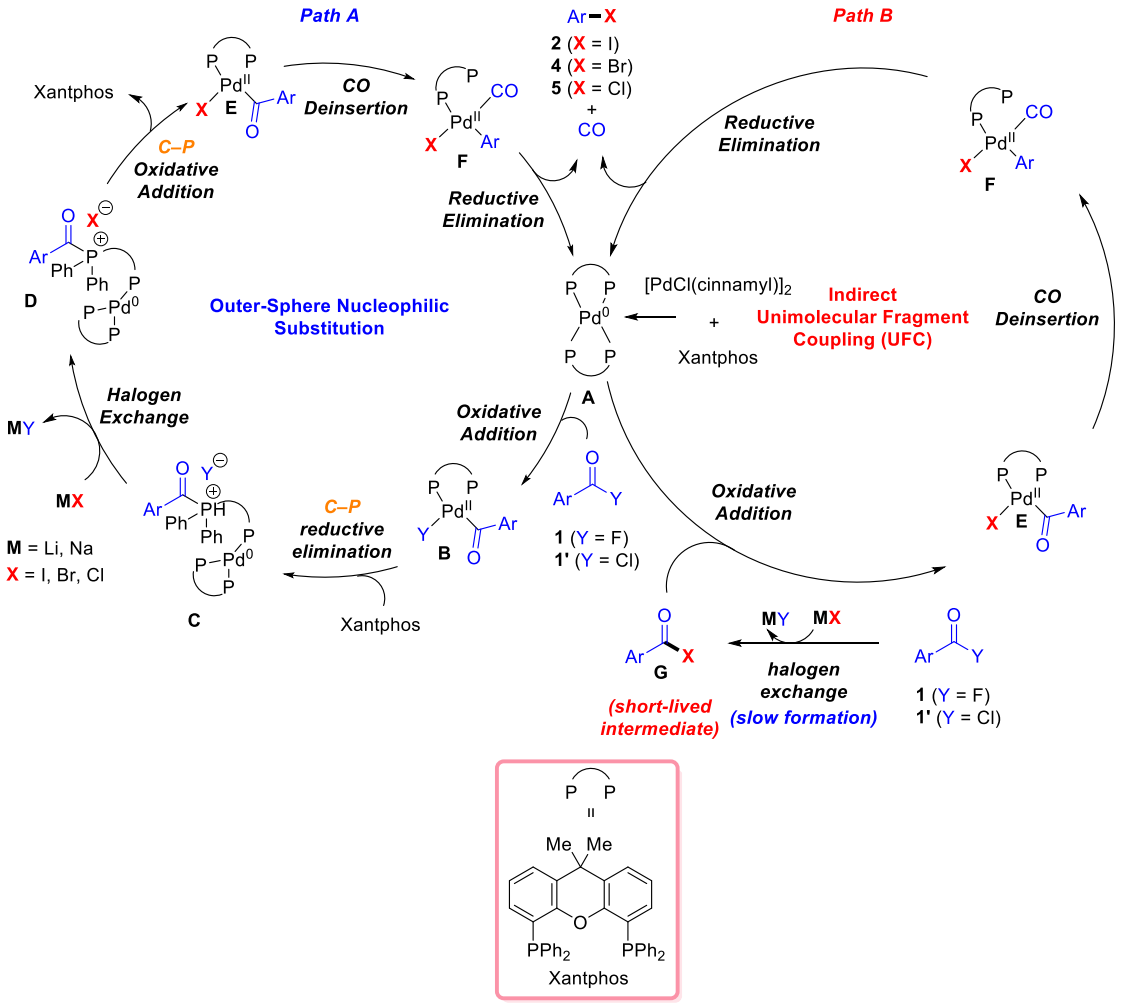

In pathway B, acyl fluoride **1** or chloride **1'** reacts directly with alkali metal halides, gradually forming the corresponding acyl halides **G** (notably acyl iodides) in situ. These reactive species undergo oxidative addition with Pd(0), forming the acyl complex **E**. Subsequent CO deinsertion generates the aryl complex **F**, followed by reductive elimination of the C−X bond to produce the desired halogenated products. An alternative mechanism could involve direct oxidative addition of acyl fluoride **1** or chloride **1'** to palladium, followed by halogen exchange on the palladium center. However, as demonstrated in **Scheme 2-11**, no palladium−fluoride species were detected in the $^{31}P\{^{1}H\}$ NMR spectrum. Furthermore, the stoichiometric reaction of acyl fluoride

1 with the palladium complex in the absence of iodine did not yield any oxidative adduct. Thus, this pathway can be excluded at this stage.

2-3 Summary

In summary, the Authors have successfully established a practical and adaptable palladium-catalyzed method for decarbonylative nucleophilic halogenation of acyl fluorides and chlorides. This catalytic system, utilizing palladium and the large-bite-angle ligand Xantphos, effectively facilitated the challenging reductive elimination of Ar−I, Ar−Br, and Ar−Cl bonds, enabling the efficient synthesis of a wide range of aryl halides. The use of inexpensive lithium and sodium halides as halogen sources not only enhances economic feasibility but also adheres to green chemistry principles, as these inorganic salts are low-cost and exhibit minimal toxicity.

From a mechanistic perspective, Xantphos served dual functions: acting as a ligand to promote the reductive elimination of C−X bonds and as an active additive facilitating unique outer-sphere nucleophilic substitution through the formation of phosphonium halides. Decarbonylation was a critical component of this process, with the coordination of CO released during the reaction to Pd accelerating the reductive elimination step. Furthermore, the interaction of surplus Xantphos with the Pd(0) species likely inhibited its reversion to (Xantphos)Pd(Ar)X, favoring progression through the catalytic cycle.

Scheme 2-24. Summary of Palladium-catalyzed Decarbonylative Nucleophilic Halogenation of Acyl Halides.

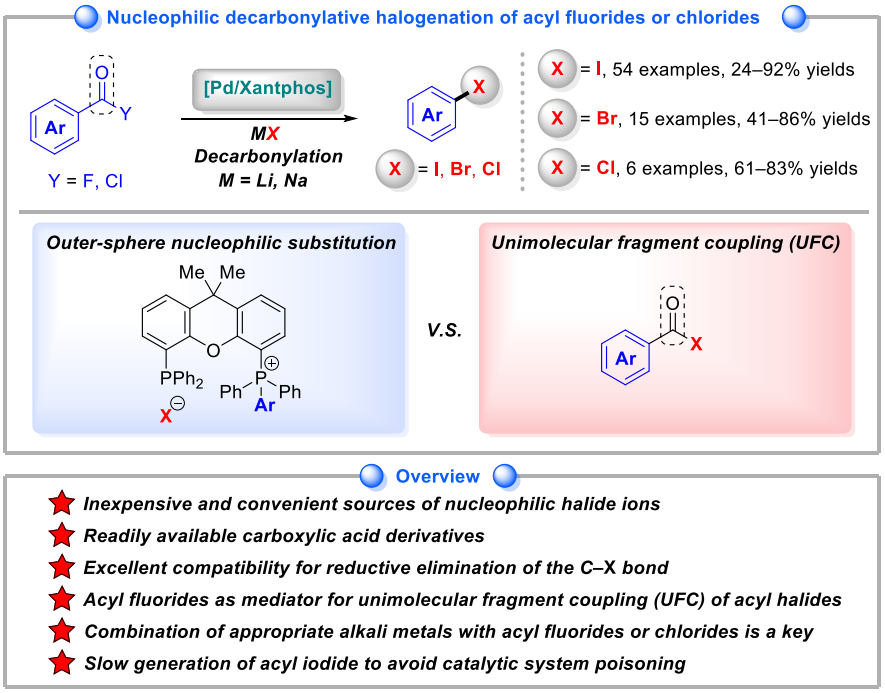

The identification of acyl iodides as key intermediates is a noteworthy advancement. Using stable acyl fluorides and chlorides as precursors, acyl iodides were generated in situ, enabling indirect UFC under mild and practical conditions. The principle of "controlled generation," where highly reactive intermediates are formed and consumed simultaneously, proved to be an effective approach to maintaining catalyst activity and preventing deactivation (**Scheme 2-24**). This synthetic framework offers valuable insights for future studies aimed at tackling complex chemical transformations.

2-4 Experimental Section

2-4-1 General Instrumentation and Chemicals

Instrumentation

Unless otherwise stated, all reactions were carried out under an N_2 atmosphere using standard Schlenk techniques or a glovebox. Solvents employed as eluents for routine operations, as well as dehydrated solvents, were purchased from commercial suppliers and used without any further purification. Glassware was dried in an oven at 130 °C and evacuated before use. Merck precoated TLC plates (silica gel 60 F_{254}, 0.25 mm) were used for thin-layer chromatography (TLC) analyses throughout this work. Silica gel column chromatography was carried out using Silica gel 60 N (spherical, neutral, 40–100 μm) from Kanto Chemicals Co., Ltd. NMR spectra (^{1}H, ^{13}C{1H}, ^{19}F{^{1}H}, and ^{31}P{^{1}H}) were recorded on Mercury-400 (400 MHz) or Mercury-600 (600 MHz) spectrometers. Chemical shifts (δ) are reported in parts per million relative to $CDCl_3$ at 7.26 ppm for ^{1}H and at 77.16 ppm for ^{13}C{^{1}H}, respectively. The ^{19}F{^{1}H} NMR spectra were referenced using CCl_3F (δ = 0.00 ppm) as an external standard. GC yields were determined by analyzing the crude mixture using n-dodecane as an internal standard on a Shimadzu GC-14A equipped with a flame ionization detector, using Shimadzu Capillary Column (CBP1-M25-025) and Shimadzu C-R6A-Chromatopac integrator. Infrared spectra were recorded on a Shimadzu IR Prestige-21 spectrophotometer. Elemental analyses were carried out with a Perkin-Elmer 2400 CHN elemental analyzer at Okayama University. High-resolution mass spectra were obtained on a JEOL JMS-700 spectrometer in the electron ionization (EI) mode.

Chemicals

Unless specified otherwise, materials obtained from commercial suppliers were used without further purification. Palladium(II)(π-cinnamyl) chloride dimer ($[PdCl(cinnamyl)]_2$) (purity > 97%) was purchased from Tokyo Chemical Industry Co., Ltd. and Sigma-Aldrich Co. LLC. 4,5-Bis(diphenylphosphino)-9,9-dimethylxanthene (Xantphos) (purity > 98%) was purchased from Tokyo Chemical Industry Co., Ltd. Lithium iodide (purity > 97%) and sodium iodide (purity > 99.5%) were purchased from FUJIFILM Co., Ltd. Lithium bromide (purity > 95%) was purchased from Kanto

Chemical Co., Inc. Lithium chloride (purity > 98%) was purchased from Tokyo Chemical Industry Co., Ltd. Toluene (super dehydrated) was purchased from FUJIFILM Co., Ltd. Benzoyl fluoride (**1b**) (purity > 98%), benzoyl chloride (**1b**') (purity > 98%) and 1-naphthoyl chloride (**1a'**) ((purity > 98%) were purchased from Tokyo Chemical Industry Co., Ltd.

2-4-2 Experimental Procedures of Synthesis of Starting Materials

Aroyl fluorides, aroyl chlorides, an ester, and an amide were purchased from commercial suppliers or synthesized according to the methods described below (**Schemes 2-25, 26, and 27**).

Scheme 2-25. Commercially Available or Synthesized Aroyl Fluorides (**1**).

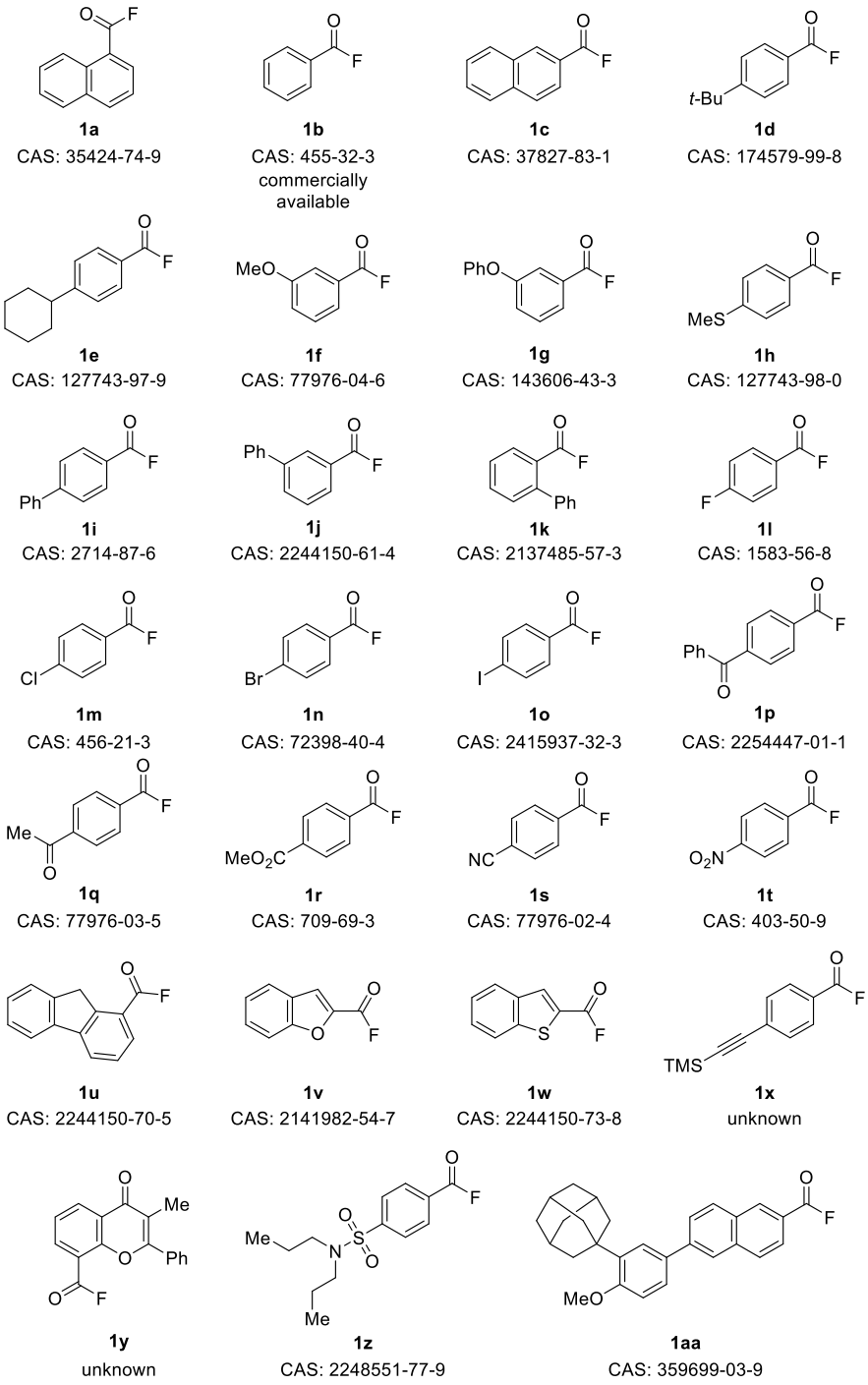

Scheme 2-26. Commercially Available or Synthesized Aroyl Chlorides (**1'**).

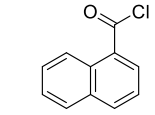

1a'
CAS: 879-18-5
commercially
available

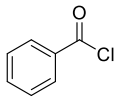

1b'
CAS: 98-88-4
commercially
available

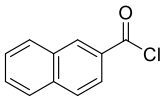

1c'
CAS: 2243-83-6
commercially
available

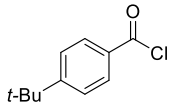

1d'
CAS: 19692-45-6
commercially
available

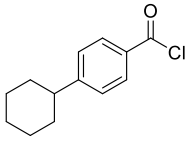

1e'
CAS: 121193-16-6

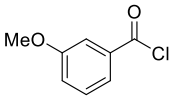

1f'
CAS: 1711-05-3
commercially
available

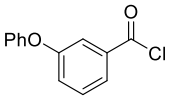

1g'
CAS: 3586-15-0

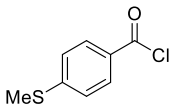

1h'
CAS: 1442-06-4

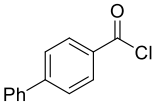

1i'
CAS: 14002-51-8
commercially
available

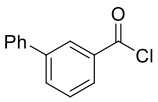

1j'
CAS: 42498-44-2

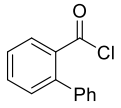

1k'
CAS: 14002-52-9

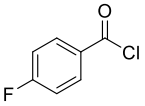

1l'
CAS: 403-43-0
commercially
available

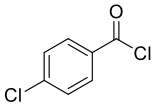

1m'
CAS: 122-01-0
commercially
available

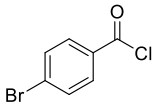

1n'
CAS: 586-75-4
commercially
available

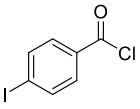

1o'
CAS: 1711-02-0
commercially
available

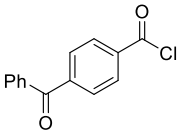

1p'
CAS: 39148-58-8

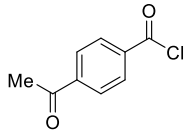

1q'
CAS: 31076-84-3

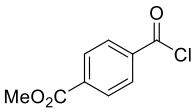

1r'
CAS: 7377-26-6
commercially
available

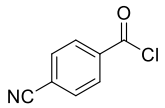

1s'
CAS: 6068-72-0
commercially
available

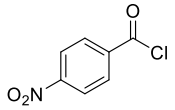

1t'
CAS: 122-04-3
commercially
available

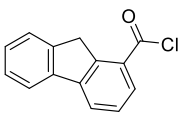

1u'
CAS: 55341-64-5

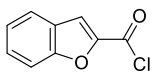

1v'
CAS: 55341-64-5

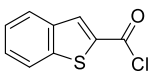

1w'
CAS: 39827-11-7

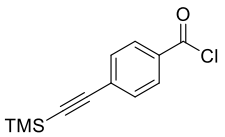

1x'
CAS: 1470024-92-0

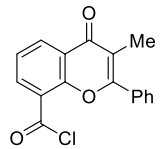

1y'
CAS: 51950-71-1

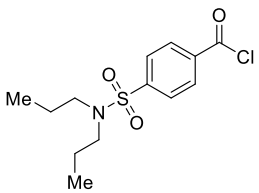

1z'
CAS: 29171-72-0

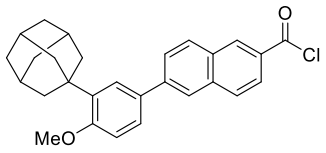

1aa'
CAS: 106685-64-7

Scheme 2-27. Synthesized Ester and Amide.

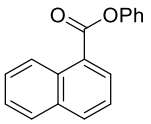

Ester
CAS: 36773-67-8

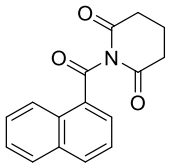

Amide
CAS: 2098569-26-5

Procedure A: General Procedure for the Synthesis of **1a**–**1f**, **1h**–**1o**, **1q**–**1t**, **1w**, and **1z**[23]

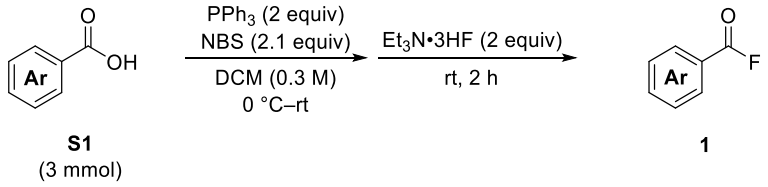

S1
(3 mmol)

1

On the bench-top, carboxylic acid **S1** (1 equiv, 3 mmol), PPh_3 (2 equiv, 6 mmol, 1.57 g), and anhydrous dichloromethane (DCM) (10 mL, 0.3 M) were added to an oven-dried flask equipped with a magnetic stir bar. The flask was sealed with a rubber septum and cooled to 0 °C using an ice-bath. *N*-Bromosuccinimide (NBS) (2.1 equiv, 6.3 mmol, 1.12 g) was then added in one portion. After stirring for two min, the ice-bath was removed, and the solution was allowed to reach room temperature over the course of 15 min. To the reaction mixture, $Et_3N \cdot 3HF$ (2 equiv, 6 mmol, 961 μL) was added dropwise *via* a syringe and stirred for 2 h at room temperature. Upon completion of the reaction, the mixture was diluted with hexane (250 mL) and stirred for 10 min to precipitate large amounts of succinimide and triphenylphosphine oxide. The solids were removed by filtration through a short pad of silica gel (3–5 cm thick x 3 cm diameter) using dichloromethane and hexane as eluents. All volatiles were evaporated under reduced pressure to afford pure acyl fluorides **1**, which were utilized in the catalytic reactions without further purification.

Procedure B: General Procedure for the Synthesis of **1g**, **1p**, **1u**, **1v**, **1y**, and **1aa**[24]

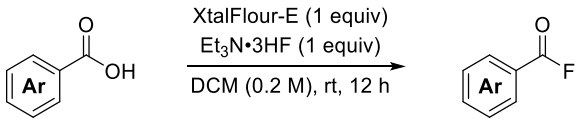

S1
(3 mmol)

1

In a nitrogen-filled glovebox, an oven-dried Schlenck tube containing diethylaminodifluorosulfinium tetrafluoroborate (XtalFluor-E) (1 equiv, 3 mmol, 687 mg) and a magnetic stir bar was sealed with a rubber septum. The tube was then taken out

from the glovebox and connected to nitrogen pipeline. Subsequently, carboxylic acid **S1** (1 equiv, 3 mmol) and anhydrous dichloromethane (15 mL, 0.2 M) were added to the tube, followed by sequential dropwise addition of $Et_3N{\cdot}3HF$ (1 equiv, 3 mmol, 480 μL) *via* a syringe. The resulting mixture was stirred for 12 h at room temperature. Afterward, the mixture was transferred into a flask containing hexane (250 mL) and stirred for 15 min. The precipitates were removed by filtration through a short pad of silica gel (3–5 cm thick x 3 cm diameter) using dichloromethane and hexane as eluents. All volatiles were evaporated under reduced pressure to afford pure acyl fluorides **1**, which were employed in the catalytic reactions without further purification.

Procedure C: Procedure for the synthesis of **1x**[23,25]

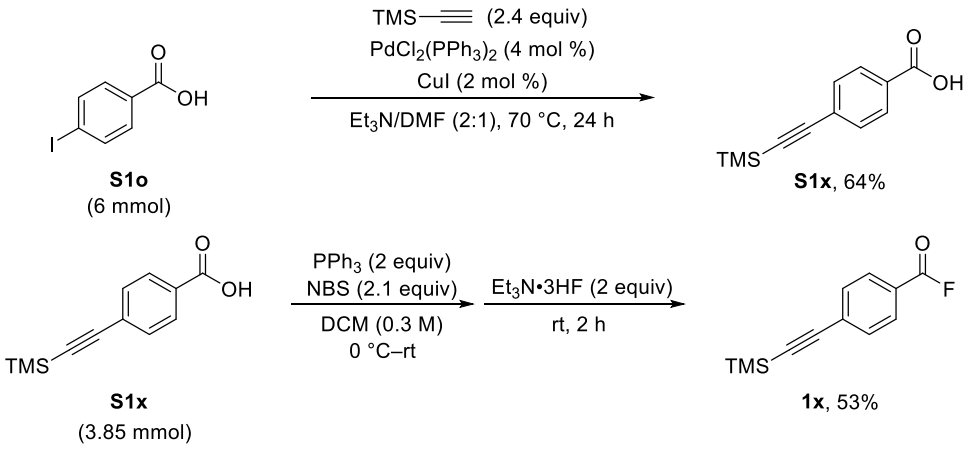

In a Schlenk tube, 4-iodobenzoic acid (**S1o**) (1 equiv, 6 mmol, 1.49 g), $PdCl_2(PPh_3)_2$ (4 mol %, 0.24 mmol, 169 mg), and CuI (2 mol %, 0.12 mmol, 22.9 mg) were dissolved in a mixture of Et_3N (8 mL) and *N*,*N*-dimethylformamide (DMF, 4 mL). Then, trimethylsilylacetylene (2.4 equiv, 14.4 mmol, 2 mL) was added to the tube. The mixture was heated at 70 °C for 24 h. After cooling to room temperature, the resulting suspension was filtered through a short pad of celite and rinsed with ethyl acetate (EtOAc) (20 mL) and dichloromethane (20 mL). The solvents were removed by rotary evaporation, and the obtained slurry was dissolved in EtOAc (20 mL), washed with water (2 x 10 mL) and brine (2 x 10 mL), dried over anhydrous $MgSO_4$, and filtered. The organic layer was concentrated *in vacuo*, and the crude product was purified by column

chromatography on silica gel (dichloromethane:methanol = 100:0 to 95:5) to yield the desired product **S1x** as a yellow solid (840 mg, 64%).

The obtained **S1x** was employed as a substrate for procedure A, affording **1x** as a beige solid (441 mg, 53%).

Procedure D: General Procedure for the Synthesis of Aroyl Chlorides[13]

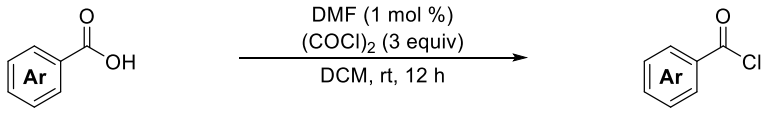

S1
(3 mmol)

1'

In the presence of air, an oven-dried round-bottomed flask equipped with a stirring bar was charged with carboxylic acid **S1** (1 equiv, 3 mmol), dichloromethane (9 mL), and *N,N*-dimethylformamide (DMF, 1 mol %, 0.03 mmol, 2.3 μL). Oxalyl chloride (3 equiv, 9 mmol, 772 μL) was added dropwise using a syringe. A rubber stopper was placed over the flask to release pressure. The reaction mixture was stirred at room temperature for 12 h. The solvent and unreacted oxalyl chloride were removed under reduced pressure. The obtained aroyl chlorides **1'** were used without further purification.

Procedure E: Procedure for the Synthesis of **1y'**[26]

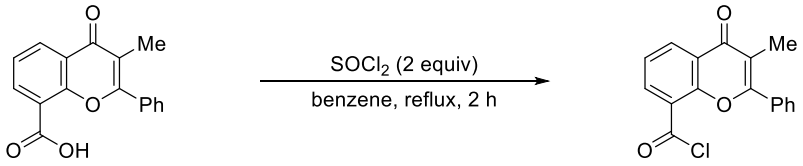

S1y
(3 mmol)

1y', quant.

In the presence of air, an oven-dried round-bottomed flask equipped with a stirring bar was charged with 3-methylflavone-8-carboxylic acid (**S1y**) (1 equiv, 3 mmol, 841 mg) and benzene (15 mL). Thionyl chloride (2 equiv, 6 mmol, 433 μL) was added dropwise using a syringe. A reflux condenser was placed over the flask. Then, the reaction mixture

was refluxed for 2 h. The solvent and unreacted thionyl chloride were removed under reduced pressure. The obtained acyl chloride **1y'** (891 mg, quantitative) were used without further purification.

Procedure F: Procedure for the Synthesis of **Ester**[27]

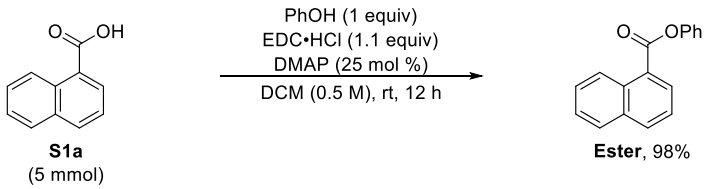

To a Schlenk tube equipped with a stirring bar, 1-naphthoic acid (**S1a**) (1 equiv, 5 mmol, 861 mg), phenol (1 equiv, 5 mmol, 471 mg), 1-(3-dimethylaminopropyl)-3-ethylcarbodiimide hydrochloride (EDC·HCl) (1.1 equiv, 5.5 mmol, 1.05 g), *N,N*-dimethyl-4-aminopyridine (DMAP) (0.25 equiv, 1.25 mmol, 153 mg), and dichloromethane (10 mL, 0.5 M) were added. After stirring the mixture for 12 h at room temperature, the reaction was quenched with saturated sodium bicarbonate ($NaHCO_3$) (aq.) and extracted three times with EtOAc. The combined organic layer was dried over anhydrous $MgSO_4$, filtrated, and concentrated under reduced pressure. The residue was purified by flash column chromatography on silica gel (EtOAc/hexane = 1:5) to afford the desired product (1.21 g, 98%) as a white solid.

Procedure G: Procedure for the Synthesis of Amide[28]

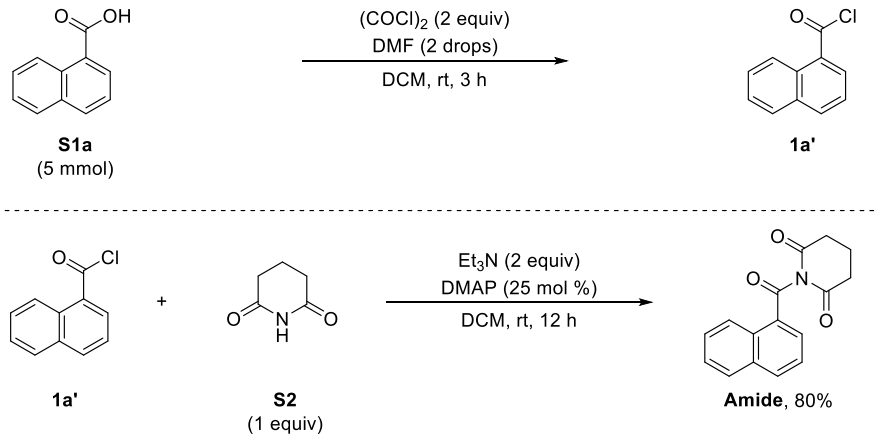

To a round-bottomed flask equipped with a magnetic stirrer were added 1-naphthoic acid (**S1a**) (1 equiv, 5 mmol, 861 mg) and dichloromethane (DCM) (10 mL). Oxalyl chloride (2 equiv, 10 mmol, 858 μL) was then added dropwise at 0 °C. A couple of drops of DMF were added, and the reaction mixture was allowed to reach room temperature. Stirring was continued until gas evolution ceased (typically 3 h). After this period, the mixture was concentrated under reduced pressure to remove hydrogen chloride (HCl) and excess oxalyl chloride, yielding the corresponding 1-naphthoyl chloride (**1a'**), which was used in the next step without further purification.

In a separate round-bottomed flask, a mixture of glutarimide (**S2**) (1 equiv, 5 mmol, 566 mg), Et_3N (2 equiv, 10 mmol 1.39 mL), DMAP (25 mol %, 1.25 mmol, 153 mg), and DCM (10 mL) was cooled to 0 °C, and **1a'** was added dropwise. The reaction mixture was allowed to reach room temperature and stirred for 16 h. After this period, the mixture was diluted with DCM (20 mL) and washed with HCl (1 M aq., 25 mL), water (25 mL), and brine (25 mL). The organic layer was then dried with anhydrous $MgSO_4$, filtered, and concentrated under reduced pressure to afford the crude product, which was purified by recrystallisation from toluene to afford the desired product (1.08 g, 80%) as a beige solid.

1-Naphthoyl Fluoride (1a)

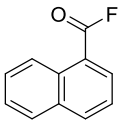

1a

Prepared according to procedure A (376 mg, 72%) as a white solid. R_f = 0.5 (DCM/hexane = 1/10). ^{1}H NMR (400 MHz, $CDCl_3$): δ 9.02 (dt, J = 8.7, 1.0 Hz, 1H), 8.35 (d, J = 7.4 Hz, 1H), 8.19–8.16 (m, 1H), 7.94 (d, J = 8.4 Hz, 1H), 7.74–7.70 (m, 1H), 7.64–7.54 (m, 2H); ^{19}F{^{1}H} NMR (376 MHz, $CDCl_3$): δ 29.89.

These data align with previously published reports in the literature.[29]

2-Naphthoyl Fluoride (1c)

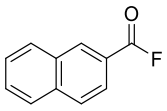

1c

Prepared according to procedure A (385 mg, 74%) as a white solid. R_f = 0.5 (DCM/hexane = 1/10). ^{1}H NMR (400 MHz, $CDCl_3$): δ 8.64–8.64 (m, 1H), 8.02–7.91 (m, 4H), 7.69 (ddd, J = 8.2, 6.9, 1.3 Hz, 1H), 7.61 (ddd, J = 8.2, 6.9, 1.3 Hz, 1H); ^{19}F{^{1}H} NMR (376 MHz, $CDCl_3$): δ 18.05.

These data align with previously published reports in the literature.[12b]

4-*tert*-Butylbenzoyl Fluoride (1d)

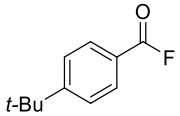

1d

Prepared according to procedure A (442 mg, 82%) as a colorless liquid. R_f = 0.55 (DCM/hexane = 1/10). ^{1}H NMR (400 MHz, $CDCl_3$): δ 8.00–7.96 (m, 2H), 7.56–7.52 (m, 2H), 1.36 (s, 9H); ^{19}F{^{1}H} NMR (376 MHz, $CDCl_3$): δ 17.63.

These data align with previously published reports in the literature.[30]

4-Cyclohexylbenzoyl Fluoride (1e)

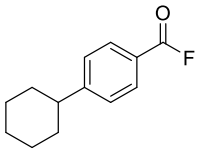

1e

Prepared according to procedure A (477 mg, 77%) as a white solid. R_f = 0.55 (DCM/hexane = 1/10). ^{1}H NMR (400 MHz, $CDCl_3$): δ 7.96 (dt, J = 8.4, 2.0 Hz, 2H), 7.37–7.33 (m, 2H), 2.64–2.57 (m, 1H), 1.91–1.84 (m, 4H), 1.80–1.75 (m, 1H), 1.49–1.35 (m, 4H), 1.32–1.23 (m, 1H); ^{19}F{^{1}H} NMR (376 MHz, $CDCl_3$): δ 17.43.

These data align with previously published reports in the literature.[31]

3-Methoxybenzoyl Fluoride (1f)

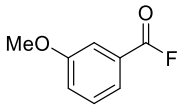

1f

Prepared according to procedure A (242 mg, 52%) as a colorless liquid. R_f = 0.4 (DCM/hexane = 1/5). ^{1}H NMR (400 MHz, $CDCl_3$): δ 7.66–7.63 (m, 1H), 7.53–7.52 (m, 1H), 7.45–7.41 (m, 1H), 7.23 (ddd, J = 8.3, 2.7, 1.0 Hz, 1H), 3.87 (s, 3H); ^{19}F{^{1}H} NMR (376 MHz, $CDCl_3$): δ 18.57.

These data align with previously published reports in the literature.[30]

3-Phenoxybenzoyl Fluoride (1g)

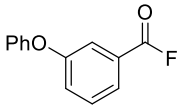

1g

Prepared according to procedure B (586 mg, 90%) as a colorless oil. R_f = 0.5 (DCM/hexane = 1/5). ^{1}H NMR (400 MHz, $CDCl_3$): δ 7.79–7.76 (m, 1H), 7.63–7.62 (m, 1H), 7.51–7.46 (m, 1H), 7.43–7.37 (m, 2H), 7.34 (ddd, J = 8.3, 2.6, 1.1 Hz, 1H), 7.22–7.18 (m, 1H), 7.07–7.03 (m, 2H); ^{19}F{^{1}H} NMR (376 MHz, $CDCl_3$): δ 19.11.

These data align with previously published reports in the literature.[24]

4-(Methylthio)benzoyl Fluoride (1h)

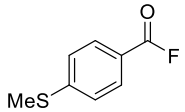

1h

Prepared according to procedure A (308 mg, 60%) as a white solid. R_f = 0.4 (DCM/hexane = 1/5). ^{1}H NMR (400 MHz, $CDCl_3$): δ 7.92–7.89 (m, 2H), 7.30–7.28 (m, 2H), 2.53 (s, 3H); $^{19}F\{^1H\}$ NMR (376 MHz, $CDCl_3$): δ 16.59.

These data align with previously published reports in the literature.[32]

[1,1'-Biphenyl]-4-carbonyl Fluoride (1i)

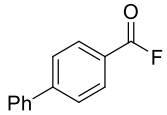

1i

Prepared according to procedure A (431 mg, 72%) as a white solid. R_f = 0.5 (DCM/hexane = 1/10). ^{1}H NMR (400 MHz, $CDCl_3$): δ 8.12 (dt, J = 8.0, 2.0 Hz, 2H), 7.76–7.73 (m, 2H), 7.66–7.63 (m, 2H), 7.53–7.42 (m, 3H); $^{19}F\{^1H\}$ NMR (376 MHz, $CDCl_3$): δ 18.12.

These data align with previously published reports in the literature.[31,32]

[1,1'-Biphenyl]-3-carbonyl Fluoride (1j)

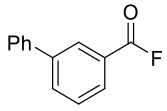

1j

Prepared according to procedure A (423 mg, 70%) as a white solid. R_f = 0.5 (DCM/hexane = 1/10). ^{1}H NMR (400 MHz, $CDCl_3$): δ 8.28 (t, J = 1.8 Hz, 1H), 8.03 (dt, J = 7.8, 1.5 Hz, 1H), 7.93 (ddd, J = 7.8, 1.9, 1.2 Hz, 1H), 7.63–7.59 (m, 3H), 7.52–7.40 (m, 2H), 7.45–7.39 (m, 1H); $^{19}F\{^1H\}$ NMR (376 MHz, $CDCl_3$): δ 18.64.

These data align with previously published reports in the literature.[12b]

[1,1'-Biphenyl]-2-carbonyl Fluoride (1k)

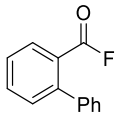

1k

Prepared according to procedure A (412 mg, 69%) as a white solid. R_f = 0.5 (DCM/hexane = 1/10). ^{1}H NMR (400 MHz, $CDCl_3$): δ 8.05 (dd, J = 7.9, 1.4 Hz, 1H), 7.68 (td, J = 7.6, 1.4 Hz, 1H), 7.51 (tt, J = 7.7, 1.3 Hz, 1H), 7.47–7.42 (m, 4H), 7.35–7.33 (m, 2H); ^{19}F{^{1}H} NMR (376 MHz, $CDCl_3$): δ 34.99.

These data align with previously published reports in the literature.[31, 32]

4-Fluorobenzoyl Fluoride (1l)

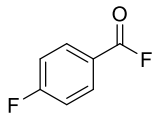

1l

Prepared according to procedure A (52.6 mg, 12%) as a colorless liquid. R_f = 0.55 (DCM/hexane = 1/10). ^{1}H NMR (400 MHz, $CDCl_3$): δ 8.11–8.06 (m, 2H), 7.24–7.18 (m, 2H); ^{19}F{^{1}H} NMR (376 MHz, $CDCl_3$): δ 17.68 (s, 1F), –100.84 to –100.91 (m, 1F).

These data align with previously published reports in the literature.[31]

4-Chlorobenzoyl Fluoride (1m)

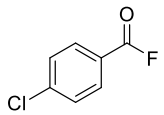

1m

Prepared according to procedure A (258 mg, 54%) as a white solid. R_f = 0.55 (DCM/hexane = 1/10). ^{1}H NMR (400 MHz, $CDCl_3$): δ 8.00–7.96 (m, 2H), 7.53–7.49 (m, 2H); ^{19}F{^{1}H} NMR (376 MHz, $CDCl_3$): δ 18.39.

These data align with previously published reports in the literature.[31]

4-Bromobenzoyl Fluoride (1n)

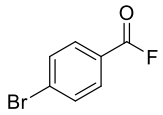

1n

Prepared according to procedure A (382 mg, 63%) as a white solid. R_f = 0.55 (DCM/hexane = 1/10). ^{1}H NMR (400 MHz, $CDCl_3$): δ 7.91–7.88 (m, 2H), 7.70–7.66 (m, 2H); $^{19}F\{^1H\}$ NMR (376 MHz, $CDCl_3$): δ 18.41.

These data align with previously published reports in the literature.[32]

4-Iodobenzoyl Fluoride (1o)

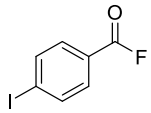

1o

Prepared according to procedure A (408 mg, 54%) as a white solid. R_f = 0.55 (DCM/hexane = 1/10). ^{1}H NMR (400 MHz, $CDCl_3$): δ 7.92–7.89 (m, 2H), 7.75–7. 72 (m, 2H); $^{19}F\{^1H\}$ NMR (376 MHz, $CDCl_3$): δ 18.27.

These data align with previously published reports in the literature.[32]

4-Benzoylbenzoyl Fluoride (1p)

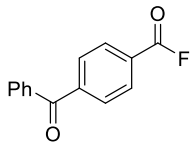

1p

Prepared according to procedure B (621 mg, 91%) as a white solid. R_f = 0.4 (DCM/hexane = 1/2). ^{1}H NMR (400 MHz, $CDCl_3$): δ 8.16 (dt, J = 8.4, 1.6 Hz, 2H), 7.91–7.88 (m, 2H), 7.82–7.79 (m, 2H), 7.66–7.62 (m, 1H), 7.54–7.49 (m, 2H); $^{19}F\{^1H\}$ NMR (376 MHz, $CDCl_3$): δ 19.94.

These data align with previously published reports in the literature.[12b]

4-Acetylbenzoyl Fluoride (1q)

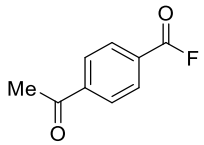

1q

Prepared according to procedure A (256 mg, 51%) as a yellow solid. R_f = 0.3 (DCM/hexane = 1/2). ^{1}H NMR (400 MHz, $CDCl_3$): δ 8.13–8.10 (m, 2H), 8.07–8.04 (m, 2H), 2.65 (s, 3H); $^{19}F\{^1H\}$ NMR (376 MHz, $CDCl_3$): δ 20.15.

These data align with previously published reports in the literature.[33]

Methyl 4-(Fluorocarbonyl)benzoate (1r)

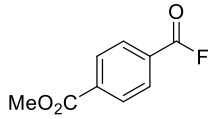

1r

Prepared according to procedure A (325 mg, 60%) as a white solid. R_f = 0.6 (EtOAc/hexane = 1/5). ^{1}H NMR (400 MHz, $CDCl_3$): δ 8.18–8.15 (m, 2H), 8.11–8.08 (m, 2H), 3.96 (s, 3H); $^{19}F\{^1H\}$ NMR (376 MHz, $CDCl_3$): δ 20.00.

These data align with previously published reports in the literature.[12b]

4-Cyanobenzoyl Fluoride (1s)

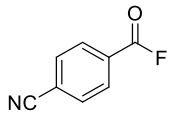

1s

Prepared according to procedure A (221 mg, 49%) as a white solid. R_f = 0.6 (EtOAc/hexane = 1/5). ^{1}H NMR (400 MHz, $CDCl_3$): δ 8.18–8.15 (m, 2H), 7.86–7.83 (m, 2H); $^{19}F\{^1H\}$ NMR (376 MHz, $CDCl_3$): δ 20.20.

These data align with previously published reports in the literature.[12b]

4-Nitrobenzoyl Fluoride (1t)

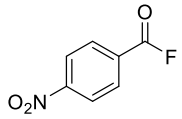

1t

Prepared according to procedure A (220 mg, 43%) as a beige solid. R_f = 0.4 (DCM/hexane = 1/2). ^{1}H NMR (400 MHz, $CDCl_3$): δ 8.40–8.37 (m, 2H), 8.27–8.24 (m, 2H); $^{19}F\{^1H\}$ NMR (376 MHz, $CDCl_3$): δ 21.31.

These data align with previously published reports in the literature.[31]

9*H*-Fluorene-1-carbonyl Fluoride (1u)

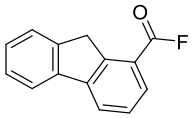

1u

Prepared according to procedure B (593 mg, 93%) as a white solid. R_f = 0.5 (DCM/hexane = 1/10). ^{1}H NMR (400 MHz, $CDCl_3$): δ 8.06 (d, J = 7.6 Hz, 1H), 7.96 (dd, J = 7.8, 1.0 Hz, 1H), 7.82–7.79 (m, 1H), 7.62–7.59 (m, 1H), 7.53 (t, J = 8.0 Hz, 1H), 7.44–7.37 (m, 2H), 4.21 (s, 2H); $^{19}F\{^1H\}$ NMR (376 MHz, $CDCl_3$): δ 25.17.

These data align with previously published reports in the literature.[12a]

Benzofuran-2-carbonyl Fluoride (1v)

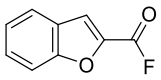

1v

Prepared according to procedure B (441 mg, 90%) as a white solid. R_f = 0.5 (DCM/hexane = 1/10). ^{1}H NMR (400 MHz, $CDCl_3$): δ 7.77–7.74 (m, 2H), 7.62 (dq, J = 8.5, 1.0 Hz, 1H), 7.58–7.54 (m, 1H), 7.38 (ddd, J = 8.0, 7.0, 1.1 Hz, 1H); $^{19}F\{^1H\}$ NMR (376 MHz, $CDCl_3$): δ 17.35.

These data align with previously published reports in the literature.[10a]

Benzo[*b*]thiophene-2-carbonyl Fluoride (1w)

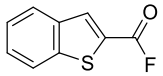

1w

Prepared according to procedure A (284 mg, 52%) as a white solid. R_f = 0.5 (DCM/hexane = 1/10). ^{1}H NMR (400 MHz, $CDCl_3$): δ 8.20 (s, 1H), 7.95 (dt, J = 8.0, 1.1 Hz, 1H), 7.91 (dq, J = 8.2, 0.9 Hz, 1H), 7.55 (ddd, J = 8.3, 7.1, 1.3 Hz, 1H), 7.48 (ddd, J = 8.1, 7.1, 1.1 Hz, 1H); ^{19}F{^{1}H} NMR (376 MHz, $CDCl_3$): δ 25.10.

These data align with previously published reports in the literature.[12a]

4-((Trimethylsilyl)ethynyl)benzoyl Fluoride (1x)

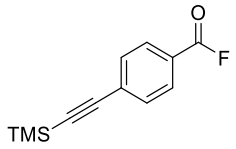

1x

Prepared according to procedure C (441 mg, 53%) as a beige solid. mp: 66–68 °C. R_f = 0.5 (DCM/hexane = 1/10). ^{1}H NMR (600 MHz, $CDCl_3$): δ 7.98–7.96 (m, 2H), 7.58–7.57 (m, 2H), 0.27 (s, 9H); ^{13}C{^{1}H} NMR (151 MHz, $CDCl_3$): δ 157.0 (d, $^1J_{C–F}$ = 344.3 Hz), 132.5, 131.3 (d, $^3J_{C–F}$ = 3.6 Hz), 130.5, 124.4 (d, $^2J_{C–F}$ = 61.9 Hz), 103.4, 100.2, –0.1; ^{19}F{^{1}H} NMR (376 MHz, $CDCl_3$): δ 18.41. FT-IR (cm^{-1}): 2956 (s), 2160 (s), 1805 (s), 1604 (s), 1410 (s), 1251 (m), 1175 (s), 1032 (s), 1010 (s), 858 (m), 759 (s). Anal. Calcd for $C_{12}H_{13}FOSi$: C, 65.42; H, 5.95%; Found: C, 65.45; H, 6.09%.

3-Methyl-4-oxo-2-phenyl-4*H*-chromene-8-carbonyl Fluoride (1y)

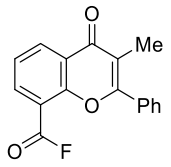

1y

Prepared according to procedure B (786 mg, 93%) as a white solid. mp: 128–130 °C. R_f = 0.4 (DCM/hexane = 1/1). ^{1}H NMR (400 MHz, $CDCl_3$): δ 8.57 (ddd, J = 7.9, 1.8, 1.0 Hz, 1H), 8.31 (dd, J = 7.6, 1.7 Hz, 1H), 7.82–7.76 (m, 2H), 7.56–7.48 (m, 4H), 2.25 (s, 3H); ^{13}C{^{1}H} NMR (101 MHz, $CDCl_3$): δ 177.1, 161.1, 155.7 (d, $^3J_{C-F}$ = 3.1 Hz), 153.5 (d, $^1J_{C-F}$ = 345.5 Hz), 137.9 (d, $^4J_{C-F)}$ = 2.1 Hz), 134.0, 132.5, 130.9, 129.4, 128.6, 124.3, 123.6 (d, $^4J_{C-F}$ = 2.2 Hz), 118.3, 114.6 (d, $^2J_{C-F}$ = 62.7 Hz), 11.9; ^{19}F{^{1}H} NMR (376 MHz, $CDCl_3$): δ 32.93. FT-IR (cm^{-1}): 1824 (s), 1790 (s), 1649 (s), 1622 (s), 1598 (s), 1477 (s), 1442 (s), 1390 (s), 1371 (s), 1271 (m), 1061 (m), 1018 (s), 754 (m), 695 (m). Anal. Calcd for $C_{17}H_{11}FO_3$: C, 72.34; H, 3.93%; Found: C, 72.40; H, 3.85%.

4-(*N*,*N*-Dipropylsulfamoyl)benzoyl Fluoride (1z)

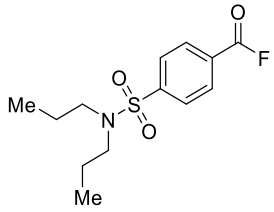

1z

Prepared according to procedure A (615 mg, 71%) as a white solid. R_f = 0.3 (DCM/hexane = 1/2). ^{1}H NMR (400 MHz, $CDCl_3$): δ 8.17–8.14 (m, 2H), 7.96–7.93 (m, 2H), 3.12–3.08 (m, 4H), 1.54 (hept, J = 7.4 Hz, 4H), 0.85 (t, J = 7.4 Hz, 6H); ^{19}F{^{1}H} NMR (376 MHz, $CDCl_3$): δ 20.16.

These data align with previously published reports in the literature.[10a]

6-(3-(Adamantan-1-yl)-4-methoxyphenyl)-2-naphthoyl Fluoride (1aa)

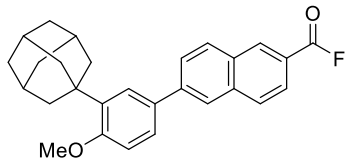

1aa

Prepared according to procedure B (224 mg, 90%) (0.6 mmol scale) as a white solid. R_f = 0.5 (DCM/hexane = 1/5). ^{1}H NMR (400 MHz, $CDCl_3$): δ 8.64 (s, 1H), 8.05–7.97 (m, 4H), 7.86 (dd, J = 8.6, 1.8 Hz, 1H), 7.61_4–7.60_8 (m, 1H), 7.56 (dd, J = 8.4, 2.4 Hz, 1H), 7.01 (d, J = 8.4 Hz, 1H), 3.92 (s, 3H), 2.19_2–2.18_5 (m, 6H), 2.11 (t, J = 2.8 Hz, 3H), 1.81 (t, J = 3.1 Hz, 6H); ^{19}F{^{1}H} NMR (376 MHz, $CDCl_3$): δ 17.64.

These data align with previously published reports in the literature.[34]

4-Cyclohexylbenzoyl Chloride (1e')

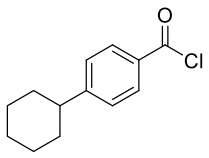

1e'

Prepared according to procedure D (666 mg, quantitative) as a colorless oil. ^{1}H NMR (600 MHz, $CDCl_3$): δ 8.05–8.03 (m, 2H), 7.35–7.33 (m, 2H), 2.62–2.58 (m, 1H), 1.91–1.84 (m, 4H), 1.80–1.75 (m, 1H), 1.47–1.37 (m, 4H), 1.32–1.23 (m, 1H); ^{13}C{^{1}H} NMR (151 MHz, $CDCl_3$): δ 168.2, 156.6, 131.8, 130.9, 127.6, 44.9, 34.0, 26.7, 26.0.

3-Phenoxybenzoyl Chloride (1g')

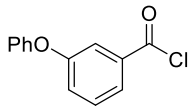

1g'

Prepared according to procedure D (697 mg, quantitative) as a colorless liquid. ^{1}H NMR (600 MHz, $CDCl_3$): δ 7.87–7.85 (m, 1H), 7.72 (t, J = 2.4 Hz, 1H), 7.47 (t, J = 8.0 Hz, 1H), 7.42–7.39 (m, 2H), 7.32 (ddd, J = 8.2, 2.5, 1.0 Hz, 1H), 7.20 (tt, J = 7.3, 1.1 Hz, 1H), 7.07–7.04 (m, 2H); ^{13}C{^{1}H} NMR (151 MHz, $CDCl_3$): δ 167.9, 158.2, 156.1, 134.9, 130.3, 130.2, 126.0, 125.3, 124.5, 120.6, 119.5.

4-(Methylthio)benzoyl Chloride (1h')

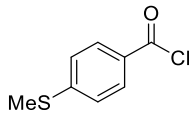

1h'

Prepared according to procedure D (566 mg, quantitative) as a beige solid. ^{1}H NMR (400 MHz, $CDCl_3$): δ 8.00–7.97 (m, 2H), 7.28–7.25 (m, 2H), 2.53 (s, 3H); $^{13}C\{^{1}H\}$ NMR (101 MHz, $CDCl_3$): δ 167.6, 149.9, 131.7, 128.9, 124.9, 14.7.

These data align with previously published reports in the literature.[35]

[1,1'-Biphenyl]-3-carbonyl Chloride (1j')

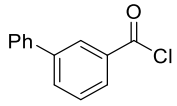

1j'

Prepared according to procedure D (655 mg, quantitative) as a colorless oil. ^{1}H NMR (600 MHz, $CDCl_3$): δ 8.34–8.33 (m, 1H), 8.11 (ddd, J = 7.9, 1.9, 1.1 Hz, 1H), 7.91 (ddd, J = 7.7, 1.9, 1.1 Hz, 1H), 7.63–7.58 (m, 3H), 7.51–7.48 (m, 2H), 7.44–7.41 (m, 1H); $^{13}C\{^{1}H\}$ NMR (151 MHz, $CDCl_3$): δ 168.6, 142.4, 139.3, 134.0, 133.9, 130.3, 130.0, 129.6, 129.2, 128.4, 127.3.

These data align with previously published reports in the literature.[36]

[1,1'-Biphenyl]-2-carbonyl Chloride (1k')

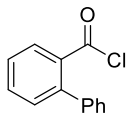

1k'

Prepared according to procedure D (659 mg, quantitative) as a colorless oil. ^{1}H NMR (600 MHz, $CDCl_3$): δ 8.04 (dt, J = 7.9, 1.3 Hz, 1H), 7.63 (tt, J = 7.6, 1.1 Hz, 1H), 7.50 (tt, J = 7.6, 1.1 Hz, 1H), 7.47–7.40 (m, 4H), 7.37–7.35 (m, 2H); $^{13}C\{^{1}H\}$ NMR (151 MHz, $CDCl_3$): δ 168.5, 142.8, 139.8, 134.5, 133.2, 131.4, 131.2, 128.8, 128.6, 128.1, 127.6.

These data align with previously published reports in the literature.[37]

4-Benzoylbenzoyl Chloride (1p')

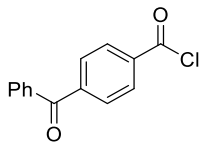

1p'

Prepared according to procedure D (738 mg, quantitative) as a white solid. ^{1}H NMR (600 MHz, $CDCl_3$): δ 8.24–8.22(m, 2H), 7.89–7.87 (m, 2H), 7.81–7.79 (m, 2H), 7.64 (tt, J = 7.2, 1.2 Hz, 1H), 7.53–7.50 (m, 2H); ^{13}C{^{1}H} NMR (151 MHz, $CDCl_3$): δ 195.4, 168.0, 143.4, 136.5, 135.9, 133.5, 131.3, 130.2$_2$, 130.1$_5$, 128.7.

These data align with previously published reports in the literature.[38]

4-Acetylbenzoyl Chloride (1q')

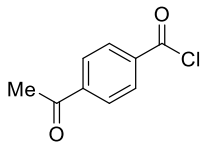

1q'

Prepared according to procedure D (570 mg, quantitative) as a yellow solid. ^{1}H NMR (600 MHz, $CDCl_3$): δ 8.19–8.17 (m, 2H), 8.05–8.03 (m, 2H), 2.65 (s, 3H); ^{13}C{^{1}H} NMR (151 MHz, $CDCl_3$): δ 197.1, 167.9, 141.8, 136.5, 131.6, 128.7, 27.1.

These data align with previously published reports in the literature.[35]

9*H*-Fluorene-1-carbonyl Chloride (1u')

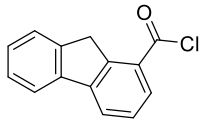

1u'

Prepared according to procedure D (702 mg, quantitative) as a white solid. ^{1}H NMR (400 MHz, $CDCl_3$): δ 8.19 (dd, J = 7.9, 1.0 Hz, 1H), 8.03 (d, J = 7.6 Hz, 1H), 7.80–7.78 (m, 1H), 7.59–7.53 (m, 2H), 7.43–7.35 (m, 2H), 4.15 (s, 2H); ^{13}C{^{1}H} NMR (151 MHz, $CDCl_3$): δ 167.6, 146.5, 143.6, 143.3, 139.7, 131.8, 129.8, 128.0, 127.9, 127.1, 126.2, 125.2, 120.2, 40.0.

These data align with previously published reports in the literature.[39]

Benzofuran-2-carbonyl Chloride (1v')

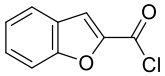

1v'

Prepared according to procedure D (535 mg, quantitative) as a white solid. ^{1}H NMR (400 MHz, $CDCl_3$): δ 7.86 (d, J = 7.6 Hz, 1H), 7.76 (dt, J = 7.6, 1.2 Hz, 1H), 7.63–7.55 (m, 2H), 7.38 (ddd, J = 8.0, 6.8, 1.3 Hz, 1H); ^{13}C{^{1}H} NMR (151 MHz, $CDCl_3$): δ 157.4, 157.2, 146.7, 130.1, 126.6, 124.8, 123.9, 120.7, 112.9.

These data align with previously published reports in the literature.[40]

Benzo[*b*]thiophene-2-carbonyl Chloride (1w')

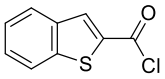

1w'

Prepared according to procedure D (582 mg, quantitative) as a white solid. ^{1}H NMR (600 MHz, $CDCl_3$): δ 8.24 (s, 1H), 7.93 (dt, J = 8.1, 1.1 Hz, 1H), 7.85 (dq, J = 8.2, 1.0 Hz, 1H), 7.54 (ddd, J = 8.3, 7.1, 1.2 Hz, 1H), 7.46 (ddd, J = 8.1, 7.1, 1.0 Hz, 1H); ^{13}C{^{1}H} NMR (151 MHz, $CDCl_3$): δ 161.2, 144.1, 138.1, 136.6, 136.0, 128.9, 126.8, 125.8, 123.0.

These data align with previously published reports in the literature.[41]

4-((Trimethylsilyl)ethynyl)benzoyl Chloride (1x')

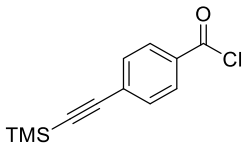

1x'

Prepared according to procedures C (step 1) and D (909 mg, quantitative) (3.8 mmol scale) as a yellow solid. ^{1}H NMR (600 MHz, $CDCl_3$): δ 8.05–8.03 (m, 2H), 7.57–7.55 (m, 2H), 0.27 (s, 9H); ^{13}C{^{1}H} NMR (151 MHz, $CDCl_3$): δ 167.8, 132.5, 132.4, 131.3, 130.5, 103.4, 100.5, –0.1.

These data align with previously published reports in the literature.[13]

3-Methyl-4-oxo-2-phenyl-4*H*-chromene-8-carbonyl Chloride (1y')

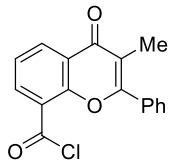

1y'

Prepared according to procedure E (891 mg, quantitative) as a white solid. ^{1}H NMR (600 MHz, $CDCl_3$): δ 8.53 (dd, J = 7.9, 1.7 Hz, 1H), 8.47 (dd, J = 7.7, 1.7 Hz, 1H), 7.79–7.76 (m, 2H), 7.56–7.52 (m, 3H), 7.50 (t, J = 6.0 Hz, 1H), 2.24 (s, 3H); ^{13}C{^{1}H} NMR (151 MHz, $CDCl_3$): δ 177.6, 162.9, 161.1, 154.0, 138.6, 133.5, 132.4, 130.9, 129.4, 128.6, 124.2, 123.4, 123.1, 118.3, 11.9.

4-(*N*,*N*-Dipropylsulfamoyl)benzoyl Chloride (1z')

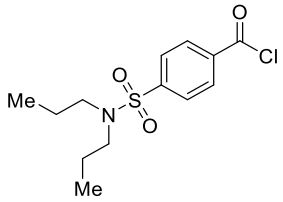

1z'

Prepared according to procedure D (908 mg, quantitative) as a white solid. ^{1}H NMR (600 MHz, $CDCl_3$): δ 8.23–8.21 (m, 2H), 7.94–7.92 (m, 2H), 3.12–3.09 (m, 4H), 1.53 (h, J = 7.4 Hz, 4H), 0.85 (t, J = 7.4 Hz, 6H); ^{13}C{^{1}H} NMR (151 MHz, $CDCl_3$): δ 167.5, 146.5, 136.1, 131.9, 127.5, 50.0, 22.0, 11.2.

These data align with previously published reports in the literature.[13]

6-(3-(Adamantan-1-yl)-4-methoxyphenyl)-2-naphthoyl Chloride (1aa')

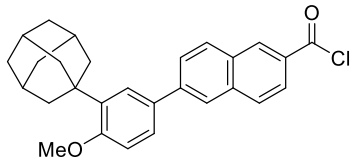

1aa'

Prepared according to procedure D (255 mg, quantitative) (0.6 mmol scale) as a white solid. ^{1}H NMR (600 MHz, $CDCl_3$): δ 8.75 (d, J = 2.2 Hz, 1H), 8.07–8.04 (m, 3H), 7.95 (d, J = 8.7 Hz, 1H), 7.87 (dd, J = 8.5, 1.8 Hz, 1H), 7.62 (d, J = 2.4 Hz, 1H), 7.56 (dd, J = 8.4, 2.4 Hz, 1H), 7.01 (d, J = 8.4 Hz, 1H), 3.92 (s, 3H), 2.19$_2$–2.18$_7$ (m, 6H), 2.11 (quint, J = 3.1 Hz, 3H), 1.81 (t, J = 3.1 Hz, 6H); ^{13}C{^{1}H} NMR (151 MHz, $CDCl_3$): δ 168.5, 159.4, 143.2, 139.3, 137.1, 134.8, 132.1, 131.1, 130.5, 129.9, 129.0, 127.3, 126.2, 126.0, 125.9, 124.8, 112.3, 55.3, 40.7, 37.4, 37.2, 29.2.

These data align with previously published reports in the literature.[13]

Phenyl 1-naphthoate (Ester)

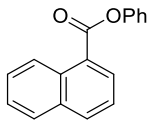

Ester

Prepared according to procedure F (1.21 g, 98%) as a white solid. ^{1}H NMR (400 MHz, $CDCl_3$): δ 9.09 (d, J = 8.4 Hz, 1H), 8.51 (dd, J = 7.3, 1.3 Hz, 1H), 8.12 (dt, J = 8.2, 1.1 Hz, 1H), 7.95 (ddt, J = 8.2, 1.3, 0.6 Hz, 1H), 7.68 (ddd, J = 8.6, 6.8, 1.5 Hz, 1H), 7.61–7.57 (m, 2H), 7.53–7.48 (m, 2H), 7.36–7.31 (m, 3H); ^{13}C{^{1}H} NMR (101 MHz, $CDCl_3$): δ 165.9, 151.1, 134.4, 134.0, 131.8, 131.3, 129.7, 128.8, 128.3, 126.5, 126.1, 126.0, 125.9, 124.6, 122.0.

These data align with previously published reports in the literature.[27,42]

1-(1-Naphthoyl)piperidine-2,6-dione (Amide)

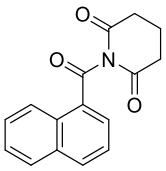

Amide

Prepared according to procedure G (1.08 g, 80%) as a beige solid. ^{1}H NMR (400 MHz, $CDCl_3$): δ 9.09–9.06 (m, 1H), 8.09 (d, J = 8.0 Hz, 1H), 7.91–7.89 (m, 1H), 7.84 (dd, J = 7.4, 1.2 Hz, 1H), 7.71 (ddd, J = 8.6, 6.9, 1.4 Hz, 1H), 7.59 (ddd, J = 8.0, 6.8, 1.6 Hz, 1H), 7.47 (dd, J = 8.2, 7.3 Hz, 1H), 2.76 (t, J = 6.6 Hz, 4H), 2.12 (quint, J = 6.4 Hz, 2H); ^{13}C{^{1}H} NMR (101 MHz, $CDCl_3$): δ 172.3, 170.8, 136.1, 134.1, 132.0, 131.4, 129.4, 128.8, 128.6, 127.1, 125.9, 124.5, 32.6, 17.5.

These data align with previously published reports in the literature.[43]

2-4-3 Experimental Procedures of Catalytic Decarbonylative Halogenation

2-4-3-1 General Procedure for Screening of the Reaction Conditions

An oven-dried 5-mL microwave vial, fitted with a magnetic stirring bar, was loaded with Pd or Ni catalysts (2.5 or 5 mol %), a ligand (12.5 or 25 mol %), and either 1-naphthoyl fluoride (**1a**), 1-naphthoyl chloride (**1a'**), or other carboxylic acid derivatives (**amide** or **ester**) (0.2 mmol, 1 equiv) under ambient air. A halogen source (0.2–0.6 mmol, 1–3 equiv) and anhydrous solvent (1 mL, 0.2 M) were added inside a nitrogen-filled glovebox. The vial was sealed securely and heated in a preheated block at 100–170 °C for 12–24 h with constant stirring. After cooling to room temperature, the reaction mixture was transferred to an oven-dried round-bottom flask. The vial was rinsed with dichloromethane (5 × 2 mL), and the combined solution was concentrated under reduced pressure. Dibromomethane (CH_2Br_2) was then added as an internal standard, and product yields were quantified using ^1H NMR spectroscopy.

2-4-3-2 General Procedure for Experimental Procedures and Spectroscopic Data for the Products

Procedure H (closed system):

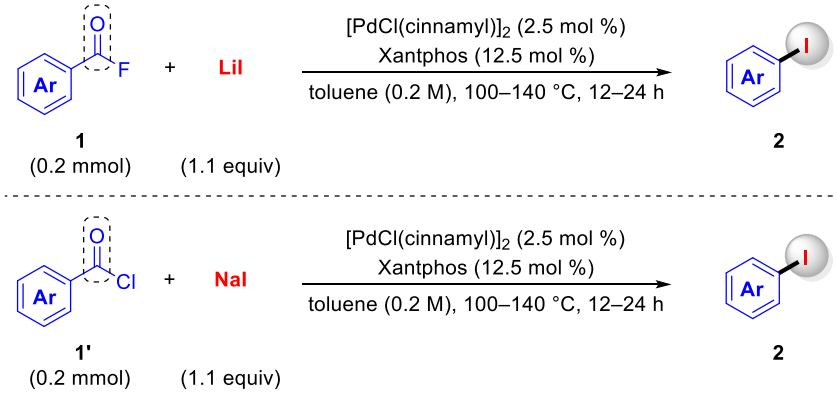

An oven-dried 5-mL microwave vial equipped with a magnetic stirring bar was loaded with $[PdCl(cinnamyl)]_2$ (2.5 mol %, 5 μmol, 2.6 mg), Xantphos (12.5 mol %, 0.025 mmol, 14.5 mg), and either acyl fluorides **1** or acyl chlorides **1** (0.2 mmol, 1 equiv) under ambient air. Lithium iodide (for **1**) or sodium iodide (for **1'**) (0.22 mmol, 1.1 equiv, 29.4 mg or 33.0 mg, respectively) and anhydrous toluene (1 mL, 0.2 M) were added in a nitrogen-filled glovebox. The vial was securely sealed and heated in a preheated block at 100–140 °C for 12–24 h with continuous stirring. After the reaction mixture cooled to room temperature, it was purified by silica gel column chromatography using ethyl acetate or dichloromethane/hexane as the eluent to obtain the desired product **2**. Yields of volatile products (**2b** and **2l**) were determined via GC analysis of the reaction mixture, using *n*-dodecane as an internal standard.

Procedure I (open system):

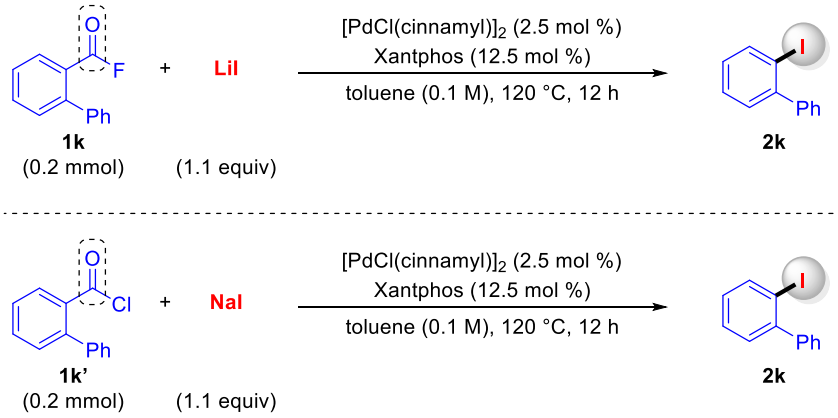

An oven-dried 5-mL microwave vial equipped with a magnetic stirring bar was loaded with $[PdCl(cinnamyl)]_2$ (2.5 mol %, 5 μmol, 2.6 mg), Xantphos (12.5 mol %, 0.025 mmol, 14.5 mg), and either [1,1'-biphenyl]-2-carbonyl fluoride (**1k**, 0.2 mmol, 1 equiv, 40.0 mg) or [1,1'-biphenyl]-2-carbonyl chloride (**1k'**, 0.2 mmol, 1 equiv, 43.3 mg) under ambient air. Lithium iodide (for **1k**, 0.22 mmol, 1.1 equiv, 29.4 mg) or sodium iodide (for **1k'**, 0.22 mmol, 1.1 equiv, 33.0 mg) and anhydrous toluene (2 mL, 0.1 M) were introduced in a nitrogen-filled glovebox. The vial was securely sealed, and the septum was pierced with a needle for pressure equilibration (a depiction of the reaction setup is provided below). The vial was then placed in a preheated heating block at 120 °C and stirred for 12 h. After cooling to room temperature, the reaction mixture was purified by silica gel column chromatography using hexane as the eluent, yielding the desired product **2k**.

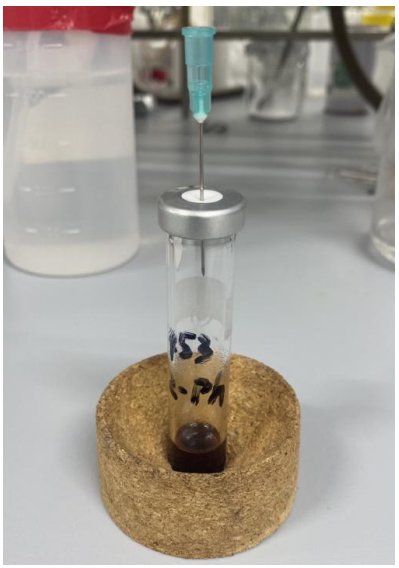

Procedure J:

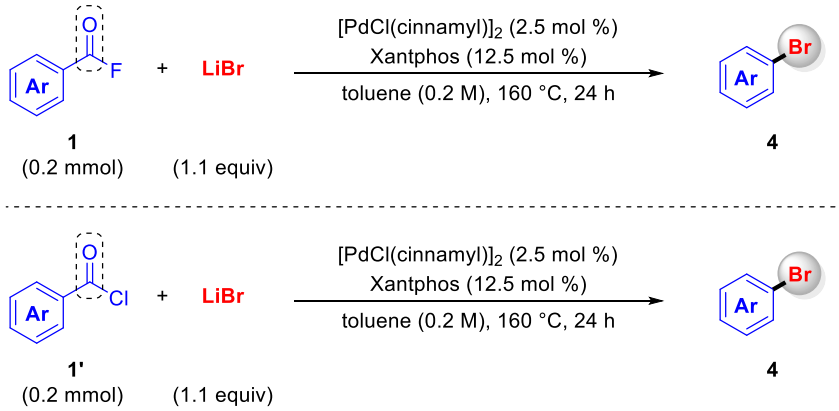

An oven-dried 5-mL microwave vial equipped with a magnetic stirring bar was loaded with $[PdCl(cinnamyl)]_2$ (2.5 mol %, 5 μmol, 2.6 mg), Xantphos (12.5 mol %, 0.025 mmol, 14.5 mg), and either acyl fluorides **1** or acyl chlorides **1'** (0.2 mmol, 1 equiv) under ambient air. Lithium bromide (0.22 mmol, 1.1 equiv, 19.1 mg) and anhydrous toluene (1 mL, 0.2 M) were added to a nitrogen-filled glovebox. The vial was securely sealed and heated in a preheated block at 160 °C for 24 h with continuous stirring. (***Safety Note****: The reaction must be conducted in a fume hood. Due to the high reaction temperature exceeding toluene's boiling point and the generation of CO gas, there is a potential risk of the reaction cap detaching under pressure.*) Once the reaction mixture cooled to room temperature, it was purified by silica gel column chromatography using a dichloromethane/hexane mixture as the eluent to obtain the desired product **4**.

Procedure K:

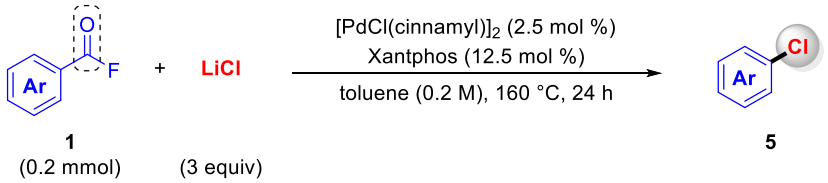

An oven-dried 5-mL microwave vial equipped with a magnetic stirring bar was charged with $[PdCl(cinnamyl)]_2$ (2.5 mol %, 5 μmol, 2.6 mg), Xantphos (12.5 mol %, 0.025 mmol, 14.5 mg), and acyl fluorides 1 (0.2 mmol, 1 equiv) under ambient air. Lithium chloride

(0.6 mmol, 3 equiv, 25.4 mg) and anhydrous toluene (1 mL, 0.2 M) were added inside a nitrogen-filled glovebox. The vial was securely sealed and heated in a preheated block at 160 °C for 24 h with continuous stirring. (***Safety Note****: This procedure must be performed in a fume hood. The high reaction temperature exceeds the boiling point of toluene, and the reaction generates CO gas, increasing the potential risk of cap detachment due to pressure buildup.*) After cooling the reaction mixture to room temperature, it was purified using silica gel column chromatography with a dichloromethane/hexane eluent to isolate the desired product **5**.

Procedure L (Scale-up Experiment):

Synthesis of 1-Iodo-9H-fluorene (2u) on 2 mmol Scale

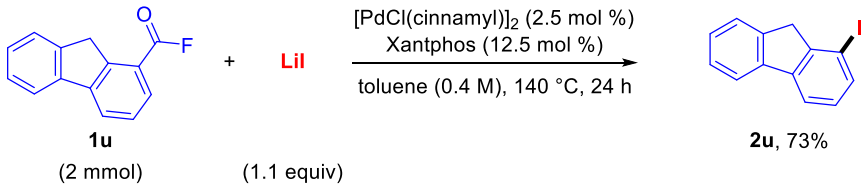

An oven-dried 20-mL microwave vial equipped with a magnetic stirring bar was loaded with [PdCl(cinnamyl)]$_2$ (2.5 mol %, 0.05 mmol, 25.9 mg), Xantphos (12.5 mol %, 0.25 mmol, 144.7 mg), and 9*H*-fluorene-1-carbonyl fluoride (**1u**, 2 mmol, 1 equiv, 424.4 mg) under ambient air. Lithium iodide (2.2 mmol, 1.1 equiv, 294.5 mg) and anhydrous toluene (5 mL, 0.4 M) were added inside a nitrogen-filled glovebox. The vial was securely sealed and heated in a preheated block at 140 °C for 24 h with stirring. After allowing the reaction to cool to room temperature, the mixture was purified by silica gel column chromatography using hexane as the eluent, yielding 1-iodo-9*H*-fluorene (**2u**) as a white solid with a 73% yield (0.43 g).

Spectroscopic Data for the Products

1-Iodonaphthalene (2a)

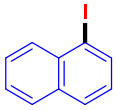

2a

Prepared according to procedure H as a colorless oil. R_f = 0.60 (hexane). Isolated yields were 92% (46.6 mg) from **1a**, and 90% (45.5 mg) from **1a'**, respectively. ^{1}H NMR (400 MHz, $CDCl_3$): δ 8.16–8.10 (m, 2H), 7.85 (d, J = 8.3 Hz, 1H), 7.79 (d, J = 7.9 Hz, 1H), 7.64–7.58 (m, 1H), 7.57–7.52 (m, 1H), 7.19 (t, J = 7.8 Hz, 1H); ^{13}C{^{1}H} NMR (101 MHz, $CDCl_3$): δ 137.5, 134.4, 134.2, 132.2, 129.1, 128.6, 127.8, 126.9, 126.8, 99.7.
These data align with previously published reports in the literature.[14]

2-Iodonaphthalene (2c)

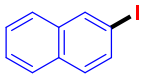

2c

Prepared according to procedure H as a white solid. R_f = 0.60 (hexane). Isolated yields were 67% (33.9 mg) from **1c** and 62% (31.4 mg) from **1c'**, respectively. ^{1}H NMR (400 MHz, $CDCl_3$): δ 8.25 (d, J = 1.4 Hz, 1H), 7.82–7.78 (m, 1H), 7.74–7.70 (m, 2H), 7.59–7.57 (m, 1H), 7.52–7.48 (m, 2H); ^{13}C{^{1}H} NMR (101 MHz, $CDCl_3$): δ 136.7, 135.1, 134.5, 132.2, 129.6, 128.0, 126.9, 126.8, 126.6, 91.6.
These data align with previously published reports in the literature.[14]

1-*tert*-Butyl-4-iodobenzene (2d)

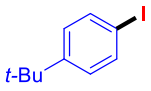

2d

Prepared according to procedure H as a colorless oil. R_f = 0.80 (hexane). Isolated yields were 57% (29.7 mg) from **1d** and 60% (31.3 mg) from **1d'**, respectively. ^{1}H NMR (400 MHz, $CDCl_3$): δ 7.63–7.60 (m, 2H), 7.16–7.13 (m, 2H), 1.30 (s, 9H); ^{13}C{^{1}H} NMR (101 MHz, $CDCl_3$): δ 151.0, 137.2, 127.7, 90.8, 34.7, 31.3.
These data align with previously published reports in the literature.[44]

1-Cyclohexyl-4-iodobenzene (2e)

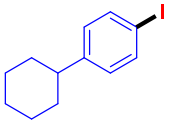

2e

Prepared according to procedure H as a colorless oil. R_f = 0.80 (hexane). Isolated yields were 31% (17.6 mg) from **1e** and 62% (35.2 mg) from **1e'**, respectively. ^{1}H NMR (400 MHz, $CDCl_3$): δ 7.63–7.59 (m, 2H), 6.99–6.96 (m, 2H), 2.49–2.42 (m, 1H), 1.89–1.81 (m, 4H), 1.78–1.73 (m, 1H), 1.44–1.33 (m, 4H), 1.30–1.21 (m, 1H); ^{13}C{^{1}H} NMR (151 MHz, $CDCl_3$): δ 147.8, 137.4, 129.1, 90.8, 44.2, 34.4, 26.9, 26.2.

These data align with previously published reports in the literature.[45]

1-Iodo-3-methoxybenzene (2f)

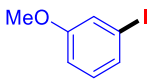

2f

Prepared according to procedure H as a colorless oil. R_f = 0.40 (DCM/hexane = 1/10). Isolated yields were 42% (19.6 mg) from **1f** and 38% (17.8 mg) from **1f'**, respectively. ^{1}H NMR (400 MHz, $CDCl_3$): δ 7.29 (ddd, J = 7.7, 1.6, 0.9 Hz, 1H), 7.26–7.25 (m, 1H), 7.00 (t, J = 8.0 Hz, 1H), 6.87 (ddd, J = 8.4, 2.5, 1.0 Hz, 1H), 3.78 (s, 3H); ^{13}C{^{1}H} NMR (101 MHz, $CDCl_3$): δ 160.3, 130.9, 129.7, 123.1, 113.9, 94.5, 55.5.

These data align with previously published reports in the literature.[14]

1-Iodo-3-phenoxybenzene (2g)

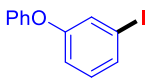

2g

Prepared according to procedure H as a colorless oil. R_f = 0.40 (hexane). Isolated yields were 71% (42.1 mg) from **1g** and 60% (35.6 mg) from **1g'**, respectively. ^{1}H NMR (600 MHz, $CDCl_3$): δ 7.45–7.43 (m, 1H), 7.39–7.36 (m, 3H), 7.18–7.14 (m, 1H), 7.07–7.02 (m, 3H), 7.00–6.97 (m, 1H); ^{13}C{^{1}H} NMR (151 MHz, $CDCl_3$): δ 158.1, 156.5, 132.3, 131.1, 130.0, 127.7, 124.0, 119.4, 118.1, 94.4.

These data align with previously published reports in the literature.[46]

4-Iodophenyl methyl sulfide (2h)

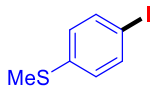

2h

Prepared according to procedure H as a white solid. R_f = 0.50 (DCM/hexane = 1/10). Isolated yields were 44% (22.1 mg) from **1h** and 37% (18.6 mg) from **1h'**, respectively. ^{1}H NMR (400 MHz, $CDCl_3$): δ 7.59–7.56 (m, 2H), 7.00–6.97 (m, 2H), 2.46 (s, 3H); $^{13}C\{^1H\}$ NMR (101 MHz, $CDCl_3$): δ 138.8, 137.8, 128.4, 89.3, 15.8.

These data align with previously published reports in the literature.[14]

4-Iodo-1,1'-biphenyl (2i)

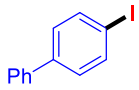

2i

Prepared according to procedure H as a white solid. R_f = 0.55 (hexane). Isolated yields were 70% (39.4 mg) from **1i** and 65% (36.7 mg) from **1i'**, respectively. ^{1}H NMR (400 MHz, $CDCl_3$): δ 7.79–7.76 (m, 2H), 7.57–7.54 (m, 2H), 7.47–7.42 (m, 2H), 7.39–7.32 (m, 3H); $^{13}C\{^1H\}$ NMR (101 MHz, $CDCl_3$): δ 140.9, 140.2, 138.0, 129.2, 129.0, 127.8, 127.0, 93.2.

These data align with previously published reports in the literature.[14]

3-Iodo-1,1'-biphenyl (2j)

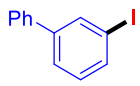

2j

Prepared according to procedure H as a colorless oil. R_f = 0.55 (hexane). Isolated yields were 78% (43.9 mg) from **1j** and 69% (38.7 mg) from **1j'**, respectively. ^{1}H NMR (400 MHz, $CDCl_3$): δ 7.97–7.95 (m, 1H), 7.71–7.67 (m, 1H), 7.57–7.54 (m, 3H), 7.48–7.43 (m, 2H), 7.41–7.36 (m, 1H), 7.18 (t, J = 7.8 Hz, 1H); $^{13}C\{^1H\}$ NMR (101 MHz, $CDCl_3$): δ 143.6, 139.8, 136.3$_1$, 136.2$_8$, 130.5, 129.0, 128.0, 127.2, 126.5, 94.9.

These data align with previously published reports in the literature.[47]

2-Iodo-1,1'-biphenyl (2k)

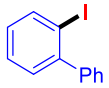

2k

Prepared according to procedure I as a colorless oil. R_f = 0.55 (hexane). Isolated yields were 32% (18.2 mg) from **1k** and 61% (34.4 mg) from **1k'**, respectively. ^{1}H NMR (600 MHz, $CDCl_3$): δ 7.97 (dd, J = 7.9, 1.2 Hz, 1H), 7.46–7.43 (m, 2H), 7.42–7.39 (m, 2H), 7.37–7.35 (m, 2H), 7.32 (dd, J = 7.6, 1.8 Hz, 1H), 7.05 (ddd, J = 7.9, 7.3, 1.7 Hz, 1H); ^{13}C{^{1}H} NMR (151 MHz, $CDCl_3$): δ 146.7, 144.3, 139.6, 130.2, 129.4, 128.9, 128.2, 128.1, 127.8, 98.8.

These data align with previously published reports in the literature.[44]

1-Chloro-4-iodobenzene (2m)

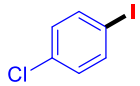

2m

Prepared according to procedure H as a white solid. R_f = 0.80 (hexane). Isolated yields were 44% (21.0 mg) from **1m** and 28% (13.5 mg) from **1m'**, respectively. ^{1}H NMR (400 MHz, $CDCl_3$): δ 7.62–7.59 (m, 2H), 7.10–7.07 (m, 2H); ^{13}C{^{1}H} NMR (101 MHz, $CDCl_3$): δ 138.9, 134.3, 130.7, 91.3.

These data align with previously published reports in the literature.[14]

1-Bromo-4-iodobenzene (2n)

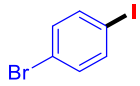

2n

Prepared according to procedure H as a white solid. R_f = 0.80 (hexane). Isolated yields were 46% (26.1 mg) from **1n** and 50% (28.4 mg) from **1n'**, respectively. ^{1}H NMR (400 MHz, $CDCl_3$): δ 7.56–7.53 (m, 2H), 7.25–7.21 (m, 2H); ^{13}C{^{1}H} NMR (151 MHz, $CDCl_3$): δ 139.2, 133.6, 122.3, 92.2.

These data align with previously published reports in the literature.[14]

1,4-Diiodobenzene (2o)

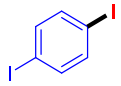

2o

Prepared according to procedure H as a white solid. R_f = 0.80 (hexane). Isolated yields were 50% (32.7 mg) from **1o** and 65% (42.9 mg) from **1o'**, respectively. ^{1}H NMR (400 MHz, $CDCl_3$): δ 7.41 (s, 4H); $^{13}C\{^1H\}$ NMR (101 MHz, $CDCl_3$): δ 139.5, 93.5.
These data align with previously published reports in the literature.[44]

4-Iodobenzophenone (2p)

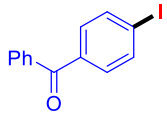

2p

Prepared according to procedure H as a white solid. R_f = 0.40 (DCM/hexane = 1/1). Isolated yields were 63% (38.7 mg) from **1p** and 68% (41.7 mg) from **1p'**, respectively. ^{1}H NMR (400 MHz, $CDCl_3$): δ 7.86–7.83 (m, 2H), 7.79–7.76 (m, 2H), 7.60 (ddt, J = 8.1, 6.9, 1.4 Hz, 1H), 7.54–7.46 (m, 4H); $^{13}C\{^1H\}$ NMR (101 MHz, $CDCl_3$): δ 196.0, 137.7, 137.2, 137.0, 132.8, 131.6, 130.1, 128.5, 100.3.
These data align with previously published reports in the literature.[48]

1-(4-Iodophenyl)ethan-1-one (2q)

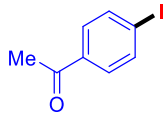

2q

Prepared according to procedure H as a yellow solid. R_f = 0.30 (DCM/hexane = 1/1). Isolated yields were 58% (28.6 mg) from **1q** and 62% (30.4 mg) from **1q'**, respectively. ^{1}H NMR (400 MHz, $CDCl_3$): δ 7.84–7.81 (m, 2H), 7.67–7.64 (m, 2H), 2.57 (s, 3H); $^{13}C\{^1H\}$ NMR (101 MHz, $CDCl_3$): δ 197.5, 138.0, 136.4, 129.9, 101.3, 26.6.
These data align with previously published reports in the literature.[14]

Methyl 4-Iodobenzoate (2r)

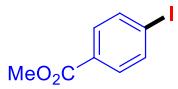

2r

Prepared according to procedure H as a white solid. R_f = 0.40 (DCM/hexane = 1/1). Isolated yields were 67% (35.0 mg) from **1r** and 68% (35.9 mg) from **1r'**, respectively. ^{1}H NMR (400 MHz, $CDCl_3$): δ 7.81–7.78 (m, 2H), 7.75–7.72 (m, 2H), 3.90 (s, 3H); $^{13}C\{^1H\}$ NMR (151 MHz, $CDCl_3$): δ 166.7, 137.8, 131.2, 129.7, 100.9, 52.4.

These data align with previously published reports in the literature.[14]

4-Iodobenzonitrile (2s)

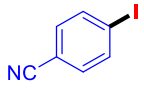

2s

Prepared according to procedure H as a white solid. R_f = 0.30 (DCM/hexane = 1/1). Isolated yields were 80% (36.7 mg) from **1s** and 63% (28.9 mg) from **1s'**, respectively. ^{1}H NMR (400 MHz, $CDCl_3$): δ 7.86–7.83 (m, 2H), 7.38–7.35 (m, 2H); $^{13}C\{^1H\}$ NMR (101 MHz, $CDCl_3$): δ 138.6, 133.3, 118.3, 111.8, 100.4.

These data align with previously published reports in the literature.[14]

1-Iodo-4-nitrobenzene (2t)

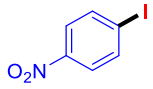

2t

Prepared according to procedure H as a white solid. R_f = 0.50 (DCM/hexane = 1/1). Isolated yield was 81% (40.6 mg) from **1t'**. ^{1}H NMR (600 MHz, $CDCl_3$): δ 7.95–7.90 (m, 4H); $^{13}C\{^1H\}$ NMR (151 MHz, $CDCl_3$): δ 147.9, 138.8, 125.0, 102.8.

These data align with previously published reports in the literature.[49]

1-Iodo-9*H*-fluorene (2u)

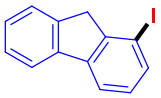

2u

Prepared according to procedure H as a white solid. R_f = 0.55 (hexane). Isolated yields were 87% (50.7 mg) from **1u** and 83% (48.5 mg) from **1u'**, respectively. ^{1}H NMR (400 MHz, $CDCl_3$): δ 7.76–7.73 (m, 2H), 7.68 (dd, J = 7.8, 1.0 Hz, 1H), 7.59–7.56 (m, 1H), 7.42–7.32 (m, 2H), 7.14–7.09 (m, 1H), 3.81 (s, 2H); ^{13}C{^{1}H} NMR (151 MHz, $CDCl_3$): δ 147.9, 142.5, 142.2, 141.7, 135.9, 128.8, 127.5, 127.1, 125.1, 120.7, 119.7, 94.1, 42.5.
These data align with previously published reports in the literature.[50]

2-Iodobenzofuran (2v)

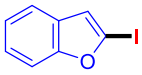

2v

Prepared according to procedure H as a colorless oil. R_f = 0.60 (hexane). Isolated yields were 30% (14.5 mg) from **1v** and 37% (36.0 mg) from **1v'**, respectively. ^{1}H NMR (600 MHz, $CDCl_3$): δ 7.53–7.50 (m, 1H), 7.50–7.46 (m, 1H), 7.24–7.20 (m, 2H), 6.96 (s, 1H); ^{13}C{^{1}H} NMR (151 MHz, $CDCl_3$): δ 158.3, 129.3, 124.4, 123.3, 119.8, 117.4, 111.0, 96.0.
These data align with previously published reports in the literature.[51]

2-Iodobenzo[*b*]thiophene (2w)

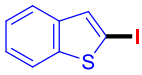

2w

Prepared according to procedure H and bulb-to-bulb distillation to remove benzo[*b*]thiophene, as a colorless oil. R_f = 0.60 (hexane). Isolated yields were 24% (12.4 mg) from **1w** and 31% (32.7 mg) from **1w'**, respectively. ^{1}H NMR (600 MHz, $CDCl_3$): δ 7.78–7.76 (m, 1H), 7.72–7.71 (m, 1H), 7.54 (s, 1H), 7.33–7.27 (m, 2H); ^{13}C{^{1}H} NMR (151 MHz, $CDCl_3$): δ 144.5, 140.9, 133.9, 124.7, 124.5, 122.4, 121.4, 78.6.
These data align with previously published reports in the literature.[51]

((4-Iodophenyl)ethynyl)trimethylsilane (2x)

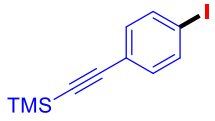

2x

Prepared according to procedure H as a white solid. R_f = 0.65 (hexane). Isolated yields were 58% (34.8 mg) from **1x** and 47% (28.3 mg) from **1x'**, respectively. ^{1}H NMR (600 MHz, $CDCl_3$): δ 7.65–7.63 (m, 2H), 7.19–7.17 (m, 2H), 0.25 (s, 9H); $^{13}C\{^1H\}$ NMR (151 MHz, $CDCl_3$): δ 137.5, 133.6, 122.8, 104.1, 96.0, 94.6, 0.0.

These data align with previously published reports in the literature.[14]

8-Iodo-3-methyl-2-phenyl-4*H*-chromen-4-one (2y)

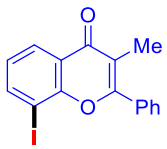

2y

Prepared according to procedure H as a white solid. R_f = 0.20 (DCM/hexane = 2/1). Isolated yields were 55% (39.8 mg) from **1y** and 84% (61.0 mg) from **1y'**, respectively. ^{1}H NMR (600 MHz, $CDCl_3$): δ 8.22 (dd, J = 7.9, 1.5 Hz, 1H), 8.11 (dd, J = 7.6, 1.5 Hz, 1H), 7.79–7.77 (m, 2H), 7.57–7.52 (m, 3H), 7.15 (t, J = 7.7 Hz, 1H), 2.23 (s, 3H); $^{13}C\{^1H\}$ NMR (151 MHz, $CDCl_3$): δ 178.7, 161.3, 155.1, 143.2, 133.0, 130.6, 129.5, 128.6, 126.5, 126.3, 123.2, 117.6, 85.1, 12.1.

These data align with previously published reports in the literature.[14]

4-Iodo-*N*,*N*-dipropylbenzenesulfonamide (2z)

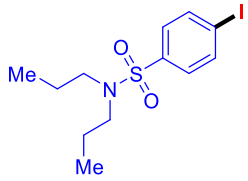

2z

Prepared according to procedure H as a white solid. R_f = 0.40 (DCM/hexane = 2/1). Isolated yields were 76% (55.8 mg) from **1z** and 75% (54.8 mg) from **1z'**, respectively. ^{1}H NMR (400 MHz, $CDCl_3$): δ 7.86–7.81 (m, 2H), 7.52–7.48 (m, 2H), 3.07–3.03 (m, 4H), 1.59–1.48 (m, 4H), 0.88–0.83 (m, 6H); $^{13}C\{^1H\}$ NMR (101 MHz, $CDCl_3$): δ 140.0, 138.3, 128.6, 99.5, 50.1, 22.1, 11.3.

These data align with previously published reports in the literature.[14]

1-(5-(6-Iodonaphthalen-2-yl)-2-methoxyphenyl)adamantane (2aa)

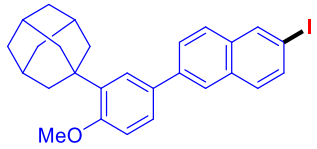

2aa

Prepared according to procedure H as a white solid. R_f = 0.50 (CH_2Cl_2/hexane = 1/10). Isolated yields were 32% (31.4 mg) from **1aa** and 47% (46.3 mg) from **1aa'**, respectively. ^{1}H NMR (600 MHz, $CDCl_3$): δ 8.24 (s, 1H), 7.94 (s, 1H), 7.77–7.71 (m, 3H), 7.62 (d, J = 9.0 Hz, 1H), 7.59 (d, J = 2.4 Hz, 1H), 7.52 (dd, J = 8.4, 2.4 Hz, 1H), 6.99 (d, J = 8.4 Hz, 1H), 3.91 (s, 3H), 2.20 (d, J = 3.0 Hz, 6H), 2.12 (t, J = 3.0 Hz, 3H), 1.82 (t, J = 3.0 Hz, 6H); $^{13}C\{^1H\}$ NMR (151 MHz, $CDCl_3$): δ 158.9, 139.7, 139.1, 136.5, 134.8, 133.9, 132.8, 132.6, 129.7, 127.3, 126.6, 126.0, 125.7, 125.0, 112.2, 91.0, 55.3, 40.7, 37.3$_2$, 37.2$_6$, 29.2.

These data align with previously published reports in the literature.[14]

1-Bromonaphthalene (4a)

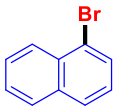

4a

Prepared according to procedure J as a colorless oil. R_f = 0.60 (hexane). Isolated yields were 86% (35.5 mg) from **1a** and 79% (32.6 mg) from **1a'**, respectively. ^{1}H NMR (400 MHz, $CDCl_3$): δ 8.31–8.29 (m, 1H), 7.87–7.81 (m, 3H), 7.66–7.61 (m, 1H), 7.58–7.54 (m, 1H), 7.34 (t, J = 7.6 Hz, 1H); $^{13}C\{^1H\}$ NMR (151 MHz, $CDCl_3$): δ 134.7, 132.1, 130.0, 128.4, 128.1, 127.5, 127.2, 126.8, 126.3, 123.0.

These data align with previously published reports in the literature.[52]

2-Bromonaphthalene (4b)

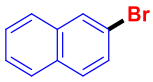

4b

Prepared according to procedure J as a white solid. R_f = 0.60 (hexane). Isolated yield was 61% (25.2 mg) from **1b**. ^{1}H NMR (400 MHz, $CDCl_3$): δ 8.02–8.01 (m, 1H), 7.84–7.79 (m, 1H), 7.78–7.74 (m, 1H), 7.73–7.70 (m, 1H), 7.55 (dd, J = 8.7, 2.0 Hz, 1H), 7.53–7.47 (m, 2H); $^{13}C\{^1H\}$ NMR (101 MHz, $CDCl_3$): δ 134.6, 131.9, 130.0, 129.7, 129.4, 128.0, 127.1, 127.0, 126.4, 119.9.

These data align with previously published reports in the literature.[53]

1-Bromo-3-phenoxybenzene (4d)

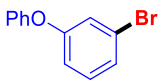

4d

Prepared according to procedure J as a colorless oil. R_f = 0.40 (hexane). Isolated yields were 70% (34.7 mg) from **1d** and 61% (30.5 mg) from **1d'**, respectively. ^{1}H NMR (400 MHz, $CDCl_3$): δ 7.40–7.35 (m, 2H), 7.25–7.19 (m, 2H), 7.18–7.14 (m, 2H), 7.05–7.01 (m, 2H), 6.94 (ddd, J = 7.7, 2.4, 1.4 Hz, 1H); $^{13}C\{^1H\}$ NMR (101 MHz, $CDCl_3$): δ 158.5, 156.4, 130.9, 130.1, 126.2, 124.1, 123.0, 121.8, 119.5, 117.3.

These data align with previously published reports in the literature.[54]

4-Bromo-1,1'-biphenyl (4e)

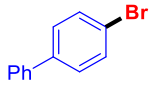

4e

Prepared according to procedure J as a white solid. R_f = 0.55 (hexane). Isolated yields were 64% (29.7 mg) from **1e** and 65% (30.5 mg) from **1e'**, respectively. ^{1}H NMR (400 MHz, $CDCl_3$): δ 7.59–7.55 (m, 4H), 7.48–7.43 (m, 4H), 7.40–7.36 (m, 1H); $^{13}C\{^1H\}$ NMR (101 MHz, $CDCl_3$): δ 140.3, 140.1, 132.0, 129.0, 128.9, 127.8, 127.1, 121.7.
These data align with previously published reports in the literature.[52]

3-Bromo-1,1'-biphenyl (4f)

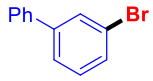

4f

Prepared according to procedure J as a colorless oil. R_f = 0.55 (hexane). Isolated yield was 74% (34.5 mg) from **1f**. ^{1}H NMR (400 MHz, $CDCl_3$): δ 7.76 (t, J = 1.8 Hz, 1H), 7.59–7.55 (m, 2H), 7.54–7.51 (m, 1H), 7.50–7.44 (m, 3H), 7.41–7.37 (m, 1H), 7.32 (t, J = 7.8 Hz, 1H); $^{13}C\{^1H\}$ NMR (101 MHz, $CDCl_3$): δ 143.5, 139.8, 130.4, 130.3$_4$, 130.3$_0$, 129.0, 128.0, 127.2, 125.9, 123.0.
These data align with previously published reports in the literature.[55]

4-Bromobenzophenone (4g)

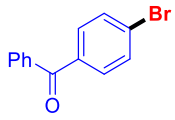

4g

Prepared according to procedure J as a white solid. R_f = 0.40 (DCM/hexane = 1/1). Isolated yield was 70% (36.9 mg) from **1g**. ^{1}H NMR (400 MHz, $CDCl_3$): δ 7.79–7.76 (m, 2H), 7.69–7.66 (m, 2H), 7.64–7.58 (m, 3H), 7.51–7.46 (m, 2H); $^{13}C\{^1H\}$ NMR (101 MHz, $CDCl_3$): δ 195.8, 137.3, 136.4, 132.8, 131.7$_3$, 131.6$_9$, 130.1, 128.5, 127.6.
These data align with previously published reports in the literature.[56]

4-Bromobenzonitrile (4h)

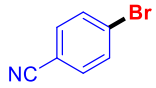

4h

Prepared according to procedure J as a white solid. R_f = 0.25 (DCM/hexane = 1/1). Isolated yield was 59% (21.5 mg) from **1h**. ^{1}H NMR (400 MHz, $CDCl_3$): δ 7.65–7.61 (m, 2H), 7.54–7.51 (m, 2H); $^{13}C\{^1H\}$ NMR (101 MHz, $CDCl_3$): δ 133.5, 132.8, 128.1, 118.2, 111.3.

These data align with previously published reports in the literature.[52]

Methyl 4-Bromobenzoate (4i)

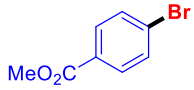

4i

Prepared according to procedure J as a white solid. R_f = 0.40 (DCM/hexane = 1/1). Isolated yield was 41% (17.6 mg) from **1i**. ^{1}H NMR (400 MHz, $CDCl_3$): δ 7.91–7.88 (m, 2H), 7.59–7.56 (m, 2H), 3.91 (s, 3H); $^{13}C\{^1H\}$ NMR (101 MHz, $CDCl_3$): δ 166.5, 131.9, 131.3, 129.2, 128.2, 52.4.

These data align with previously published reports in the literature.[52]

1-Bromo-9*H*-fluorene (4j)

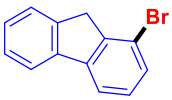

4j

Prepared according to procedure J as a white solid. mp: 64–67 °C. R_f = 0.55 (hexane). Isolated yield was 84% (41.3 mg) from **1j**. ^{1}H NMR (400 MHz, $CDCl_3$): δ 7.77–7.75 (m, 1H), 7.71 (dd, J = 7.5, 0.9 Hz, 1H), 7.58 (ddt, J = 7.1, 1.7, 0.9 Hz, 1H), 7.46 (dd, J = 7.9, 0.9 Hz, 1H), 7.41 (tdt, J = 7.4, 1.4, 0.7 Hz, 1H), 7.36 (td, J = 7.3, 1.3 Hz, 1H), 7.27 (tt, J = 7.8, 0.8 Hz, 1H), 3.87 (s, 2H); $^{13}C\{^1H\}$ NMR (101 MHz, $CDCl_3$): δ 143.5$_3$, 143.4$_6$, 142.5, 141.4, 129.7, 128.7, 127.5, 127.1, 125.2, 120.5, 120.3, 118.9, 38.8. FT-IR (cm^{-1}): 3049 (s), 2889 (s), 1560 (s), 1446 (s), 1424 (s), 1130 (s), 1031 (s), 1014 (s), 751 (s), 727 (s), 659 (s). Anal. Calcd for $C_{13}H_9Br$: C, 63.70; H, 3.70%; Found: C, 63.98; H, 3.88%.

4-Bromo-*N*,*N*-dipropylbenzenesulfonamide (4k)

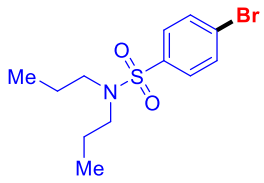

4k

Prepared according to procedure J as a white solid. R_f = 0.40 (DCM/hexane = 2/1). Isolated yield was 68% (43.4 mg) from **1k**. ^{1}H NMR (400 MHz, $CDCl_3$): δ 7.67–7.61 (m, 4H), 3.08–3.04 (m, 4H), 1.54 (hept, J = 7.4 Hz, 4H), 0.86 (t, J = 7.4 Hz, 6H); $^{13}C\{^1H\}$ NMR (101 MHz, $CDCl_3$): δ 139.4, 132.3, 128.7, 127.2, 50.1, 22.1, 11.3.

These data align with previously published reports in the literature.[57]

1-Chloronaphthalene (5a)

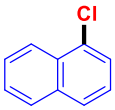

5a

Prepared according to procedure K as a colorless oil. R_f = 0.55 (hexane). Isolated yield was 75% (24.3 mg). ^{1}H NMR (400 MHz, $CDCl_3$): δ 8.30–8.28 (m, 1H), 7.88–7.86 (m, 1H), 7.78 (d, J = 8.0 Hz, 1H), 7.63–7.53 (m, 3H), 7.42–7.38 (m, 1H); ^{13}C{^{1}H} NMR (101 MHz, $CDCl_3$): δ 134.7, 132.1, 130.9, 128.4, 127.3, 127.2, 126.8, 126.3, 125.9, 124.5. These data align with previously published reports in the literature.[17]

1-Chloro-3-phenoxybenzene (5b)

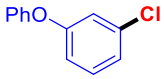

5b

Prepared according to procedure K as a colorless oil. R_f = 0.60 (DCM/hexane = 1/10). Isolated yield was 62% (25.4 mg). ^{1}H NMR (600 MHz, $CDCl_3$): δ 7.39–7.36 (m, 2H), 7.25 (t, J = 8.4 Hz, 1H), 7.17–7.15 (m, 1H), 7.07 (ddt, J = 8.0, 1.7, 0.7 Hz, 1H), 7.05–7.02 (m, 2H), 6.99 (t, J = 2.2 Hz, 1H), 6.90 (ddt, J = 8.2, 2.4, 0.7 Hz, 1H); ^{13}C{^{1}H} NMR (151 MHz, $CDCl_3$): δ 158.5, 156.4, 135.2, 130.6, 130.1, 124.1, 123.3, 119.6, 118.9, 116.8. These data align with previously published reports in the literature.[58]

3-Chloro-1,1'-biphenyl (5c)

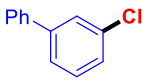

5c

Prepared according to procedure K as a colorless oil. R_f = 0.55 (hexane). Isolated yield was 61% (23.1 mg). ^{1}H NMR (600 MHz, $CDCl_3$): δ 7.60–7.57 (m, 3H), 7.49–7.45 (m, 3H), 7.40–7.37 (m, 2H), 7.33 (ddd, J = 8.0, 2.1, 1.2 Hz, 1H); ^{13}C{^{1}H} NMR (151 MHz, $CDCl_3$): δ 143.2, 139.9, 134.8, 130.1, 129.0, 128.0, 127.4$_3$, 127.3$_9$, 127.3, 125.4. These data align with previously published reports in the literature.[55]

4-Chlorobenzophenone (5d)

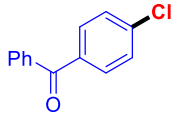

5d

Prepared according to procedure K as a white solid. R_f = 0.30 (DCM/hexane = 1/1). Isolated yield was 80% (34.6 mg). ^{1}H NMR (600 MHz, $CDCl_3$): δ 7.78–7.74 (m, 4H), 7.61–7.58 (m, 1H), 7.50–7.45 (m, 4H); $^{13}C\{^1H\}$ NMR (151 MHz, $CDCl_3$): δ 195.6, 139.0, 137.3, 136.0, 132.8, 131.6, 130.0, 128.7, 128.5.

These data align with previously published reports in the literature.[17]

1-Chloro-9*H*-fluorene (5e)

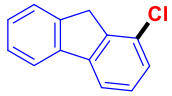

5e

Prepared according to procedure K as a white solid. R_f = 0.55 (hexane). Isolated yield was 70% (28.2 mg). ^{1}H NMR (600 MHz, $CDCl_3$): δ 7.78 (d, J = 7.5 Hz, 1H), 7.68 (d, J = 7.5 Hz, 1H), 7.58 (dt, J = 7.3, 1.0 Hz, 1H), 7.41 (td, J = 7.5, 1.0 Hz, 1H), 7.37–7.33 (m, 2H), 7.30–7.29 (m, 1H), 3.92 (s, 2H); $^{13}C\{^1H\}$ NMR (151 MHz, $CDCl_3$): δ 143.6, 142.8, 141.2$_9$, 141.2$_7$, 131.2, 128.6, 127.5, 127.1, 126.8, 125.3, 120.5, 118.3, 36.7.

These data align with previously published reports in the literature.[59]

4-Chloro-*N*,*N*-dipropylbenzenesulfonamide (5f)

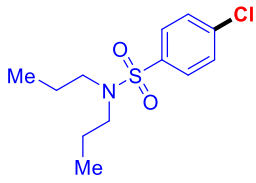

5f

Prepared according to procedure K as a colorless oil. R_f = 0.40 (DCM/hexane = 2/1). Isolated yield was 83% (46 mg). ^{1}H NMR (600 MHz, $CDCl_3$): δ 7.74–7.72 (m, 2H), 7.47–7.45 (m, 2H), 3.07–3.05 (m, 4H), 1.54 (hept, J = 7.2 Hz, 4H), 0.86 (t, J = 7.4 Hz, 6H); $^{13}C\{^1H\}$ NMR (151 MHz, $CDCl_3$): δ 138.9, 138.7, 129.4, 128.6, 50.1, 22.1, 11.3.

These data align with previously published reports in the literature.[60]

2-4-4 Experimental Procedures of Mechanistic Study

2-4-4-1 Catalytic and Stoichiometric Time-Course Experiments

Catalytic reaction

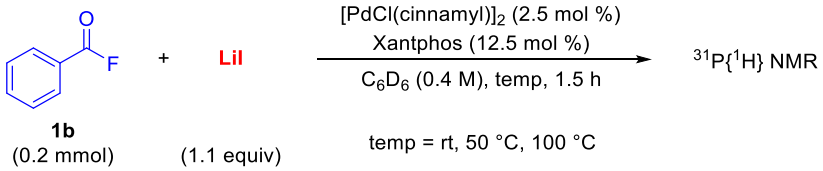

An oven-dried J. Young NMR tube was loaded with $[PdCl(cinnamyl)]_2$ (2.5 mol %, 5 μmol, 2.6 mg), Xantphos (12.5 mol %, 0.025 mmol, 14.5 mg), lithium iodide (0.22 mmol, 1.1 equiv, 29.4 mg), benzoyl fluoride (**1b**, 0.2 mmol, 1 equiv, 22 μL), and benzene-d_6 (0.5 mL, 0.4 M) in a nitrogen-filled glovebox. The tube was securely sealed and kept at room temperature for 1.5 h before being heated at 50 °C for 1.5 h, followed by an additional heating step at 100 °C for 1.5 h in an oil bath, with manual shaking every 5 min. $^{31}P\{^1H\}$ NMR spectra were recorded at each stage to monitor the reaction progress, as reported in **Scheme 2-11**.

Stoichiometric reaction

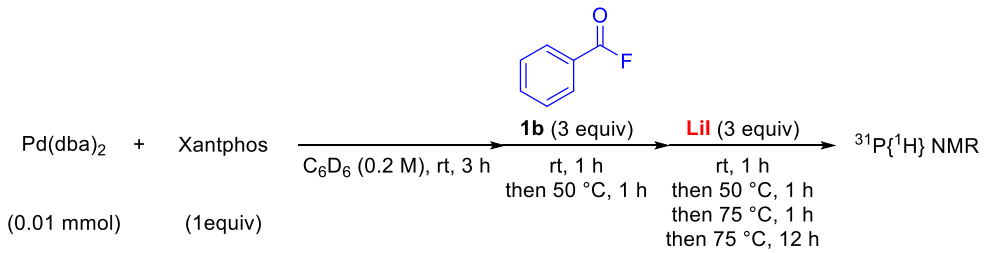

An oven-dried J. Young NMR tube was loaded with $Pd(dba)_2$ (0.01 mmol, 1 equiv, 5.2 mg), Xantphos (0.01 mmol, 1 equiv, 5.8 mg), and benzene-d_6 (0.5 mL, 0.2 M) inside a

nitrogen-filled glovebox. The tube was securely sealed, and a $^{31}P\{^{1}H\}$ NMR spectrum was immediately recorded. After the tube was kept at room temperature for 3 h, benzoyl fluoride (**1b**, 0.03 mmol, 3 equiv, 3.2 μL) was added in the glovebox. The reaction mixture was then left at room temperature for 1 hour and subsequently heated at 50 °C for 1 hour. Following this, lithium iodide (0.03 mmol, 3 equiv, 4.0 mg) was added in the glovebox. The reaction tube was kept at room temperature for 1 hour, then heated sequentially at 50 °C for 1 hour, 75 °C for 1 hour, and finally for 12 h with manual shaking every 5 min. $^{31}P\{^{1}H\}$ NMR spectra were recorded at each stage to monitor the reaction progress, as reported in **Scheme 2-12**.

2-4-4-2 Synthesis of Pd Complexes 6 and 7

***Trans*-(Xantphos)Pd(COPh)I (6):**

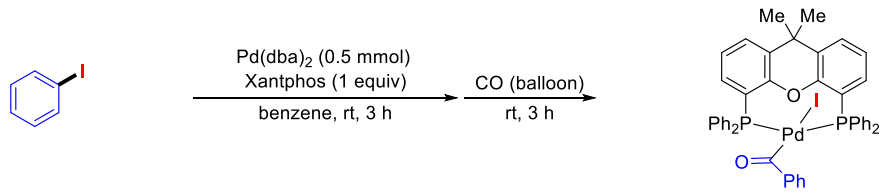

2b
(19 equiv)

6, 63%

Following a procedure reported in the literature,[14,19] an oven-dried 50-mL Schlenk tube equipped with a magnetic stirring bar was loaded with $Pd(dba)_2$ (0.5 mmol, 1 equiv, 287.5 mg), Xantphos (0.5 mmol, 1 equiv, 289.3 mg), iodobenzene (**2b**, 9.5 mmol, 19 equiv, 1.1 mL), and anhydrous benzene (10 mL, 0.05 M) inside a nitrogen-filled glovebox. The tube was sealed with a glass stopper and stirred at room temperature for 3 h. Subsequently, the sidearm of the Schlenk tube was connected to a carbon monoxide (CO) balloon, and the reaction mixture was stirred continuously at room temperature for an additional 3 h. Upon completion, the solvent was reduced to approximately 2 mL under vacuum, and diethyl ether (10 mL) was added to the residue. The resulting mixture was filtered, and the solid was washed with diethyl ether (3 × 10 mL). The collected solid was dissolved in dichloromethane (10 mL) and passed through a short Celite column. The filtrate was concentrated under reduced pressure, yielding complex **6** as a red powder (289 mg, 63%).

^{1}H NMR (600 MHz, $CDCl_3$): δ 7.71–7.70 (m, 2H), 7.55 (dd, J = 7.8, 1.5 Hz, 2H), 7.40–7.37 (m, 8H), 7.25 (t, J = 7.0 Hz, 4H), 7.18 (tt, J = 7.2, 1.3 Hz, 1H), 7.13 (t, J = 7.8 Hz, 8H), 7.05 (dt, J = 16.3, 7.6 Hz, 4H), 6.78–6.74 (m, 2H), 1.67 (s, 6H); ^{13}C{^{1}H} NMR (151 MHz, $CDCl_3$): δ 154.8 (t, J = 5.1 Hz), 140.7 (t, J = 11.9 Hz), 134.4 (t, J = 6.2 Hz), 133.5, 132.5, 131.9 (t, J = 19.6 Hz), 131.0, 130.8, 129.7, 128.1 (t, J = 4.8 Hz), 127.4, 127.3, 124.3, 121.1 (t, J = 15.7 Hz), 35.9, 28.7; ^{31}P{^{1}H} NMR (162 MHz, $CDCl_3$): δ 0.50 (s). These data align with previously published reports in the literature.[19]

***Trans*-(Xantphos)Pd(Ph)I (7):**

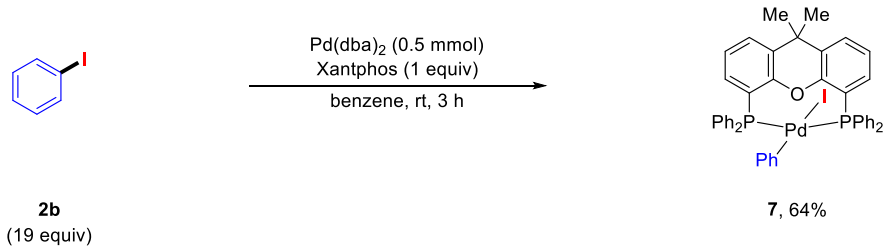

2b
(19 equiv)

7, 64%

Following the procedure described in the literature,[14] an oven-dried 50-mL Schlenk tube equipped with a magnetic stirring bar was loaded with $Pd(dba)_2$ (0.5 mmol, 1 equiv, 287.5 mg), Xantphos (0.5 mmol, 1 equiv, 289.3 mg), iodobenzene (**2b**, 9.5 mmol, 19 equiv, 1.1 mL), and anhydrous benzene (10 mL, 0.05 M) inside a nitrogen-filled glovebox. The tube was sealed with a glass stopper and stirred at room temperature for 3 h. After stirring, the solvent was concentrated to approximately 2 mL under vacuum, and diethyl ether (10 mL) was added to the residue. The resulting mixture was filtered, and the collected solid was washed with diethyl ether (3 × 10 mL). The solid was then dissolved in dichloromethane (10 mL) and passed through a short column of Celite. The filtrate was concentrated under reduced pressure to yield complex **7** as an orange powder (285 mg, 64%).

^{1}H NMR (600 MHz, $CDCl_3$): δ 7.61 (d, J = 7.6 Hz, 2H), 7.40–7.32 (m, 8H), 7.26–7.21 (m, 6H), 7.16 (t, J = 7.8 Hz, 2H), 7.13 (t, J = 7.8 Hz, 8H), 6.52–6.51 (m, 2H), 6.30 (t, J = 7.2 Hz, 1H), 6.14 (t, J = 7.6 Hz, 2H), 1.80 (s, 6H); ^{13}C{^{1}H} NMR (151 MHz, $CDCl_3$): δ 158.5, 155.6 (t, J = 5.6 Hz), 135.3 (t, J = 6.2 Hz), 134.8 (t, J = 2.4 Hz), 134.2 (t, J = 2.9 Hz), 131.7 (t, J = 22.5 Hz), 131.2, 129.7, 127.9 (t, J = 5.1 Hz), 127.1, 126.6, 124.3 (t, J = 3.0 Hz), 123.3, 121.1, 36.2, 28.4; ^{31}P{^{1}H} NMR (162 MHz, $CDCl_3$): δ 9.49 (s).
These data align with previously published reports in the literature.[14]

2-4-4-3 Catalytic Activity of Complexes 6 and 7

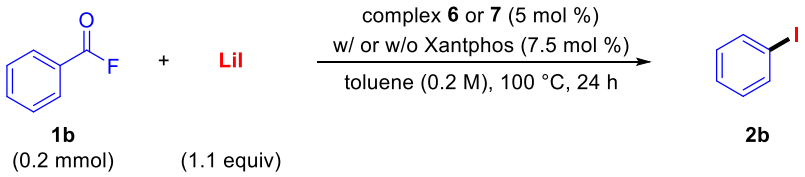

An oven-dried 5-mL microwave vial equipped with a magnetic stirring bar was loaded with Pd complex **6** or **7** (5 mol %, 0.01 mmol, 9.2 mg or 8.9 mg, respectively) and Xantphos (7.5 mol %, 0.015 mmol, 8.7 mg) under ambient air. Lithium iodide (0.22 mmol, 1.1 equiv, 29.4 mg) and anhydrous toluene (1 mL, 0.2 M) were introduced in a nitrogen-filled glovebox. The vial was tightly sealed, and benzoyl fluoride (**1b**, 0.2 mmol, 1 equiv, 22 μL) was added via syringe through the septum of the cap. The sealed vial was placed in a preheated block at 100 °C and stirred for 24 h. After cooling to room temperature, *n*-dodecane was added as an internal standard. The yield of iodobenzene (**2b**) was quantified through GC analysis of the reaction mixture, as reported in **Table 2-10**.

2-4-4-4 Catalytic Inactivity of (Xantphos)PdI_2

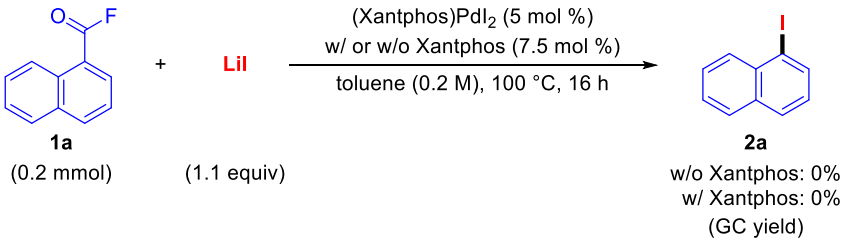

An oven-dried 5-mL microwave vial equipped with a magnetic stirring bar was charged with (Xantphos)PdI_2 (5 mol %, 0.01 mmol, 9.4 mg), prepared according to a reported method,[19] and Xantphos (7.5 mol %, 0.015 mmol, 8.7 mg) under ambient air. 1-Naphthoyl fluoride (**1a**, 0.2 mmol, 1 equiv, 34.8 mg), lithium iodide (0.22 mmol, 1.1 equiv, 29.4 mg), and anhydrous toluene (1 mL, 0.2 M) were then added in a nitrogen-filled glovebox. The vial was securely sealed and heated in a preheated block at 100 °C for 16 h with stirring. After cooling to room temperature, *n*-dodecane was introduced as an internal standard. GC analysis of the reaction mixture revealed that no 1-iodonaphthalene (**2a**) was detected, irrespective of the presence of Xantphos, as reported in **Scheme 2-13**.

2-4-4-5 Synthesis of Acyl Iodides (11)

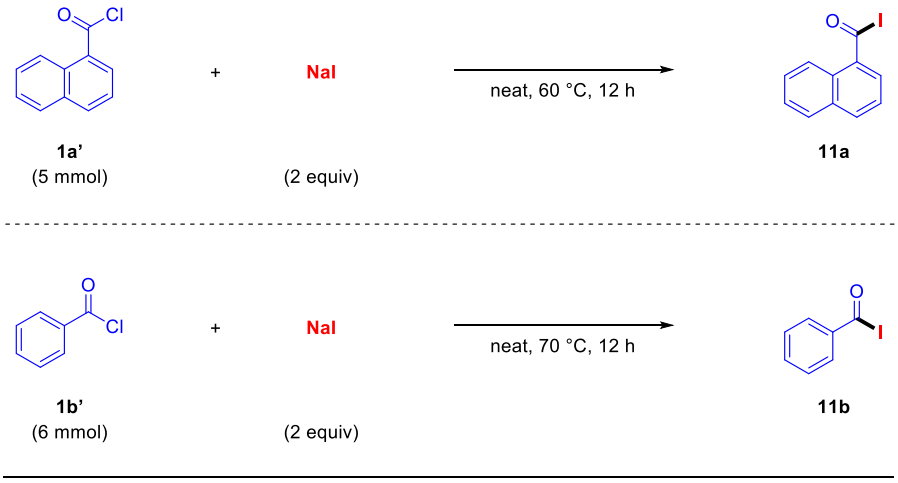

Following the reported method,[61] an oven-dried 5-mL microwave vial equipped with a magnetic stirring bar was loaded with sodium iodide (10 mmol or 12 mmol, 2 equiv, 1.5 g or 1.8 g, respectively) and freshly distilled 1-naphthoyl chloride (**1a'**, 5 mmol, 1 equiv, 751 μL) or benzoyl chloride (**1b'**, 6 mmol, 1 equiv, 691 μL) inside a nitrogen-filled glovebox. The vial was securely sealed and heated in a preheated block at 60 °C (for **1a'**) or 70 °C (for **1b'**) for 12 h with continuous stirring. After cooling to room temperature, the vial was brought back into the glovebox. The reaction mixture was filtered through a 0.2 μm PTFE filter, and the filtrate was further filtered through a fresh filter to yield the desired product, **11a** or **11b**, as an orange-red liquid in quantitative yield. Compounds **11a** and **11b** were stable when stored in a light-protected vial inside the glovebox for over one month without any noticeable changes in appearance or reactivity.

1-Naphthoyl chloride (1a')

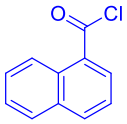

1a'

^{1}H NMR (400 MHz, $CDCl_3$): δ 8.79–8.76 (m, 1H), 8.58 (dd, J = 7.5, 1.2 Hz, 1H), 8.14 (d, J = 8.0 Hz, 1H), 7.94–7.92 (m, 1H), 7.70 (ddd, J = 8.6, 6.9, 1.5 Hz, 1H), 7.62–7.56 (m, 2H); ^{13}C{^{1}H} NMR (101 MHz, $CDCl_3$): δ 167.6, 136.4, 135.5, 133.8, 130.8, 129.6$_4$, 129.6$_1$, 129.0, 127.2, 125.2, 124.7.

This reagent was purchased from TCI.

1-Naphthoyl iodide (11a)

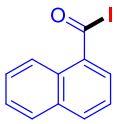

11a

^{1}H NMR (400 MHz, $CDCl_3$): δ 8.58 (d, J = 8.7 Hz, 1H), 8.37 (d, J = 7.5 Hz, 1H), 8.11 (d, J = 8.2 Hz, 1H), 7.92 (d, J = 8.1 Hz, 1H), 7.72–7.67 (m, 1H), 7.65–7.58 (m, 2H); ^{13}C{^{1}H} NMR (101 MHz, $CDCl_3$): δ 158.9, 139.5, 136.2, 133.6, 132.9, 129.8, 128.6, 127.6, 127.4, 124.7, 124.6.

Benzoyl chloride (1b')

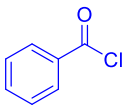

1b'

^{1}H NMR (600 MHz, $CDCl_3$): δ 8.13–8.11 (m, 2H), 7.69 (tt, J = 7.8, 1.3 Hz, 1H), 7.54–7.50 (m, 2H); ^{13}C{^{1}H} NMR (151 MHz, $CDCl_3$): δ 168.6, 135.5, 133.4, 131.6, 129.1.

This reagent was purchased from TCI.

Benzoyl iodide (11b)

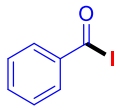

11b

^{1}H NMR (600 MHz, $CDCl_3$): δ 7.93–7.91 (m, 2H), 7.68 (td, J = 7.5, 2.2 Hz, 1H), 7.49–7.46 (m, 2H); $^{13}C\{^{1}H\}$ NMR (151 MHz, $CDCl_3$): δ 160.2, 137.0, 135.8, 132.5, 129.0. These data align with previously published reports in the literature.[62]

2-4-4-6 Pd-Catalyzed Unimolecular Fragment Coupling (UFC) of Acyl Iodides

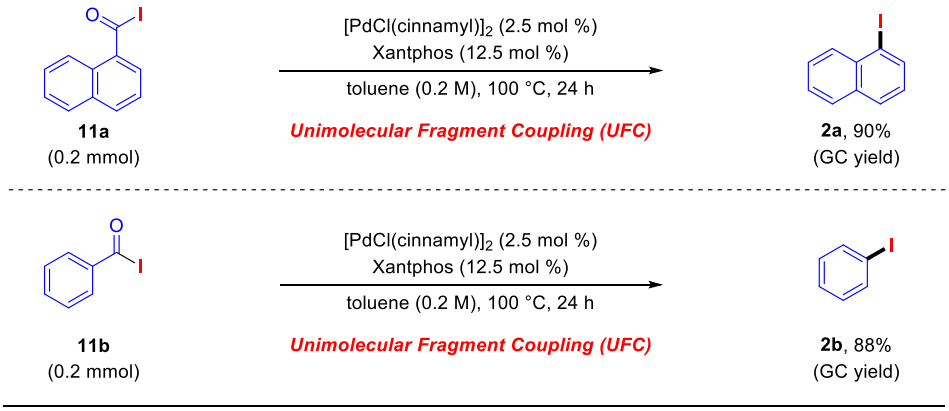

An oven-dried 5-mL microwave vial equipped with a magnetic stirring bar was loaded with $[PdCl(cinnamyl)]_2$ (2.5 mol %, 5 μmol, 2.6 mg) and Xantphos (12.5 mol %, 0.025 mmol, 14.5 mg) under ambient air. Acyl iodide (**11a**, 0.2 mmol, 1 equiv, 56.4 mg) or (**11b**, 0.2 mmol, 1 equiv, 46.4 mg) and anhydrous toluene (1 mL, 0.2 M) were introduced in a nitrogen-filled glovebox. The vial was securely sealed and heated in a preheated block at 100 °C for 24 h with continuous stirring. After cooling to room temperature, *n*-dodecane was added as an internal standard. The yields of aryl iodides **2a** and **2b** were quantified using GC, resulting in 90% and 88% yields, respectively, as reported in **Scheme 2-17**.

2-4-4-7 Stepwise Reaction of Acyl Chlorides and Metal Iodides

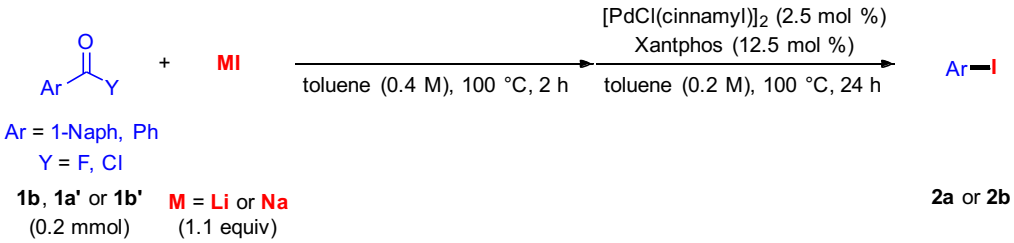

An oven-dried 5-mL microwave vial equipped with a magnetic stirring bar was loaded with benzoyl fluoride (**1a**, 0.2 mmol, 1 equiv, 22 µL), 1-naphthoyl chloride (**1a'**, 0.2 mmol, 1 equiv, 30 µL), or benzoyl chloride (**1b'**, 0.2 mmol, 1 equiv, 23 µL), along with lithium iodide (0.22 mmol, 1.1 equiv, 29.4 mg) or sodium iodide (0.22 mmol, 1.1 equiv, 33.0 mg) and toluene (0.5 mL, 0.4 M) in a nitrogen-filled glovebox. The vial was securely sealed and heated in a preheated block at 100 °C for 2 h with stirring. Once the reaction mixture cooled to room temperature, the vial was returned to the glovebox. The reaction mixture was then transferred to a new oven-dried 5-mL microwave vial containing a magnetic stirring bar, $[PdCl(cinnamyl)]_2$ (2.5 mol %, 5 µmol, 2.6 mg), and Xantphos (12.5 mol %, 0.025 mmol, 14.5 mg), using an additional 0.5 mL of toluene. The vial was tightly sealed and heated again at 100 °C for 24 h with continuous stirring. After cooling to room temperature, *n*-dodecane or *n*-pentadecane was added as an internal standard, and the yield of 1-iodonaphthalene (**2a**) or iodobenzene (**2b**) was determined using GC analysis of the reaction mixture, as reported in **Table 2-11**.

2-4-4-8 Stepwise Reaction of 1-Naphthoyl Chloride (1a') and Lithium Iodide Including Vacuum Process

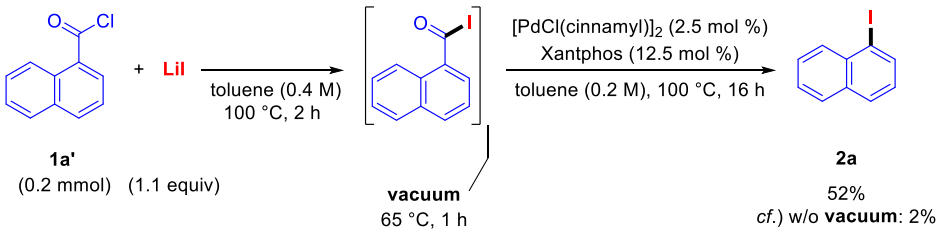

An oven-dried 5-mL microwave vial equipped with a magnetic stirring bar was loaded with 1-naphthoyl chloride (**1a'**, 0.2 mmol, 1 equiv, 30 µL), lithium iodide (0.22 mmol, 1.1 equiv, 29.4 mg), and anhydrous toluene (0.5 mL, 0.4 M) inside a nitrogen-filled glovebox. The vial was tightly sealed and heated in a preheated block at 100 °C for 2 h with continuous stirring. After the reaction mixture cooled to room temperature, it was filtered through a syringe filter in the glovebox. The filtrate was concentrated under reduced pressure at 65 °C for 1 hour. The residue was redissolved in toluene (0.5 mL) and filtered again through a syringe filter, and the solid on the filter was washed with an additional 0.5 mL of toluene. The combined filtrates were transferred to a new oven-dried 5-mL microwave vial containing a magnetic stirring bar, $[PdCl(cinnamyl)]_2$ (2.5 mol %, 5 µmol, 2.6 mg), and Xantphos (12.5 mol %, 0.025 mmol, 14.5 mg). The vial was securely sealed and heated in a preheated block at 100 °C for 16 h with stirring. After the reaction cooled to room temperature, n-dodecane was added as an internal standard. GC analysis of the reaction mixture revealed a 52% yield of 1-iodonaphthalene (**2a**), as reported in **Scheme 2-19**.

2-4-4-9 $^{31}P\{^{1}H\}$ NMR Monitoring of Decarbonylative Iodination of Acyl Chloride

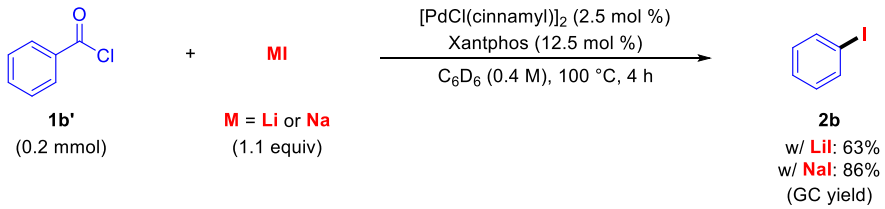

An oven-dried J. Young NMR tube was loaded with $[PdCl(cinnamyl)]_2$ (2.5 mol %, 5 μmol, 2.6 mg), Xantphos (12.5 mol %, 0.025 mmol, 14.5 mg), lithium iodide (0.22 mmol, 1.1 equiv, 29.4 mg) or sodium iodide (0.22 mmol, 1.1 equiv, 33.0 mg), benzoyl chloride (**1b'**, 0.2 mmol, 1 equiv, 23 μL), and benzene-d_6 (0.5 mL, 0.4 M) inside a nitrogen-filled glovebox. The tube was tightly sealed and heated in an oil bath at 100 °C for 4 h, with manual shaking every 5 min. After the reaction, $^{31}P\{^{1}H\}$ NMR spectra were recorded. Subsequently, *n*-dodecane was added as an internal standard. GC analysis of the reaction mixture showed that the yield of iodobenzene (**2b**) was 63% when LiI was used and 86% when NaI was employed, as reported in **Scheme 2-18**.

2-4-4-10 Control Experiment of Iodine as a Catalyst Poison

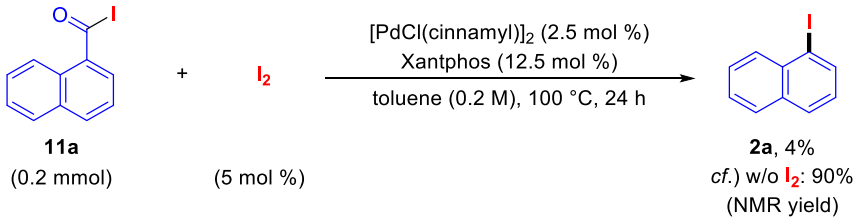

An oven-dried 5-mL microwave vial equipped with a magnetic stirring bar was charged with $[PdCl(cinnamyl)]_2$ (2.5 mol %, 5 μmol, 2.6 mg) and Xantphos (12.5 mol %, 0.025 mmol, 14.5 mg) under ambient air. 1-Naphthoyl iodide (**11a**, 0.2 mmol, 1 equiv, 56.4 mg), iodine in toluene (0.02 M, 5 mol %, 0.01 mmol, 0.5 mL), and anhydrous toluene (0.5 mL, 0.2 M) were added inside a nitrogen-filled glovebox. The vial was securely sealed and heated in a preheated block at 100 °C for 24 h with stirring. After cooling to room temperature, the reaction mixture was transferred to an oven-dried round-bottom flask. The vial was rinsed with dichloromethane (5 × 2 mL), and the combined solution was concentrated under reduced pressure. Dibromomethane was added as an internal standard, and the yield of 1-iodonaphthalene (**2a**) was determined to be 4% using ^{1}H NMR analysis, as reported in **Scheme 2-20**.

2-4-4-11 $^{31}P\{^{1}H\}$ NMR Monitoring the Decarbonylation of Acyl Iodide for the UFC Process

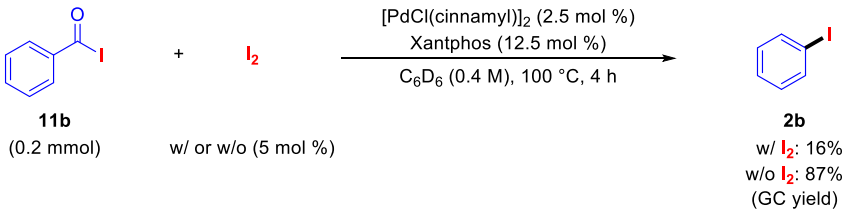

An oven-dried 5-mL microwave vial equipped with a magnetic stirring bar was charged with $[PdCl(cinnamyl)]_2$ (2.5 mol %, 5 μmol, 2.6 mg) and Xantphos (12.5 mol %, 0.025 mmol, 14.5 mg) under ambient air. Benzoyl iodide (**11b**, 0.2 mmol, 1 equiv, 46.4 mg) and benzene-d_6 (0.5 mL, 0.4 M) or iodine in benzene-d_6 (0.02 M, 5 mol %, 0.01 mmol, 0.5 mL) were added in a nitrogen-filled glovebox. The vial was securely sealed and heated in a preheated block at 100 °C for 4 h with stirring. After cooling to room temperature, the reaction mixture was transferred to an NMR tube inside the glovebox. $^{31}P\{^{1}H\}$ NMR analysis was performed (as reported in **Scheme 2-21**), followed by the addition of *n*-dodecane as an internal standard. GC analysis of the reaction mixture revealed that the yield of iodobenzene (**2b**) was 16% in the presence of I_2 and 87% in its absence.

2-4-4-12 Time-Course Study of the Formation of Acyl Iodide from Acyl Fluoride and Acyl Chloride

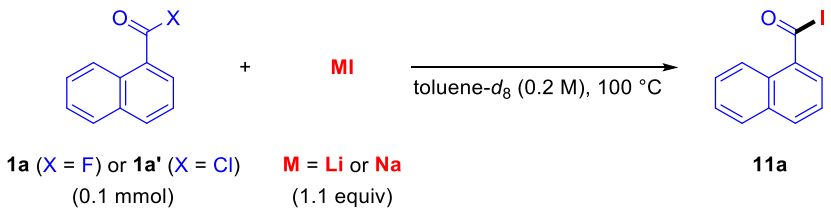

An oven-dried J. Young NMR tube was loaded with 1-naphthoyl fluoride (**1a**, 0.1 mmol, 1 equiv, 17.4 mg) or 1-naphthoyl chloride (**1a'**, 0.1 mmol, 1 equiv, 15.0 μL), lithium iodide (0.11 mmol, 1.1 equiv, 14.7 mg) or sodium iodide (0.11 mmol, 1.1 equiv, 16.5 mg), toluene-d_8 (0.5 mL, 0.2 M), and dibromomethane as an internal standard in a nitrogen-filled glovebox. The tube was sealed and heated in a preheated oil bath at 100 °C. After the reaction mixture cooled to room temperature, it was analyzed by ^{1}H NMR at various time points, as detailed in **Tables 2-12, 13, and 14**.

2-4-4-13 Effects of Li Salts on Pd-Catalyzed UFC of Acyl Iodide

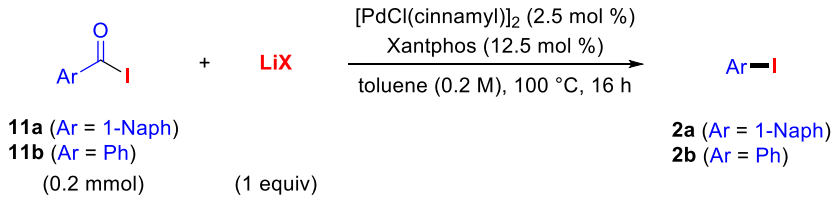

An oven-dried 5-mL microwave vial equipped with a magnetic stirring bar was charged with $[PdCl(cinnamyl)]_2$ (2.5 mol %, 5 μmol, 2.6 mg) and Xantphos (12.5 mol %, 0.025 mmol, 14.5 mg) under ambient air. The corresponding lithium salt (0.2 mmol, 1 equiv), 1-naphthoyl iodide (**11a**, 0.2 mmol, 1 equiv, 56.4 mg) or benzoyl iodide (**11b**, 0.2 mmol, 1 equiv, 46.4 mg), and anhydrous toluene (1 mL, 0.2 M) were added in a nitrogen-filled glovebox. The vial was securely sealed and heated in a preheated block at 100 °C for 16 h with continuous stirring. After cooling to room temperature, *n*-dodecane or *n*-pentadecane was added as an internal standard. The yield of each product (**2a** or **2b**) was determined by GC analysis, as reported in **Table 2-15**.

2-4-4-14 Effects of Lithium Iodide on Pd-Catalyzed UFC of Benzoyl Iodide (11b) in a Stepwise Procedure

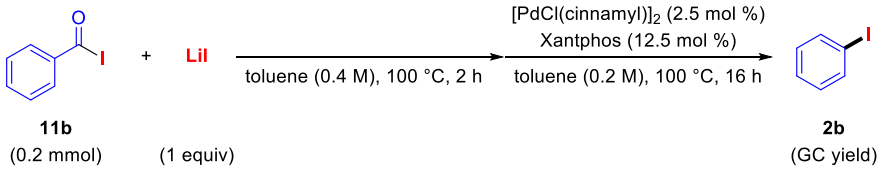

An oven-dried 5-mL microwave vial equipped with a magnetic stirring bar was loaded with benzoyl iodide (**11b**, 0.2 mmol, 1 equiv, 46.4 mg) and/or lithium iodide (0.2 mmol, 1 equiv, 26.8 mg), along with toluene (0.5 mL, 0.4 M) in a nitrogen-filled glovebox. The vial was securely sealed and heated in a preheated block at 100 °C for 2 h with stirring. After cooling to room temperature, the vial was brought back into the glovebox, and the reaction mixture was transferred to a second oven-dried 5-mL microwave vial containing a magnetic stirring bar, $[PdCl(cinnamyl)]_2$ (2.5 mol %, 5 μmol, 2.6 mg), and Xantphos (12.5 mol %, 0.025 mmol, 14.5 mg) using an additional 0.5 mL of toluene. The vial was tightly sealed and heated again at 100 °C for 16 h with stirring. After cooling to room temperature, *n*-dodecane was added as an internal standard, and GC analysis revealed the yield of iodobenzene (**2b**) was 15% when lithium iodide was present. Under the same conditions, the yield increased to 89% in the absence of lithium iodide, as reported in **Table 2-16**.

2-4-5 Copies of NMR Charts for All the Compounds

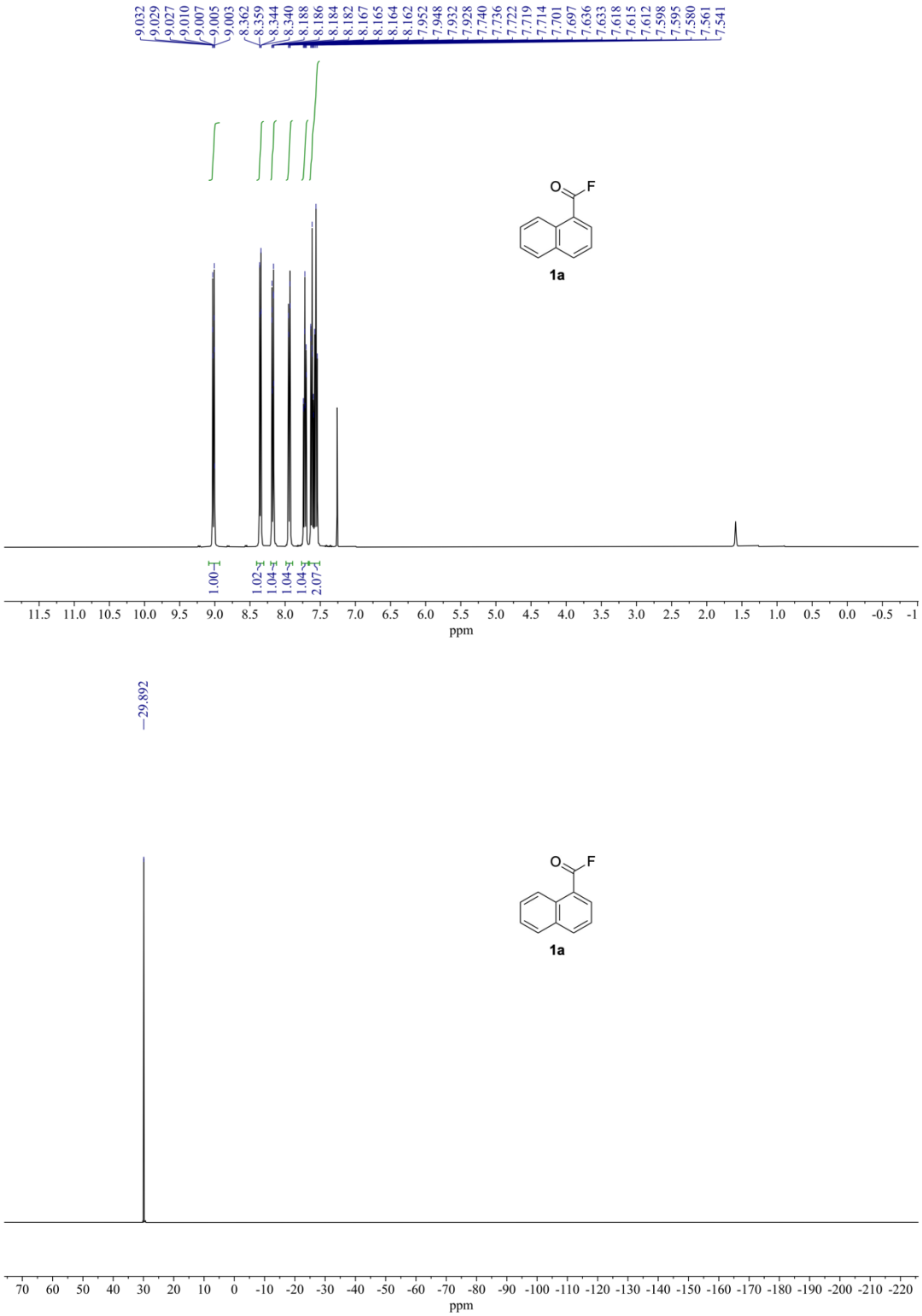

^{1}H NMR (400 MHz) and ^{19}F{^{1}H} NMR (376 MHz) spectra of **1a** (rt, $CDCl_3$).

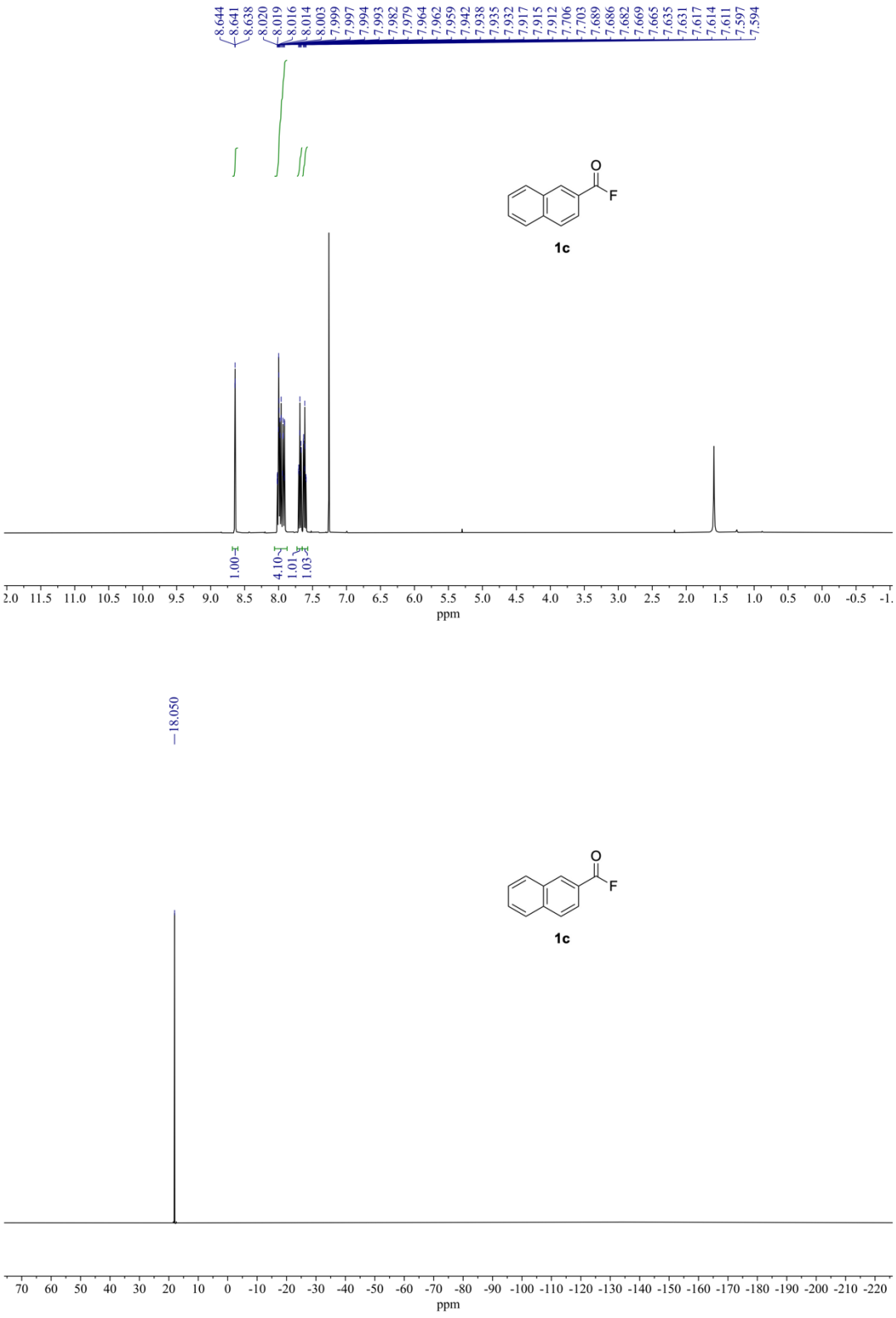

^{1}H NMR (400 MHz) and ^{19}F{^{1}H} NMR (376 MHz) spectra of **1c** (rt, $CDCl_3$).

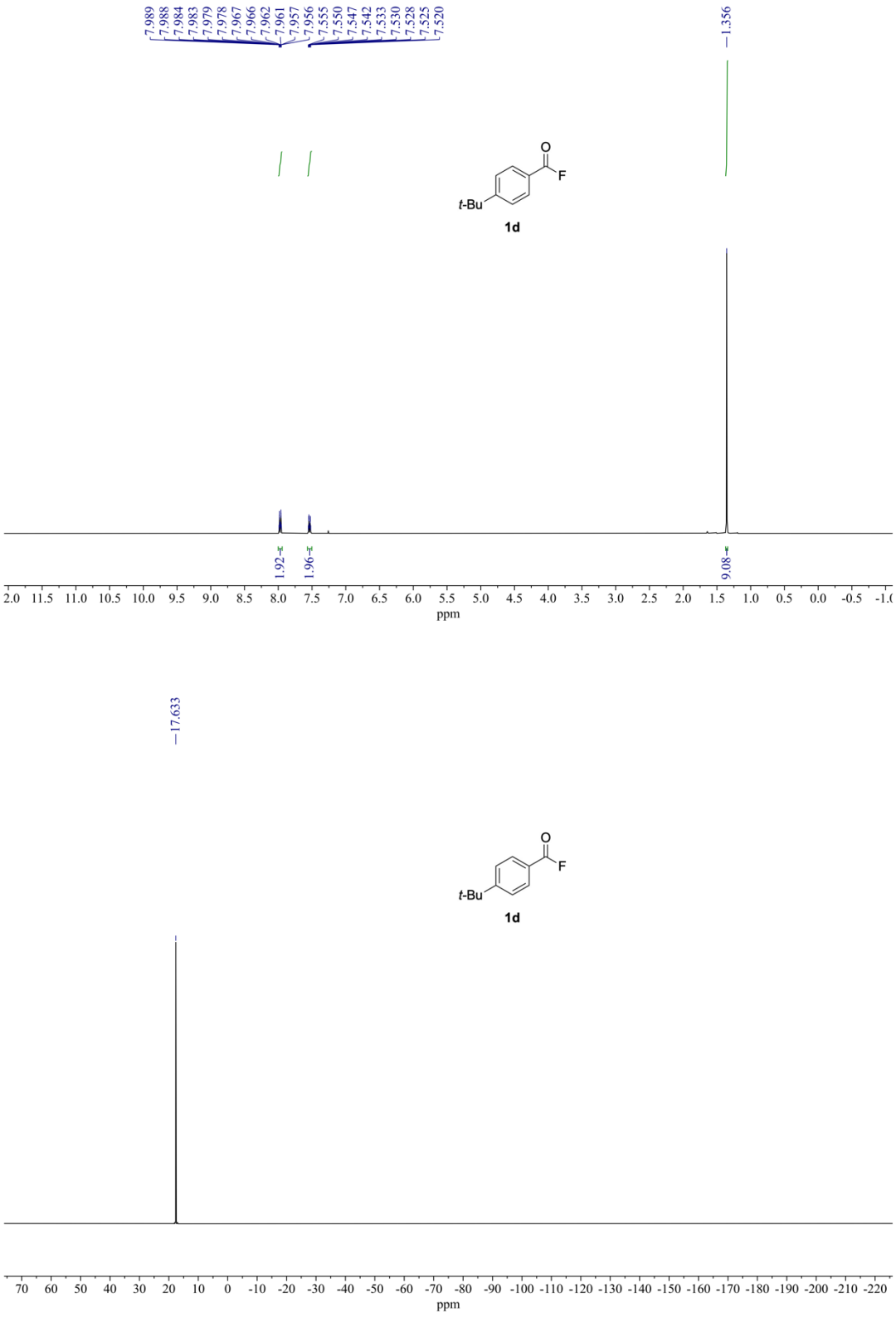

^{1}H NMR (400 MHz) and ^{19}F{^{1}H} NMR (376 MHz) spectra of **1d** (rt, $CDCl_3$).

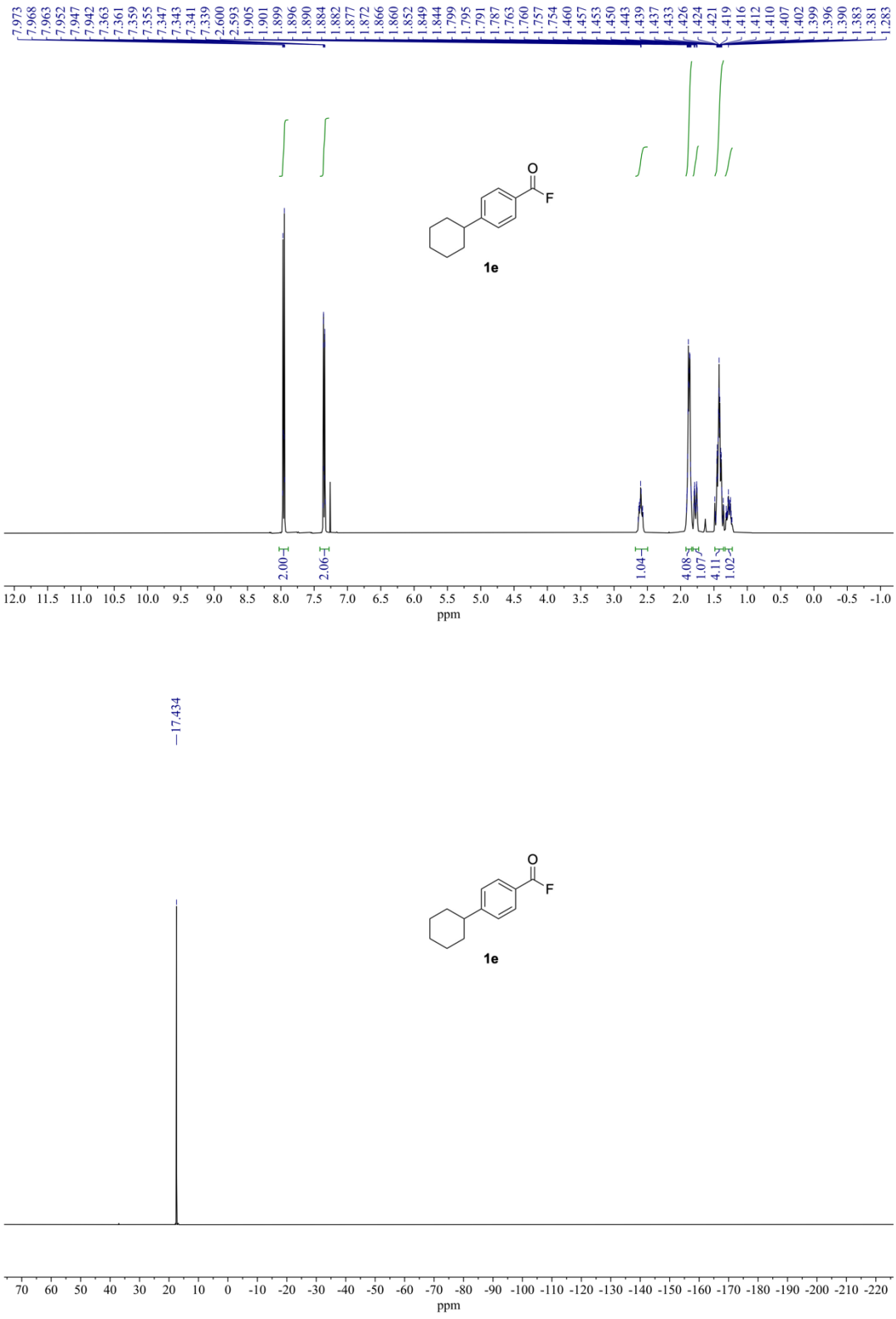

^{1}H NMR (400 MHz) and ^{19}F{^{1}H} NMR (376 MHz) spectra of **1e** (rt, $CDCl_3$).

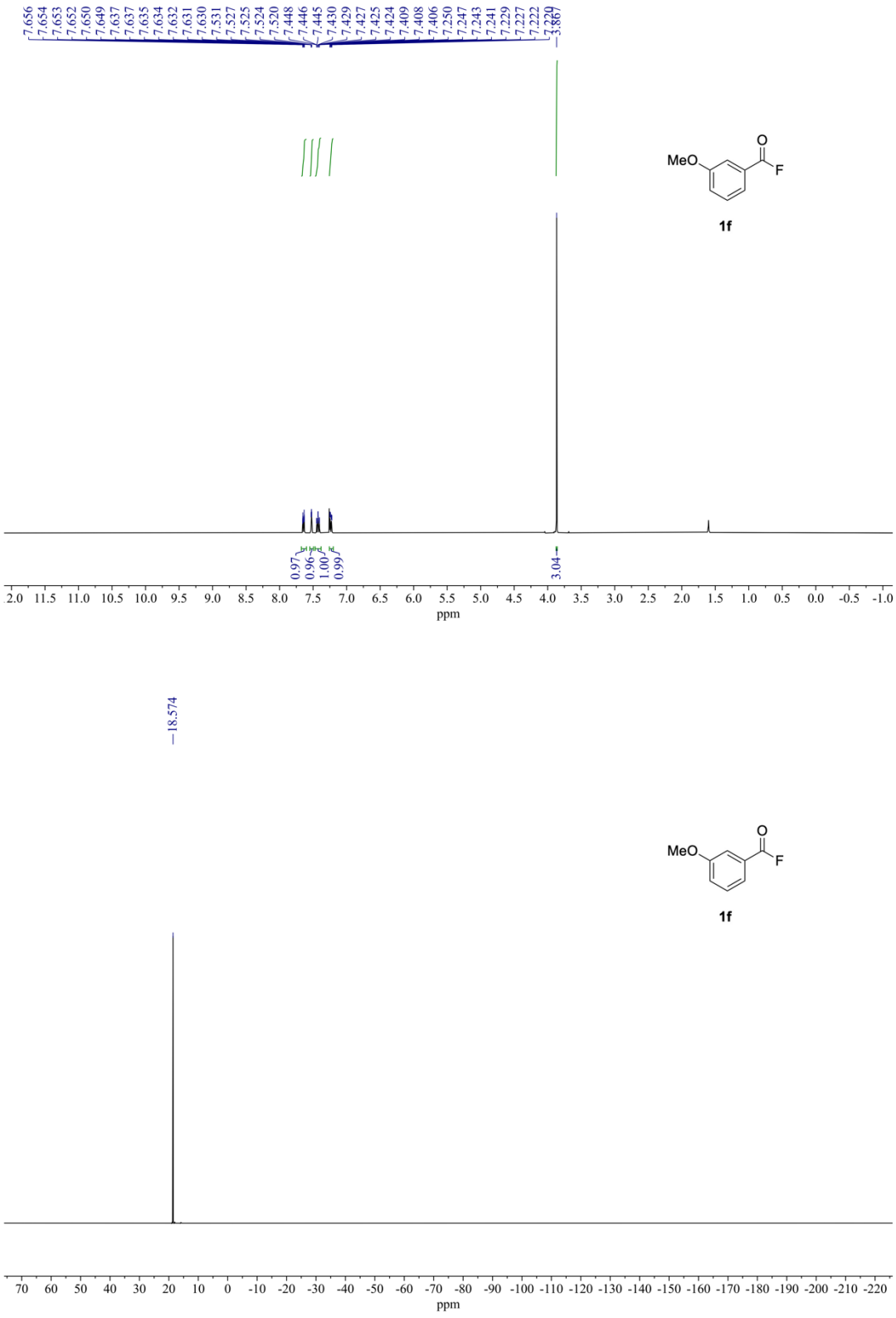

^{1}H NMR (400 MHz) and ^{19}F{^{1}H} NMR (376 MHz) spectra of **1f** (rt, $CDCl_3$).

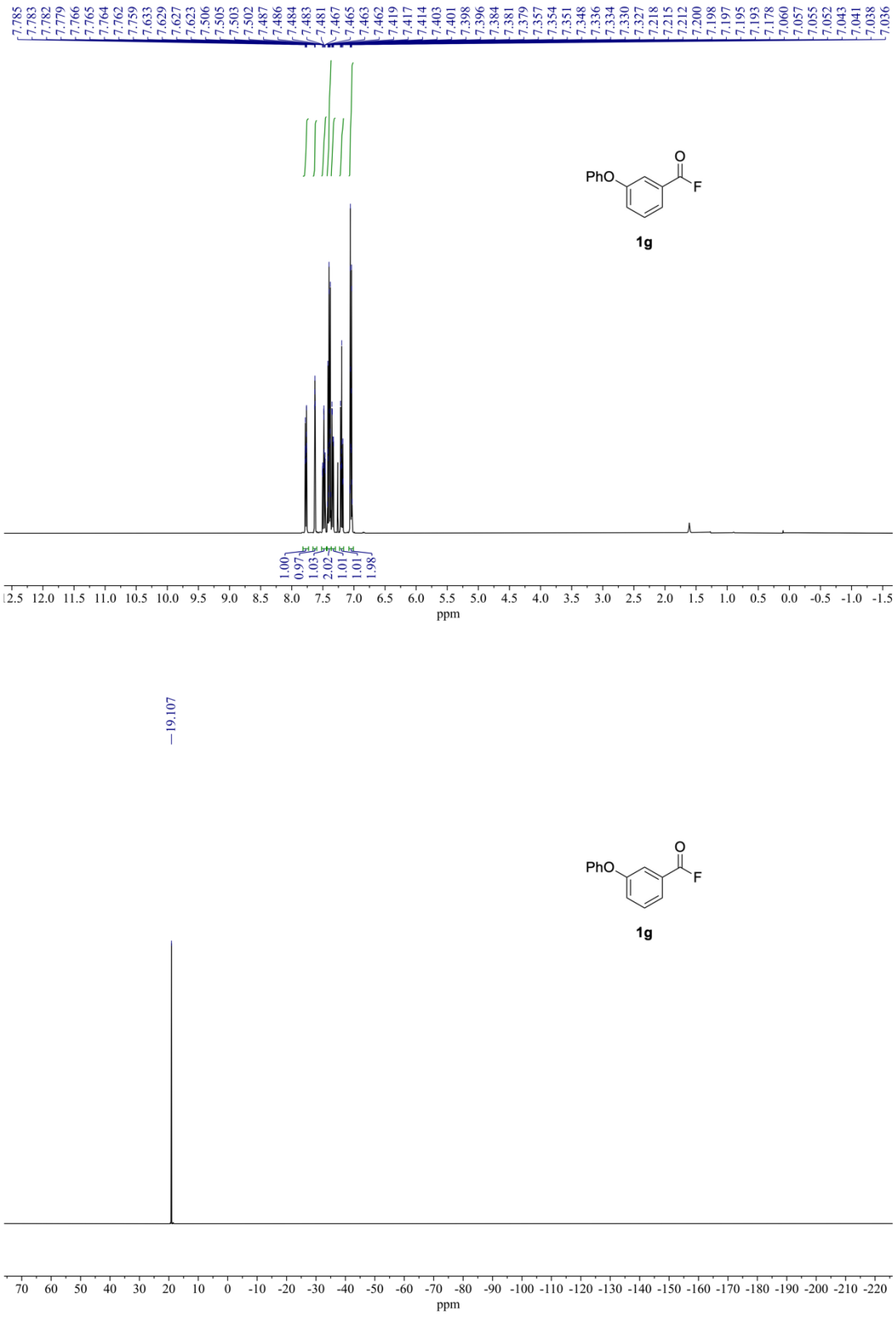

^{1}H NMR (400 MHz) and ^{19}F{^{1}H} NMR (376 MHz) spectra of **1g** (rt, $CDCl_3$).

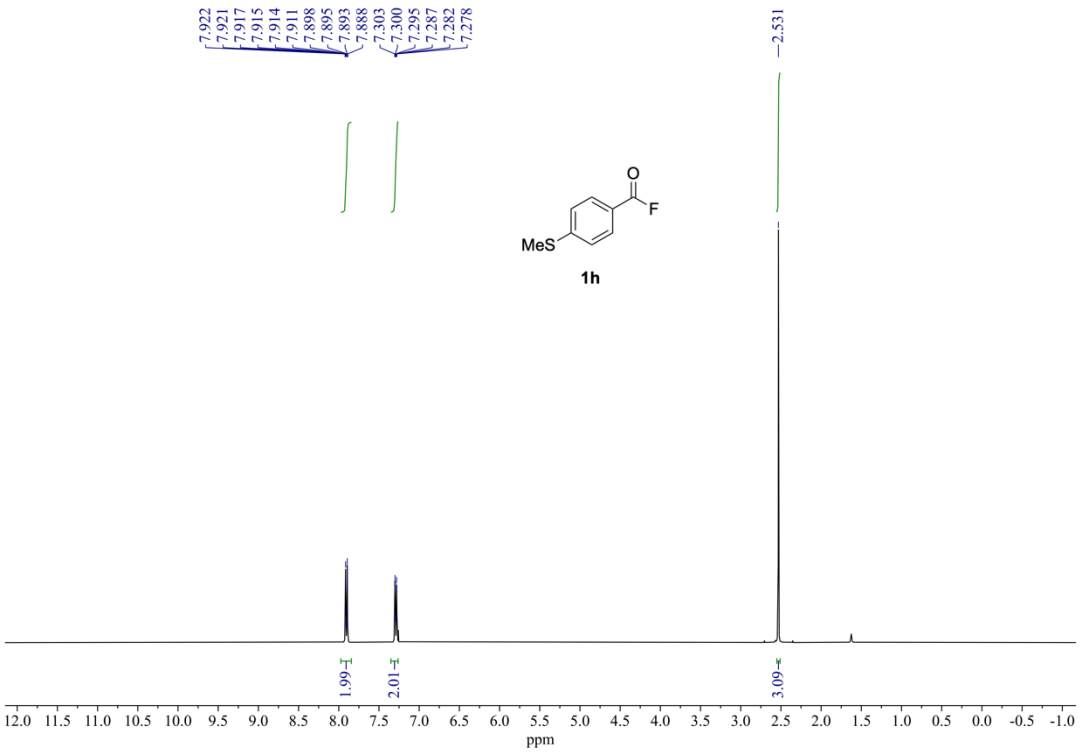

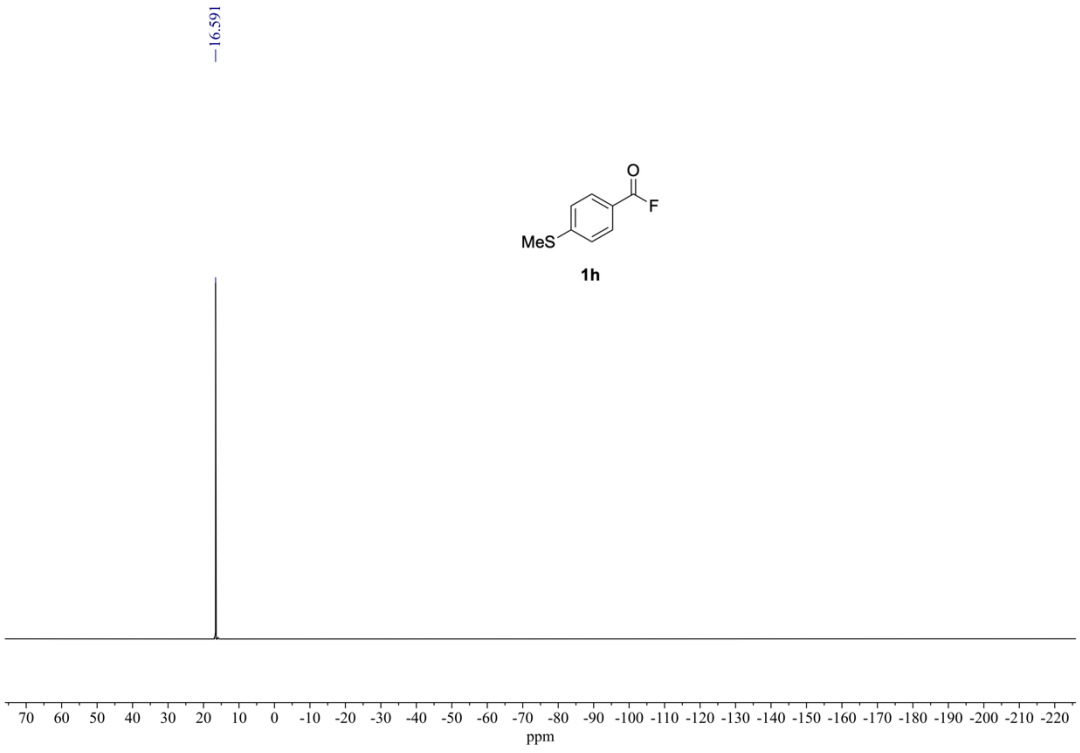

^{1}H NMR (400 MHz) and ^{19}F{^{1}H} NMR (376 MHz) spectra of **1h** (rt, $CDCl_3$).

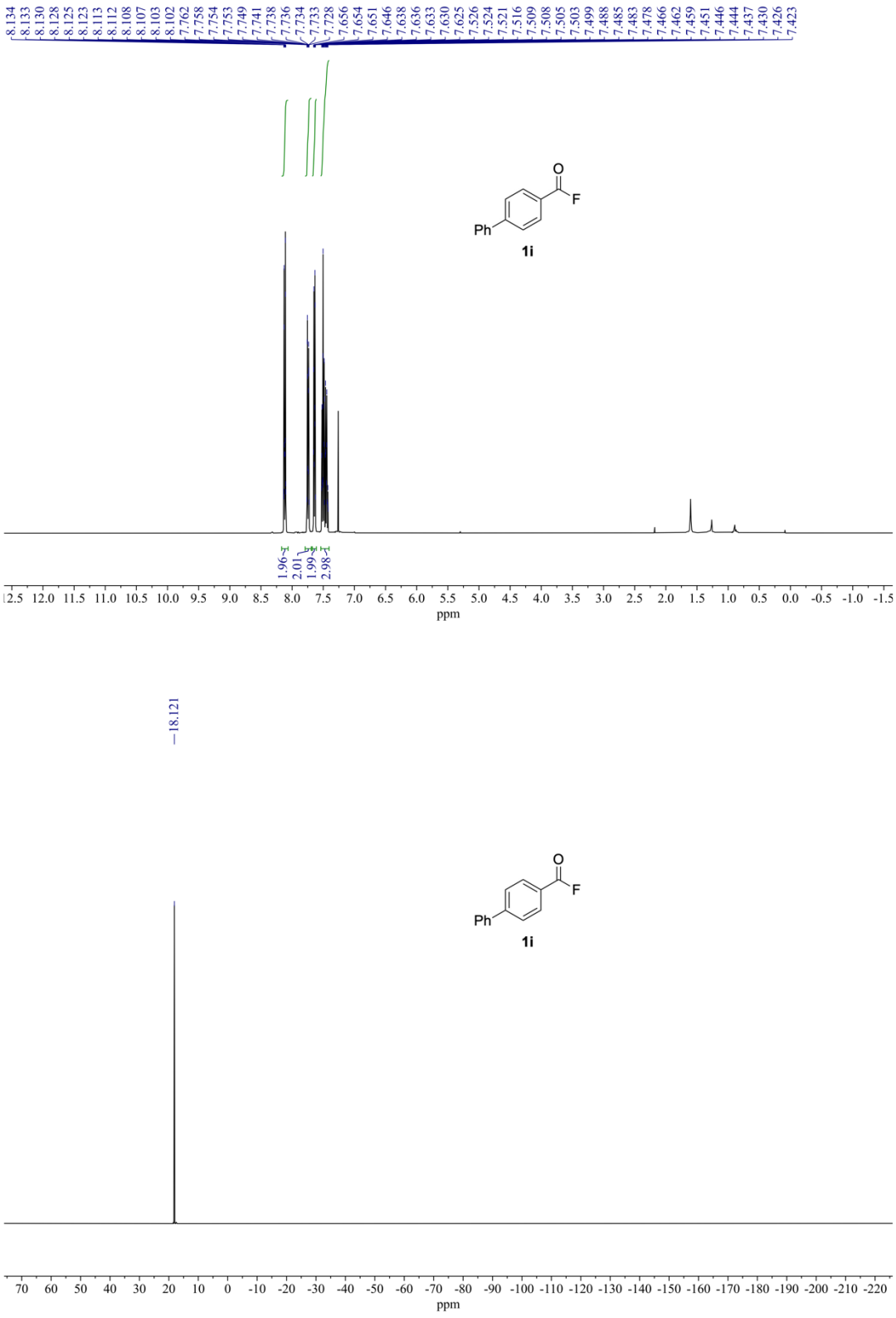

^{1}H NMR (400 MHz) and ^{19}F{^{1}H} NMR (376 MHz) spectra of **1i** (rt, $CDCl_3$).

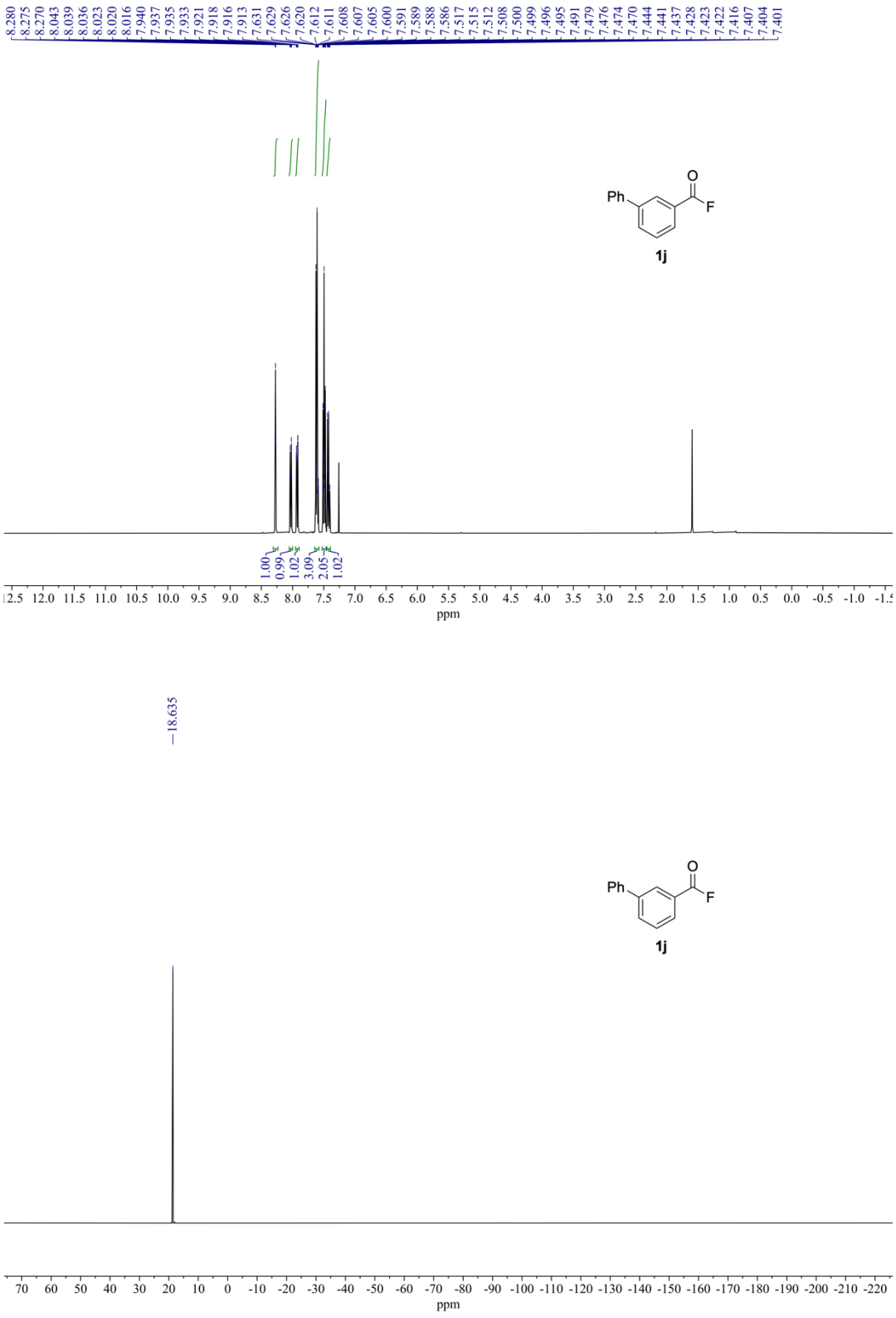

^{1}H NMR (400 MHz) and ^{19}F{^{1}H} NMR (376 MHz) spectra of **1j** (rt, $CDCl_3$).

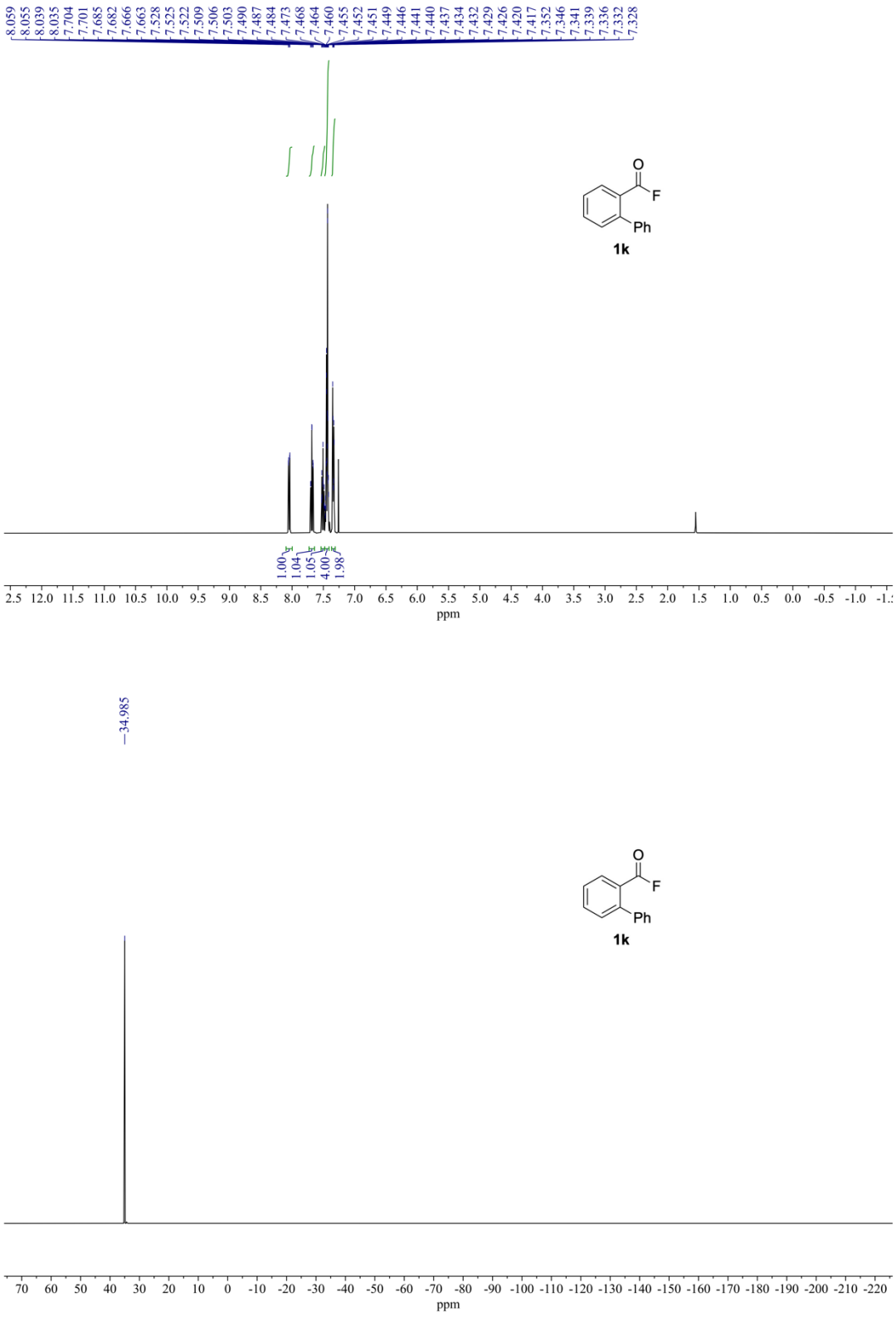

^{1}H NMR (400 MHz) and ^{19}F{^{1}H} NMR (376 MHz) spectra of **1k** (rt, $CDCl_3$).

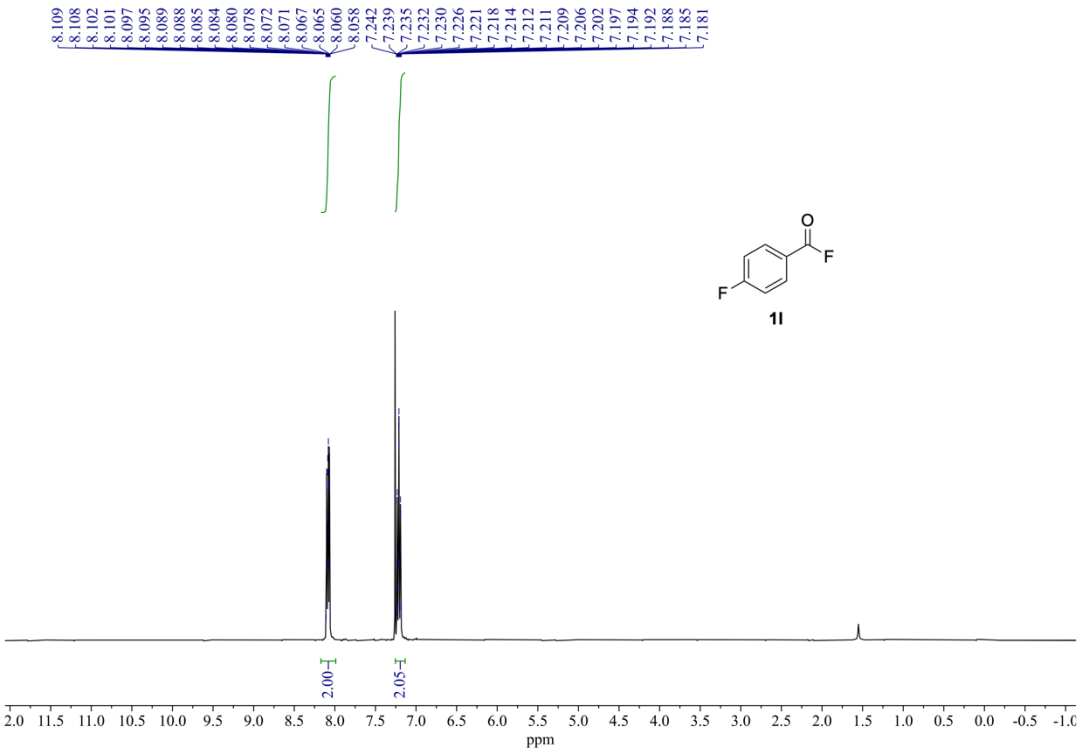

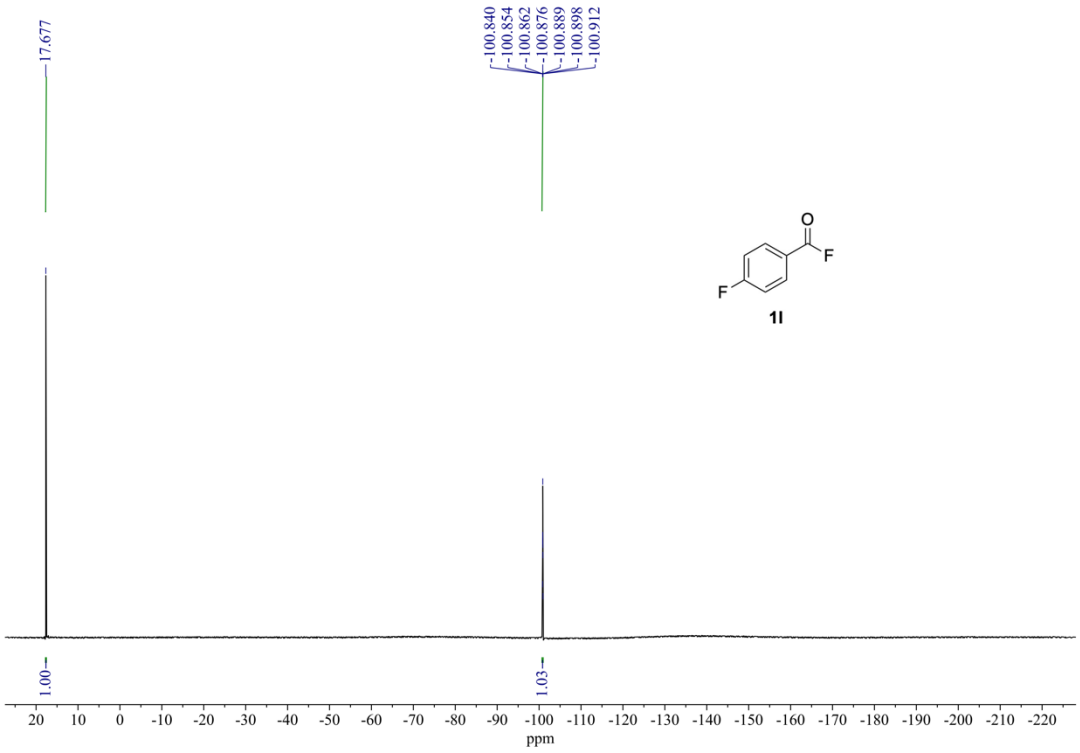

^{1}H NMR (400 MHz) and ^{19}F{^{1}H} NMR (376 MHz) spectra of **1l** (rt, $CDCl_3$).

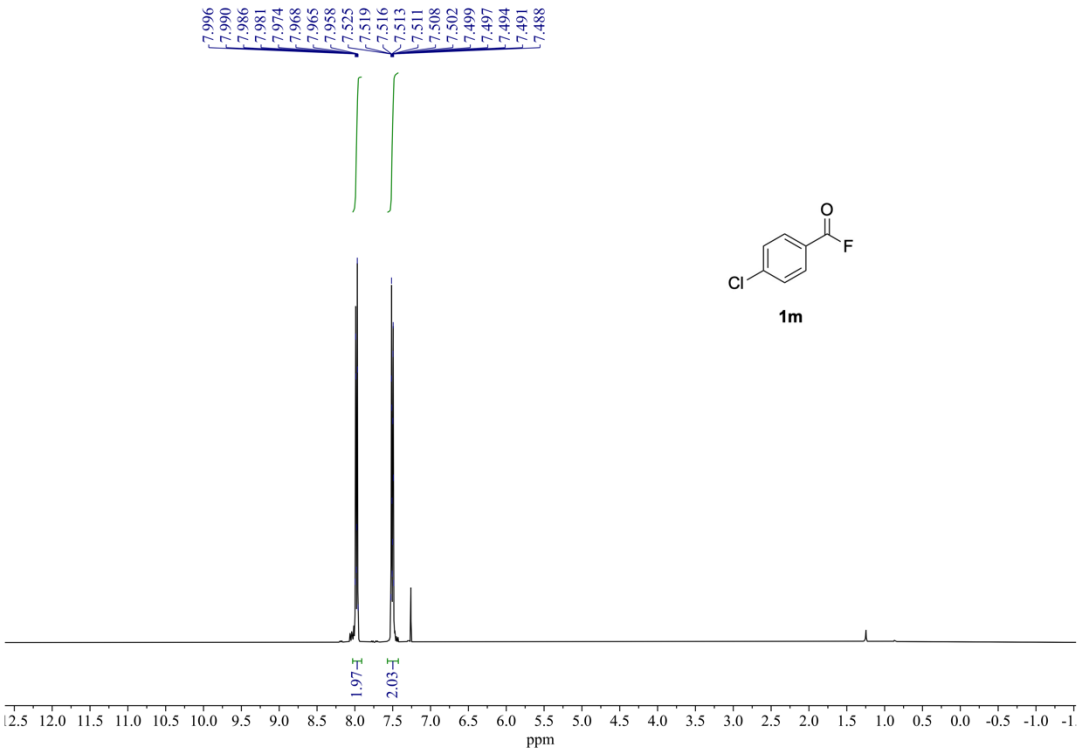

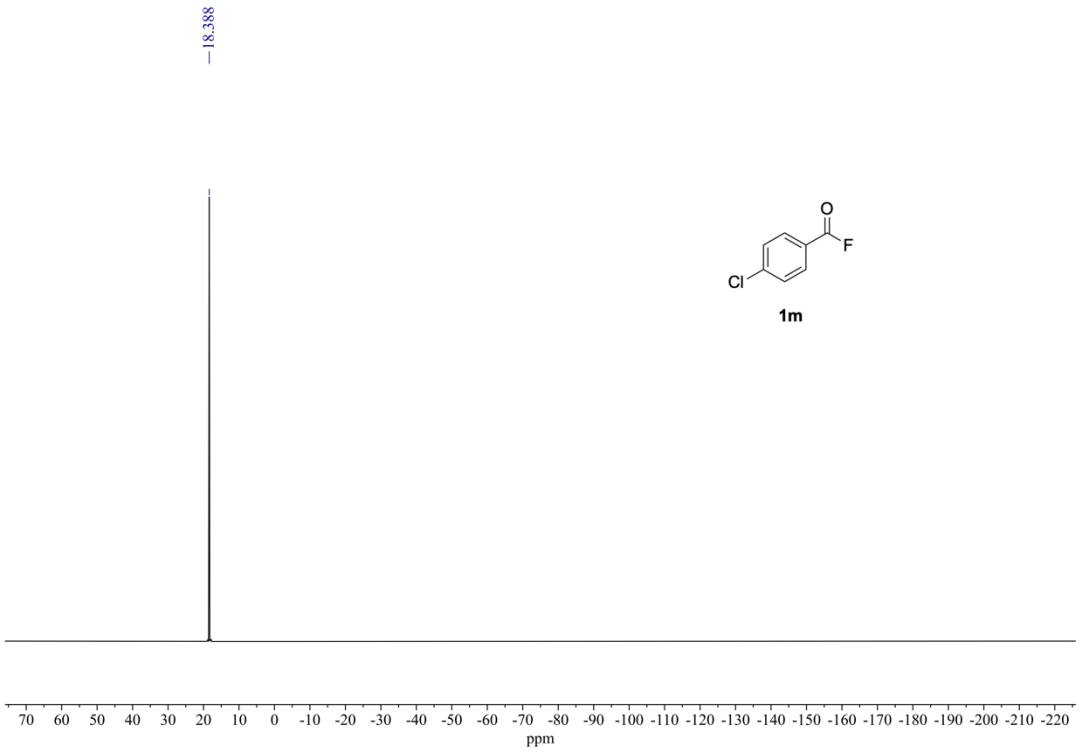

^{1}H NMR (400 MHz) and ^{19}F{^{1}H} NMR (376 MHz) spectra of **1m** (rt, $CDCl_3$).

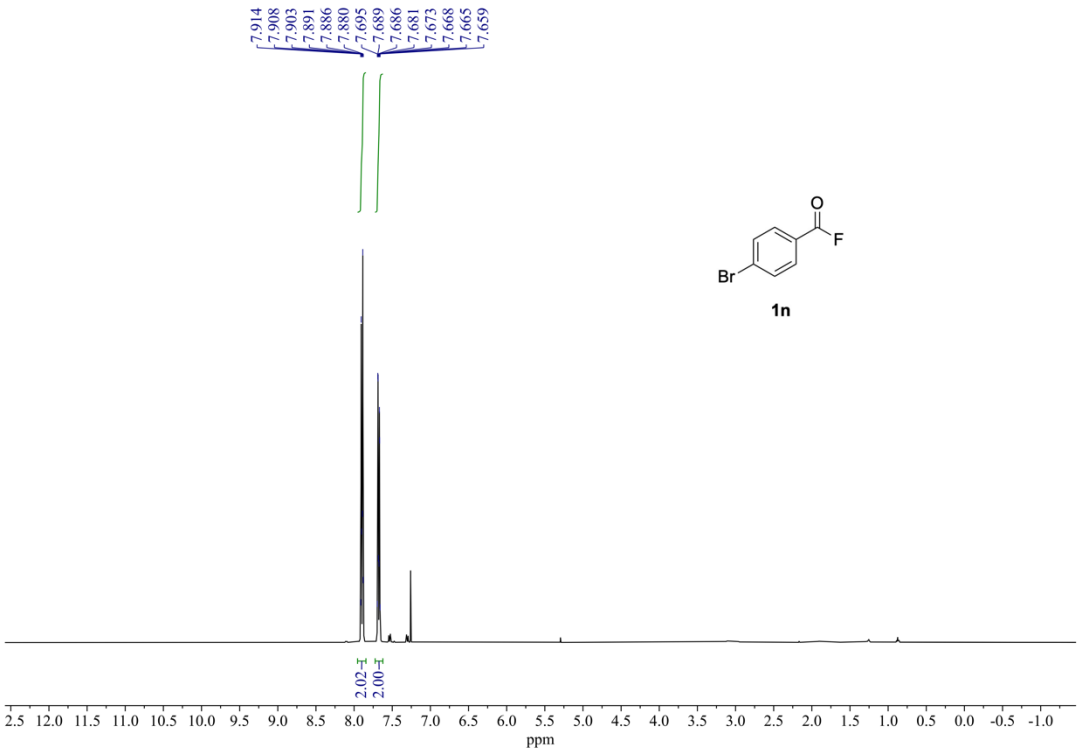

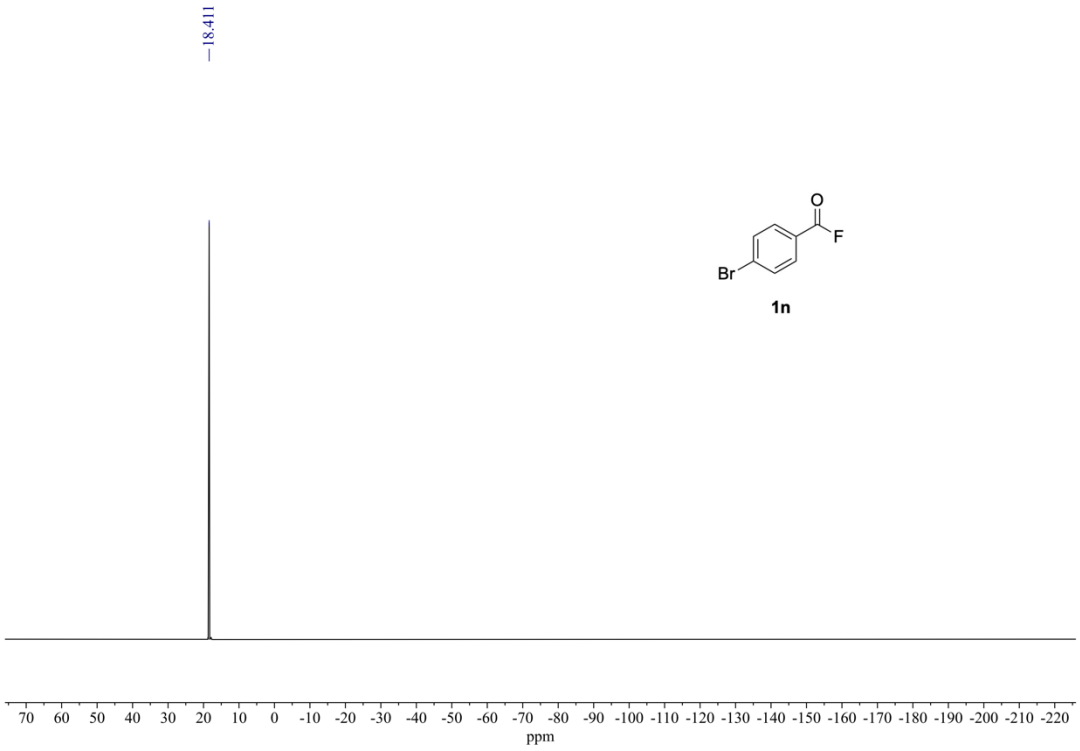

^{1}H NMR (400 MHz) and ^{19}F{^{1}H} NMR (376 MHz) spectra of **1n** (rt, $CDCl_3$).

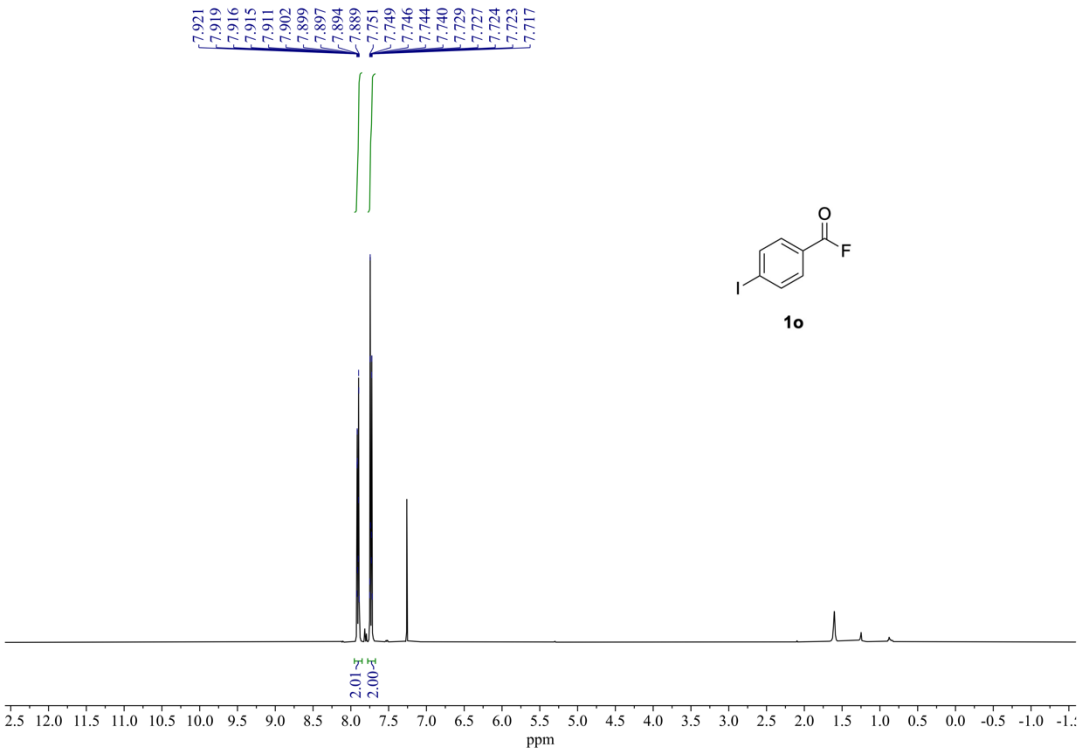

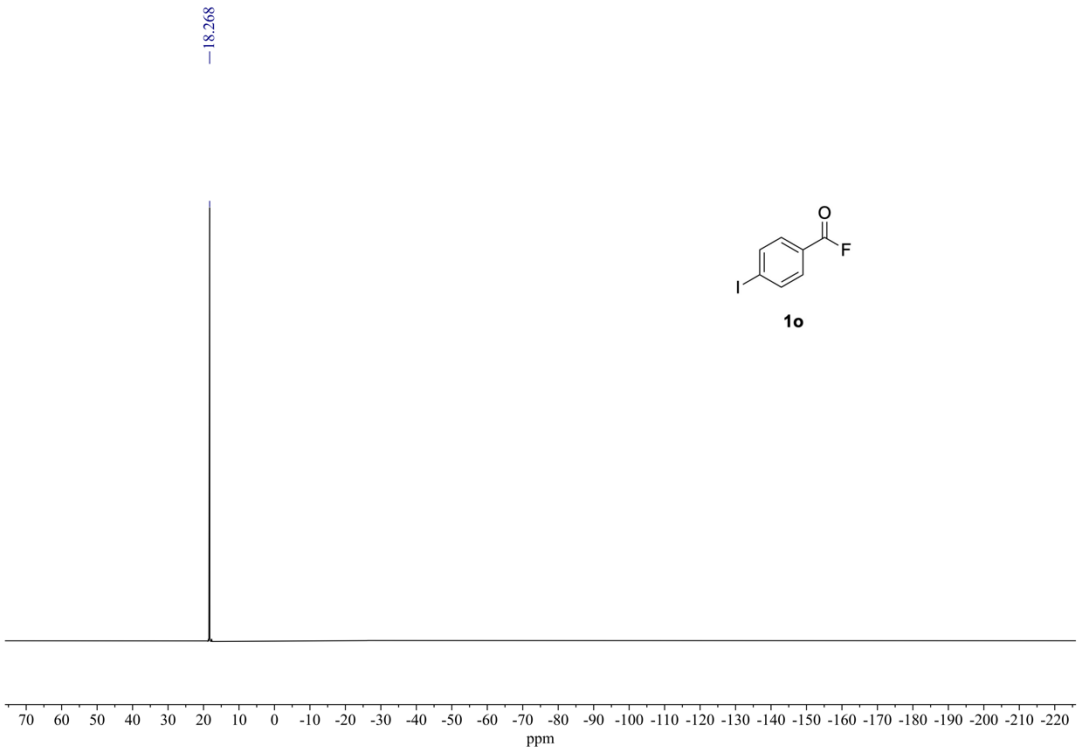

^{1}H NMR (400 MHz) and ^{19}F{^{1}H} NMR (376 MHz) spectra of **1o** (rt, $CDCl_3$).

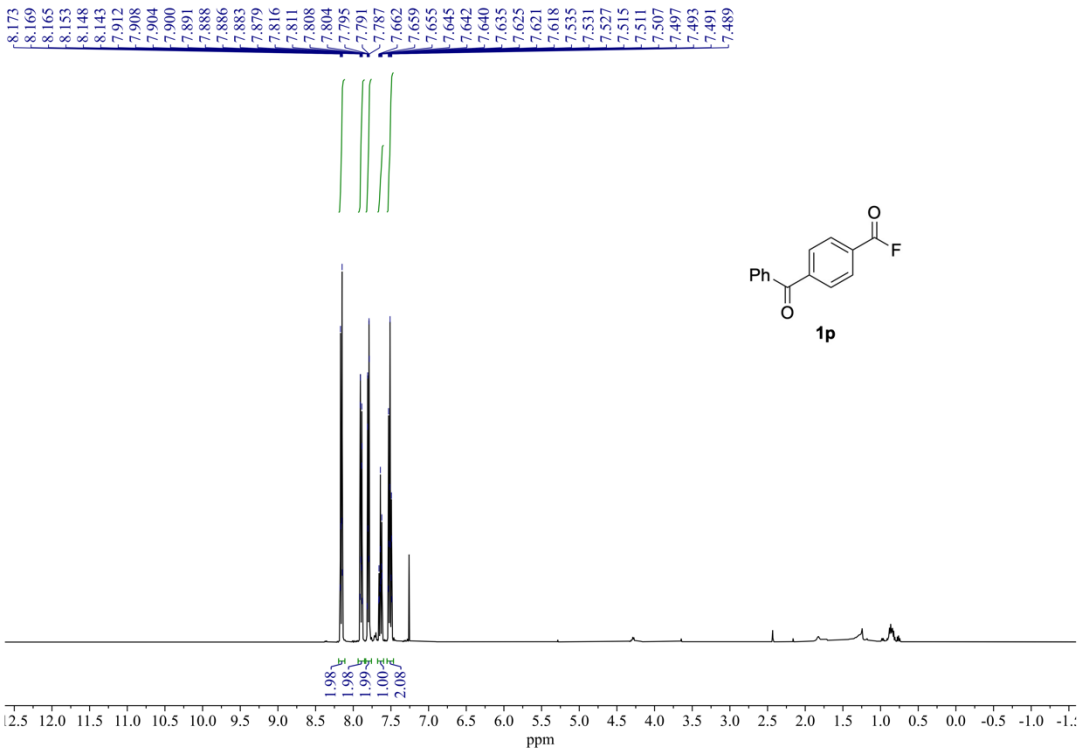

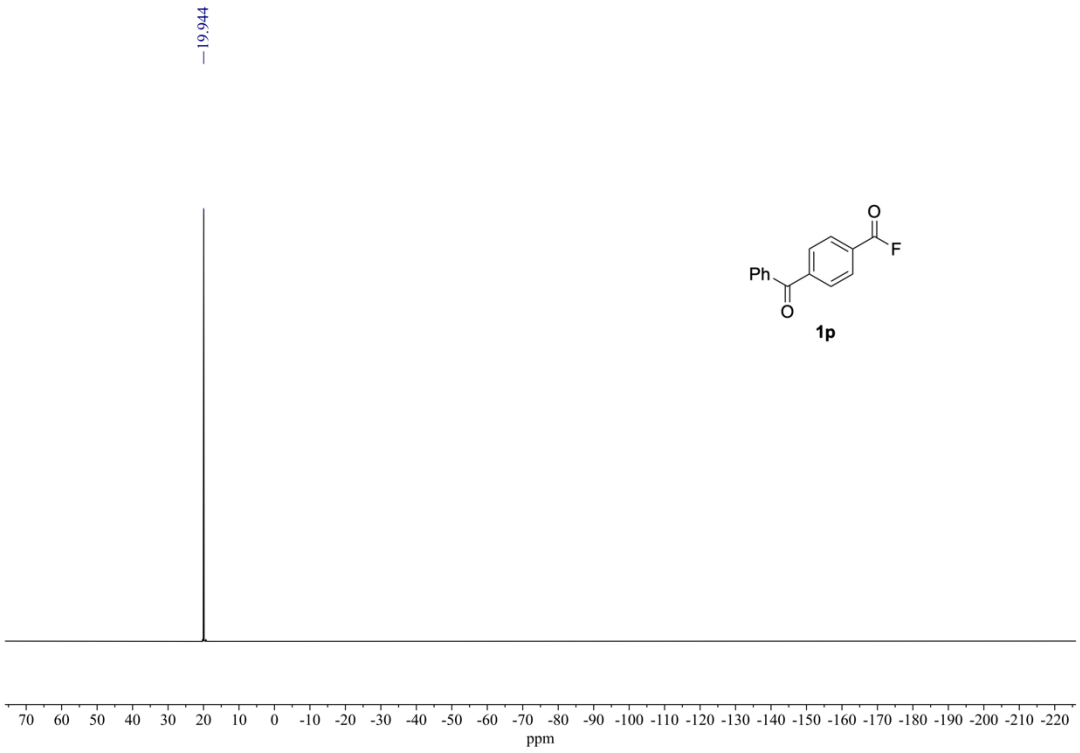

^{1}H NMR (400 MHz) and ^{19}F{^{1}H} NMR (376 MHz) spectra of **1p** (rt, $CDCl_3$).

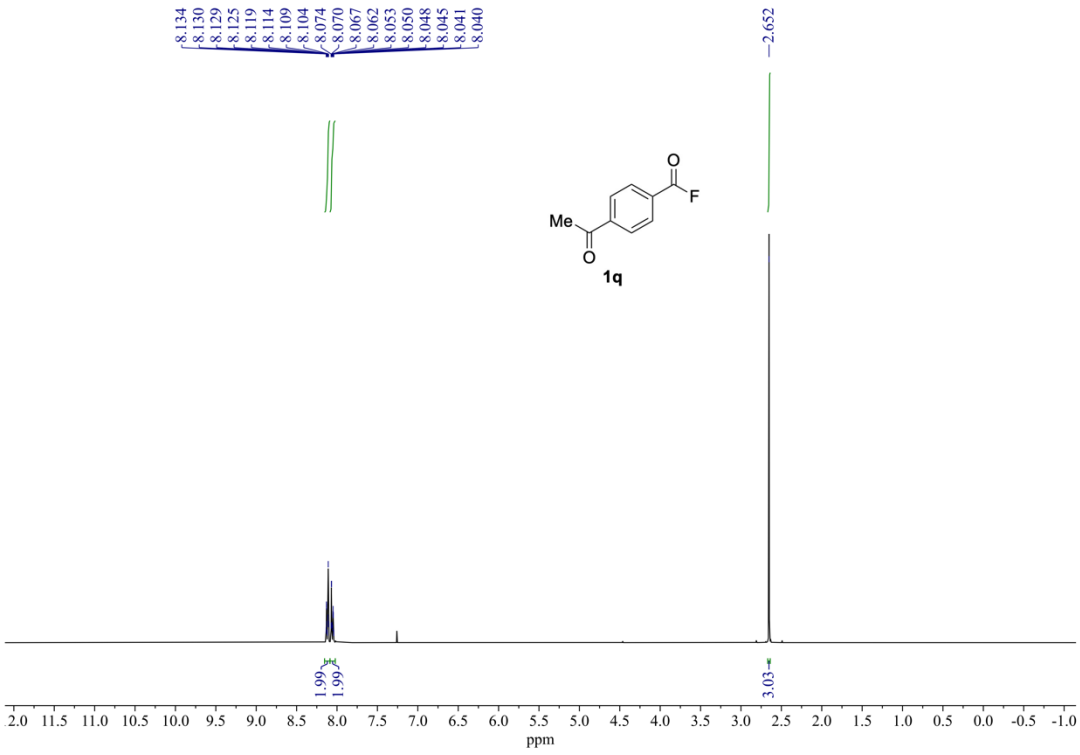

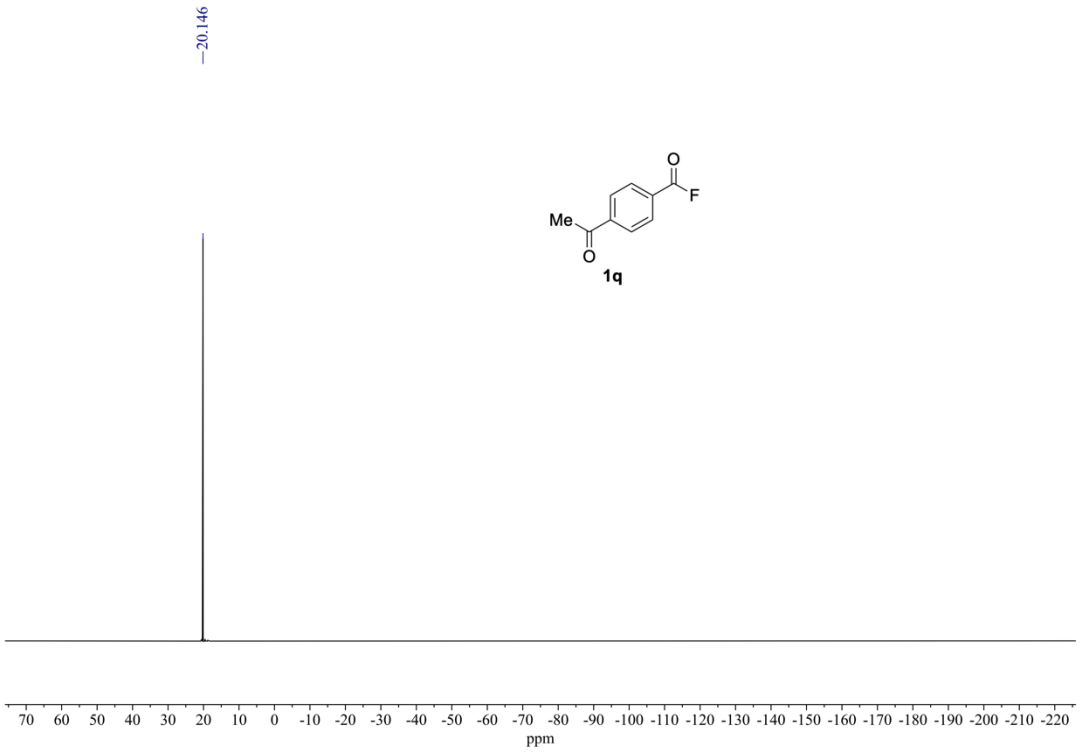

^{1}H NMR (400 MHz) and ^{19}F{^{1}H} NMR (376 MHz) spectra of **1q** (rt, $CDCl_3$).

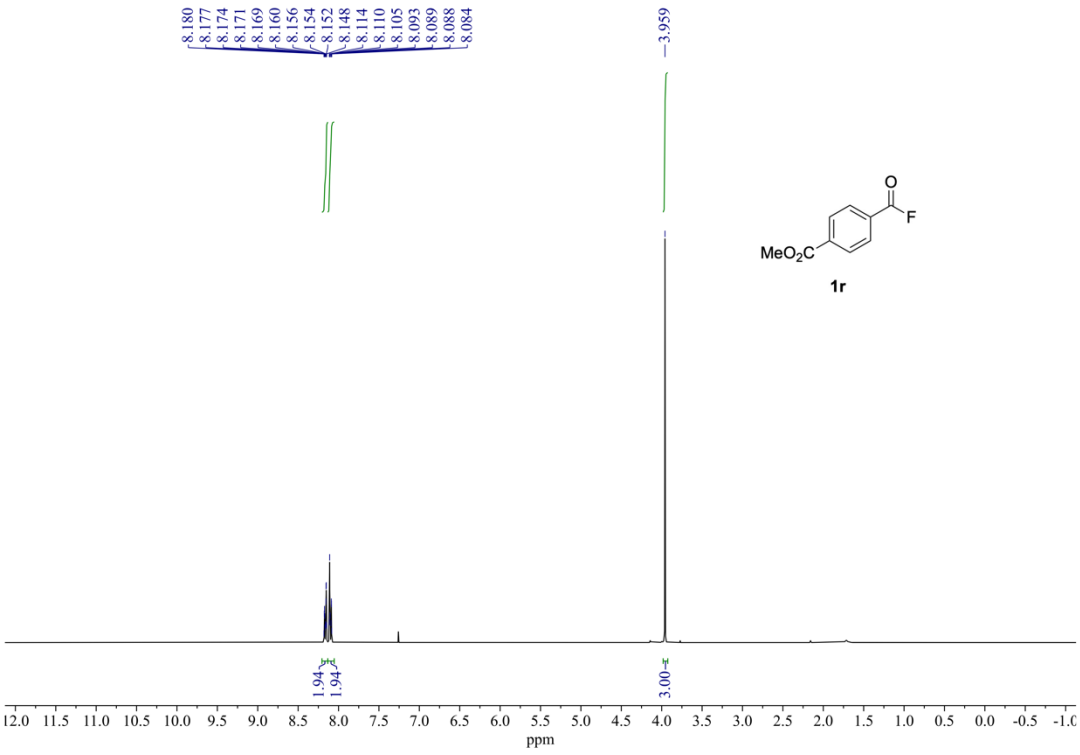

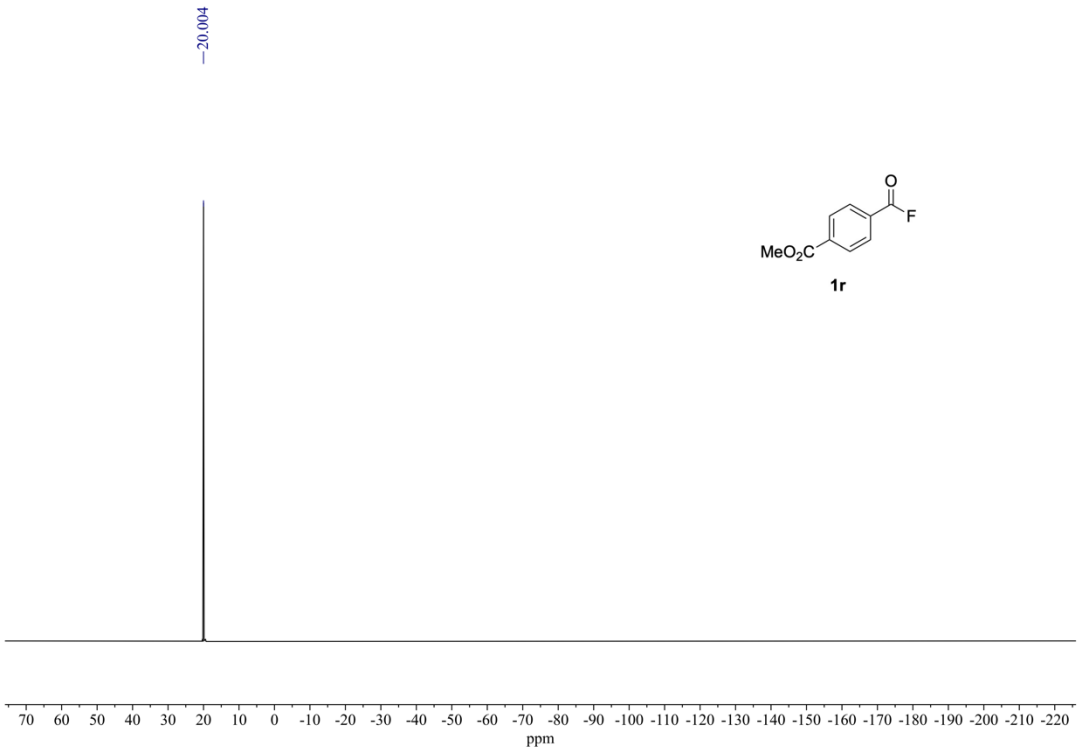

^{1}H NMR (400 MHz) and ^{19}F{^{1}H} NMR (376 MHz) spectra of **1r** (rt, $CDCl_3$).

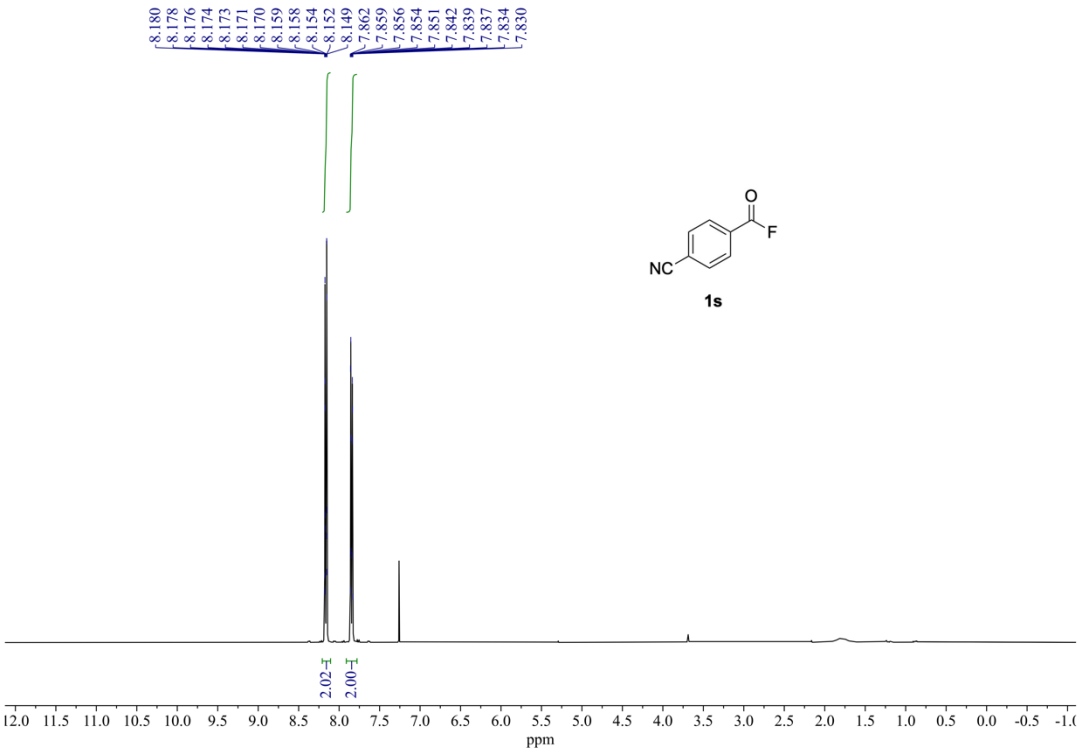

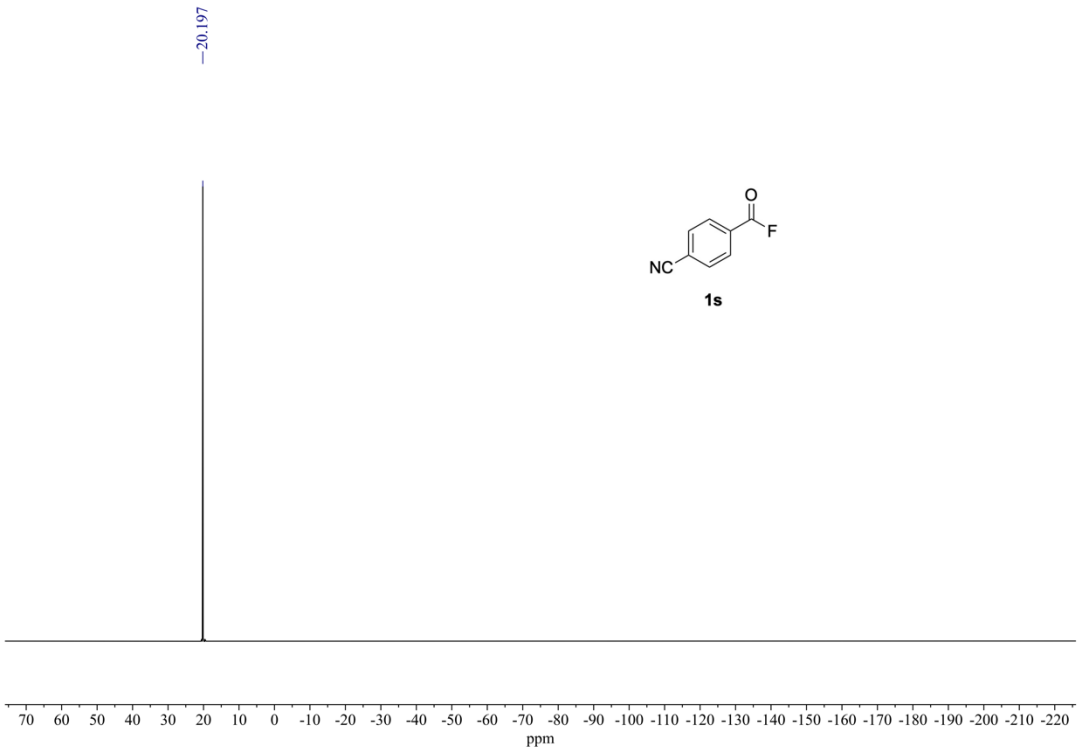

^{1}H NMR (400 MHz) and ^{19}F{^{1}H} NMR (376 MHz) spectra of **1s** (rt, $CDCl_3$).

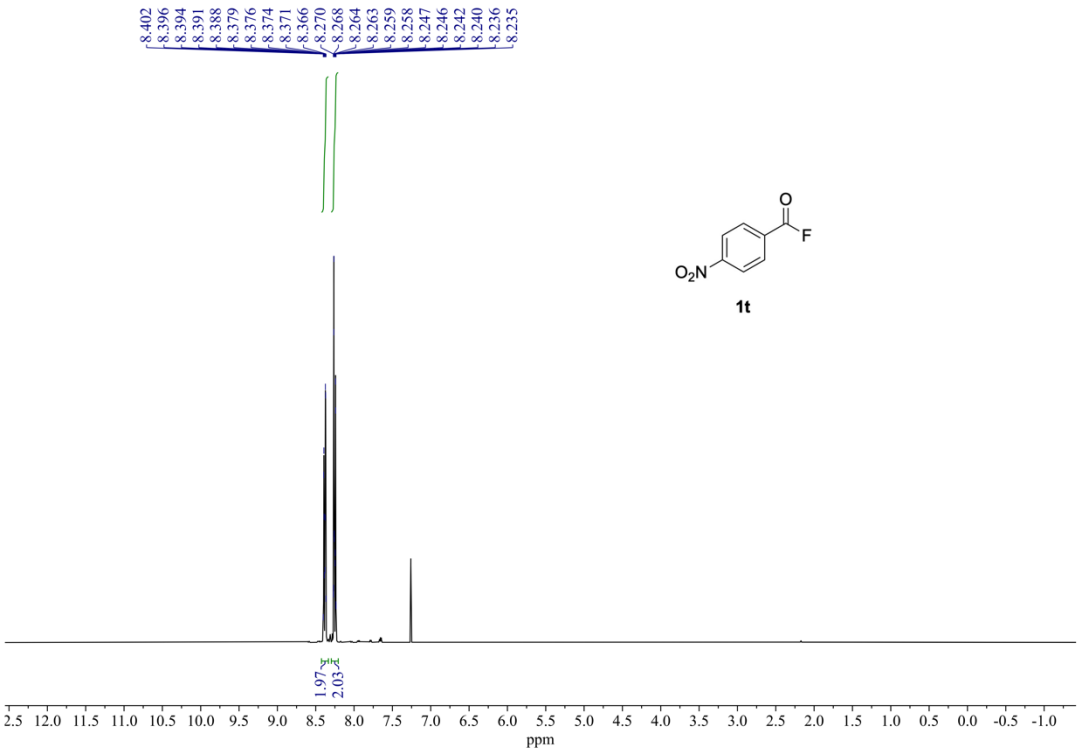

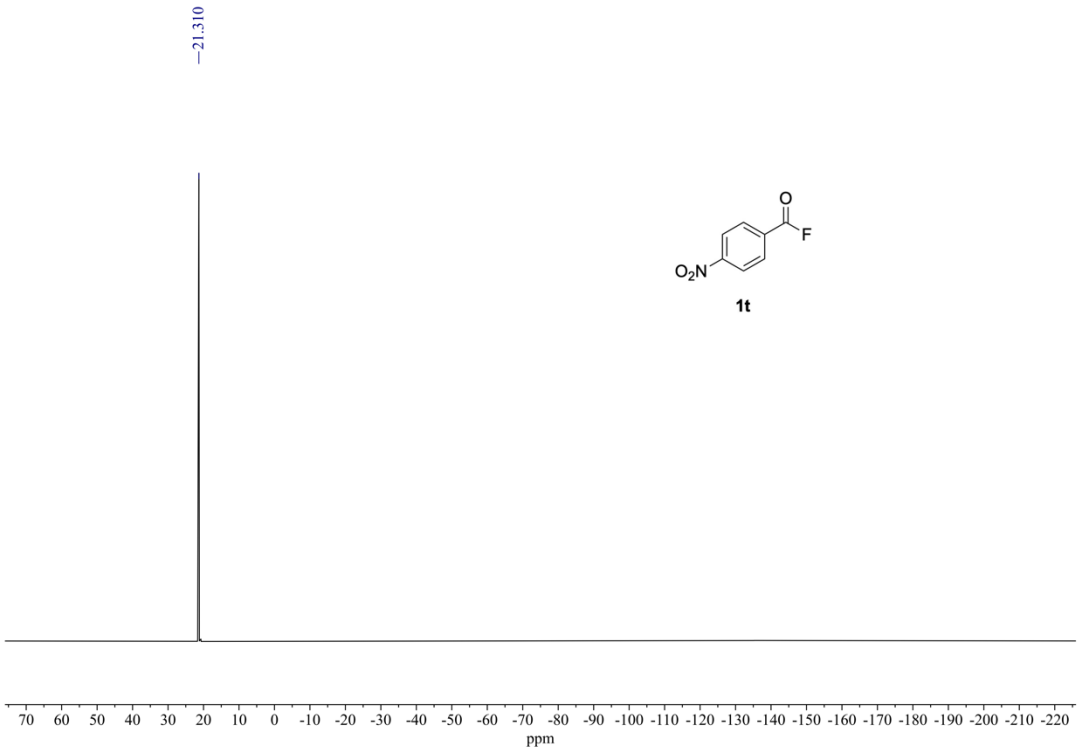

^{1}H NMR (400 MHz) and ^{19}F{^{1}H} NMR (376 MHz) spectra of **1t** (rt, $CDCl_3$).

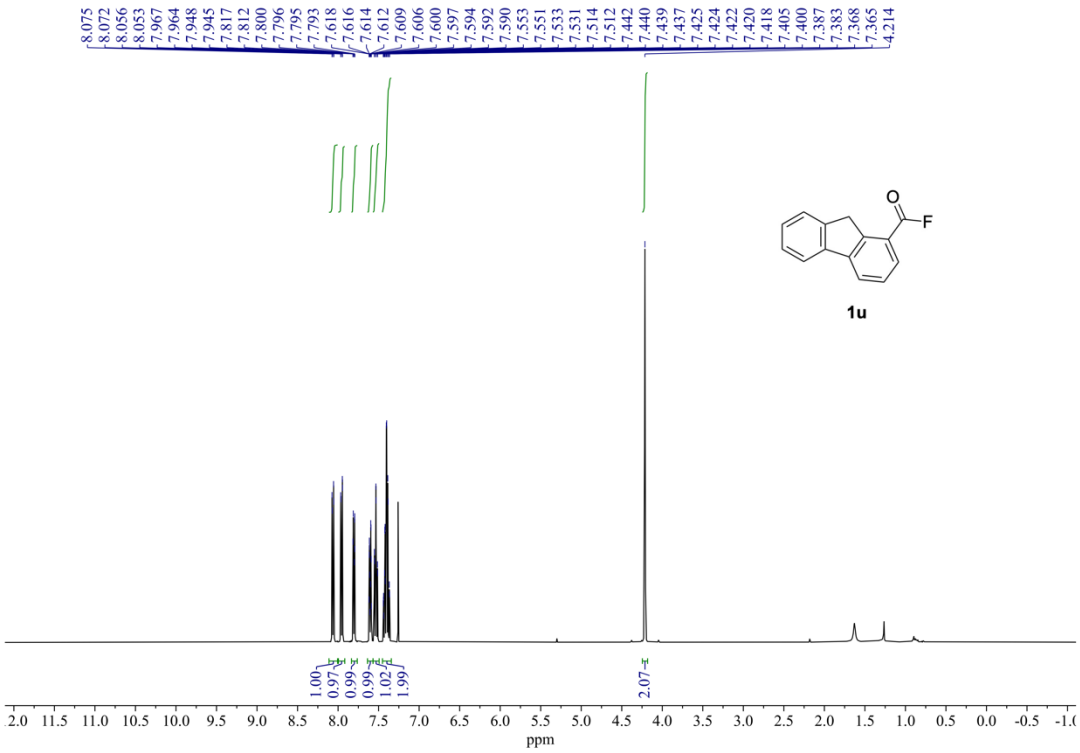

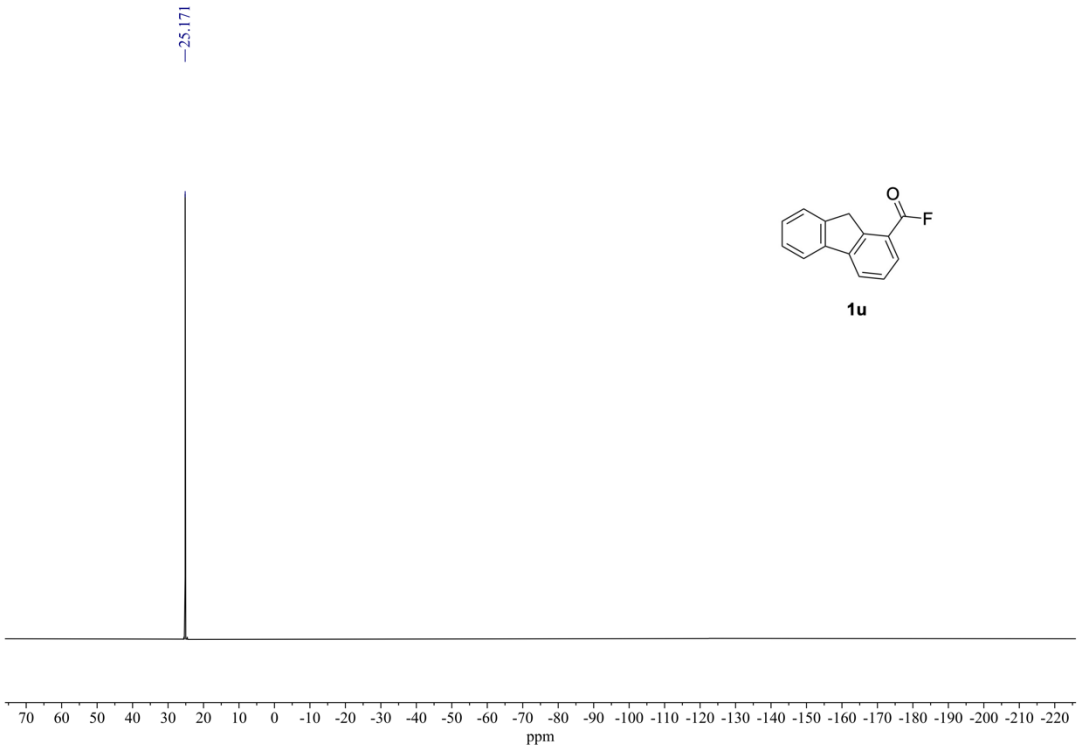

^{1}H NMR (400 MHz) and ^{19}F{^{1}H} NMR (376 MHz) spectra of **1u** (rt, $CDCl_3$).

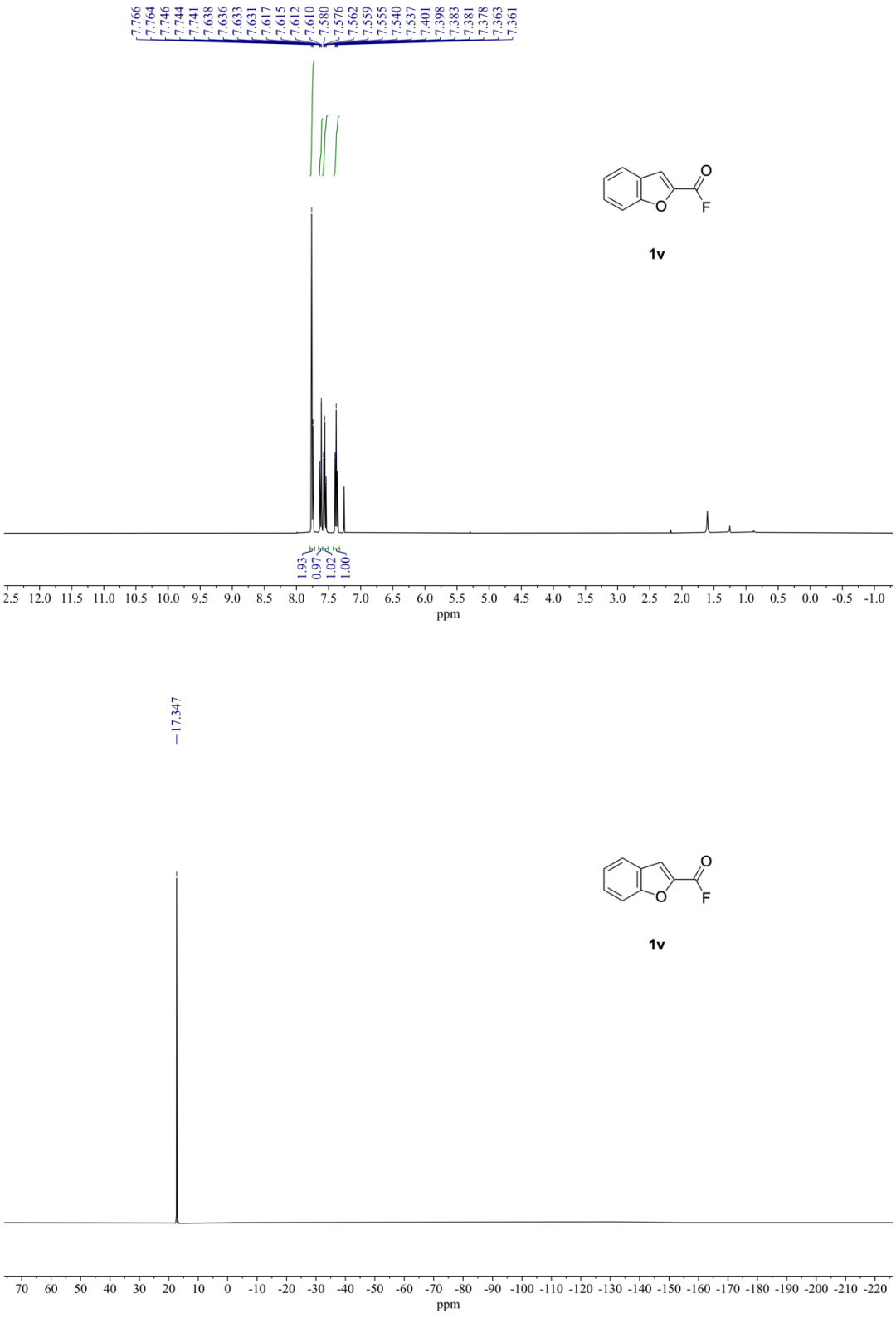

^{1}H NMR (400 MHz) and ^{19}F{^{1}H} NMR (376 MHz) spectra of **1v** (rt, $CDCl_3$).

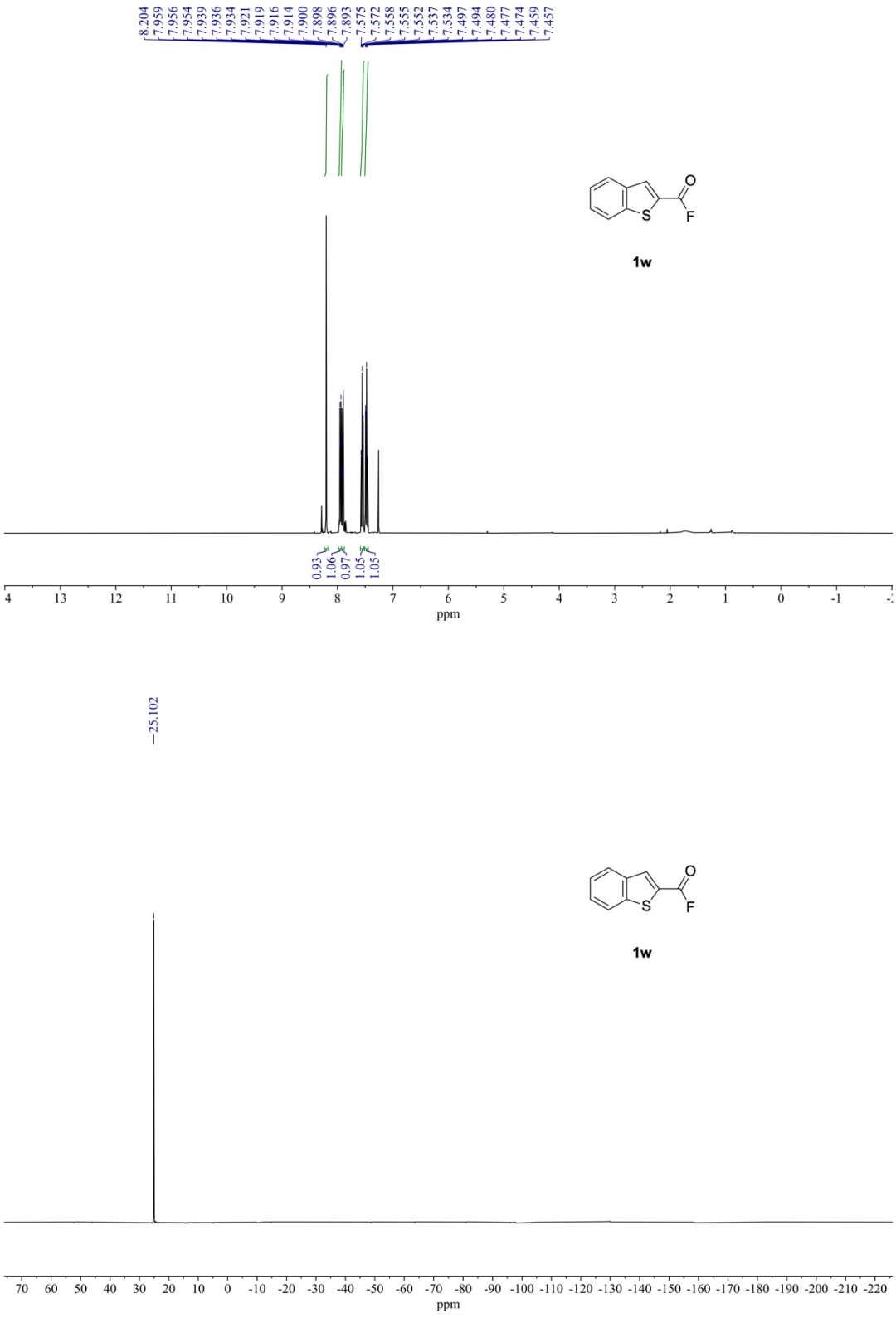

^{1}H NMR (400 MHz) and ^{19}F{^{1}H} NMR (376 MHz) spectra of **1w** (rt, $CDCl_3$).

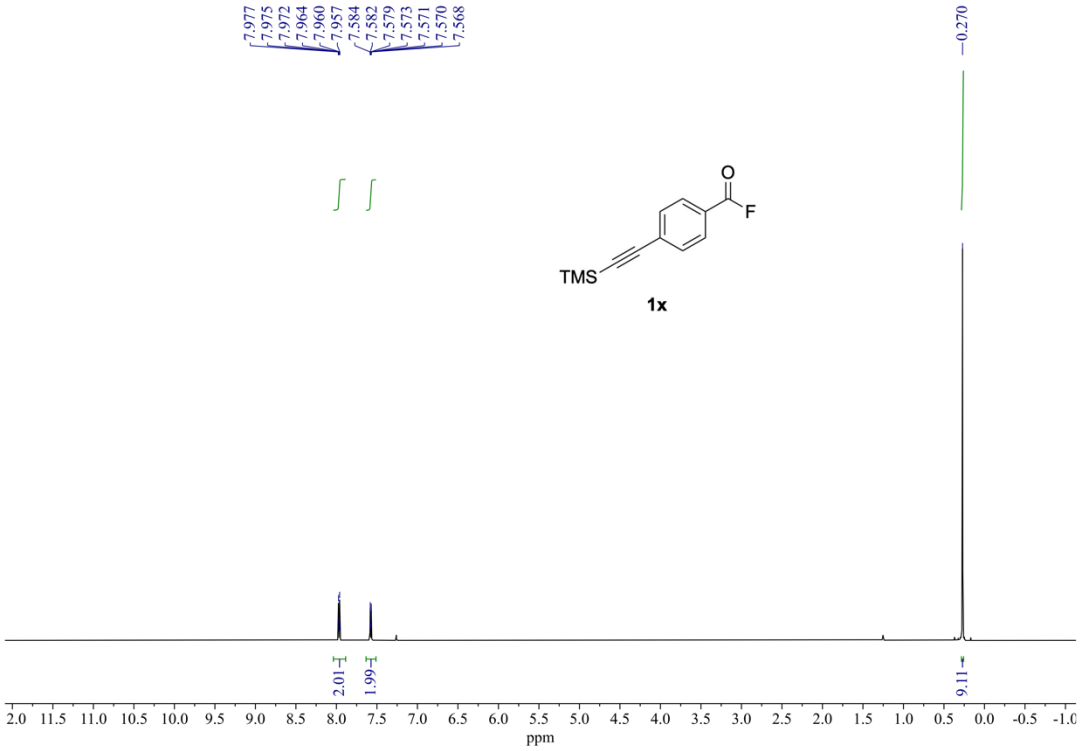
7.977
7.975
7.972
7.964
7.960
7.957
7.584
7.582
7.579
7.573
7.571
7.570
7.568
-0.270
O
F
TMS
1x
2.01
1.99
9.11
ppm

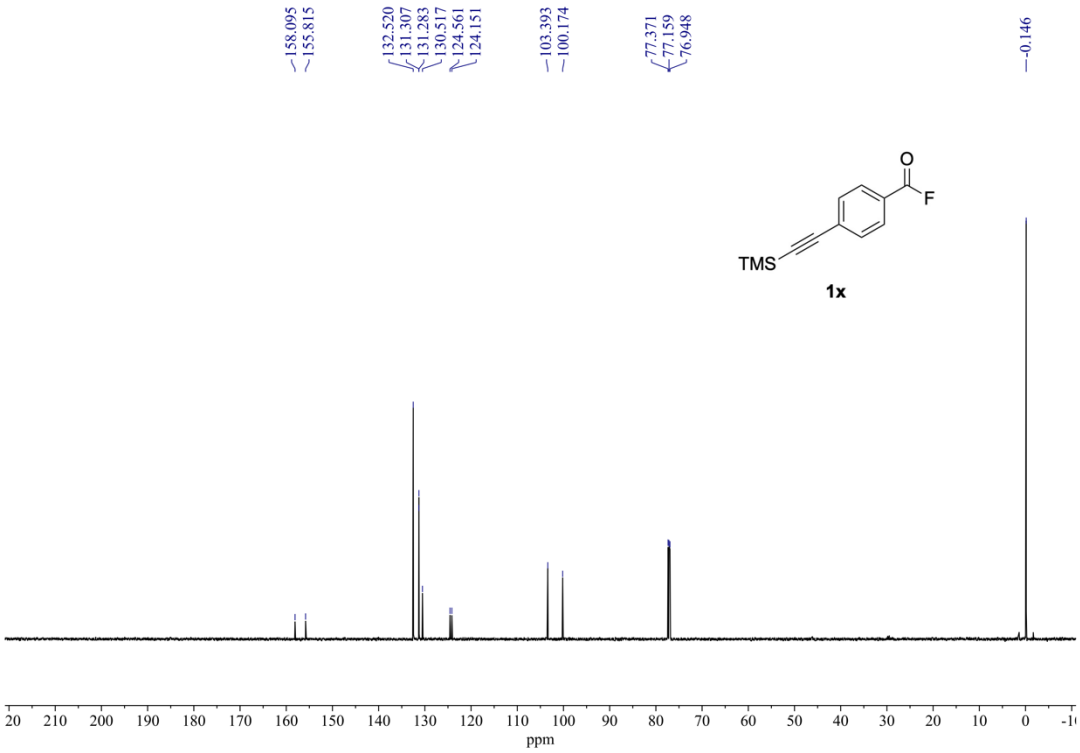
158.095
155.815
132.520
131.307
131.283
130.517
124.561
124.151
103.393
100.174
77.371
77.159
76.948
-0.146
O
F
TMS
1x
ppm

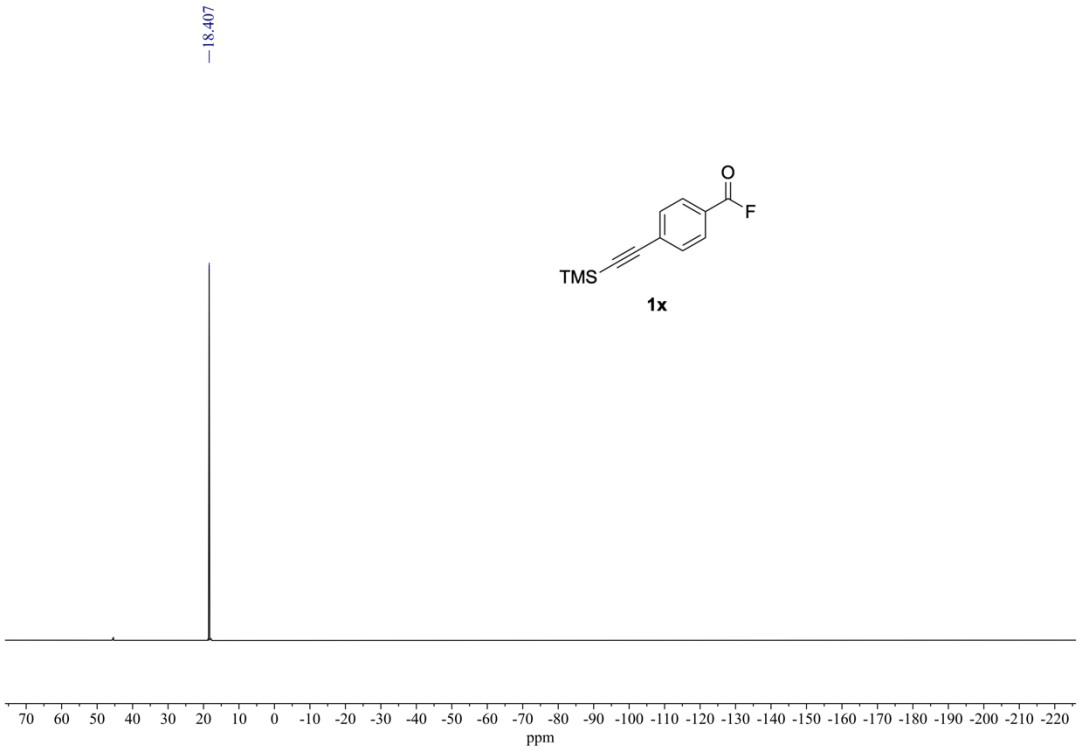

^{1}H NMR (600 MHz), ^{13}C{^{1}H} NMR (151 MHz) and ^{19}F{^{1}H} NMR (376 MHz) spectra of **1x** (rt, $CDCl_3$).

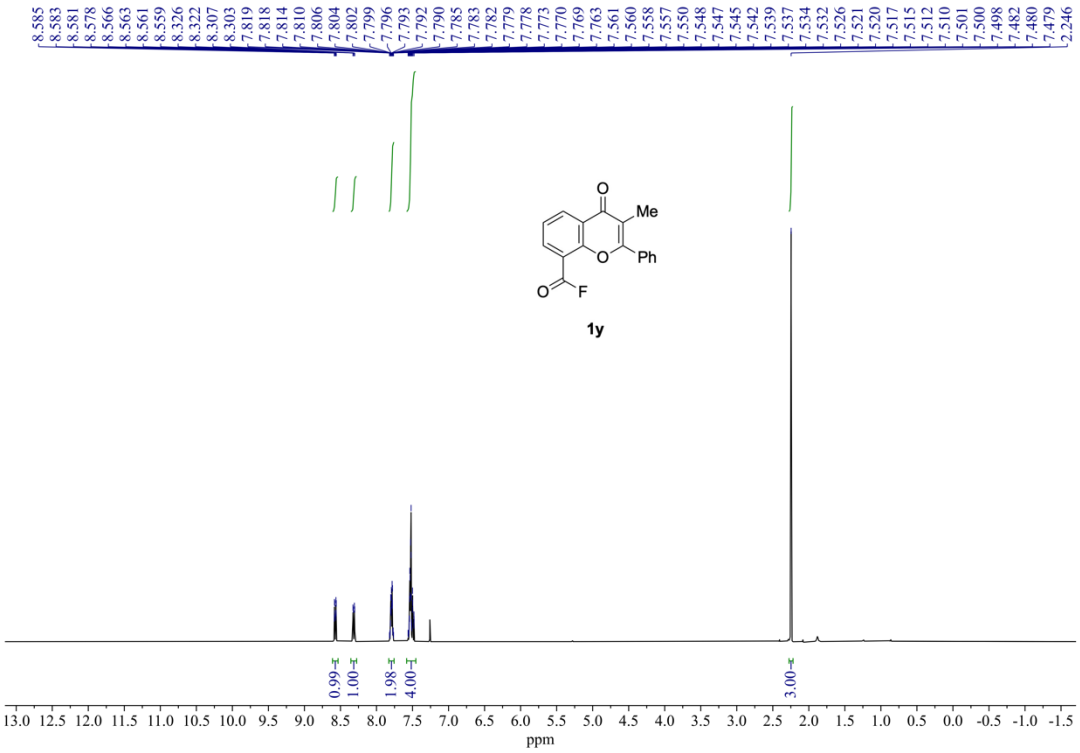
8.585
8.583
8.581
8.578
8.566
8.563
8.561
8.559
8.326
8.322
8.307
8.303
7.819
7.818
7.814
7.810
7.806
7.804
7.802
7.799
7.796
7.793
7.792
7.790
7.785
7.783
7.782
7.779
7.778
7.773
7.770
7.769
7.763
7.561
7.560
7.558
7.557
7.550
7.548
7.547
7.545
7.542
7.539
7.537
7.534
7.532
7.526
7.521
7.520
7.517
7.515
7.512
7.510
7.501
7.500
7.498
7.482
7.480
7.479
2.246
O
Me
O
Ph
O
F
1y
0.99
1.00
1.98
4.00
3.00
13.0 12.5 12.0 11.5 11.0 10.5 10.0 9.5 9.0 8.5 8.0 7.5 7.0 6.5 6.0 5.5 5.0 4.5 4.0 3.5 3.0 2.5 2.0 1.5 1.0 0.5 0.0 -0.5 -1.0 -1.5
ppm

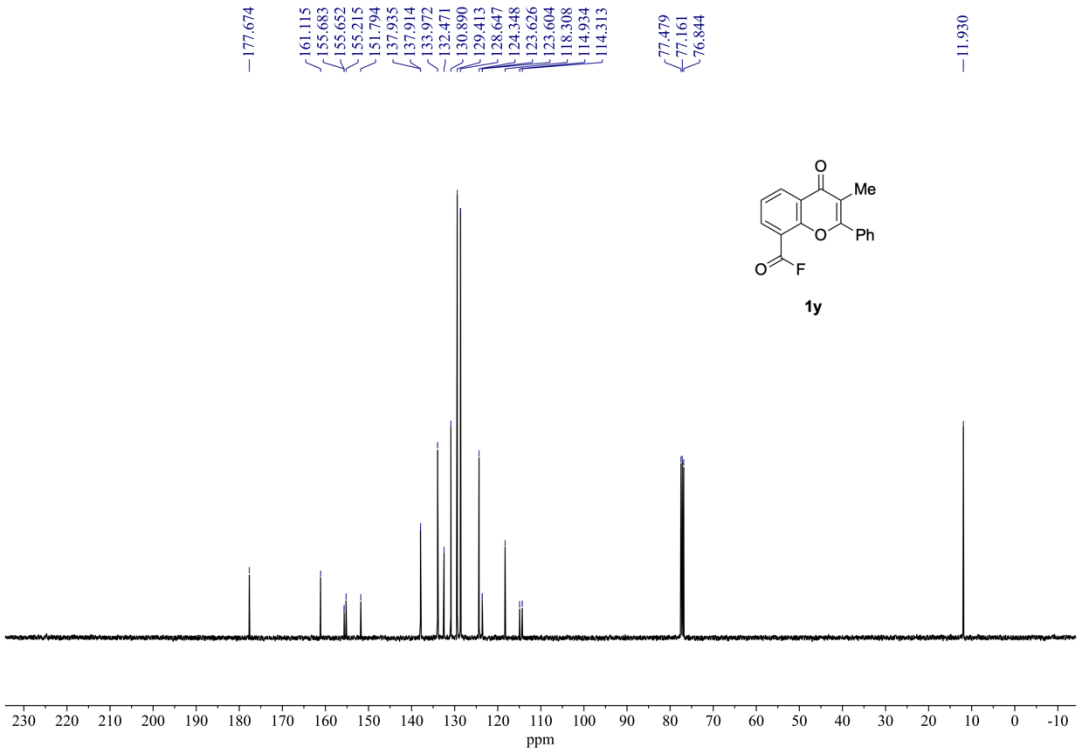
177.674
161.115
155.683
155.652
155.215
151.794
137.935
137.914
133.972
132.471
130.890
129.413
128.647
124.348
123.626
123.604
118.308
114.934
114.313
77.479
77.161
76.844
11.930
O
Me
O
Ph
O
F
1y
230 220 210 200 190 180 170 160 150 140 130 120 110 100 90 80 70 60 50 40 30 20 10 0 -10
ppm

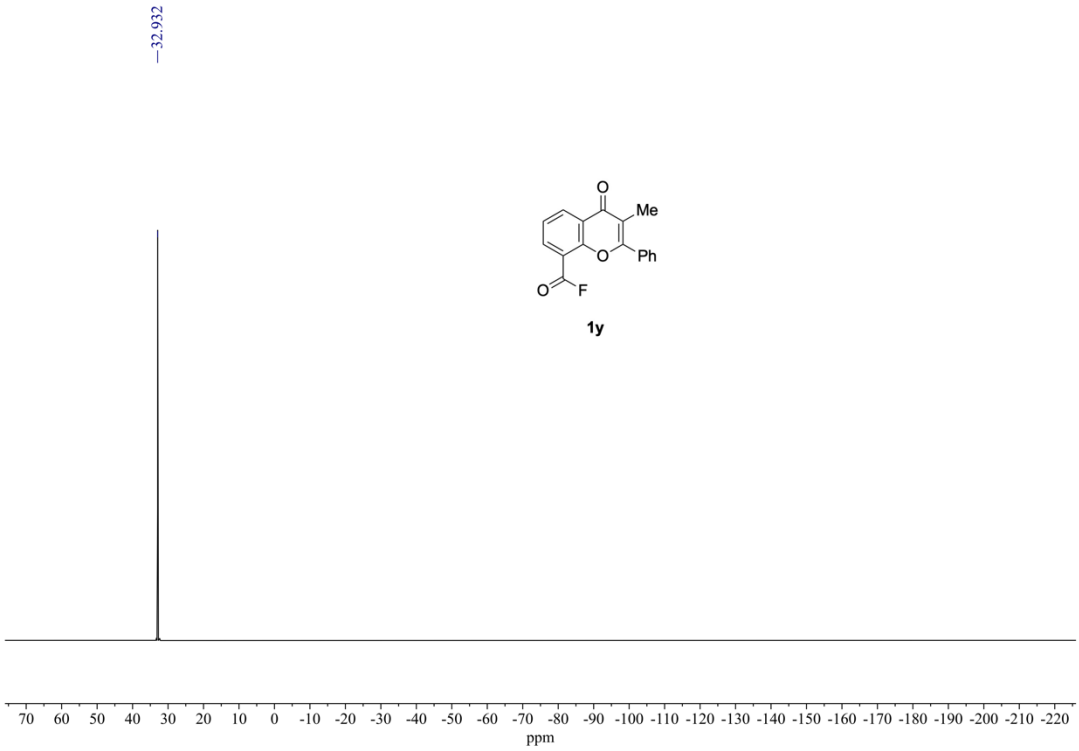

^{1}H NMR (400 MHz), ^{13}C{^{1}H} NMR (101 MHz) and ^{19}F{^{1}H} NMR (376 MHz) spectra of **1y** (rt, $CDCl_3$).

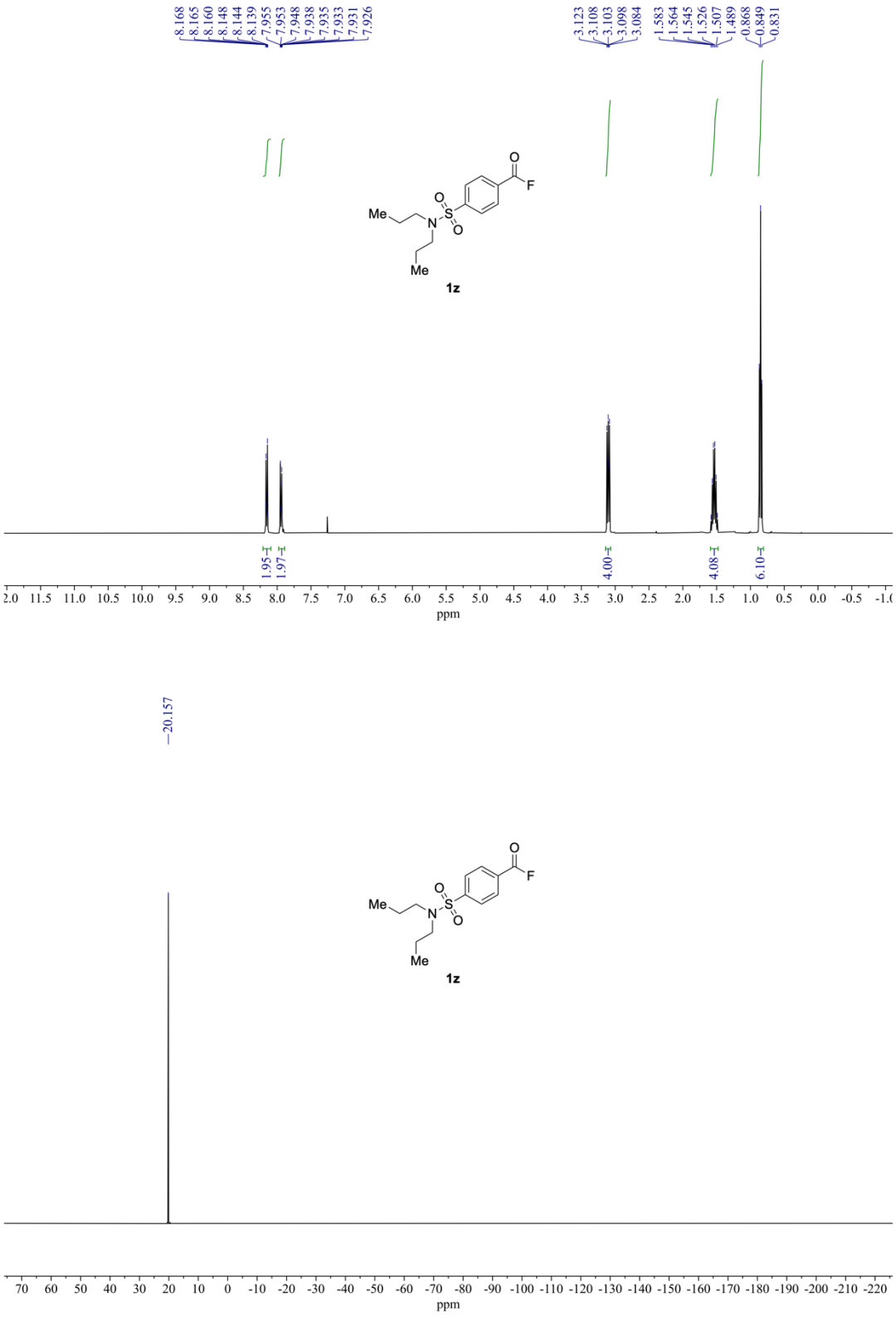

^{1}H NMR (400 MHz) and ^{19}F{^{1}H} NMR (376 MHz) spectra of **1z** (rt, $CDCl_3$).

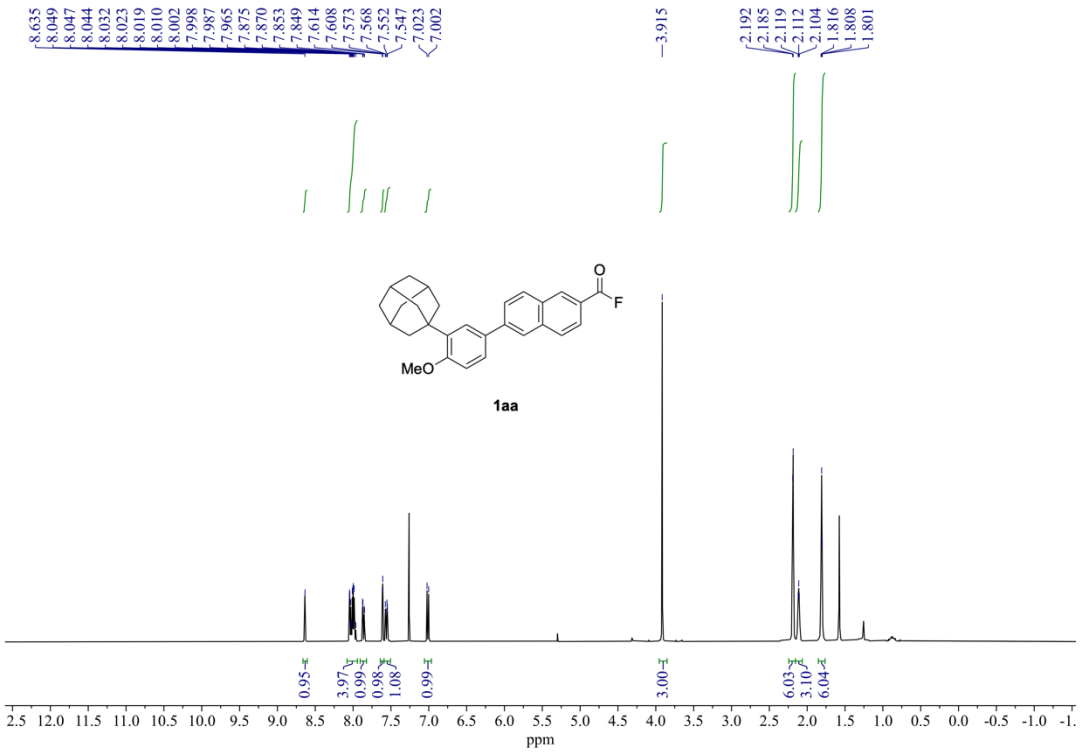

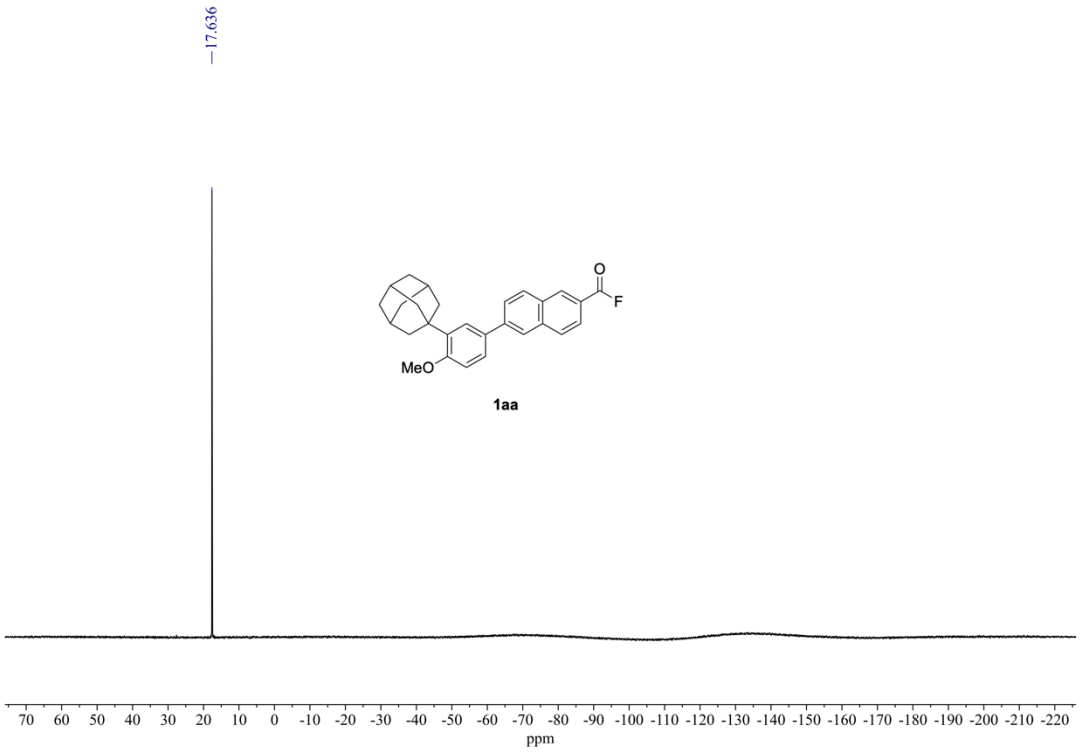

^{1}H NMR (400 MHz) and ^{19}F{^{1}H} NMR (376 MHz) spectra of **1aa** (rt, $CDCl_3$).

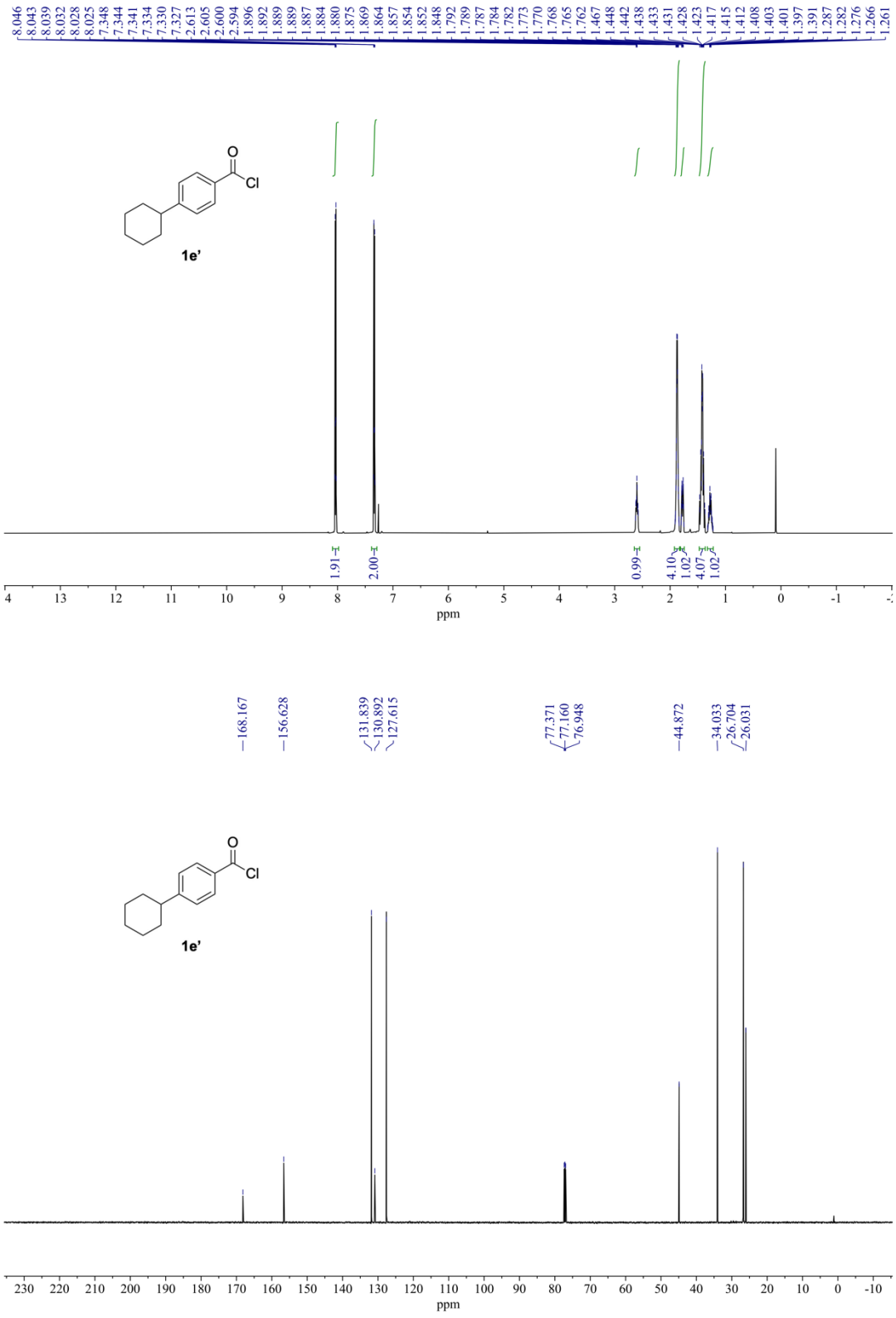

^{1}H NMR (600 MHz) and ^{13}C{^{1}H} NMR (151 MHz) spectra of **1e'** (rt, $CDCl_3$).

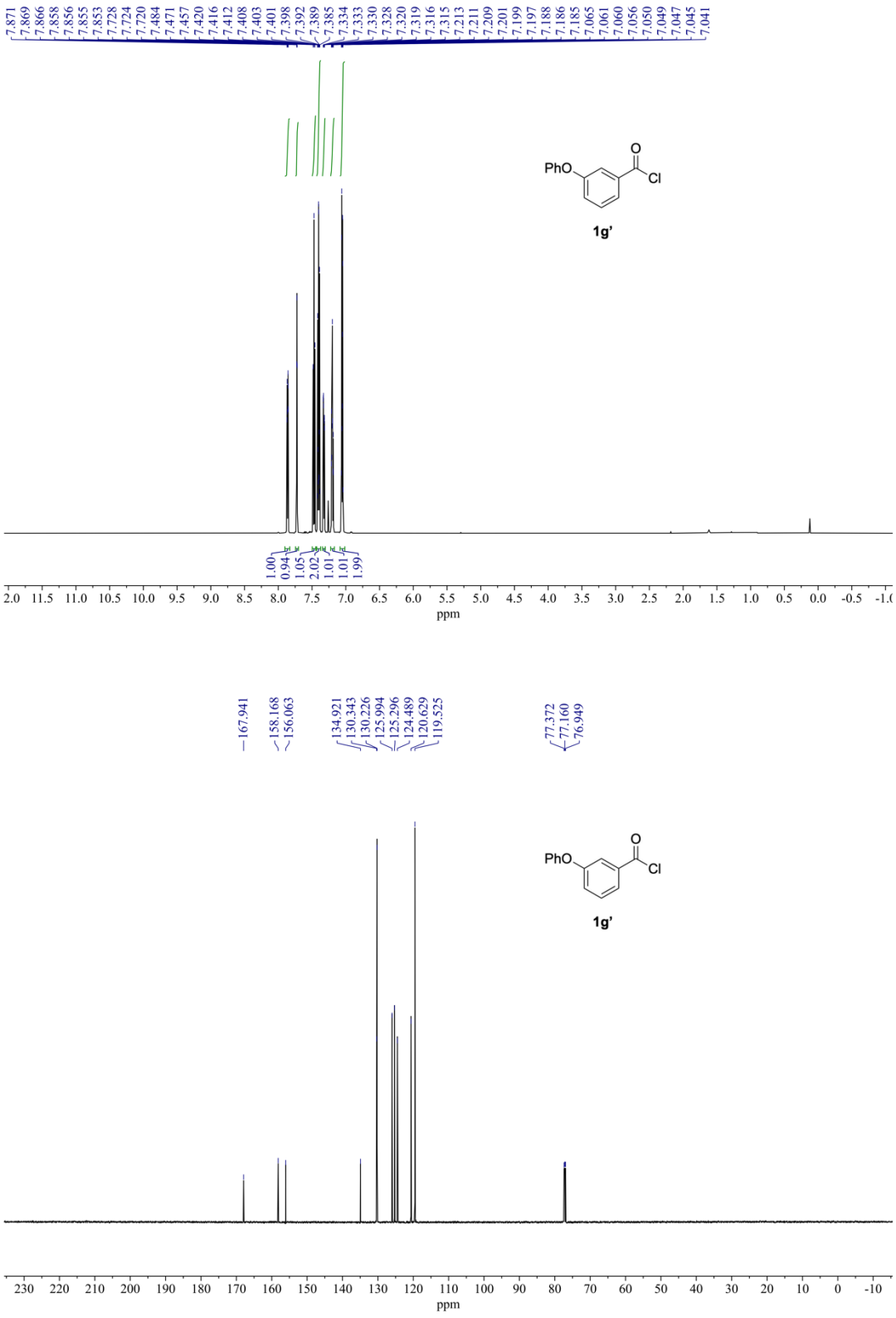

^{1}H NMR (600 MHz) and ^{13}C{^{1}H} NMR (151 MHz) spectra of **1g'** (rt, $CDCl_3$).

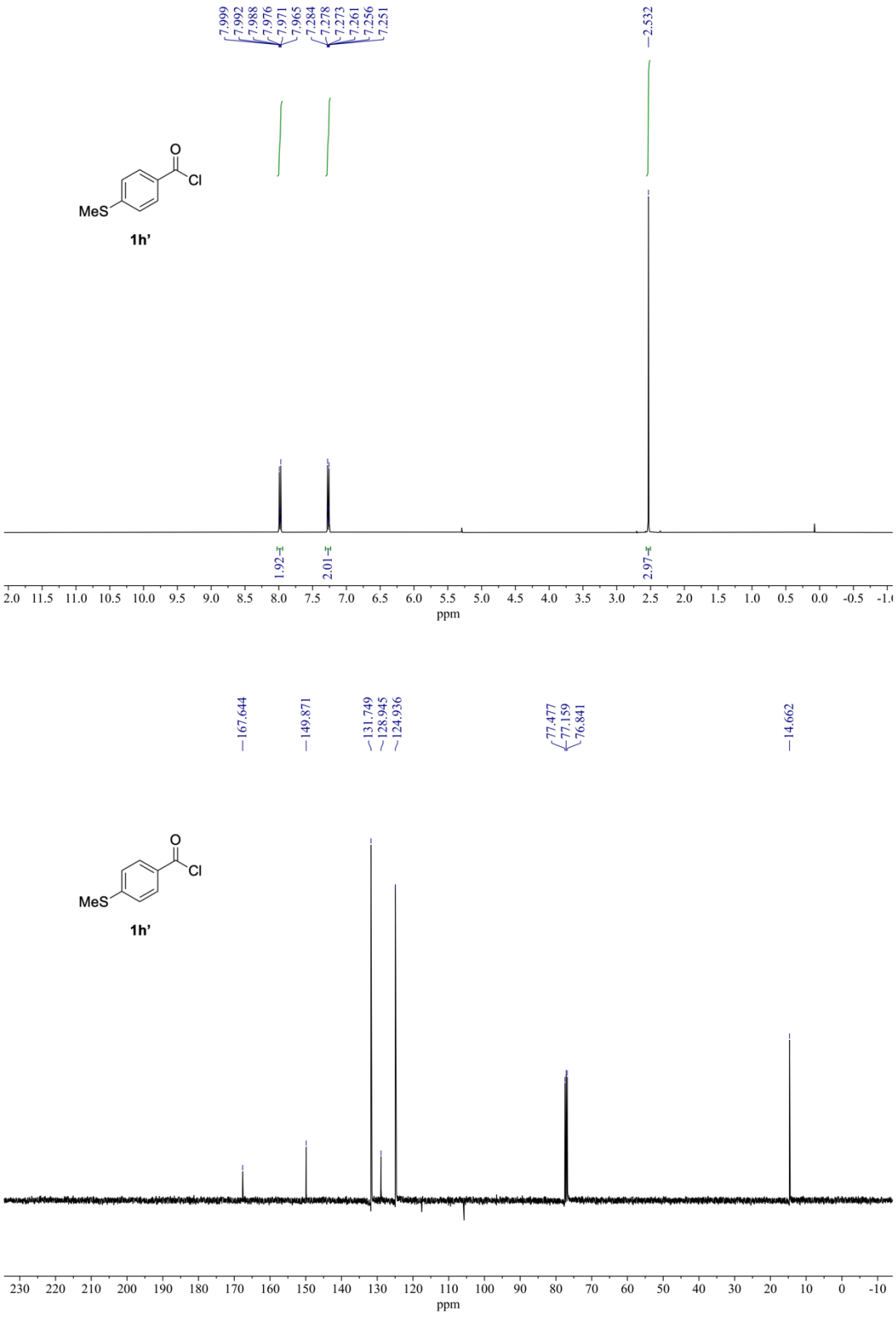

^{1}H NMR (400 MHz) and ^{13}C{^{1}H} NMR (101 MHz) spectra of **1h'** (rt, $CDCl_3$).

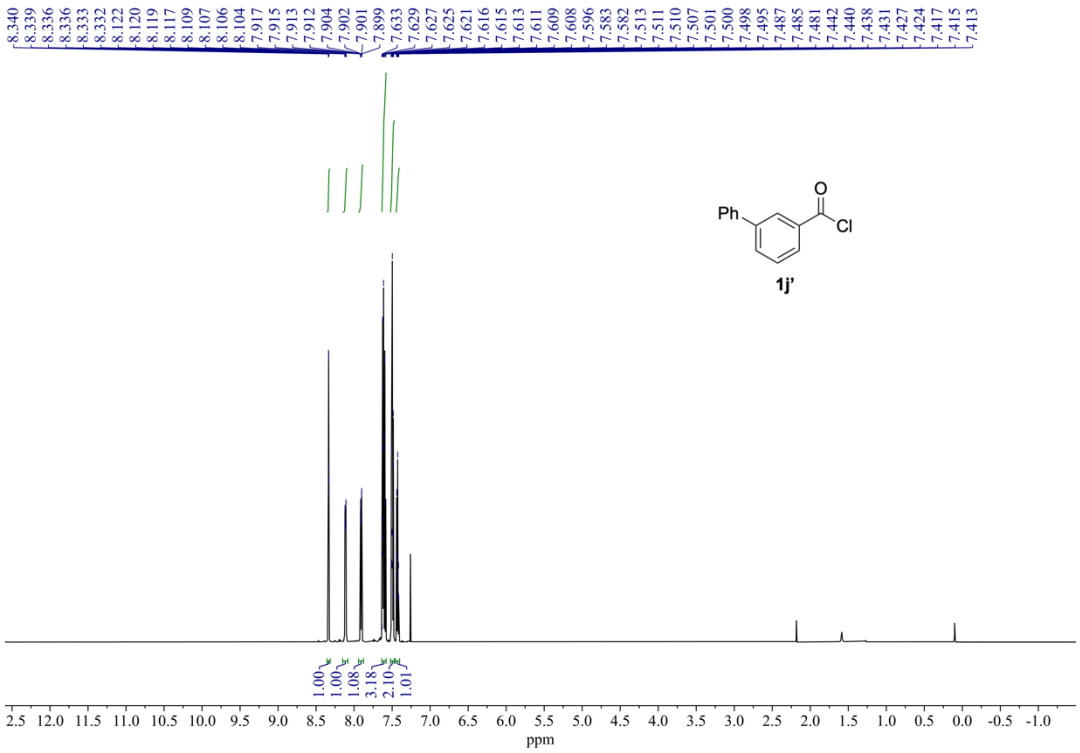

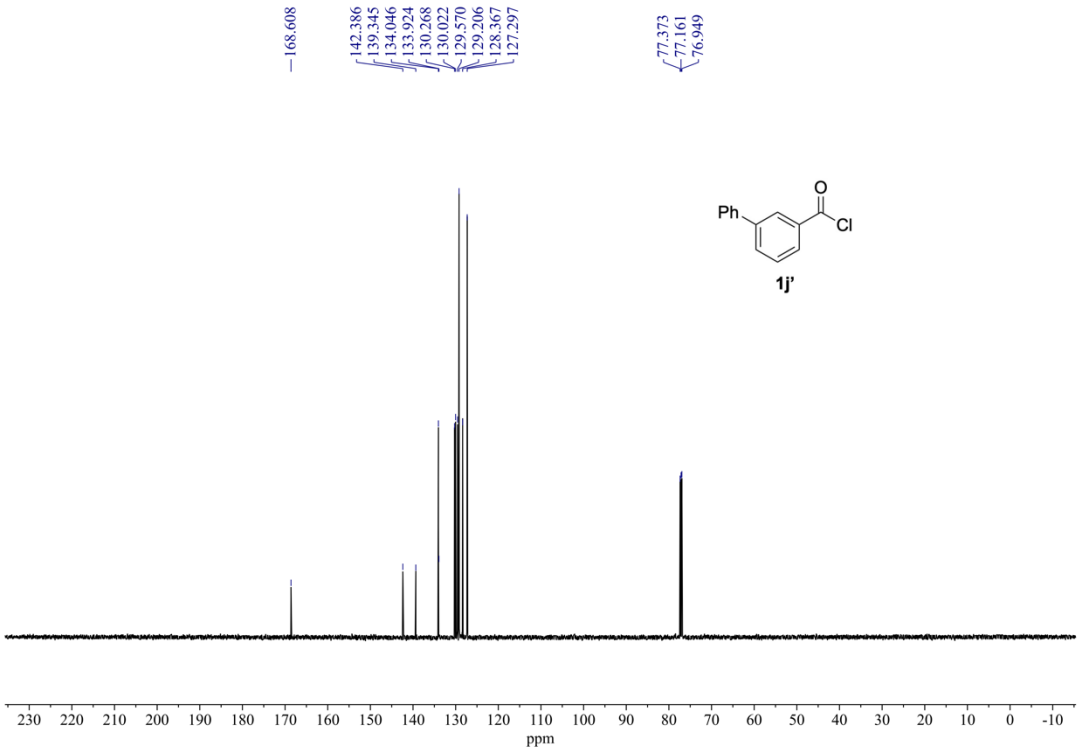

^{1}H NMR (600 MHz) and ^{13}C{^{1}H} NMR (151 MHz) spectra of **1j'** (rt, $CDCl_3$).

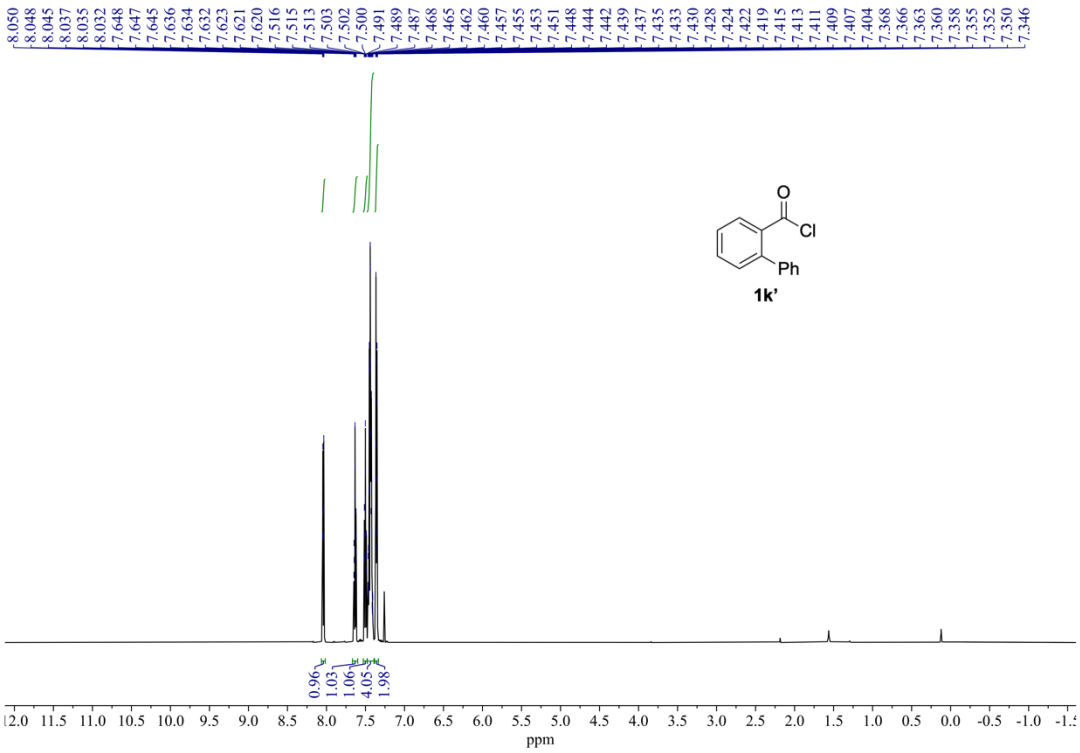

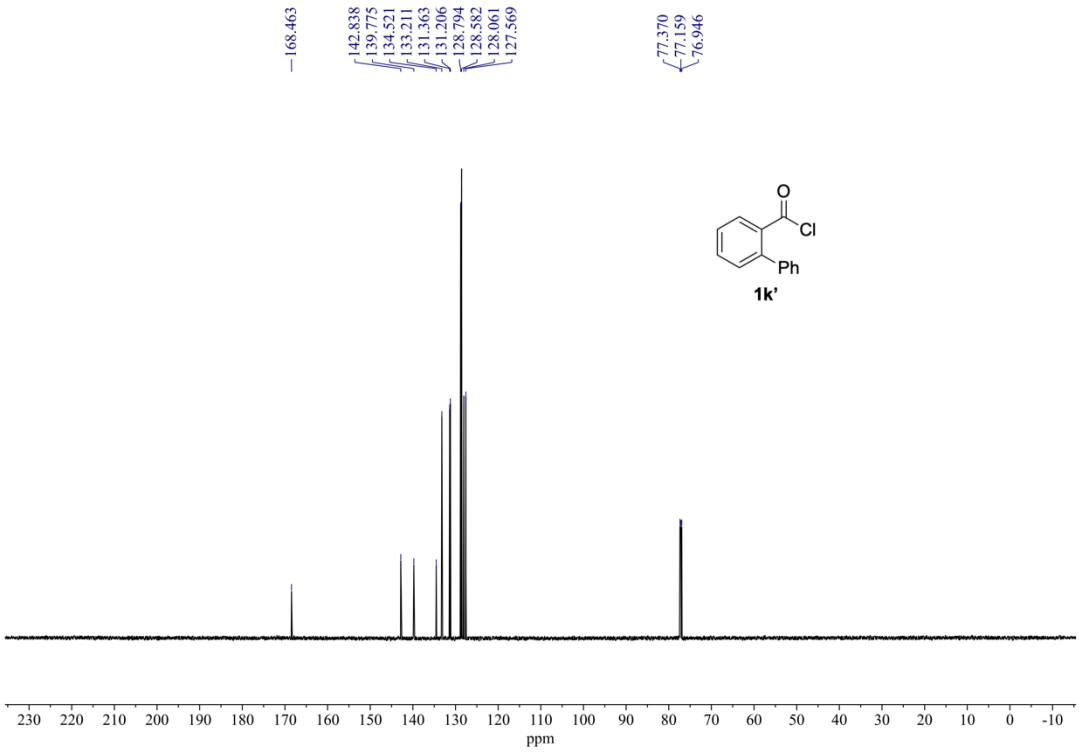

^{1}H NMR (600 MHz) and ^{13}C{^{1}H} NMR (151 MHz) spectra of **1k'** (rt, $CDCl_3$).

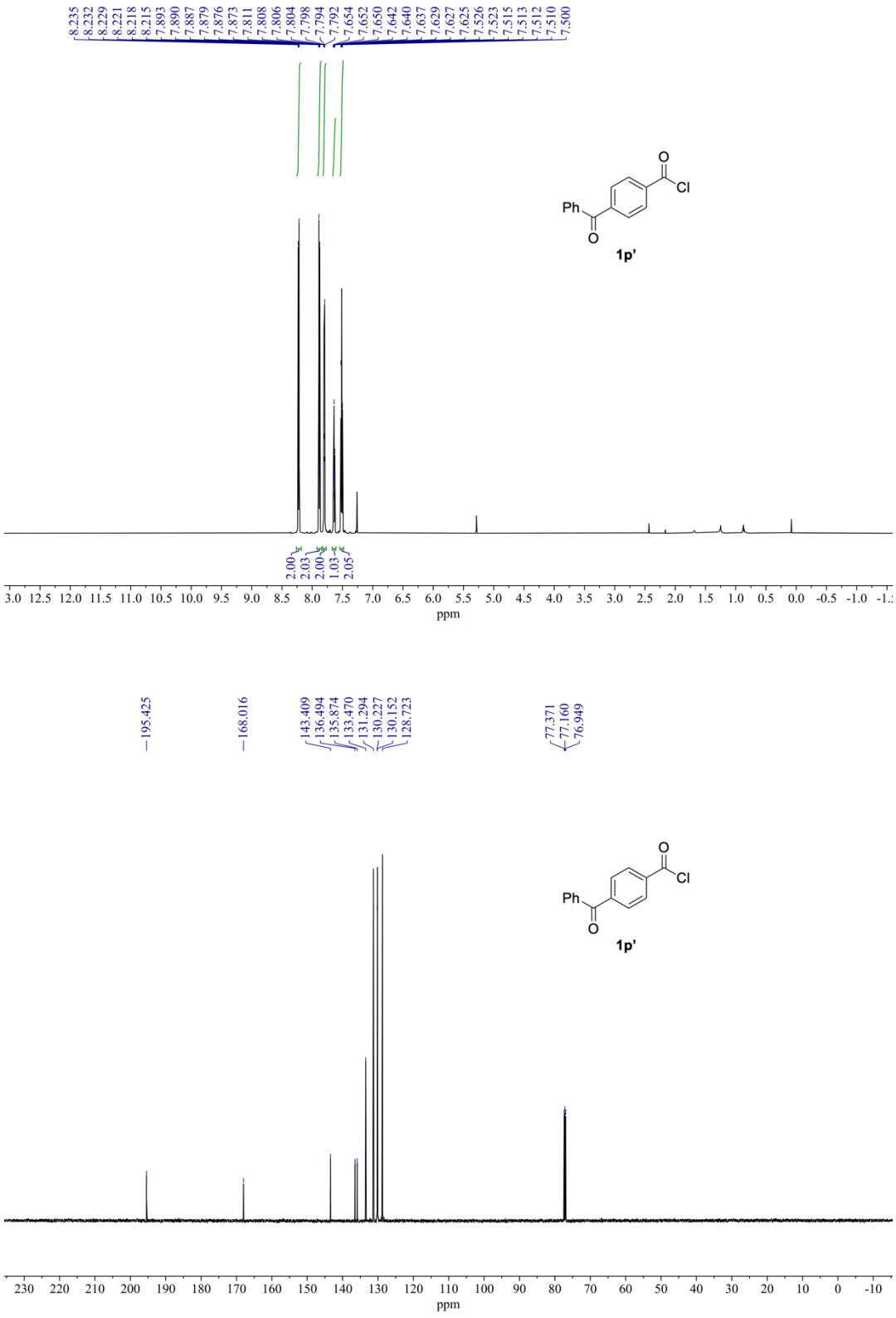

^{1}H NMR (600 MHz) and ^{13}C{^{1}H} NMR (151 MHz) spectra of **1p'** (rt, $CDCl_3$).

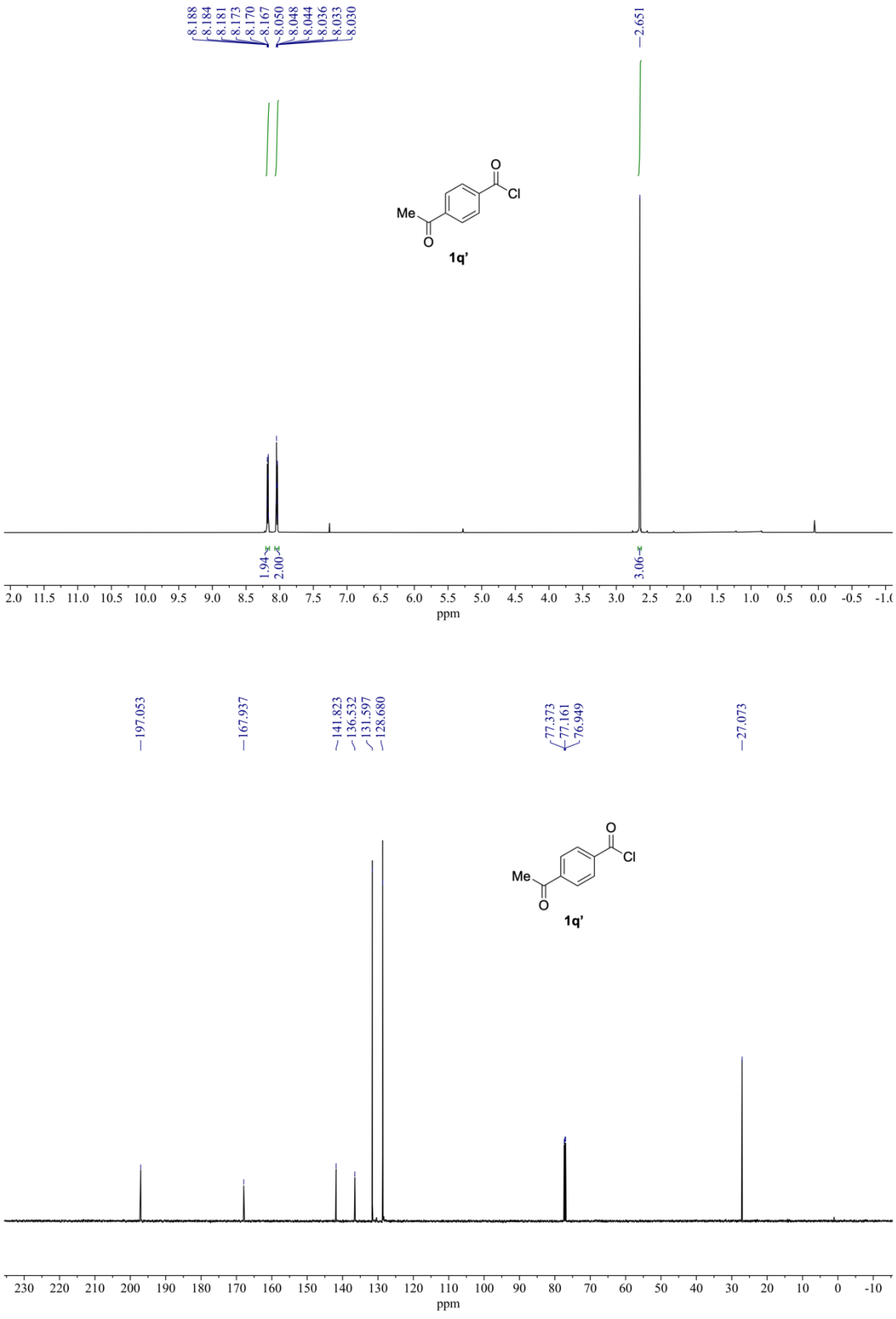

^{1}H NMR (600 MHz) and ^{13}C{^{1}H} NMR (151 MHz) spectra of **1q'** (rt, $CDCl_3$).

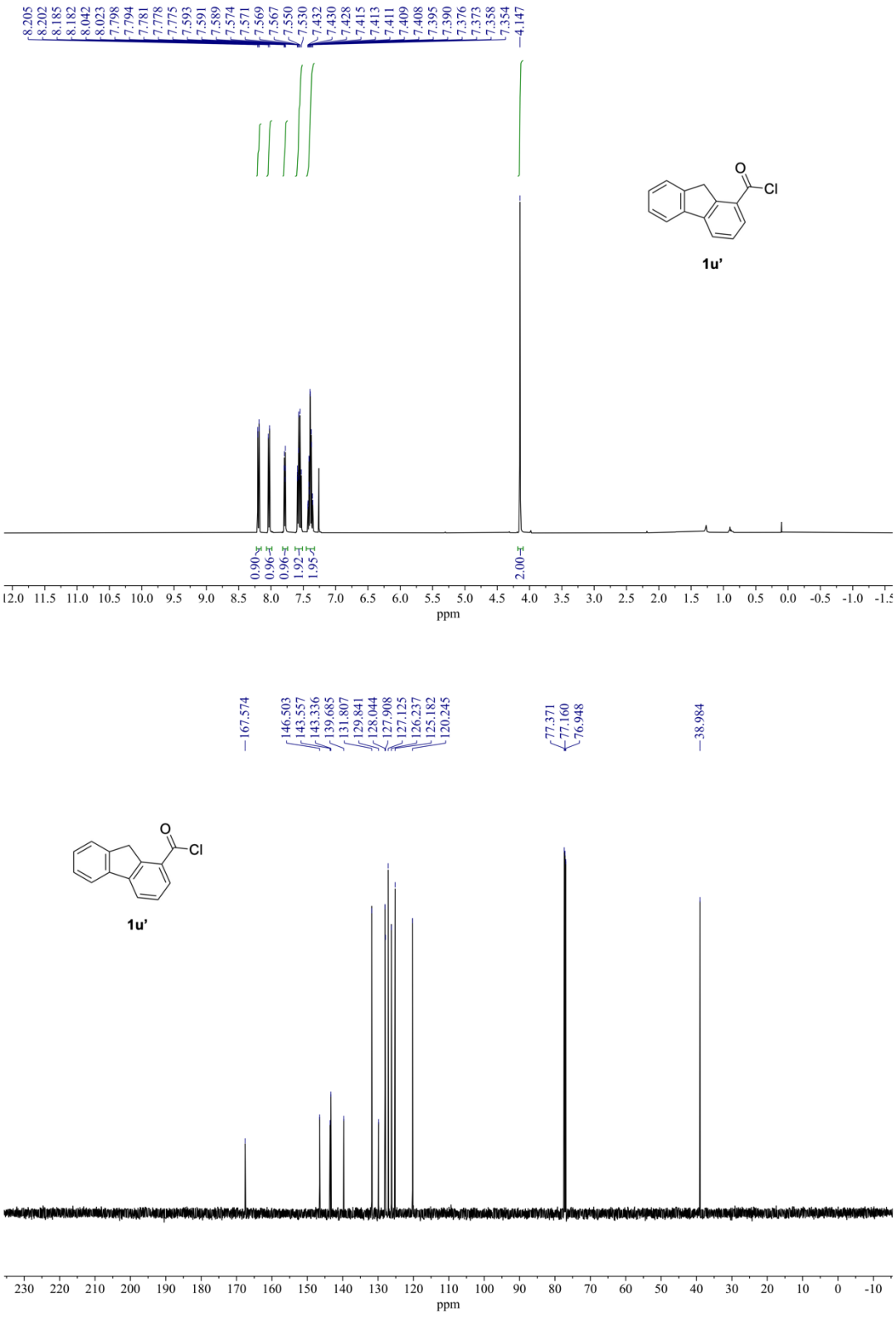

^{1}H NMR (400 MHz) and ^{13}C{^{1}H} NMR (151 MHz) spectra of **1u'** (rt, $CDCl_3$).

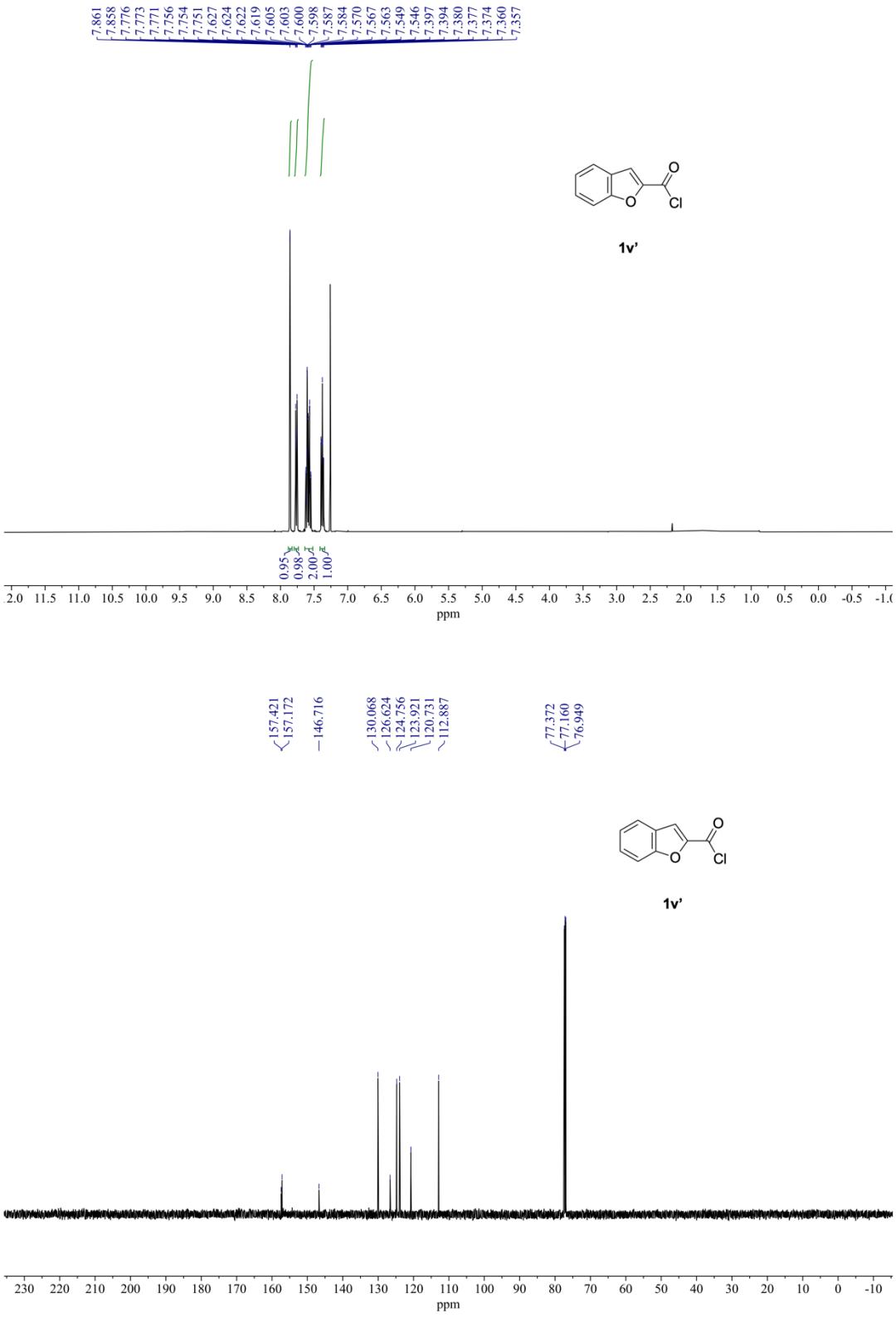

^{1}H NMR (400 MHz) and ^{13}C{^{1}H} NMR (151 MHz) spectra of **1v'** (rt, $CDCl_3$).

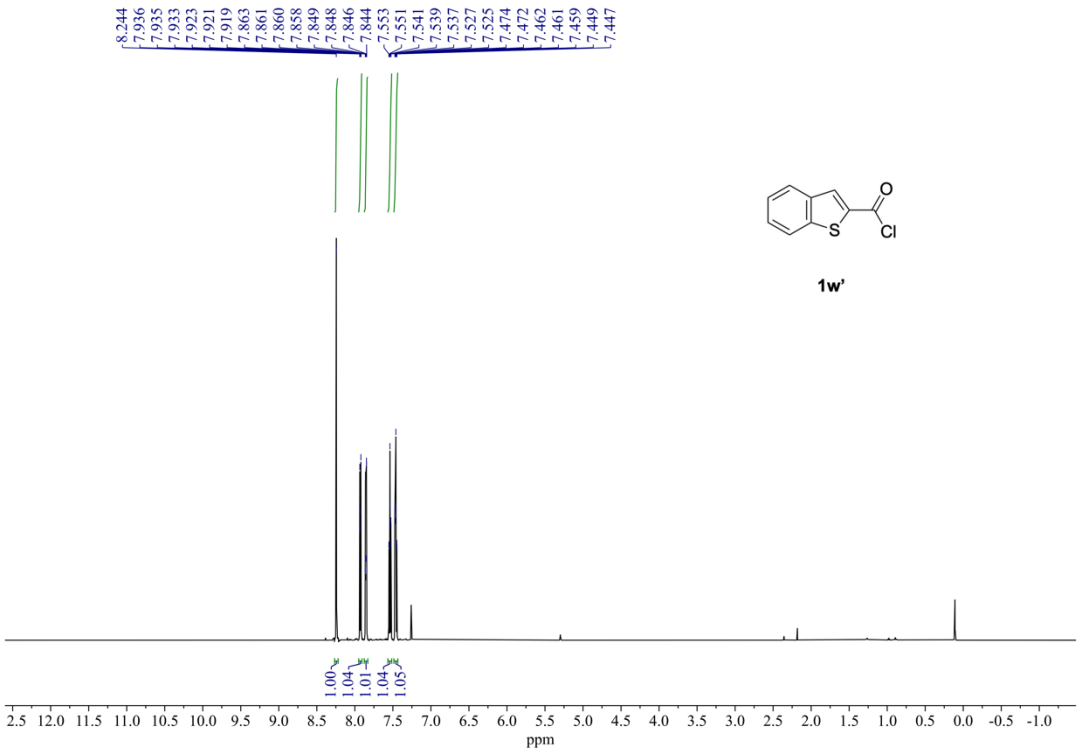

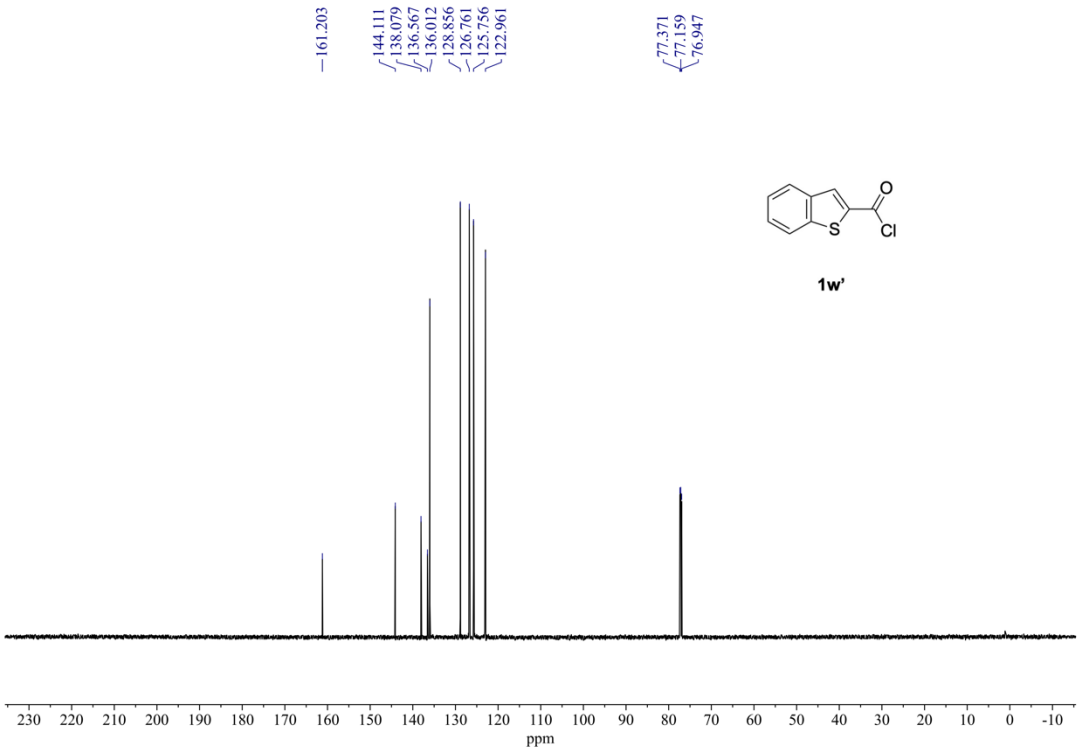

^{1}H NMR (600 MHz) and ^{13}C{^{1}H} NMR (151 MHz) spectra of **1w'** (rt, $CDCl_3$).

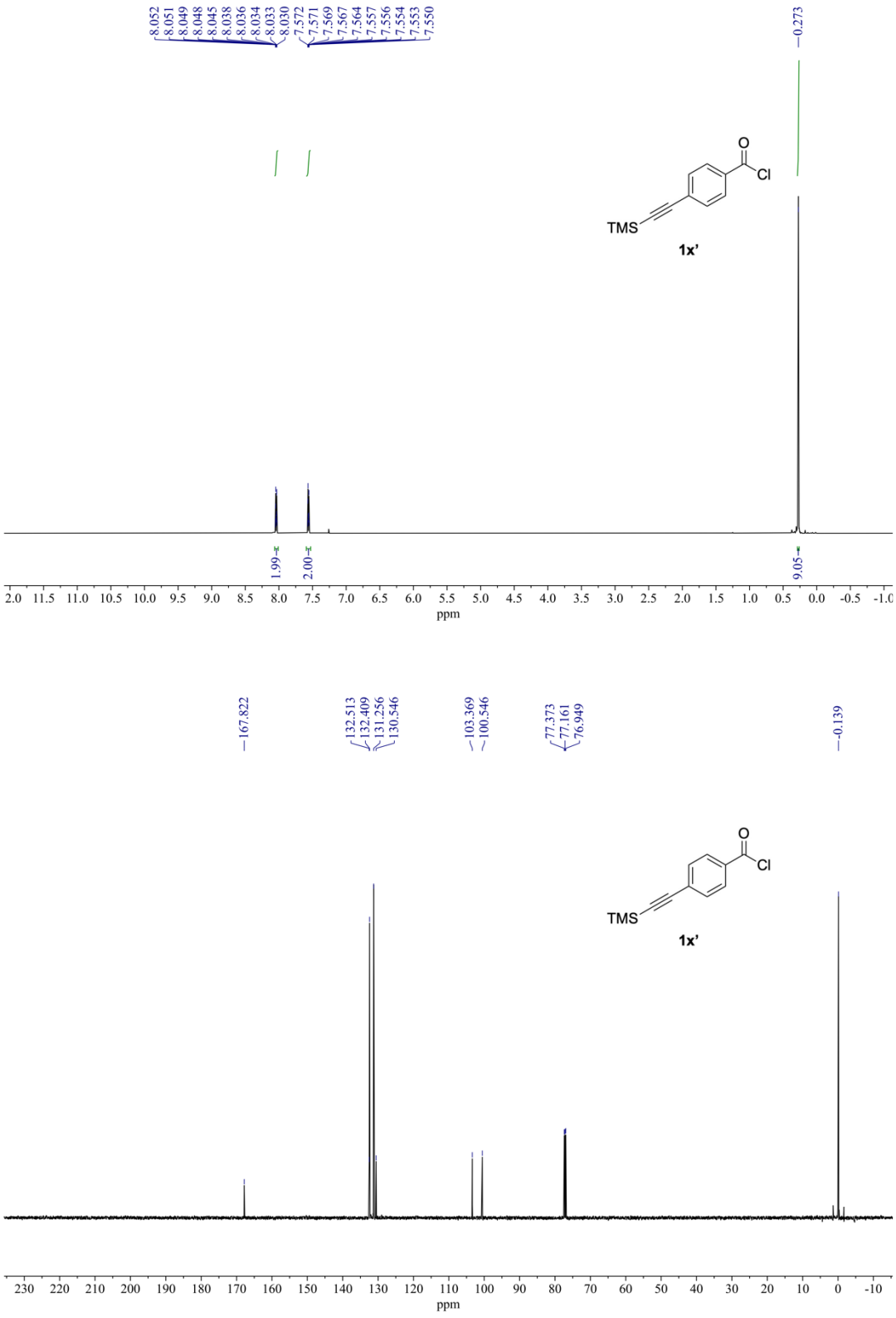

^{1}H NMR (600 MHz) and ^{13}C{^{1}H} NMR (151 MHz) spectra of **1x'** (rt, $CDCl_3$).

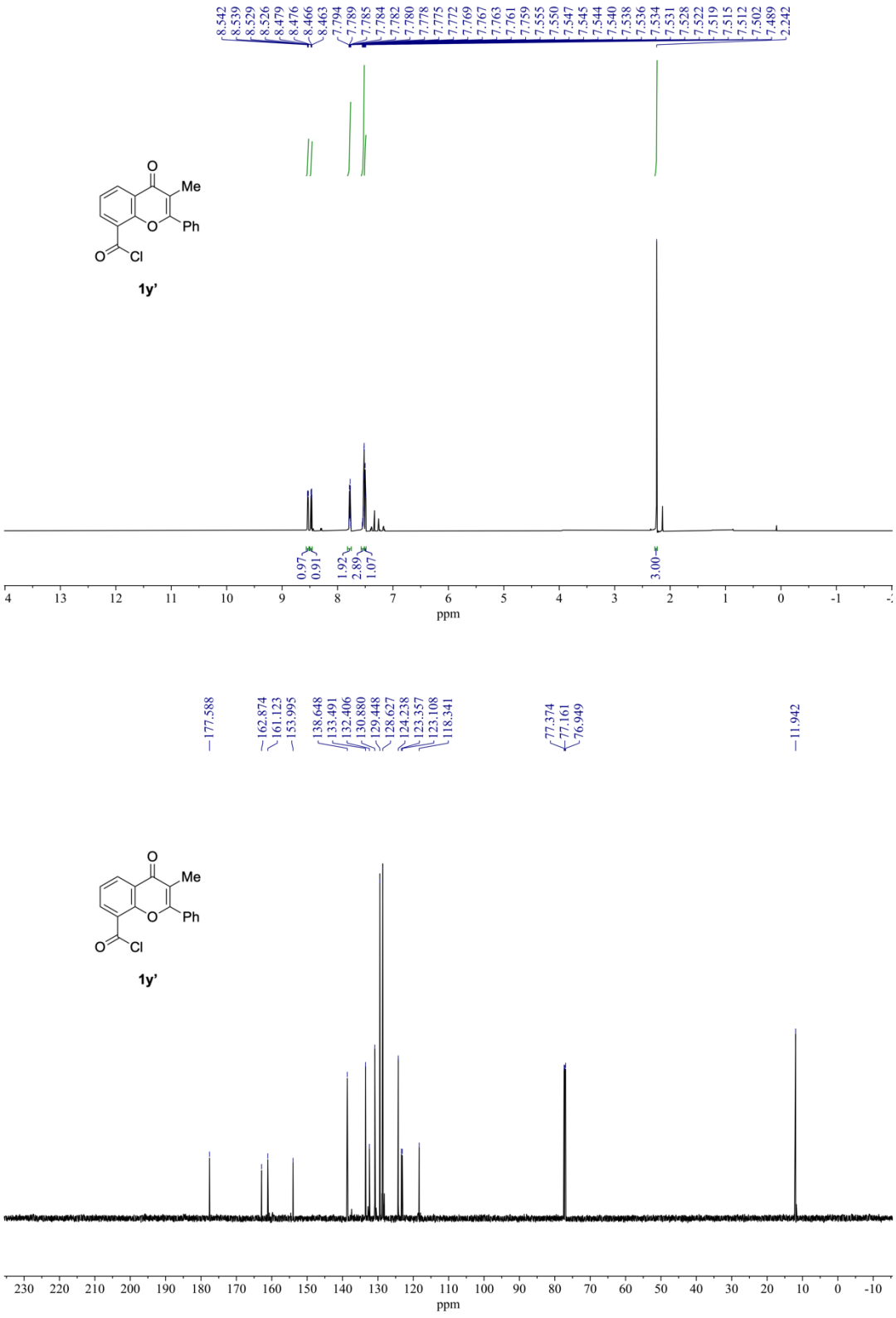

^{1}H NMR (600 MHz) and ^{13}C{^{1}H} NMR (151 MHz) spectra of **1y'** (rt, $CDCl_3$).

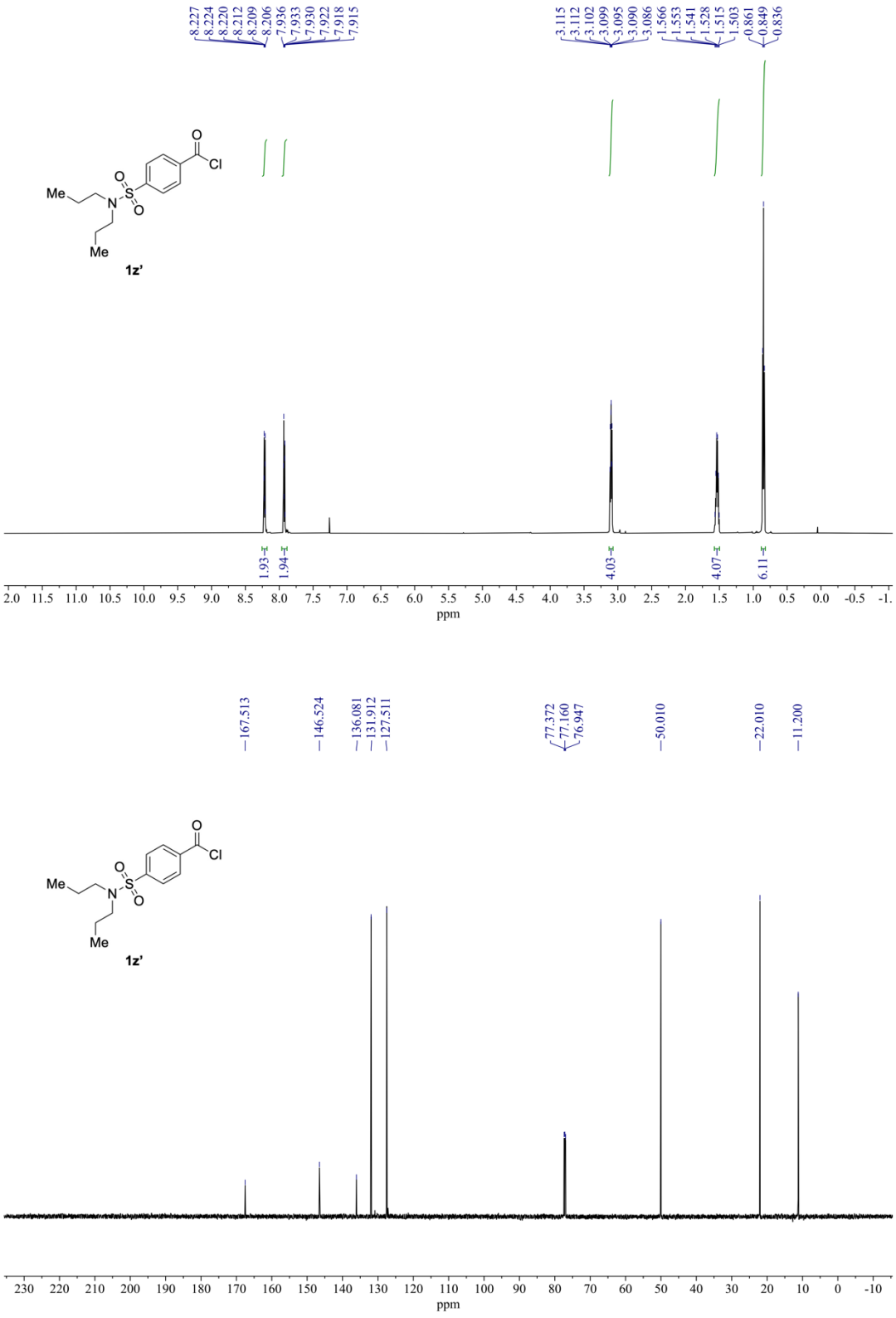

^{1}H NMR (600 MHz) and ^{13}C{^{1}H} NMR (151 MHz) spectra of **1z'** (rt, $CDCl_3$).

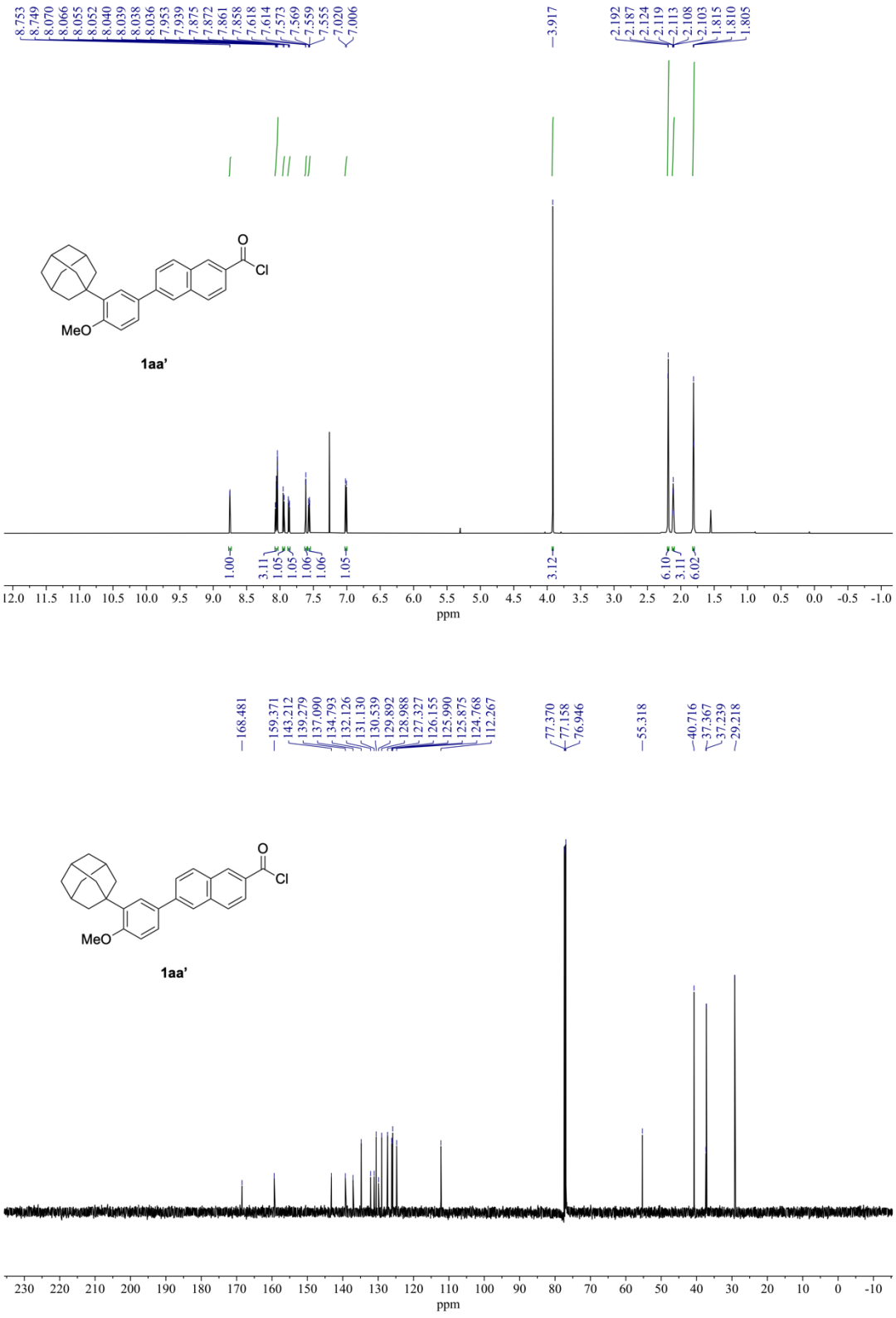

^{1}H NMR (600 MHz) and ^{13}C{^{1}H} NMR (151 MHz) spectra of **1aa'** (rt, $CDCl_3$).

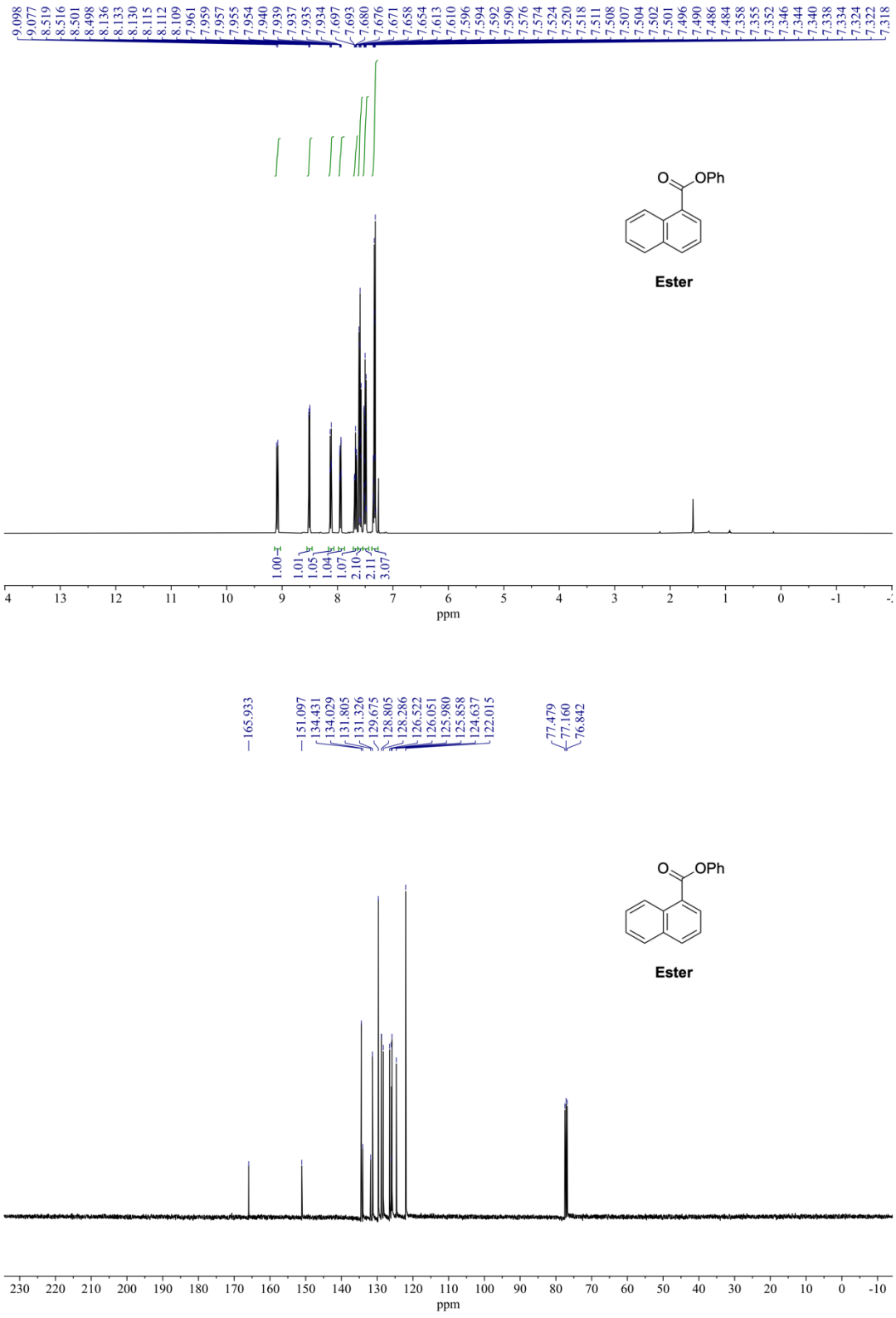

^{1}H NMR (400 MHz) and ^{13}C{^{1}H} NMR (101 MHz) spectra of **Ester** (rt, $CDCl_3$).

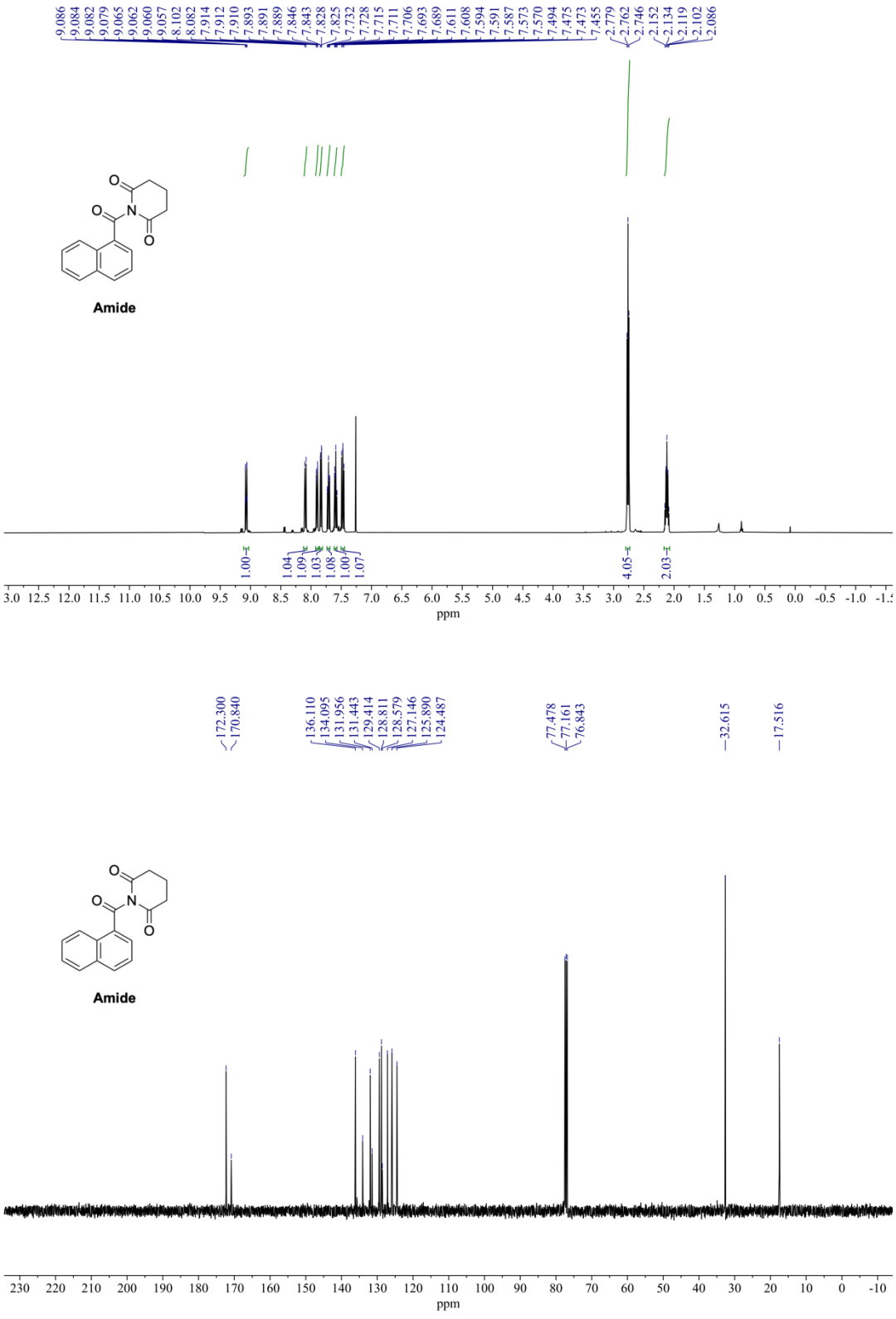

^{1}H NMR (400 MHz) and ^{13}C{^{1}H} NMR (101 MHz) spectra of **Amide** (rt, $CDCl_3$).

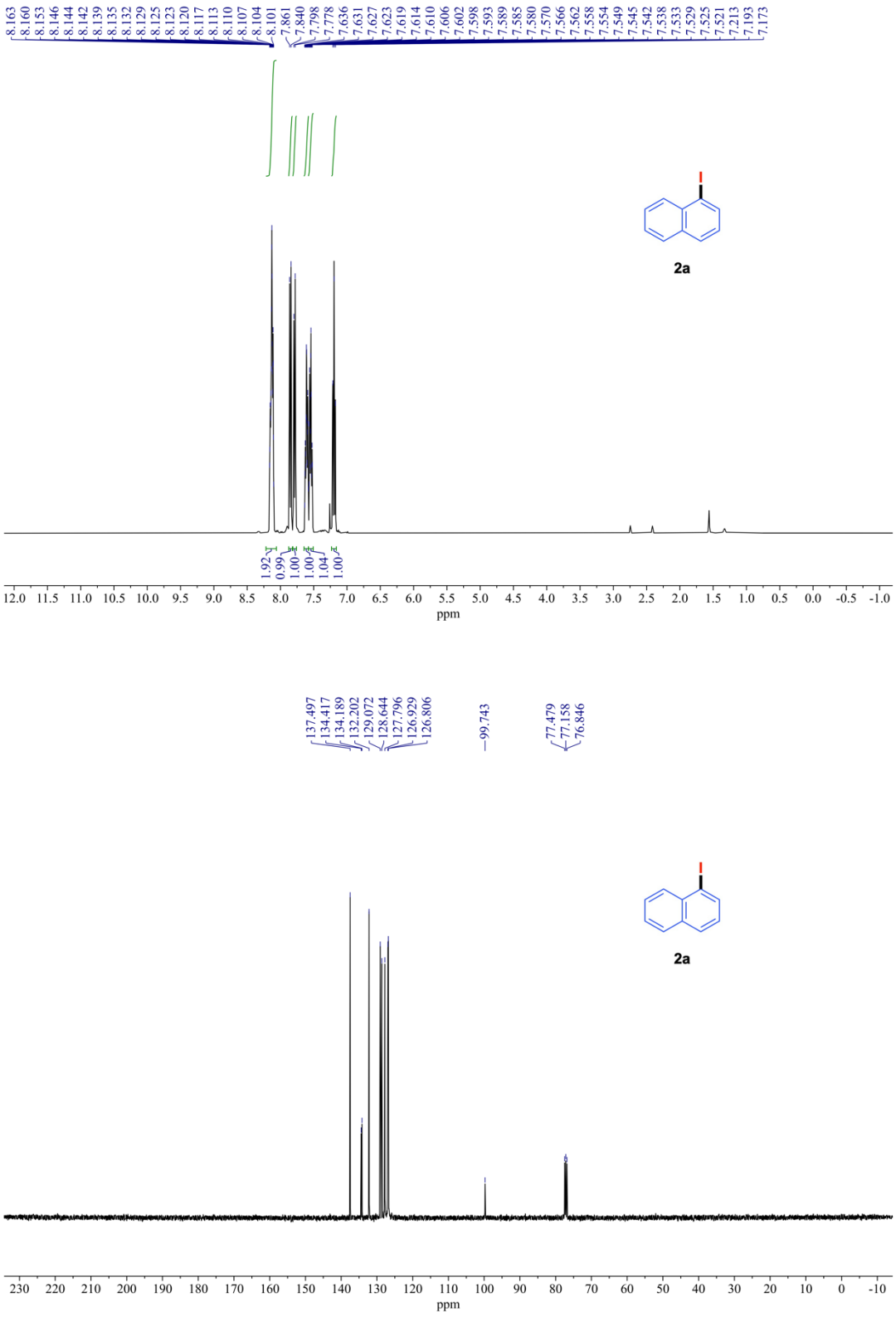

^{1}H NMR (400 MHz) and ^{13}C{^{1}H} NMR (101 MHz) spectra of **2a** (rt, $CDCl_3$).

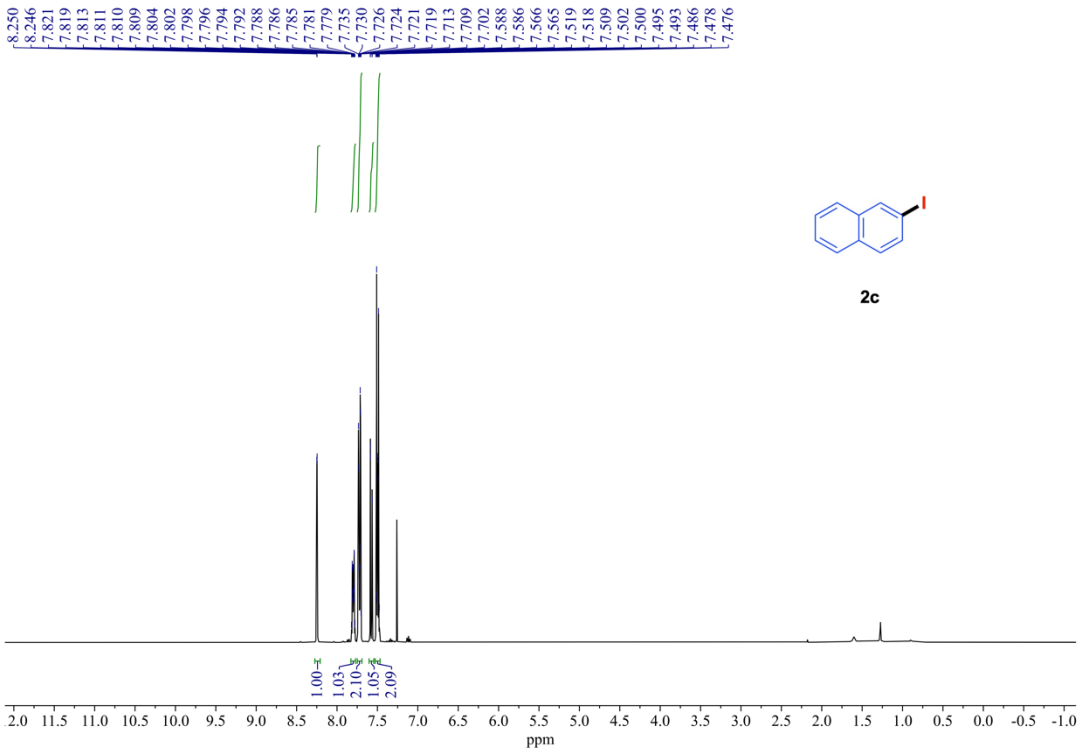

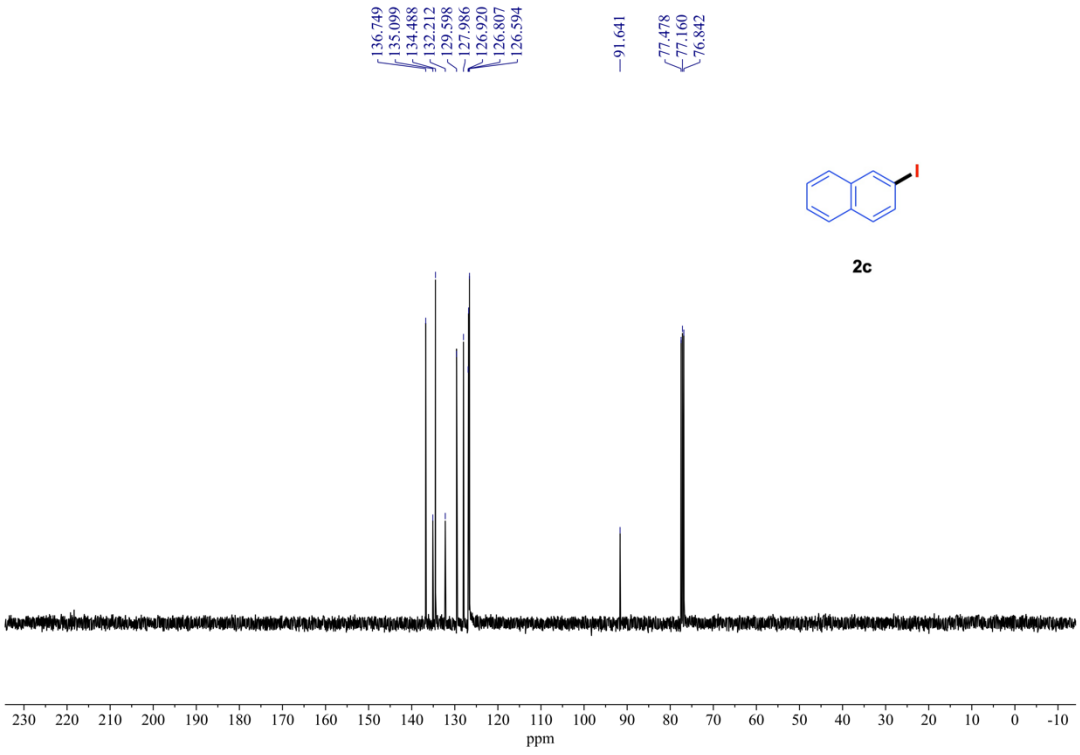

^{1}H NMR (400 MHz) and ^{13}C{^{1}H} NMR (101 MHz) spectra of **2c** (rt, $CDCl_3$).

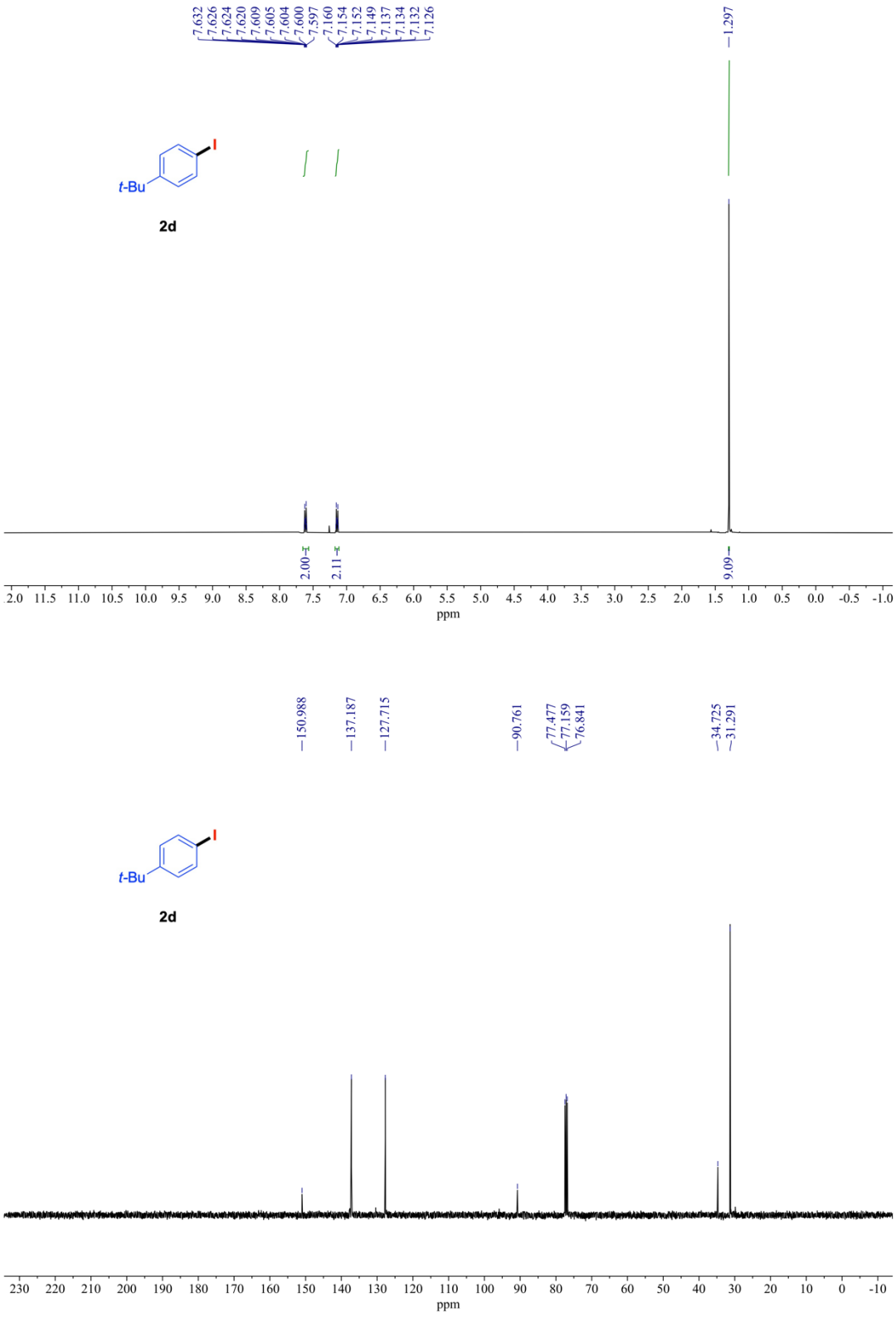

^{1}H NMR (400 MHz) and ^{13}C{^{1}H} NMR (101 MHz) spectra of **2d** (rt, $CDCl_3$).

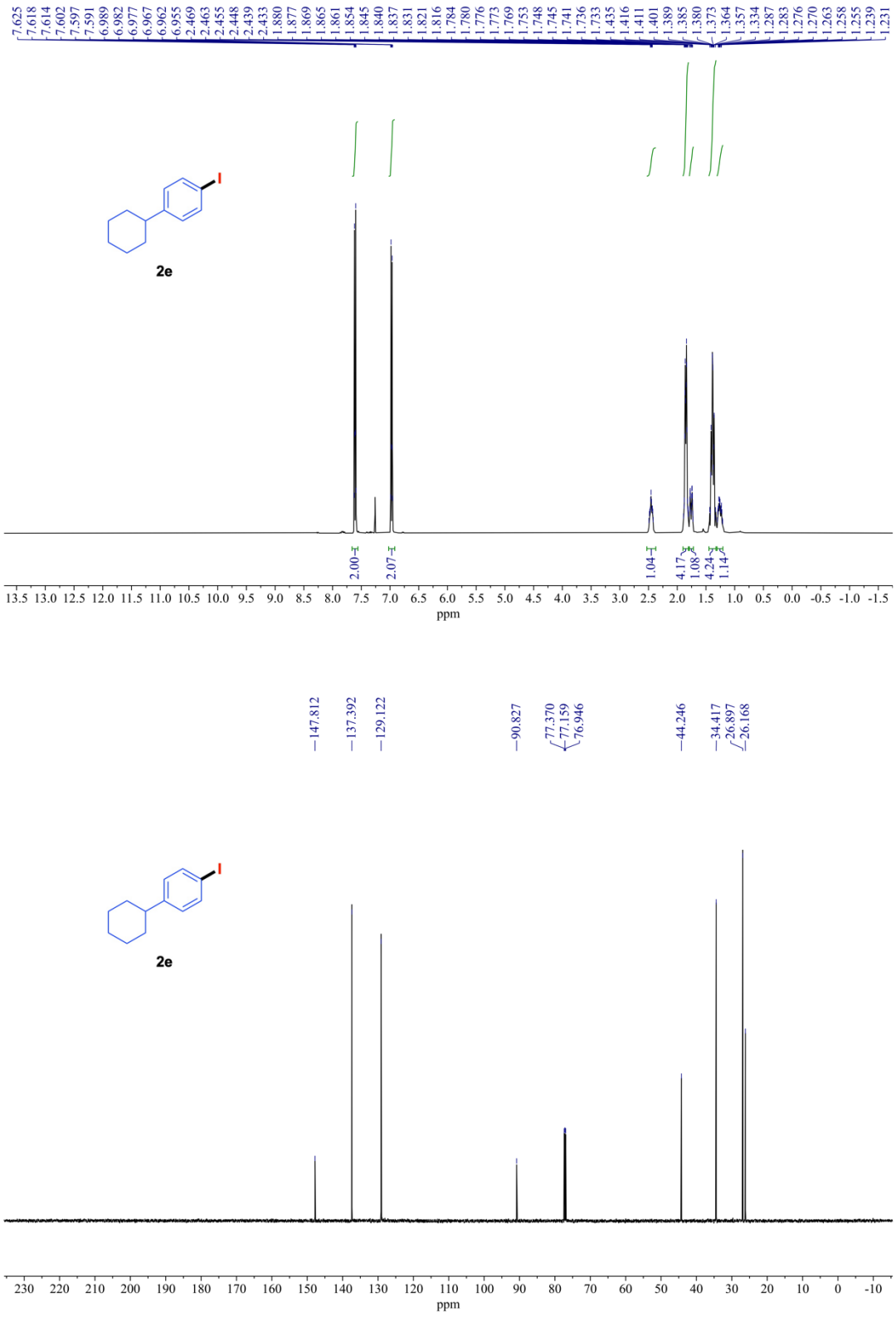

^{1}H NMR (400 MHz) and ^{13}C{^{1}H} NMR (151 MHz) spectra of **2e** (rt, $CDCl_3$).

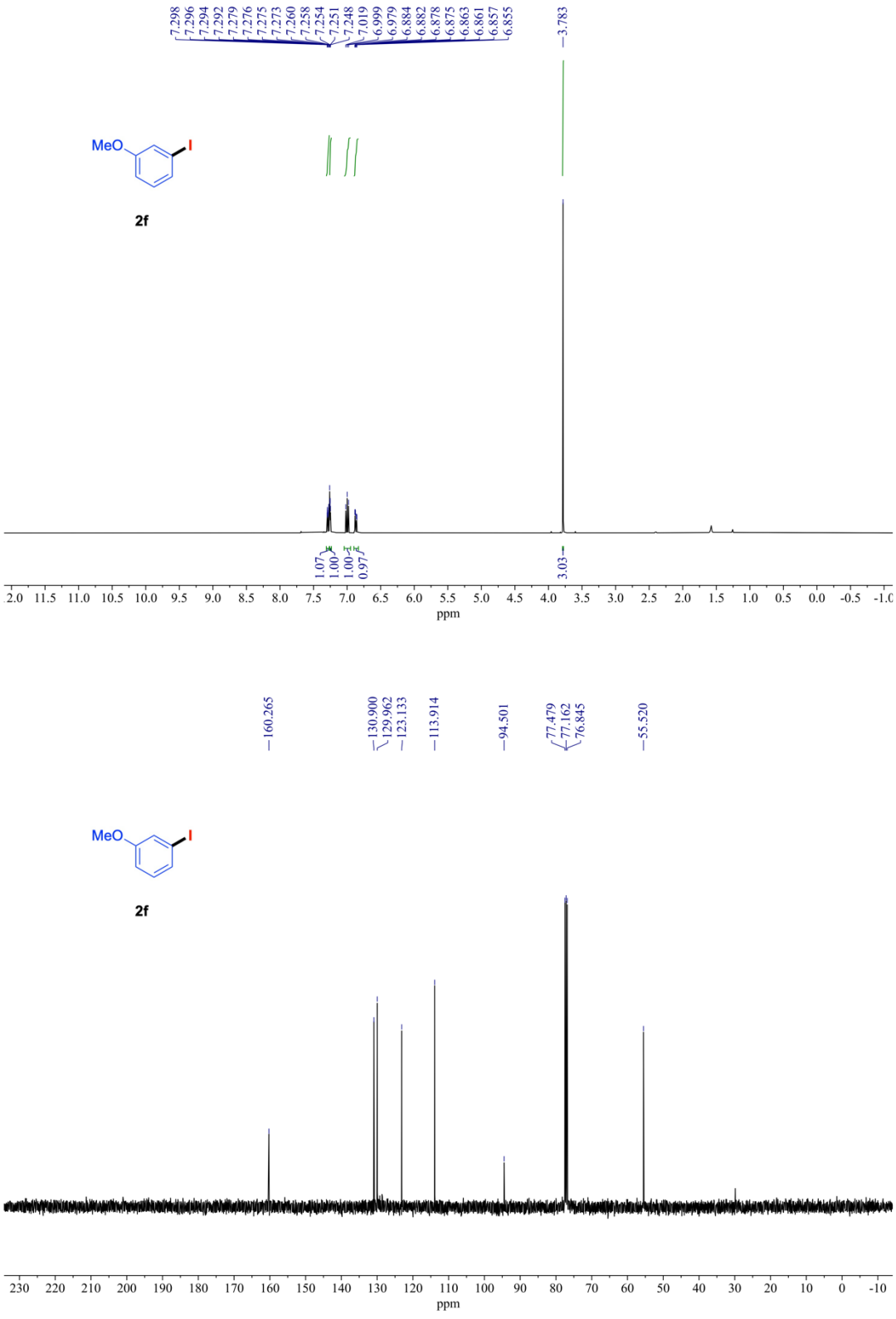

^{1}H NMR (400 MHz) and ^{13}C{^{1}H} NMR (101 MHz) spectra of **2f** (rt, $CDCl_3$).

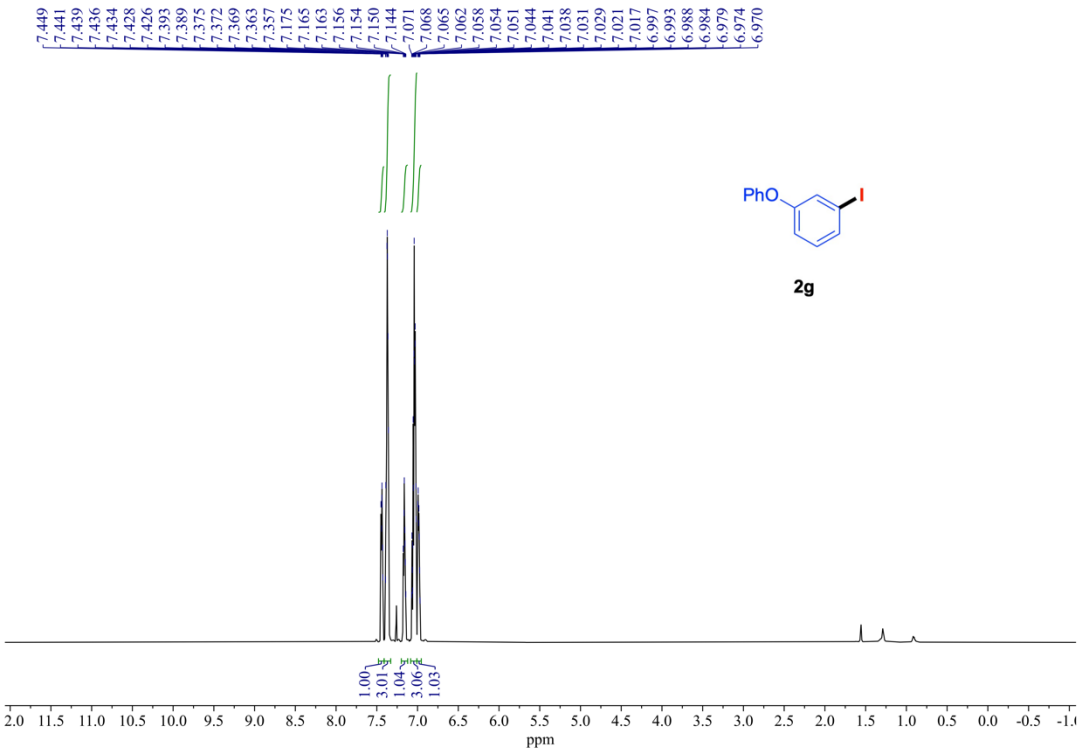

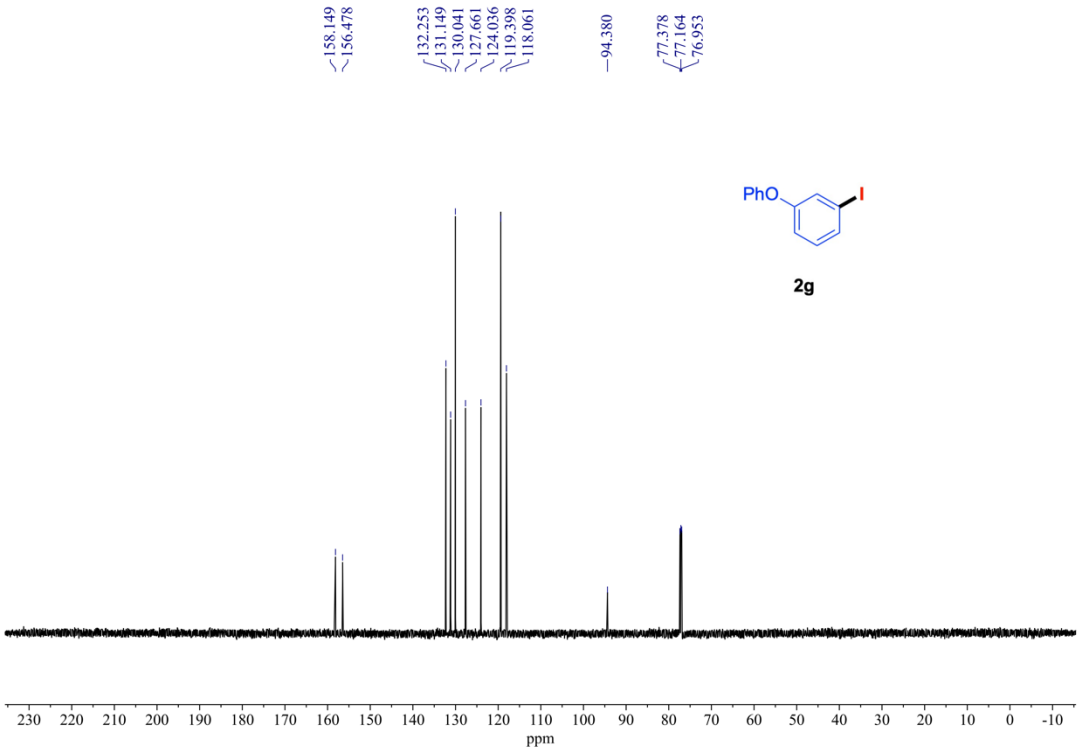

^{1}H NMR (600 MHz) and ^{13}C{^{1}H} NMR (151 MHz) spectra of **2g** (rt, $CDCl_3$).

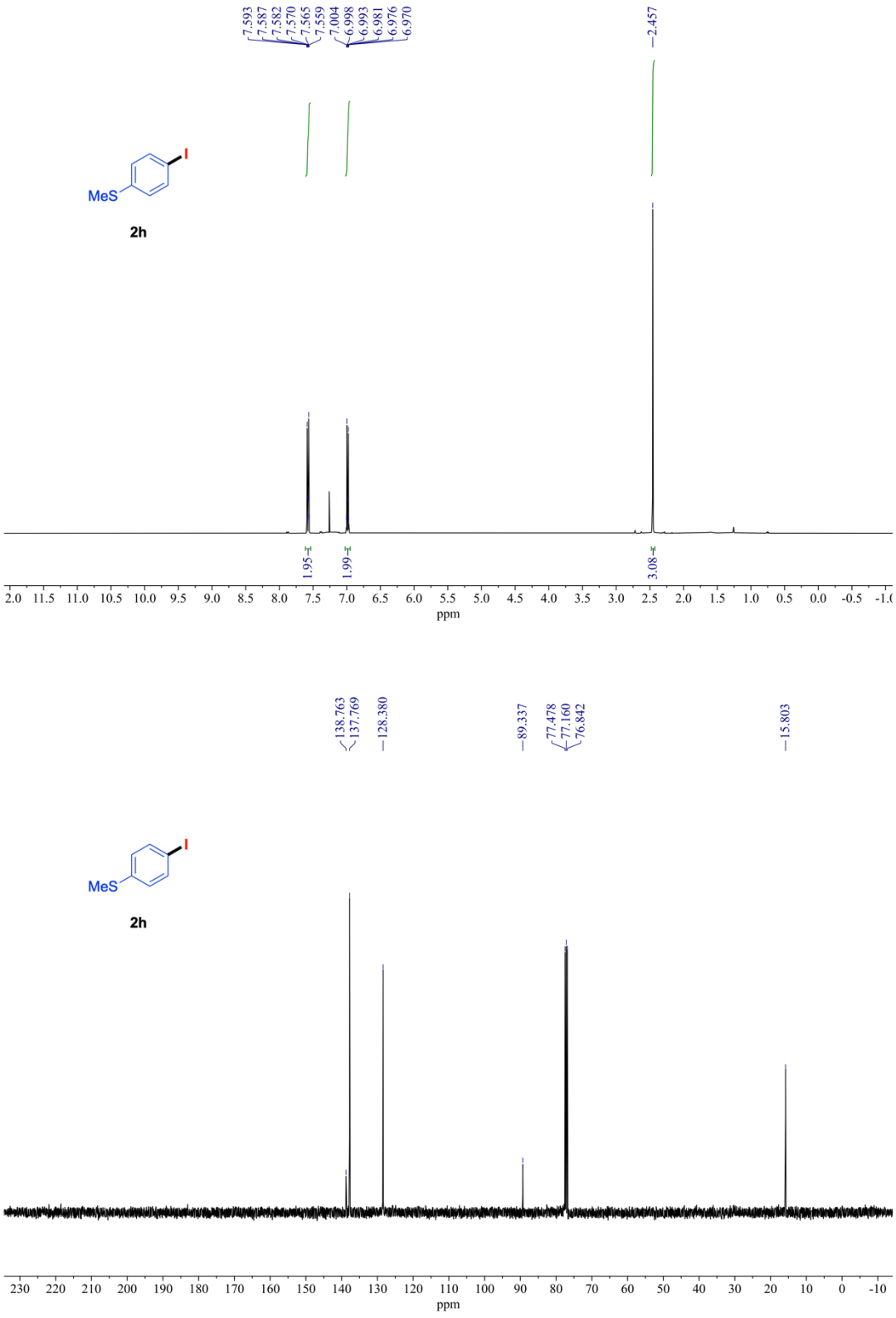

^{1}H NMR (400 MHz) and ^{13}C{^{1}H} NMR (101 MHz) spectra of **2h** (rt, $CDCl_3$).

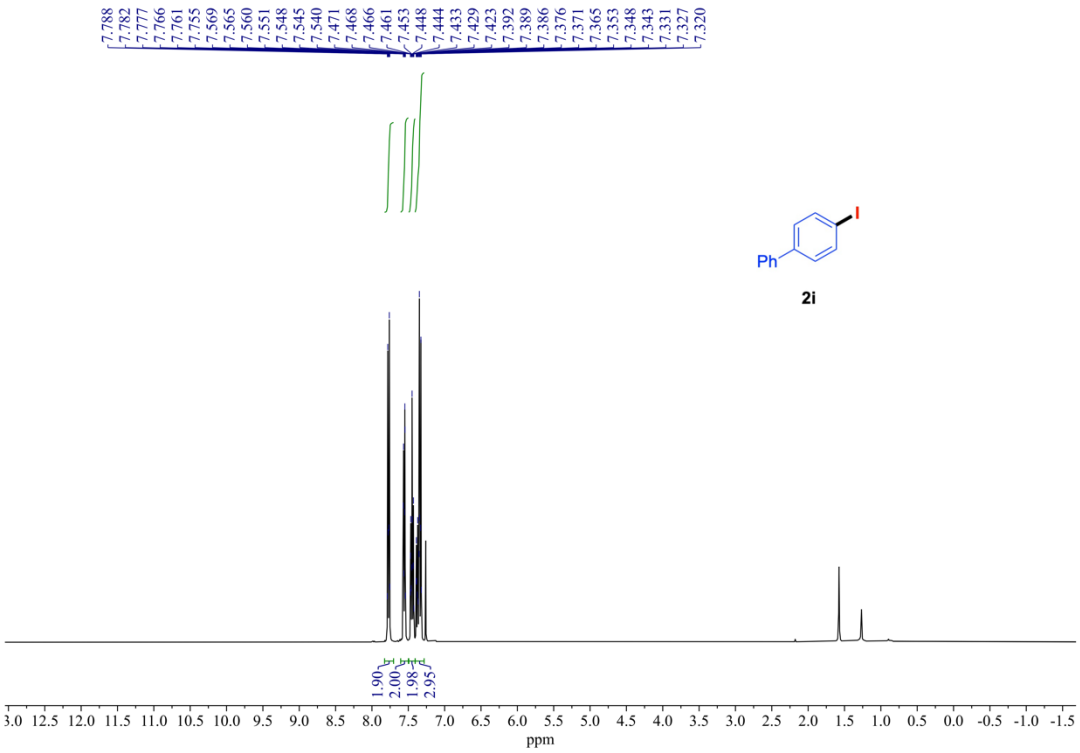

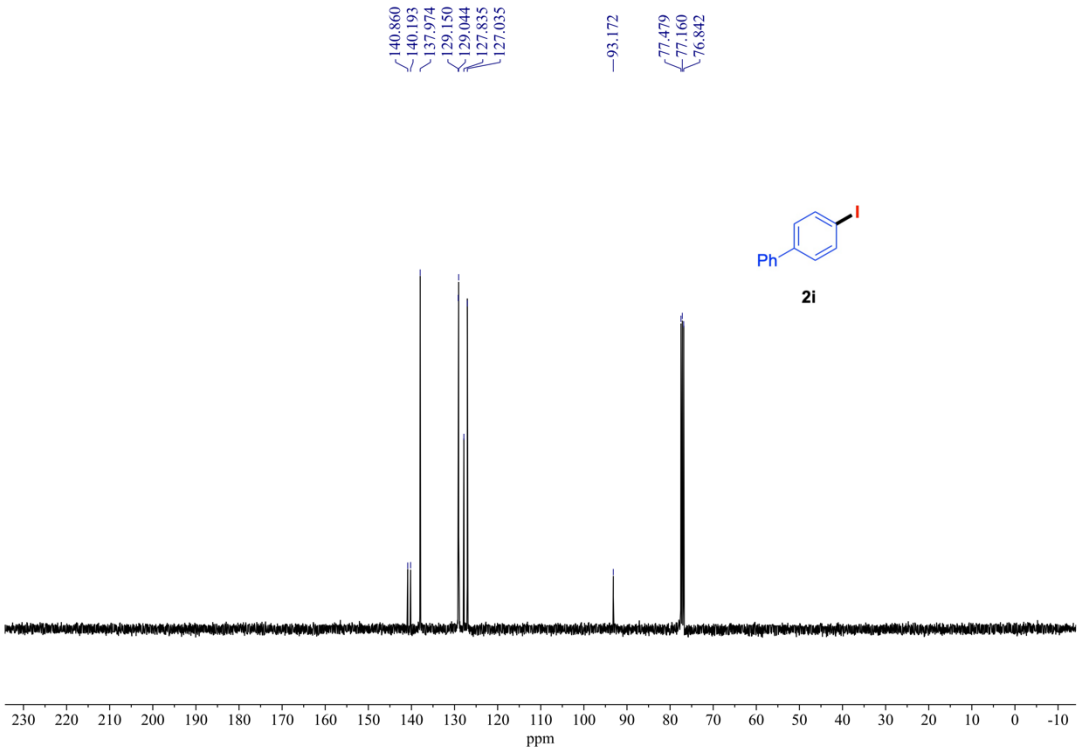

^{1}H NMR (400 MHz) and ^{13}C{^{1}H} NMR (101 MHz) spectra of **2i** (rt, $CDCl_3$).

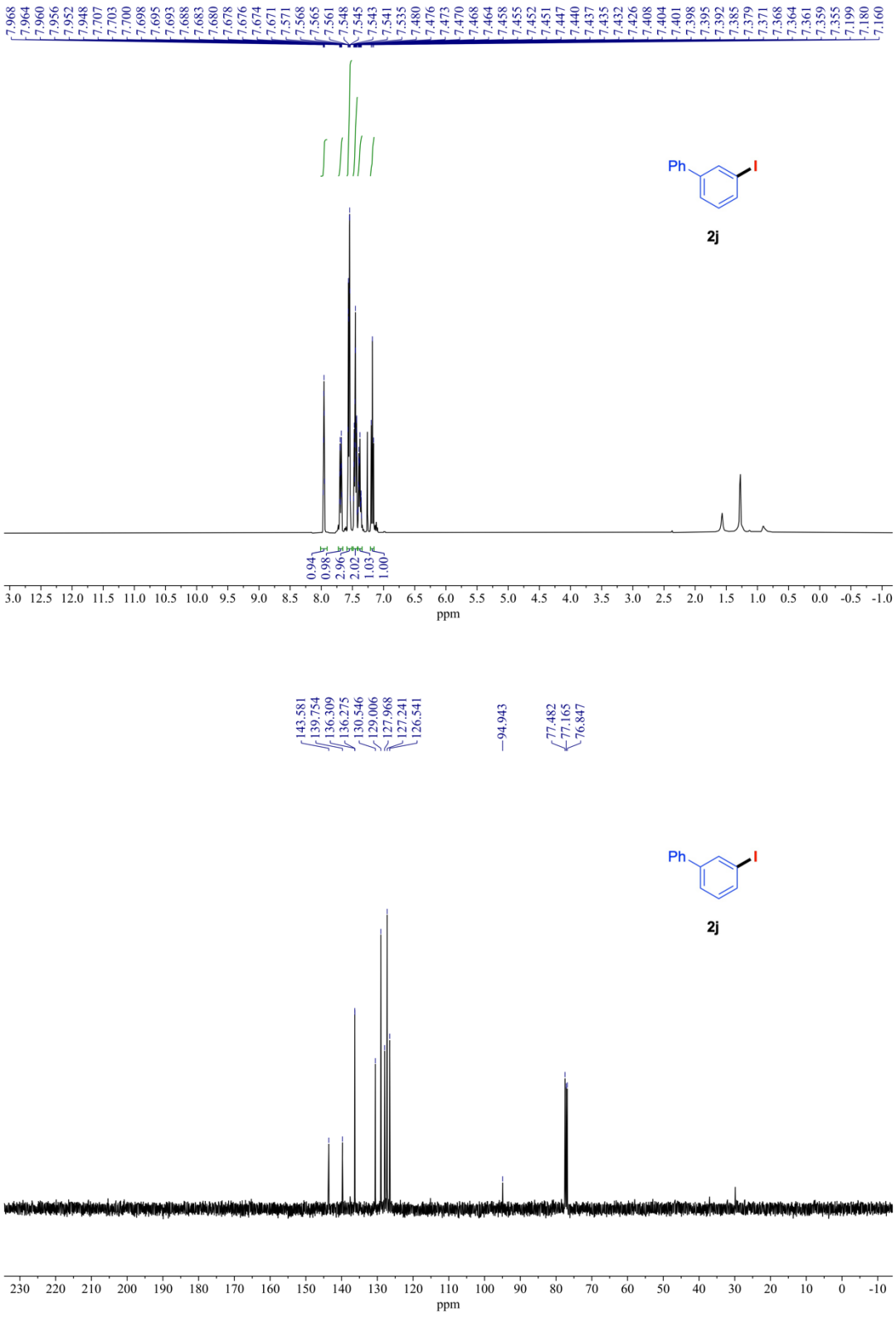

^{1}H NMR (400 MHz) and ^{13}C{^{1}H} NMR (101 MHz) spectra of **2j** (rt, $CDCl_3$).

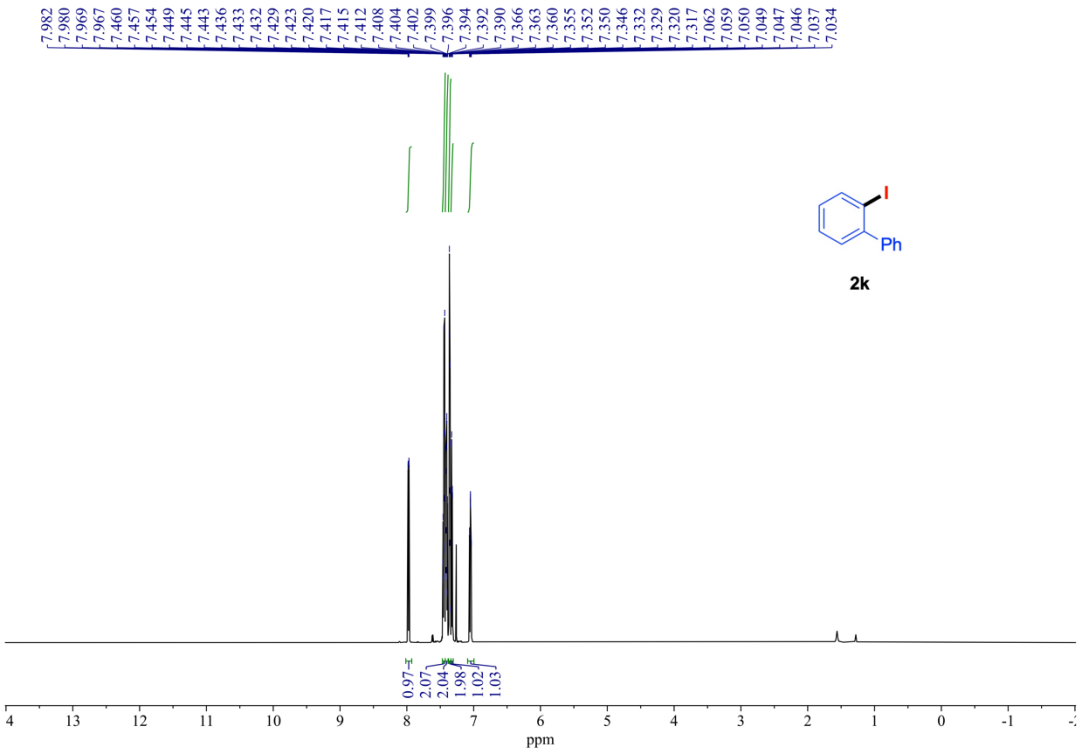

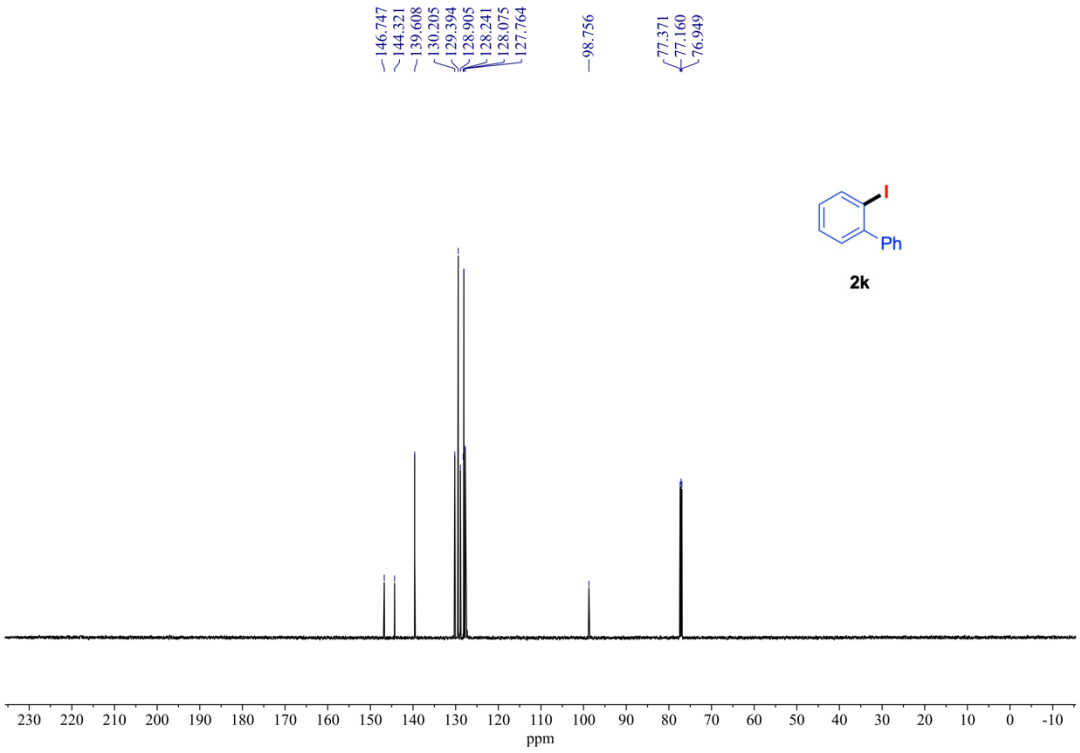

^{1}H NMR (600 MHz) and ^{13}C{^{1}H} NMR (151 MHz) spectra of **2k** (rt, $CDCl_3$).

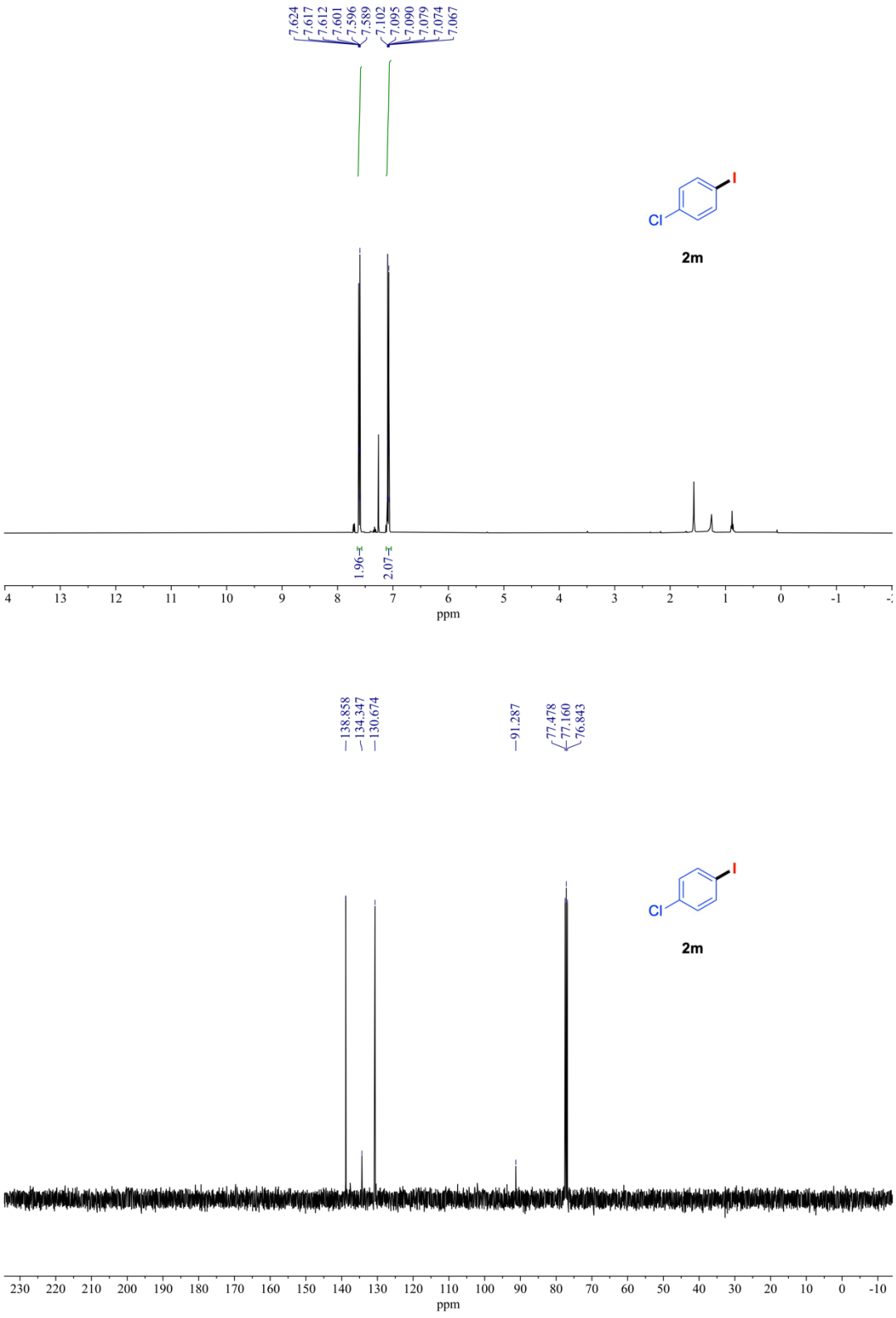

^{1}H NMR (400 MHz) and ^{13}C{^{1}H} NMR (101 MHz) spectra of **2m** (rt, $CDCl_3$).

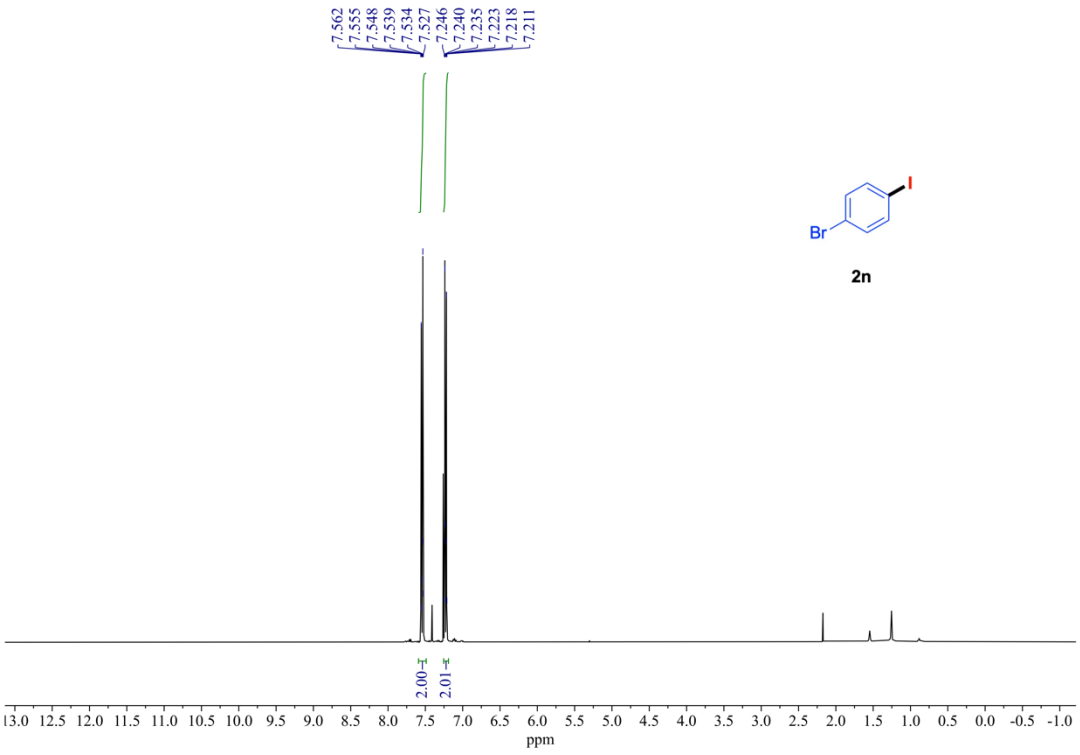

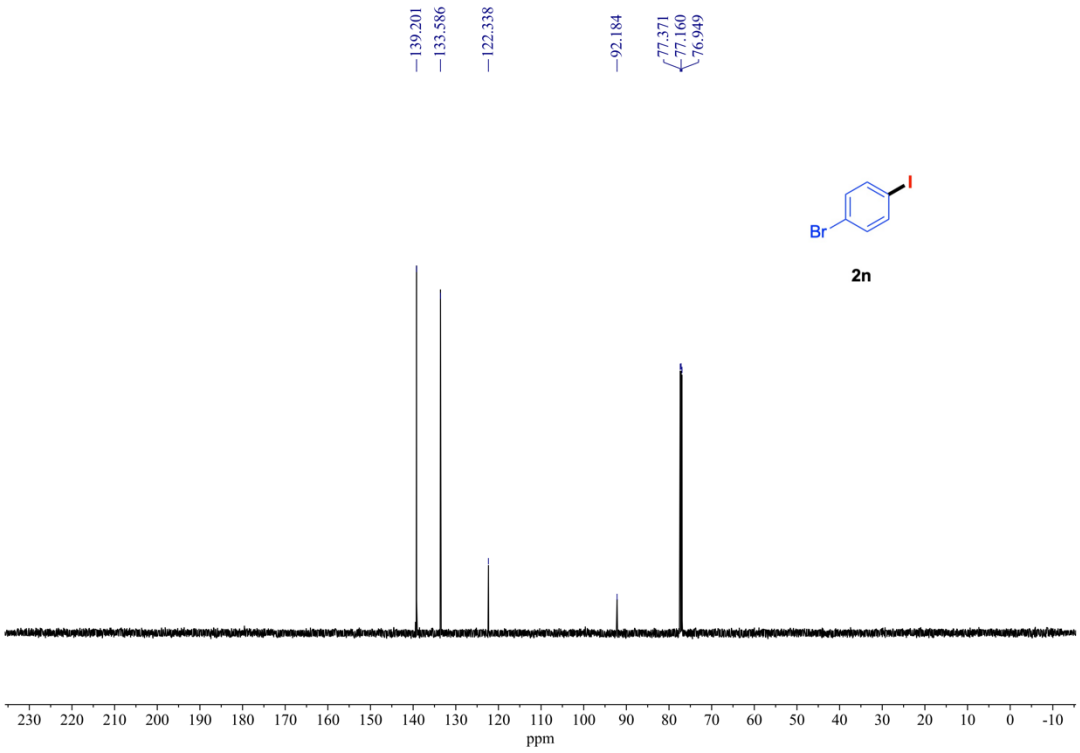

^{1}H NMR (400 MHz) and ^{13}C{^{1}H} NMR (151 MHz) spectra of **2n** (rt, $CDCl_3$).

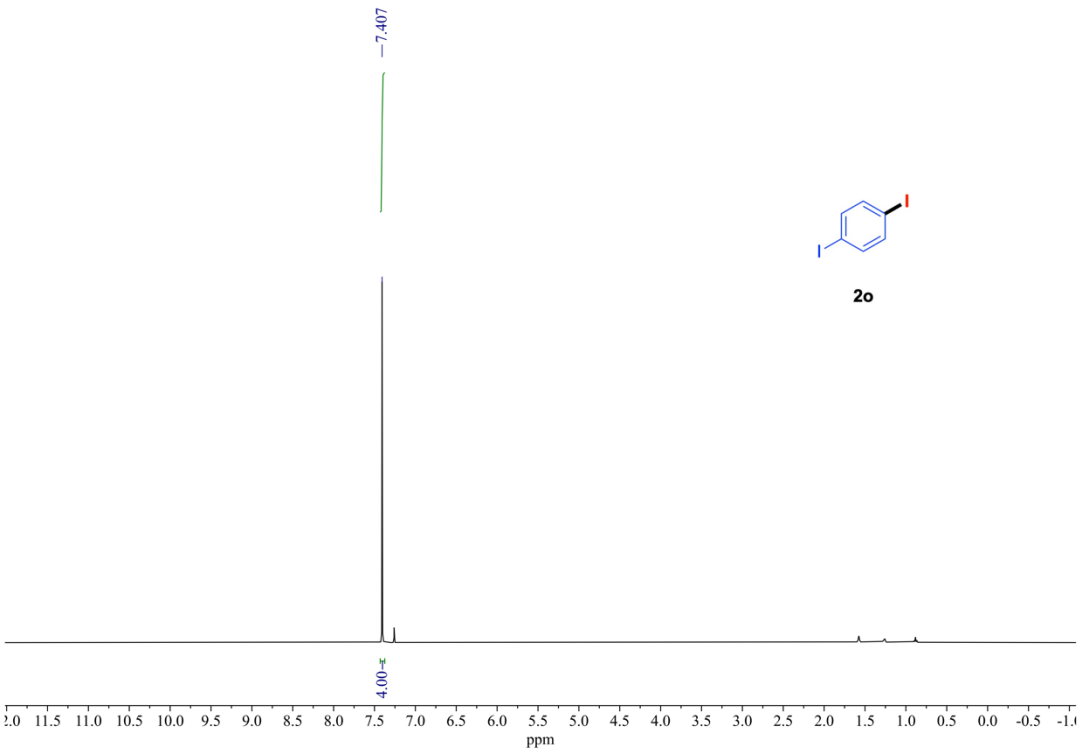

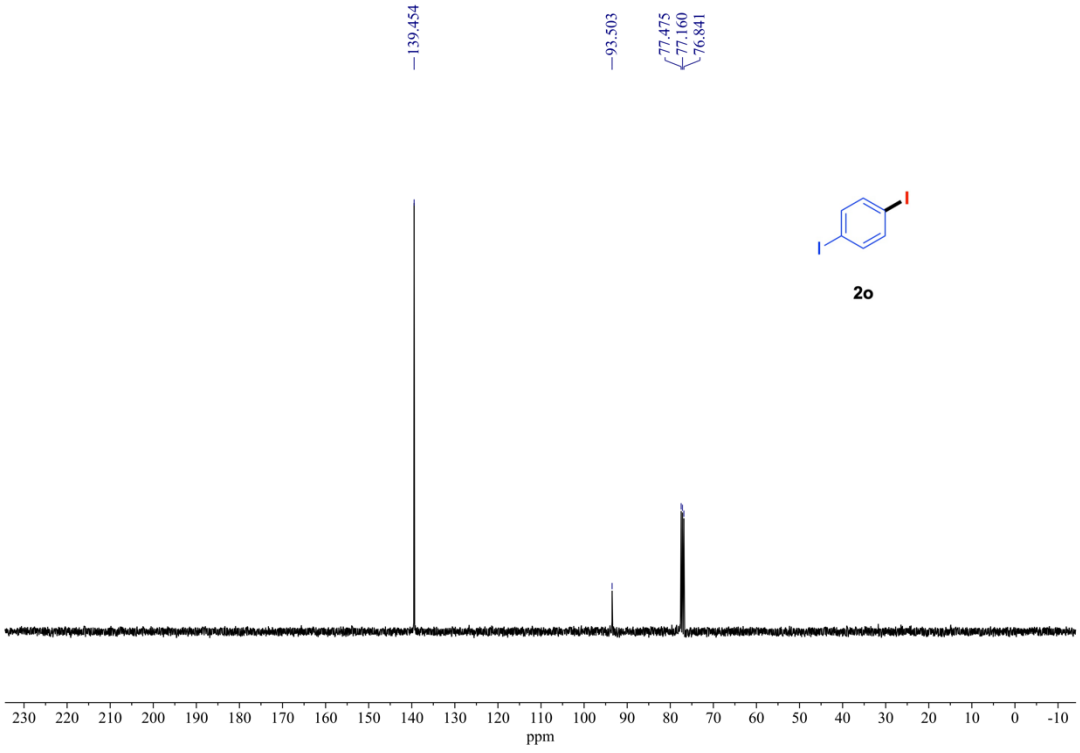

^{1}H NMR (400 MHz) and $^{13}C\{^{1}H\}$ NMR (101 MHz) spectra of **2o** (rt, $CDCl_3$).

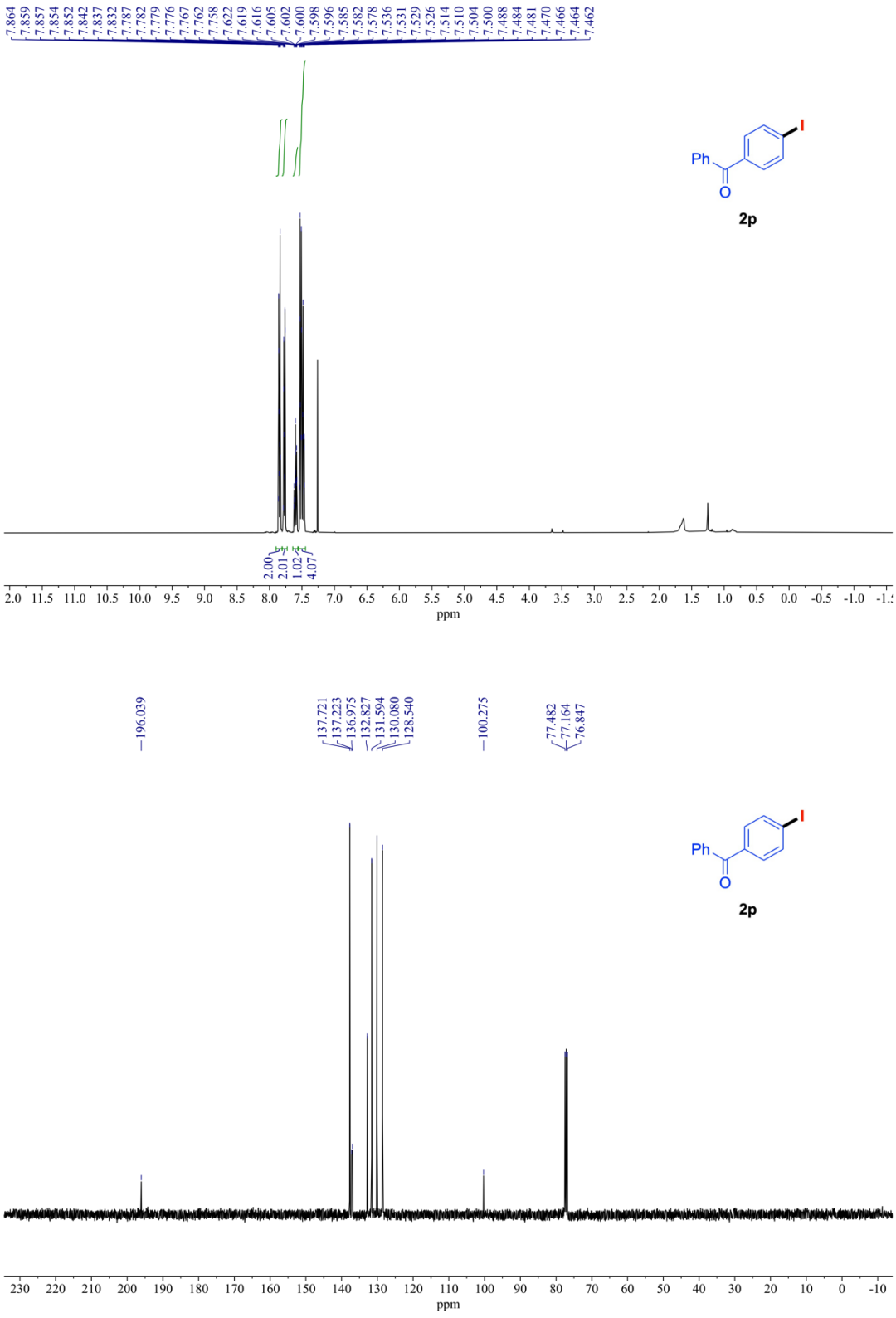

^{1}H NMR (400 MHz) and ^{13}C{^{1}H} NMR (101 MHz) spectra of **2p** (rt, $CDCl_3$).

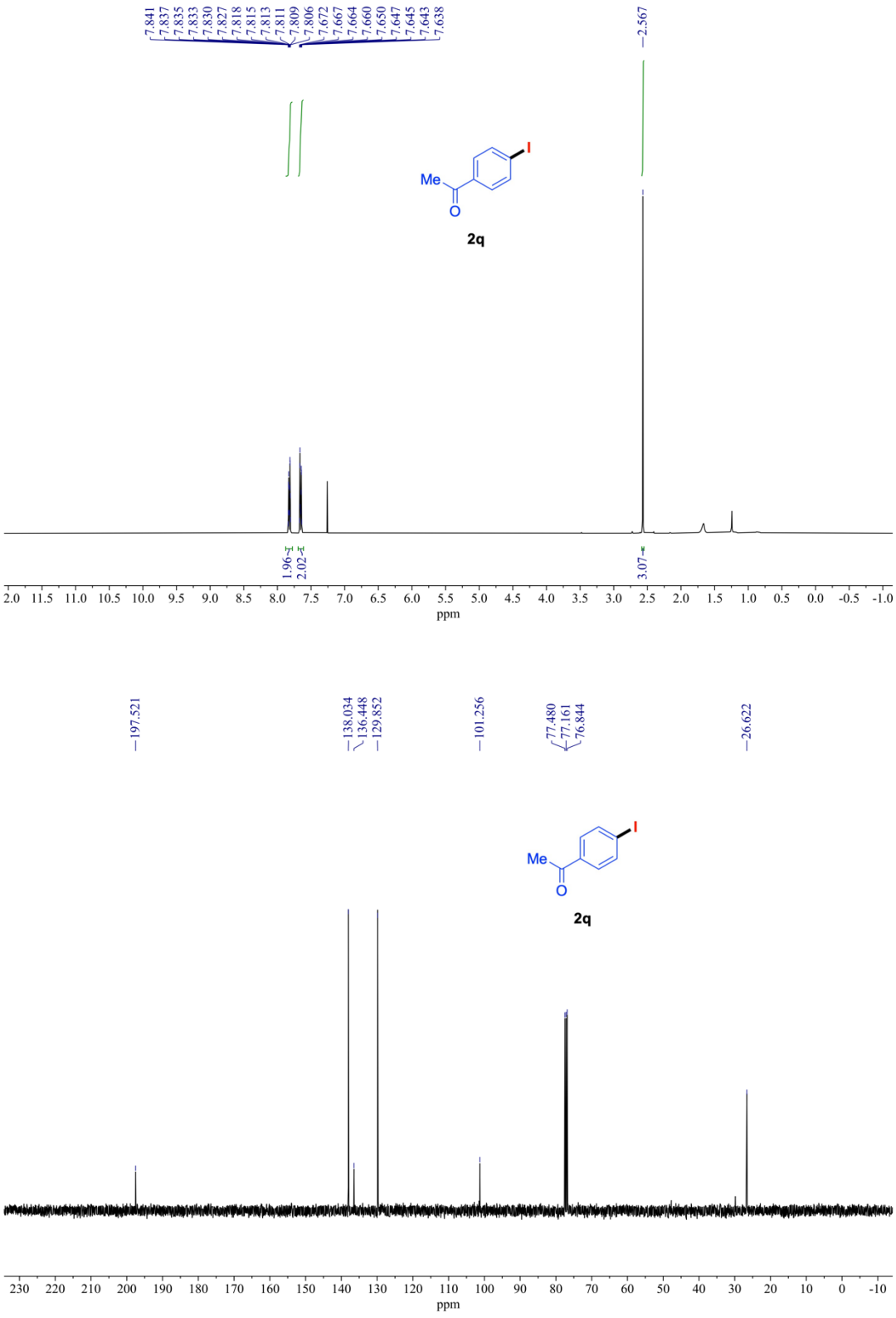

^{1}H NMR (400 MHz) and ^{13}C{^{1}H} NMR (101 MHz) spectra of **2q** (rt, $CDCl_3$).

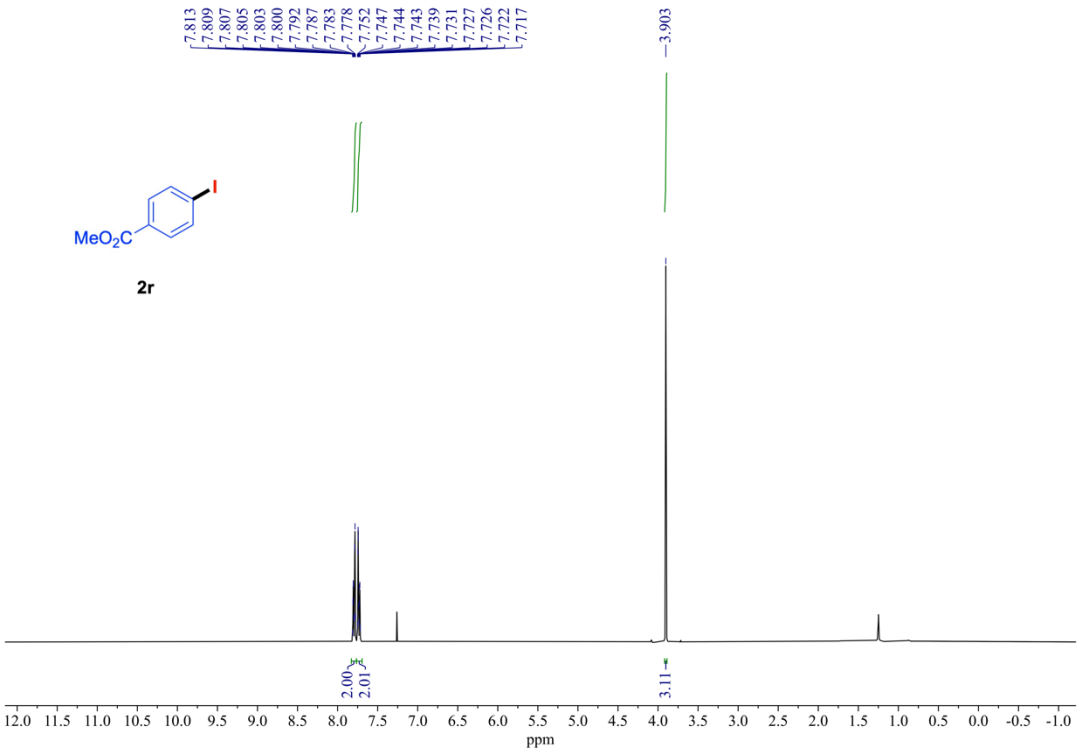

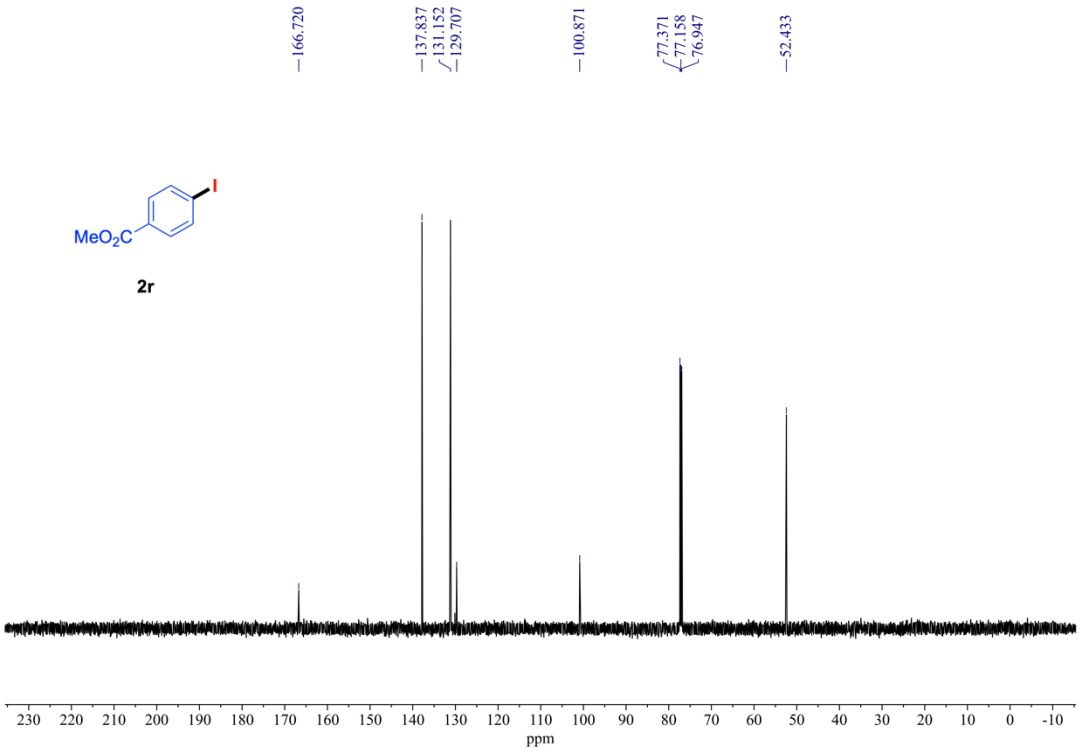

^{1}H NMR (400 MHz) and ^{13}C{^{1}H} NMR (151 MHz) spectra of **2r** (rt, $CDCl_3$).

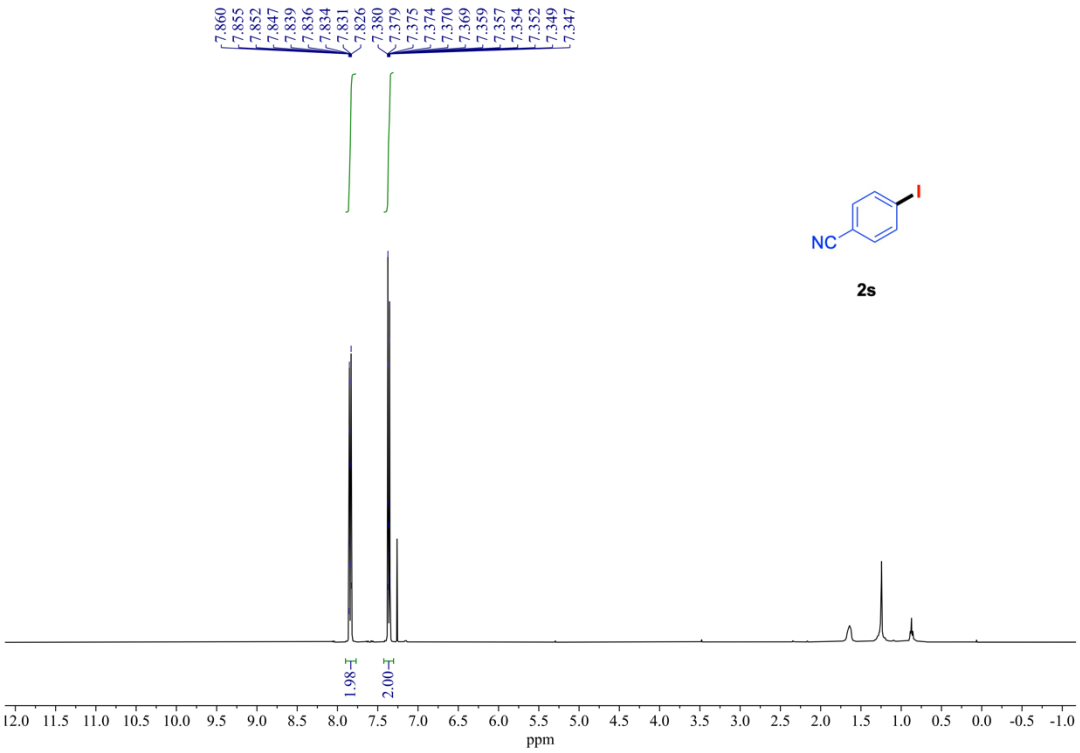

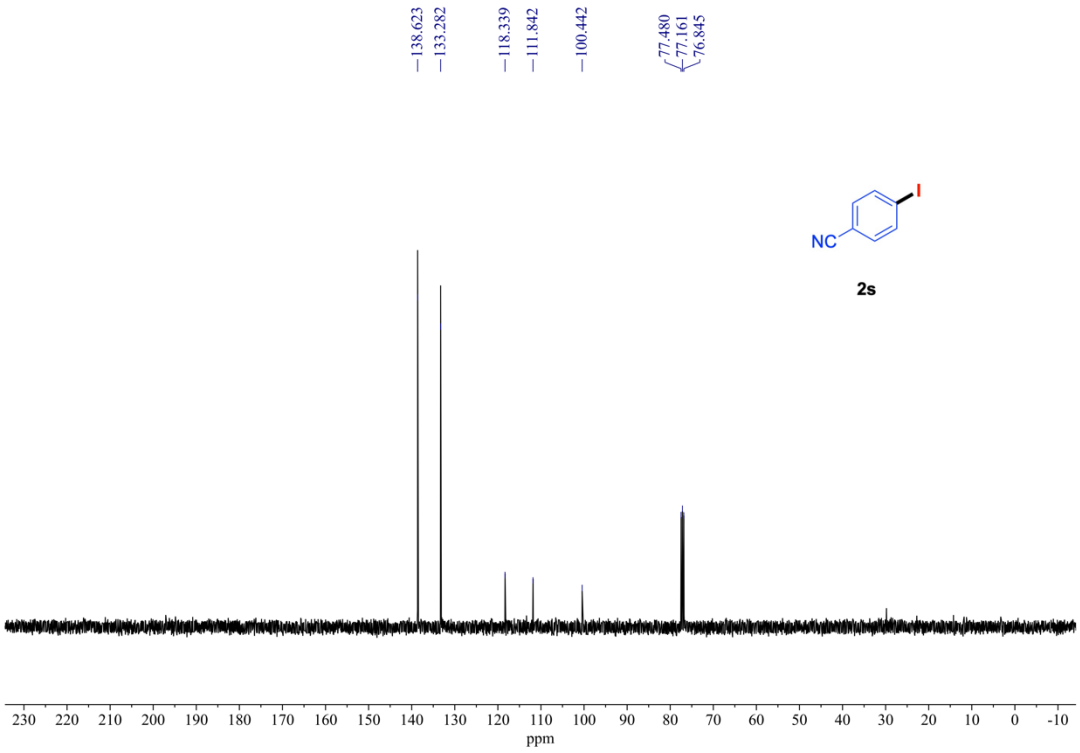

^{1}H NMR (400 MHz) and ^{13}C{^{1}H} NMR (101 MHz) spectra of **2s** (rt, $CDCl_3$).

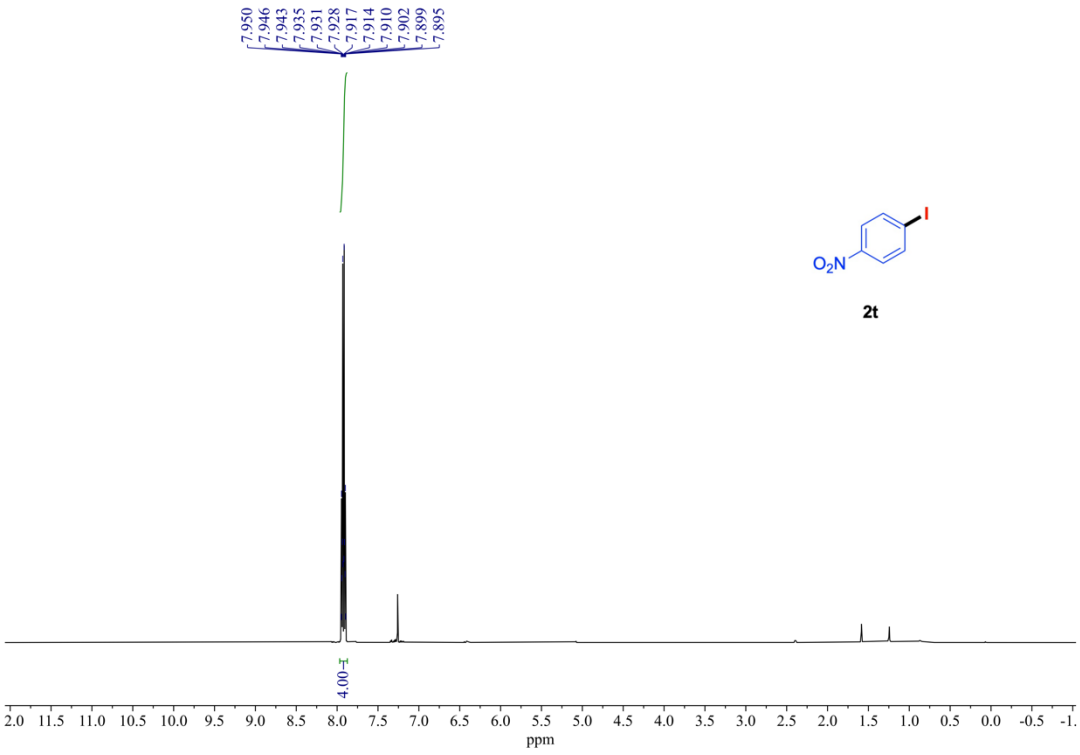

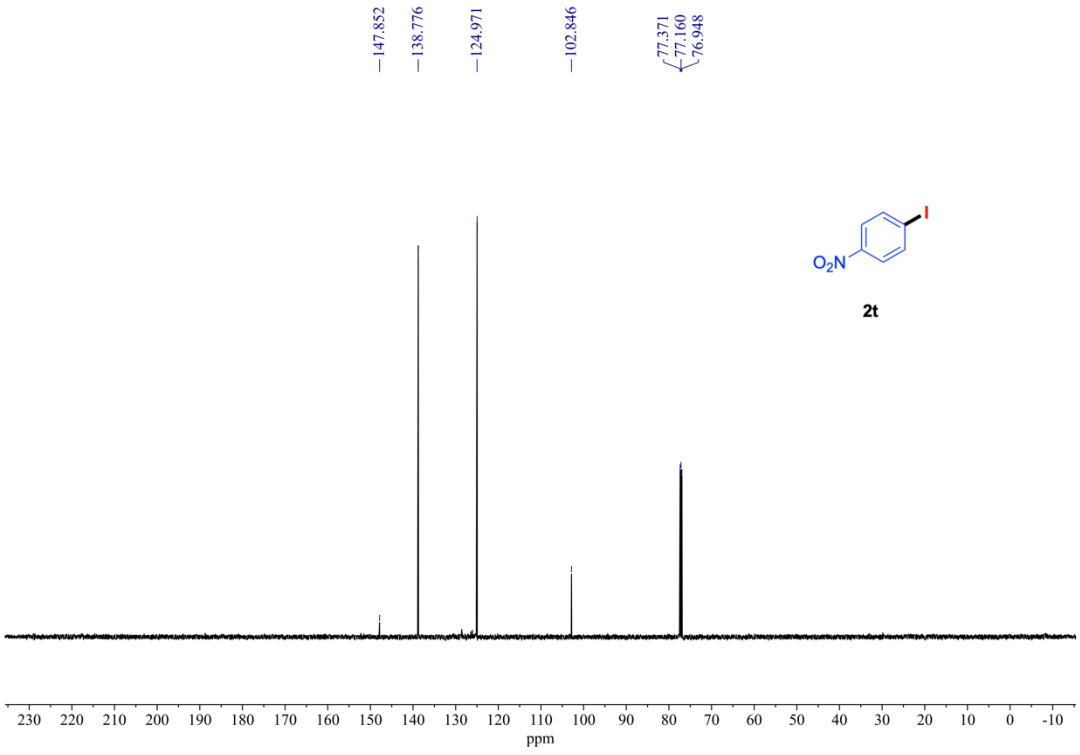

^{1}H NMR (600 MHz) and ^{13}C{^{1}H} NMR (151 MHz) spectra of **2t** (rt, $CDCl_3$).

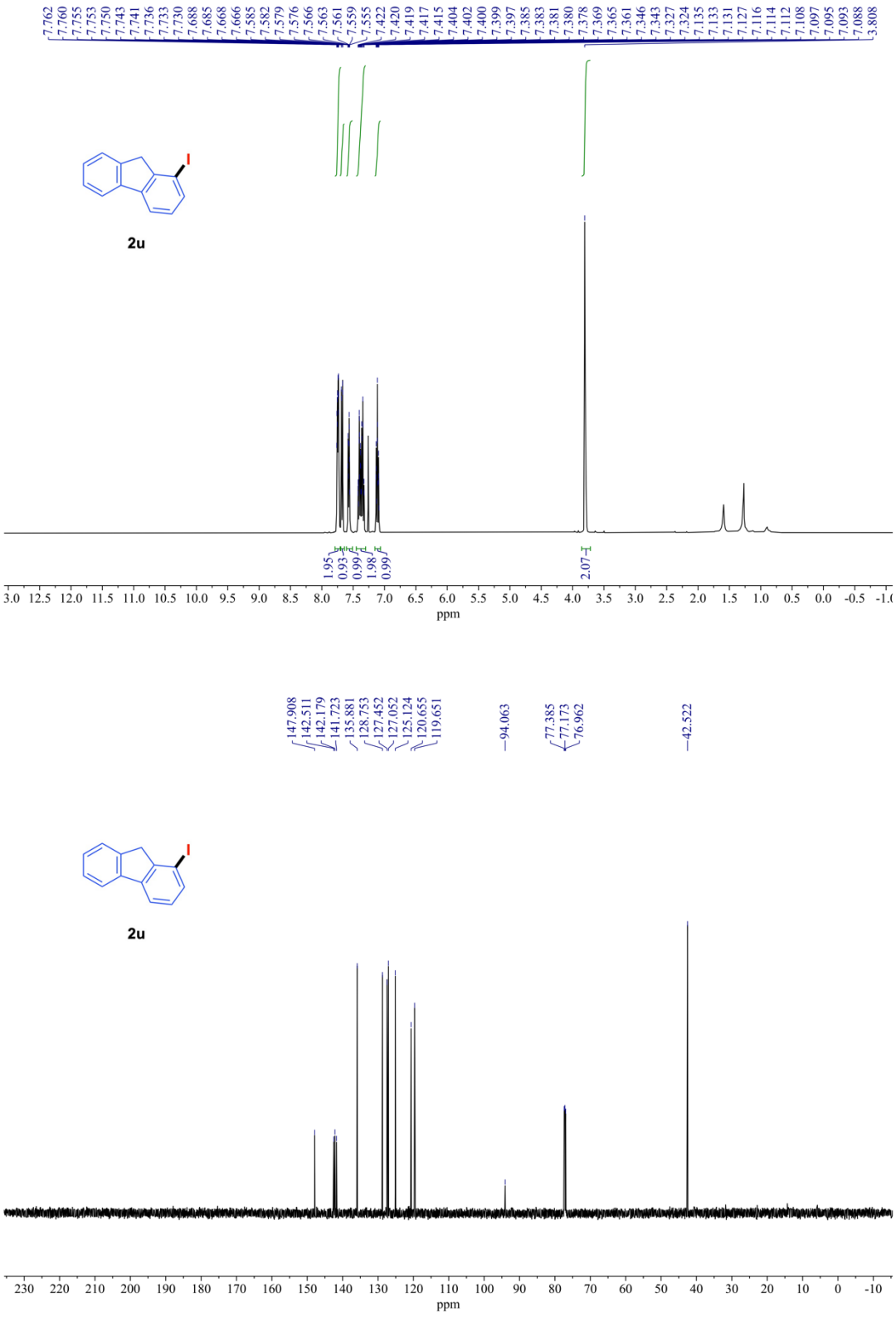

^{1}H NMR (400 MHz) and ^{13}C{^{1}H} NMR (151 MHz) spectra of **2u** (rt, $CDCl_3$).

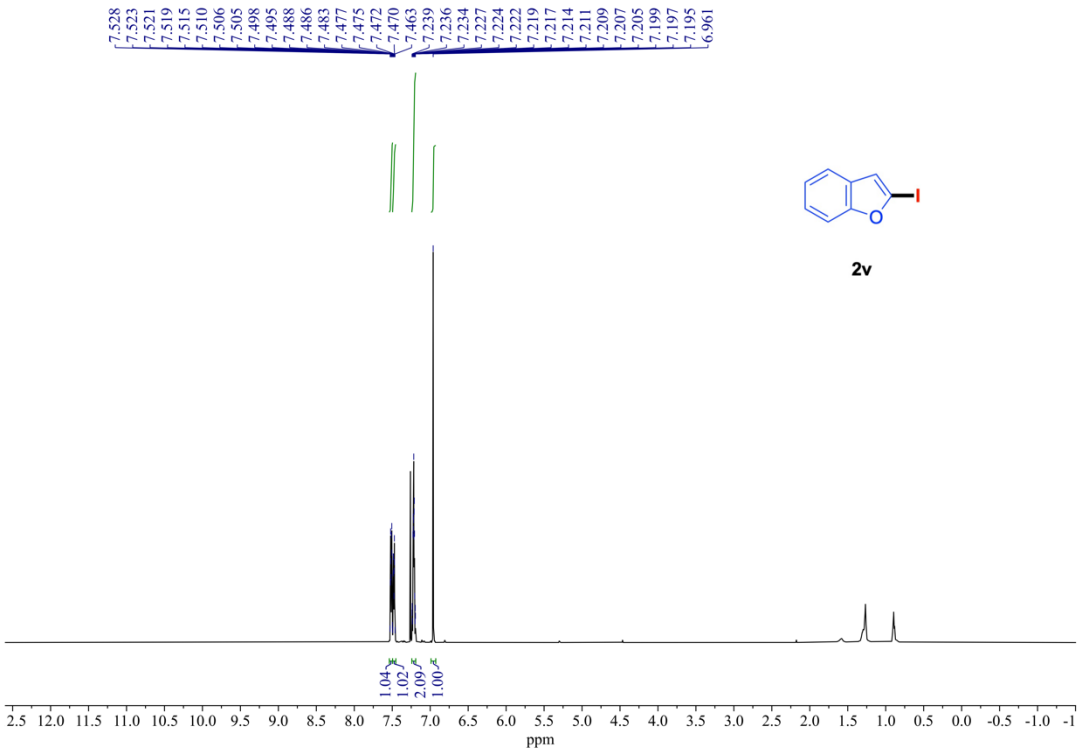

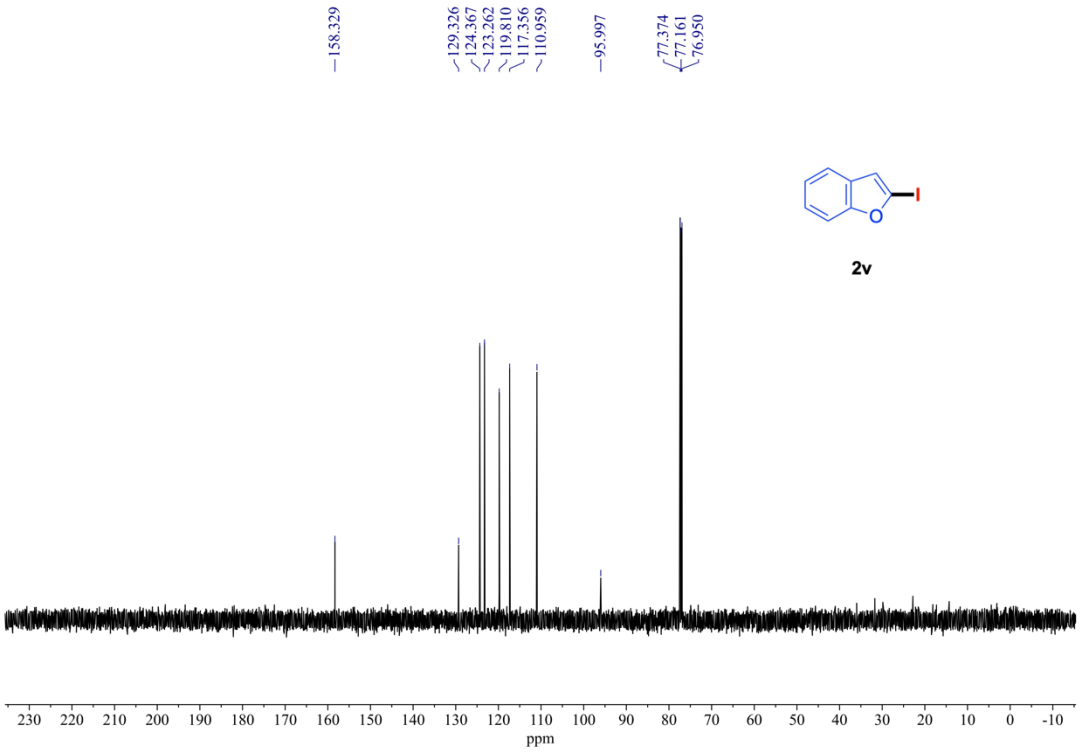

2v

^{1}H NMR (600 MHz) and ^{13}C{^{1}H} NMR (151 MHz) spectra of **2v** (rt, $CDCl_3$).

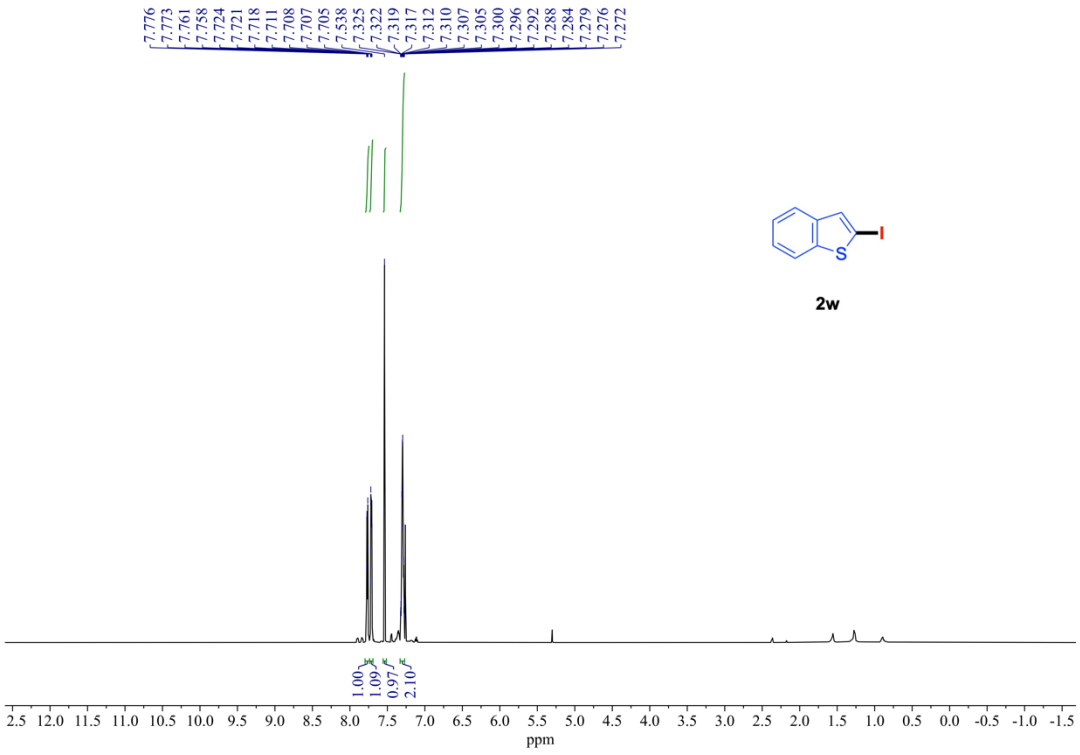

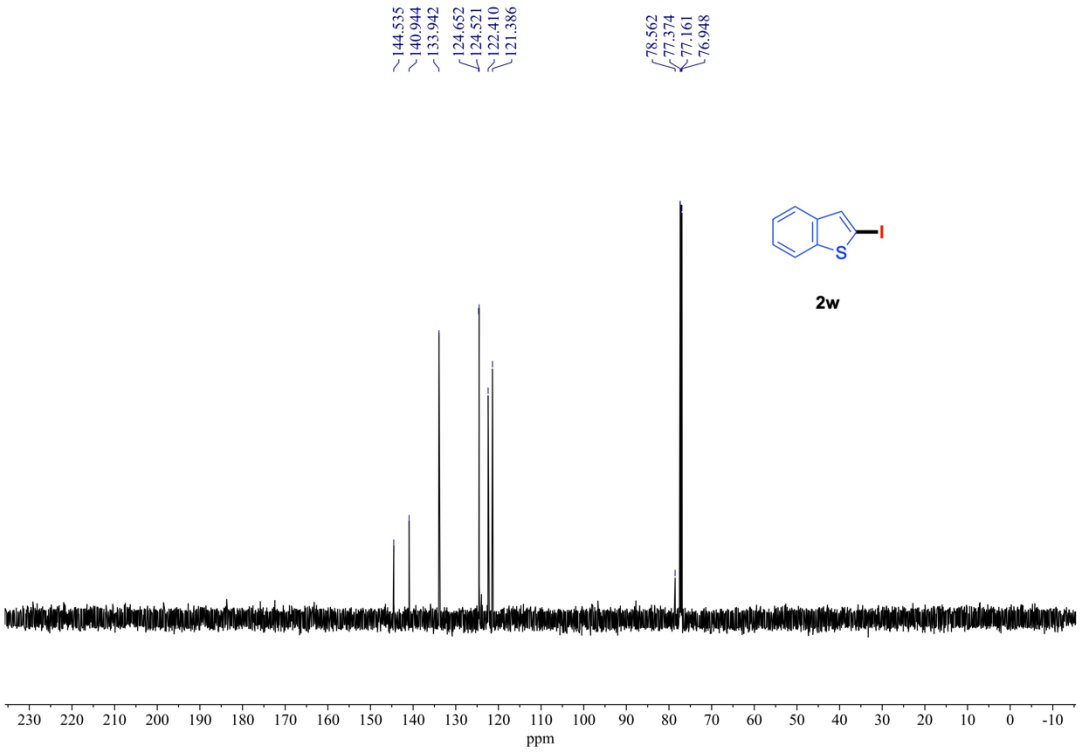

^{1}H NMR (600 MHz) and ^{13}C{^{1}H} NMR (151 MHz) spectra of **2w** (rt, $CDCl_3$).

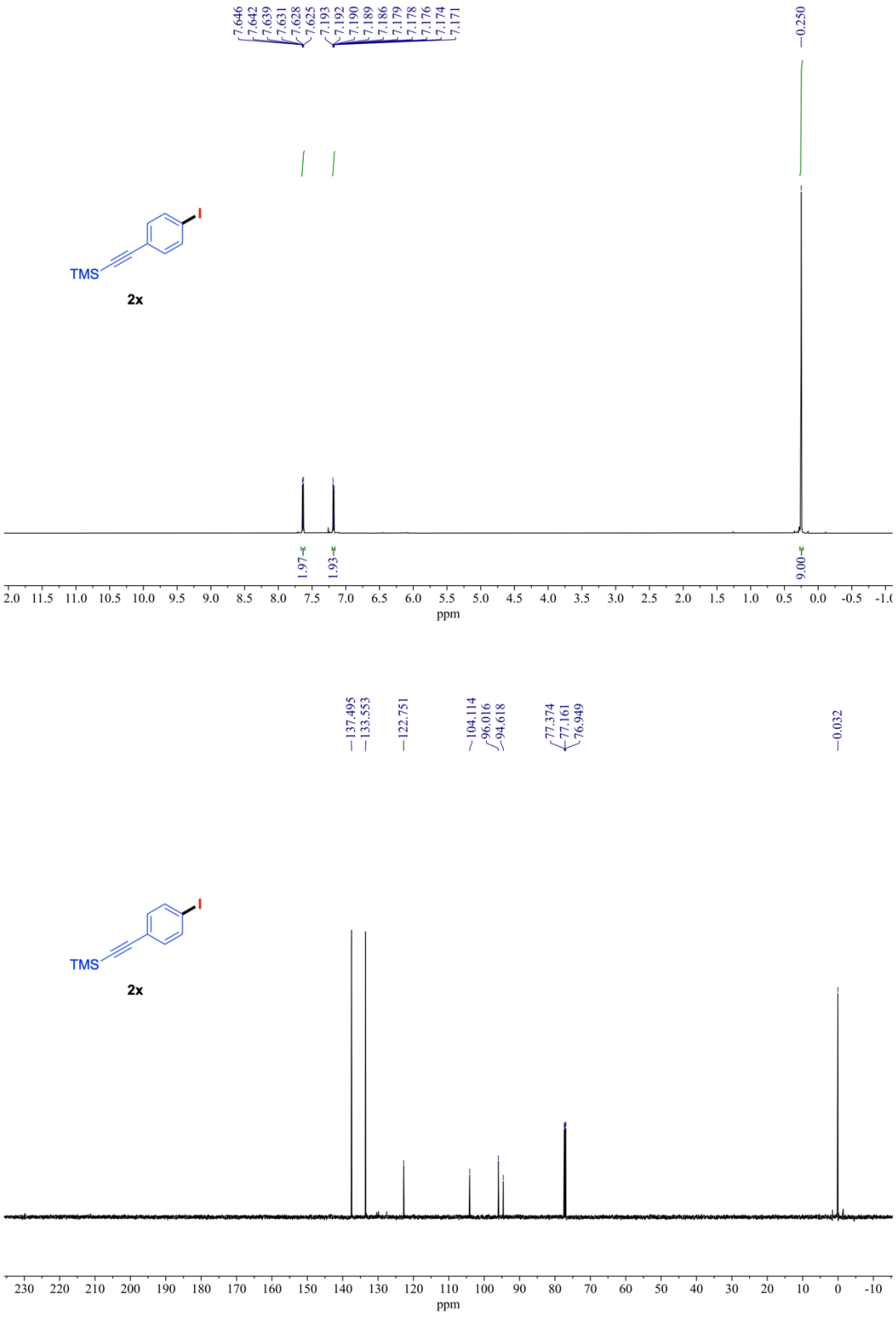

^{1}H NMR (600 MHz) and ^{13}C{^{1}H} NMR (151 MHz) spectra of **2x** (rt, $CDCl_3$).

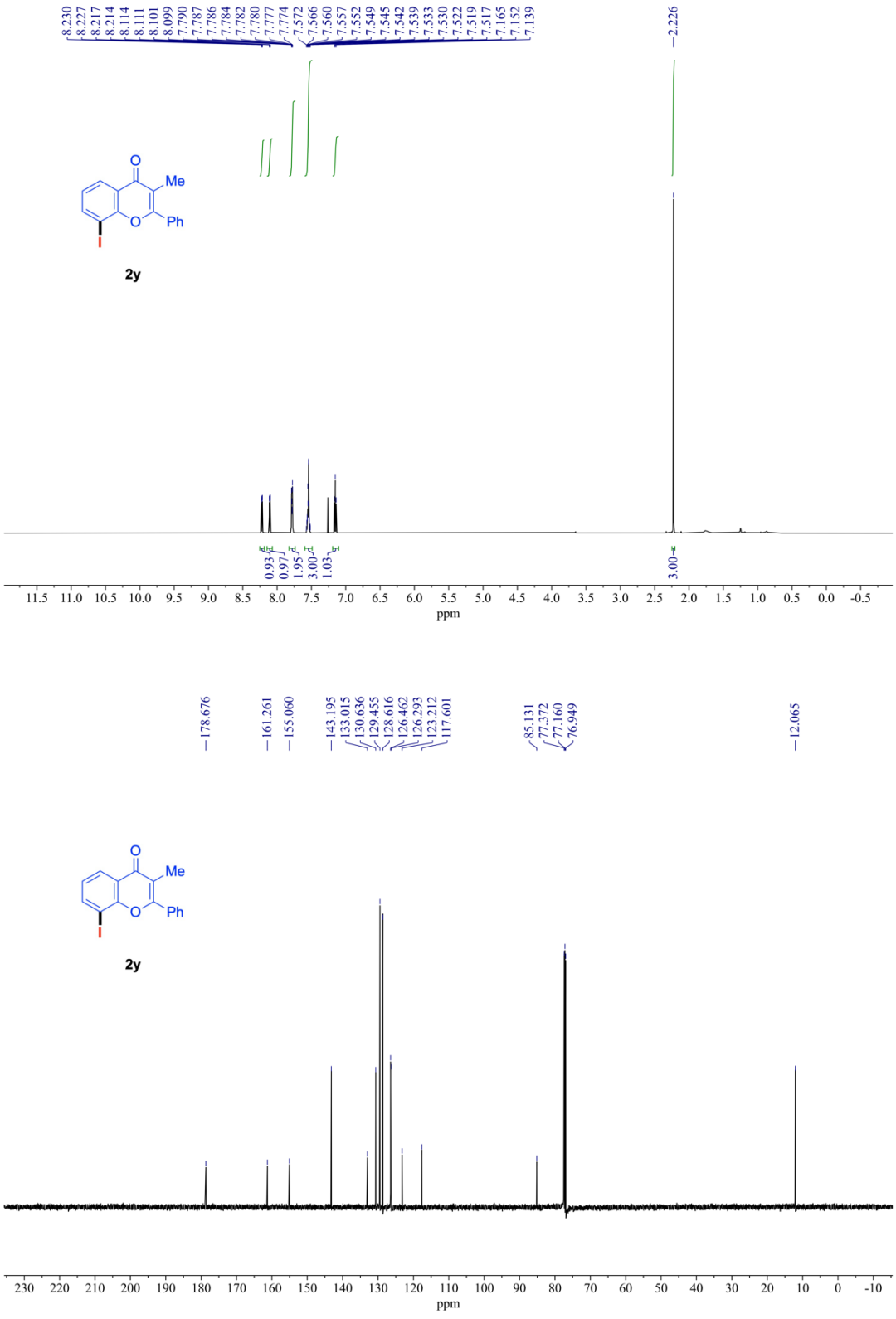

^{1}H NMR (600 MHz) and ^{13}C{^{1}H} NMR (151 MHz) spectra of **2y** (rt, $CDCl_3$).

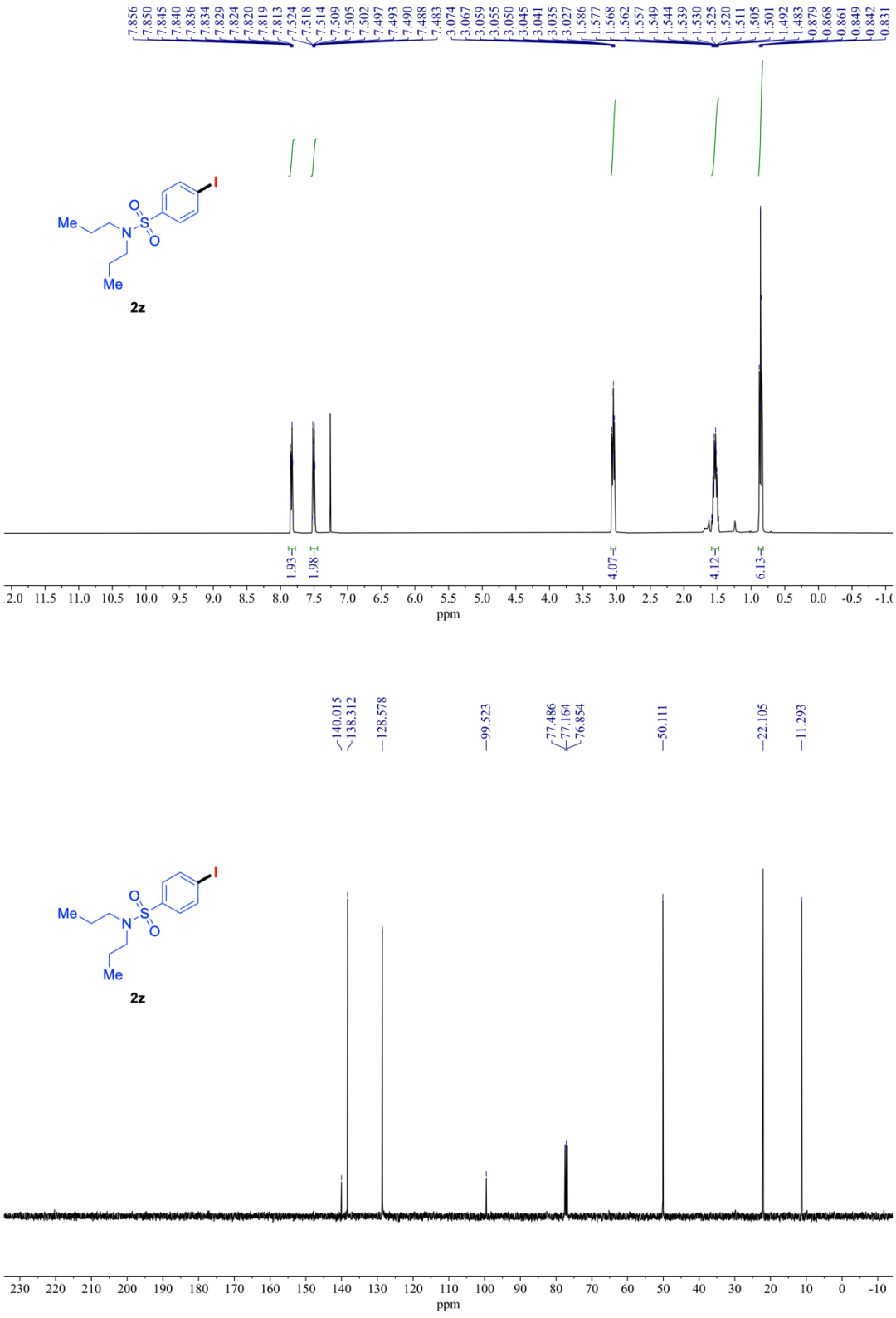

^{1}H NMR (400 MHz) and ^{13}C{^{1}H} NMR (101 MHz) spectra of **2z** (rt, $CDCl_3$).

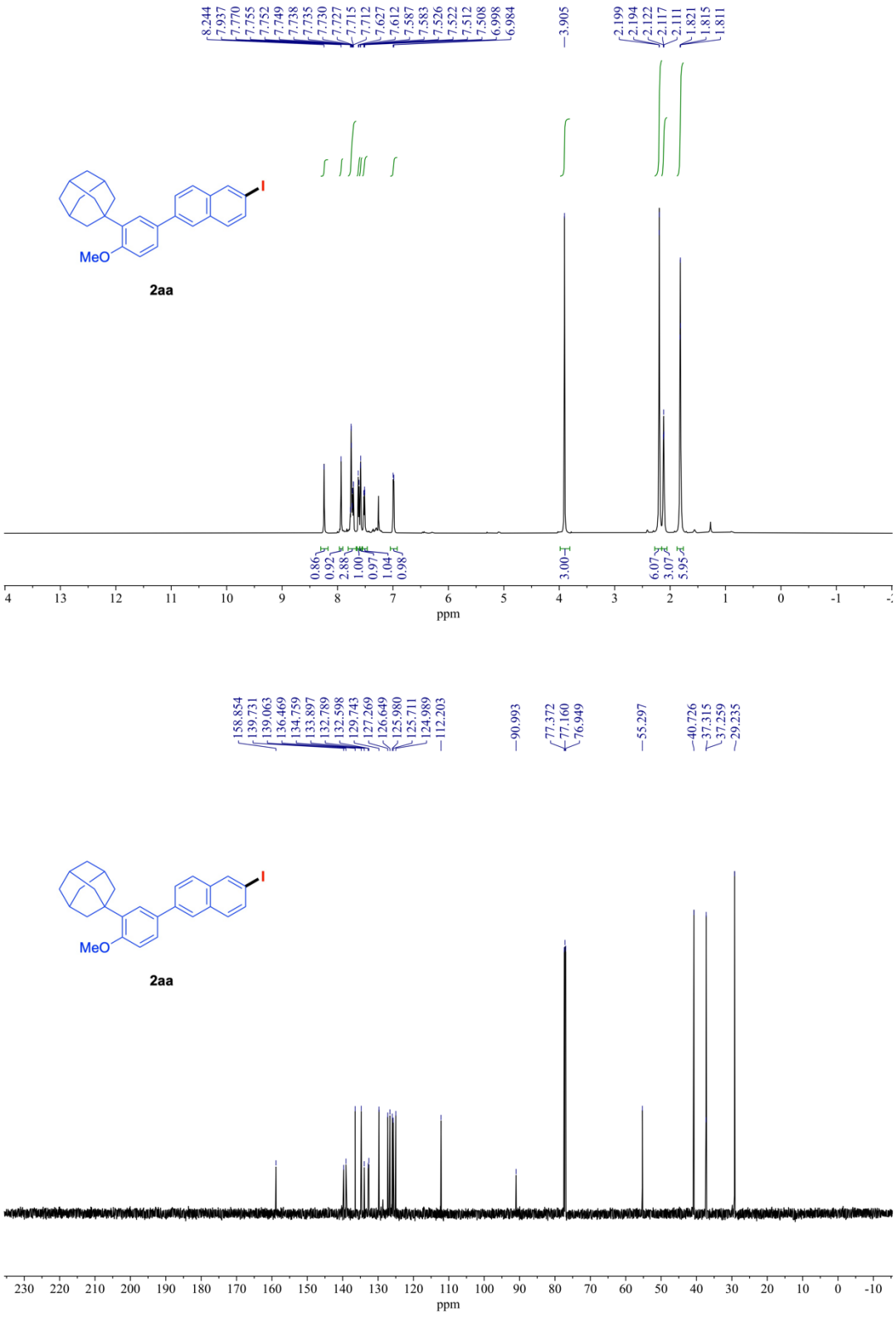

^{1}H NMR (600 MHz) and ^{13}C{^{1}H} NMR (151 MHz) spectra of **2aa** (rt, $CDCl_3$).

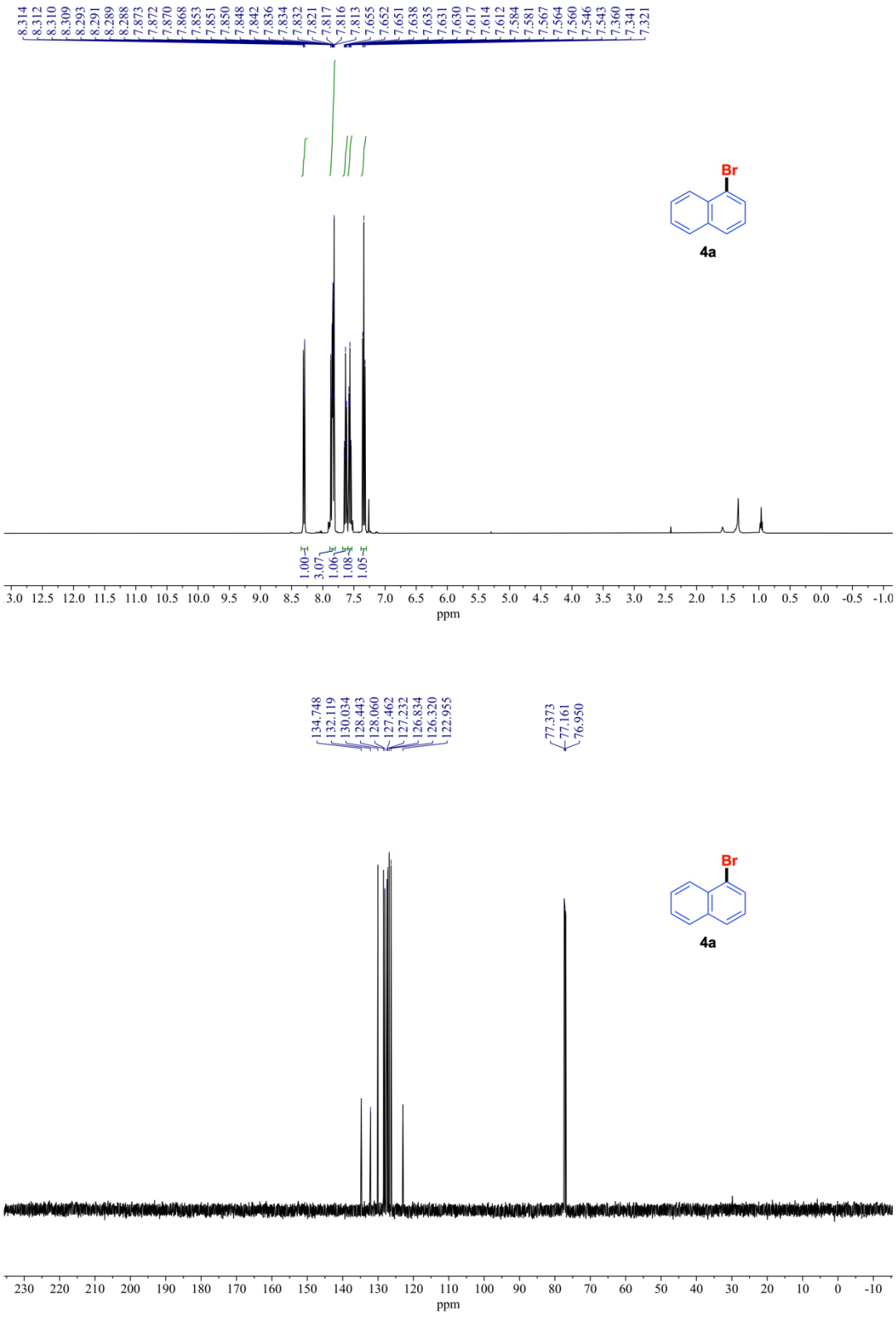

^{1}H NMR (400 MHz) and ^{13}C{^{1}H} NMR (151 MHz) spectra of **4a** (rt, $CDCl_3$).

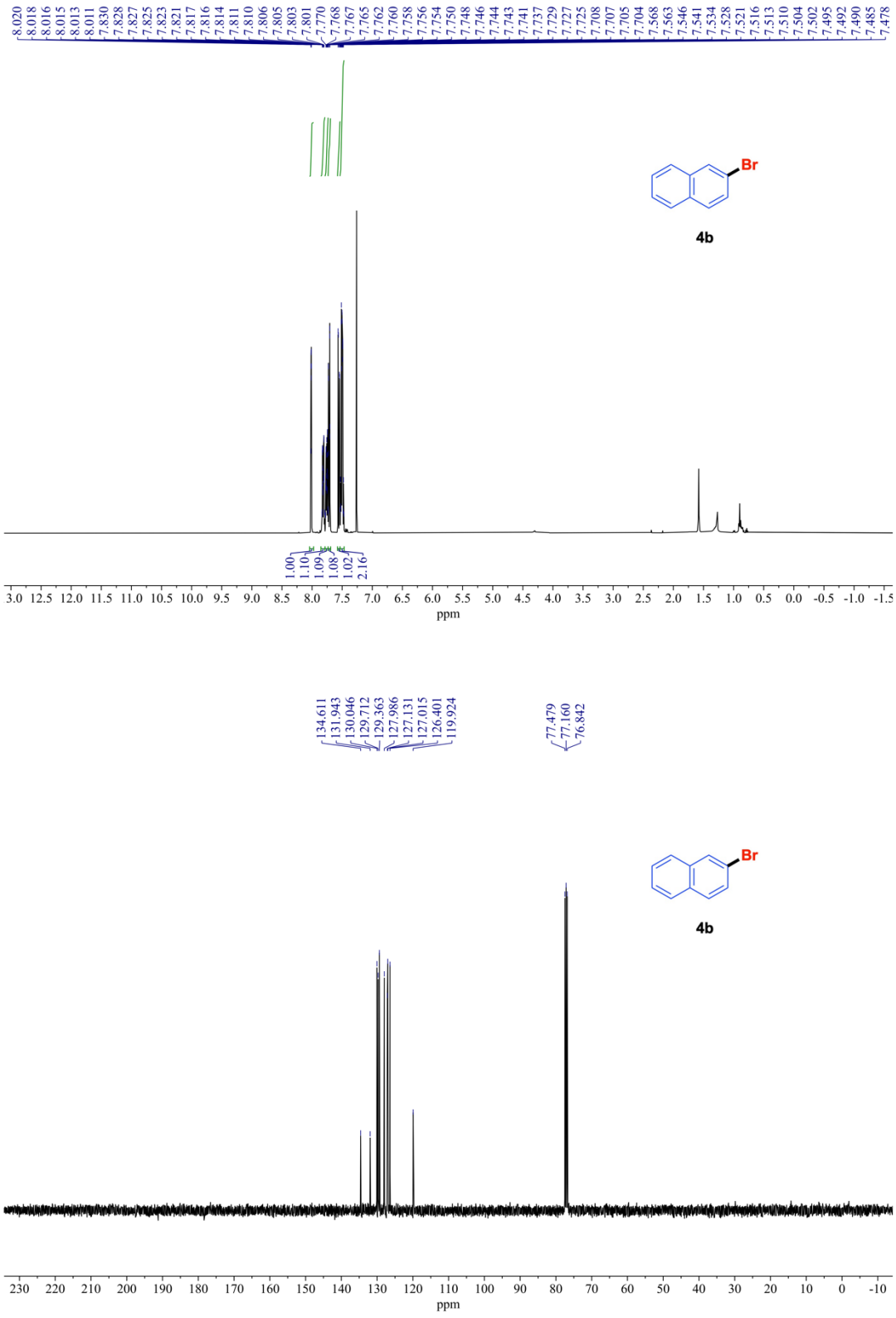

^{1}H NMR (400 MHz) and ^{13}C{^{1}H} NMR (101 MHz) spectra of **4b** (rt, $CDCl_3$).

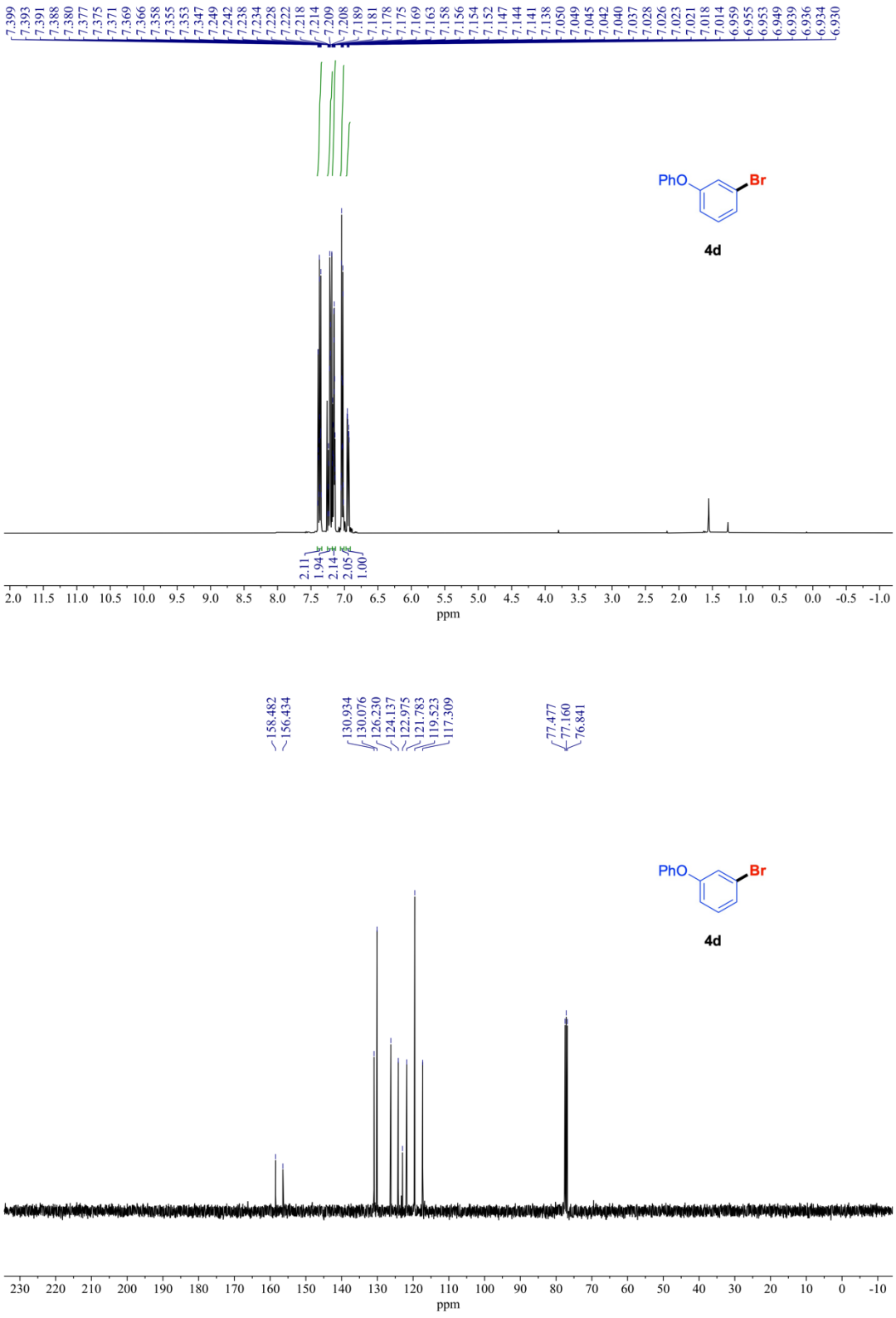

^{1}H NMR (400 MHz) and ^{13}C{^{1}H} NMR (101 MHz) spectra of **4d** (rt, $CDCl_3$).

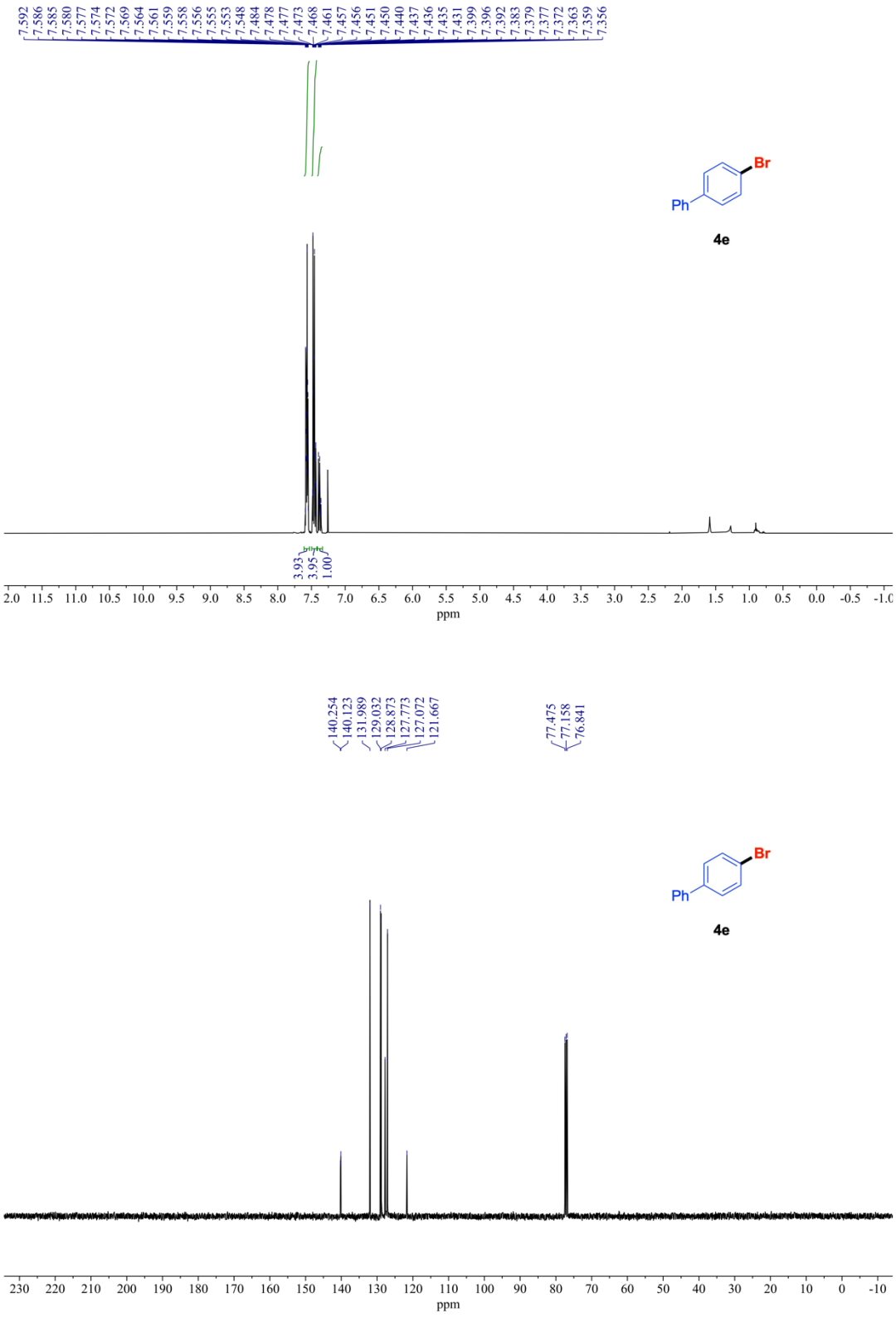

^{1}H NMR (400 MHz) and ^{13}C{^{1}H} NMR (101 MHz) spectra of **4e** (rt, $CDCl_3$).

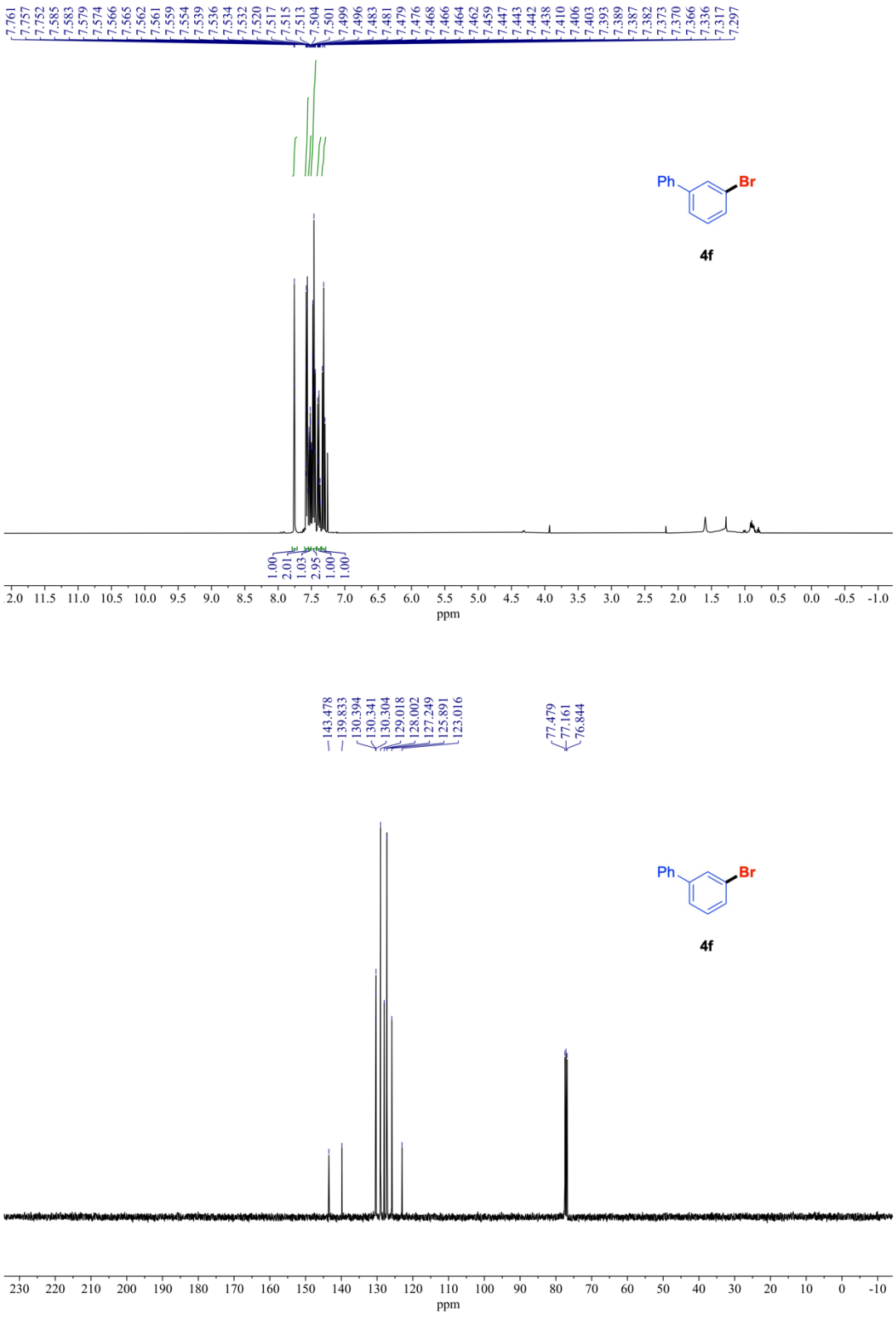

^{1}H NMR (400 MHz) and ^{13}C{^{1}H} NMR (101 MHz) spectra of **4f** (rt, $CDCl_3$).

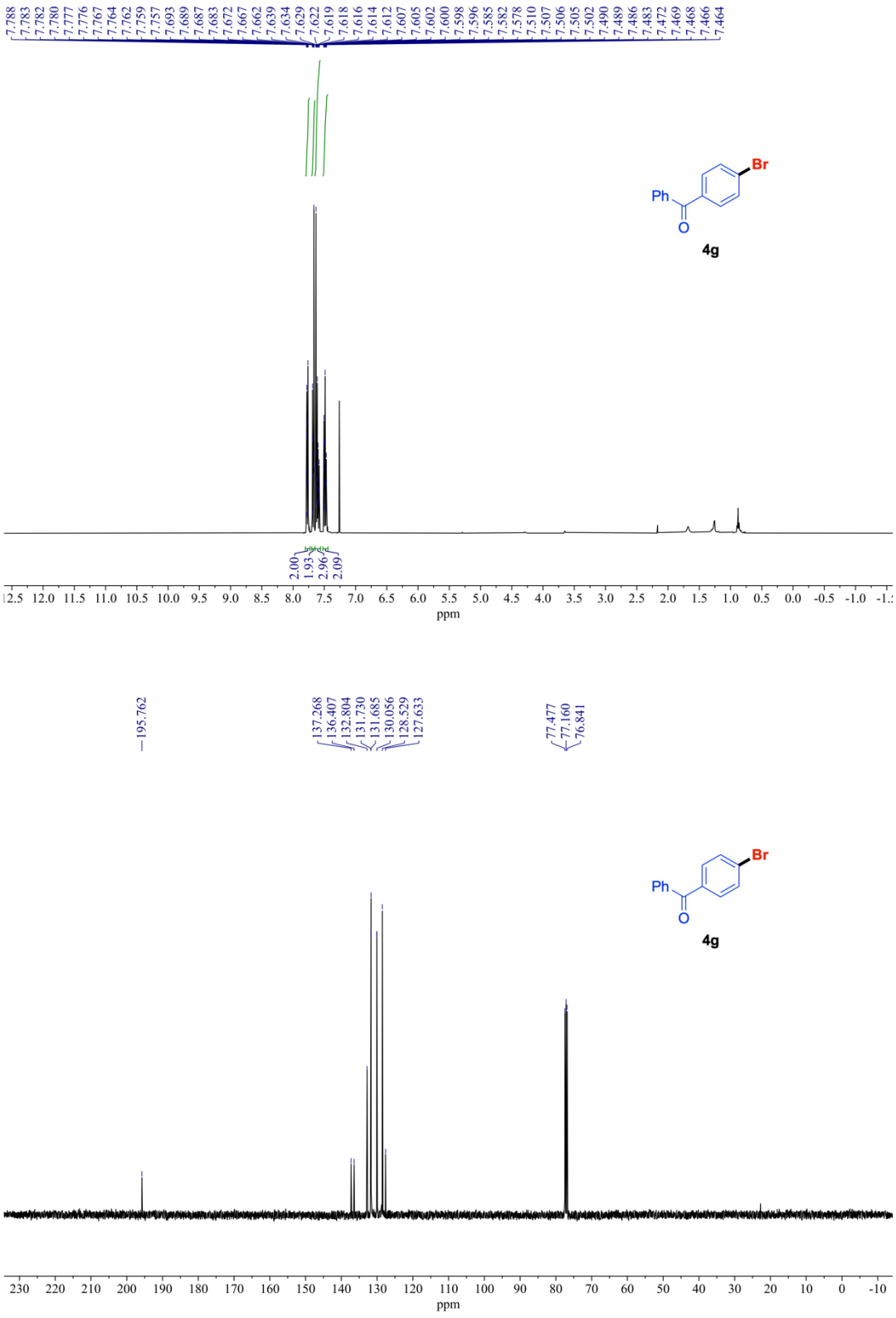

^{1}H NMR (400 MHz) and ^{13}C{^{1}H} NMR (101 MHz) spectra of **4g** (rt, $CDCl_3$).

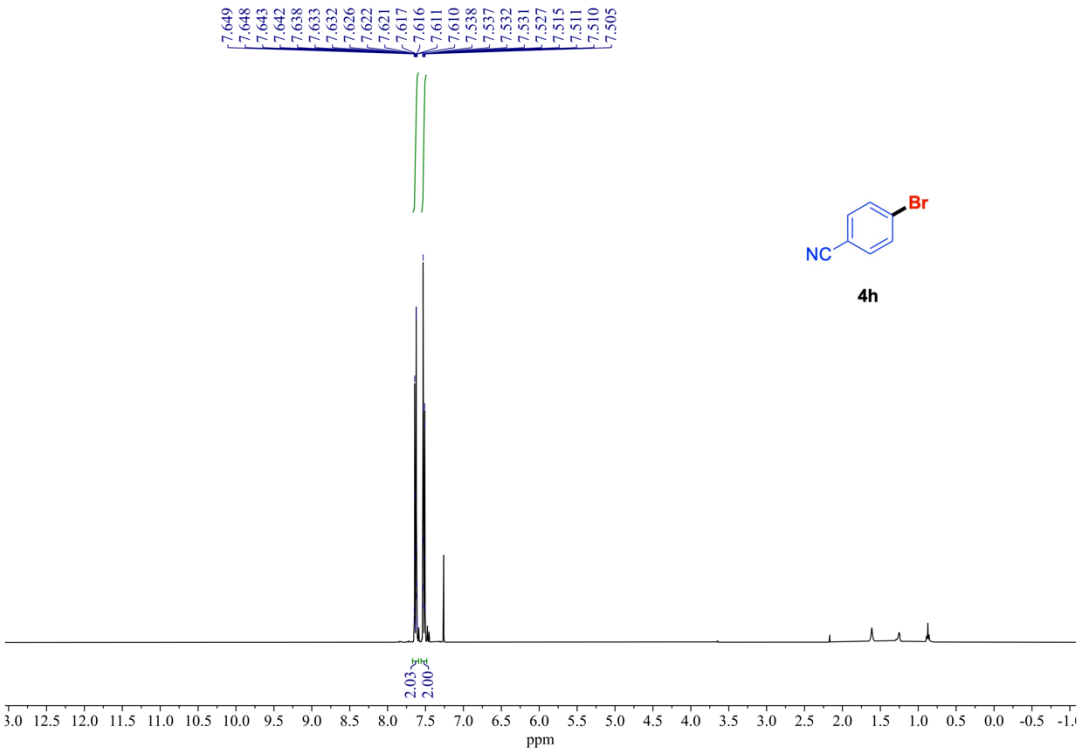

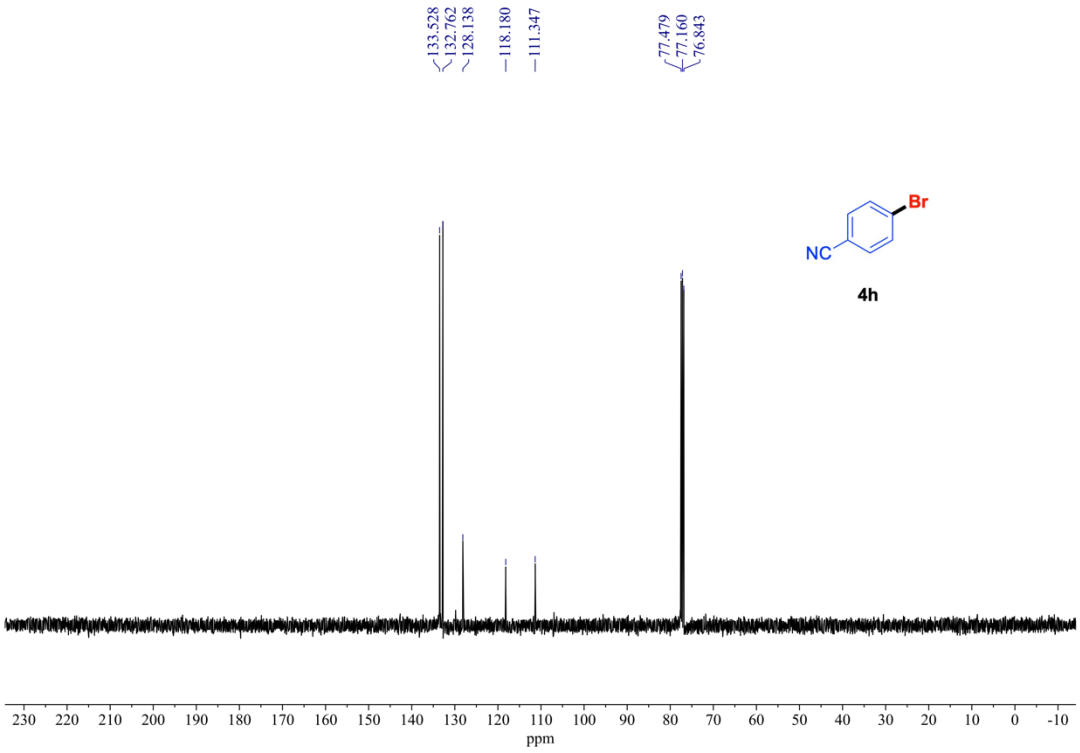

^{1}H NMR (400 MHz) and ^{13}C{^{1}H} NMR (101 MHz) spectra of **4h** (rt, $CDCl_3$).

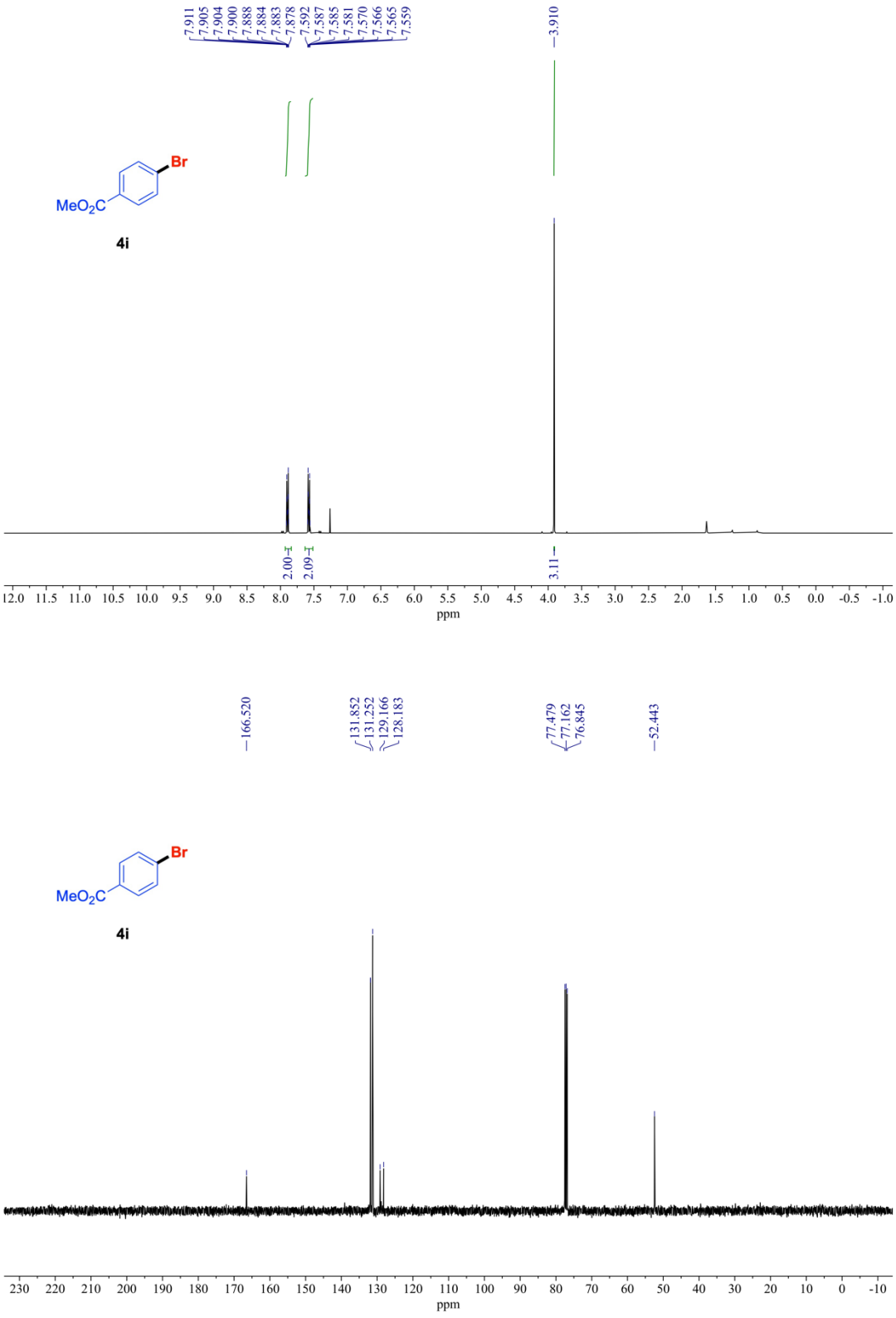

^{1}H NMR (400 MHz) and ^{13}C{^{1}H} NMR (101 MHz) spectra of **4i** (rt, $CDCl_3$).

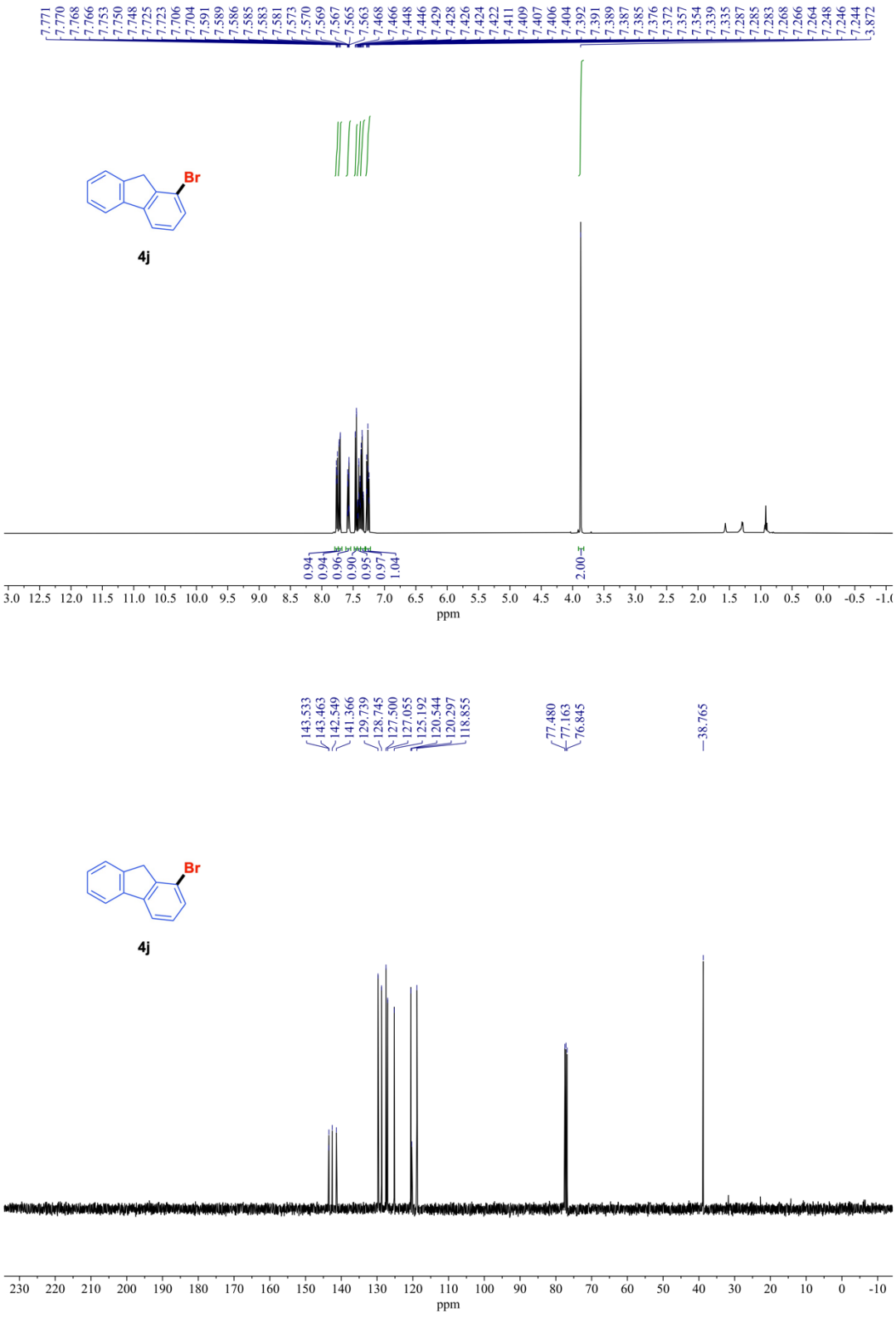

^{1}H NMR (400 MHz) and ^{13}C{^{1}H} NMR (101 MHz) spectra of **4j** (rt, $CDCl_3$).

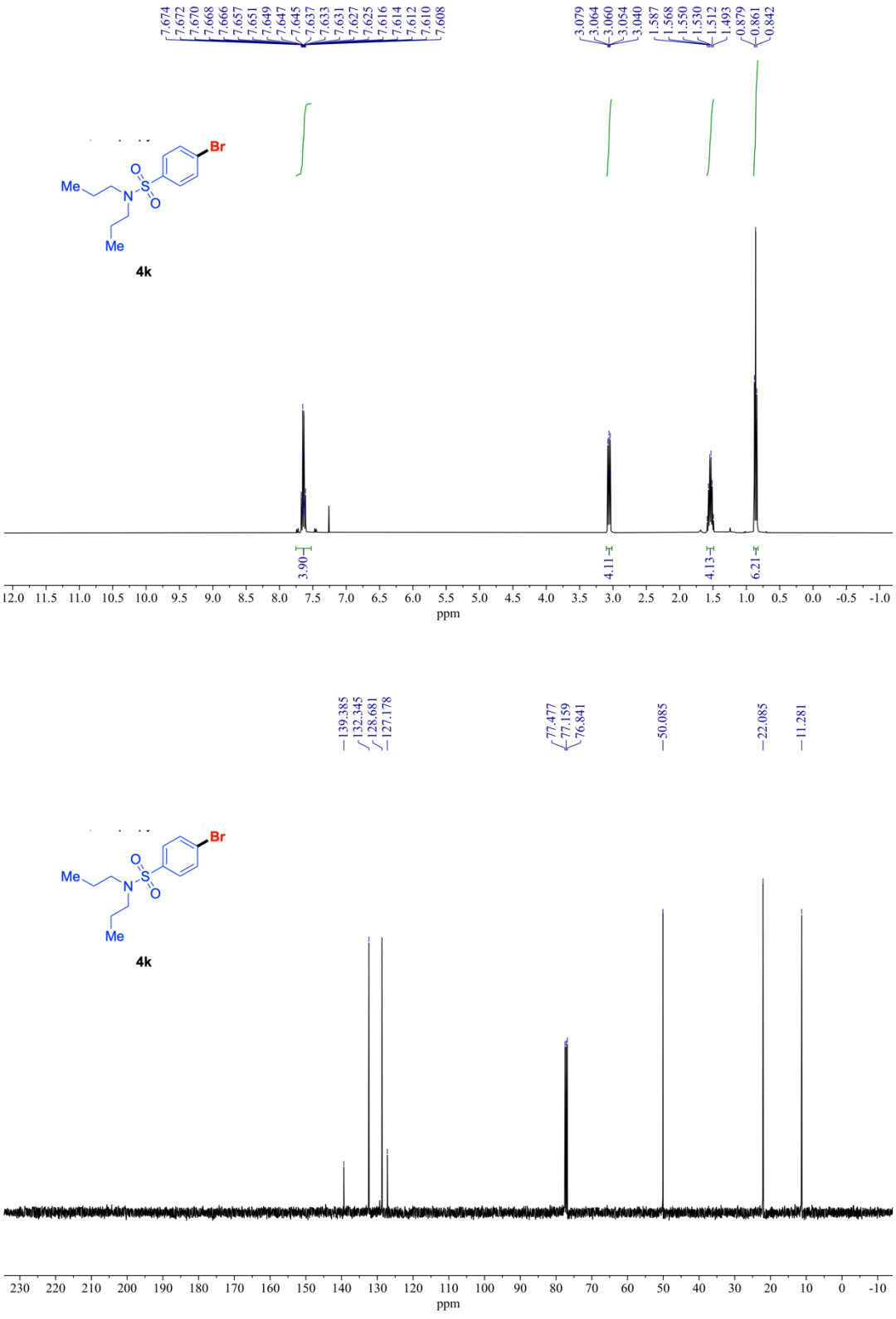

^{1}H NMR (400 MHz) and ^{13}C{^{1}H} NMR (101 MHz) spectra of **4k** (rt, $CDCl_3$).

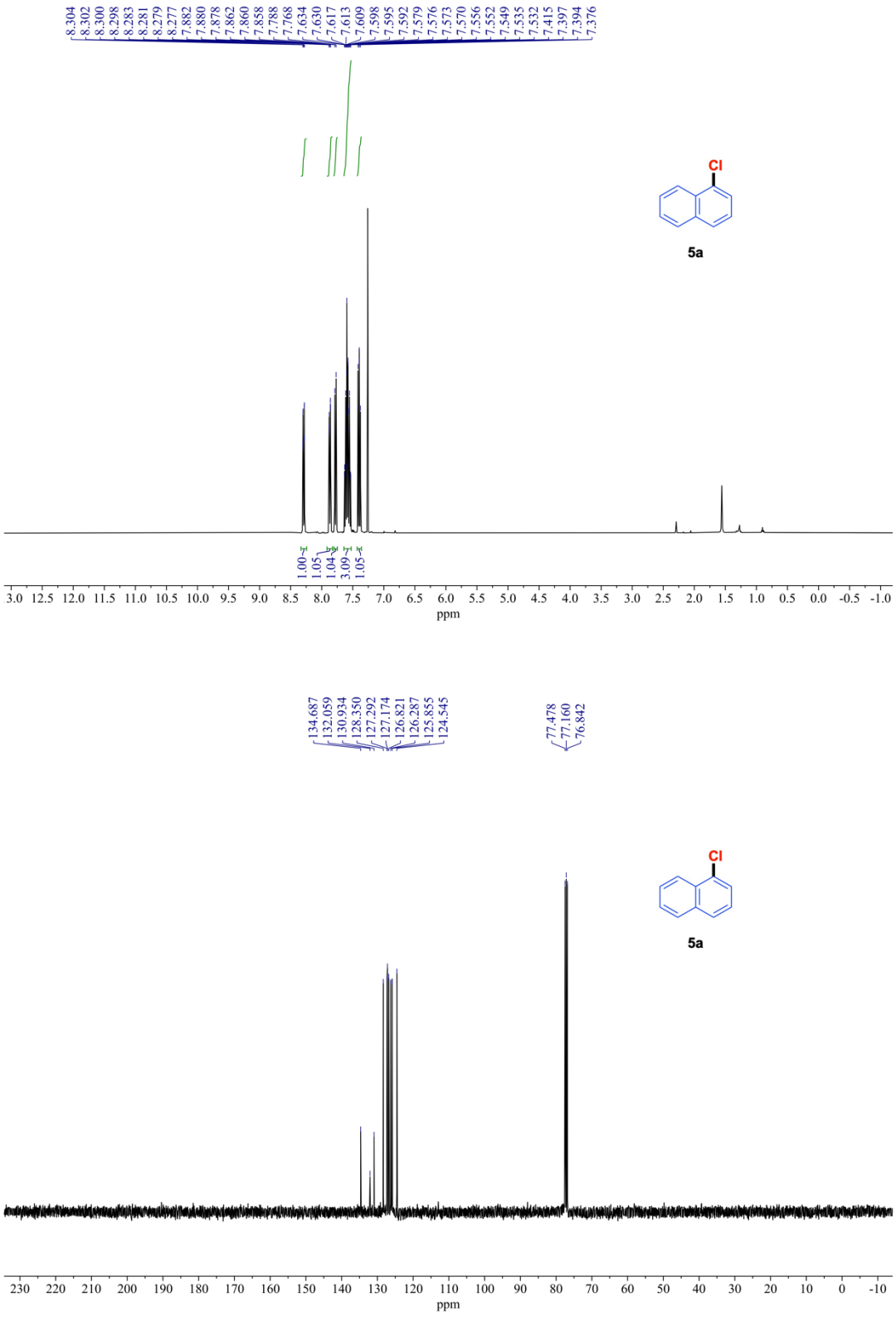

^{1}H NMR (400 MHz) and ^{13}C{^{1}H} NMR (101 MHz) spectra of **5a** (rt, $CDCl_3$).

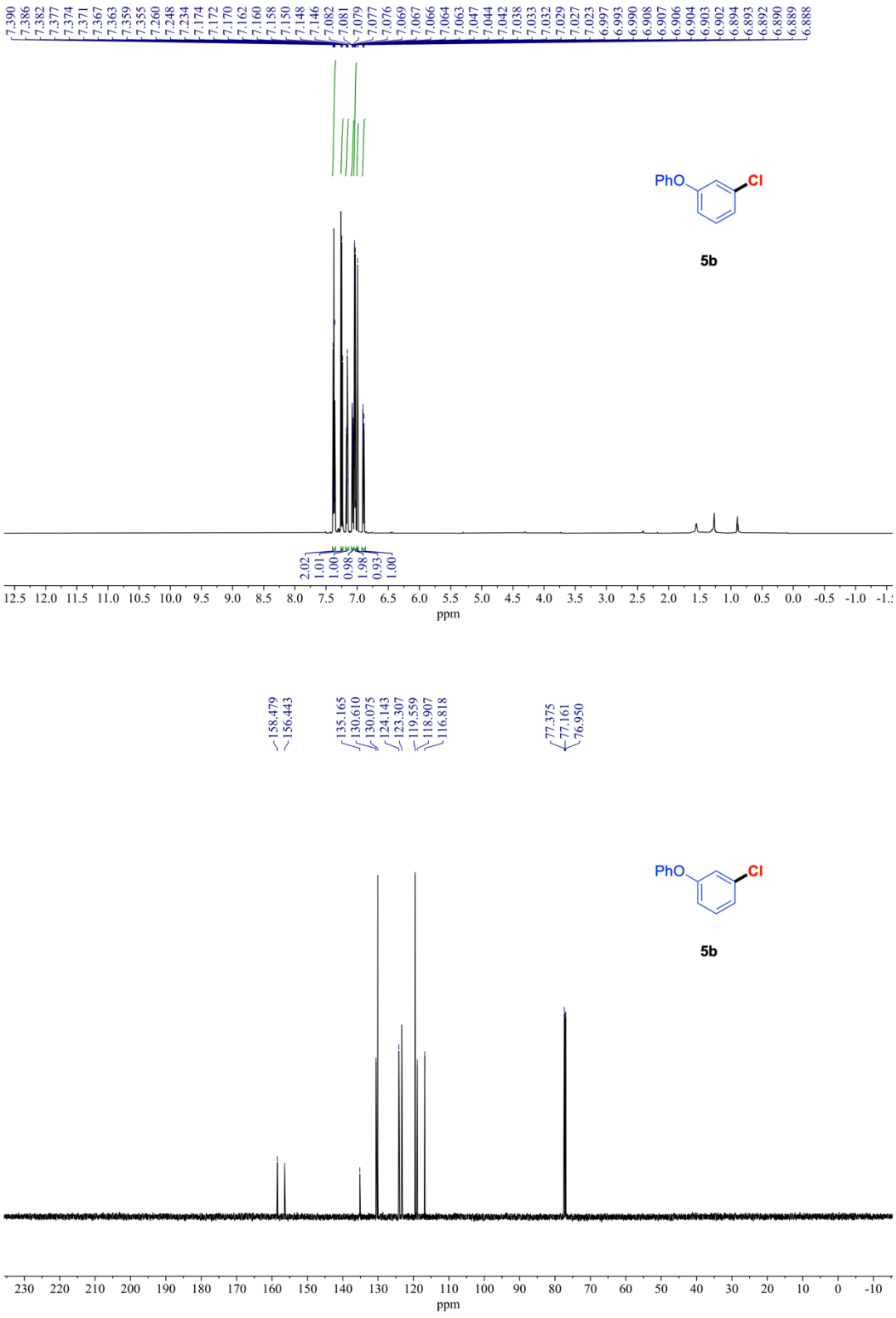

^{1}H NMR (600 MHz) and ^{13}C{^{1}H} NMR (151 MHz) spectra of **5b** (rt, $CDCl_3$).

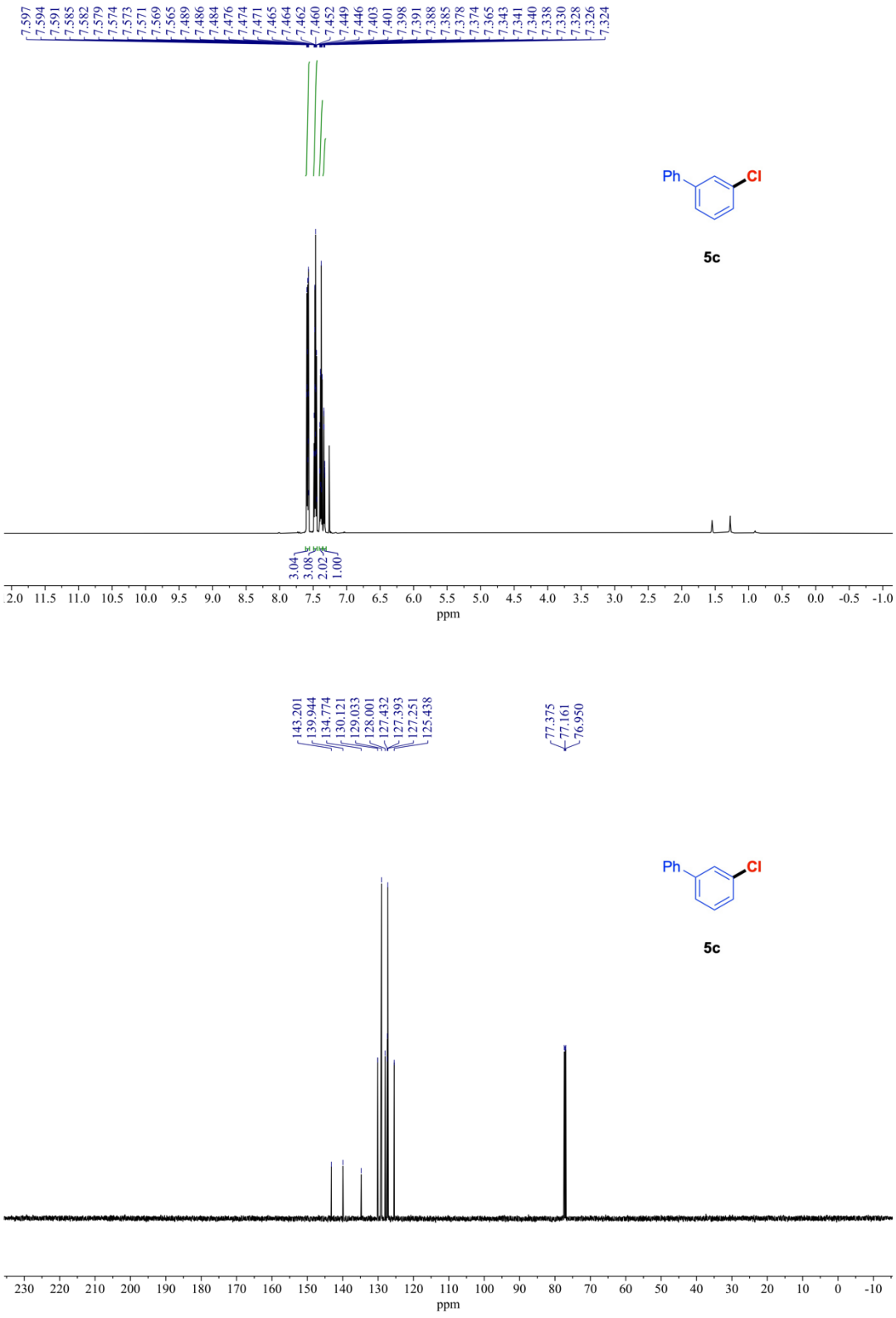

^{1}H NMR (600 MHz) and ^{13}C{^{1}H} NMR (151 MHz) spectra of **5c** (rt, $CDCl_3$).

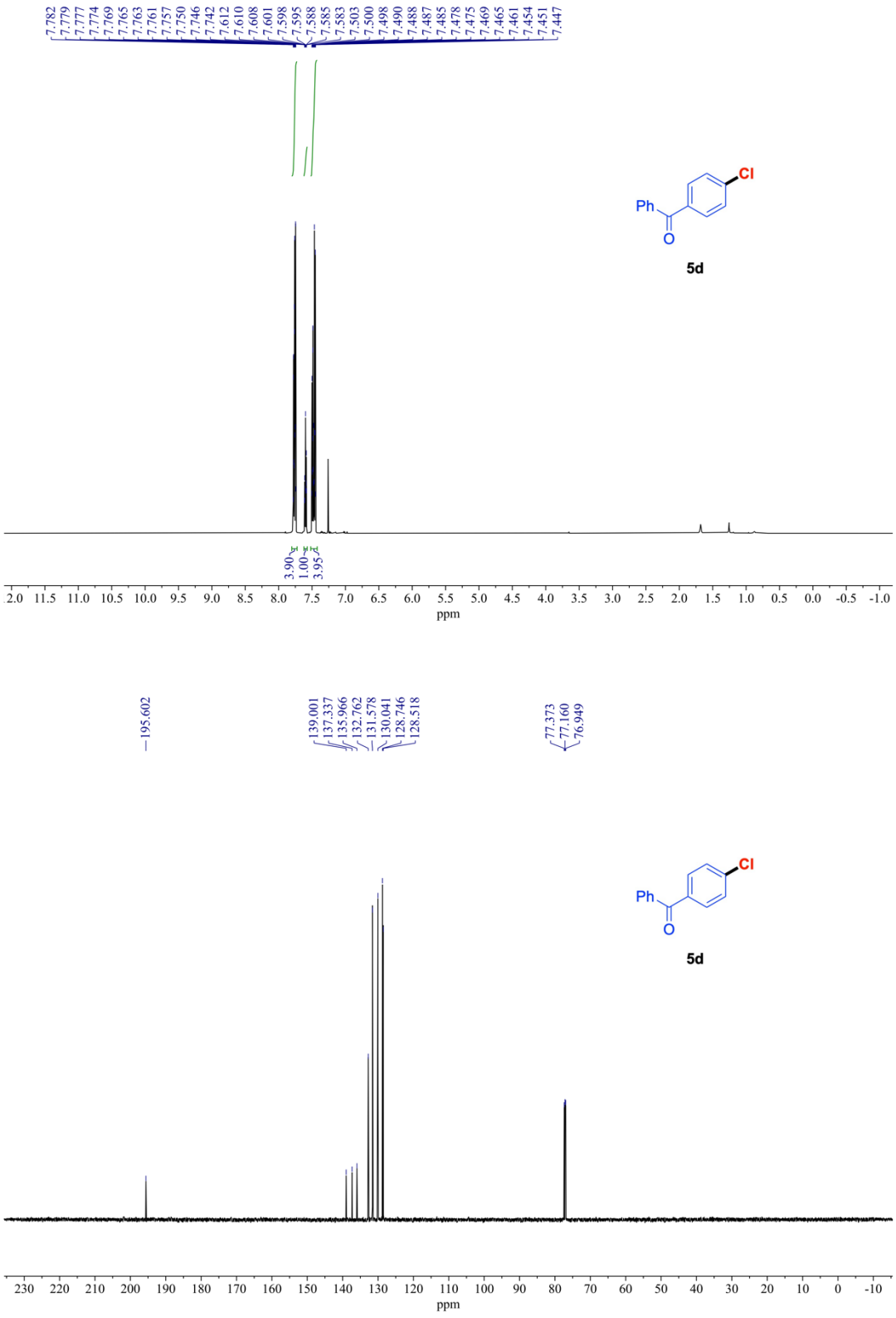

^{1}H NMR (600 MHz) and ^{13}C{^{1}H} NMR (151 MHz) spectra of **5d** (rt, $CDCl_3$).

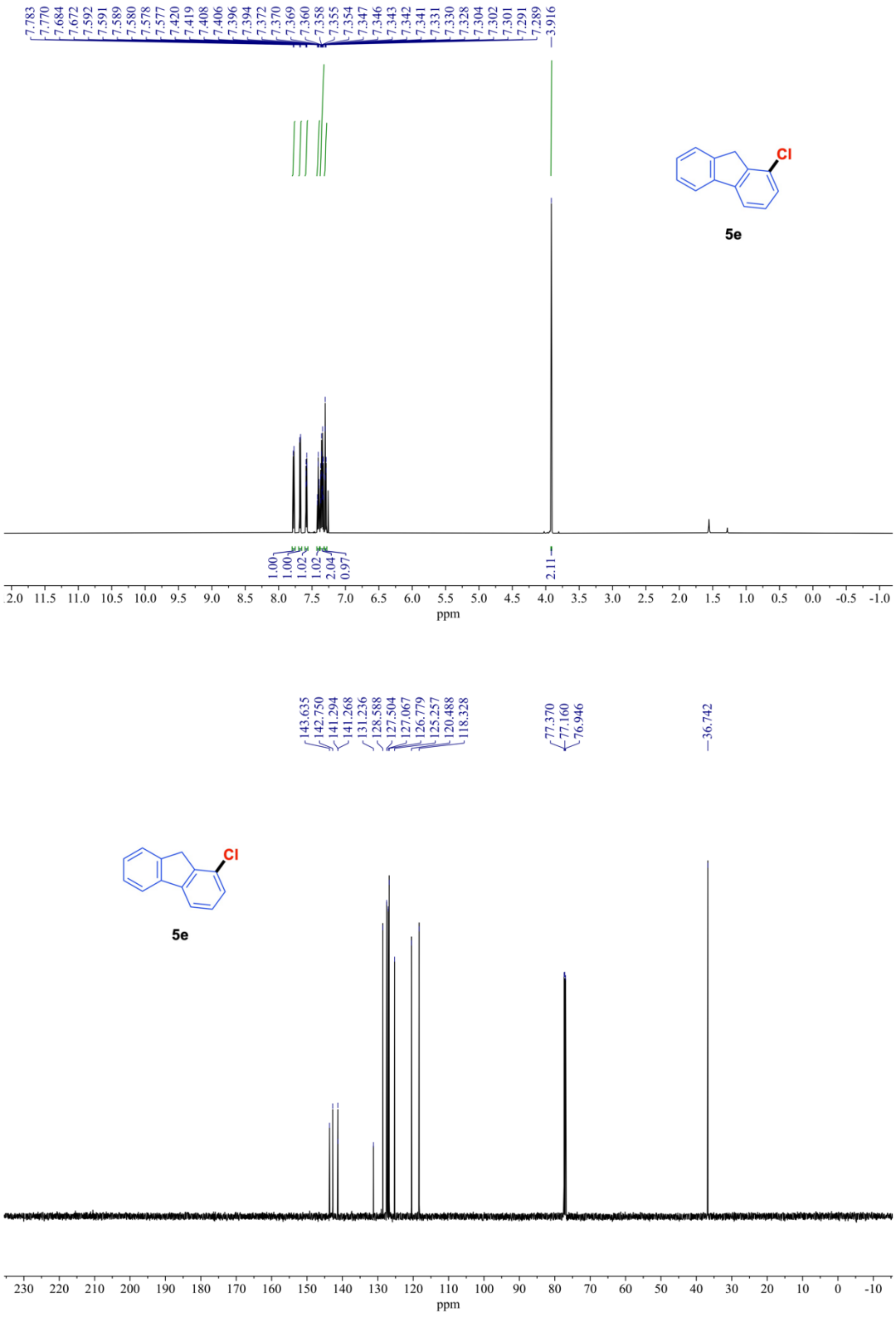

^{1}H NMR (600 MHz) and ^{13}C{^{1}H} NMR (151 MHz) spectra of **5e** (rt, $CDCl_3$).

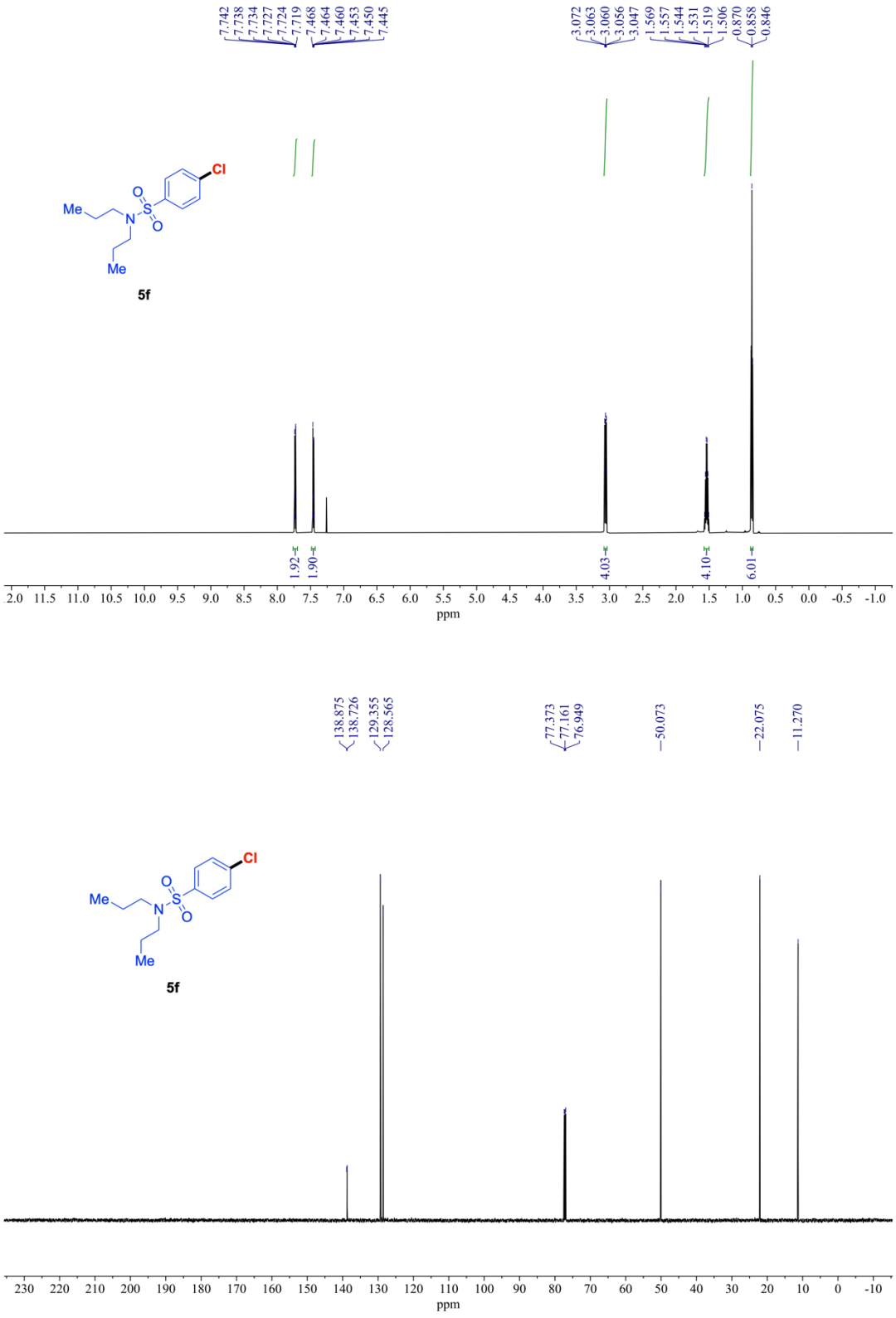

^{1}H NMR (600 MHz) and ^{13}C{^{1}H} NMR (151 MHz) spectra of **5f** (rt, $CDCl_3$).

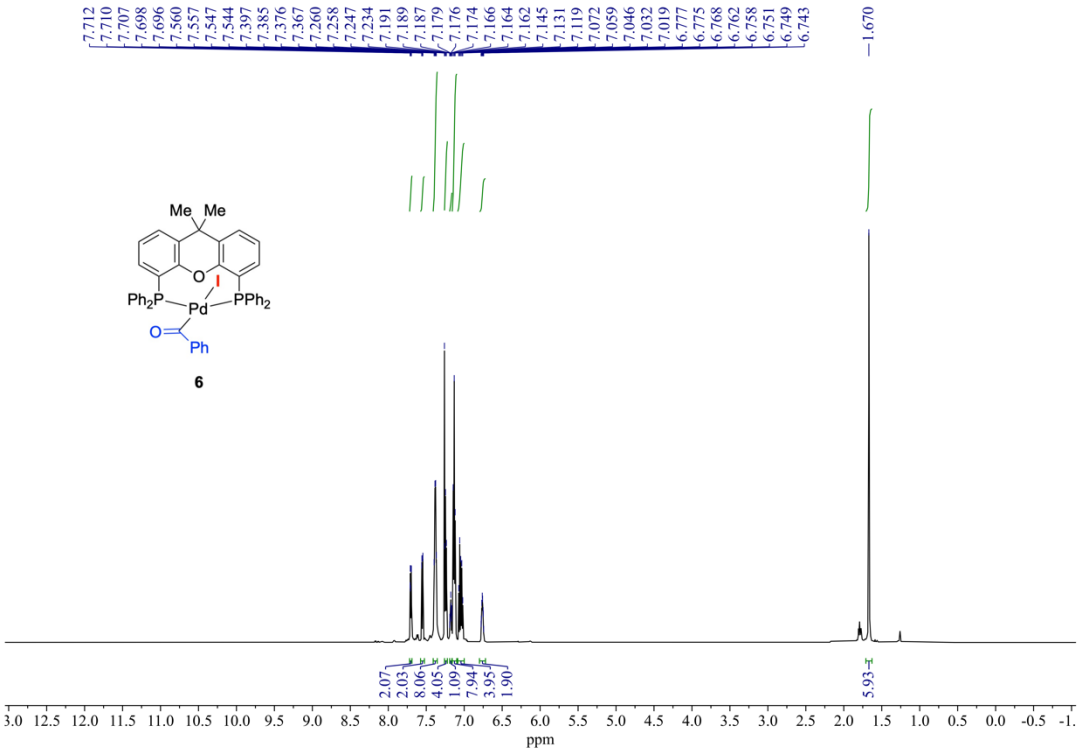
7.712
7.710
7.707
7.698
7.696
7.560
7.557
7.547
7.544
7.397
7.385
7.376
7.367
7.260
7.258
7.247
7.234
7.191
7.189
7.187
7.179
7.176
7.174
7.166
7.164
7.162
7.145
7.131
7.119
7.072
7.059
7.046
7.032
7.019
6.777
6.775
6.768
6.762
6.758
6.751
6.749
6.743
1.670
Me Me
O
I
Ph2P
Pd
PPh2
O
Ph
6
2.07
2.03
8.06
4.05
1.09
7.94
3.95
1.90
5.93
3.0 12.5 12.0 11.5 11.0 10.5 10.0 9.5 9.0 8.5 8.0 7.5 7.0 6.5 6.0 5.5 5.0 4.5 4.0 3.5 3.0 2.5 2.0 1.5 1.0 0.5 0.0 -0.5 -1.
ppm

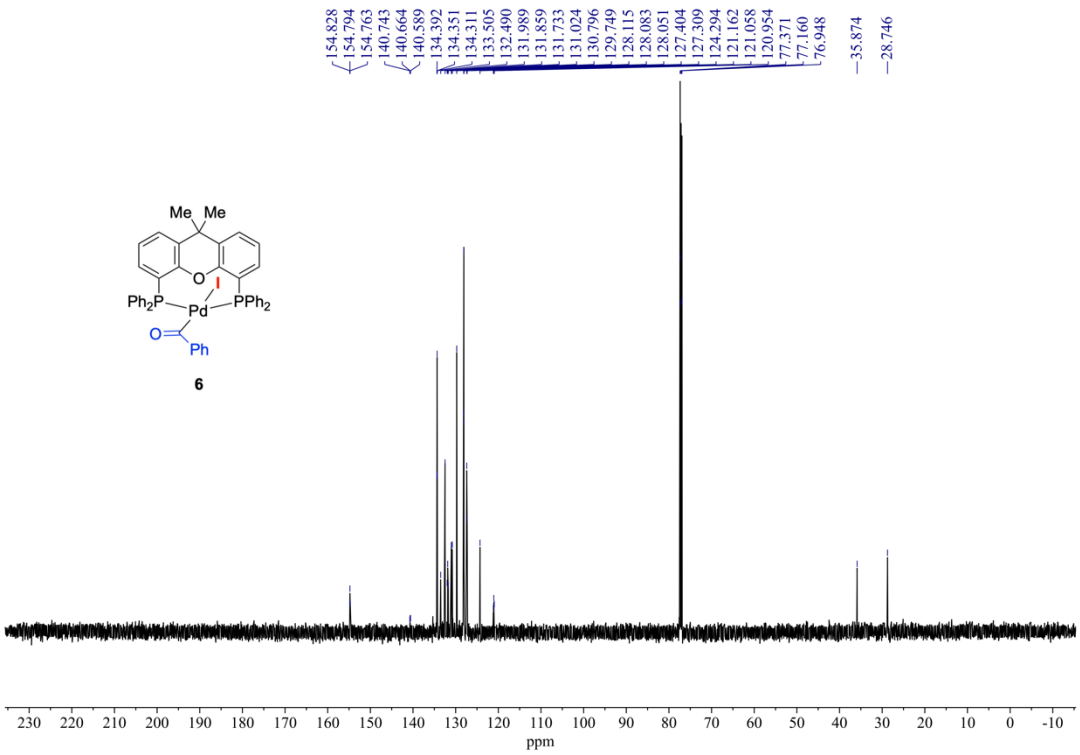
154.828
154.794
154.763
140.743
140.664
140.589
134.392
134.351
134.311
133.505
132.490
131.989
131.859
131.733
131.024
130.796
129.749
128.115
128.083
128.051
127.404
127.309
124.294
121.162
121.058
120.954
77.371
77.160
76.948
35.874
28.746
Me Me
O
I
Ph2P
Pd
PPh2
O
Ph
6
230 220 210 200 190 180 170 160 150 140 130 120 110 100 90 80 70 60 50 40 30 20 10 0 -10
ppm

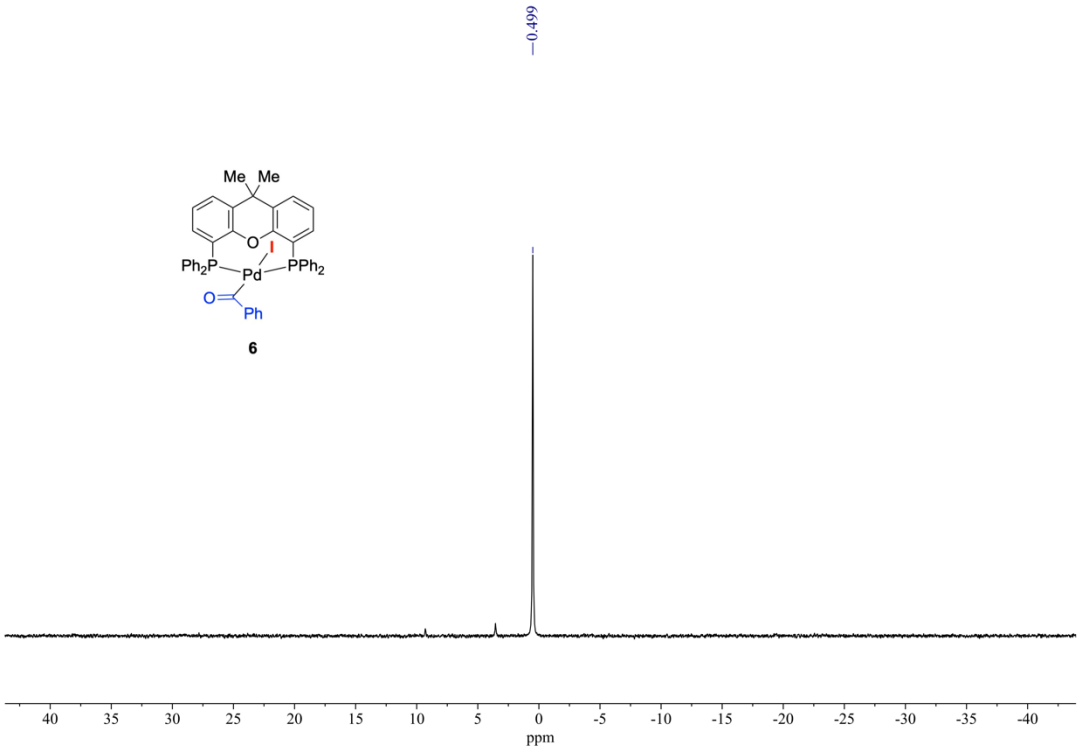

^{1}H NMR (600 MHz), ^{13}C{^{1}H} NMR (151 MHz) and ^{31}P{^{1}H} NMR (162 MHz) spectra of **6** (rt, $CDCl_3$).

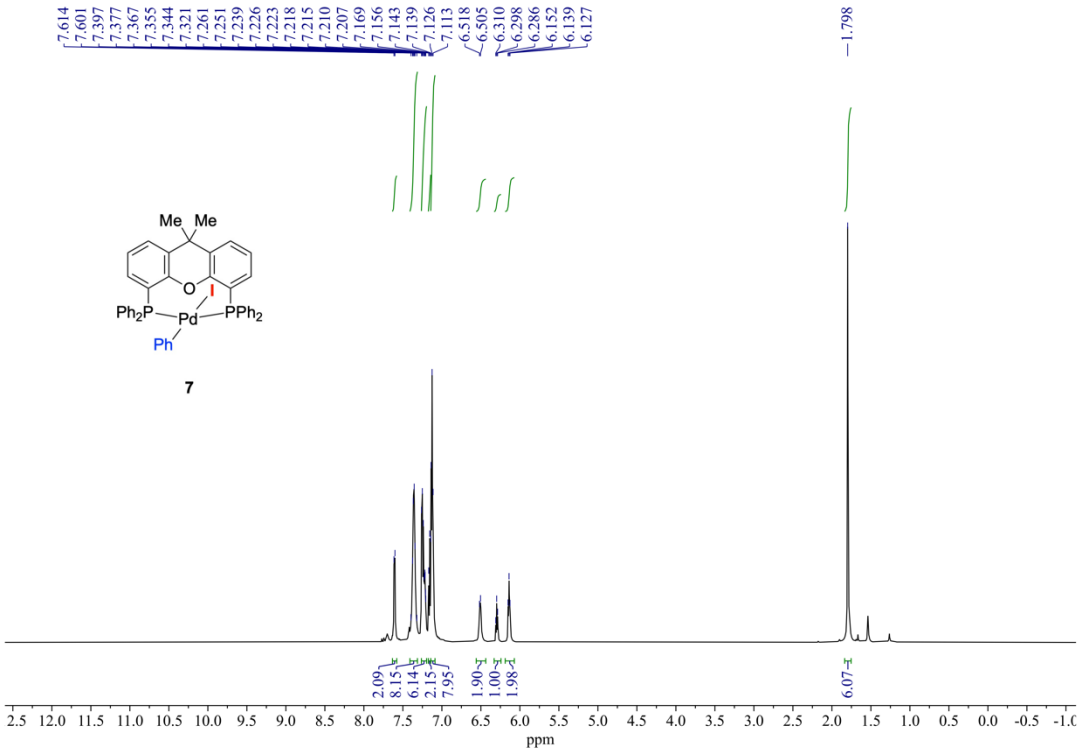
7.614
7.601
7.397
7.377
7.367
7.355
7.344
7.321
7.261
7.251
7.239
7.226
7.223
7.218
7.215
7.210
7.207
7.169
7.156
7.143
7.139
7.126
7.113
6.518
6.505
6.310
6.298
6.286
6.152
6.139
6.127
1.798
Me Me
O
I
Ph2P
Pd
PPh2
Ph
7
2.09
8.15
6.14
2.15
7.95
1.90
1.00
1.98
6.07
2.5 12.0 11.5 11.0 10.5 10.0 9.5 9.0 8.5 8.0 7.5 7.0 6.5 6.0 5.5 5.0 4.5 4.0 3.5 3.0 2.5 2.0 1.5 1.0 0.5 0.0 -0.5 -1.0
ppm

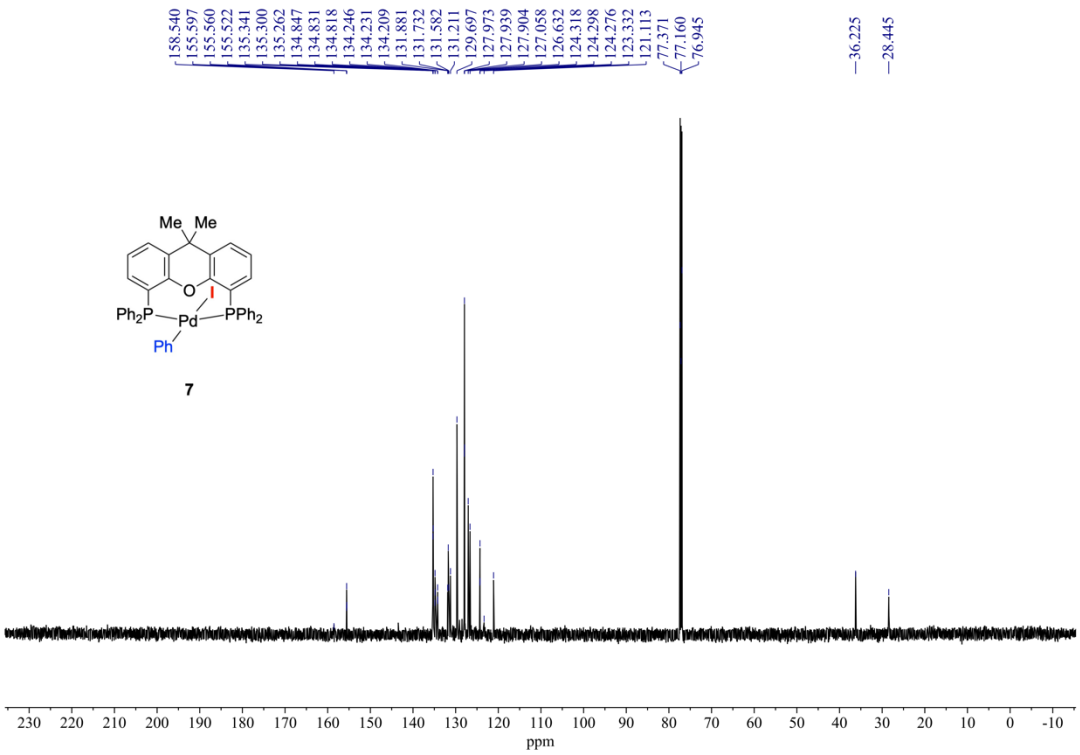
158.540
155.597
155.560
155.522
135.341
135.300
135.262
134.847
134.831
134.818
134.246
134.231
134.209
131.881
131.732
131.582
131.211
129.697
127.973
127.939
127.904
127.058
126.632
124.318
124.298
124.276
123.332
121.113
77.371
77.160
76.945
36.225
28.445
Me Me
O
I
Ph2P
Pd
PPh2
Ph
7
230 220 210 200 190 180 170 160 150 140 130 120 110 100 90 80 70 60 50 40 30 20 10 0 -10
ppm

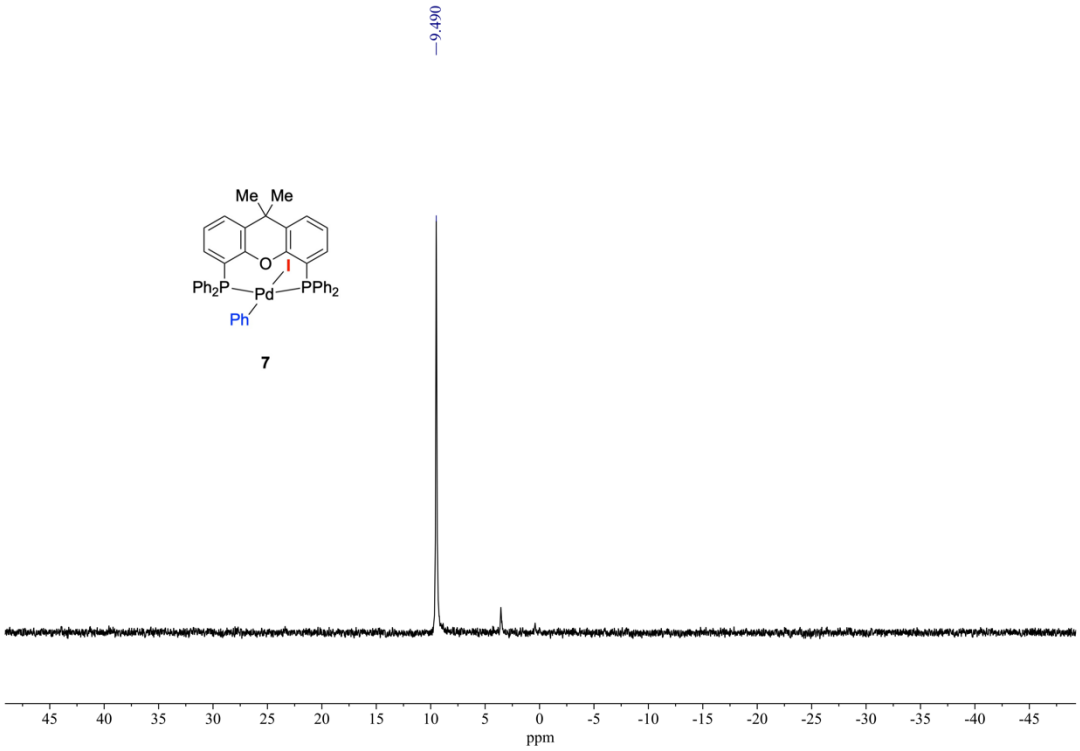

^{1}H NMR (600 MHz), ^{13}C{^{1}H} NMR (151 MHz) and ^{31}P{^{1}H} NMR (162 MHz) spectra of **7** (rt, $CDCl_3$).

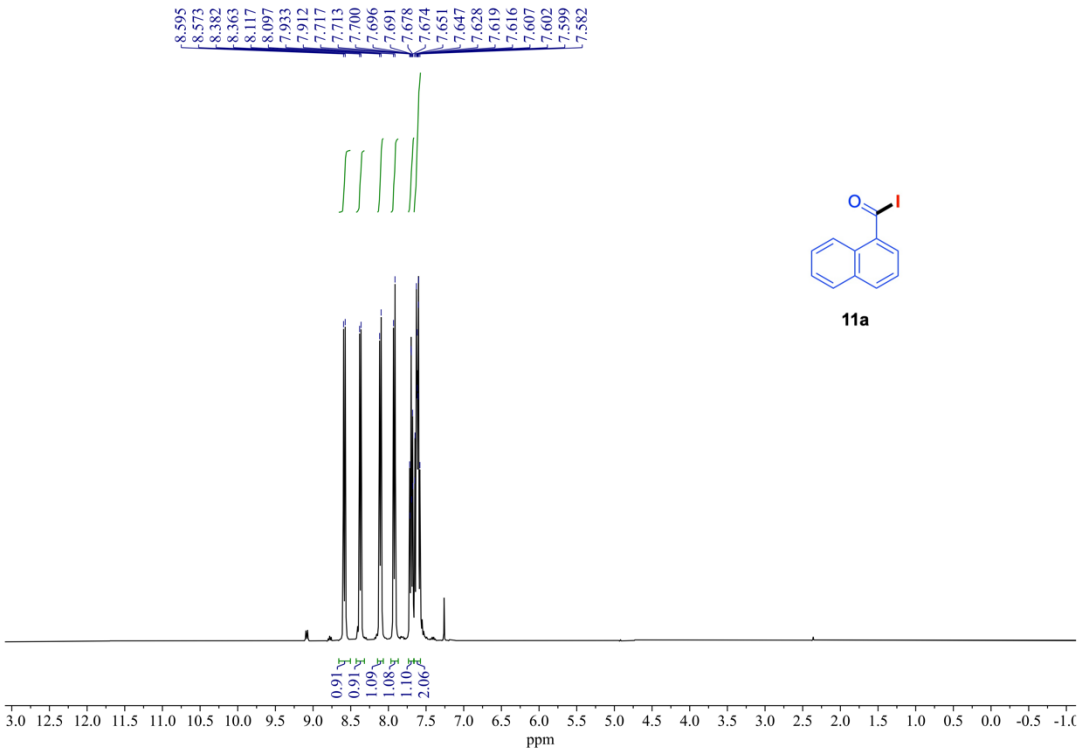

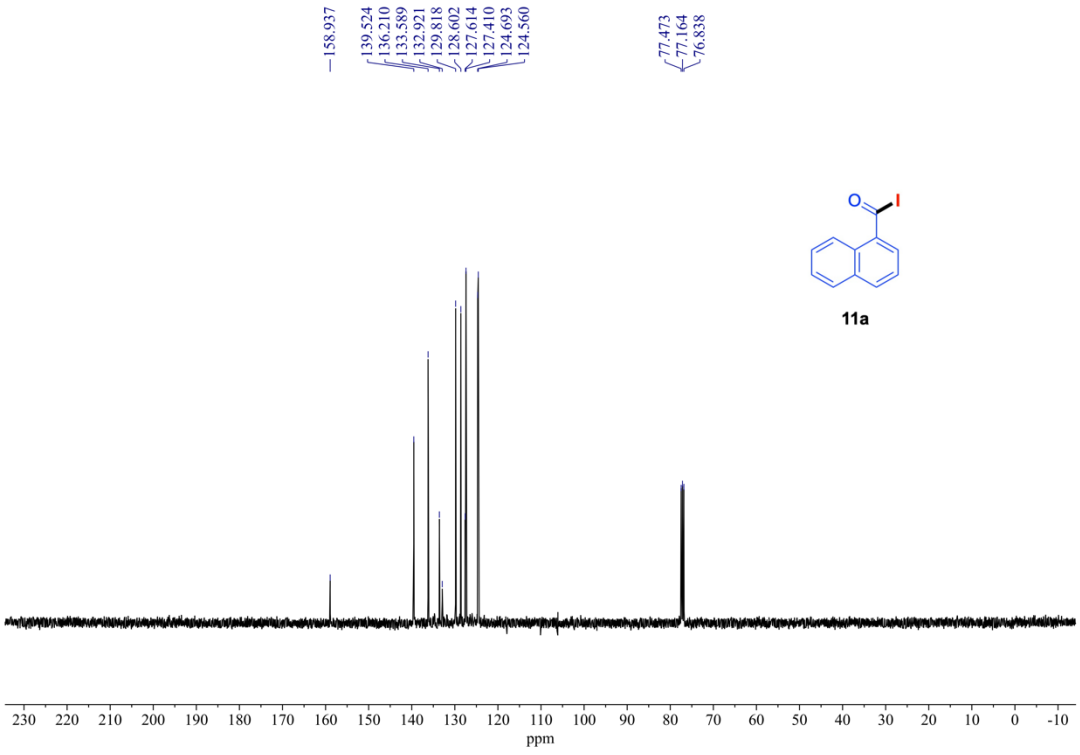

^{1}H NMR (400 MHz) and ^{13}C{^{1}H} NMR (101 MHz) spectra of **11a** (rt, $CDCl_3$).

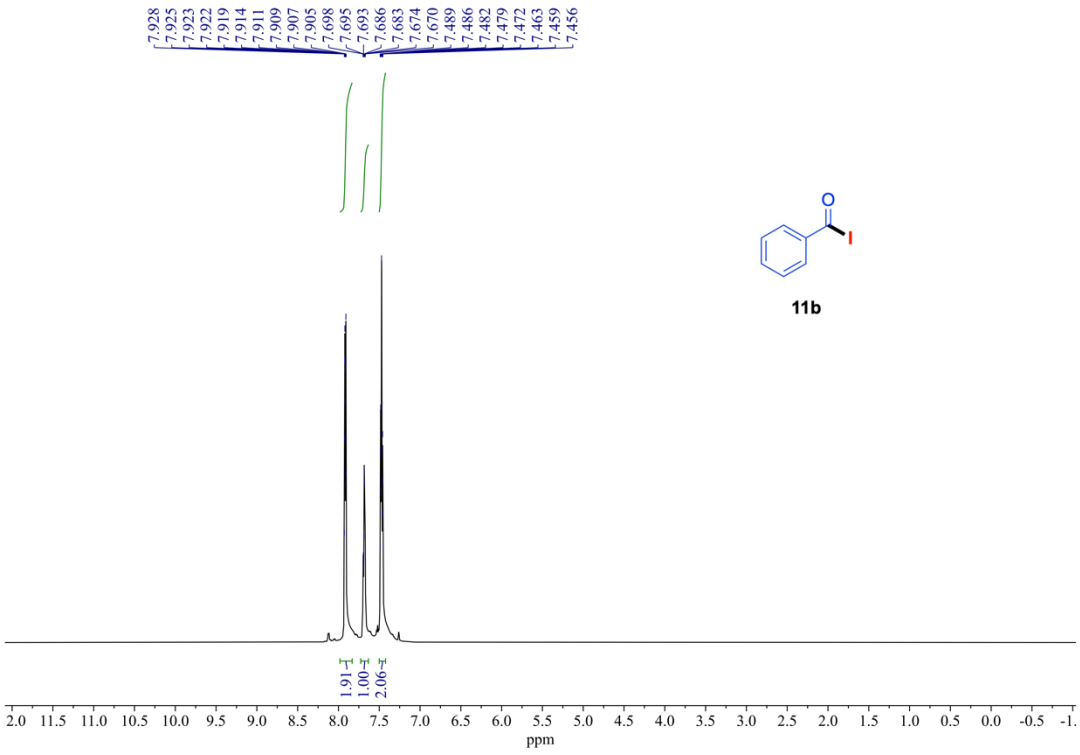

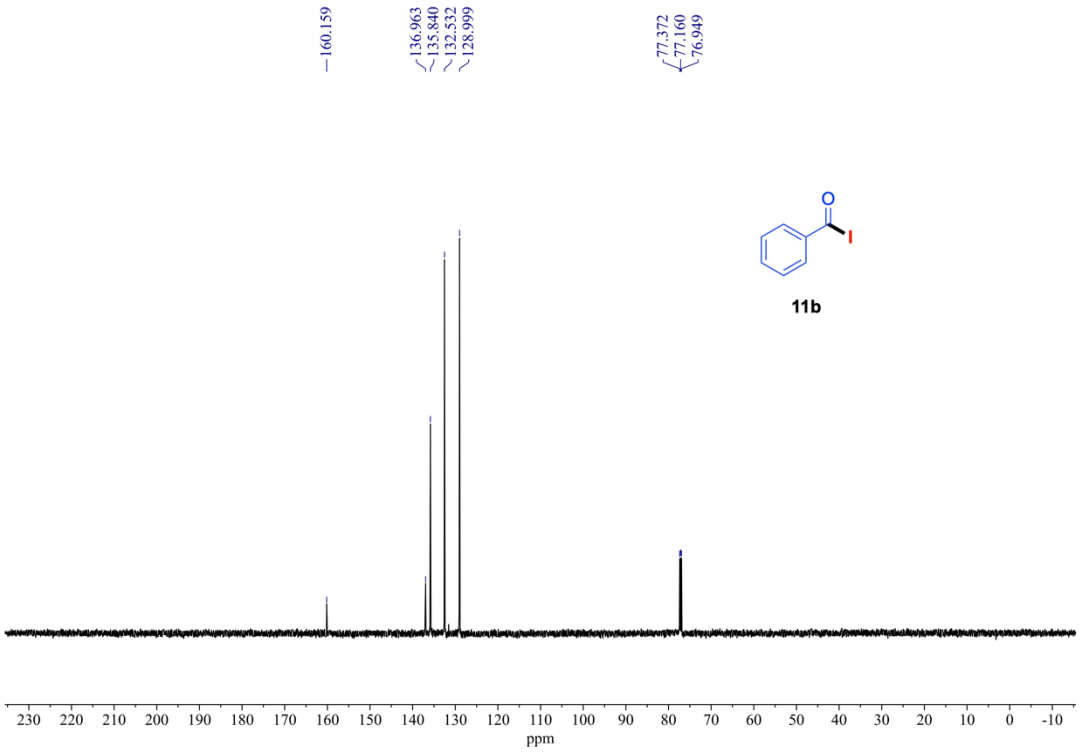

^{1}H NMR (600 MHz) and ^{13}C{^{1}H} NMR (151 MHz) spectra of **11b** (rt, $CDCl_3$).

2-5 References

1. Cui, B.; Jia, S.; Tokunaga, E.; Shibata, N. *Nat. Commun.* **2018**, *9*, 4393.
2. For several selected papers, see: (a) Watson, D. A.; Su, M.; Teverovskiy, G.; Zhang, Y.; GarcíaFortanet, J.; Kinzel, T.; Buchwald, S. L. *Science* **2009**, *325*, 1661. (b) Shen, X.; Hyde, A. M.; Buchwald, S. L. *J. Am. Chem. Soc.* **2010**, *132*, 14076. (c) Pan, J.; Wang, X.; Zhang, Y.; Buchwald, S. L. *Org. Lett.* **2011**, *13*, 4974. For several selected reviews, see: (d) Sather, A. C.; Buchwald, S. L. *Acc. Chem. Res.* **2016**, *49*, 2146. (e) Brown, J. M.; Gouverneur, V. *Angew. Chem., Int. Ed.* **2009**, *48*, 8610; *Angew. Chem.* **2009**, *121*, 8762.
3. For several selected reviews, see: (a) Jones, D. J.; Lautens, M.; McGlacken, G. P. *Nat. Catal.* **2019**, *2*, 843. (b) Petrone, D. A.; Ye, J.; Lautens, M. *Chem. Rev.* **2016**, *116*, 8003. (c) Chen, C.; Tong, X. *Org. Chem. Front.* **2014**, *1*, 439.
4. (a) Torres, G. M.; Liu, Y.; Arndtsen, B. A. *Science* **2020**, *368*, 318. (b) Kinney, R. G.; Tjutrins, J.; Torres, G. M.; Liu, N. J.; Kulkarni, O.; Arndtsen, B. A. *Nat. Chem.* **2018**, *10*, 193.
5. (a) Gooßen, L. J.; Rodríguez, N.; Gooßen, K. *Angew. Chem., Int. Ed.* **2008**, *47*, 3100; *Angew. Chem.* **2008**, *120*, 3144. (b) Qin, T.; Cornella, J.; Li, C.; Malins, L. R.; Edwards, J. T.; Kawamura, S.; Maxwell, B. D.; Eastgate, M. D.; Baran, P. S. *Science* **2016**, *352*, 801. (c) Noble, A.; McCarver, S. J.; Macmillan, D. W. C. *J. Am. Chem. Soc.* **2015**, *137*, 624.
6. For selected reviews and reports, see: (a) Rodríguez, N.; Goossen, L. J. *Chem. Soc. Rev.* **2011**, *40*, 5030. (b) Cornella, J.; Larrosa, I. *Synthesis* **2012**, *44*, 653. (c) Edwards, J. T.; Merchant, R. R.; McClymont, K. S.; Knouse, K. W.; Qin, T.; Malins, L. R.; Vokits, B.; Shaw, S. A.; Bao, D. H.; Wei, F.-L.; Zhou, T.; Eastgate, M. D.; Baran, P. S. *Nature* **2017**, *545*, 213. (d) Zuo, Z.; Ahneman, D. T.; Chu, L.; Terrett, J. A.; Doyle, A. G.; MacMillan, D. W. C. *Science* **2014**, *345*, 437. (e) Gooßen, L. J.; Deng, G.; Levy, L. M. *Science* **2006**, *313*, 662. (f) Cornella, J.; Lu, P.; Larrosa, I. *Org. Lett.* **2009**, *11*, 5506.
7. For selected reviews and reports, see: (a) Zhao, Q.; Szostak, M. *ChemSusChem* **2019**, *12*, 2983. (b) Guo, L.; Rueping, M. *Chem.—Eur. J.* **2018**, *24*, 7794. (c) Lu, H.; Yu, T.-Y.; Xu, P.-F.; Wei, H. *Chem. Rev.* **2021**, *121*, 365. (d) Amaike, K.; Muto, K.; Yamaguchi, J.; Itami, K. *J. Am. Chem. Soc.* **2012**, *134*, 13573. (e) Gooßen, L. J.; Paetzold, J. *Adv. Synth. Catal.* **2004**, *346*, 1665. (f) Zhou, T.; Xie, P.-P.; Ji, C.-L.; Hong, X.; Szostak, M. *Org. Lett.* **2020**, *22*, 6434. (g) Weires, N. A.; Baker, E. L.; Garg, N. K. *Nat. Chem.* **2016**, *8*, 75. (h) Meng, G.; Szostak, M. *Angew. Chem., Int. Ed.* **2015**, *54*, 14518; *Angew. Chem.* **2015**, *127*, 14726. (i) Sugihara, T.; Satoh, T.; Miura, M.; Nomura, M.

Angew. Chem., Int. Ed. **2003**, *42*, 4672; *Angew. Chem.* **2003**, *115*, 4820. (j) Gooßen, L. J.; Paetzold, J. *Angew. Chem., Int. Ed.* **2002**, *41*, 1237; *Angew. Chem.* **2002**, *114*, 1285. (k) Pan, F.; Boursalian, G. B.; Ritter, T. *Angew. Chem., Int. Ed.* **2018**, *57*, 16871; *Angew. Chem.* **2018**, *130*, 17113.

8. For several selected reviews, see: (a) Blanchard, N.; Bizet, V. *Angew. Chem., Int. Ed.* **2019**, *58*, 6814; *Angew. Chem.* **2019**, *131*, 6886. (b) Ogiwara, Y.; Sakai, N. *Angew. Chem., Int. Ed.* **2020**, *59*, 574; *Angew. Chem.* **2020**, *132*, 584. (c) Wang, Z.; Wang, X.; Nishihara, Y. *Chem.—Asian J.* **2020**, *15*, 1234. (d) Fu, L.; Chen, Q.; Nishihara, Y. *Chem. Rec.* **2021**, *21*, 3394. (e) Tian, T.; Chen, Q.; Li, Z.; Nishihara, Y. *Synthesis* **2022**, *54*, 3667.
9. Keaveney, S. T.; Schoenebeck, F. *Angew. Chem., Int. Ed.* **2018**, *57*, 4073; *Angew. Chem.* **2018**, 130, 4137.
10. (a) Malapit, C. A.; Bour, J. R.; Brigham, C. E.; Sanford, M. S. *Nature* **2018**, *563*, 100. (b) Lalloo, N.; Malapit, C. A.; Taimoory, S. M.; Brigham, C. E.; Sanford, M. S. *J. Am. Chem. Soc.* **2021**, *143*, 18617. (c) Malapit, C. A.; Bour, J. R.; Laursen, S. R.; Sanford, M. S. *J. Am. Chem. Soc.* **2019**, *141*, 17322. (d) Fehér, P. P.; Stirling, A. *Organometallics* **2020**, *39*, 2774.
11. (a) Ogiwara, Y.; Sakurai, Y.; Hattori, H.; Sakai, N. *Org. Lett.* **2018**, *20*, 4204. (b) Sakurai, S.; Yoshida, T.; Tobisu, M. *Chem. Lett.* **2019**, *48*, 94. (c) Kayumov, M.; Zhao, J.-N.; Mirzaakhmedov, S.; Wang, D.-Y.; Zhang, A. *Adv. Synth. Catal.* **2020**, *362*, 776. (d) Sakurai, S.; Tobisu, M. *Chem. Lett.* **2021**, *50*, 151. (e) He, B.; Liu, X.; Li, H.; Zhang, X.; Ren, Y.; Su, W. *Org. Lett.* **2021**, *23*, 4191.
12. (a) Okuda, Y.; Xu, J.; Ishida, T.; Wang, C.-A.; Nishihara, Y. *ACS Omega* **2018**, *3*, 13129. (b) Wang, Z.; Wang, X.; Nishihara, Y. *Chem. Commun.* **2018**, *54*, 13969. (c) Wang, X.; Wang, Z.; Liu, L.; Asanuma, Y.; Nishihara, Y. *Molecules* **2019**, *24*, 1671. (d) Wang, X.; Wang, Z.; Nishihara, Y. *Chem. Commun.* **2019**, *55*, 10507. (e) Fu, L.; Chen, Q.; Wang, Z.; Nishihara, Y. *Org. Lett.* **2020**, *22*, 2350. (f) Chen, Q.; Fu, L.; Nishihara, Y. *Chem. Commun.* **2020**, *56*, 7977. (g) Chen, Q.; Fu, L.; You, J.; Nishihara, Y. *Synlett* **2021**, *32*, 1560. (h) You, J.; Chen, Q.; Nishihara, Y. *Synthesis* **2021**, *53*, 3045. (i) Chen, Q.; Li, Z.; Nishihara, Y. *Org. Lett.* **2022**, *24*, 385. (j) Chen, Q.; You, J.; Tian, T.; Li, Z.; Kashihara, M.; Mori, H.; Nishihara, Y. *Org. Lett.* **2022**, *24*, 9259.
13. Lee, Y. H.; Morandi, B. *Nat. Chem.* **2018**, *10*, 1016.
14. Boehm, P.; Martini, T.; Lee, Y. H.; Cacherat, B.; Morandi, B. *Angew. Chem., Int. Ed.* **2021**, *60*, 17211; *Angew. Chem.* **2021**, *133*, 17348.
15. De La Higuera Macias, M.; Arndtsen, B. A. *J. Am. Chem. Soc.* **2018**, *140*, 10140.

16. For several selected reviews, see: (a) Durand, D. J.; Fey, N. *Chem. Rev.* **2019**, *119*, 6561. (b) Kamer, P. C. J.; van Leeuwen, P. W. N. M.; Reek, J. N. H. *Acc. Chem. Res.* **2001**, *34*, 895. (c) Niksch, T.; Gorls, H.; Weigand, W. *Eur. J. Inorg. Chem.* **2010**, *2010*, 95.
17. Malapit, C. A.; Ichiishi, N.; Sanford, M. S. *Org. Lett.* **2017**, *19*, 4142.
18. For several selected reviews, see: (a) Meng, G.; Zhang, J.; Szostak, M. *Chem. Rev.* **2021**, *121*, 12746. (b) Li, G.; Ma, S.; Szostak, M. *Trends Chem.* **2020**, *2*, 914. (c) Gao, P.; Rahman, M. M.; Zamalloa, A.; Feliciano, J.; Szostak, M. *J. Org. Chem.* **2023**, *88*, 13371. (d) Liu, C.; Szostak, M. *Org. Biomol. Chem.* **2018**, *16*, 7998.
19. (a) Miloserdov, F. M.; Grushin, V. V. *Angew. Chem., Int. Ed.* **2012**, *51*, 3668; *Angew. Chem.* **2012**, *124*, 3728. (b) Johns, A. M.; Utsunomiya, M.; Incarvito, C. D.; Hartwig, J. F. *J. Am. Chem. Soc.* **2006**, *128*, 1828. (c) Miloserdov, F. M.; McMullin, C. L.; Belmonte, M. M.; Benet-Buchholz, J.; Bakhmutov, V. I.; Macgregor, S. A.; Grushin, V. V. *Organometallics* **2014**, *33*, 736.
20. For several selected examples, see: (a) Garrou, P. E.; Heck, R. F. *J. Am. Chem. Soc.* **1976**, *98*, 4115. (b) Quesnel, J. S.; Arndtsen, B. A. *J. Am. Chem. Soc.* **2013**, *135*, 16841.
21. For several selected examples, see: (a) Blum, J.; Oppenheimer, E.; Bergmann, E. D. *J. Am. Chem. Soc.* **1967**, *89*, 2338. (b) Blum, J.; Rosenman, H.; Bergmann, E. D. *J. Org. Chem.* **1968**, *33*, 1928. (c) Ohno, K.; Tsuji, J. *J. Am. Chem. Soc.* **1968**, *90*, 99. (d) Tsuji, J.; Ohno, K. *J. Am. Chem. Soc.* **1966**, *88*, 3452. (e) Blum, J. *Tetrahedron Lett.* **1966**, *7*, 1605. (f) Tsuji, J.; Ohno, K.; Kajimoto, T. *Tetrahedron Lett.* **1965**, *6*, 4565.
22. For several selected examples, see: (a) Fujimoto, H.; Kodama, T.; Yamanaka, M.; Tobisu, M. *J. Am. Chem. Soc.* **2020**, *142*, 17323. (b) Fujimoto, H.; Kusano, M.; Kodama, T.; Tobisu, M. *J. Am. Chem. Soc.* **2021**, *143*, 18394. (c) Fujimoto, H.; Yamamura, S.; Takenaka, N.; Tobisu, M. *Synthesis* **2023**, *55*, 899. (d) Fujimoto, H.; Yamamura, S.; Kusano, M.; Tobisu, M. *Org. Lett.* **2023**, *25*, 336. (e) Fujimoto, H.; Yasui, K.; Tobisu, M. *Bull. Chem. Soc. Jpn.* **2023**, *96*, 872.
23. Munoz, S. B.; Dang, H.; Ispizua-Rodriguez, X.; Mathew, T.; Prakash, G. K. S. *Org. Lett.* **2019**, *21*, 1659.
24. (a) Kim, J.; Jang, J.; Lee, Y.; Shin, K. *Org. Lett.* **2022**, *24*, 5412. (b) Boreux, A.; Indukuri, K.; Gagosz, F.; Riant, O. *ACS Catal.* **2017**, *7*, 8200. (c) Beaulieu, F.; Bauregard, L.-P.; Courchesne, G.; Couturier, M.; LaFlamme, F.; L'Heureux, A. *Org. Lett.* **2009**, *11*, 5050.
25. Dine, T. M. E.; Jimmidi, R.; Diaconu, A.; Fransolet, M.; Michiels, C.; Winter, J. D.; Gillon, E.; Imberty, A.; Coenye, T.; Vincent, S. P. *J. Med. Chem.* **2021**, *64*, 14728.

26. Re, P. D.; Verlicchi, L.; Setnikar, I. *J. Med. Pharm. Chem.* **1960**, *2*, 263.
27. Pu, X.; Hu, J.; Zhao, Y.; Shi, Z. *ACS Catal.* **2016**, *6*, 6692.
28. Jones, A. C.; Williams, M. T. J.; Morrill, L. C.; Browne, D. L. *ACS Catal.* **2022**, *12*, 13681.
29. (a) Ogiwara, Y.; Hosaka, S.; Sakai, N. *Organometallics* **2020**, *39*, 856. (b) Ogiwara, Y.; Sakino, D.; Sakurai, Y.; Sakai, N. *Eur. J. Org. Chem.* **2017**, *2017*, 4324.
30. Song, H.-X.; Tian, Z.-Y.; Xiao, J.-C.; Zhang, C.-P. *Chem.—Eur. J.* **2020**, *26*, 16261.
31. Liang, Y.; Zhao, Z.; Taya, A.; Shibata, N. *Org. Lett.* **2021**, *23*, 847.
32. Zhu, C.; Zhumagazy, S.; Yue, H.; Rueping, M. *Org. Chem. Front.* **2022**, *9*, 342.
33. Mahmoud, E. M.; Mori, S.; Sumii, Y.; Shibata, N. *Org. Lett.* **2023**, *25*, 2810.
34. Wu, F.-W.; Mao, Y.-J.; Pu, J.; Li, H.-L.; Ye, P.; Xu, Z.-Y.; Lou, S.-J.; Xu, D.-Q. *Org. Biomol. Chem.* **2022**, *20*, 4091.
35. (a) Xiao, J.; Han, L.-B. *J. Chem. Res.* **2019**, *43*, 205. (b) Patel, M. V.; Bell, R.; Majest, S.; Henry, R.; Kolasa, T. *J. Org. Chem.* **2004**, *69*, 7058.
36. Herschhorn, A.; Lerman, L.; Weitman, M.; Gleenberg, I. O.; Nudelman, A.; Hizi, A. *J. Med. Chem.* **2007**, *50*, 2370.
37. Branca, M.; Pena, S.; Guillot, R.; Gori, D.; Alezra, V.; Kouklovsky, C. *J. Am. Chem. Soc.* **2009**, *131*, 10711.
38. Schuler, A.-K.; Prucker, O.; Rühe, J. *Macromol. Chem. Phys.* **2016**, *217*, 1457.
39. (a) Grunewald, G. L.; Carter, A. E.; Sall, D. J.; Monn, J. A. *J. Med. Chem.* **1988**, *31*, 60. (b) Bergmann, E. D.; Ikan, R. *J. Am. Chem. Soc.* **1956**, *78*, 2821.
40. Ozcan, S.; Kazi, A.; Marsilio, F.; Fang, B.; Guida, W. C.; Koomen, J.; Lawrence, H. R.; Sebti, S. M. *J. Med. Chem.* **2013**, *56*, 3783.
41. Cheng, K.; Wang, X.; Yin, H. *J. Am. Chem. Soc.* **2011**, *133*, 3764.
42. Gautam, P.; Kathe, P.; Bhanage, B. M. *Green Chem.* **2017**, *19*, 823.
43. Srimontree, W.; Chatupheeraphat, A.; Liao, H.-H.; Rueping, M. *Org. Lett.* **2017**, *19*, 3091.
44. Liu, W.; Yang, X.; Gao, Y.; Li, C.-J. *J. Am. Chem. Soc.* **2017**, *139*, 8621.
45. Ni, S.; Yan, J.; Tewari, S.; Reijerse, E. J.; Ritter, T.; Cornella, J. *J. Am. Chem. Soc.* **2023**, *145*, 9988.
46. Zhao, J.; Larock, R. C. *J. Org. Chem.* **2006**, *71*, 5340.
47. Li, L.; Liu, W.; Zeng, H.; Mu, X.; Cosa, G.; Mi, Z.; Li, C.-J. *J. Am. Chem. Soc.* **2015**, *137*, 8328.
48. Meng, M.; Yang, L.; Cheng, K.; Qi, C. *J. Org. Chem.* **2018**, *83*, 3275.

49. Kim, M. H.; Kim, J. *J. Org. Chem.* **2018**, *83*, 1673.
50. Zhu, D.; Peng, H.; Sun, Y.; Wu, Z.; Wang, Y.; Luo, B.; Yu, T.; Hu, Y.; Huang, P.; Wen, S. *Green Chem.* **2021**, *23*, 1972.
51. Perry, G. J. P.; Quibell, J. M.; Panigrahi, A.; Larrosa, I. *J. Am. Chem. Soc.* **2017**, *139*, 11527.
52. Feng, Y.; Luo, H.; Zheng, W.; Matsunaga, S.; Lin, L. *ACS Catal.* **2022**, *12*, 11089.
53. Zarate, C.; Nakajima, M.; Martin, R. *J. Am. Chem. Soc.* **2017**, *139*, 1191.
54. Sundalam, S. K.; Stuart, D. R. *J. Org. Chem.* **2015**, *80*, 6456.
55. (a) Kumar, A.; Shah, B. A. *Org. Lett.* **2015**, *17*, 5232. (b) Kan, J.; Huang, S.; Lin, J.; Zhang, M.; Su, W. *Angew. Chem., Int. Ed.* **2015**, *54*, 2199; *Angew. Chem.* **2015**, *127*, 2227.
56. Wang, X.; Huang, Y.; Xu, Y.; Tang, X.; Wu, W.; Jiang, H. *J. Org. Chem.* **2017**, *82*, 2211.
57. Yin, C.; Liao, Y.; He, B.; Li, H.; Su, W. *Chem.—Eur. J.* **2023**, *29*, e202300184.
58. Best, D.; Jean, M.; van de Weghe, P. *J. Org. Chem.* **2016**, *81*, 7760.
59. Xu, L.; Yang, W.; Zhang, L.; Miao, M.; Yang, Z.; Xu, X.; Ren, H. *J. Org. Chem.* **2014**, *79*, 9206.
60. Cai, Y.; Zhang, R.; Sun, D.; Xu, S.; Zhou, Q. *Synlett* **2017**, *28*, 1630.
61. (a) Toso, S.; Baranov, D.; Giannini, C.; Manna, L. *ACS Nano* **2021**, *15*, 20341. (b) Blum, J.; Rosenman, H.; Bergmann, E. D. *J. Org. Chem.* **1968**, *33*, 1928.
62. (a) Imran, M.; Caligiuri, V.; Wang, M.; Goldoni, L.; Prato, M.; Krahne, R.; Trizio, L. D.; Manna, L. *J. Am. Chem. Soc.* **2018**, *140*, 2656. (b) Acharyya, P.; Maji, K.; Kundu, K.; Biswas, K. *ACS Appl. Nano Mater.* **2020**, *3*, 877. (c) Hoffmann, H. M. R.; Haase, K. *Synthesis* **1981**, *1981*, 715.

CHAPTER 3

Palladium-Catalyzed Decarbonylative Halogenation of Acid Anhydrides

3-1 Introduction

Undoubtedly, the Author's in-depth exploration of the nucleophilic halogenation mode in the previous chapter will open up a new era for subsequent transition metal-catalyzed nucleophilic halogenation. After all, carboxylic acids and their derivatives, which are inexpensive, air-stable, and highly operable, have been used as candidates for the synthesis of aromatic halides decades ago.[1] However, the halogenation mode in the classical category focuses on the decarboxylation electrophilic halogenation of carboxylic acids. On this basis, a series of decarboxylation halogenations of carboxylic acids have been reported, including the renowned Hunsdiecker−Borodin decarboxylation electrophilic halogenation.[2] Highly active electrophilic halogen reagents (including nucleophilic halogen reagents + oxidants) have shown great potential to directly assemble halogen atoms on the carboxylic acid moiety with the realization of decarboxylation (**Scheme 3-1**).[3,4] In addition, due to the nature of the transformation, carboxylic acids can be considered as traceless activating groups and meet the atom economy requirements of modern organic synthesis. Nevertheless, many deep-rooted limitations and challenges remain difficult to overcome. In particular, unlike aliphatic carboxylic acids, relatively stable aromatic carboxylic acids are difficult to achieve electrophilic decarboxylation halogenation. Simultaneously, many halogenation decarboxylation schemes are based on stepwise processes,[5] using heavy or toxic metals and highly toxic, corrosive or strongly oxidizing reagents, [6] using complicated electrophilic halogenating agents or environmentally un-friendly halogenated solvents,[7] and involving tedious separation of the final organic halide,[4] wherein directly leads to a limited substrate scope. Although similar protocols carried out under transition metal catalysis can improve these stubborn problems to some extent, they cannot fundamentally overcome these inherent challenges.[8] In addition, the utilization of bespoke catalysts,[9] and challenges related to suboptimal selectivity also led to the formation of undesirable byproducts.[10] In contrast, the transition metal-catalyzed decarbonylative nucleophilic halogenation strategy of carboxylic acid derivatives can significantly improve this relatively embar-rassing situation. Unfortunately, there are two insurmountable gaps based on this design. One is the weak nucleophilicity of the nucleophilic halogen reagent, and the other is the

thermodynamically unfavorable reductive elimination of C–X bond mediated by transition metals.[11]

Scheme 3-1. Two Halogenation Modes of Carboxylic Acids and Carboxylic Acid Derivatives.

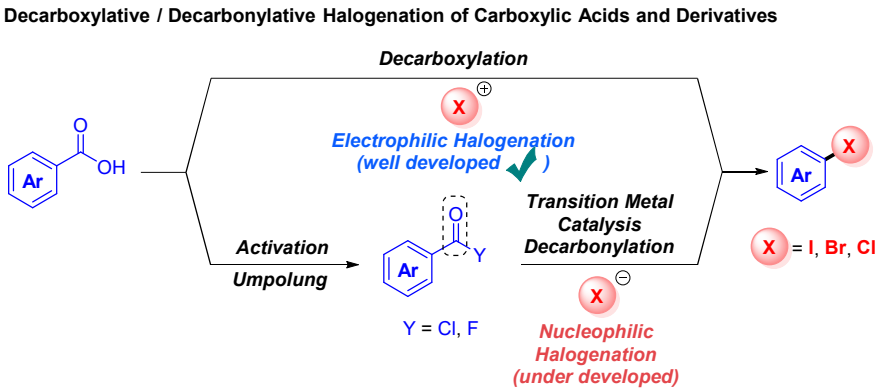

Excitedly, after the Author's in-depth mechanistic study of the palladium-catalyzed decarbonylation nucleophilic halogenation of acyl halides in the previous stage, we have gained a fairly deep understanding of this catalytic transformation. Therefore, it is urgent to continue to expand the application potential and value of this research field. Nevertheless, there are several insuperable gaps in the research in the previous chapter that need to be overcome and broken through. Especially, the stability of acyl chlorides, the high cost of acyl fluorides, and the incompatibility of substrates with electron-donating groups (such as 4-anisyl). Therefore, in order to further develop a more practical, easier to operate and more cost-effective decarbonylation mode, the author is eager to find a new unique trick to break through this obstacle and dilemma.

Scheme 3-2. Transition Metal Catalyzed Decarbonylative Transformations of Acid Anhydrides.

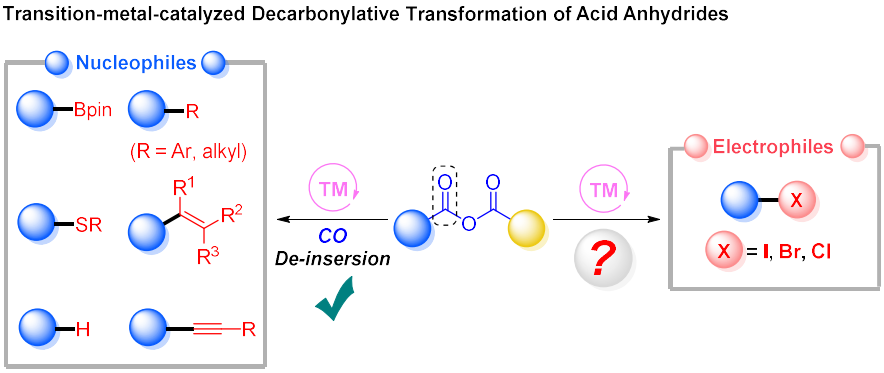

Acid anhydrides as “activated carboxylic acids” open new doors for organic synthesis as active, inexpensive and stable electrophiles after umpolung from corresponding acid. The simplest acid anhydride, acetic anhydride (Ac_2O), has reached a production scale of about 3 million tons/year due to its industrial application.[12] More importantly, acid anhydrides can undergo facile oxidative addition and decarbonylation under transition metal catalysis, thus providing endless possibilities for subsequent transformations.[13] Indeed, transition metal-catalyzed decarbonylation of carboxylic acid derivatives has been systematically developed by chemists in recent years.[14] Nevertheless, considering the worrying stability of acyl chlorides and the inertness of esters and amides, chemists have developed acyl fluorides as new electrophiles with both reactivity and stability, and recently.[15] However, the relatively expensive synthesis cost of acyl fluorides has also limited the appreciation they have won to a certain extent. Therefore, in order to balance the reactivity, stability and cost, anhydrides are a potential candidate with their unique characteristics. Since Blum and Lipshes reported the intramolecular decarbonylative cyclization protocol of acid anhydrides under transition metal catalysis in 1969 by using Wilkinson's catalyst,[16] the decarbonylative transformation of acid anhydrides under transition metal catalysis has been involved in four-dimensional research modes, including elimination,[17] insertion and annulation,[18] C–H bond functionalization,[19] and cross-coupling reactions. Especially the decarbonylative cross-coupling reaction mode, a series of Mizoroki-Heck coupling,[20] Negishi coupling,[21] Suzuki-Miyaura coupling,[22] Sonogashira-Hagihara coupling,[23] Miyaura borylatioin,[24] thioetherification,[25] and reduction[26] of acid anhydrides have been revealed successively, and a variety of new nucleophilic reagents have been constructed. How to use the decarbonylation mode of acid anhydrides to construct new electrophilic reagents, especially aryl halides, still needs to be developed (**Scheme 3-2**). Therefore, combined with the Author's research experience in the previous chapter,[27] we tried to develop inexpensive and stable anhydrides as perfect reaction substrate candidates for palladium-catalyzed decarbonylation nucleophilic halogenation. To the author's delight, after a series of explorations, the author developed a protocol for Pd-catalyzed decarbonylative nucleophilic halogenation of acid anhydrides, among which the bulky Xantphos once again demonstrated the high compatibility and universality of Pd-mediated reductive elimination of C–I, C–Br and C–Cl bonds using inexpensive lithium halides (LiX) as the

halogen sources (**Scheme 3-3**). Crucially, we successfully allowed the removal of generated CO, which shifts the equilibrium toward product formation, through the design of a simple open system, significantly improving reaction efficiency, especially for substrates with electron-donating substituents, and constructed a series of aryl iodides, aryl bromides and aryl chlorides with good yields.

Scheme 3-3. Pd-catalyzed Decarbonylative Nucleophilic Halogenation of Acid Anhydrides.

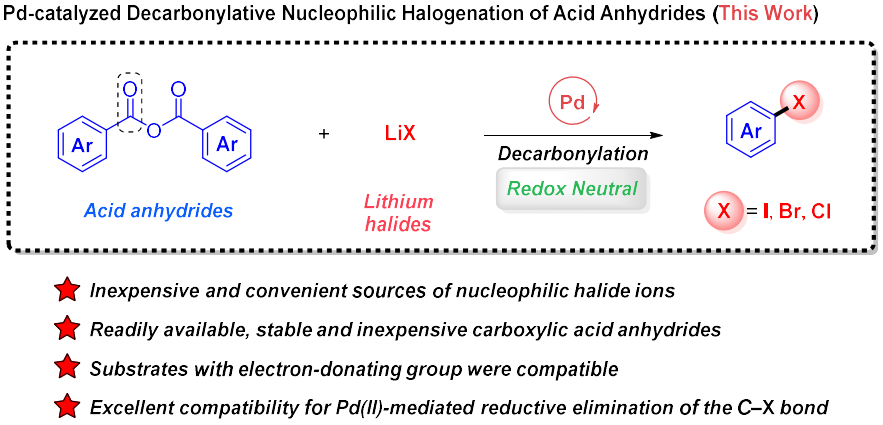

3-2 Results and Discussion

3-2-1 Optimization of Reaction Condition for Acid Anhydrides

Based on previous experience, the Author first built a $[PdCl(cinnamyl)]_2$/Xantphos catalytic system to verify its catalytic activity. Meanwhile, the Author selected 1-naphthoic anhydride (**1a**) as a substrate and lithium iodide (LiI) as an iodine source partner, using toluene as a solvent and reacting at 100 °C for 24 h. To the excitement of the Author, the expected decarbonylative nucleophilic iodination product 1-iodonaphthalene (**2a**) was obtained in a yield of 57% with 25% of the raw material remaining (Table 3-1, entry 1). Subsequently, in order to improve the conversion rate of the starting material, the Author increased the amount of LiI. When LiI (1.5 equiv) was added as an iodide source, the acid anhydride **1a** was completely consumed and the yield of the desired product 1-iodonaphthalene (**2a**) was increased to 87% (Table 3-1, entry 2). However, further increasing the amount of LiI did not further improve the yield of decarbonylative iodination. To the Author's delight, when the catalyst loading was slightly increased, the catalytic efficiency almost reached the highest level, and the decarbonylative iodination product **2a** was obtained with a yield of 97% (Table 3-1, entry 4). In addition, if the catalyst loading was further increased, the reaction yield would not be significantly affected (Table 3-1, entries 5 and 6). Based on this, the appropriate catalyst loading (3 mol %) and LiI dosage (1.5 equiv) were determined for further investigations to optimize the reaction conditions.

Table 3-1. Effect of the Amount of LiI and Pd catalyst in Catalytic Decarbonylative Iodination of **1a**.

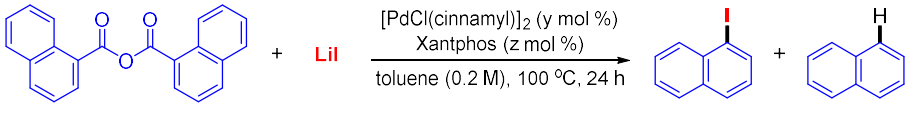

1a (0.2 mmol) (x equiv) **2a** **3a**

entry	**LiI (x equiv)**	**Pd/Xantphos (1:5) (y/z mol %)**	**1a** (%)[a]	yield (%)[a]	
				2a	**3a**
1	1.1	2.5/12.5	25	57	<1
2	1.5	2.5/12.5	0	86	<1
3	2	2.5/12.5	0	83	<1
4	**1.5**	**3/15**	**0**	**97**	**<1**
5	1.5	3.5/17.5	0	95	<1
6	1.5	4/20	0	96	<1

Reaction condition: **1a** (0.2 mmol, 1 equiv), $[PdCl(cinnamyl)]_2$ (y mol %), Xantphos (z mol %), LiI (x equiv), toluene (0.2 M), 24 h, under N_2. [a] NMR yields were determined by ^1H NMR using dibromomethane as the internal standard.

On the other hand, the author tried to screen out a matching iodine source, so a series of nucleophilic iodine reagents were considered, including NaI, KI, tetrabutylammonium iodide (TBAI) and 1-iodobutane in addition to LiI (Table 3-2, entries 2–5). However, other iodine sources were not compatible with the catalytic system due to their weak nucleophilicity. Therefore, LiI was once again used as the only nucleophilic iodine source for the decarbonylation iodination of anhydrides with its excellent properties.

Table 3-2. Effect of Iodine Sources in Catalytic Decarbonylative Iodination of **1a**.

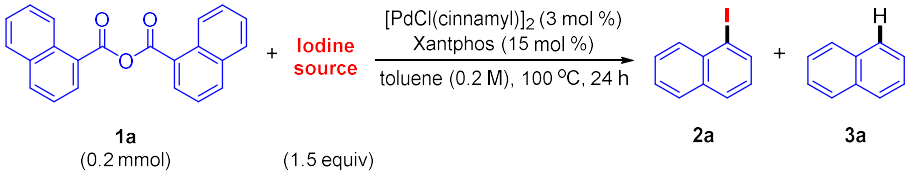

1a (0.2 mmol) (1.5 equiv) **2a** **3a**

entry	iodine source	**1a** (%)[a]	yield (%)[a]	
			2a	**3a**
1	**LiI**	**0**	**97**	**<1**
2	NaI	87	<5	<1
3	KI	91	<5	<1
4	tetrabutylammonium iodide (TBAI)	80	<5	<1
5	1-iodobutane	86	<5	<1

Reaction condition: **1a** (0.2 mmol, 1 equiv), $[PdCl(cinnamyl)]_2$ (3 mol %), Xantphos (15 mol %), toluene (0.2 M), 100 °C, 24 h, under N_2. [a] NMR yields were determined by ^1H NMR using dibromomethane as the internal standard.

In the next stage, the authors started to explore and investigate the anti-interference ability of the catalytic system. The first thing to be considered was different ligands, especially bidentate phosphine ligands with large bite angles similar to Xantphos. Therefore, after a series of screening of bidentate phosphine ligands, it was found (Table 3-3, entries 1–11) that, similar to the decarbonylation iodination of acyl halides, only DPEphos and dtbpf could give moderate yields in the designed catalytic transformation (Table 3-3, entries 4 and 11), and the remaining bidentate ligands were not suitable for the expected transformation. In addition, after screening different monodentate phosphine ligands, the author found (Table 3-3, entries 12–19) that neither bulky nor normal monodentate phosphine ligands were compatible with the catalytic system. On this basis, Xantphos deserves to be named as the only suitable ligand due to its strong charm, which not only relies on its steric hindrance effect, but also may be related to its non-innocence, in other words, it is helpful to generate the phosphonium salts, to some extent, to mediate the outer-sphere nucleophilic substitution step and accelerate nucleophilic iodination.

Table 3-3. Effect of Ligands in Catalytic Decarbonylative Iodination of **1a**.

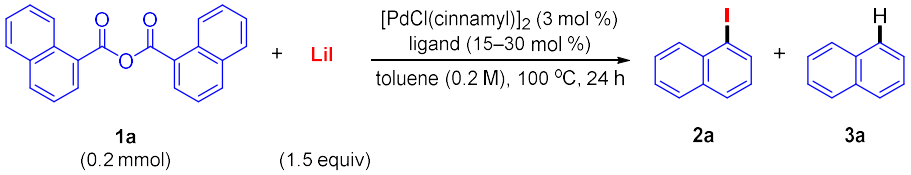

1a (0.2 mmol) (1.5 equiv) **2a** **3a**

entry	ligand	**1a** (%)[a]	yield (%)[a]	
			2a	**3a**
1	**Xantphos (15 mol %)**	**0**	**97**	**<1**
2	CyXantphos (15 mol %)	54	<1	<1
3	*t*-BuXantphos (15 mol %)	62	<1	<1
4	DPEphos (15 mol %)	46	34	<1
5	dpppent (15 mol %)	46	<1	<1
6	dppb (15 mol %)	64	<1	<1
7	dppp (15 mol %)	58	<1	<1
8	dppe (15 mol %)	38	<1	<1
9	dcype (15 mol %)	53	<1	<1
10	dppf (15 mol %)	43	13	<1
11	dtbpf (15 mol %)	10	37	<1
12	PPh_3 (30 mol %)	68	<1	<1
13	PCy_3 (30 mol %)	94	<1	<1
14	$P(t\text{-}Bu)_3 \cdot HBF_4$ (30 mol %)	7	<1	<1
15	BrettPhos (30 mol %)	23	5	<1
16	SPhos (30 mol %)	40	<1	<1
17	RuPhos (30 mol %)	30	4	<1
18	*t*-BuXPhos (30 mol %)	60	<1	<1
19	XPhos (30 mol %)	51	3	2

Reaction condition: **1a** (0.2 mmol, 1 equiv), $[PdCl(cinnamyl)]_2$ (3 mol %), LiI (0.3 mmol), toluene (0.2 M), 100 °C, 24 h, under N_2. [a] NMR yields were determined by ^1H NMR using dibromomethane as the internal standard.

Regularly, the Author also investigated different Pd catalyst precursors. The results indicated that the remaining Pd(II) catalyst precursors, $PdCl_2$ and $Pd(OAc)_2$, are completely incompatible with this transformation (Table 3-4, entries 2 and 3). Precisely, two common Pd(0) species, $Pd(dba)_2$ and $Pd_2(dba)_3$, can be used for the designed catalytic decarbonylative transformation, but they are less efficient than $[PdCl(cinnamyl)]_2$,

affording the desired product 1-iodonaphthalene (**2a**) in 57% and 68% yields, respectively (Table 3-4, entries 4 and 5). Finally, the Author also wondered whether the Pd catalyst could be replaced by a more inexpensive but similar Ni catalyst, so the Author screened several common Ni(0) or Ni(II) species and suggested that they were completely unsuitable for catalyzing decarbonylative iodination (Table 3-4, entries 6–8). Therefore, the [PdCl(cinnamyl)]$_2$/Xantphos catalytic system was selected as a suitable catalytic system.

Table 3-4. Effect of Transition Metal Precursors in Catalytic Decarbonylative Iodination of **1a**.

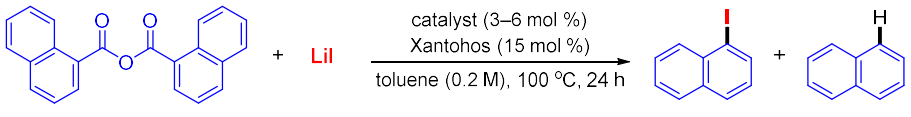

1a (0.2 mmol) (1.5 equiv) **2a** **3a**

entry	**catalyst**	**1a** (%)[a]	yield (%)[a]	
			2a	**3a**
1[b]	**[PdCl(cinnamyl)]$_2$**	**0**	**97**	**<1**
2[c]	$PdCl_2$	45	<1	<1
3[c]	$Pd(OAc)_2$	60	<1	<1
4[c]	$Pd(dba)_2$	8	57	<1
5[b]	$Pd_2(dba)_3$	1	68	<1
6[c]	$Ni(cod)_2$	49	<1	<1
7[c]	$NiCl_2$	48	<1	<1
8[c]	$Ni(acac)_2$	48	<1	<1

Reaction condition: **1a** (0.2 mmol, 1 equiv), catalyst (3–6 mol %), Xantphos (15 mol %), LiI (0.3 mmol), toluene (0.2 M), 100 °C, 24 h, under N_2. [a] NMR yields were determined by ^{1}H NMR using dibromomethane as the internal standard. [b] Catalyst (3 mol %). [c] Catalyst (6 mol %).

In addition, the Author also explored the effect of solvent on decarbonylative nucleophilic iodination of acid anhydrides. By investigating four solvents other than toluene, namely THF, 1-4-dioxane, 1,2-dichloroethane (DCE), and *N*,*N*-dimethylformamide (DMF), the results indicated that although ether solvents can

construct the desired product 1-iodonaphthalene (**2a**) with moderate yields (Table 3-5, entries 3 and 4), their own ring-opening reaction as a side reaction in this system will dramatically reduce the chemoselectivity. The remaining DCE and DMF as solvents are completely inconsistent with the transformation mode (Table 3-5, entries 2 and 5). Therefore, the appropriate solvent was determined to be toluene.

Table 3-5. Solvent Effect in Catalytic Decarbonylative Iodination of **1a**.

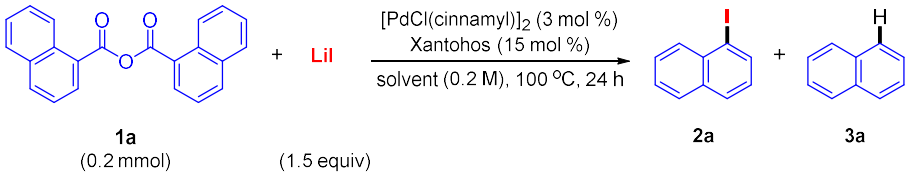

entry	**solvent**	**1a** (%)[a]	yield (%)[a]	
			2a	**3a**
1	**toluene**	**0**	**97**	**<1**
2	DCE	65	3	<1
3	THF	0	30	<1
4	1,4-dioxane	0	33	<1
5	DMF	45	0	<1

Reaction condition: **1a** (0.2 mmol, 1 equiv), [PdCl(cinnamyl)]$_2$ (3 mol %), Xantphos (15 mol %), LiI (0.3 mmol), 100 °C, 24 h, under N_2. [a] NMR yields were determined by ^{1}H NMR using dibromomethane as the internal standard.

In summary, the optimized reaction conditions can be basically determined: [PdCl(cinnamyl)]$_2$ (3 mol %)/Xantphos (15 mol %) is used as a satisfactory catalytic system, 1-naphthoic anhydride (**1a**) is used as a substrate, LiI (1.5 equiv) is used as an iodine source, and toluene is used as a solvent. The reaction is carried out at 100 °C for 24 h to obtain the expected decarbonylative nucleophilic iodination product 1-iodonaphthalene (**2a**) with nearly quantitative yield and good chemoselectivity.

Finally, in order to investigate the sensitivity and influencing factors of the established reaction conditions, the authors conducted several control experiments (Table 3-6): Initially, the Author found that reducing the amount of the ligand Xanphos from 15 mol % to 6 mol % would lead to a significant decrease in the yield of the decarbonylative iodination product 1-iodonaphthalene (**2a**) (Table 3-6, entry 2). This once again emphasizes that the catalytic system is sensitive to the amount of ligand used. Excessive ligand helps to form tetracoordinated $(Xantphos)_2Pd(0)$ species, thereby improving the stability of the catalytic system and inhibiting the reverse reaction of the formed aryl iodide. In addition, the authors found that reducing the reaction temperature from 100 °C to 80 °C also caused a dramatic decrease in conversion efficiency (Table 3-6, entry 3). Moreover, the Author also wondered the necessity of using symmetrical acid anhydrides. Therefore, the authors synthesized a mixed anhydride with good activity, 1-naphthoic pivalic anhydride (**1o**), as a substrate to verify its reactivity (Table 3-6, entry 4). The results indicated that only 25% of the decarbonylative iodination product 1-iodonaphthalene (**2a**) was obtained. Therefore, the addition of symmetrical acid anhydrides is necessary in the designed catalytic system. Finally, the reaction did not proceed at all in the absence of $[PdCl(cinnamyl)]_2$/Xantphos (Table 3-6, entry 5).

Table 3-6. Control Experiments in Catalytic Decarbonylative Iodination of **1a**.

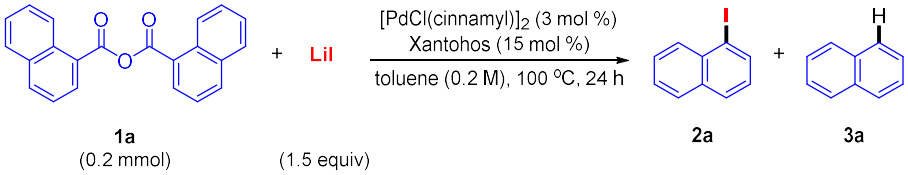

1a (0.2 mmol) (1.5 equiv) 2a 3a

entry	deviations from standard conditions	yield (%)[a]	
		2a	**3a**
1	**none**	**97**	**<1**
2	Xantphos (6 mol %) instead of Xantphos (15 mol %)	70	<1
3	80°C instead of 100°C	55	<1
4	1-naphthoic pivalic anhydride (**1o**) instead of **1a**	25	<1
5	w/o [PdCl(cinnamyl)]$_2$ and Xantphos	0	0

Reaction condition: **1a** (0.2 mmol, 1 equiv), [PdCl(cinnamyl)]$_2$ (3 mol %), Xantphos (15 mol %), LiI (0.3 mmol), toluene (0.2 M), 100 °C, 24 h, under N_2. [a] NMR yields were determined by ^{1}H NMR using dibromomethane as the internal standard.

Subsequently, after establishing a suitable catalytic system, the Author tried to measure its compatibility first, especially for substrates with electron-donating groups, which were proven to be difficult to be compatible with in the previous chapter. Therefore, the Author selected 3-methoxybenzoic anhydride (**1d**) as the reaction substrate to verify its reactivity under standard conditions (Table 3-7, entry 1). Unfortunately, the designed catalytic system can only afford the expected product 3-methoxyiodobenzene (**2d**) in a yield of 36%. In order to further overcome this limitation, the Author briefly optimized the protocol. Firstly, the Author empirically increased the reaction temperature due to the sluggish oxidative addition of acid anhydrides with electron-donating substituents, but this change did not effectively improve the reaction yield (Table 3-7, entry 2). Crucially, when the Author slightly increased the amount of catalyst/ligand, the desired nucleophilic iodination product could be dramatically improved, and **2d** was obtained in 53% yield (Table 3-7, entry 3). Based on this, the Author postulated that the cause of this result

might be due to catalyst poisoning. Therefore, in order to further weaken the catalyst deactivation, an open system was introduced into the protocol, which was expected to promote the escape of possible catalyst poisons, molecular iodine (I_2), due to the volatility of iodine. To the Author's delight, this measure effectively improved the catalytic efficiency, and the desired decarbonylative iodination product **2d** was obtained in 71% yield (Table 3-7, entry 4).

Table 3-7. Optimized Reaction Condition for Decarbonylative Iodination of 3-Methoxybenzoic Anhydride (**1d**).

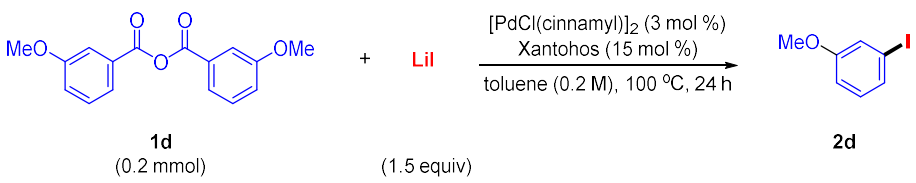

entry	**deviations from standard conditions**	yield of **2d** (%)[a]
1	none	36
2	140 °C instead of 100 °C	29
3	[PdCl(cinnamyl)]$_2$ (3.5 mol %)/Xantphos (17.5 mol %)	53
4[b]	**[PdCl(cinnamyl)]$_2$ (3.5 mol %)/Xantphos (17.5 mol %)**	**71**

Reaction condition: **1b** (0.2 mmol, 1 equiv), [PdCl(cinnamyl)]$_2$ (3 mol %), Xantphos (15 mol %), LiI (0.3 mmol), toluene (0.2 M), 100 °C, 24 h, under N_2. [a] NMR yields were determined by ^{1}H NMR using dibromomethane as the internal standard. [b] Open system.

From another perspective, the Author tried to further investigation whether the established Pd-catalyzed decarbonylative iodination system could still be extended to decarbonylative bromination and chlorination when acid anhydride was used as a substrate. Therefore, the Authors once again used 1-naphthoic anhydride (**1a**) as a substrate and LiBr as a bromination partner to explore the optimized reaction conditions (Table 3-8). To the authors' delight, the Pd-catalyzed system can be perfectly applied to the decarbonylative

bromination mode by simply increasing the reaction temperature (Table 3-8, entry 4), and the expected decarbonylative bromination product 1-bromonaphthalene (**4a**) can be obtained in nearly quantitative yield.

Table 3-8. Effect of Temperature for Catalytic Decarbonylative Bromination of **1a**.

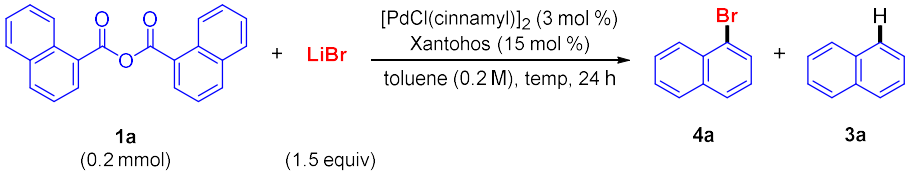

1a (0.2 mmol) (1.5 equiv) **4a** **3a**

entry	**temp (°C)**	**1a** (%)[a]	yield (%)[a]	
			4a	**3a**
1	100	>99	<1	<1
2	120	41	33	<1
3	140	2	77	<1
4	**160**	**0**	**95**	**<1**

Reaction condition: **1a** (0.2 mmol, 1 equiv), [PdCl(cinnamyl)]$_2$ (3 mol %), Xantphos (15 mol %), LiBr (0.3 mmol), 24 h, under N_2. [a] NMR yields were determined by ^{1}H NMR using dibromomethane as the internal standard.

However, for decarbonylation chlorination, although it can be achieved with high chemoselectivity, the conversion rate of this protocol is relatively low due to the weak nucleophilicity and low solubility of LiCl. When LiCl (3 equiv) is added, the decarbonylative chlorination product 1-chloronaphthalene (**5a**) can be afforded in 56% yield with 41% of the starting material remaining (Table 3-9, entry 2). However, even the continuous increase in the amount of LiCl still does not improve the efficiency of decarbonylative conversion (Table 3-9, entries 3–6). Nevertheless, although further increasing the temperature to 180 °C leads to a slight increase in yield (Table 3-9, entry 7), it will make the reaction operation impractical and therefore not ideal. Therefore, the Author still kept the reaction temperature at 160 °C and changed the concentration of LiCl, but even diluting the catalytic system would not affect the expected decarbonylative

nucleophilic chlorination (Table 3-9, entries 8–10). Therefore, the authors determined the amount of LiCl to be 3 equivalents and kept the temperature and concentration unchanged, thus taking this as the optimal reaction condition.

Table 3-9. Effect of Temperature, Concentration, and the Amount of LiCl for Catalytic Decarbonylative Chlorination of **1a**.

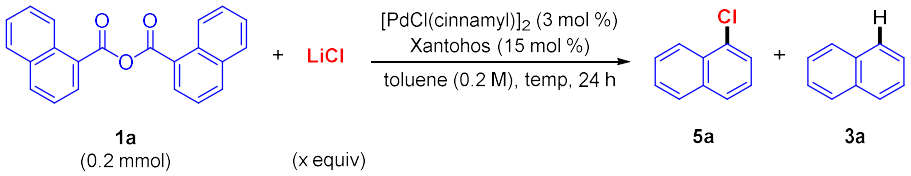

entry	LiCl (x equiv)	1a (%)[a]	yield (%)[a]	
			5a	3a
1	1.5	47	49	<1
2	**3**	**41**	**56**	**<1**
3	4	40	56	<1
4	6	40	58	<1
5	8	39	55	<1
6	10	39	56	<1
7[b]	3	29	64	<1
8[c]	3	42	53	<1
9[d]	3	40	53	<1
10[e]	3	34	39	<1

Reaction condition: **1a** (0.2 mmol, 1 equiv), $[PdCl(cinnamyl)]_2$ (3 mol %), Xantphos (15 mol %), 160 °C, 24 h, under N_2. [a] NMR yields were determined by ^1H NMR using dibromomethane as the internal standard. [b] 180 °C. [c] Toluene (0.5 mL). [d] Toluene (2 mL). [e] Toluene (3 mL).

3-2-2 Substrate Scope of Decarbonylative Halogenation

In the subsequent phase, the author initiated a comprehensive study on the substrate compatibility for decarbonylative iodination (**Scheme 3-4**). Initially, several redox-neutral anhydrides demonstrated excellent compatibility with the optimized

conditions, such as 1-naphthoic anhydride (**1a**), benzoic anhydride (**1b**), and 2-naphthoic anhydride (**1c**). These substrates yielded the corresponding decarbonylative iodination products, namely 1-iodonaphthalene (**2a**), iodobenzene (**2b**), and 2-iodonaphthalene (**2c**), in satisfactory yields.

Next, attention was directed towards evaluating the influence of electronic effects on substrate performance in this reaction. Specifically, the focus was on the applicability of anhydrides bearing electron-donating substituents within this catalytic framework, such as 3-methoxy (**1d**) and 4-methoxy-benzoic anhydrides (**1e**). Under the optimized conditions, these substrates only produced the desired iodinated products in low yields due to catalyst deactivation caused by poisoning. To mitigate this adverse effect, an unexpected yet effective solution was discovered—employing an open reaction system. This adjustment significantly improved the yields of 3-methoxy-iodobenzene (**2d**) and 4-methoxy-iodobenzene (**2e**), resulting in yields of 71% and 32%, respectively. This improvement is attributed to the open system allowing the removal of generated CO, which shifts the equilibrium toward product formation.

Furthermore, the compatibility of additional electron-donating substituents was explored, including 4-*t*-Bu, 4-Ph, and 3-Ph groups. Notably, raising the reaction temperature enabled these substrates to undergo decarbonylative transformation with high efficiency, delivering the corresponding iodinated products—4-*tert*-butyl iodobenzene (**2f**), 4-iodobiphenyl (**2g**), and 3-iodobiphenyl (**2h**)—in yields of 60%, 55%, and 81%, respectively. The enhanced reactivity observed at elevated temperatures is likely due to the increased energy requirement for facilitating the thermodynamically less favorable oxidative addition of anhydrides containing electron-donating groups.

Scheme 3-4. Substrate Scope for Decarbonylative Nucleophilic Halogenation of Acid Anhydrides **1**.

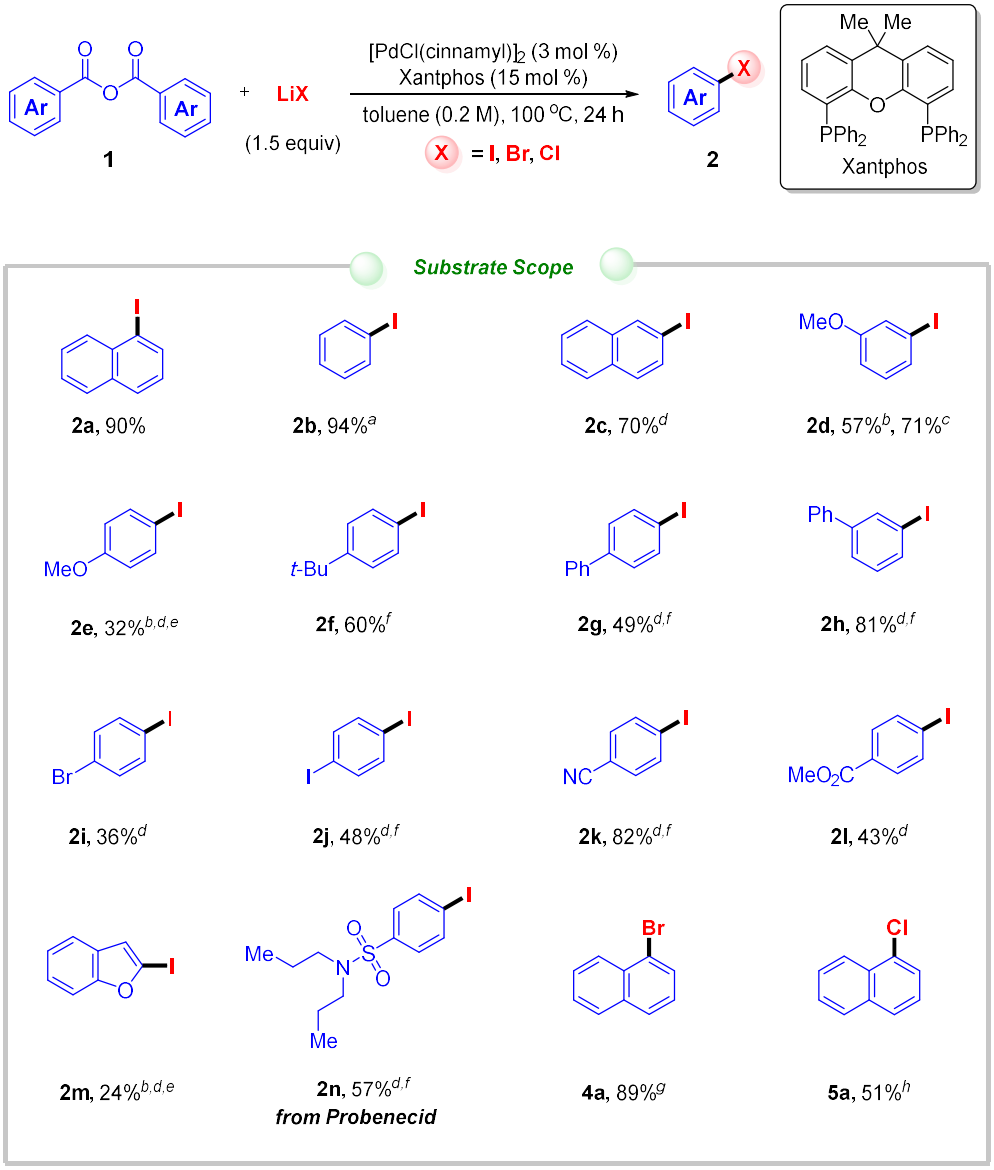

Reaction conditions: acid anhydrides **1** (0.2 mmol, 1 equiv), [PdCl(cinnamyl)]$_2$ (3 mol%), Xantphos (15 mol%), LiI (1.5 equiv), toluene (0.2 M), 100 °C, 24 h. Isolated yields are shown unless otherwise indicated. [a] GC yield was determined using *n*-dodecane as an internal standard. [b] open system; toluene (0.1 M). [c] NMR yield was determined by ^{1}H NMR, using dibromomethane as an internal standard. [d] [PdCl(cinnamyl)]$_2$ (3.5 mol%), Xantphos (17.5 mol%). [e] 120 °C, 12 h. [f] 140 °C, 12 h. [g] 160 °C, LiBr (0.3 mmol, 1.5 equiv). [h] 160 °C, LiCl (0.6 mmol, 3 equiv).

Conversely, the Author examined the influence of electron-withdrawing substituents on this catalytic decarbonylation system. To our satisfaction, benzoic anhydrides containing

highly reactive bromine and iodine substituents proved unexpectedly suitable for this reaction. Specifically, they successfully delivered the corresponding decarbonylative iodinated products, 4-bromoiodobenzene (**2i**) and 1,4-diiodobenzene (**2j**), with moderate yields and high chemoselectivity. Moreover, anhydrides bearing strong electron-withdrawing groups, such as 4-CN and 4-CO_2Me, did not hinder the nucleophilic iodination process. These substrates afforded 4-iodobenzonitrile (**2k**) and methyl 4-iodobenzoate (**2l**) in yields of 82% and 43%, respectively, further underscoring the remarkable efficiency of this catalytic system.

Next, the Author tested the compatibility of heteroaromatic anhydrides, including benzofuran-2-carboxylic anhydride, with this decarbonylative transformation. Although the reaction proceeded, the yield of the corresponding iodinated product was somewhat reduced due to the simultaneous formation of decarbonylative reduction byproduct benzofuran. Finally, to illustrate the practical utility of this method in pharmaceutical synthesis, we explored Probenecid derivatives and found that they could still undergo successful nucleophilic iodination, delivering product **2m** in 57% yield.

Importantly, the Author discovered that this newly developed Pd-catalyzed system could be further adapted for constructing C–Br and C–Cl bonds by simply increasing the reaction temperature, owing to the highly endothermic nature of C–X bond reductive elimination. Notably, decarbonylative bromination produced 1-bromonaphthalene (**4a**) in an excellent 89% yield. However, the analogous chlorination reaction yielded 1-chloronaphthalene (**5a**) in only 51%, even when using 3 equivalents of LiCl as the chlorine source. Despite this lower yield, the catalytic system exhibited robust performance, with a conversion rate of 59%, likely limited by the weak nucleophilicity and poor solubility of LiCl.

3-2-3 Mechanistic Study

The Author conducted mechanistic studies based on their hypotheses to gain a deeper un-derstanding of the catalytic transformation. First of all, the Author performed time-course studies and monitored the $^{31}P\{^{1}H\}$ NMR spectra for the stoichiometric Pd-mediated decarbonylative nucleophilic iodination process to identify potential intermediates (**Scheme 3-5**).

Scheme 3-5. Monitoring the Stoichiometric Iodination of **1b** at Room Temperature, 50, and 75 °C by $^{31}P\{^{1}H\}$ NMR.

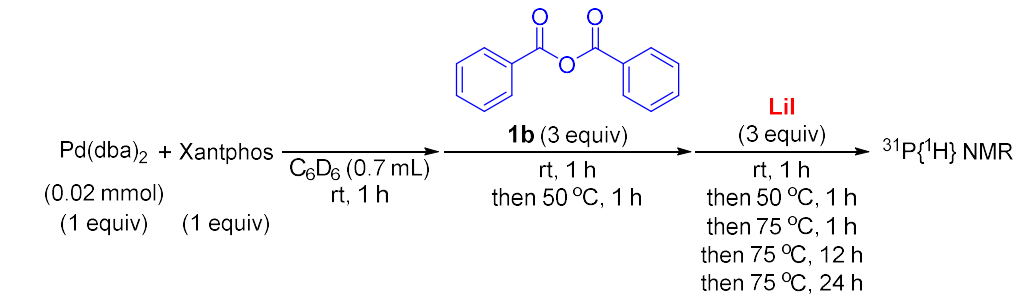

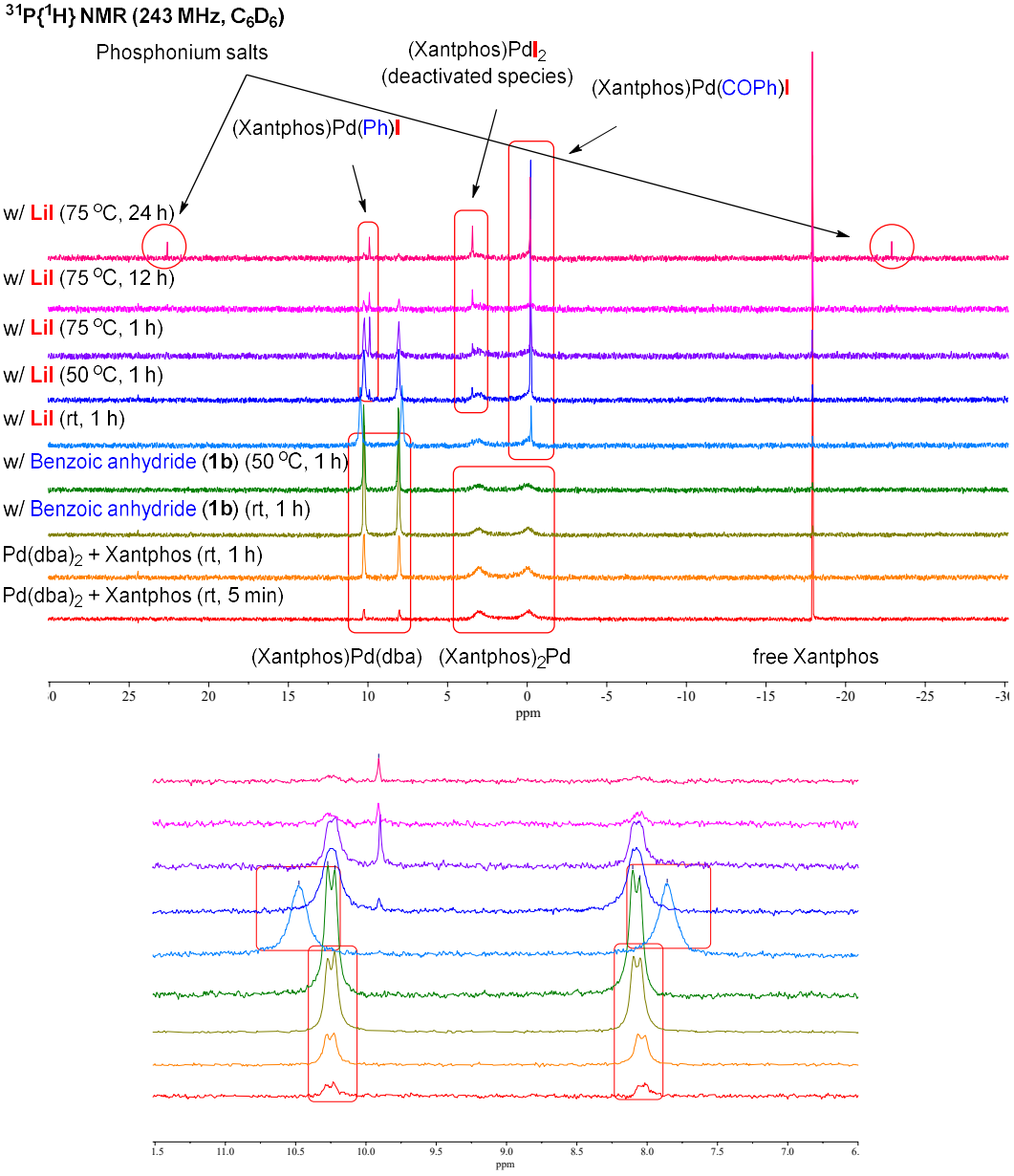

Initially, when $Pd(dba)_2$ and Xantphos were mixed, the previously reported $(Xantphos)_2Pd$ (two broad singlets at −0.1 and 3.1 ppm) and (Xantphos)Pd(dba) (two doublets at 8.1 and 10.2 ppm) were observed.[28] Upon the addition of benzoic anhydride (**1b**), the mixture was monitored to determine whether the expected oxidative addition had occurred. However, no significant changes were observed even when the temperature was increased from room temperature to 50 °C. Subsequently, upon adding LiI into the reaction mixture, the oxidative adduct *trans*-(Xantphos)Pd(II)(COPh)I[29] was detected at room temperature after 1 h. As the temperature was further increased (from 50 °C to 75 °C), the decarbonylative complex, *trans*-(Xantphos)Pd(II)(Ph)I,[29] was detected via the carbonyl de-insertion process. Based on the identification of these two key intermediates, we proposed a unimolecular fragment coupling (UFC) mechanism.[30] The core of this mechanism involves the in situ formation of acyl iodide, a transient intermediate, via nucleophilic substitution of the acid anhydride **1** with LiI. Crucially, as they have previously discussed,[27] the key to the success of this pathway lies in the rate of acyl iodide formation, which must occur slowly and gradually to ensure efficient conversion and avoid catalyst poisoning. Therefore, the Author monitored the reaction using ^1H NMR spectroscopy at room temperature, 50 °C, and 100 °C to investigate whether acyl iodide forms from the mixture of 1-naphthoic anhydride (**1a**) and LiI (**Tables 3-9–11**).

Table 3-9. Time-Course Study for the Reaction of 1-Naphthoic Anhydride (**1a**) with LiI at rt.

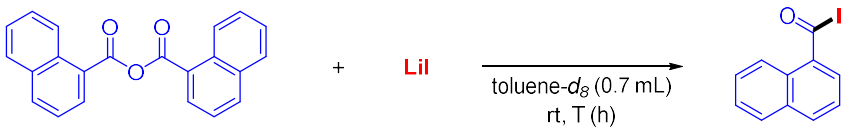

1a (0.05 mmol) + LiI (1.5 equiv) → **6**

entry	time (h)	yield of **1a** (%)[a]	yield of **6** (%)[a]
1	0	>99	0
2	1	>99	0
3	2	>99	0
4	3	>99	0
5	6	>99	0

Reaction conditions: **1a** (0.05 mmol, 1 equiv), LiI (0.075 mmol), toluene (0.2 M), rt, under N_2. [a] NMR yields were determined by ^{1}H NMR using dibromomethane as an internal standard.

Table 3-10. Time-Course Study for the Reaction of 1-Naphthoic Anhydride (**1a**) with LiI at 50 °C.

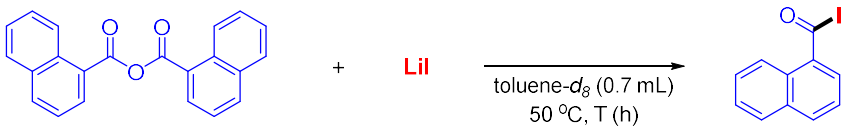

1a (0.05 mmol) + LiI (1.5 equiv) → **6**

entry	time (h)	yield of **1a** (%)[a]	yield of **6** (%)[a]
1	0	>99	0
2	1	>99	<1
3	2	>99	<1
4	3	>99	<1
5	6	>99	<1

Reaction conditions: **1a** (0.05 mmol, 1 equiv), LiI (0.075 mmol), toluene (0.2 M), 50 °C, under N_2. [a] NMR yields were determined by ^{1}H NMR using dibromomethane as an internal standard.

Table 3-11. Time-Course Study for the Reaction of 1-Naphthoic Anhydride (**1a**) with LiI at 100 °C.

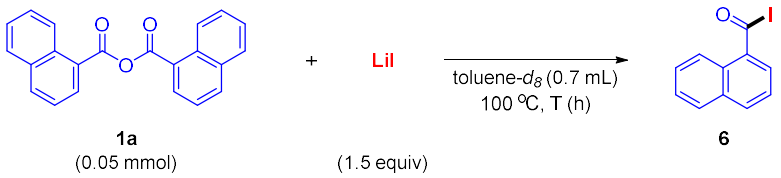

1a (0.05 mmol) (1.5 equiv) **6**

entry	time (h)	yield of **1a** (%)[a]	yield of **6** (%)[a]
1	0	>99	0
2	1	96	4
3	2	90	10
4	3	81	13
5	6	61	25
6	12	27	42
7	24	<1	47

Reaction conditions: **1a** (0.05 mmol, 1 equiv), LiI (0.075 mmol), toluene (0.2 M), 100 °C, under N_2. [a] NMR yields were determined by ^1H NMR using dibromomethane as an internal standard.

However, no acyl iodide (**6**) was detected at room temperature (**Tables 3-9**), and only trace amounts were observed at 50 °C (**Tables 3-10**). At 100 °C, only 4% of 1-naphthoyl iodide (**6**) was formed after 1 h, and the yield remained low at 47% even after 24 h. Additionally, a white solid, identified as lithium 1-naphthoate (**7**), precipitated due to its low solubility in toluene (**Tables 3-11**).

Nevertheless, this result contradicts the experimental observation that no reaction occurred when benzoic anhydride (**1b**) was added to the $Pd(dba)_2$/Xantphos mixture. Yet, upon subsequent addition of LiI, the *trans*-(Xantphos)Pd(II)(COPh)I signal was detected even at room temperature. To investigate further, we added LiI to the $Pd(dba)_2$/Xantphos mixture and recorded the $^{31}P\{^1H\}$ NMR spectrum (**Scheme 3-6**). After 1 h at room temperature, the signal for $(Xantphos)_2Pd$ remained largely unchanged, while the signal as signable to (Xantphos)Pd(dba) disappeared, and two new singlets at 7.4 and 11.0 ppm emerged. Furthermore, when benzoic anhydride (**1b**) was added to this mixture, the *trans*-(Xantphos)Pd(II)(COPh)I signal appeared at room temperature after 1 h. These results suggest that LiI does not react with acid anhydride **1** at room temperature without

the catalyst, but in the presence of the catalyst, an apparent oxidative addition of the acyl iodide occurs.

Scheme 3-6. Monitoring the Stoichiometric Iodination of **1b** at Room Temperature, 50, 75, and 100 °C by $^{31}P\{^{1}H\}$ NMR.

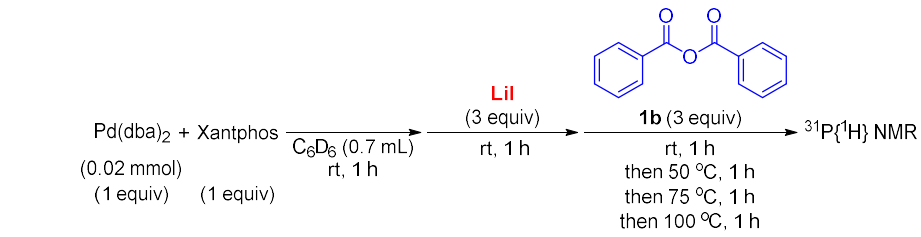

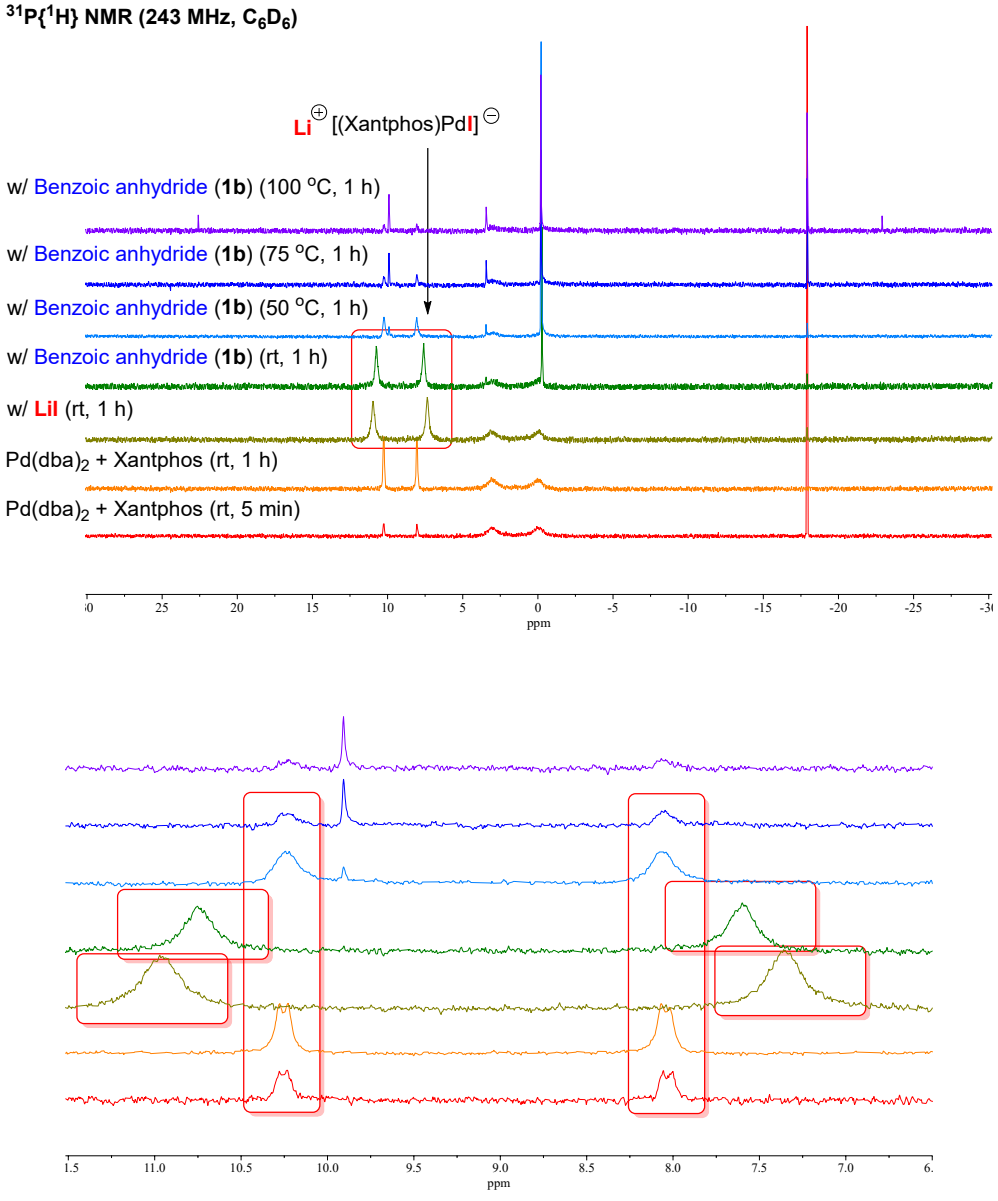

3-2-4 Proposed Mechanism

Based on a brief mechanistic study, we propose two possible mechanisms (**Scheme 3-7**). The first mechanism follows a decarbonylative unimolecular fragment coupling (UFC) pathway (Path A). Initially, LiI-mediated nucleophilic substitution of the acid anhydride **1** generates acyl halide intermediate **B**. This acyl halide then undergoes oxidative addition with the active Pd(0) complex **A**, forming the acyl–Pd–X intermediate **C**. Subsequent carbonyl de-insertion and reductive elimination generate the desired decarbonylative halogenated product **2** while regenerating the active Pd(0) catalyst **A**. In an alternative mechanism (Path B), the palladium catalyst is converted into the anionic palladate complex **E** in the presence of lithium halide.[31] This anionic complex **E**, being electron-rich, facilitates the facile oxidative addition of acid anhydride **1**, leading to the formation of the common intermediate **C**. The subsequent steps proceed similarly to Path A.

Scheme 3-7. Two Plausible Reaction Mechanisms.

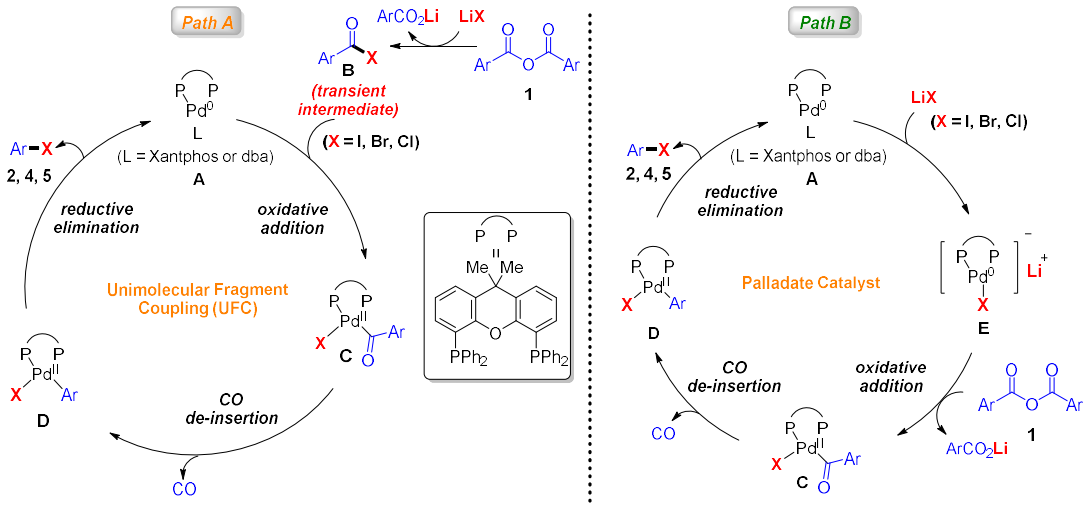

Finally, regarding the outer-sphere nucleophilic substitution mechanism mentioned in the previous chapter,[32] according to the current experimental results, this does not seem to be the most likely reaction mechanism. Although when 1-naphthoic anhydride (**1a**) is used as a reaction substrate for decarbonylative nucleophilic halogenation, we can detect the corresponding iodobenzene, bromobenzene and chlorobenzene by GC-MS under

standard conditions, their sources may be either the scrambling of the phenyl group in the outer-sphere nucleophilic substitution step or the over-reaction. Considering that the nucleophilicity of the iodine anion in LiI seems to be sufficient for transmetalation, it seems unnecessary to generate the phosphonium salts through C–P bond reductive elimination and then perform outer-sphere nucleophilic substitution. Therefore, we are currently unable to determine the identity of the phosphonium salts, whether it is a reaction intermediate or an over-reaction product. Based on this, we will not discuss and introduce this postulation in detail in this chapter.

3-3 Summary

In summary, the Author have disclosed an efficient Pd-catalyzed decarbonylative nucleophilic halogenation model for acid anhydrides, in which anhydrides, with their unique metastable advantages, avoid the inconvenience caused by the instability of acyl chlorides and the high cost of expensive acyl fluorides, demonstrating their great potential in the future of synthetic chemistry and related fields. In addition, the bulky and low-cost Xantphos is once again proposed as a highly universal and compatible ligand for thermodynamically and kinetically unfavorable processes – Pd(II)-mediated reductive elimination of C–X bond – and can facilely mediate the palladium-catalyzed reductive elimination of C–Cl bonds, C–Br bonds, and even C–I bonds and efficiently mediate a series of decarbonylative nucleophilic chlorinations, brominations, and even iodinations and the construction of a series of aryl chlorides, aryl bromides, and even aryl iodides with good efficiency. Crucially, this protocol uses an open system, to some extent, to accelerate the removal of generated CO, which shifts the equilibrium toward product formation, then improving the compatibility of substrates with electron-donating substituents, especially anise substrates. Finally, through the study of the mechanism, the Author described two plausible mechanisms, including indirect unimolecular fragment coupling (IUFC) mechanism via decarbonylation (path A) and palladate-mediated facile oxidative addition of acid anhydrides (path B). The rate of generation of the transient intermediate acyl iodide in the process is the key to the success of the protocol in path A. The unique characteristics of the anhydride can form corresponding lithium carboxylates with the iodine salt, thereby significantly reducing the formation rate of acyl iodide to ensure high catalytic efficiency. The Author is convinced that this research model will provide strong support and help for the subsequent development of related fields.

3-4 Experimental Section

3-4-1 General Instrumentation and Chemicals

Instrumentation

Unless otherwise stated, all reactions were carried out under an N_2 atmosphere using standard Schlenk techniques or a glovebox. Solvents employed as eluents for routine operations, as well as dehydrated solvents, were purchased from commercial suppliers and used without any further purification. Glassware was dried in an oven at 130 °C and evacuated before use. Merck precoated TLC plates (silica gel 60 F_{254}, 0.25 mm) were used for thin-layer chromatography (TLC) analyses throughout this work. Silica gel column chromatography was carried out using Silica gel 60 N (spherical, neutral, 40–100 μm) from Kanto Chemicals Co., Ltd. NMR spectra (^{1}H, ^{13}C{1H}, ^{19}F{^{1}H}, and ^{31}P{^{1}H}) were recorded on Mercury-400 (400 MHz) or Mercury-600 (600 MHz) spectrometers. Chemical shifts (δ) are reported in parts per million relatives to $CDCl_3$ at 7.26 ppm for ^{1}H and at 77.16 ppm for ^{13}C{^{1}H}, respectively. The ^{19}F{^{1}H} NMR spectra were referenced using CCl_3F (δ = 0.00 ppm) as an external standard. GC yields were determined by analyzing the crude mixture using n-dodecane as an internal standard on a Shimadzu GC-14A equipped with a flame ionization detector, using Shimadzu Capillary Column (CBP1-M25-025) and Shimadzu C-R6A-Chromatopac integrator. Infrared spectra were recorded on a Shimadzu IR Prestige-21 spectrophotometer. Elemental analyses were carried out with a Perkin-Elmer 2400 CHN elemental analyzer at Okayama University. High-resolution mass spectra were obtained on a JEOL JMS-700 spectrometer in the electron ionization (EI) mode.

Chemicals

Unless specified otherwise, materials obtained from commercial suppliers were used without further purification. Palladium(II)(π-cinnamyl) chloride dimer ([PdCl(cinnamyl)]$_2$) (purity > 97%) was purchased from Tokyo Chemical Industry Co., Ltd. and Sigma-Aldrich Co. LLC. 4,5-Bis(diphenylphosphino)-9,9-dimethylxanthene (Xantphos) (purity > 98%) was purchased from Tokyo Chemical Industry Co., Ltd. Lithium iodide (purity > 97%) was purchased from FUJIFILM Co., Ltd. Lithium bromide (purity > 99%) and lithium chloride (purity > 98%) were purchased from Tokyo

Chemical Industry Co., Ltd.　Toluene (super dehydrated) was purchased from FUJIFILM Co., Ltd.　Benzoic anhydride (**1b**) (purity > 97%) weas purchased from Tokyo Chemical Industry Co., Ltd.

3-4-2 Experimental Procedures of Synthesis of Starting Materials

Acid anhydrides were purchased from commercial suppliers or synthesized according to the methods described below (**Scheme 3-6**).

Scheme 3-6. Commercially Available or Synthesized Acid Anhydrides (**1**).

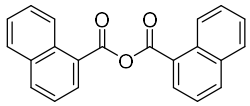

1a
CAS: 64985-86-0

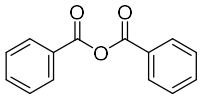

1b
CAS: 93-97-0
Commercially available

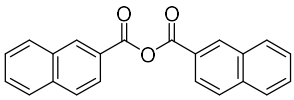

1c
CAS: 20176-11-8

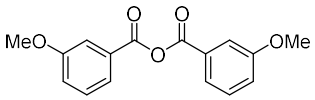

1d
CAS: 94611-94-6

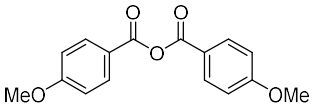

1e
CAS: 794-94-5

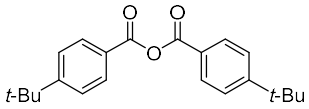

1f
CAS: 22201-45-2

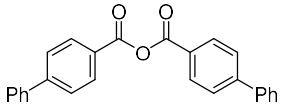

1g
CAS: 25327-57-5

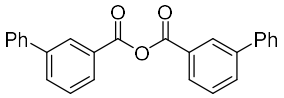

1h
CAS: 500690-59-5

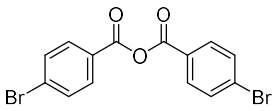

1i

CAS: 1633-33-6

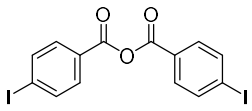

1j

CAS: 75474-06-5

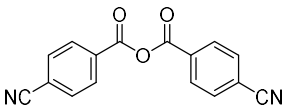

1k

CAS: 16657-25-3

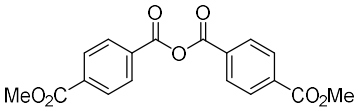

1l

CAS: 860708-87-8

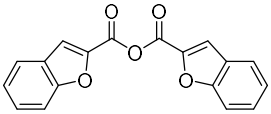

1m

CAS: 51885-74-6

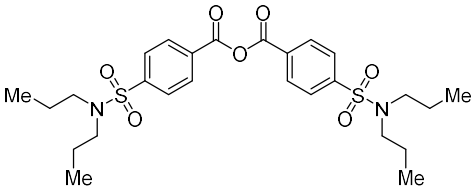

1n

CAS: 2734045-29-3

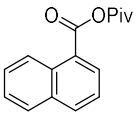

1o

unknown

Procedure A: General Procedure for the Synthesis of **1a**–**1j** and **1l**–**1n**[33]

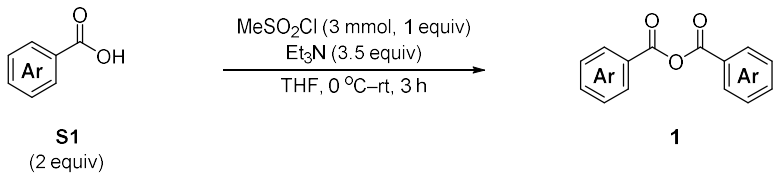

In a Schlenk tube, carboxylic acid (**S1**) (2 equiv, 6 mmol) was dissolved in super dehydrated THF (20 mL). Then the reaction tube was cooled to 0 °C. Methanesulfonyl chloride (1 equiv, 3 mmol, 232 μL) and Et_3N (3.5 equiv, 10.5 mmol, 1.5 mL) were then added dropwise at 0 °C *via* syringes. The resulting mixture was stirred for 3 h at room temperature. Subsequently, the reaction was quenched with saturated sodium bicarbonate ($NaHCO_3$) (aq.) and extracted three times with EtOAc (3 x 30 mL). The combined organic layer was dried over anhydrous $MgSO_4$, filtrated, and concentrated under reduced pressure. The residue was purified by filtration through a short pad of silica gel (3–5 cm thick x 3 cm diameter) using dichloromethane and hexane as eluents. All volatiles were evaporated under reduced pressure to afford pure acid anhydrides **1**, which were employed in the catalytic reactions without further purification.

Procedure B: General Procedure for the Synthesis of **1k**[34]

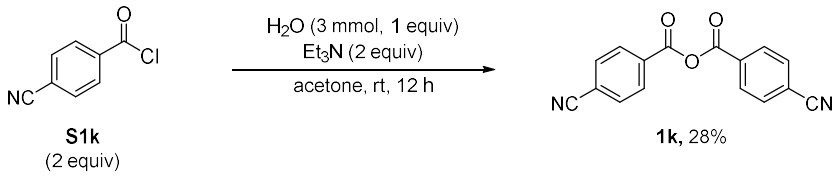

4-Cyanobenzoyl chloride (**S1k**, 2 equiv, 6 mmol, 993.5 mg) and water (1 equiv, 3 mmol, 54 μL) were added into an oven-dried flask equipped with a magnetic stir bar, and than mixed in 15 ml of acetone. Triethylamine (2 equiv, 6 mmol, 0.84 mL) was gradually introduced over a period of 1–2 min. The resulting mixture was stirred for 12 h at room temperature. Upon completion of the reaction, the resulting triethylamine hydrochloride precipitate was removed by filtration. The collected triethylamine hydrochloride was

rinsed with an additional 3 x 15–20 ml of acetone. The combined filtrates were dried over anhydrous $MgSO_4$, filtrated, and concentrated under reduced pressure. The residue was purified by filtration through a short pad of silica gel (3–5 cm thick x 3 cm diameter) using dichloromethane and hexane as eluents. All volatiles were evaporated under reduced pressure to afford pure 4-cyanobenzoic anhydride **1k** as the white solid with the yield of 28% (235.6 mg), which was employed in the catalytic reactions without further purification.

Procedure C: Procedure for the synthesis of **1o**[35]

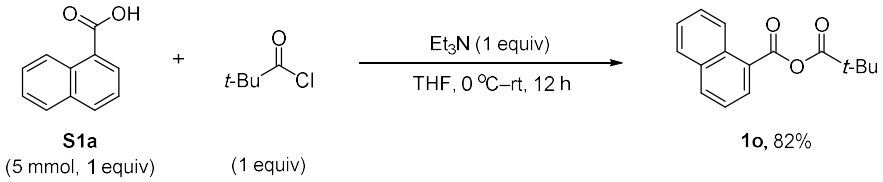

S1a
(5 mmol, 1 equiv)

(1 equiv)

1o, 82%

In a Schlenk tube, 1-naphthoic acid (**S1a**) (1 equiv, 5 mmol, 861 mg) was dissolved in super dehydrated THF (20 mL). Then the reaction tube was cooled to –15 °C. Freshly distilled pivaloyl chloride (1 equiv, 5 mmol, 0.61 mL) and Et_3N (1 equiv, 5 mmol, 0.7 mL) were then added dropwise at –15 °C *via* syringes. The resulting mixture was stirred for 12 h at room temperature. Subsequently, upon completion of the reaction, the resulting triethylamine hydrochloride precipitate was removed by filtration. The collected triethylamine hydrochloride was rinsed with an additional 3 x 20–25 ml of dichloromethane. The residue was purified by filtration through a short pad of neutral silica gel (3–5 cm thick x 3 cm diameter) using dichloromethane and hexane as eluents. All volatiles were evaporated under reduced pressure to afford pure mixed acid anhydrides **1o** as a colorless oil (1.0524 g, 82%), which were employed in the catalytic reactions without further purification.

1-Naphthoic anhydride (1a)

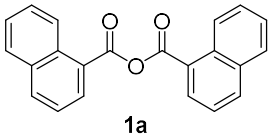

1a

Prepared according to procedure A (1.6207 g, 90%) (5.5 mmol scale) as a white solid. R_f = 0.5 (DCM/hexane = 1/1). 1H NMR (600 MHz, $CDCl_3$): δ 9.19 (d, J = 8.7 Hz, 2H), 8.44 (dd, J = 7.4, 1.3 Hz, 2H), 8.13 (d, J = 8.2 Hz, 2H), 7.93 (dd, J = 8.2, 1.4 Hz, 2H), 7.71 (ddd, J = 8.5, 6.8, 1.4 Hz, 2H), 7.61 (t, J = 7.5 Hz, 2H), 7.55 (t, J = 7.7 Hz, 2H); $^{13}C\{^1H\}$ NMR (151 MHz, $CDCl_3$): δ 163.02, 135.65, 134.00, 132.22, 131.94, 128.91, 128.89, 126.83, 125.69, 124.86, 124.54.

These data align with previously published reports in the literature.[36]

2-Naphthoic anhydride (1c)

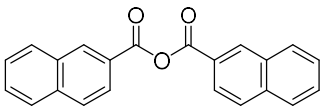

1c

Prepared according to procedure A (790.1 mg, 81%) as a white solid. R_f = 0.5 (DCM/hexane = 1/1). ^1H NMR (600 MHz, $CDCl_3$): δ 8.78 (d, J = 1.8 Hz, 2H), 8.19 (dd, J = 8.5, 1.8 Hz, 2H), 8.03–7.92 (m, 6H), 7.67 (ddd, J = 8.2, 6.8, 1.3 Hz, 2H), 7.60 (ddd, J = 8.1, 6.8, 1.2 Hz, 2H); $^{13}C\{^1H\}$ NMR (151 MHz, $CDCl_3$): δ 162.86, 136.32, 132.91, 132.53, 129.77, 129.35, 128.95, 128.03, 127.24, 126.16, 125.48.

These data align with previously published reports in the literature.[37]

3-Methoxybenzoic anhydride (1d)

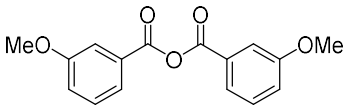

1d

Prepared according to procedure A (714.5 mg, 45%) (5.5 mmol scale) as a white solid. R_f = 0.3 (DCM/hexane = 1/1). ^1H NMR (600 MHz, $CDCl_3$): δ 7.73 (dt, J = 7.7, 1.3 Hz, 2H), 7.64 (dd, J = 2.7, 1.5 Hz, 2H), 7.42 (t, J = 7.9 Hz, 2H), 7.21 (ddd, J = 8.3, 2.7, 1.0 Hz, 2H), 3.87 (s, 6H); $^{13}C\{^1H\}$ NMR (151 MHz, $CDCl_3$): δ 162.34, 159.96, 130.13, 129.99, 122.98, 121.14, 115.02, 55.64.

These data align with previously published reports in the literature.[37]

4-Methoxybenzoic anhydride (1e)

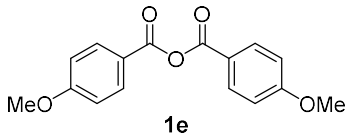

1e

Prepared according to procedure A (1.3168 g, 84%) (5.5 mmol scale) as a white solid. R_f = 0.3 (DCM/hexane = 1/1). ^{1}H NMR (600 MHz, $CDCl_3$): δ 8.11–8.05 (m, 4H), 6.99–6.93 (m, 4H), 3.88 (s, 6H); $^{13}C\{^1H\}$ NMR (151 MHz, $CDCl_3$): δ 164.67, 162.37, 132.89, 121.28, 114.22, 55.67.

These data align with previously published reports in the literature.[36]

4-(*tert*-butyl)benzoic anhydride (1f)

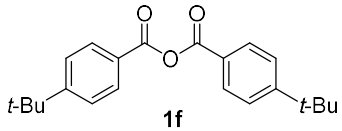

1f

Prepared according to procedure A (971.8 mg, 96%) as a white solid. R_f = 0.35 (DCM/hexane = 1/2). ^{1}H NMR (600 MHz, $CDCl_3$): δ 8.12–8.08 (m, 4H), 7.56–7.51 (m, 4H), 1.36 (s, 18H).; $^{13}C\{^1H\}$ NMR (151 MHz, $CDCl_3$): δ 162.45, 158.42, 130.51, 126.15, 125.86, 35.26, 31.03.

These data align with previously published reports in the literature.[36]

[1,1'-biphenyl]-4-carboxylic anhydride (1g)

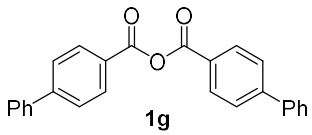

1g

Prepared according to procedure A (956.3 mg, 84%) as a white solid. R_f = 0.45 (DCM/hexane = 1/1). ^{1}H NMR (600 MHz, $CDCl_3$): δ 8.28–8.23 (m, 4H), 7.79–7.74 (m, 4H), 7.69–7.64 (m, 4H), 7.51 (dd, J = 8.5, 6.9 Hz, 4H), 7.46–7.42 (m, 2H); $^{13}C\{^1H\}$ NMR (151 MHz, $CDCl_3$): δ 162.45, 147.41, 139.65, 131.26, 129.17, 128.69, 127.64, 127.60, 127.47.

These data align with previously published reports in the literature.[38]

[1,1'-biphenyl]-3-carboxylic anhydride (1h)

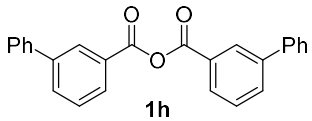

1h

Prepared according to procedure A (604 mg, 53%) as a white solid. R_f = 0.45 (DCM/hexane = 1/1). ^{1}H NMR (600 MHz, $CDCl_3$): δ 8.41 (t, J = 1.9 Hz, 2H), 8.16 (dt, J = 7.8, 1.5 Hz, 2H), 7.91 (dt, J = 7.8, 1.5 Hz, 2H), 7.67–7.60 (m, 6H), 7.52–7.46 (m, 4H), 7.44–7.39 (m, 2H).; ^{13}C{^{1}H} NMR (151 MHz, $CDCl_3$): δ 162.52, 142.27, 139.75, 133.35, 129.53, 129.51, 129.38, 129.33, 129.16, 128.19, 127.32. FT-IR (cm^{-1}): 1784 (s), 1724 (s), 1477 (s), 1418 (s), 1289 (s), 1200 (m), 1088 (m), 1045 (s), 733 (m), 613 (s). Anal. Calcd for $C_{26}H_{18}O_3$: C, 82.52; H, 4.79%; Found: C, 82.40; H, 4.79%.

4-Bromobenzoic anhydride (1i)

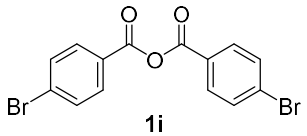

1i

Prepared according to procedure A (273 mg, 24%) as a white solid. R_f = 0.4 (DCM/hexane = 1/2). ^{1}H NMR (600 MHz, CD_2Cl_2): δ 8.01–7.99 (m, 4H), 7.72–7.10 (m, 4H).; ^{13}C{^{1}H} NMR (151 MHz, CD_2Cl_2): δ 161.8, 132.8, 132.3, 130.4, 128.0.
These data align with previously published reports in the literature.[36]

4-Iodobenzoic anhydride (1j)

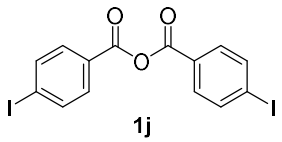

1j

Prepared according to procedure A (183.9 mg, 13%) as a white solid. R_f = 0.4 (DCM/hexane = 1/2). ^{1}H NMR (600 MHz, $CDCl_3$): δ 7.92–7.88 (m, 4H), 7.84–7.81 (m, 4H)·; ^{13}C{^{1}H} NMR (151 MHz, $CDCl_3$): δ 161.90, 138.54, 131.87, 128.22, 103.27.
These data align with previously published reports in the literature.[36]

4-Cyanobenzoic anhydride (1k)

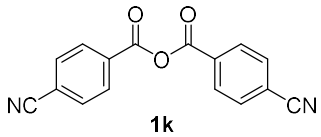

1k

Prepared according to procedure B (235.6 mg, 28%) as a white solid. R_f = 0.3 (DCM/hexane = 2/1). ^{1}H NMR (600 MHz, $CDCl_3$): δ 8.28–8.22 (m, 4H), 7.88–7.83 (m, 4H)·; $^{13}C\{^1H\}$ NMR (151 MHz, $CDCl_3$): δ 160.34, 132.91, 132.13, 131.09, 118.39, 117.53.

These data align with previously published reports in the literature.[19c]

4-(Methoxycarbonyl)benzoic anhydride (1l)

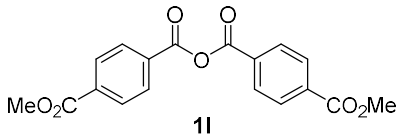

1l

Prepared according to procedure A (354.6 mg, 35%) a as a white solid. R_f = 0.45 (DCM/hexane = 3/1). ^{1}H NMR (600 MHz, $CDCl_3$): δ 8.30–8.04 (m, 8H), 3.96 (s, 6H).; $^{13}C\{^1H\}$ NMR (151 MHz, $CDCl_3$): δ 165.92, 161.35, 135.52, 132.27, 130.60, 130.11, 52.75.

These data align with previously published reports in the literature.[36]

Benzofuran-2-carboxylic anhydride (1m)

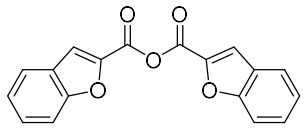

1m

Prepared according to procedure A (747.7 mg, 81%) as a white solid. R_f = 0.35 (DCM/hexane = 1/2). ^{1}H NMR (600 MHz, $CDCl_3$): δ 7.81 (s, 2H), 7.75 (d, J = 7.9 Hz, 2H), 7.62 (d, J = 8.5 Hz, 2H), 7.56–7.51 (m, 2H), 7.36 (t, J = 7.5 Hz, 2H); $^{13}C\{^1H\}$ NMR (151 MHz, $CDCl_3$): δ 156.70, 153.95, 143.49, 129.21, 126.69, 124.50, 123.52, 117.91, 112.73. FT-IR (cm^{-1}): 1786 (s), 1724 (s), 1616 (s), 1557 (s), 1476 (s), 1445 (s), 1291 (s), 1173 (m), 1087 (m), 739 (m). Anal. Calcd for $C_{18}H_{10}O_5$: C, 70.59; H, 3.29%; Found: C, 70.72; H, 3.31%.

4-(*N*,*N*-dipropylsulfamoyl)benzoic anhydride (1n)

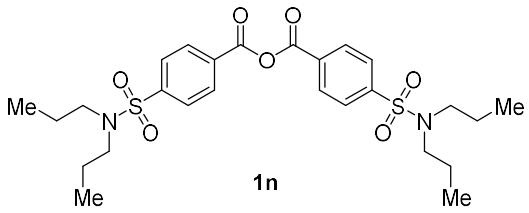

1n

Prepared according to procedure A (1.1805 mg, 71%) as a white solid. R_f = 0.45 (DCM/hexane = 10/1). ^{1}H NMR (600 MHz, $CDCl_3$): δ 8.27–8.25 (m, 4H), 7.97–7.95 (m, 4H), 3.15–3.10 (m, 8H), 1.55 (q, J = 7.5 Hz, 8H), 0.87 (t, J = 7.4 Hz, 12H); ^{13}C{^{1}H} NMR (151 MHz, $CDCl_3$): δ 160.74, 146.21, 131.64, 131.31, 127.60, 50.03, 22.03, 11.25.
These data align with previously published reports in the literature.[39]

1-Naphthoic pivalic anhydride (1o)

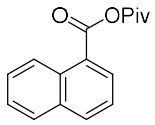

1o

Prepared according to procedure C (1.0524 g, 82%) as a colorless liquid. R_f = 0.45 (DCM/hexane = 1/1). ^{1}H NMR (600 MHz, C_6D_6): δ 9.37–9.29 (m, 1H), 8.04 (d, J = 7.3 Hz, 1H), 7.58 (d, J = 8.2 Hz, 1H), 7.49 (d, J = 8.3 Hz, 1H), 7.32 (ddd, J = 8.4, 6.8, 1.5 Hz, 1H), 7.18 (t, J = 7.5 Hz, 1H), 7.02 (dddd, J = 9.0, 6.4, 3.1, 1.5 Hz, 1H), 1.13 (s, 9H); ^{13}C{^{1}H} NMR (151 MHz, C_6D_6): δ 174.06, 163.25, 135.28, 134.24, 132.27, 131.83, 128.96, 128.92, 128.35, 126.88, 126.11, 124.47, 40.12, 26.50. FT-IR (cm^{-1}): 1796 (s), 1726 (s), 1576 (s), 1510 (s), 1479 (s), 1397 (s), 1370 (s), 1234 (m), 1052 (m), 962 (m), 806 (m), 777 (m), 647 (s). Anal. Calcd for $C_{16}H_{16}O_3$: C, 74.98; H, 6.29%; Found: C, 75.35; H, 6.30%.

3-4-3 Experimental Procedures of Catalytic Decarbonylative Halogenation

3-4-3-1 General Procedure for Screening of the Reaction Conditions

An oven-dried 5-mL microwave vial, fitted with a magnetic stirring bar, was loaded with Pd or Ni catalysts, a ligand, and acid anhydride (0.2 mmol, 1 equiv) under ambient air. A halogen source and anhydrous solvent (1 mL, 0.2 M) were added inside a nitrogen-filled glovebox. The vial was sealed securely and heated in a preheated block at 100–180 °C for 24 h with constant stirring. After cooling to room temperature, the reaction mixture was transferred to an oven-dried round-bottom flask. The vial was rinsed with dichloromethane (5 × 2 mL), and the combined solution was concentrated under reduced pressure. Dibromomethane (CH_2Br_2) was then added as an internal standard, and product yields were quantified using ^1H NMR spectroscopy.

3-4-3-2 General Procedure for Experimental Procedures and Spectroscopic Data for the Products

Procedure D (closed system):

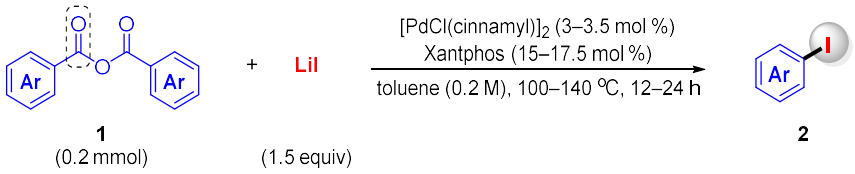

1 (0.2 mmol) (1.5 equiv) **2**

An oven-dried 5-mL microwave vial equipped with a magnetic stirring bar was loaded with [PdCl(cinnamyl)]$_2$ (3–3.5 mol %, 6–7 μmol, 3.1–3.6 mg), Xantphos (15 – 17.5 mol %, 0.03–0.035 mmol, 17.4–20.3 mg), and acid anhydrides **1** (0.2 mmol, 1 equiv) under ambient air. Lithium iodide (0.3 mmol, 1.5 equiv, 40.2 mg) and anhydrous toluene (1 mL, 0.2 M) were added in a nitrogen-filled glovebox. The vial was securely sealed and heated in a preheated block at 100–140 °C for 12–24 h with continuous stirring. After the reaction mixture cooled to room temperature, it was purified by silica gel column chromatography using ethyl acetate or dichloromethane/hexane as the eluent to obtain the desired product **2**. Yields of volatile product (**2b**) was determined via GC analysis of the reaction mixture, using *n*-dodecane as an internal standard.

Procedure E (open system):

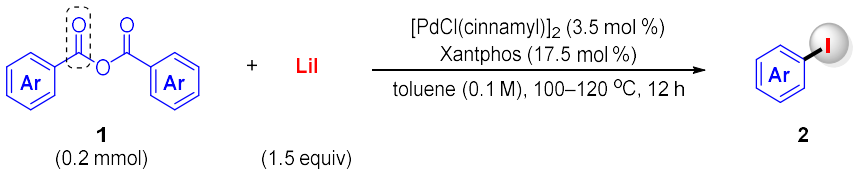

1 (0.2 mmol) (1.5 equiv) **2**

An oven-dried 5-mL microwave vial equipped with a magnetic stirring bar was loaded with [PdCl(cinnamyl)]$_2$ (3.5 mol %, 7 μmol, 3.6 mg), Xantphos (17.5 mol %, 0.035 mmol, 20.3 mg), and acid anhydrides **1** (0.2 mmol, 1 equiv) under ambient air. Lithium iodide (0.3 mmol, 1.5 equiv, 40.2 mg) and anhydrous toluene (2 mL, 0.1 M) were introduced in a nitrogen-filled glovebox. The vial was securely sealed, and the septum was pierced with a needle for pressure equilibration (*a depiction of the reaction setup is provided in **Chapter 2***). The vial was then placed in a preheated heating block at 100–120 °C and

stirred for 12 h. After cooling to room temperature, the reaction mixture was purified by silica gel column chromatography using a dichloromethane/hexane mixture or pure hexane as the eluent, yielding the desired products.

Procedure F:

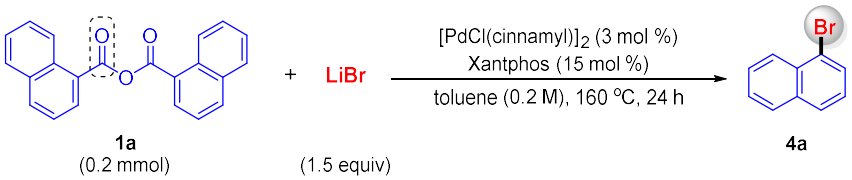

An oven-dried 5-mL microwave vial equipped with a magnetic stirring bar was loaded with [PdCl(cinnamyl)]$_2$ (3 mol %, 6 μmol, 3.1 mg), Xantphos (15 mol %, 0.03 mmol, 17.4 mg), and 1-naphthoic anhydride **1a** (0.2 mmol, 1 equiv, 65.3 mg) under ambient air. Lithium bromide (0.3 mmol, 1.5 equiv, 26.1 mg) and anhydrous toluene (1 mL, 0.2 M) were added in a nitrogen-filled glovebox. The vial was securely sealed and heated in a preheated block at 160 °C for 24 h with continuous stirring. (***Safety Note****: The reaction must be conducted in a fume hood. Due to the high reaction temperature exceeding toluene's boiling point and the generation of CO gas, there is a potential risk of the reaction cap detaching under pressure.*) Once the reaction mixture cooled to room temperature, it was purified by silica gel column chromatography using pure mixture as the eluent to obtain the desired product **4a**.

Procedure G:

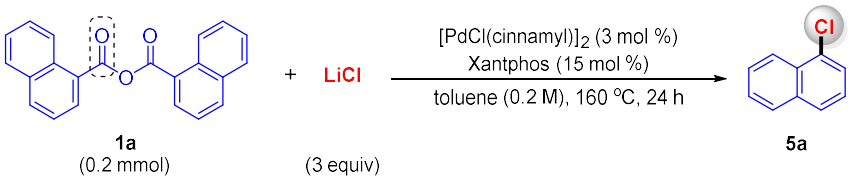

An oven-dried 5-mL microwave vial equipped with a magnetic stirring bar was charged with [PdCl(cinnamyl)]$_2$ (3 mol %, 6 μmol, 3.1 mg), Xantphos (15 mol %, 0.03 mmol, 17.4 mg), and 1-naphthoic anhydride **1a** (0.2 mmol, 1 equiv, 65.3 mg) under ambient air. Lithium chloride (0.6 mmol, 3 equiv, 25.4 mg) and anhydrous toluene (1 mL, 0.2 M) were

added inside a nitrogen-filled glovebox. The vial was securely sealed and heated in a preheated block at 160 °C for 24 h with continuous stirring. (***Safety Note****: This procedure must be performed in a fume hood. The high reaction temperature exceeds the boiling point of toluene, and the reaction generates CO gas, increasing the potential risk of cap detachment due to pressure buildup.*) After cooling the reaction mixture to room temperature, it was purified using silica gel column chromatography with hexane as the eluent to isolate the desired product **5a**.

Spectroscopic Data for the Products

1-Iodonaphthalene (2a)

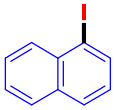

2a

Prepared according to procedure D as a yellow oil. R_f = 0.60 (hexane). Isolated yield was 90% (45.9 mg) from **1a**. ^{1}H NMR (600 MHz, $CDCl_3$) : δ 8.11 (t, J = 7.9 Hz, 2H), 7.85 (d, J = 8.2 Hz, 1H), 7.81–7.75 (m, 1H), 7.60 (t, J = 7.6 Hz, 1H), 7.53 (t, J = 7.5 Hz, 1H), 7.19 (t, J = 7.8 Hz, 1H).; ^{13}C{^{1}H} NMR (151 MHz, $CDCl_3$): δ 137.53, 134.46, 134.23, 132.23, 129.10, 128.67, 127.82, 126.96, 126.83, 99.72.

These data align with previously published reports in the literature.[27]

2-Iodonaphthalene (2c)

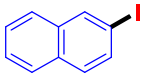

2c

Prepared according to procedure D as a white solid. R_f = 0.60 (hexane). Isolated yield was 40% (20.2 mg) from **1c**. ^{1}H NMR (400 MHz, $CDCl_3$): δ 8.25 (d, J = 1.7 Hz, 1H), 7.83–7.76 (m, 1H), 7.76–7.69 (m, 2H), 7.58 (d, J = 8.6 Hz, 1H), 7.50 (dt, J = 6.3, 3.5 Hz, 2H); ^{13}C{^{1}H} NMR (101 MHz, $CDCl_3$): δ 136.76, 135.11, .134.50, 132.22, 129.61, 128.00, 126.93, 126.82, 126.60, 91.63.

These data align with previously published reports in the literature.[27]

1-Iodo-3-methoxybenzene (2d)

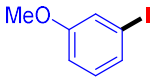

2d

Prepared according to procedure E as a colorless oil. R_f = 0.40 (DCM/hexane = 1/10). Isolated yield was 57% (26.8 mg) from **1d**. ^{1}H NMR (600 MHz, $CDCl_3$): δ 7.63–7.60 (m, 2H), 7.16–7.13 (m, 2H), 1.30 (s, 9H); ^{13}C{^{1}H} NMR (151 MHz, $CDCl_3$): δ 160.26, 130.90, 129.96, 123.13, 113.91, 94.50, 55.52.

These data align with previously published reports in the literature.[27]

1-Iodo-4-methoxybenzene (2e)

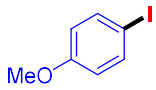

2e

Prepared according to procedure E as a colorless oil. R_f = 0.40 (DCM/hexane = 1/10). Isolated yield was 32% (15.2 mg) from **1e**. ^{1}H NMR (600 MHz, $CDCl_3$): δ 7.59–7.52 (m, 2H), 6.72–6.65 (m, 2H), 3.78 (s, 3H).; $^{13}C\{^1H\}$ NMR (151 MHz, $CDCl_3$): 159.59, 138.33, 116.49, 82.82, 55.45.

These data align with previously published reports in the literature.[27]

1-(*tert*-butyl)-4-iodobenzene (2f)

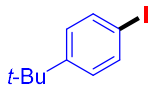

2f

Prepared according to procedure D as a white solid. R_f = 0.80 (hexane). Isolated yield was 60% (31.1 mg) from **1f**. ^{1}H NMR (400 MHz, $CDCl_3$): δ 7.66–7.57 (m, 2H), 7.18–7.11 (m, 2H), 1.30 (s, 9H); $^{13}C\{^1H\}$ NMR (101 MHz, $CDCl_3$): δ 150.98, 137.19, 127.71, 90.76, 34.72, 31.29.

These data align with previously published reports in the literature.[27]

4-Iodo-1,1'-biphenyl (2g)

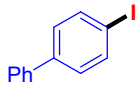

2g

Prepared according to procedure D as a white solid. R_f = 0.55 (hexane). Isolated yield was 55% (31.7 mg) from **1g**. ^{1}H NMR (600 MHz, $CDCl_3$): δ 7.82–7.72 (m, 2H), 7.58–7.53 (m, 2H), 7.47–7.42 (m, 2H), 7.39–7.35 (m, 1H), 7.35–7.32 (m, 2H).; $^{13}C\{^1H\}$ NMR (151 MHz, $CDCl_3$): δ 140.86, 140.19, 137.98, 129.15, 129.05, 127.83, 127.04, 93.17.

These data align with previously published reports in the literature.[27]

3-Iodo-1,1'-biphenyl (2h)

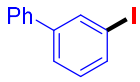

2h

Prepared according to procedure D as a colorless oil. R_f = 0.55 (hexane). Isolated yield was 81% (45.1 mg) from **1h**. ^{1}H NMR (600 MHz, $CDCl_3$): δ 7.95 (t, J = 1.7 Hz, 1H), 7.68 (ddd, J = 7.9, 1.8, 1.0 Hz, 1H), 7.57–7.53 (m, 3H), 7.48–7.43 (m, 2H), 7.40–7.35 (m, 1H), 7.18 (t, J = 7.8 Hz, 1H); ^{13}C{^{1}H} NMR (151 MHz, $CDCl_3$): δ 143.59, 139.77, 136.32, 136.28, 130.55, 129.01, 127.97, 127.25, 126.55, 94.93.

These data align with previously published reports in the literature.[27]

1-Bromo-4-iodobenzene (2i)

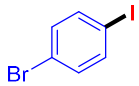

2i

Prepared according to procedure D as a white solid. R_f = 0.80 (hexane). Isolated yield was 36% (20.3 mg) from **1i**. ^{1}H NMR (600 MHz, $CDCl_3$): δ 7.58–7.51 (m, 2H), 7.25–7.19 (m, 2H).; ^{13}C{^{1}H} NMR (151 MHz, $CDCl_3$): δ 139.21, 133.59, 122.34, 92.16.

These data align with previously published reports in the literature.[27]

1,4-Diiodobenzene (2j)

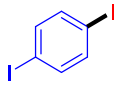

2j

Prepared according to procedure D as a white solid. R_f = 0.80 (hexane). Isolated yield was 48% (31.1 mg) from **1j**. ^{1}H NMR (600 MHz, $CDCl_3$): δ 7.41 (s, 4H); ^{13}C{^{1}H} NMR (151 MHz, $CDCl_3$): δ 139.47, 93.49.

These data align with previously published reports in the literature.[27]

4-Iodobenzonitrile (2k)

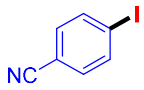

2k

Prepared according to procedure D as a white solid. R_f = 0.30 (DCM/hexane = 1/1). Isolated yield was 82% (37.3 mg) from **1k**. ^{1}H NMR (600 MHz, $CDCl_3$): δ 7.90–7.79 (m, 2H), 7.40–7.33 (m, 2H); $^{13}C\{^1H\}$ NMR (151 MHz, $CDCl_3$): δ 138.64, 133.29, 118.34, 111.87, 100.43.

These data align with previously published reports in the literature.[27]

Methyl 4-Iodobenzoate (2l)

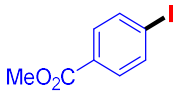

2l

Prepared according to procedure D as a white solid. R_f = 0.40 (DCM/hexane = 1/1). Isolated yield was 70% (36.9 mg) from **1l**. ^{1}H NMR (600 MHz, $CDCl_3$): δ 7.82–7.77 (m, 2H), 7.77–7.72 (m, 2H), 3.91 (s, 3H); $^{13}C\{^1H\}$ NMR (151 MHz, $CDCl_3$): δ 166.75, 137.86, 131.17, 129.75, 100.86, 52.44.

These data align with previously published reports in the literature.[27]

2-Iodobenzofuran (2m)

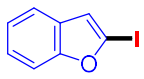

2m

Prepared according to procedure E as a colorless oil. R_f = 0.60 (hexane). Isolated yield was 24% (11.8 mg) from **1m**. ^{1}H NMR (600 MHz, $CDCl_3$): δ 7.53–7.49 (m, 1H), 7.49–7.46 (m, 1H), 7.23–7.19 (m, 2H), 6.96 (s, 1H); $^{13}C\{^1H\}$ NMR (151 MHz, $CDCl_3$): δ 158.35, 129.34, 124.37, 123.27, 119.81, 117.37, 110.96, 95.98.

These data align with previously published reports in the literature.[27]

4-Iodo-*N*,*N*-dipropylbenzenesulfonamide (2n)

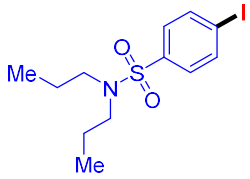

2n

Prepared according to procedure D as a white solid. R_f = 0.40 (DCM/hexane = 2/1). Isolated yield was 57% (41.8 mg) from **1n**. ^{1}H NMR (400 MHz, $CDCl_3$): δ 7.89–7.79 (m, 2H), 7.55–7.45 (m, 2H), 3.09–3.02 (m, 4H), 1.54 (dq, J = 14.9, 7.4 Hz, 4H), 0.86 (t, J = 7.4 Hz, 6H); ^{13}C{^{1}H} NMR (101 MHz, $CDCl_3$): δ 140.03, 138.31, 128.58, 99.51, 50.11, 22.11, 11.29.

These data align with previously published reports in the literature.[27]

1-Bromonaphthalene (4a)

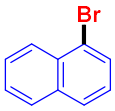

4a

Prepared according to procedure F as a colorless oil. R_f = 0.60 (hexane). Isolated yield was 89% (36.7 mg) from **1a**. ^{1}H NMR (400 MHz, $CDCl_3$): δ 8.28 (d, J = 8.4 Hz, 1H), 7.89–7.78 (m, 3H), 7.62 (ddd, J = 8.5, 6.9, 1.5 Hz, 1H), 7.56 (td, J = 7.5, 6.8, 1.4 Hz, 1H), 7.34 (t, J = 7.8 Hz, 1H); ^{13}C{^{1}H} NMR (151 MHz, $CDCl_3$): δ 134.73, 132.11, 130.01, 128.42, 128.04, 127.44, 127.21, 126.81, 126.29, 122.94.

These data align with previously published reports in the literature.[27]

1-Chloronaphthalene (5a)

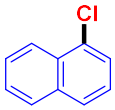

5a

Prepared according to procedure G as a colorless oil. R_f = 0.55 (hexane). Isolated yield was 51% (16.5 mg) from **1a**. ^{1}H NMR (400 MHz, $CDCl_3$): δ 8.38–8.24 (m, 1H), 7.88 (d, J = 8.0 Hz, 1H), 7.79 (d, J = 8.2 Hz, 1H), 7.68–7.52 (m, 3H), 7.44–7.37 (m, 1H); $^{13}C\{^1H\}$ NMR (101 MHz, $CDCl_3$): δ 134.67, 132.04, 130.92, 128.34, 127.28, 127.16, 126.80, 126.27, 125.84, 124.53.

These data align with previously published reports in the literature.[27]

2-4-4 Experimental Procedures of Mechanistic Study

2-4-4-1 Time-Course Experiment of Stoichiometric Reaction

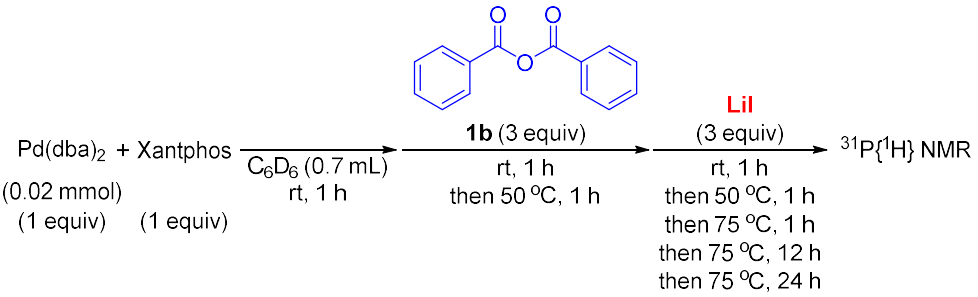

An oven-dried J.Young NMR tube was charged with $Pd(dba)_2$ (1 equiv, 0.02 mmol, 11.5 mg), Xantphos (1 equiv, 0.02 mmol, 11.6 mg), and benzene-d_6 (0.7 mL) inside a nitrogen-filled glovebox. The tube was tightly closed, and $^{31}P\{^1H\}$ NMR measurements were performed immediately. After allowing the reaction tube to stand at room temperature for 1 h, benzoic anhydride (**1b**) (3 equiv, 0.06 mmol, 13.6 mg) was added in the glovebox. The reaction tube was then left at room temperature for 1 h and heated at 50 °C for 1 h. Subsequently, lithium iodide (3 equiv, 0.06 mmol, 8.0 mg) was added in the glovebox. The tube was left at room temperature for 1 h, followed by heating at 50 °C for 1 h, at 75 °C for 1 h, then for 12 h, and finally for 24 h. The $^{31}P\{^1H\}$ NMR measurements were performed at each time point (**Scheme 3-5**).

Stoichiometric reaction 2

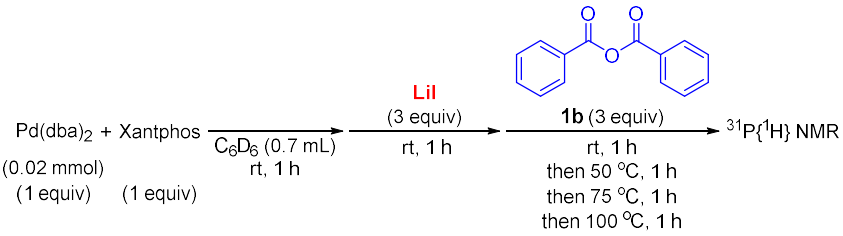

An oven-dried J.Young NMR tube was charged with $Pd(dba)_2$ (1 equiv, 0.02 mmol, 11.5 mg), Xantphos (1 equiv, 0.02 mmol, 11.6 mg), and benzene-d_6 (0.7 mL) inside a nitrogen-filled glovebox. The tube was tightly closed, and $^{31}P\{^{1}H\}$ NMR measurements were performed immediately. After allowing the reaction tube to stand at room temperature for 1 h, lithium iodide (3 equiv, 0.06 mmol, 8.0 mg) was added in a glovebox. The reaction tube was then left at room temperature for 1 h. Subsequently, benzoic anhydride (**1b**) (3 equiv, 0.06 mmol, 13.6 mg) was added in the glovebox. The tube was left at room temperature for 1 h, followed by heating at 50 °C, 75 °C, and 100 °C for 1 h, respectively. The $^{31}P\{^{1}H\}$ NMR measurements were performed at each time point (**Scheme 3-6**).

2-4-4-2 Time-Course Study of the Formation of Acyl Iodide from Acid Anhydride

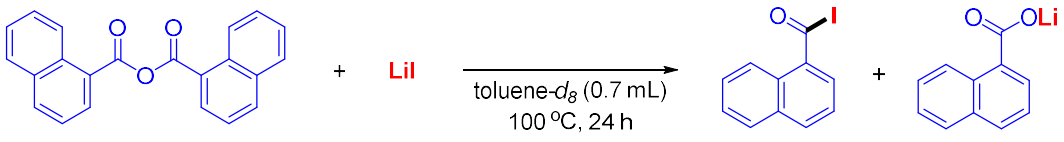

An oven-dried J.Young NMR tube was charged with 1-naphthoic anhydride (**1a**) (1 equiv, 0.05 mmol, 16.3 mg), lithium iodide (1.5 equiv, 0.075 mmol, 10.0 mg), toluene-d_8 (0.7 mL), and dibromomethane as an internal standard in a nitrogen-filled glovebox. The NMR tube was sealed and placed in a preheated oil bath at rt, 50 °C, and 100 °C. The reaction mixture was allowed to equilibrate to room temperature and analyzed by ^{1}H NMR at various time points (**Tables 3-9–11**).

2-4-5 Copies of NMR Charts for All the Compounds

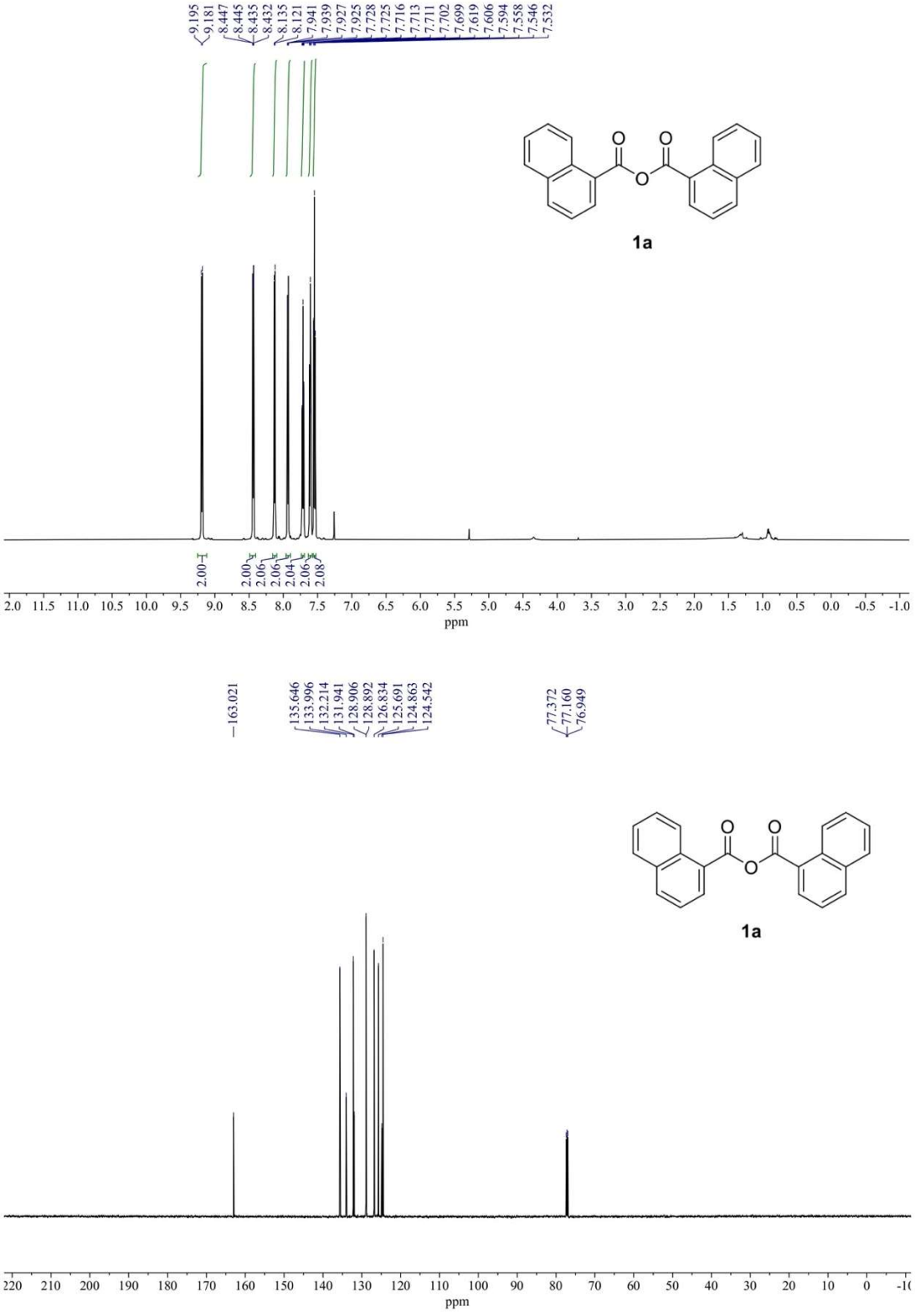

^{1}H NMR (600 MHz) and ^{13}C{^{1}H} NMR (151 MHz) spectra of **1a** (rt, $CDCl_3$).

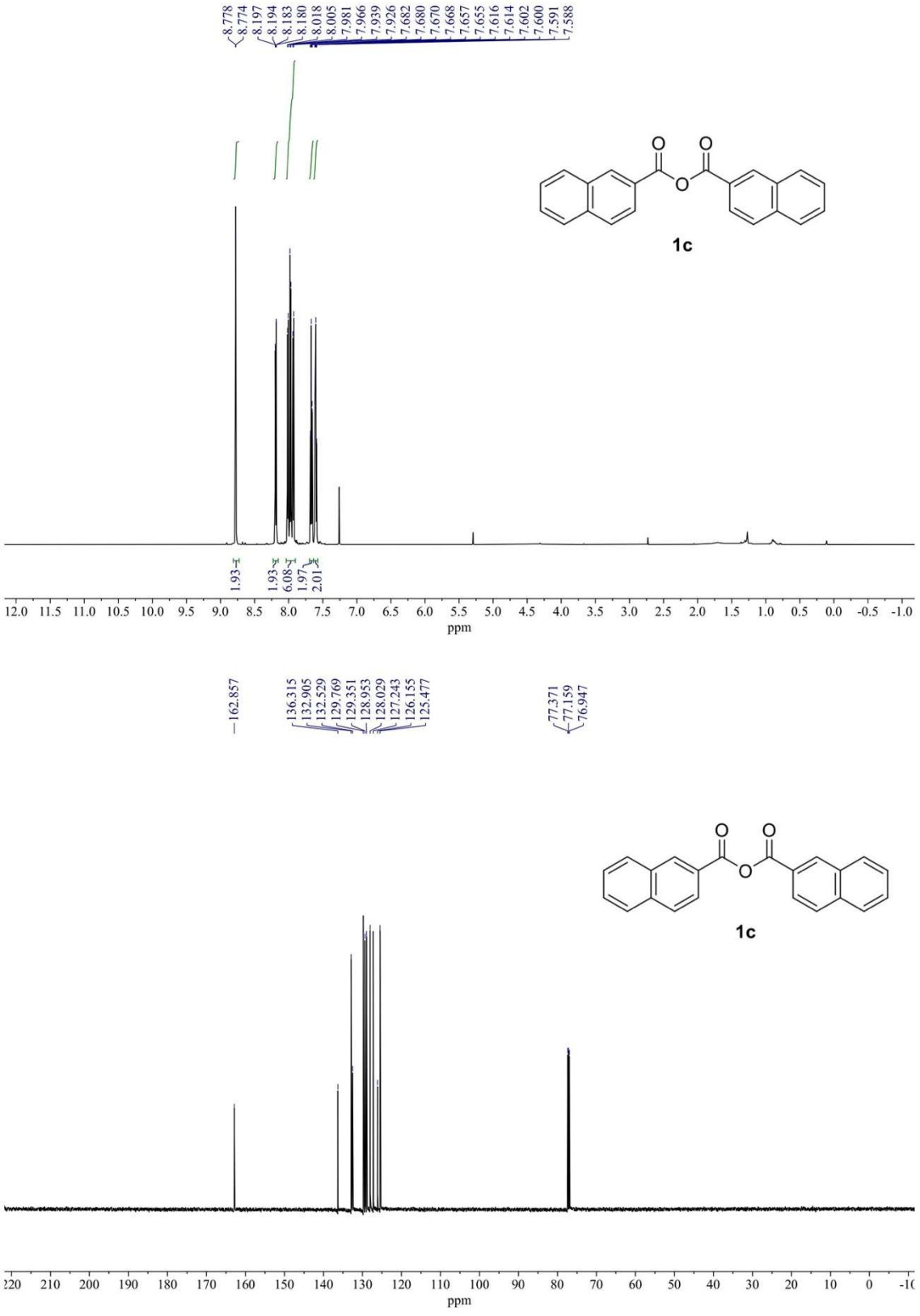

^{1}H NMR (600 MHz) and ^{13}C{^{1}H} NMR (151 MHz) spectra of **1c** (rt, $CDCl_3$).

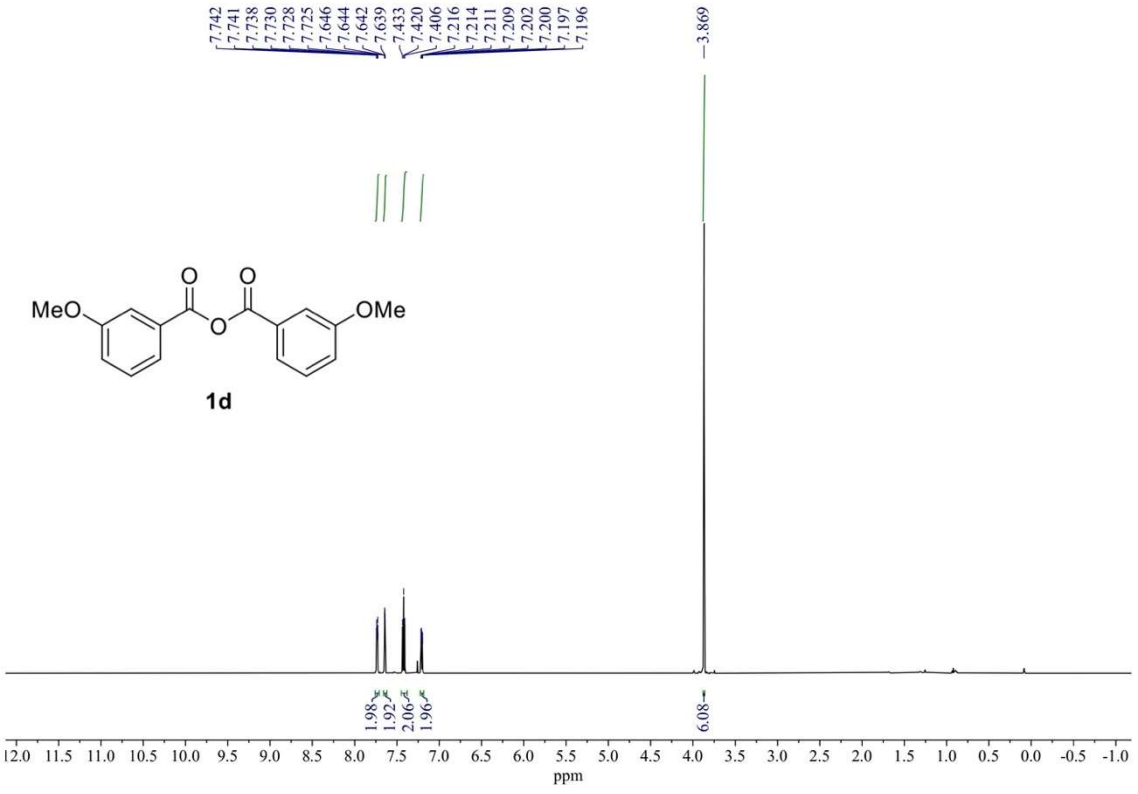

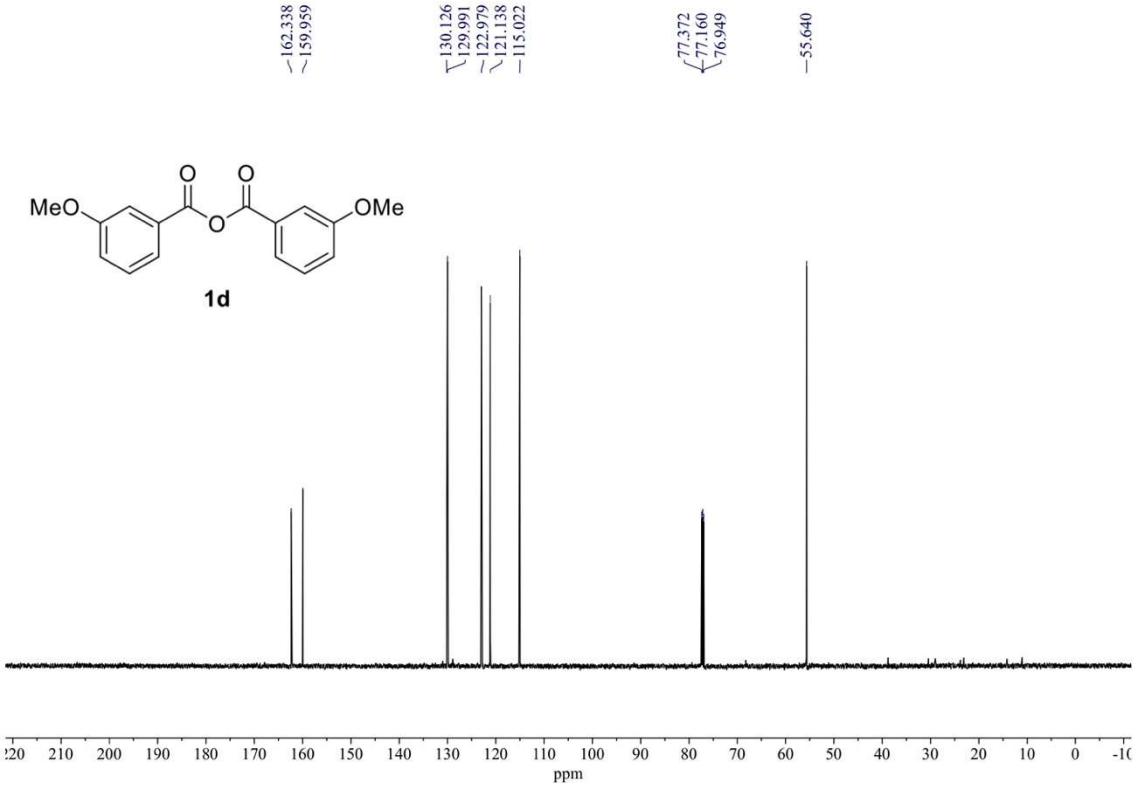

^{1}H NMR (600 MHz) and ^{13}C{^{1}H} NMR (151 MHz) spectra of **1d** (rt, $CDCl_3$).

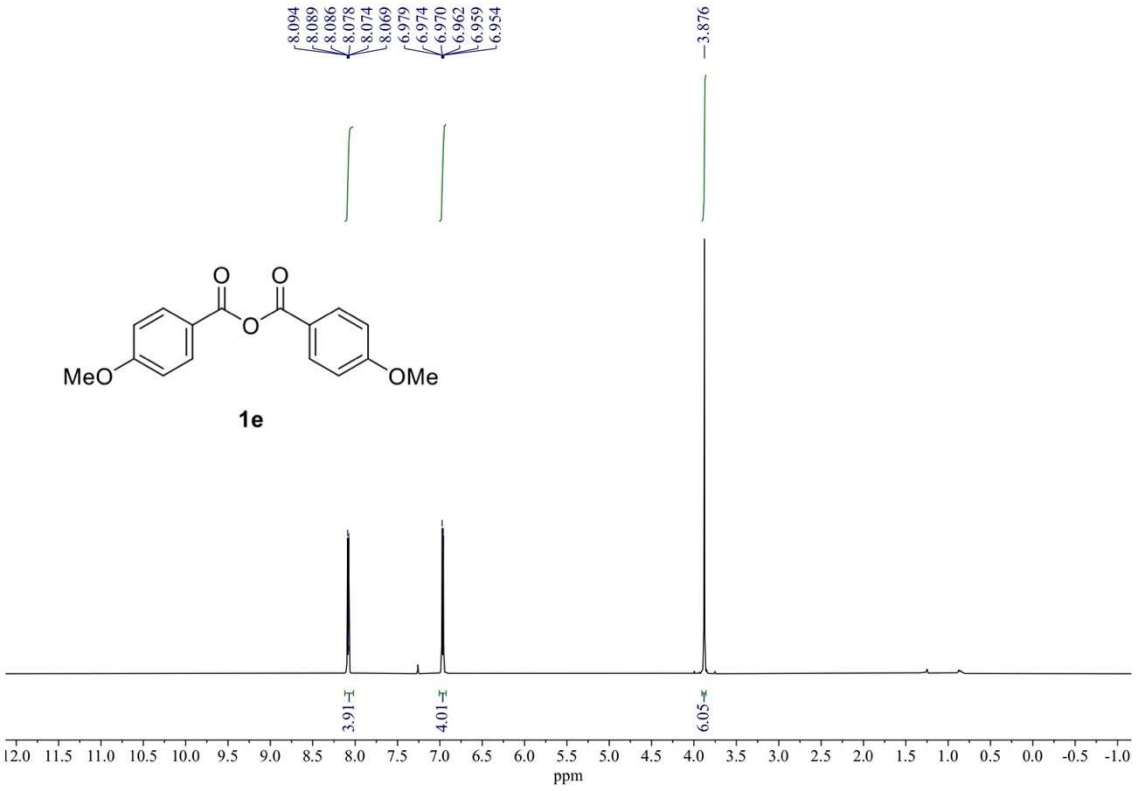

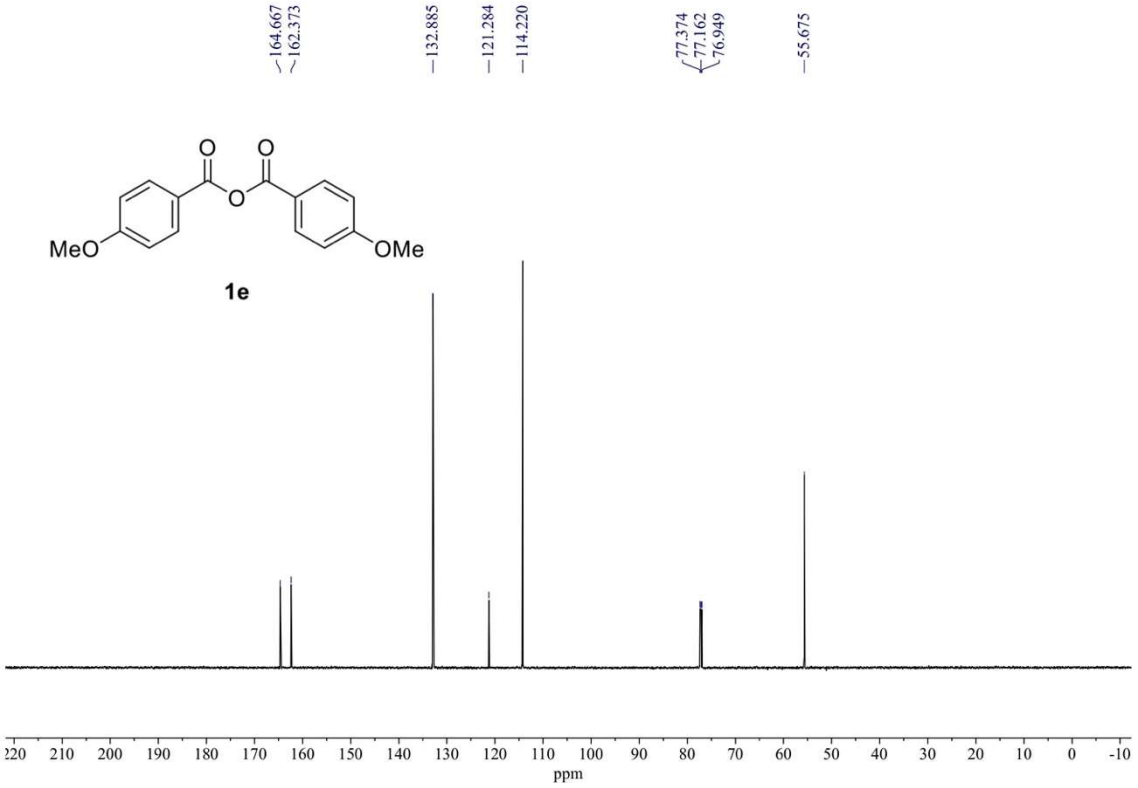

^{1}H NMR (600 MHz) and ^{13}C{^{1}H} NMR (151 MHz) spectra of **1e** (rt, $CDCl_3$).

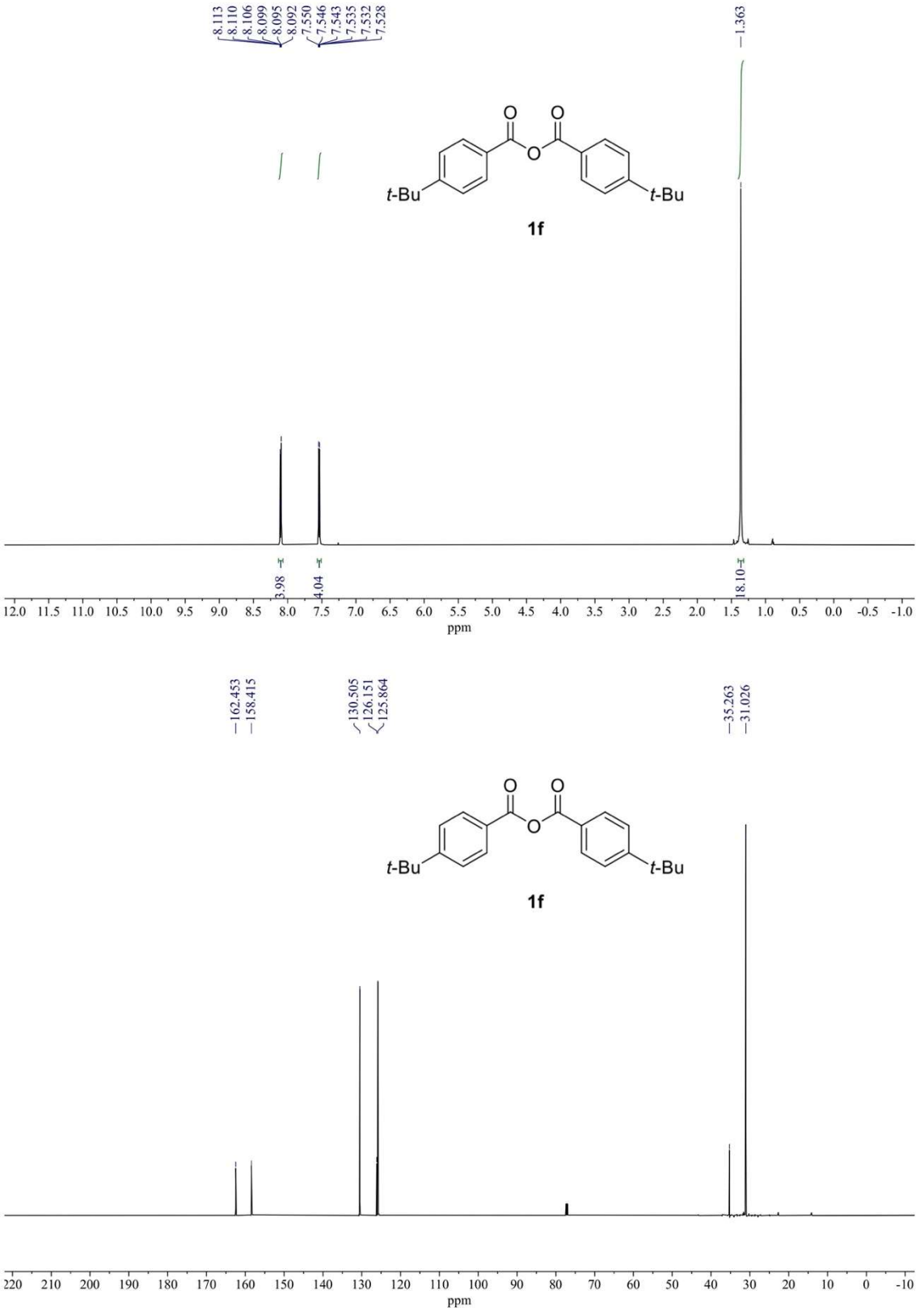

^{1}H NMR (600 MHz) and ^{13}C{^{1}H} NMR (151 MHz) spectra of **1f** (rt, $CDCl_3$).

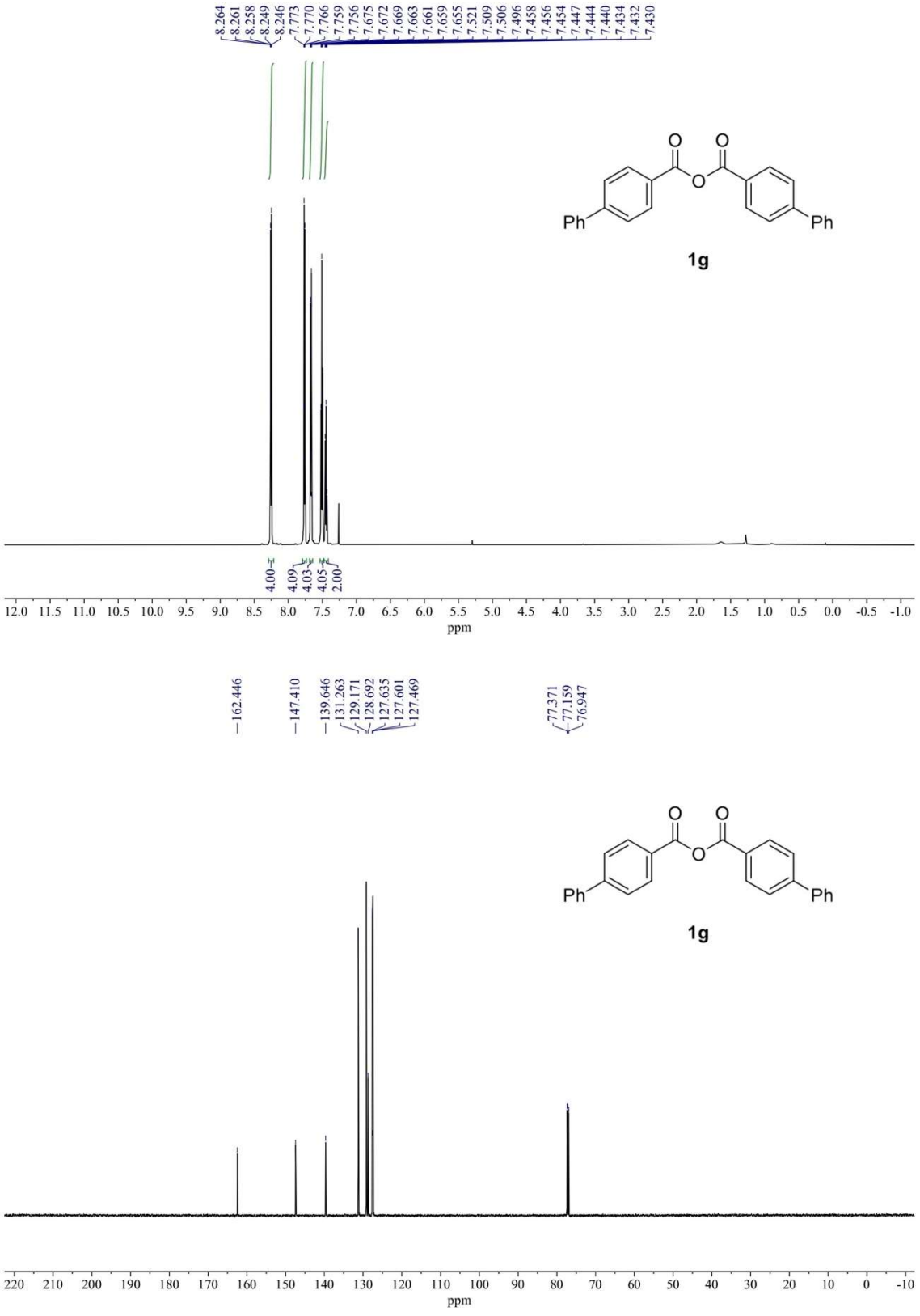

^{1}H NMR (600 MHz) and ^{13}C{^{1}H} NMR (151 MHz) spectra of **1g** (rt, $CDCl_3$).

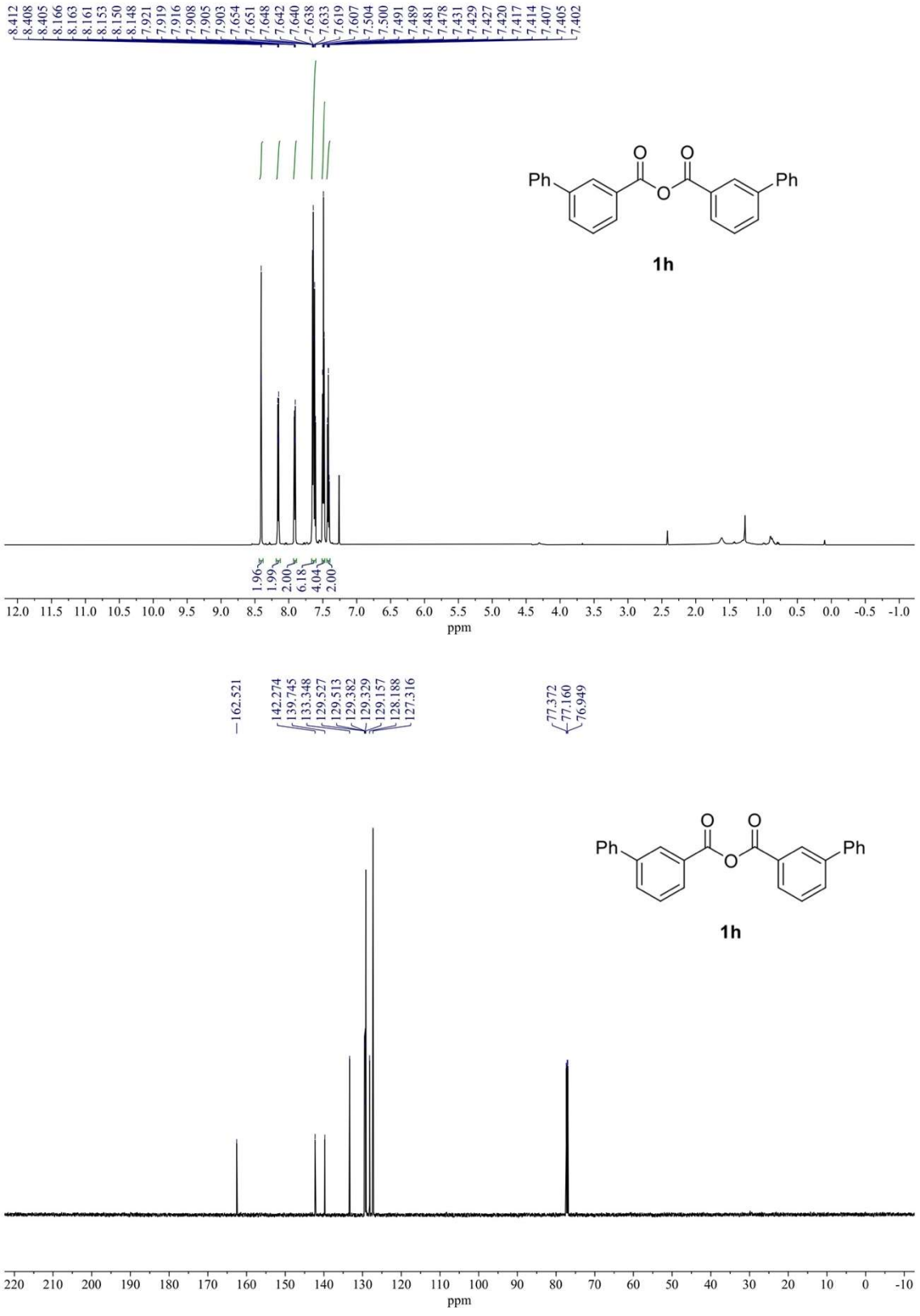

^{1}H NMR (600 MHz) and ^{13}C{^{1}H} NMR (151 MHz) spectra of **1h** (rt, $CDCl_3$).

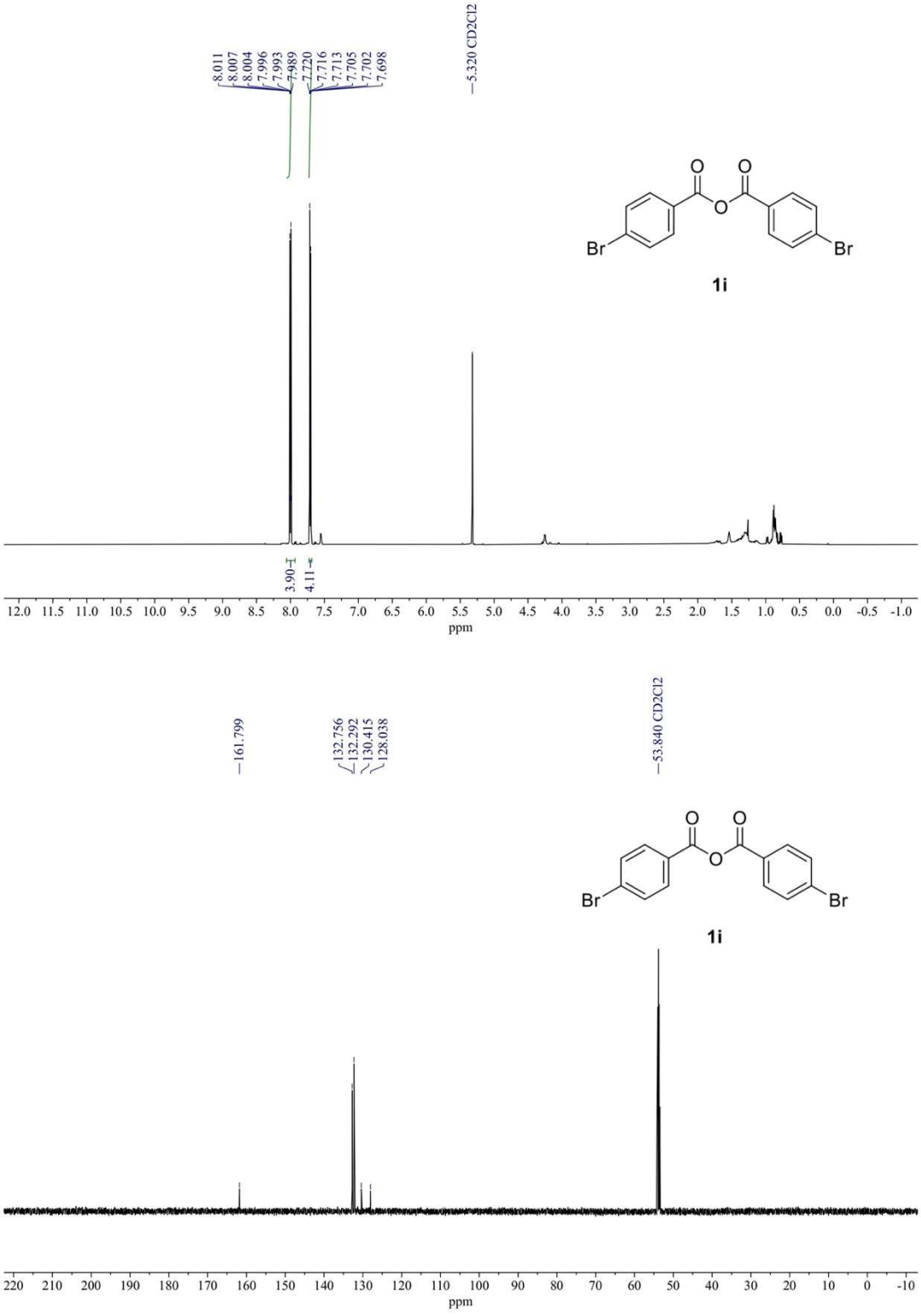

^{1}H NMR (600 MHz) and ^{13}C{^{1}H} NMR (151 MHz) spectra of **1i** (rt, CD_2Cl_2).

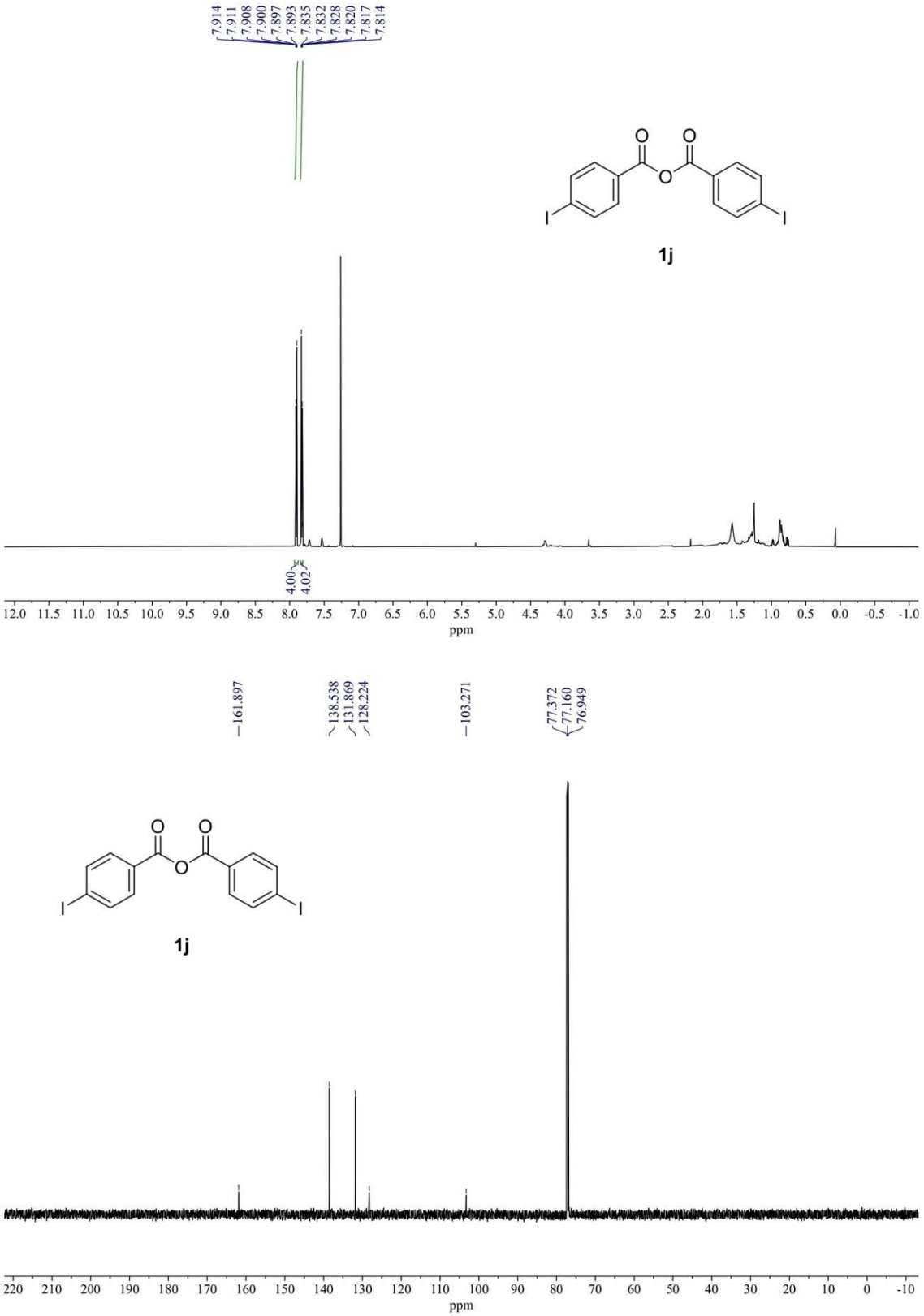

^{1}H NMR (600 MHz) and ^{13}C{^{1}H} NMR (151 MHz) spectra of **1j** (rt, $CDCl_3$).

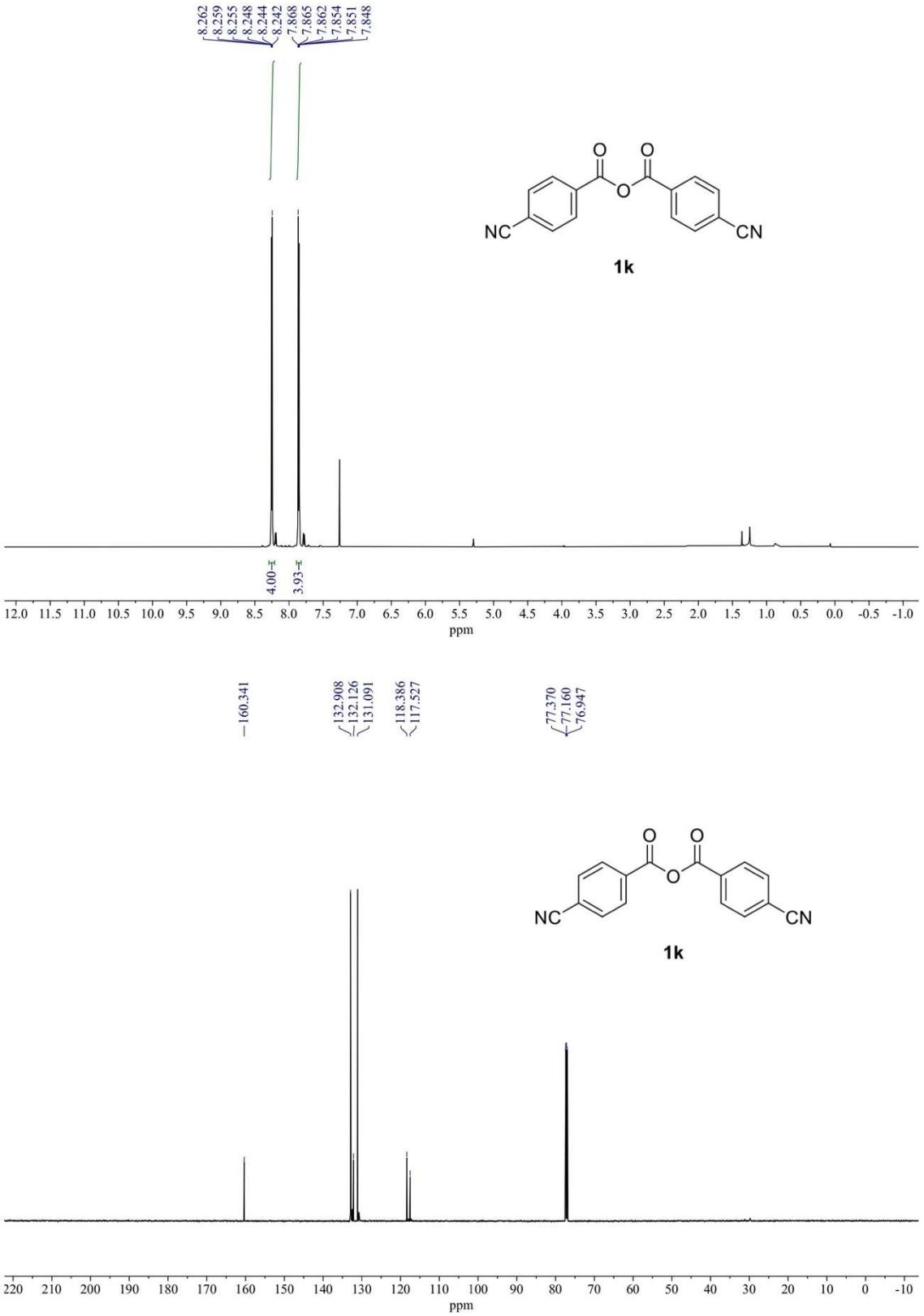

^{1}H NMR (600 MHz) and ^{13}C{^{1}H} NMR (151 MHz) spectra of **1k** (rt, $CDCl_3$).

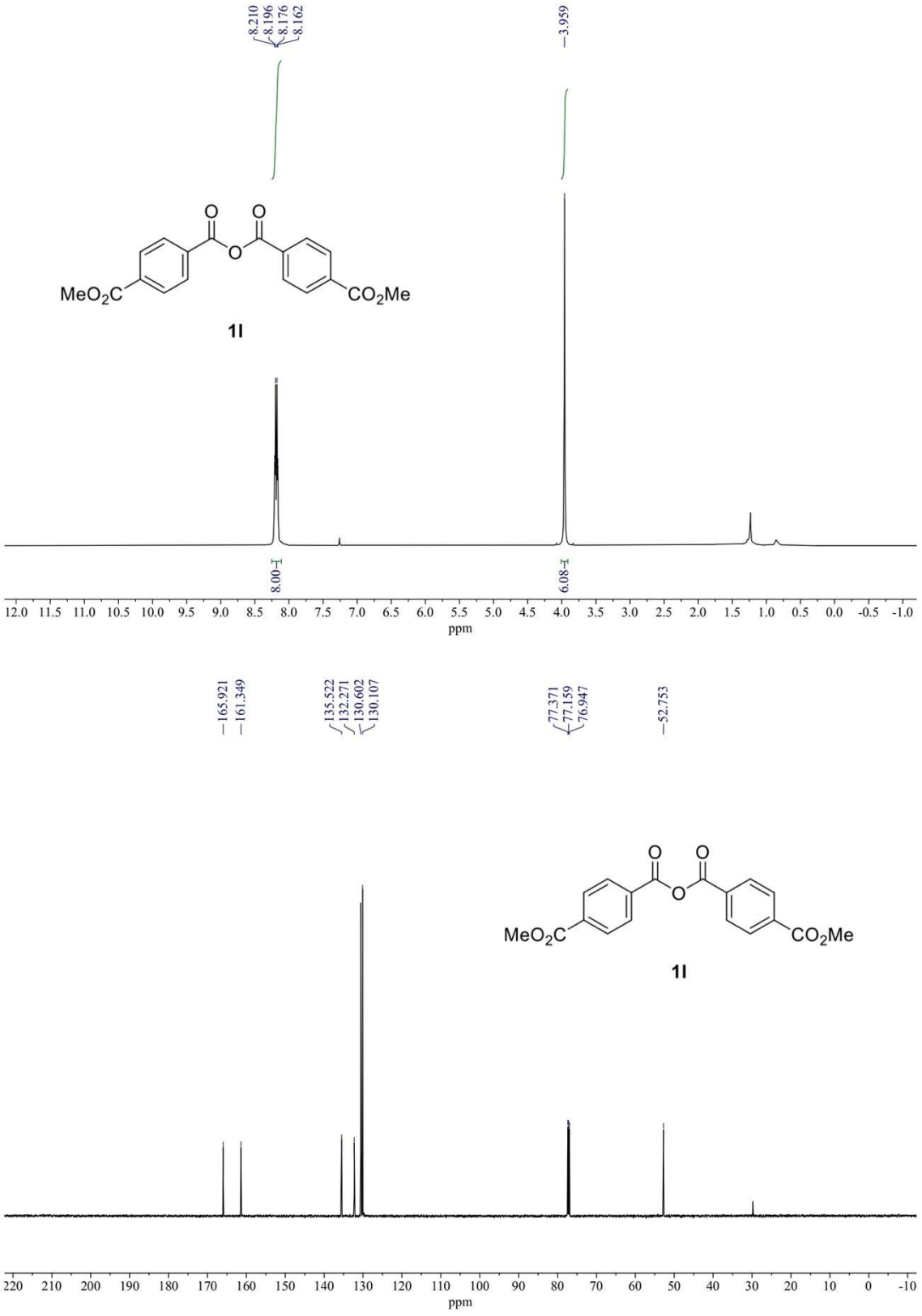

^{1}H NMR (600 MHz) and ^{13}C{^{1}H} NMR (151 MHz) spectra of **1l** (rt, $CDCl_3$).

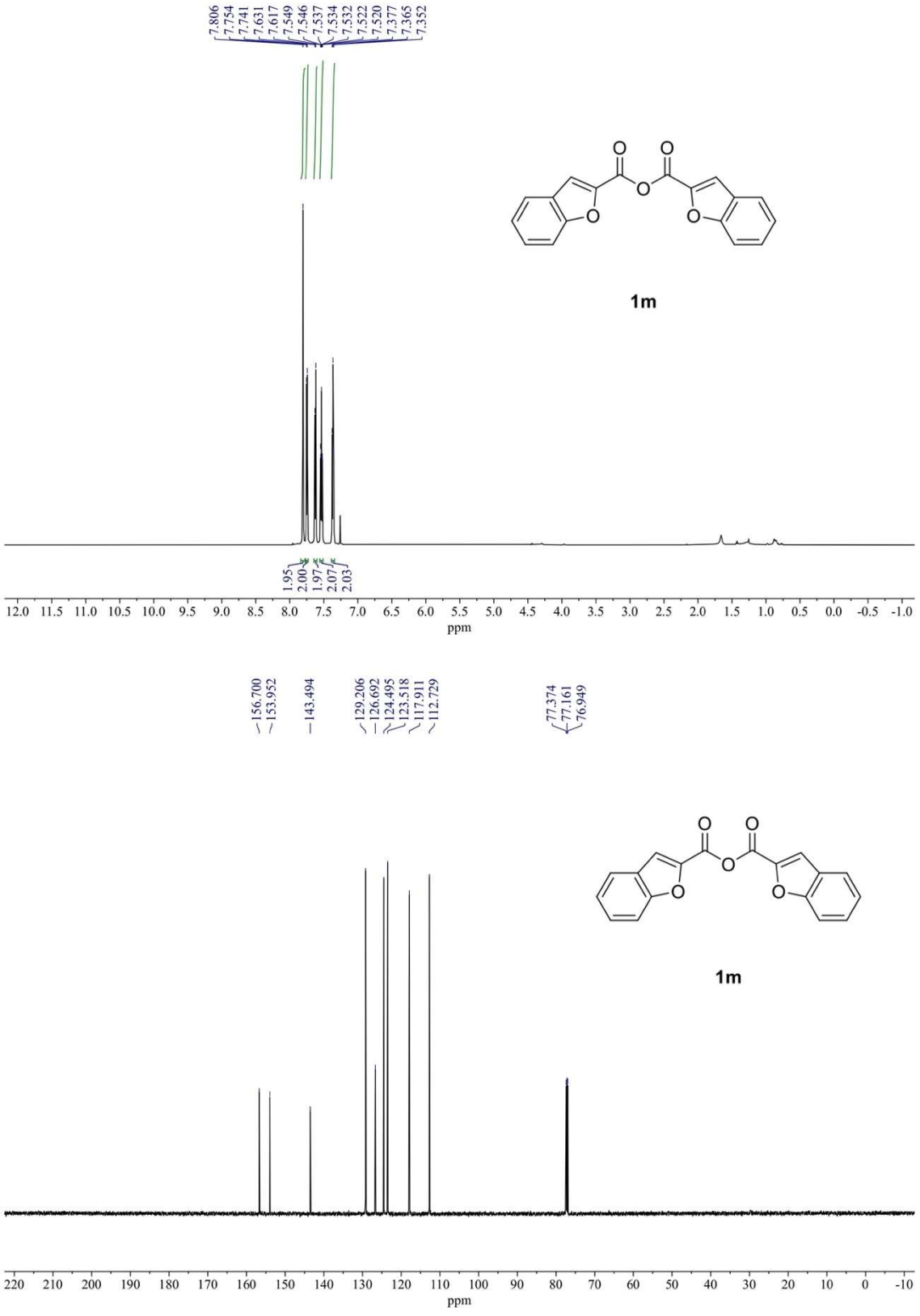

^{1}H NMR (600 MHz) and ^{13}C{^{1}H} NMR (151 MHz) spectra of **1m** (rt, $CDCl_3$).

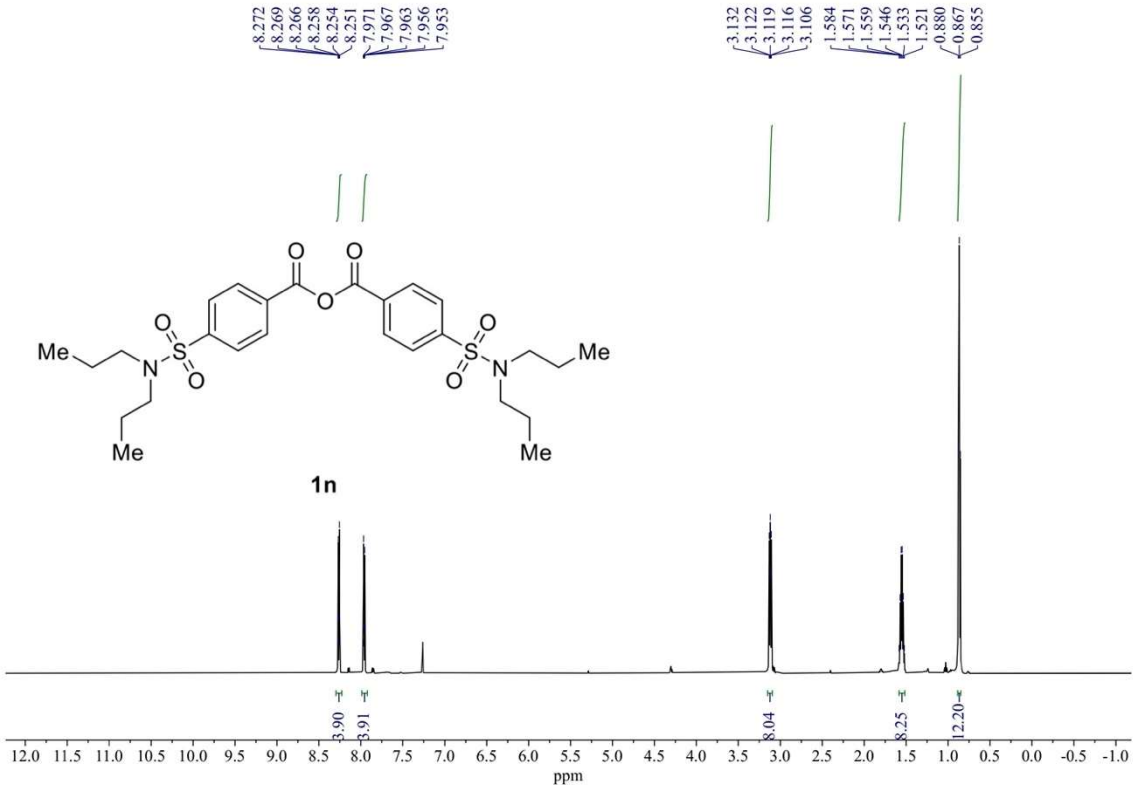

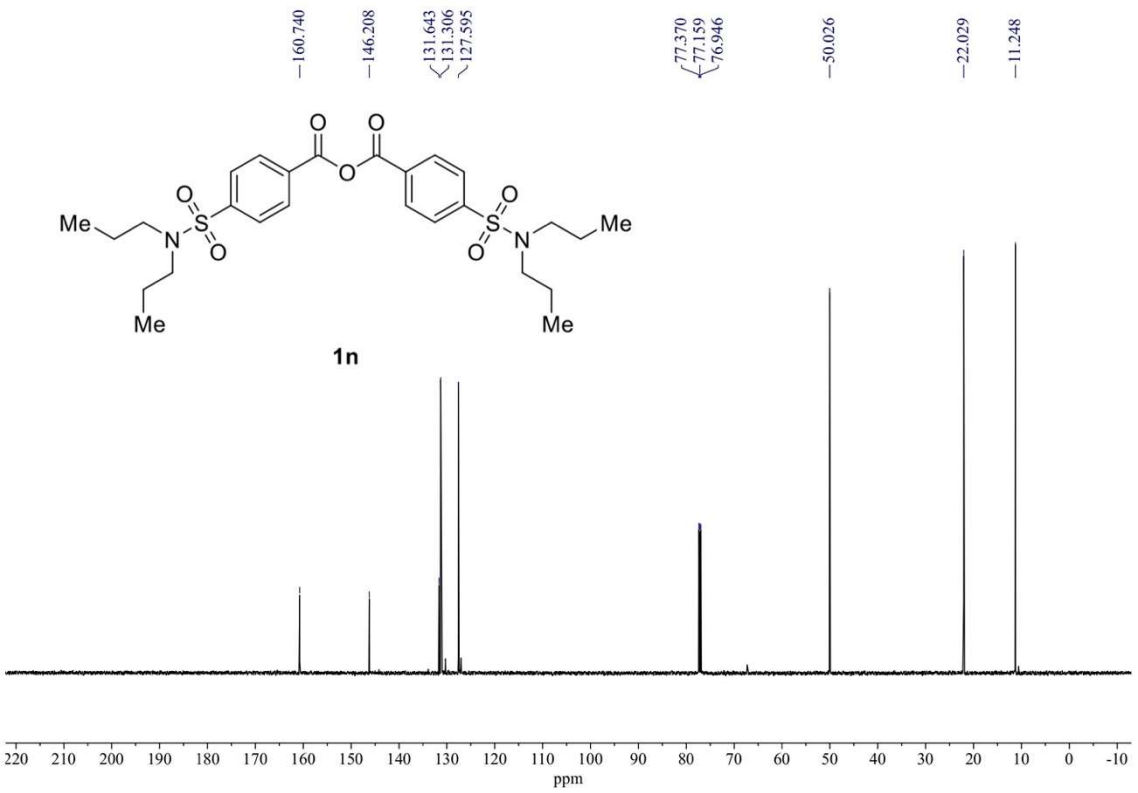

^{1}H NMR (600 MHz) and ^{13}C{^{1}H} NMR (151 MHz) spectra of **1n** (rt, $CDCl_3$).

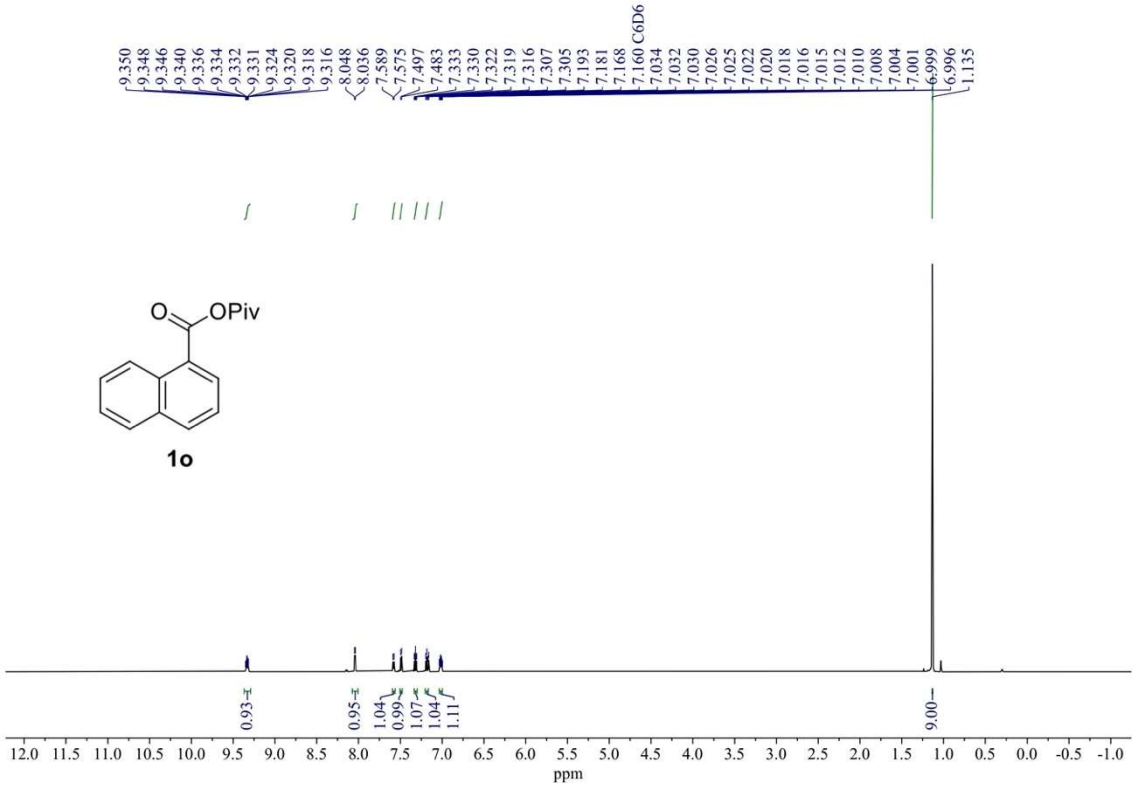

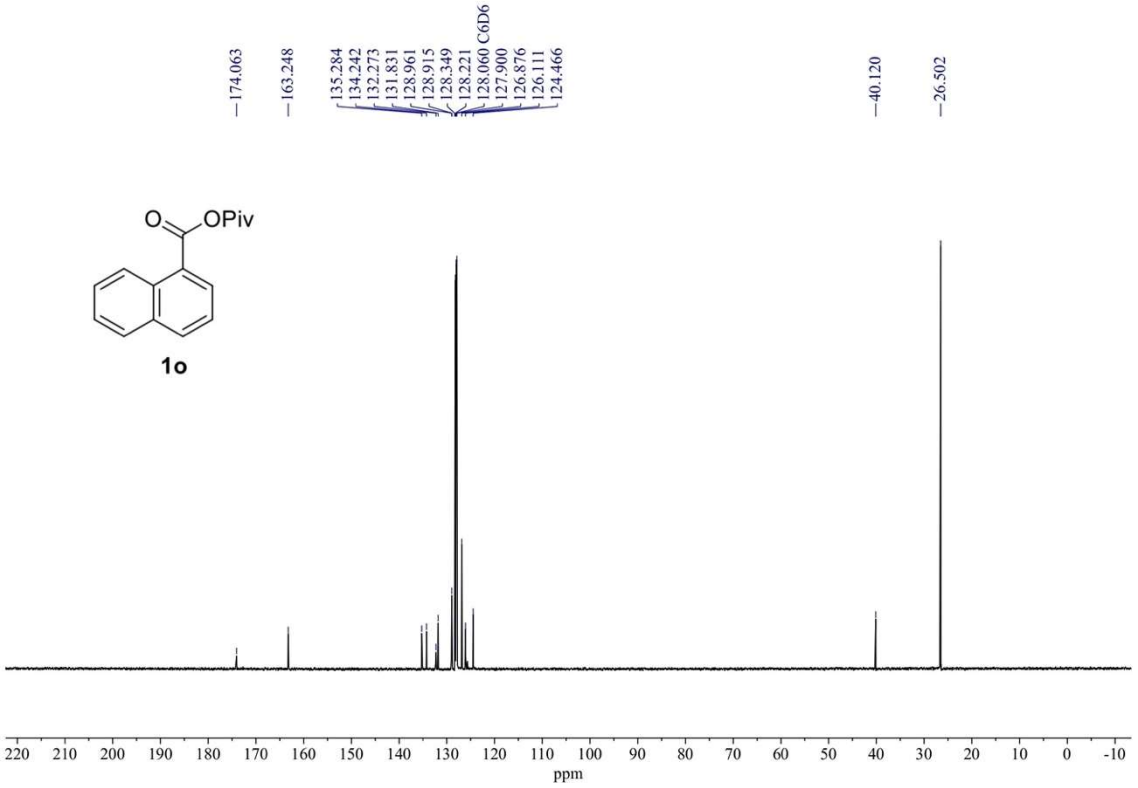

^{1}H NMR (600 MHz) and ^{13}C{^{1}H} NMR (151 MHz) spectra of **1o** (rt, C_6D_6).

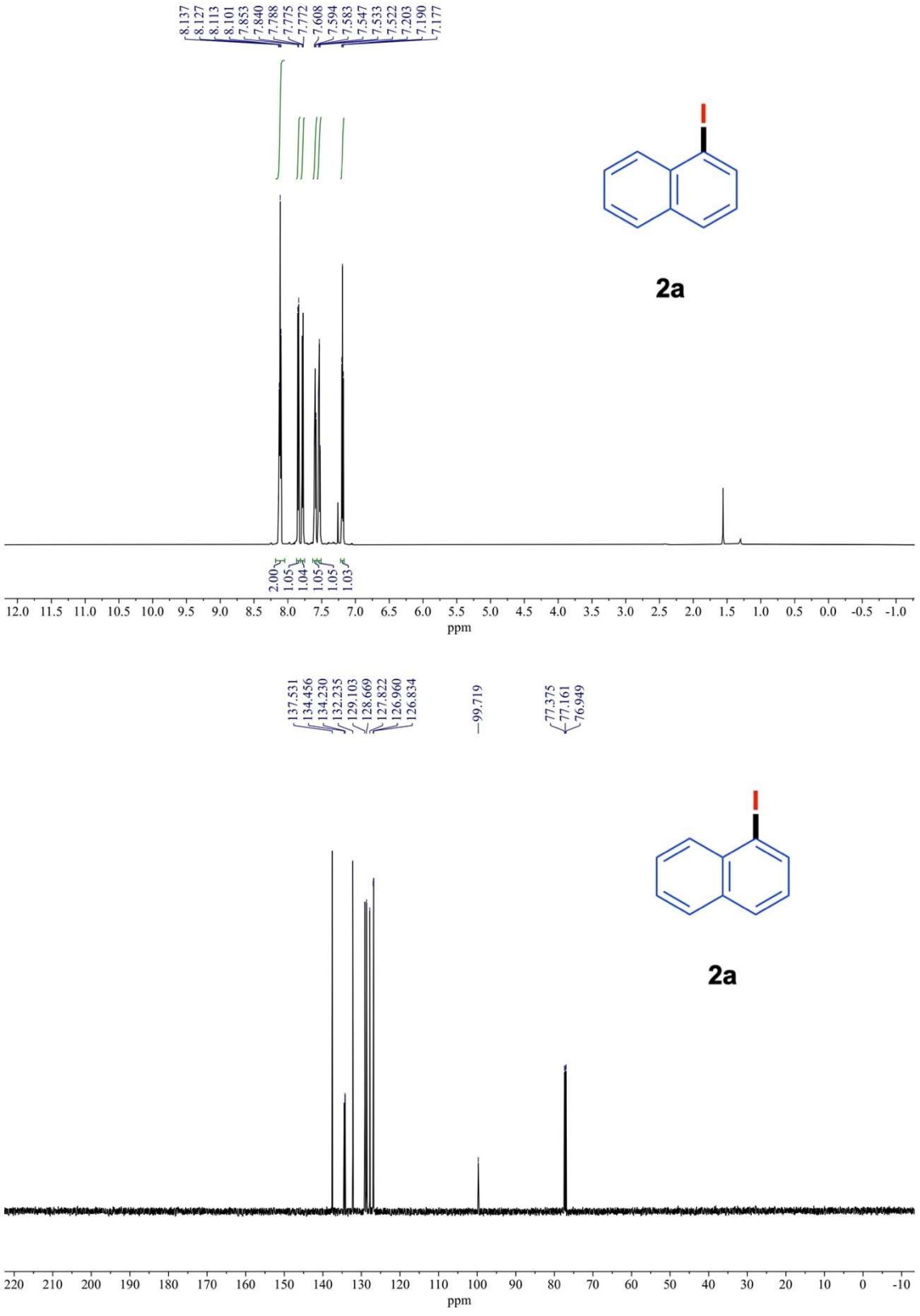

^{1}H NMR (600 MHz) and ^{13}C{^{1}H} NMR (151 MHz) spectra of **2a** (rt, $CDCl_3$).

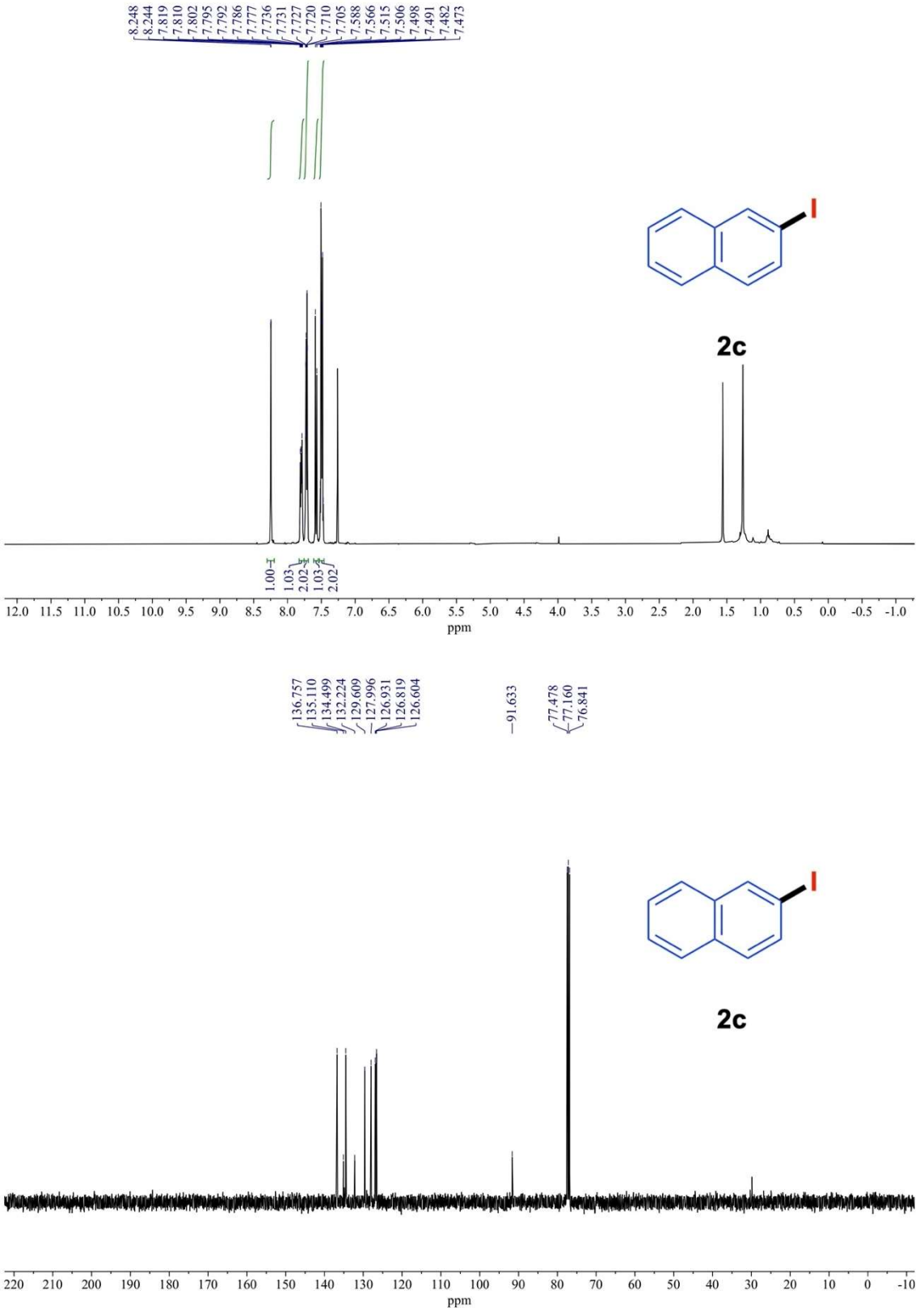

^{1}H NMR (400 MHz) and ^{13}C{^{1}H} NMR (101 MHz) spectra of **2c** (rt, $CDCl_3$).

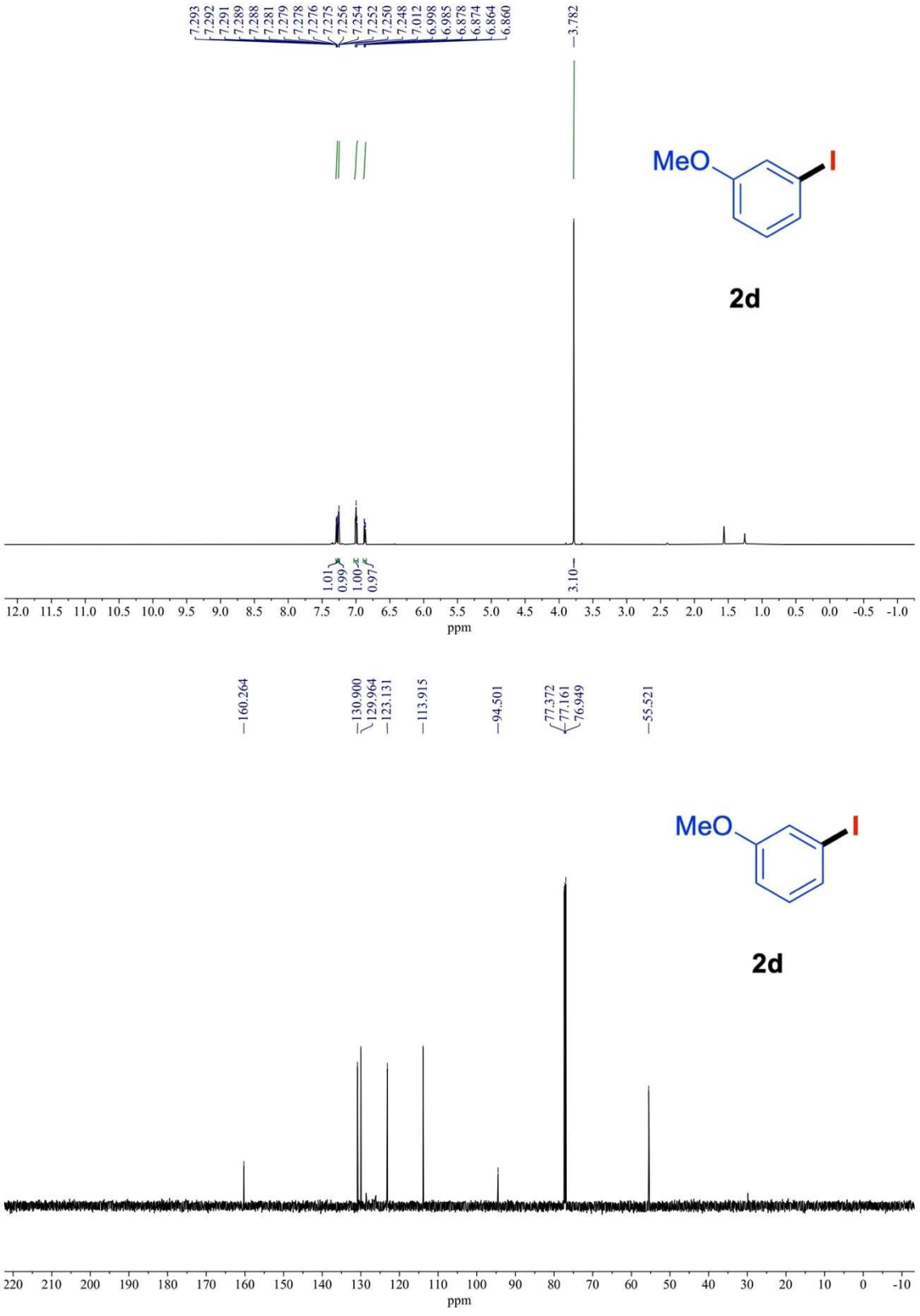

^{1}H NMR (600 MHz) and ^{13}C{^{1}H} NMR (151 MHz) spectra of **2d** (rt, $CDCl_3$).

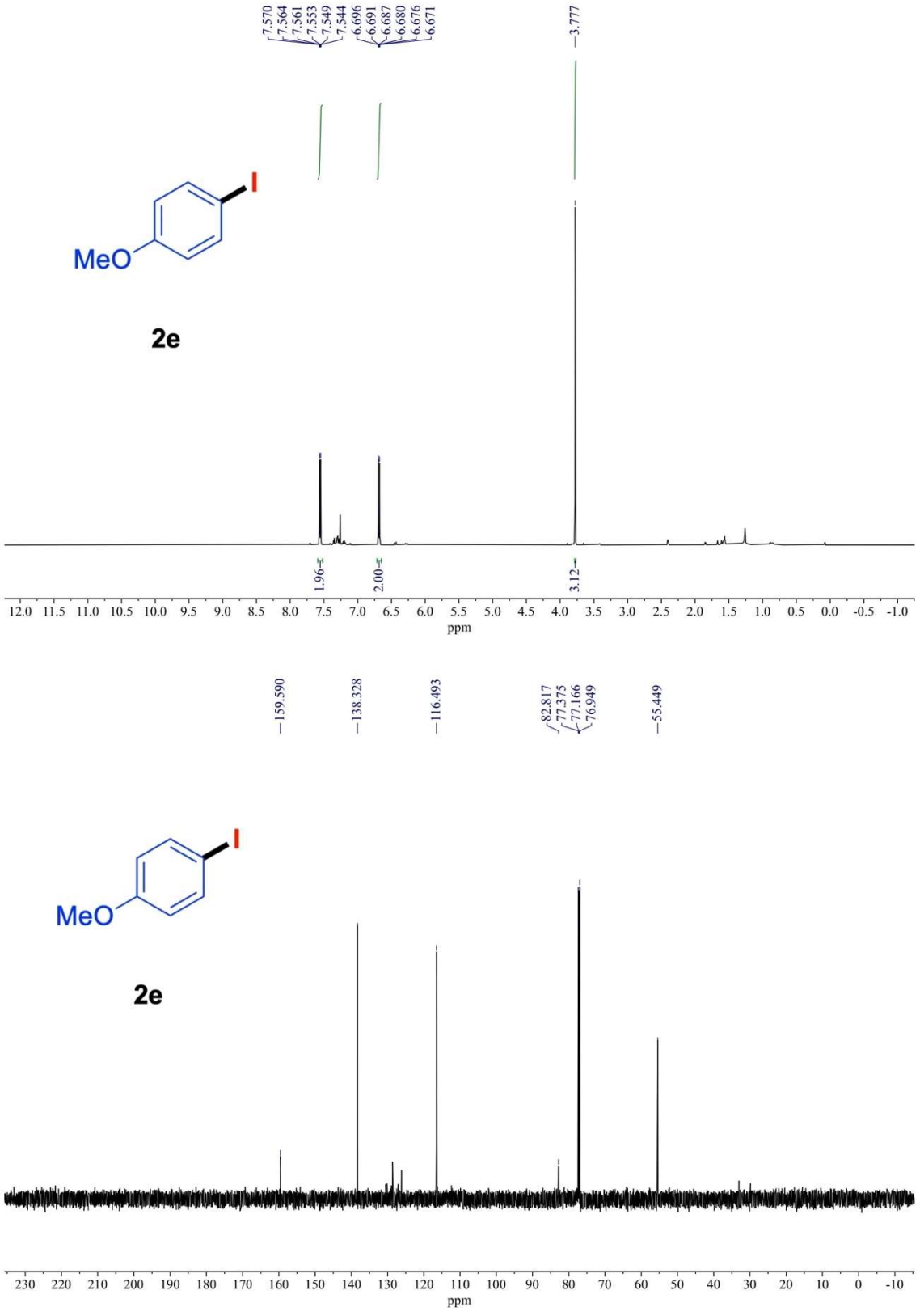

^{1}H NMR (600 MHz) and ^{13}C{^{1}H} NMR (151 MHz) spectra of **2e** (rt, $CDCl_3$).

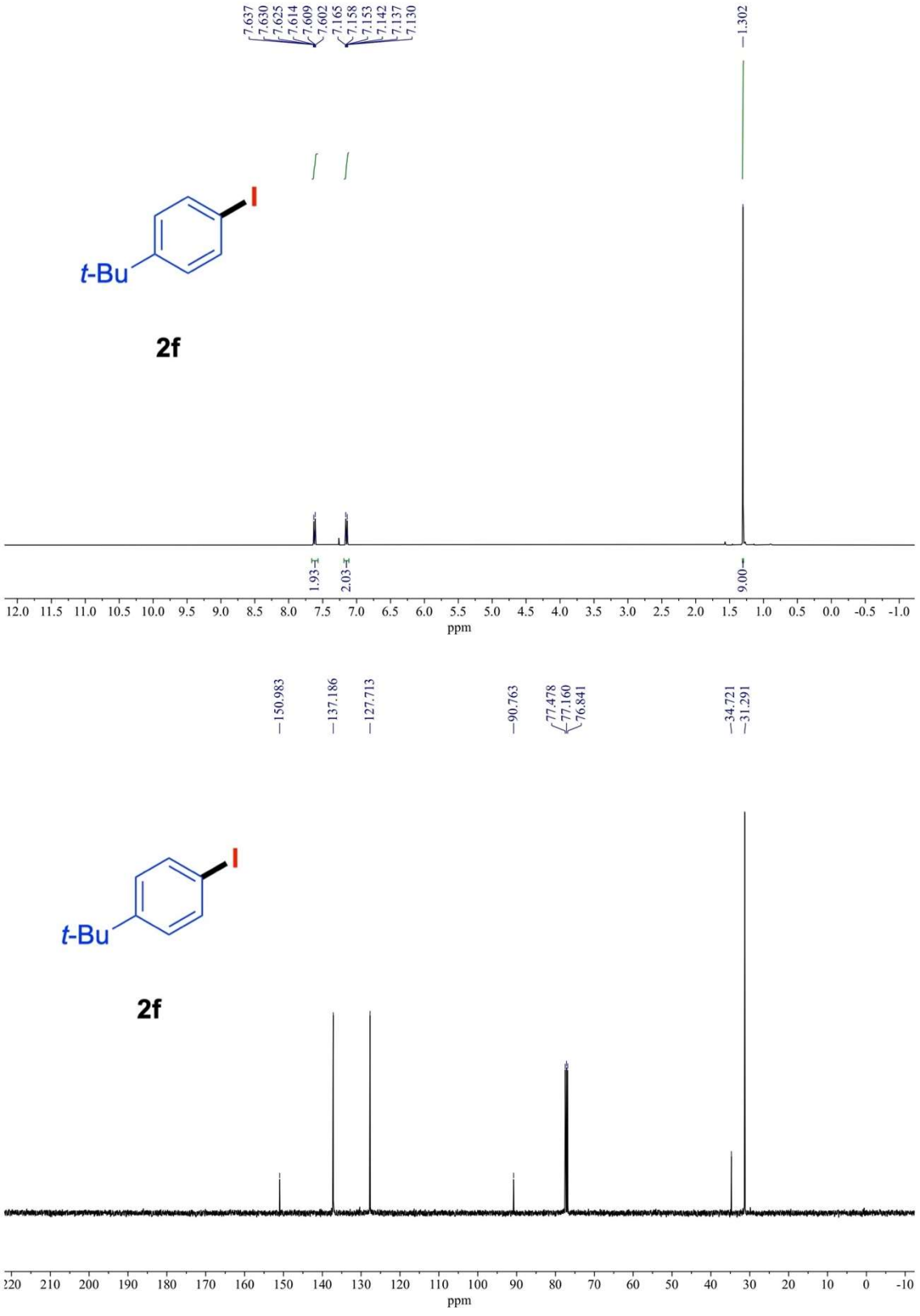

^{1}H NMR (400 MHz) and ^{13}C{^{1}H} NMR (101 MHz) spectra of **2f** (rt, $CDCl_3$).

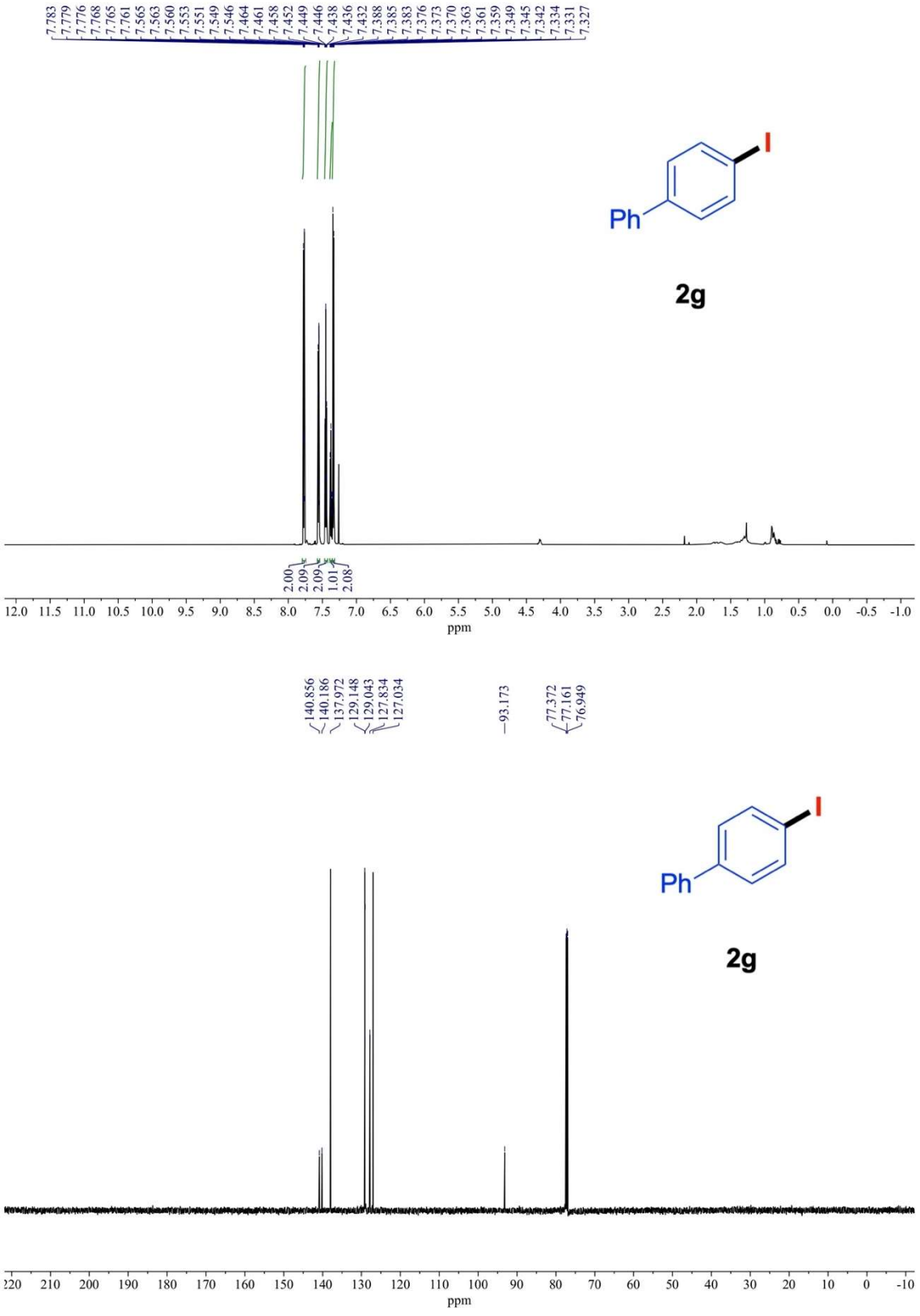

^{1}H NMR (600 MHz) and ^{13}C{^{1}H} NMR (151 MHz) spectra of **2g** (rt, $CDCl_3$).

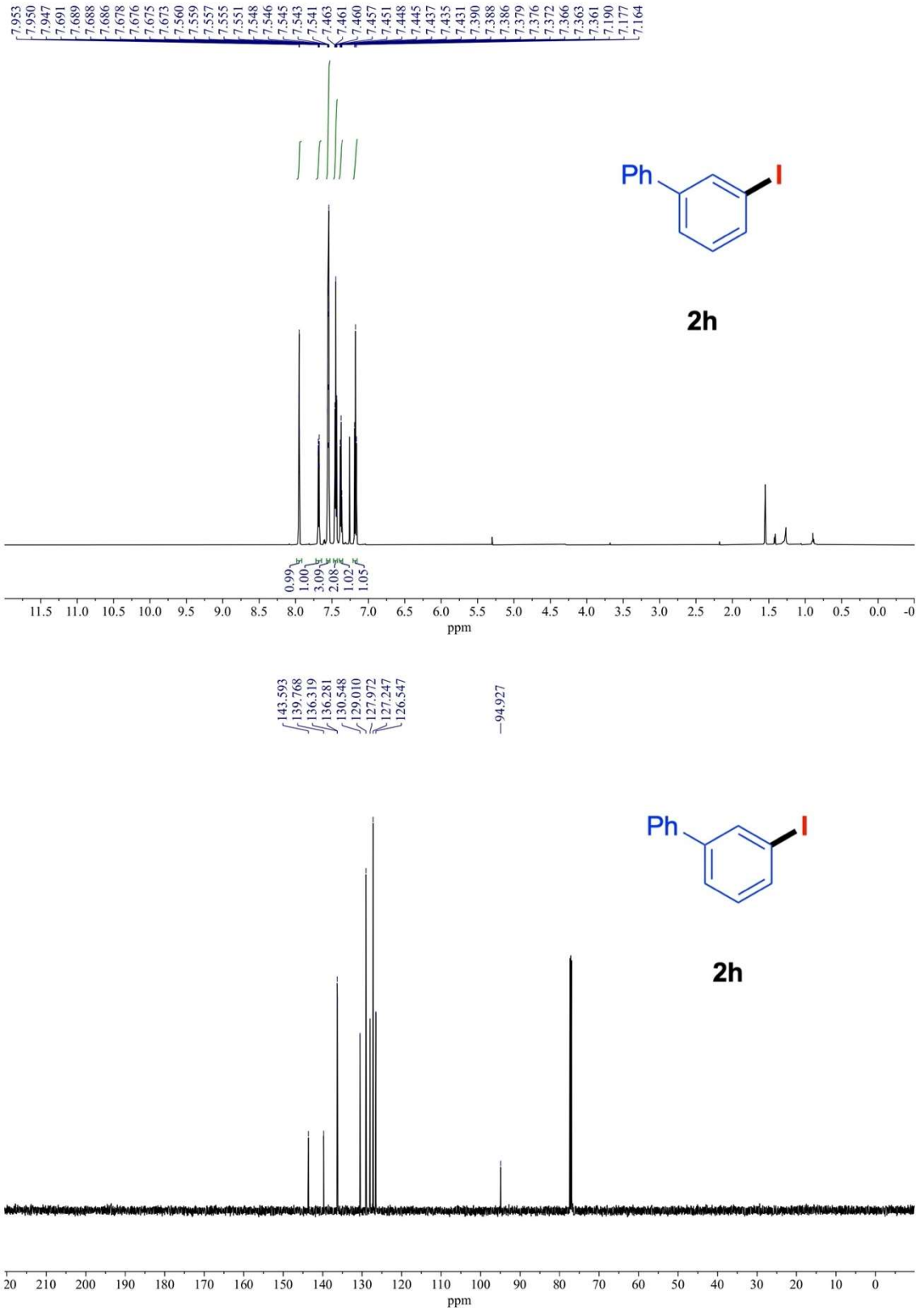

^{1}H NMR (600 MHz) and ^{13}C{^{1}H} NMR (151 MHz) spectra of **2h** (rt, $CDCl_3$).

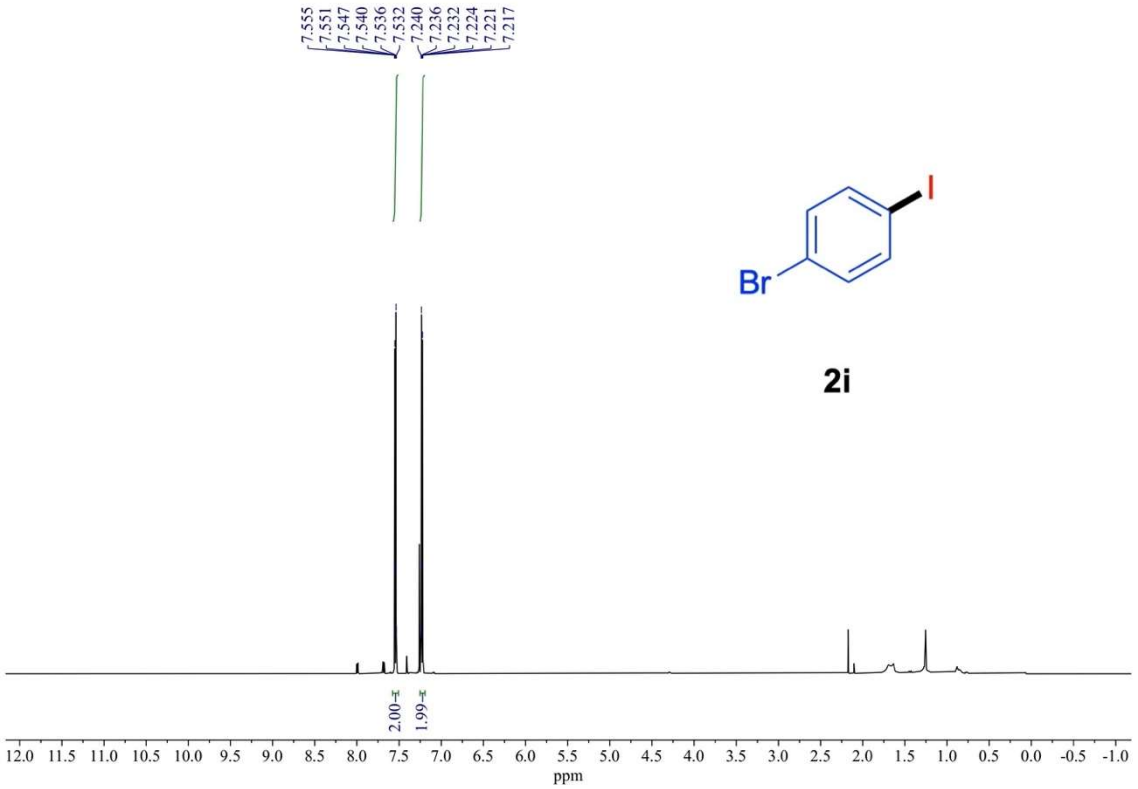

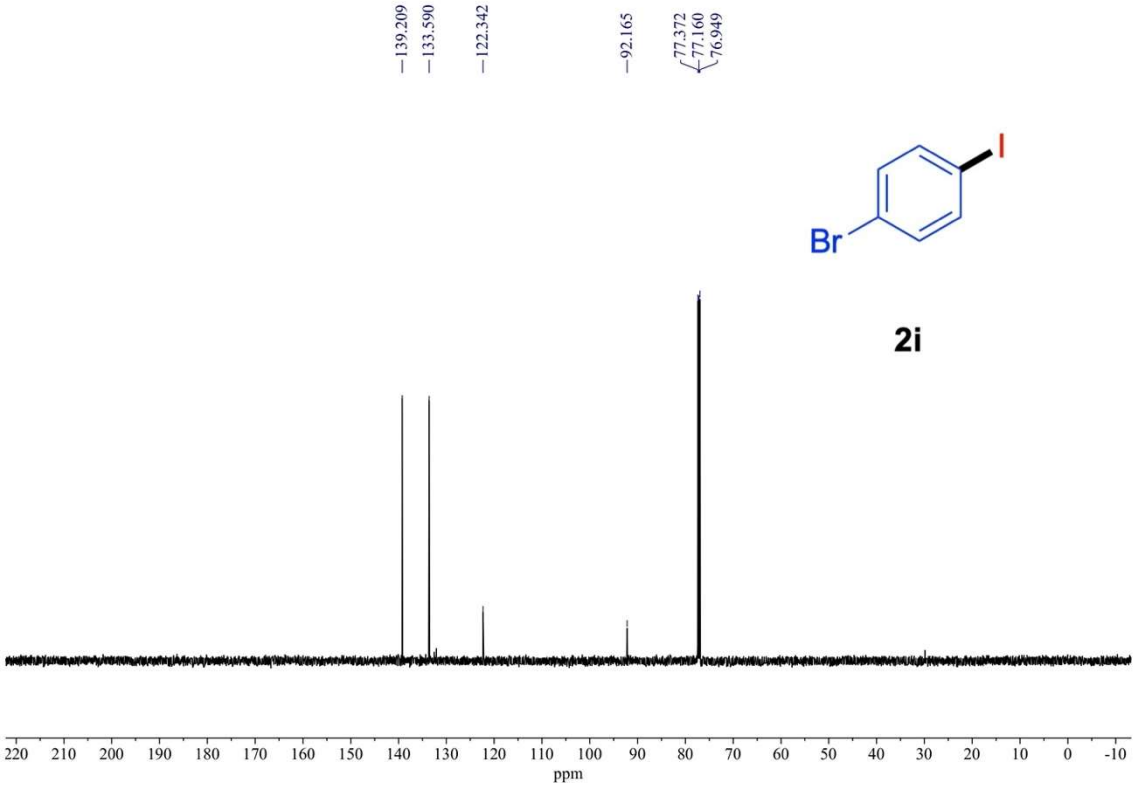

^{1}H NMR (600 MHz) and ^{13}C{^{1}H} NMR (151 MHz) spectra of **2i** (rt, $CDCl_3$).

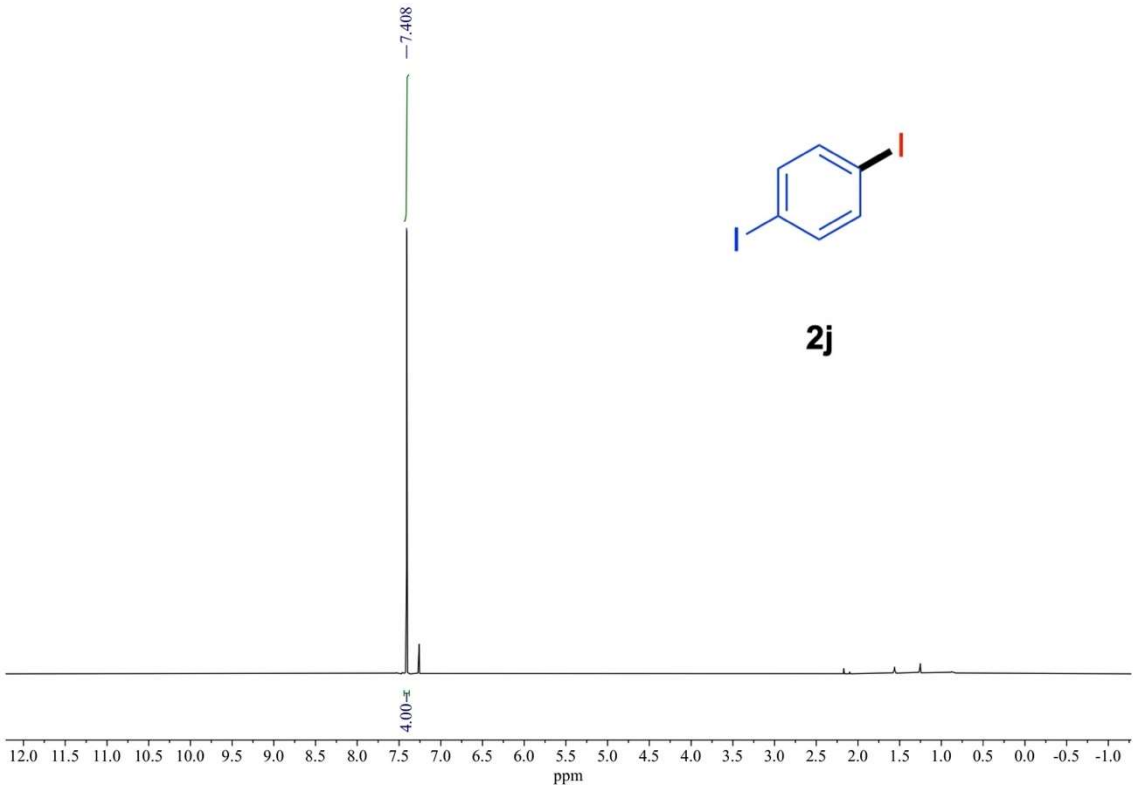

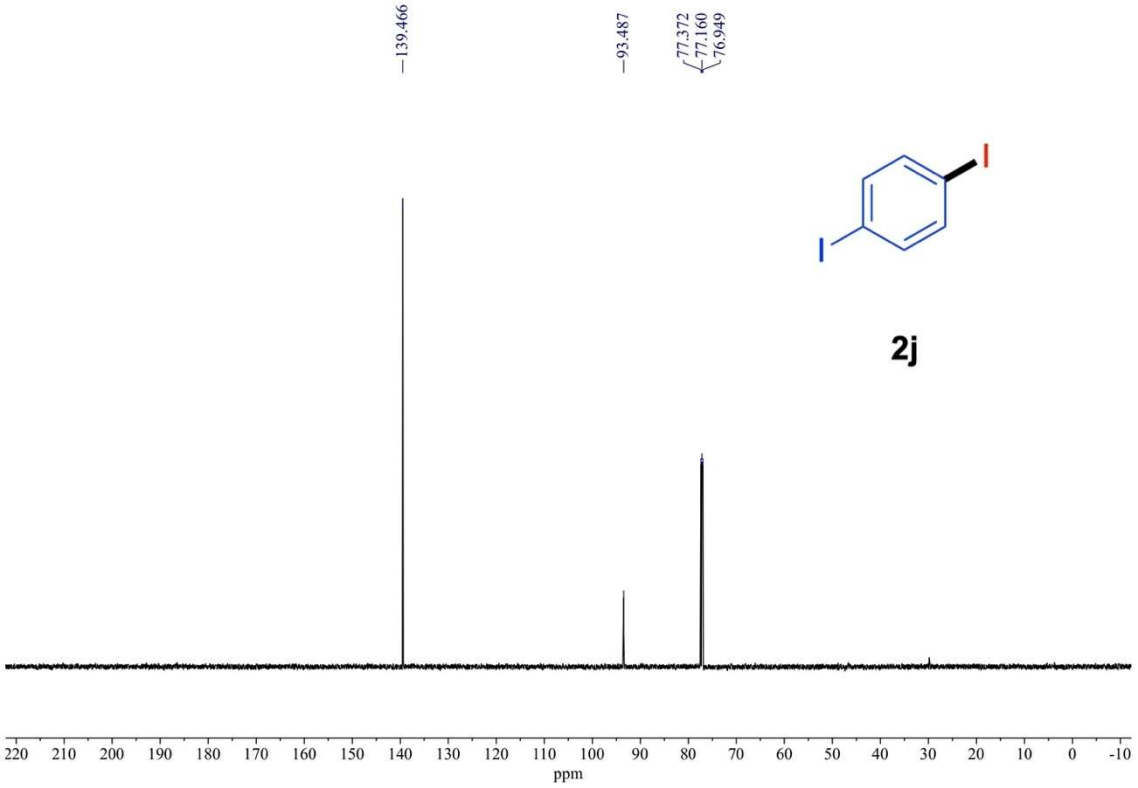

^{1}H NMR (600 MHz) and ^{13}C{^{1}H} NMR (151 MHz) spectra of **2j** (rt, $CDCl_3$).

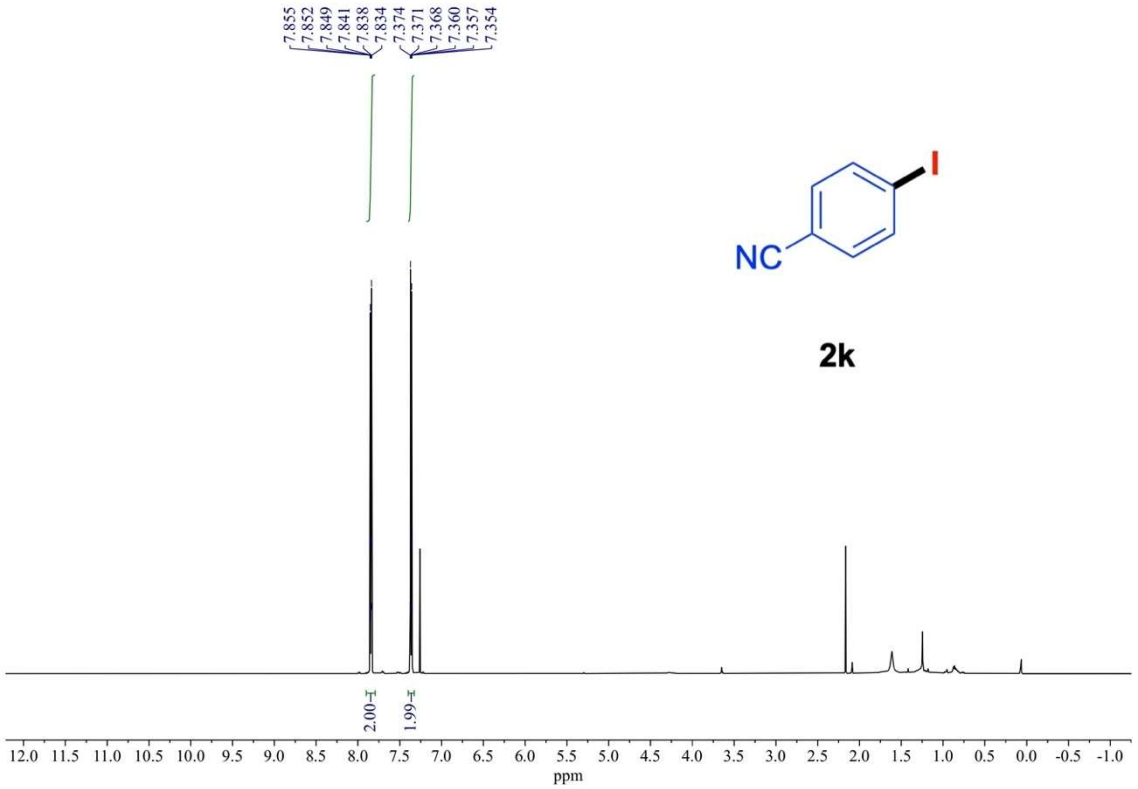

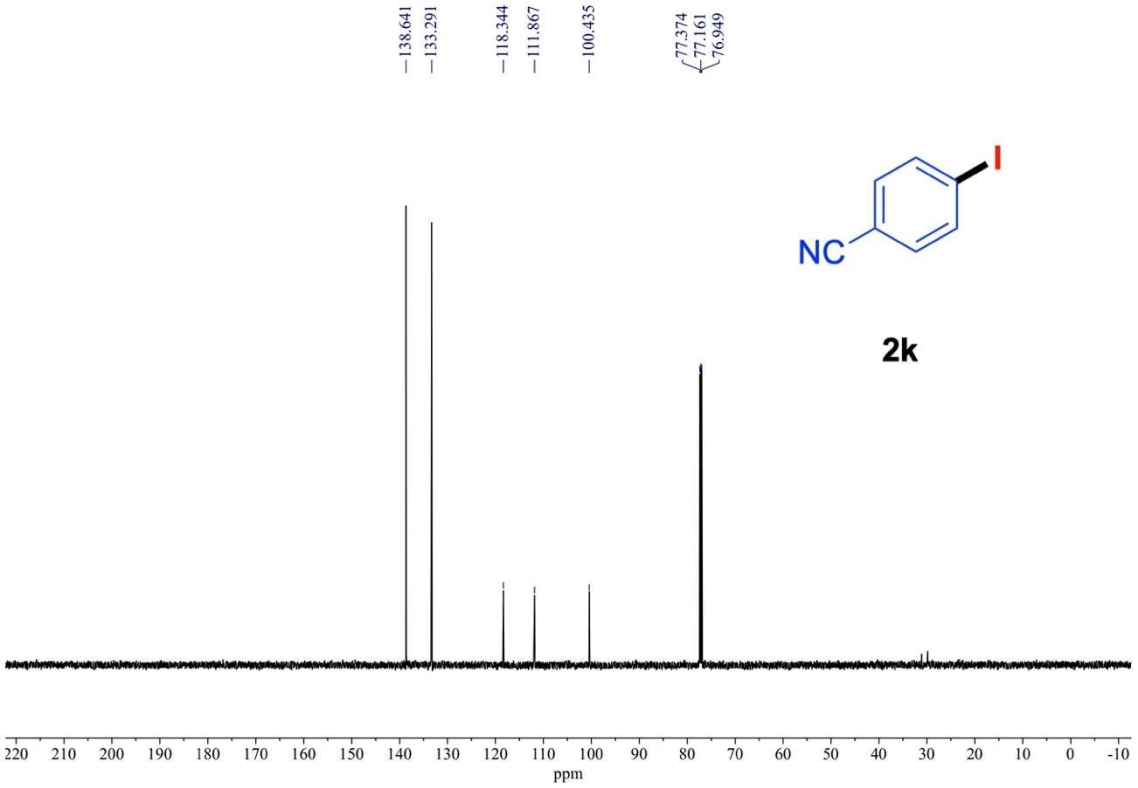

^{1}H NMR (600 MHz) and ^{13}C{^{1}H} NMR (151 MHz) spectra of **2k** (rt, $CDCl_3$).

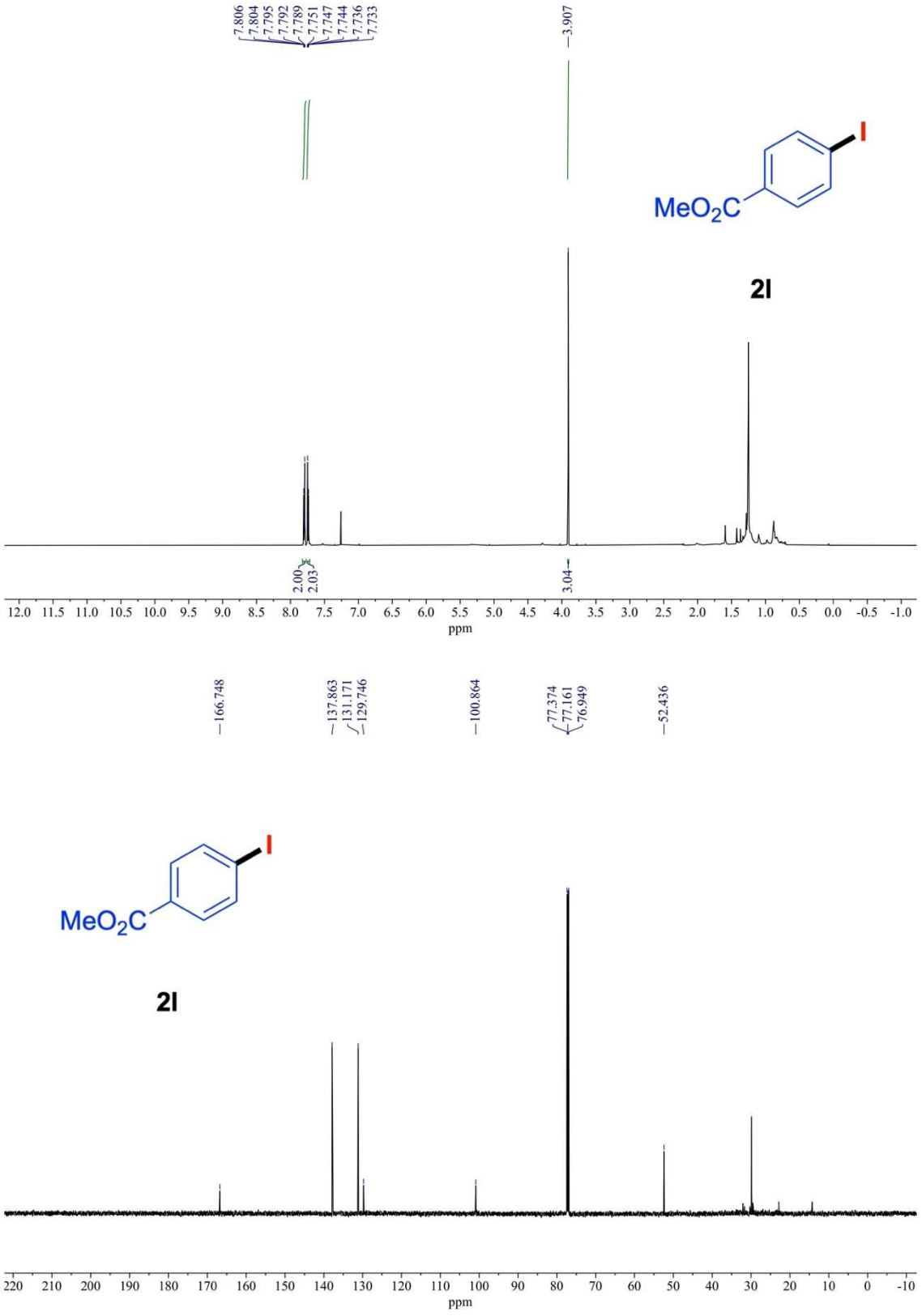

^{1}H NMR (600 MHz) and ^{13}C{^{1}H} NMR (151 MHz) spectra of **2l** (rt, $CDCl_3$).

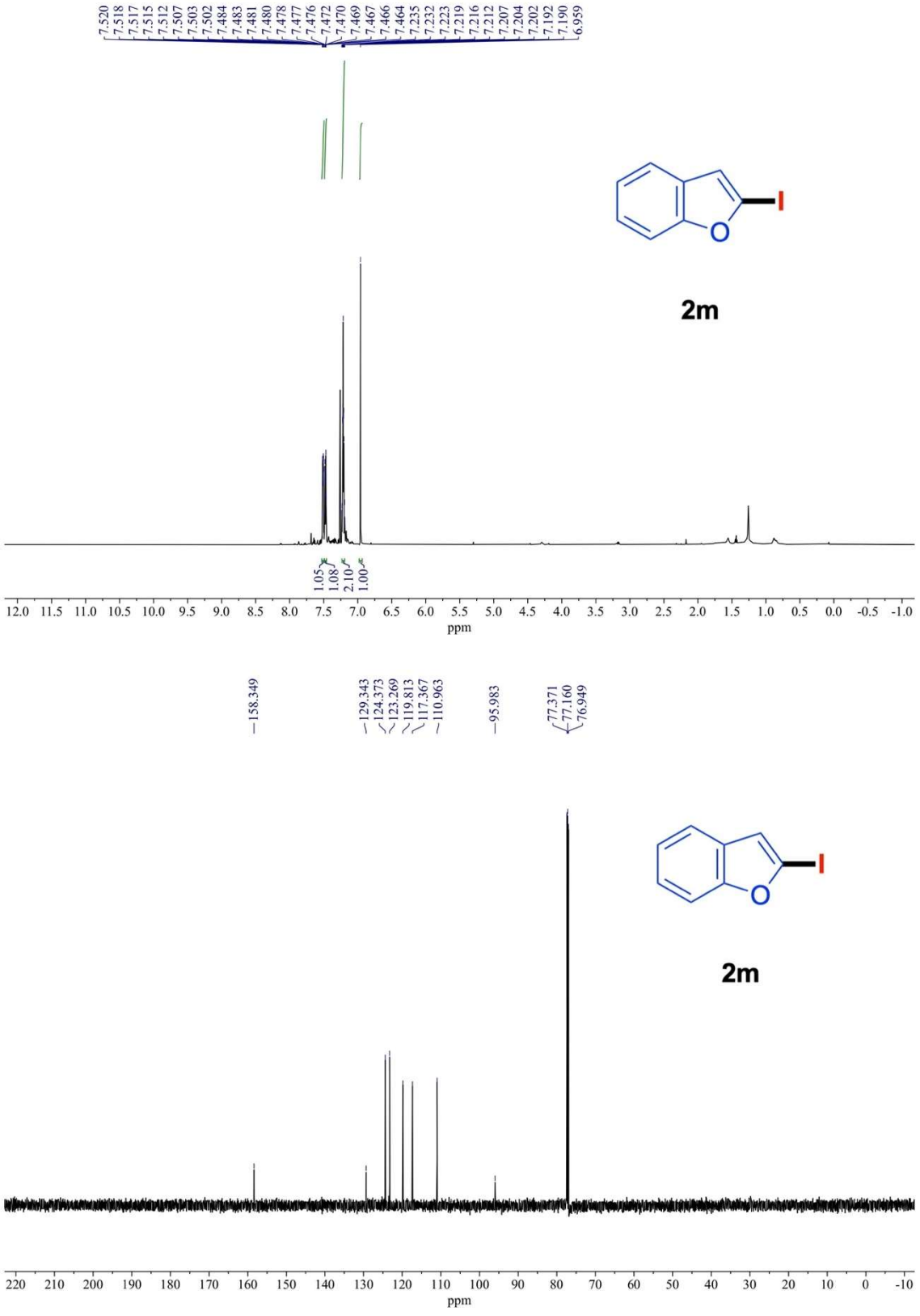

^{1}H NMR (600 MHz) and ^{13}C{^{1}H} NMR (151 MHz) spectra of **2m** (rt, $CDCl_3$).

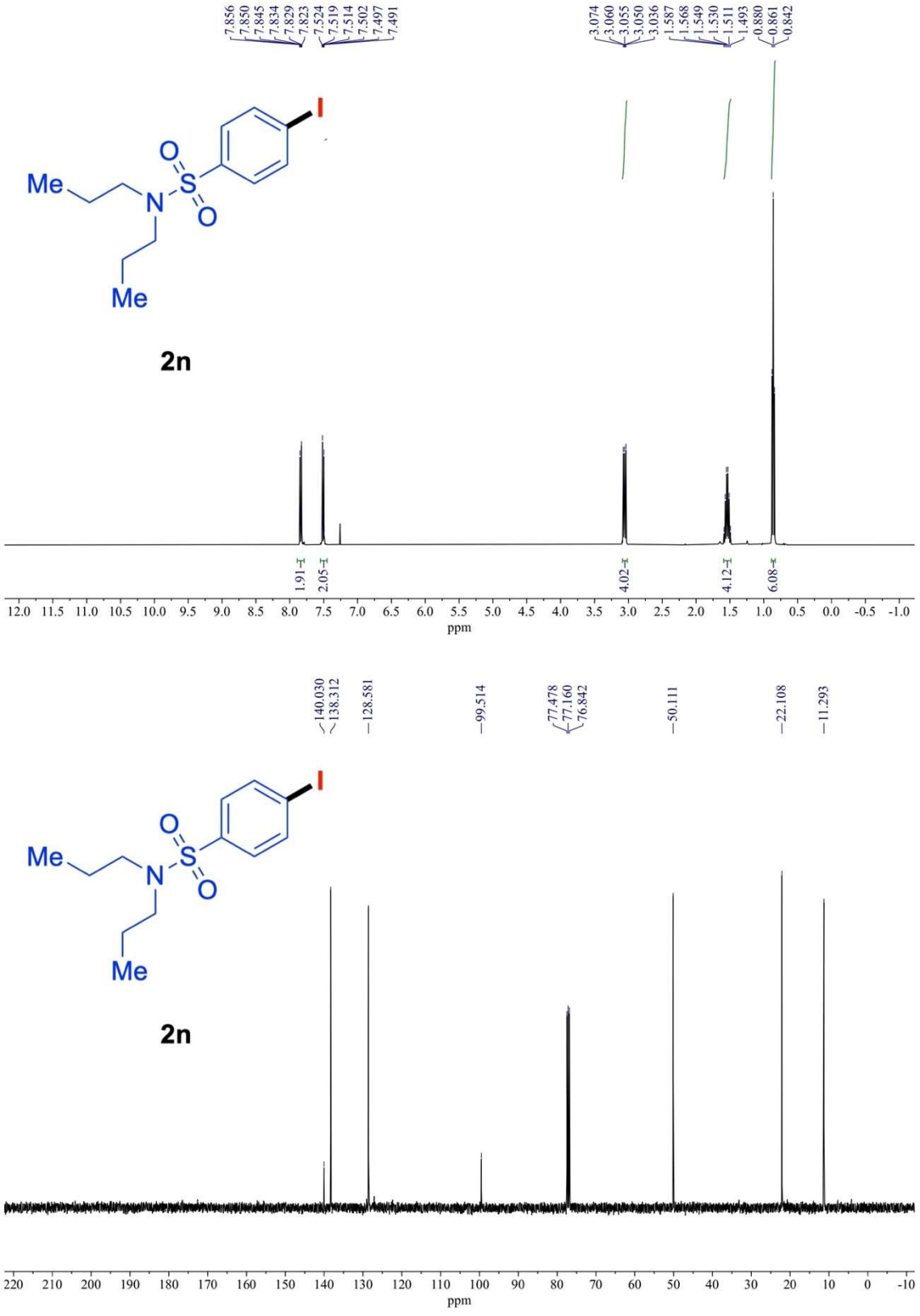

^{1}H NMR (400 MHz) and ^{13}C{^{1}H} NMR (101 MHz) spectra of **2n** (rt, $CDCl_3$).

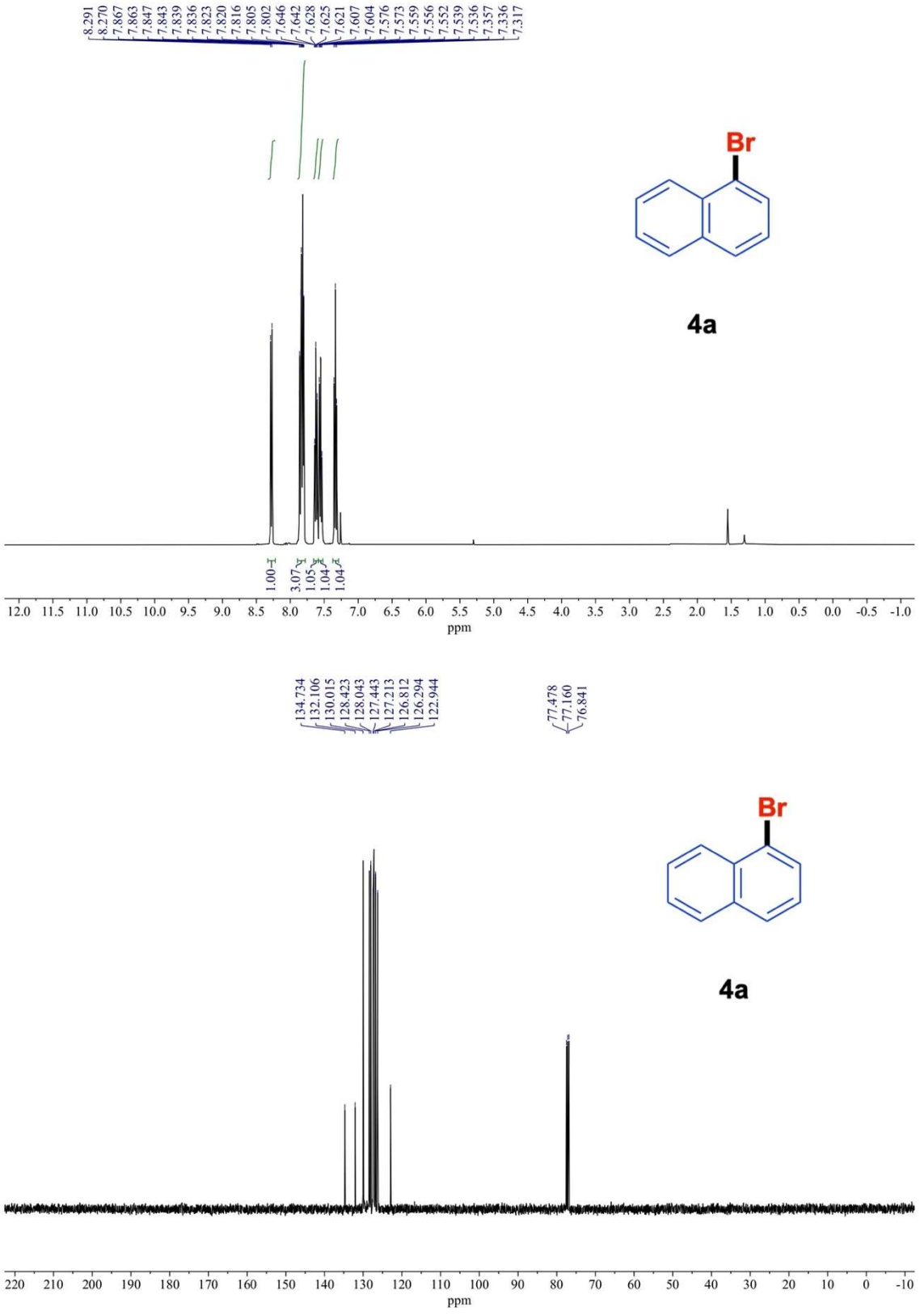

^{1}H NMR (400 MHz) and ^{13}C{^{1}H} NMR (101 MHz) spectra of **4a** (rt, $CDCl_3$).

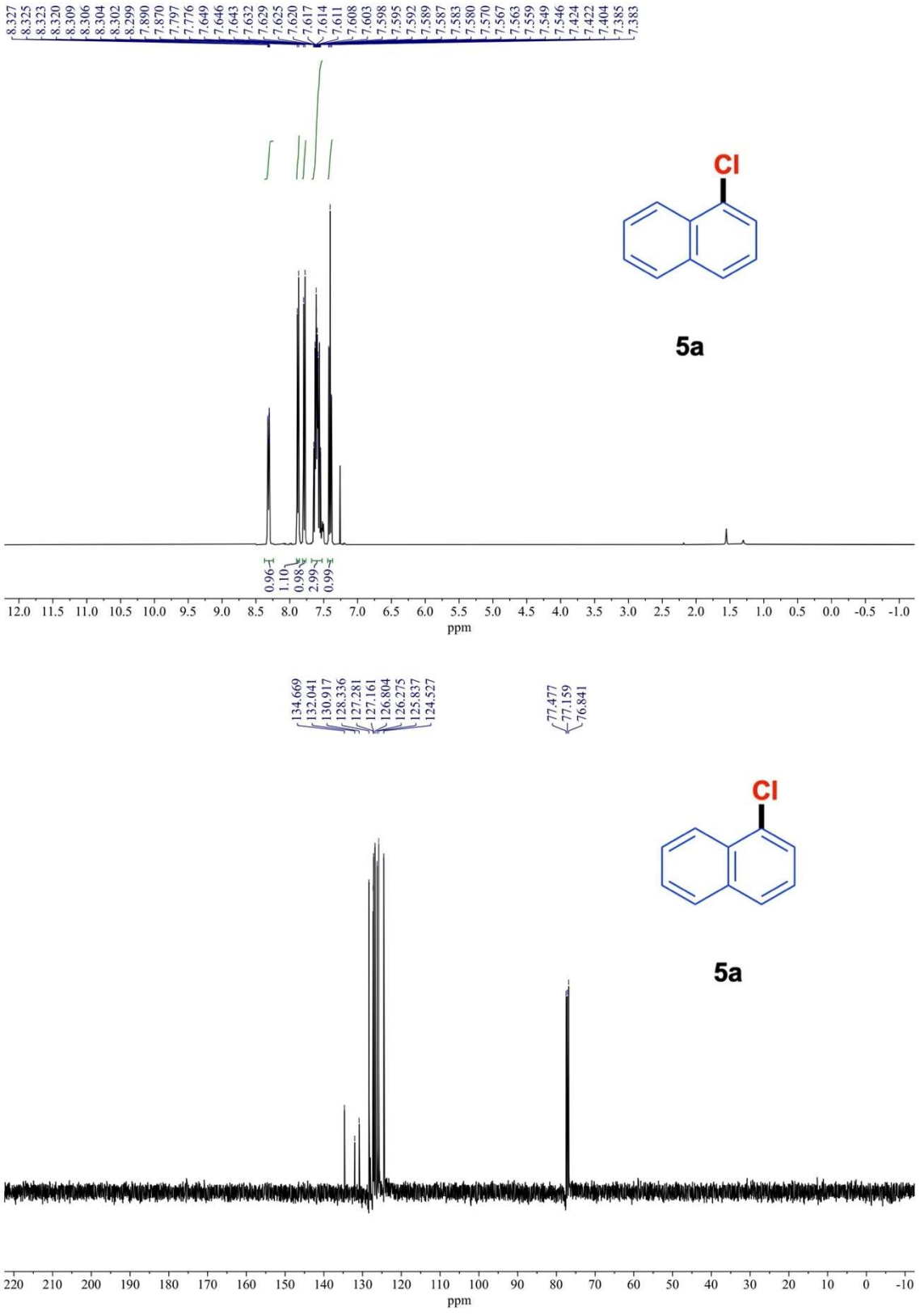

^{1}H NMR (400 MHz) and ^{13}C{^{1}H} NMR (101 MHz) spectra of **5a** (rt, $CDCl_3$).

3-5 References

1. (a) Gooßen, L. J.; Rodríguez, N.; Gooßen, K. *Angew. Chem., Int. Ed.* **2008**, *47*, 3100; *Angew. Chem.* **2008**, *120*, 3144. (b) Dzik, W. I.; Lange, P. P.; Gooßen, L. J. *Chem. Sci.* **2012**, *3*, 2671.
2. (a) Borodine, A. *Liebigs Ann.* **1861**, *119*, 121. (b) Hunsdiecker, H.; Hunsdiecker, C. *Ber. Dtsch. Chem. Ges. B* **1942**, *75*, 291. (c) Hunsdiecker, H.; Hunsdiecker, C.; Vogt, E. *HalogenContaining Organic Compounds.* US2176181, 1939.
3. Schwarz, J.; König, B. *Green Chem.* **2018**, *20*, 323.
4. Varenikov, A.; Shapiro, E.; Gandelman, M. *Chem. Rev.* **2021**, *121*, 412.
5. (a) Goncalves, R.; Brown, E. V. J. Org. Chem. 1954, 19, 4. (b) Barton, D. H. R.; Lacher, B.; Zard, S. Z. *Tetrahedron* **1987**, *43*, 4321. (c) Cornella, J.; Rosillo-Lopez, M.; Larrosa, I. *Adv. Synth. Catal.* **2011**, *353*, 1359.
6. (a) Cristol, S.; Firth, W. Jr. *J. Org. Chem.* **1961**, *26*, 280. (b) Kochi, J. K. *J. Am. Chem. Soc.* **1965**, *87*, 2500. (c) Zhan, K.; Li, Y. *Catalysts* **2017**, *7*, 314. (d) Koo, B.-S.; Kim, E.-H.; Lee, K.-J. *Synth. Commun.* **2002**, *32*, 2275.
7. (a) Kulbitski, K.; Nisnevich, G.; Gandelman, M. *Adv. Synth. Catal.* **2011**, *353*, 1438. (b) Hazarika, D.; Phukan, P. *Tetrahedron Lett.* **2018**, *59*, 4593. (c) Jayaraman, A.; Cho, E.; Kim, J.; Lee, S. *Adv. Synth. Catal.* **2018**, *360*, 3978. (d) Jayaraman, A.; Lee, S. *Org. Lett.* **2019**, *21*, 3485. (e) Zhang, X.; Feng, X.; Zhang, H.; Yamamoto, Y.; Bao, M. *Green Chem.* **2019**, *21*, 5565.
8. (a) Yang, Y.; Zhang, L.; Deng, G. J.; Gong, H. *Sci. Rep.* **2017**, *7*, 40430. (b) Peng, X.; Shao, X.-F.; Liu, Z.-Q. *Tetrahedron Lett.* **2013**, *54*, 3079. (c) Fu, Z.; Li, Z.; Song, Y.; Yang, R.; Liu, Y.; Cai, H. *J. Org. Chem.* **2016**, *81*, 2794.
9. (a) Patra, T.; Mukherjee, S.; Ma, J.; StriethKalthoff, F.; Glorius, F. *Angew. Chem., Int. Ed.* **2019**, *58*, 10514; *Angew. Chem.* **2019**, *131*, 10624. (b) Jiang, M.; Yang, H.; Jin, Y.; Ou, L.; Fu, H. *Synlett* **2018**, *29*, 1572.
10. (a) Fu, Z.; Jiang, Y.; Jiang, L.; Li, Z.; Guo, S.; Cai, H. *Tetrahedron Lett.* **2018**, *59*, 4458. (b) Li, Z.; Wang, K.; Liu, Z.-Q. *Synlett* **2014**, *25*, 2508. (c) Perry, G. J. P.; Quibell, J. M.; Panigrahi, A.; Larrosa, I. *J. Am. Chem. Soc.* **2017**, *139*, 11527. (d) Quibell, J. M.; Perry, G. J. P.; Cannas, D. M.; Larrosa, I. *Chem. Sci.* **2018**, *9*, 3860.
11. (a) Jones, D. J.; Lautens, M.; McGlacken, G. P. *Nat. Catal.* **2019**, *2*, 843. (b) Hartwig, J. F. *Organotransition Metal Chemistry: From Bonding to Catalysis*; University Science Books: Sausalito, CA, 2010. (c) Petrone, D. A.; Ye, J.; Lautens, M. *Chem. Rev.* **2016**, *116*, 8003. (d) Chen,

C.; Tong, X. *Org. Chem. Front.* **2014**, *1*, 439.

12. Tung, P.; Mankad, N. P. *J. Am. Chem. Soc.* **2023**, *145*, 9423.
13. (a) Komiya, S.; Yamamoto, A.; Yamamoto, T. *Chem. Lett.* **1981**, *10*, 193. (b) Sano, K.; Yamamoto, T.; Yamamoto, A. *Chem. Lett.* **1983**, *12*, 115. (c) Nagayama, K.; Kawataka, F.; Sakamoto, M.; Shimizu, I.; Yamamoto, A. *Chem. Lett*. **1995**, *24*, 367. (d) Sano, K.; Yamamoto, T.; Yamamoto, A. *Bull. Chem. Soc. Jpn.* **1984**, *57*, 2741. (e) Miller, J. A.; Nelson, J. A. *Organometallics* **1991**, *10*, 2958.
14. (a) Zhao, Q.; Szostak, M. *ChemSusChem* **2019**, *12*, 2983. (b) Guo, L.; Rueping, M. *Chem.—Eur. J.* **2018**, *24*, 7794. (c) Lu, H.; Yu, T.-Y.; Xu, P.-F.; Wei, H. *Chem. Rev.* **2021**, *121*, 365. (d) Lalloo, N.; Brigham, C. E.; Bunnell, A.; Sanford, M. S. *Acc. Chem. Res.* **2022**, *55*, 3430.
15. For several selected reviews, see: (a) Blanchard, N.; Bizet, V. *Angew. Chem., Int. Ed.* **2019**, *58*, 6814; *Angew. Chem.* **2019**, *131*, 6886. (b) Ogiwara, Y.; Sakai, N. *Angew. Chem., Int. Ed.* **2020**, *59*, 574; *Angew. Chem.* **2020**, *132*, 584. (c) Wang, Z.; Wang, X.; Nishihara, Y. *Chem.—Asian J.* **2020**, *15*, 1234. (d) Fu, L.; Chen, Q.; Nishihara, Y. *Chem. Rec.* **2021**, *21*, 3394. (e) Tian, T.; Chen, Q.; Li, Z.; Nishihara, Y. *Synthesis* **2022**, *54*, 3667.
16. Blum, J.; Lipshes, Z. *J. Org. Chem.* **1969**, *34*, 3076.
17. (a) Zhang, X.; Jordan, F.; Szostak, M. *Org. Chem. Front.* **2018**, *5*, 2515. (b) Trost, B. M.; Chen, F. *Tetrahedron Lett.* **1971**, *12*, 2603. (c) Miller, J. A.; Nelson, J. A.; Byrne, M. P. *J. Org. Chem.* **1993**, *58*, 18. (d) Gooßen, L. J.; Rodríguez, N. *Chem. Commun.* **2004**, 724.
18. (a) Kajita, Y.; Kurahashi, T.; Matsubara, S. *J. Am. Chem. Soc.* **2008**, *130*, 17226. (b) Matsuda, T.; Suzuki, K. *RSC Adv.* **2014**, *4*, 37138. (c) Prakash, R.; Shekarrao, K.; Gogoi, S.; Boruah, R. C. *Chem. Commun.* **2015**, *51*, 9972. (d) Mayakrishnan, S.; Arun, Y.; Maheswari, N. U.; Perumal, P. T. *Chem. Commun.* **2018**, *54*, 11889.
19. (a) Jin, W.; Yu, Z.; He, W.; Ye, W.; Xiao, W.-J. *Org. Lett.* **2009**, *11*, 1317. (b) Maetani, S.; Fukuyama, T.; Ryu, I. *Org. Lett.* **2013**, *15*, 2754. (c) Qiu, X.; Wang, P.; Wang, D.; Wang, M.; Yuan, Y.; Shi, Z. *Angew. Chem., Int. Ed.* **2019**, *58*, 1504; *Angew. Chem.* **2019**, *131*, 1518. (d) Han, X.; Yuan, Y.; Shi, Z. *J. Org. Chem.* **2019**, *84*, 12764. (e) Liu, C.; Ji, C.-L.; Zhou, T.; Hong, X.; Szostak, M. *Angew. Chem., Int. Ed.* **2021**, *60*, 10690; *Angew. Chem.* **2021**, *133*, 10785.
20. (a) Stephan, M. S.; Teunissen, A. J. J. M.; Verzijl, G. K. M.; de Vries, J. G. *Angew. Chem., Int. Ed.* **1998**, *37*, 662; *Angew. Chem.* **1998**, *37*, 688. (b) Gooßen, L. J.; Paetzold, J.; Winkel, L. *Synlett* **2002**, *10*, 1721.

21. O'Brien, E. M.; Bercot, E. A.; Rovis, T. *J. Am. Chem. Soc.* **2003**, *125*, 10498.

22. (a) Gooßen, L. J.; Paetzold, J. *Adv. Synth. Catal.* **2004**, *346*, 1665. (b) Liu, C.; Ji, C.-L.; Qin, Z.-X.; Hong, X.; Szostak, M. *iScience* **2019**, *19*, 749. (c) Ji, H.; Ma, Y.; Zhang, J.; Xing, F.; Liu, C. *Org. Biomol. Chem.* **2024**, *22*, 5578.

23. (a) Li, X.; Liu, L.; Huang, T.; Tang, Z.; Li, C.; Li, W.; Zhang, T.; Li, Z.; Chen, T. *Org. Lett.* **2021**, *23*, 3304. (b) Liu, C.; Szostak, M. *Org. Lett.* **2021**, *23*, 4726. (c) Bie, F.; Liu, X.; Szostak, M.; Liu, C. *J. Org. Chem.* **2023**, *88*, 4442. (d) Chen, L.; Ji, H.; Ding, Y.; Szostak, M.; Liu, C. *J. Org. Chem.* **2024**, *89*, 2665.

24. (a) Liu, C.; Ji, C.-L.; Hong, X.; Szostak, M. *Angew. Chem., Int. Ed.* **2018**, *57*, 16721; *Angew. Chem.* **2018**, *130*, 16963. (b) Zhang, W.; Bie, F.; Ma, J.; Zhou, F.; Szostak, M.; Liu, C. *J. Org. Chem.* **2021**, *86*, 17445. (c) Li, K.; Li, R.; Cui, Y.; Liu, C. *Org. Biomol. Chem.* **2024**, *22*, 1693.

25. (a) Zhou, J.-Y.; Tao, S.-W.; Liu, R.-Q.; Zhu, Y.-M. *J. Org. Chem.* **2019**, *84*, 11891. (b) Ji, H.; Cao, H.; Wang, G.; Xing, F.; Szostak, M.; Liu, C. *Org. Chem. Front.* **2023**, *10*, 4275.

26. Liu, C.; Qin, Z.-X.; Ji, C.-L.; Hong, X.; Szostak, M. *Chem. Sci.* **2019**, *10*, 5736.

27. Tian, T.; Kashihara, M.; Yan, W.; Nishihara, Y. *ACS Catal.* **2024**, *14*, 11905.

28. Miloserdov, F. M.; McMullin, C. L.; Belmonte, M. M.; Benet-Buchholz, J.; Bakhmutov, V. I.; Macgregor, S. A.; Grushin, V. V. *Organometallics* **2014**, *33*, 736.

29. Miloserdov, F. M.; Grushin, V. V. *Angew. Chem., Int. Ed.* **2012**, *51*, 3668; *Angew. Chem.* **2012**, *124*, 3728.

30. (a) Tian, T.; Uei, S.; Li, Z.; Nishihara, Y. *ChemCatChem* **2024**, *16*, e202401190. (b) Malapit, C. A.; Ichiishi, N.; Sanford, M. S. *Org. Lett.* **2017**, *19*, 4142.

31. Amatore, C.; Jutand, A.; Suarez, A. *J. Am. Chem. Soc.* **1993**, *115*, 9531.

32. (a) Lee, Y. H.; Morandi, B. *Nat. Chem.* **2018**, *10*, 1016. (b) Boehm, P.; Martini, T.; Lee, Y. H.; Cacherat, B.; Morandi, B. *Angew. Chem., Int. Ed.* **2021**, *60*, 17211; *Angew. Chem.* **2021**, *133*, 17348. (c) De La Higuera Macias, M.; Arndtsen, B. A. *J. Am. Chem. Soc.* **2018**, *140*, 10140.

33. (a) Liao, W.-J.; Lin, S.-Y.; Kuo, Y.-S.; Liang, C.-F. *Org. Lett.* **2022**, *24*, 4207. (b) Daskiewicz, J.-B.; Depeint, F.; Viornery, L.; Bayet, C.; Comte-Sarrazin, G.; Comte, G.; Gee, J. M.; Johnson, I. T.; Ndjoko, K.; Hostettmann, K.; Barron, D. *J. Med. Chem.* **2005**, *48*, 2790.

34. Dhimitruka, I.; SantaLucia, J. *Org. Lett.* **2006**, *8*, 47.

35. Zhang, L.; Xue, X.; Xu, C.; Pan, Y.; Zhang, G.; Xu, L.; Li, H.; Shi, Z. *ChemCatChem* **2014**, *6*, 3069.

36. Bashir, I. A.; Lee, S. *J. Org. Chem.* **2023**, *88*, 6159.
37. Khatun, N.; Santra, S. K.; Banerjee, A.; Patel, B. K. *Eur. J. Org. Chem.* **2015**, *2015*, 1309.
38. Gaspa, S.; Amura, I.; Porcheddu, A.; De Luca, L. *New J. Chem.* **2017**, *41*, 931.
39. Agrawal, S. K.; Majhi, P. K.; Goodfellow, A. S.; Tak, R. K.; Cordes, D. B.; McKay, A. P.; Kasten, K.; Bühl, M.; Smith, A. D. *Angew. Chem., Int. Ed.* **2024**, *63*, e202402909; *Angew. Chem.* **2024**, *136*, e202402909.

CHAPTER 4

Summary and Future Perspective

4-1 Summary and Conclusion

In this PhD thesis, the Author mainly focused on the Pd-catalyzed decarbonylative nucleophilic halogenation of a series of carboxylic acid derivatives through the reductive elimination pathway of the C–X bond and constructed a series of aryl iodides, aryl bromides and aryl chlorides with good efficiency and high atom utilization. As we all know, supported by previous research experience, since the discovery of this step and its confirmation by stoichiometric experiments, chemists have built a series of Pd or Ni catalytic systems and synthesized a series of organic halides by screening and designing catalytic systems, especially ligands with both electronic and steric hindrance effects. However, as Hartwig revealed in his pioneering research, the reductive elimination trends of different C(Ar)–X bonds can be derived from the equilibrium constant. Among them, the reductive elimination of C(Ar)–I bonds are the weakest, and this conclusion has also been confirmed in a large number of subsequent studies. Because the nucleophilic halogenation mode of aromatics perfectly integrates the formation of C–Br bonds, C–Cl bonds, and even C–F bonds, but only the construction of C(Ar)–I bonds remain a blank. Simultaneously, intramolecular and intermolecular carboiodination strategies undoubtedly provide a wealth of experience in the reductive elimination of C–I bonds, but all breakthroughs focus only on the reductive elimination of C(alkyl)–I and C(alkenyl)–I, therefore, the reductive elimination of C(Ar)–I bonds, which is a thermodynamically and kinetically unfavorable process, is still in high demand for further exploration and development.

Therefore, in order to further accelerate the reductive elimination of the C(Ar)–I bond, the Author expected to break through this dilemma by fundamentally regulating the electron density of the transition metal catalyst center. In other words, the Author tried to use the decarbonylation strategy to regulate the electron density of the transition metal catalyst center. Because we postulated that during the decarbonization process, the de-insertion of the carbonyl group will cause carbon monoxide (CO) to coordinate with the transition metal, which can make the transition metal more electron-deficient, so as to relatively weaken its electron density and thus, to some extent, promote the thermodynamically and kinetically unfavorable reductive elimination of C(Ar)–I bond.

Chapter 2. Palladium-Catalyzed Decarbonylative Nucleophilic Halogenation of Acyl Fluorides and Acyl Chlorides

In the Chapter 2, the Author has developed a practical and versatile palladium-catalyzed method for the decarbonylative nucleophilic halogenation of acyl fluorides and chlorides. This catalytic system, employing palladium and the large-bite-angle ligand Xantphos, efficiently facilitated the challenging reductive elimination of Ar−I, Ar−Br, and Ar−Cl bonds, thereby enabling the high-yield synthesis of a broad array of aryl halides. The use of inexpensive lithium and sodium halides as halogen sources not only improves economic viability but also aligns with green chemistry principles, as these inorganic salts are cost-effective and exhibit low toxicity.

From a mechanistic standpoint, Xantphos played a dual role: it acted as a ligand to promote the reductive elimination of C−X bonds and as an active additive facilitating a distinctive outer-sphere nucleophilic substitution via the formation of phosphonium halides. Decarbonylation was a pivotal step in the process, with the coordination of CO, released during the reaction, to Pd accelerating the reductive elimination. Additionally, the interaction of excess Xantphos with the Pd(0) species likely suppressed its reversion to (Xantphos)Pd(Ar)X, favoring efficient turnover in the catalytic cycle.

The identification of acyl iodides as crucial intermediates represents a significant advancement. By employing stable acyl fluorides and chlorides as precursors, acyl iodides were generated in situ, enabling indirect UFC under mild and practical conditions. The concept of "gradual generation," wherein highly reactive intermediates are formed and consumed simultaneously, proved to be an effective strategy for sustaining catalyst activity and minimizing deactivation. This synthetic framework offers valuable insights for future research aimed at addressing complex chemical transformations.

Some content in **Chapter 2** has been adapted with permission from the following paper:

Tian, T.; Kashihara, M.; Yan, W.; Nishihara, Y. Palladium-Catalyzed Decarbonylative Nucleophilic Halogenation of Acyl Fluorides and Chlorides: Synthesis of Aryl Halides via Reductive Elimination of the C–X (X = I, Br, and Cl) Bond and Mechanistic Implications.

ACS Catal. **2024**, *14*, 11905–11917. (© 2024 American Chemical Society) https://doi.org/10.1021/acscatal.4c03731

A direct link to the Published Work:

https://pubs.acs.org/doi/full/10.1021/acscatal.4c03731

Chapter 3. Palladium-Catalyzed Decarbonylative Nucleophilic Halogenation of Acid Anhydrides

In the Chapter 3, the Author has introduced an efficient Pd-catalyzed decarbonylative nucleophilic halogenation model for acid anhydrides. By leveraging the unique metastable properties of acid anhydrides, this approach circumvents the challenges posed by the instability of acyl chlorides and the high cost of acyl fluorides, highlighting the great potential of anhydrides in synthetic chemistry and related fields. Furthermore, the bulky and cost-effective Xantphos is once again demonstrated to be a highly versatile and compatible ligand for thermodynamically and kinetically unfavorable processes, specifically the Pd(II)-mediated reductive elimination of C–X bonds. This ligand efficiently facilitates the palladium-catalyzed reductive elimination of C–Cl, C–Br, and even C–I bonds, enabling a range of decarbonylative nucleophilic chlorination, bromination, and iodination, and the construction of aryl chlorides, aryl bromides, and aryl iodides with high efficiency.

Importantly, the use of an open system in this protocol accelerates the removal of generated CO, which shifts the equilibrium toward product formation, to significantly improves the catalytic efficiency. This improvement enhances substrate compatibility, particularly for electron-rich substrates like anisole derivatives. Mechanistic studies suggest a plausible decarbonylative unimolecular fragment coupling (UFC) pathway or an alternative route involving an anionic palladate complex. The unique properties of acid anhydrides played a crucial role in enhancing catalytic performance by modulating the reactivity of iodide salts, thereby minimizing side reactions and improving overall efficiency. These findings provide valuable insights and a strong foundation for future advancements in transition-metal-catalyzed transformations.

The Author is confident that this research model will offer strong support and valuable insights for future advancements in related fields.

Some content in **Chapter 3** has been adapted with permission from the following paper:

Tian, T.; Uei, S.; Yan, W.; Nishihara, Y. Palladium-Catalyzed Decarbonylative Nucleophilic Halogenation of Acid Anhydrides.

Catalysts **2025**, *15*, 191. (19 pages) (© 2025 Multidisciplinary Digital Publishing Institute (MDPI)) https:// doi.org/10.3390/catal15020191

A direct link to the Published Work:

https://www.mdpi.com/2073-4344/15/2/191

4-2 Future Perspective

Finally, regarding the future research direction of this research field, the author believes that the first question is whether we can use quite inexpensive, easy-to-operate and readily available esters as ideal candidates to achieve decarbonylative nucleophilic halogenation (**Scheme 4-1**). Because esters are ubiquitous structural subunits in nature, if esters can be directly manipulated to carry out the desired decarbonylative transformation, the application potential can be greatly improved. Simultaneously, the stability of esters is also quite advantageous compared to acyl chlorides, acyl fluorides and acid anhydrides. Therefore, the Author proposed a palladium-catalyzed decarbonylative nucleophilic halogenation mode of esters, which can modularly construct a series of aryl iodides, aryl bromides and aryl chlorides with quite attractive value.

Scheme 4-1. Pd-catalyzed Decarbonylative Nucleophilic Halogenation of Esters.

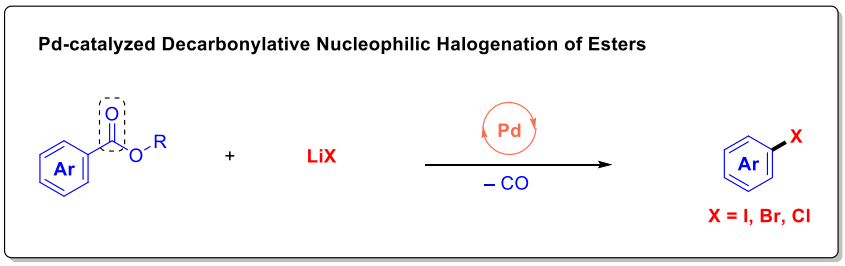

In addition, another highly anticipated breakthrough is fluorination, especially using acyl fluorides as substrates. Indeed, the transition metal-catalyzed decarbonylative unimolecular fragment coupling (UFC) of acyl fluorides is a fairy tale that is quite efficient and convenient to construct aryl fluorides. However, although palladium-mediated reductive elimination of C–F bond has been deeply revealed, the hysteresis of palladium-mediated oxidative addition of acyl fluorides still hinders the implementation of this design. Therefore, the Author proposed a photoredox/nickel co-catalyzed decarbonylative fluorination mode (**Scheme 4-2**). The design can directly obtain intermediate **C** by utilizing the facile oxidative addition and carbonyl de-insertion mode of acyl fluoride under nickel catalysis. Subsequently, the excited state photoredox catalyst excited by visible

light can single-electron oxidize Ni(II) intermediate **C** to form Ni(III) intermediate **D**, a thermodynamically favorable intermediate for reductive elimination of C–F bond. The subsequent reductive elimination of C–F bond occurs to release the desired aryl fluoride and form Ni(I) species **E**. Finally, intermediate **E** is reduced by a low-valent photoredox catalyst to regenerate the Ni(0) catalyst and the ground state photoredox catalyst.

Scheme 4-2. Photoredox/Ni co-catalyzed Decarbonylative Fluorination of Acyl Fluorides.

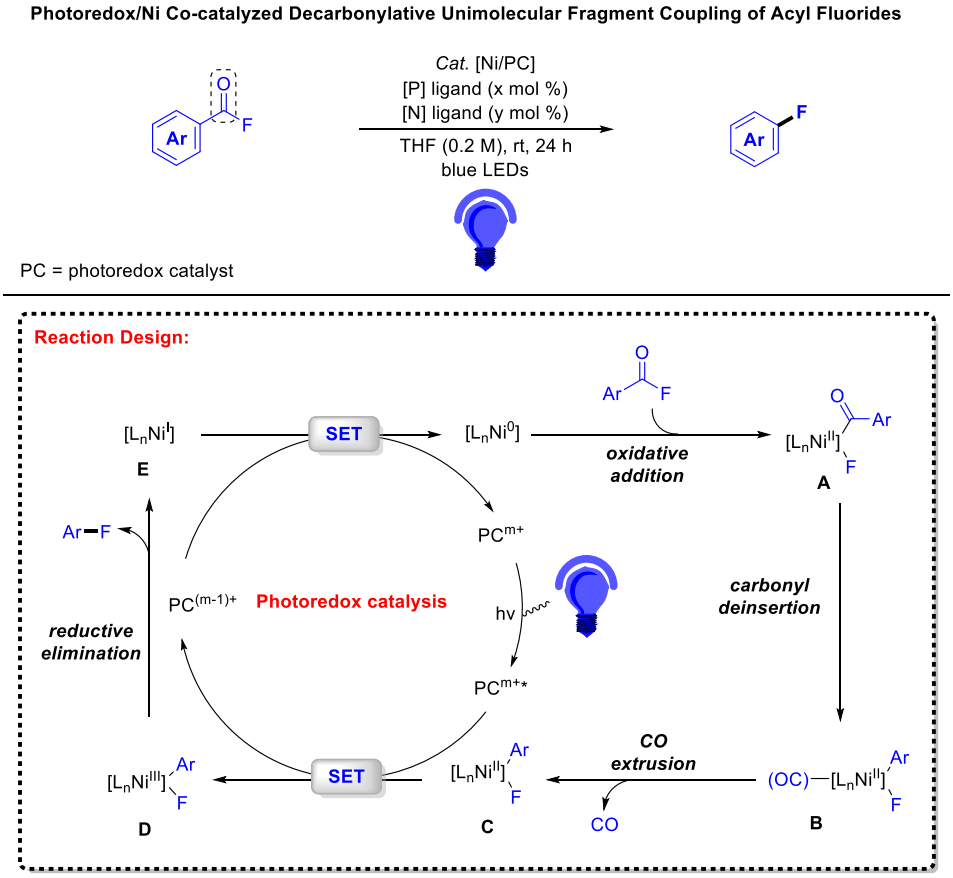

The realization of the Author's expected research results will thoroughly promote the development of related fields and provide a fairly wide range of research ideas and experience for subsequent research, and will exert great potential in the field of industrial application.

List of Publications

Publications Related to the PhD Thesis

Chapter 2

1) Palladium-Catalyzed Decarbonylative Nucleophilic Halogenation of Acyl Fluorides and Chlorides: Synthesis of Aryl Halides via Reductive Elimination of the C–X (X = I, Br, and Cl) Bond and Mechanistic Implications
Tian Tian, Myuto Kashihara, Weidan Yan, and Yasushi Nishihara*
ACS Catal. **2024***, 14,* 11905–11917.
(*This work was selected Cover Arts*)

Chapter 3

2) Palladium-Catalyzed Decarbonylative Nucleophilic Halogenation of Acid Anhydrides
Tian Tian, Shuhei Uei, Weidan Yan, and Yasushi Nishihara*
Catalysts **2025**, *15*, 191.
(*Published as Special Issue "Recent Advances in Palladium-Catalyzed Organic Synthesis"*)

Other Publications

3) Recent Advances in C–F Bond Activation of Acyl Fluorides Directed toward Catalytic Transformation by Transition Metals, *N*-Heterocyclic Carbenes, or Phosphines
Tian Tian, Qiang Chen, Zhiping Li, and Yasushi Nishihara*
Synthesis **2022***, 54,* 3667–3697.

4) Nickel-Catalyzed Decarbonylative Reductive Alkylation of Aroyl Fluorides with Alkyl Bromides
Qiang Chen, Jingwen You, Tian Tian, Zhenyao Li, Myuto Kashihara, Hiroki Mori, and Yasushi Nishihara*
Org. Lett. **2022***, 24,* 9259–9263.

5) A Highly Efficient Cross-Coupling Mode *via* the Release of Small Molecules: Transition Metal-Catalyzed Unimolecular Fragment Coupling (UFC)
Tian Tian, Shuhei Uei, Zhiping Li, and Yasushi Nishihara*
ChemCatChem **2024***, 16,* e202401190.

Presentation

1) Nickel-Catalyzed Decarbonylative Reductive Alkylation of Acyl Fluorides with Alkyl Bromides (Poster Presentation)
   Tian Tian, Qiang Chen, Jingwen You, Zhenyao Li, and Yasushi Nishihara
   The 68th Symposium on Organometallic Chemistry, No. PC-36, Division of Organometallic Chemistry, Kinka Chemical Society, Japan, On-line, September 6–8, 2022.

2) Palladium-Catalyzed Decarbonylative Halogenation of Acyl Fluorides via Reductive Elimination of the C–X Bond (Poster Presentation)
   Tian Tian, Myuto Kashihara, and Yasushi Nishihara
   The 69th Symposium on Organometallic Chemistry, No. PA-08, Division of Organometallic Chemistry, Kinka Chemical Society, Japan, Osaka University Convention Center (Osaka, Japan), September 13–15, 2023.

3) Palladium-Catalyzed Decarbonylative Halogenation of Acyl Fluorides and Chlorides via Reductive Elimination of the C–X Bond (Oral Presentation)
   Tian Tian, Myuto Kashihara, Weidan Yan, and Yasushi Nishihara
   The 124th Symposium on Organic Synthesis, No. O-08, The Society of Synthetic Organic Chemistry, Japan, Hokkaido University (Sapporo, Japan), June 27–28, 2024.

Other Presentation

1) Nickel-Catalyzed Decarbonylative Reductive Alkylation of Acyl Fluorides with Alkyl Bromides (Poster Presentation)
   Myuto Kashihara, Qiang Chen, Jingwen You, Tian Tian, Zhenyao Li, Hiroki Mori, and Yasushi Nishihara
   21st International Symposium on Organometallic Chemistry Directed Toward Organic Synthesis (OMCOS 21), No. 138, Vancouver, BC Canada (July 24–28, 2023).

2) Palladium-catalyzed decarbonylative halogenation of acid anhydrides (Poster Presentation)
   Shuhei Uei, Tian Tian, and Yasushi Nishihara
   The 12th Chugoku Shikoku Symposium of the Chemical Society of Japan, No. 1PB-03, The Chemical Society of Japan, Okayama University (Okayama, Japan), November 16–17, 2024.